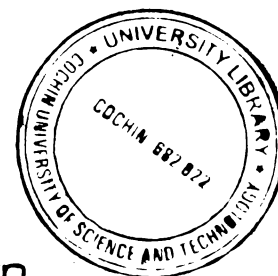Tµ77

STUDY OF FERRUGINOUS AND TITANOFERROUS IMPURITY MINERALS IN CHINA CLAY

THESIS SUBMITTED TO COCHIN UNIVERSITY OF SCIENCE AND
TECHNOLOGY IN PARTIAL FULFILMENT OF THE REQUIREMENTS FOR
THE DEGREE OF

DOCTOR OF PHILOSOPHY

IN CHEMISTRY UNDER THE FACULTY OF SCIENCE

BY

S. RAMASWAMY

UNDER THE SUPERVISION OF Dr. SATHY CHANDRASEKHAR

CHEMICAL SCIENCES DIVISION

PROCESS ENGINEERING DIVISION

NATIONAL INSTITUTE FOR INTERDISCIPLINARY SCIENCE
AND TECHNOLOGY

(Formerly Regional Research Laboratory), CSIR

THIRUVANANTHAPURAM - 695 019, KERALA, INDIA.

November – 2007

DECLARATION

I hereby declare that the matter embodied in the thesis entitled **"STUDY OF FERRUGINOUS AND TITANOFERROUS IMPURITY MINERALS IN CHINA CLAY"** is the result of investigations carried out by me in National Institute for Interdisciplinary Science and Technology (Formerly Regional Research Laboratory), CSIR, Thiruvananthapuram-695 019, under the supervision of Dr. (Mrs.) Sathy Chandrasekhar (Scientist F, Deputy Director, NIIST, Thiruvananthapuram) and the same has not been submitted elsewhere for any other degree.

S. Ramaswamy

Thiruvananthapuram
November2007

Dr. (Mrs.) Sathy Chandrasekhar
Scientist F, Deputy Director
Inorganic Material Section
Chemical Science Division

CERTIFICATE

This is to certify that the work embodied in the thesis entitled **"STUDY OF FERRUGINOUS AND TITANOFERROUS IMPURITY MINERALS IN CHINA CLAY"** is the result of investigations carried out by Mr. S. Ramaswamy, under my supervision in the Chemical Sciences and Technology Division of National Institute for Interdisciplinary Science and Technology (Formerly Regional Research Laboratory), CSIR, Thiruvananthapuram, and the same has not been submitted elsewhere for any other degree.

Dr. (Mrs.) Sathy Chandrasekhar

(Thesis Supervisor)

Thiruvananthapuram

November 2007

डॉ. (श्रीमती) सती चन्द्रशेखर
Dr. (Mrs.) SATHY CHANDRASEKHAR
वैज्ञानिक / SCIENTIST 'F'
राष्ट्रीय अंतर्विषयी विज्ञान तथा प्रौद्योगिकी संस्थान
National Institute for Interdisciplinary
Science & Technology, Govt. of India, CSIR
तिरुवनंतपुरम / Thiruvananthapuram - 695 019

ACKNOWLEDGEMENTS

PREFACE

A systematic investigation has been carried out on seven kaolin samples collected from the major deposits in India, i.e., Kasargod and Trivandrum (Kerala), Koraput (Orissa), Kutch (Gujarat), Bankura (West Bengal) and Pali (Rajasthan). The total work is presented in 7 chapters. **Chapter 1** deals with the general introduction on kaolin with respect to its formation, mineralogical and structural aspects, unique properties and industrial uses. This chapter also describes the iron minerals associated with kaolin and their effect on the optical properties. The national / international status on kaolin research is also discussed.

Chapter 2 explains the methodology adopted for characterization of clays and impurity minerals. The techniques involved are wet chemical analysis, ICP-AES, UV-Vis spectrophotometry and flame photometry for chemical assay, XRD and thermal analysis (DTA/TGA) for mineralogy, particle size distribution analysis, brightness and colour measurements, EPR, Mossbauer, FTIR and UV-Visible spectroscopy and electron microscopy (SEM, HR TEM - EDS and EPMA). Procedures for the methods adopted for concentration / removal of impurity minerals are also given.

Results on the characterization of the run-of-mine (ROM) and size classified kaolins are presented in **Chapter 3.** This chapter also gives details on the speciation of iron minerals and suggests the methods for value addition of kaolin. All clays under study are highly kaolinitic and the quantity and type of ancillary minerals vary from clay to clay. Quartz is the common impurity and micaceous, ferruginous and carbonaceous minerals also exist either singly or in combination. The three kaolin samples from Kerala are kaolinitic with impurities of quartz, rutile, anatase and iron oxides / hydroxides. Pyrite is the major iron impurity in Koraput clay whereas mica dominates in Pali and Bankura samples. The Kutch kaolin is associated with iron stained titania. Size classification increases the percentage of fine fraction. The optical properties of the clays also improve during size classification due to the removal of the coarse colored minerals. DCB treatment has given a picture of the total soluble/free iron in the samples. Kaolins from Kasargod, Trivandrum, Koraput and Bankura respond well to the DCB treatment. Pali and Kutch samples show very poor response.

1

Chapter 4 gives an account of the separation of impurity minerals by hydrocycloning, panning, alkali treatment and magnetic (hand magnet) techniques and their chemical and mineralogical characterization. The iron content in the impurity is high, but XRD analysis indicated low crystallinity. It is reasonable to think that the same minerals may be present in the clay as fine particles. Hematite and goethite are found to be major ancillary minerals present in Kasargod and Trivandrum clays with some ilmenite in one sample. Kutch clay contains mostly anatase and hematite, whereas Koraput sample contains pyrite and goethite. Goethite and mica are found in Bankura and Pali samples with some hematite in the former and calcite in the latter. It is observed that size classification removes most of the quartz but does not significantly remove the coloring impurities except in a few cases. Uniform distribution of these impurities in all size fractions is thus indicated.

Chapter 5 is on the spectroscopic (EPR, Mossbauer, Infra red and UV-Visible) and microscopic (Optical, SEM, HR TEM-EDS and EPMA) studies on selected samples. The spectroscopic and microscopic data obtained clearly substantiate the findings detailed in Chapters 3 and 4. The EPR spectral studies of selected samples were carried out at room temperature to characterize the minor components in clays that contain unpaired electrons and also to assess the effectiveness of chemical bleaching. Since the iron content in the clay samples was too low to be measured by the instrument, the impurity minerals concentrated by panning were subjected to the Mossbauer spectral studies. The characteristic isomer shift (∂), quadruple splitting (ΔE) and KOe values obtained from the spectra gave information on the type of iron impurity. FT IR studies explain the ordering in kaolinite, its crystallinity, and the presence of impurity minerals. UV-Visible spectral studies on impurity minerals concentrated by panning was carried out to identify the iron species present based on their electronic spectra i.e., (i) Fe^{+3} Ligand Field Transitions (ii) Ligand to Metal Charge Transitions and (iii) transitions resulting from the simultaneous excitation of magnetically coupled Fe^{+3} cations which occupy adjacent sites.

Electron Probe Micro Analysis (EPMA) of ROM and impurity separated by hydrocycloning gave the distribution pattern of the elements indicating the mineralogy. ROM and size classified products (SCP1 and 2) of the clays were examined under SEM

2

to understand the size and shape of the particles. Due to the uniqueness of the impurity minerals in Kutch and Koraput clays, HR TEM –EDS of selected samples from these clays were taken to get a detailed particle wise microanalysis data.

In **Chapter 6**, an attempt has been made to correlate the Fe-Ti content in the clays with their optical properties. It has been observed that the total iron content (analytical iron) cannot be directly related to the optical properties of the clay. Iron can exist in two forms, "structural" and 'free" which has been distinguished by their response to the DCB treatment. Small amount of iron in kaolinite structure does not affect the brightness because the Fe atoms are too far apart to allow any electronic transition. However, the same amount of Fe if present in the small quantities of ancillary minerals imparts color and affects the brightness of kaolin. Hence, the optical properties of kaolin are not directly related to the 'analytical" iron content, but are dependent on the species of iron present in the clay.

The investigation on Koraput kaolin has been discussed in **Chapter 7**. During the size classification studies, it was observed that the conventional method could not be adopted for this clay due to the high acidity. The clay water slurry was yellow in color and resulted in precipitation during dilution. Subsequent filtration and drying resulted in a product with yellowish brown color. Detailed study was conducted to solve this problem and a modified method has been suggested to get product clay of acceptable brightness.

Conclusions drawn out of the detailed investigations of the kaolins are given at the end. This includes results of the characterization of the ROM clay, beneficiated products and the impurity minerals, correlation of the Fe and Ti minerals with the optical properties, suggestions on the possible value addition by using advanced processing techniques and comparison of the product samples with Indian and international specifications for different applications. All the results have been published in journals and / or presented during national and international conferences.

CONTENTS

5

Abbreviations

ROM	-	Run-of-mines
SCP1	-	Size Classified Product 1
SCP2	-	Size Classified Product 2
IM1	-	Impurity Mineral 1
IM2	-	Impurity Mineral 2
IM3	-	Impurity Mineral 3
IM4	-	Impurity Mineral 4
XRD	-	X-ray Diffraction
SEM	-	Scanning Electron Microscopy
HR TEM-EDS	-	High Resolution Transmission Electron Microscopy with Energy Dispersive X-ray Spectroscopy
EPMA	-	Electron Probe Micro Analysis
EPR	-	Electron Paramagnetic Resonance spectroscopy
FTIR	-	Fourier Transformed Infra Red spectroscopy
K	-	Kaolinite
Q	-	Quartz
A	-	Anatase
R	-	Rutile
P.R	-	Pseudo Rutile
I	-	Ilmenite
H	-	Hematite
Hs	-	Hematite(Specularite
Hk	-	Hematite (Kidney ore)
G	-	Goethite
L	-	Lepidocrocite
M	-	Magnetite
Ma	-	Maghemite
Mi	-	Mica
Gr	-	Graphite
C	-	Calcite

CHAPTER 1

INTRODUCTION

Kaolin or china clay is one of the most versatile industrial minerals with wide range of applications. Minor quantities of quartzitic, ferruginous, micaceous, carbonaceous and titanoferrous minerals are generally associated with kaolin. These ancillary minerals are deleterious since they adversely affect the properties and make kaolin unsuitable for many applications. Hence their removal is of prime importance in the optimum utilization of kaolin. Physical, chemical, mineralogical, spectroscopic and microscopic techniques are generally employed for identifying and quantifying the ancillary minerals. Based on the nature and quantity of impurity minerals, beneficiation techniques for value addition are selected and sequentialized.

1.1 Clay minerals

Clay minerals are a group of hydrous aluminum silicates with a layered structure and very small (less than 0.005 mm or microscopic) particle size. They are usually produced by weathering of rocks and occur widely in mudstones, shales, marine sediments and soils. Different geologic environments produce different clay minerals from the same parent rock. The present definition (Brindley, 1972) states "clay minerals belong to the family of phyllosilicates and contain continuous two-dimensional tetrahedral sheets of composition T_2O_5 (T = Si, Al, Be etc) and are linked by sharing three corners of each tetrahedron, where the fourth corner will be pointing to any direction. Here, the tetrahedral sheets are linked in the unit structure to octahedral sheets, or to groups of coordinated cations, or individual cations."

Phyllosilicates display a two-dimensional framework of infinite sheets of SiO_4 tetrahedrons as represented in Figure 1.1. They exhibit a Si:O ratio of 2:5 resulting from the sharing of three oxygen atoms in each tetrahedron and six fold symmetry in undistorted sheets (Bailey et al., 1985). The basic structural feature of phyllosilicates is the combination of layers of psuedohexagonal network of SiO_4 tetrahedra (silica tetrahedral layer) and layers of cations in octahedral coordination (octahedral layer). The two kinds of octahedral layers are known: gibbsite and brucite layers. The gibbsite layer has a dioctahedral arrangement; ie., there are two cations of Al for each six OH ions,

whereas a brucite layer is trioctahedral there being three cations (Mg, Fe) for each layer. Composite arrangement of each of the Al octahedral and Si tetrahedral layers result in a 1:1 structure as in kaolinite (a two-layer structure); or an octahedral layer sandwiched by two tetrahedral layers resulting in a 2:1 structure (as three-layer structure), as in montmorillonite and illite. The phyllosilicate types are divided into groups on the basis of charge on the layers and on the nature of octahedral-tetrahedral layers (Bailey, 1980). The schematic representation of the common clay minerals is given in Figure 1.2. "Kaolinite" is the most versatile industrial clay mineral and abundant species of the phyllosilicate family.

Some minerals have got all charges balanced within the crystal whereas certain others contain charge unbalances within the crystal structure. These minerals are said to contain a permanent charge. Also, the tetrahedra and octahedra with which the phyllosilicates are built require a cation:oxygen radius ratio of 0.255 - 0.414 and 0.414 - 0.732 respectively. Mineral analysis over the years has indicated that many ions are found in the phyllosilicates and Table 1 gives the variety of ions which can fit into either tetrahedral or octahedral polyhedra. Aluminum is unique in that respect and it falls right on the line between the two, making it possible for the trivalent Al to replace some of the quadrivalent Si, resulting in an imbalance of "-1" for each substitution. Also at times divalent ions get substituted in the octahedral layer of dioctahedral minerals, and trivalent ions in the octahedral layer of trioctahedral minerals. In these cases there will be, respectively, a negative and positive imbalance of charge. A second source of charge on the minerals is the broken bonds found at the mineral edges. Since, the structure cannot be extended infinitely, at some point there will be oxygens without all charges satisfied by cation association. In these cases a hydrogen ion from solution will normally satisfy the requirement and it will depend entirely on the solution pH. Therefore, these charges are called either pH-dependent charge or variable charges.

1.1.1 Kaolin mineral - structure

Kaolin is tentatively defined by the International Committee on Correlation of Age and Genesis as "an earthy rock characterized by a significant content of kaolin minerals" (Keller, 1978) and the word "*kaolin*" is derived from the name of the Chinese town Kao-Ling (or Gaoling, "high ridge"), located in the Jiangxi Province of southeast

9

China, where the written description of porcelain can be found (Grim, 1968). Kaolin minerals are included under the 1:1 dioctahedral phyllosilicates of kaolin-serpentine family. Kaolinite, a clay mineral with an oxide formula of $Al_2O_3.2SiO_2.2H_2O$ and with a Si/Al ratio 1.0 is the principal mineral in kaolin. Kaolinite is chemically, $Al_2 Si_2O_5 (OH)_4$, having an ideal chemical composition of SiO_2 – 46.54%, Al_2O_3 – 39.5%, H_2O – 13.96%. It is a layered alumino-silicate mineral made of alternating sheets of octahedrally coordinated aluminum and tetrahedrally coordinated silicon that are bonded by hydroxyl groups giving it a platy hexagonally shaped crystals structure. Here silicon is in 4-fold co-ordination with oxygen ions and the resulting tetrahedra share corners to form a two dimensional sheet with all epical oxygens pointing in one direction. Octahedrally co-ordinated aluminium ions are linked to the epical oxygens of the silica sheet to form a second layer. Shared hydroxyl groups satisfy the remaining co-ordination sites of the aluminium ions . The resulting crystal is triclinic with the cell parameters

$$a = 5.139 \ A° \ ; b = 8.932 \ A° \ ; c = 7.371 \ A° \ ;$$

$$\alpha = 91.6° \ ; \ \beta = 104.8° \ ; \ \gamma = 89.9°$$

Kaolinite was first described as a mineral species in 1867 for an occurrence in the Jari River basin of Brazil.

Kaolinite occurs with varying degrees of disorder in its layer stacking (Brindley, 1980; Tchoubar et al, 1982) and has a low shrink-swell capacity and a low cation exchange capacity (1-15 meq/100g.). It is a soft, earthy, usually white mineral produced by the chemical weathering of aluminium silicate minerals like feldspar. In many parts of the world, it is colored pink-orange-red by iron oxide, giving it a distinct rust hue. Lighter concentrations yield white, yellow or light orange colours. It is mined, as kaolin, in Brazil, France, United Kingdom, Germany, India, Australia, Korea, China and USA.

Kaolinite crystals shows structural disorder due to the isomorphous substitution resulting in the incorporation of Fe, Ti and Cr (Meads and Malden, 1975; Rengaswamy, 1976; Mestdagh, 1980 and Maksimovic et al, 1981) and also from the structural defects (Plancon and Tchoubar, 1977a, b). Extensive study on the structural disorder of kaolinite under taken by Brindley et al (1986), showed that the kaolinite from each mine has a characteristic internal structural disorder which is fairly constant within the suite of the samples from a given mine. The incorporation of foreign ions into the structure of

10

kaolinite results from the variability of chemical environment during its formation. The incorporation of various cations into the structure of kaolinite and the ancillary minerals present in kaolin are of great industrial significance.

The tetrahedron and octahedron are the building blocks of kaolinite. The basic tetrahedral unit, Si - O combination has a radius ratio of 0.30, which means that the silicon ion fits nicely into a tetrahedral polyhedron. An exploded schematic diagram of this polydedron is shown in Figure 1.3a. Here the silicon ion shares its charge equally between the four oxygen ions, leaving each oxygen with an excess charge of negative one. This orthosilicate anion tends to react readily with alkali and alkali earth ions. Similarly, the SiO_4^{4-} anion does have another option open to satisfy the charges. ie., It is also possible for an oxygen ion to bond with two Si ions, and thereby have its charge balanced. Theoretically this could happen by the three face oxygen ions, the two edge oxygen ions, or the single corner oxygen ion bonding with two silicon ions. There may be several reasons that the first two options are not possible, but in the simplest explanation either faces sharing or edge sharing would bring the two highly electropositive silicon ions too close together. Thus, only a sharing of the corner oxygen ion is a viable option. Bonding of each of the four oxygen ions with two silicon ions results in a quartz crystal. In kaolinite, only one plane of oxygen ions bond with two silicon ions as indicated in Figure 1.3b. This bonding is extended in two directions to form a sheet of silicon tetrahedrons and this sheet carries unbalanced charges on the apical O ions.

The second basic building block of kaolinite is an aluminum octahedral unit. The aluminum/oxygen radius ratio is 0.41, which falls right at the maximum ratio for tetrahedral coordination and minimum ratio for octahedral coordination. Depending upon the conditions, aluminum can coordinate with either four or six oxygen ions. But within the kaolinite mineral structure, the aluminum ion is "more comfortable" in an octahedral coordination and an exploded view of the aluminum octahedral unit is demonstrated Figure 1.3c. Here aluminum shares +0.5 of its charge with each of the surrounding oxygen ions, leaving each oxygen ion with a negative 1.5 charge.

This excess negative charge on the oxygen ions needs to be balanced and the charge can at least be partially balanced if each oxygen ion is bonded with two aluminum ions. Once again, this could theoretically happen by the three face oxygen ions, the two

11

edge oxygen ions, or the single corner oxygen ion bonding with two Al ions. In this case, aluminum is slightly less electropositive than silicon and is able to approach close enough, so that corner oxygen ions can be shared. In a matrix of these octahedral units, each oxygen will be bonded to two aluminum ions, leaving it with a remaining -1 charge. The charge can be satisfied by attaching a proton (hydrogen ion) and this type of structure is continued in three dimensions leading to the formation of the gibbsite mineral (Figure 1.3d).

The other option for balancing the remaining -1 charge on the oxygen ions is to bond with the sheet of silicon tetrahedral units with apical oxygen ions still having an unbalanced charge. When the two sheets are brought together in such a way that the apical oxygen ions of the tetrahedral layer also being in the octahedral layer, the charge on these oxygen ions will get balanced by bonding to one silicon and two aluminum ions. This is the basic structure (Figure 1.3e) of the kaolinite mineral.

The kaolinite mineral is actually made up of many micelles piled one atop the other (Figure 1.3f). Since the surface on one micelle contains hydrogen ions and the other surface only oxygen ions, there is a tendency for hydrogen bonds to form between micelles. While individual hydrogen bonds are very low energy, the bonding energy is additive and the sum of the many hydrogen bonds between micelles results in the micelles being very strongly bonded together and nearly impossible to separate. Thus, kaolinite is a nonexpanding phyllosilicate and since each micelle is constructed of a layer of silicon tetrahedral units and a layer of octahedral units, kaolinite is called a 1:1 clay mineral.

1.1.2 Kaolin - Genesis

The mineral, kaolin forms in a variety of diverse environments such as (1). crystallization in cavities within the rock (2) by replacement of other minerals (3) alteration of water-laid clastic silicate parent material (4) in situ alteration of "primary" silicate crystalline rock (5) kaolinization at an unconformity (6) hydrothermal argillisation (7) in situ alteration of clay parent rock (8) sedimentary deposition of kaolin mineral (9) diagenesis and (10) formation under complex geological conditions (Keller, 1977, 1978, 1985). The two natural processes capable of kaolinisation of aluminosilicate rocks are weathering and hydrothermal alteration.

12

The formation of kaolinite and its stability depend upon the changes within its environment. Kaolin minerals tend to develop preferentially in the humid tropics. Under these climatic conditions, the fresh rocks and minerals in the presence of ample quantity of water and favorable temperatures, chemically modifies to more stable phyllosilicate phases (Weaver, 1985). Processes leading to formation of clay during chemical weathering include hydrolysis, dissolution, hydration, oxidation and chelation. An increase in rainfall, temperature and moisture enhances the amount of clay formed.

The influx of ground water has great influence on the type of clay mineral formed from a particular primary silicate. When a primary silicate hydrolyses in an environment of high acidity of H+, alkali and alkaline earth metals are removed by replacement. Then the resultant product will be a 1:1 layered pyllosiliate. In contrast, if the activities of the metal ion remain relatively high, 2:1 layer clay mineral is formed (Weaver, 1985). In addition to the above explained factors, the topography of the region also plays a major role during clay formation. For the formation of thick kaolinite deposits, a large influx of water over a long period of time is necessary. During the earlier stages of weathering, the composition of the parent material can determine the type of clay formation. In addition, the mineralogy of the parent rock, their texture, porosity, density, structure, fabric and the degree of consolidation also influence the formation of clay minerals. Kaolinite was reported to be formed from various precursor minerals and pathways of "kaolinisation ", ie., formation of kaolin by the weathering of alumino-silicate minerals or clay minerals reported by many workers are given below. Feldspars are the most abundant constituents of igneous and metamorphic rocks and the product of their weathering is the major source of kaolinite in the earth's surface. The structure of this tectosilicate consists of a continuous three-dimensional network of SiO_4 and AlO_4 tetrahedra, with the positively charges sodium, potassium and calcium situated in the interstices of the negatively charged network (Deer et al, 1976). In a study of residual kaolin derived from feldsphatic rocks in Southern Appapachians, Sand (1956) noted that kaolinite was the major mineral in Georgia sample and mica is found to be the intermediate phase during this transformation. Also, study of the alteration of K-feldspars has shown the formation of K-mica or illite as the intermediate phase between feldspar and kaolinite (Keller, 1970). Tsuzuki and Kawabe (1983) suggested that dissolution – reprecipitation mechanism is

responsible for the entire sequence of alteration of feldspars to kaolinite and Anand et al (1985) has shown the formation of kaolinite from weathered feldspars in the absence of any noncrystalline precursor. Kaolinisation of biotite (micaceous mineral) is accompanied by a change of chemical composition by exchange of some of its components such as H_2O, K^+, Mg^{+2}, Si^{+4}, Fe^{+2}, Fe^{+3} with their surroundings. Wilson (1966) and Banfield and Eggleton (1988) in their studies have reported the formation of kaolinite and goethite as end products of weathering of biotite. Heavily altered biotite from natural weathering environments is found to contain nearly completely oxidized Fe in the mineral structure during the process of kaolinisation (Gilkes et al, 1979). Muller and Bocquier (1987) found that kaolinite replacing micas in the tropics are Fe-kaolinite and with increasing weathering, it becomes richer in Fe and less well crystallized. Also, many researchers have reported the formation of kaolinite from granite (Tardy et al, 1973; Clark, 1973) and mica (Stoch and Sikora, 1976; Craw et al, 1982, Sharp et al, 1990; Banfield and Eggleton, 1990; Sing and Gillkes, 1991; Roberson et al, 1991; Pevear and Nagy, 1993 and Jeong, 1998b).

The most common parent minerals from which kaolin minerals form are feldspars and muscovite. The transformation of potassium feldspars into kaolinite results from weathering or hydrothermal alteration which leaches out potassium and silica according to the equation,

$$2KAlSi_3O_8 \quad + \quad 3H_2O \quad \longrightarrow \quad Al_2Si_2(OH)_4 \quad + \quad 4SiO_2 + \quad 2K(OH)$$

Potash Feldspar   Water   Kaolinite   Silica   Potash
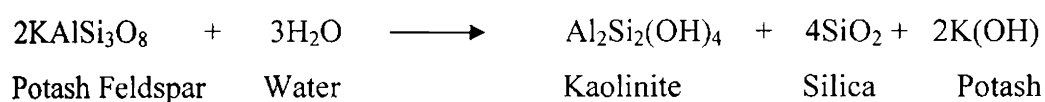
Kaolins are classified based on their mode of formation and occurrence ie., the residual and hydrothermal kaolins termed as primary and the sedimentary kaolins as secondary. Primary kaolins are those that have formed in situ usually by the alternation of crystalline rocks such as granites and rhyolites. The secondary kaolins are sedimentary which were eroded, transported and deposited as bed and most of the kaolin deposits of secondary origin are formed by the deposition of kaolinite which had been formed elsewhere. Majority of the kaolin deposits in the world are primary in nature as special geological conditions are necessary for both the deposition and preservation of secondary kaolin.

14

1.1.3 Kaolin resources

The most important kaolin resources in the world are in Devon and Cornwall in Southern England and in South Carolina and Georgia in USA. Other important deposits include those in Amazon basin in Brazil, in Brittany and Aquitaine basin in France, in Bavaria and Bohemia in Spain, Suzhou in Jingsu province in China and in parts of Eastern Europe, ie., in Germany, Czech Republic and Russia. There are very good potential deposits in Indonesia and Australia. Extensive studies on these reserves have been reported. Bristow (1968) has studied in detail the geology and genesis of the deposits in south western England. The deposits in Georgia are well described by Patterson and Murray (1975), Hurst (1979), Hurst and Pickering, 1989; Hurst et al, 1997; Schroeder et al, 2002; White et al, 1991; Schroeder and Shiflet, 2000; .Schroeder et al,2004. Storr (1983) and Konta (1980) have reviewed the properties of kaolins from Germany and Czech Republic respectively. Studies by Zheng et al (1982) show that Suzhou deposit is very large and the indicated reserves are over 20 million tons. Studies are also going on the kaolin reserves in South Western Australia and Indonesia (Singh and Gilkes, 1992 & Hart et al, 2002). An overall description of kaolin deposits through out the world was given by Keller (1977) in a series of his research publications.

The world kaolin production as reported by Roskill Information services, London for the year 2006 is approximately 27 million tones. The major producers and exporters of kaolin are USA, Brazil, UK, Germany, China and Czech Republic and account for the 66% of the total production. India, Uzbekistan and Colombia are also important producers but could only cater the needs of the national market.

Kaolin reserves in India are found in most of the states but are concentrated in Orissa, Rajastan and West Bengal. Indian kaolin deposits are classified by application and most of the known deposits contain either mixed or ceramic grades of kaolin. Known paper coating grade deposits are relatively small. The total recoverable reserves of kaolin in India are placed at 1400 million tons, which is about 56% of the total reserves. Among these 695 million tons (67%) of the total reserve falls under possible category, 301 million tons (29%) under probable category and 46 million tons (4%) under proven category. The major recoverable reserves of china clay is available in different parts of the country and the state wise resource is, West Bengal (Birbhum) – 350 Million Tons

15

(MT), Orissa (Sambalpur, Koraput) – 300 MT, Jharkhand (Shinbhum) -100 MT, Rajasthan (Chittorgarh, Jaipur, Baswada) – 180 MT, Gujarat (Kutch, Banaskantha) – 100 MT and Kerala (Trivandrum, Kundara, Kasargod) – 140 MT. Small china clay reserves are there in many other states also. Out of the above reserves, kaolin deposit from Trivandrum is found to be of superior quality.

1.2 Characterization, properties and industrial uses of kaolin

Physical, chemical, mineralogical and morphological characterization of kaolin is of utmost importance for evaluating the sample for possible applications. Physical properties include particle size, specific gravity, oil absorption capacity, acid and water solubles, optical properties such as brightness and color values. For certain high value applications, particle size distribution and brightness of the kaolin are critical. Chemical assay gives information on the concentration of the major (Si and Al) and minor (Fe, Ti, Mn, alkali and alkaline earth metals etc.) elements in the sample. The wet chemical method proposed by Bennett and Reed (1971) still holds good for the chemical characterization though more sophisticated X-ray Fluorescence analysis is also used. "Rational analysis" by calculation from the chemical composition indicates the minerals present. Mineralogical characterization of kaolin as well as identification of ancillary mineral contents is carried out by X-ray diffraction method and Brindley (1980) has given a detailed account of the same in his studies. Thermal analyses (DTA & TGA) are also used for the identification of minerals. The morphology of kaolin can be understood by scanning and transmission electron microscopy. Keller in his works (1976a, 1976b, 1976c, 1978, and 1980) has shown that morphology of the kaolinite is controlled by the source material. Electron microprobe analysis (EPMA) gives chemical assay of individual particles of even nanometer size. Spectroscopic studies also contribute to the kaolin investigations. IR and NMR spectral analysis indicates the crystallinity of kaolin as well as the presence of ancillary minerals. Even though EPR and Mossbauer spectra do not give much information on kaolinite, they have contributed greatly to the study of iron minerals in kaolin.

Kaolin is one of the versatile industrial minerals and is extensively used for many applications (Murray, 1977 and 1963). It is unique in nature because it (1) has got specific chemical composition and is chemically inert over a relatively wide pH range

16

(except for catalytic activity in some organic systems) (2) is white or near white (3) has good covering or hiding power when used as a pigment or extender in coating and filling (4) is soft and nonabrasive (5) has low conductivity of both heat and electricity (6) has got fine particle size, shape (morphology) and surface chemistry and (7) is lower in cost than most minerals with which it competes (Murray,1986) Furthermore, calcination of kaolin increases its brightness, makes its surface more compatible with organic systems, improves light scattering, enhances dielectric character and increases hardness for polishing, thereby significantly augmenting the area of application. The diverse range of applications can also be classified into six categories according to primary functions; in film formation, in fiber extension, in polymer extension and reinforcement, as a carrier, adsorbent, diluents etc and also as a polishing agent (Bundy, 1993).

Kaolin finds application in variety of industries like paper, ceramics, rubber, plastics, cement, ink, catalyst, fiber glass and also for some special uses (Figure 1.4). High value addition is achieved when the processed clay finds application as pigment in paper and paint industries (Murray, 1986). The most important use of kaolin is in papermaking, both in filling and coating, but it gets maximum value addition, when it is used for coating application. Paper is coated to improve brightness, opacity, gloss, smoothness and most importantly to improve printability. Uncoated paper is composed of largely of cellulose fibers interwoven in the random and open configuration and this paper can not be used for high end applications. The fine particle size and platelet shape of kaolin are ideal for imparting a smooth, denser and more uniformly porous surface and thereby giving better gloss, brightness, opacity and uniform ink receptivity. Kaolin is the major pigment used in coating color formulations and its properties for coating purpose have been reviewed by Bundy (1991). Kaolin with fine particle size is used in film formation as it greatly enhances the quality of films formed by polymers that are used as binders. This application in film formation includes paper coating, paint and ink. There is no naturally occurring or synthetic pigment which has got better rheology, brightness, opacity in coatings and contributes effectively to film gloss at low cost.

Though considerably less important than paper coating, paint represents a significant market for kaolin. Titanium dioxide is the dominant inorganic pigment used in the paint industry followed by calcium carbonate. Kaolin has got the remaining share in

17

the extender pigment use (Anon, 1987) and is used for exterior water based paints and oil based paints. Steig (1959) has reviewed the increased opacity of kaolin added paint films. Kaolin is the major inorganic pigment used in ink. Ink formulations are similar to those of paper coating and paint. The most important uses of kaolin in inks are to improve ink holdout and to extend both colored and white pigments (Brushwell, 1964; Stoy, 1989)

There is no critical specification for kaolin in certain applications such as in cement industry where the only concern is light color and chemical composition. Ceramic industry is a large user of kaolin in white ware, insulators and refractory. For ceramic industries, the specifications are variable as the individual users may have different requirements as to strength, plasticity, fired color, shrinkage and pyrometric cone equivalent (PCE).

Kaolin is used in rubber industries because of its reinforcing and stiffening properties. Kaolin with fine particle size gives good resistance to abrasion and is used extensively in non-black rubber goods. It finds application in plastic industry because kaolin aids in producing a smooth surface finish, reduces cracking and shrinking, obscures the fiber pattern when fiberglass is used as reinforcement, contributes to a high dielectric strength, improves resistance to chemical action and weathering. It is also used extensively in production of cracking catalysts and molecular sieves. Calcined kaolin with 90% particles less than 2 μm is used as a polishing agent in toothpaste, automobiles and soft metal polishes.

Thus kaolin possesses a broad range of properties necessary for high performance applications. Above all, the low cost of this material makes it one of most versatile industrial minerals. The approximate cost of different commercial kaolins available in Indian market is given in Table 2.

1.3 Kaolin beneficiation - International practices

Extensive research has been carried out by various research groups all over the world to identify the beneficiation methods suitable for the value addition of kaolin samples specific to a particular deposit and is still going on. The raw kaolin can be value added by employing suitable beneficiation techniques and the methods of beneficiation depend upon the quantity and nature of impurity minerals associated with it and the end use of the material. Most kaolins are usually air-floated or wet processed to get the

18

cleanest brightest products. Prior to air-floating, kaolins are crushed dried and pulverized. The pulverized material is floated in an air stream and classified with a whizzer separator. Fine particles are thus separated from the coarse kaolin. The most sophisticated wet process provides not only higher purity but enables production of a broader range of particle sizes and shapes. The general wet processing methods consist of blunging (forming clay-water suspensions), degritting (removal of coarse particles or grit), and particle size classification by hydrocycloning or centrifugation, dewatering and drying. The size classification produces different grades of kaolin with varying particle size distribution. Increase in the finer fraction can result in improved brightness due to the increase in surface area and hence more light scattering sites. During sizing, coarser (quartz) and / or denser (ilmenite, rutile etc.) impurity minerals get separated. Even small quantities of the coloring impurities in the finer fractions contaminate the clay and reduce its brightness. Hence, these impurities can be removed only by special techniques such as froth flotation, selective flocculation magnetic separation, oxidative/ reductive bleaching etc., depending upon the nature and quantity of impurities (Murray et al, 1993; Jepson, 1988). Reduction using sodium dithionite (hydros) is generally included in kaolin beneficiation to remove reducible iron impurities. Ozonation is used to oxidize the organic matter and iron complexes in "gray" kaolins and improve the brightness.

Delamination, a grinding process to cleave stacks of kaolin platelets, is generally carried out on coarse clay fractions to get high aspect ratio platelets. Calcined kaolin is produced by heating the kaolin at about 1000-1050°C for a few hours. The 'calcined' kaolin has better optical properties, but requires milling for achieving the specified particle size (Stoch, 1987; Chandrasekhar, 2002).

1.4 Iron Minerals in kaolin

Minor quantities of transition elements such as iron, titanium and manganese are generally present in kaolin as ancillary minerals which adversely affect its optical properties. The valance state of the ion and its atomic position in the structure depend on the conditions of formation of the mineral (Muller and Calas. 1993; Muller et al., 1995).The trivalent iron is the most common and most deleterious impurity present in kaolin. Iron may be present either in the form of free oxides (or hydroxides) or associated with the kaolinite / ancillary mineral structure. The common Fe-oxide minerals

in clays are hematite and goethite (Malengreau et al, 1996). Iron oxides and oxy hydroxides are present in most soils / kaolin and are the most abundant metallic oxides in most soils (Schwertmenn and Taylor, 1989). Goethite (α-FeOOH) which gives a yellow to brown colors, and hematite (α-Fe$_2$O$_3$), which gives red color, occur in many soils. They are the important constituents of the highly weathered soils of tropical and subtropical regions that contain kaolinite as the major clay mineral and are the sensitive indicators of pedogenic environments (Schwertmenn, 1985).

Other iron minerals usually found along with kaolin are pyrite, ilmenite, iron stained anatase maghemite, lepidocrocite, akaganeite and secondary mica. The form in which iron is present in the kaolin, influences it's properties and end use (Yvon et al, 1982a; Delon et al, 1982). The intimate coexistence of kaolinite, hematite and goethite in many kaolin deposits has made the study of their individual crystallo-chemical properties difficult. Mineral study is further complicated by the fact that Fe isomorphically substitutes for Al in kaolinite and Al isomorphically substitutes for Fe in goethite and hematite (Schroder et al, 1998). Fe and Ti may be present in discrete quantities in the structure of kaolinite substituting for Al or Si. Mossbauer (Malden and Meads, 1967) and EPR (Angel and Hall, 1972; Meads and Malden, 1975) techniques have provided evidence that ferric iron exists as a constituent in the octahedral layer of kaolinites. Rengasamy et al (1975b) reported the chemical composition of soil kaolinites calculated from selective dissolution data. When the extracted Fe^{+3} content were included in the octahedral composition, the SiO$_2$/R$_2$O$_3$ molar ratio obtained was near to the ideal ratio of 2.0. Also, Electron micro probe studies (Jepson and Rowse, 1975) have shown that both Fe and Ti occur possibly as isomorphous constituents in kaolinite. Substituted Ti can be distinguished from Ti oxides in a scheme of selective dissolution using hydrofluotitanic acid (Dolcater et al, 1970).

Residual white kaolins are formed by the weathering of magmatic rocks. The governing factor of their formation is the phenomenon of dissolution of relatively soluble minerals of primary rock, mainly feldspars and they are replaced by less soluble minerals such as kaolinite and other clay minerals. In the reducing environment, the iron set free in these processes is removed as soluble Fe^{+2} cation and pure white kaolin of high quality is formed (Stoch,1987). However, under certain conditions part of the iron may be

20

preserved in the kaolin and accumulation of iron in kaolins is possible due to (a) local precipitation of low soluble iron minerals under changing oxidizing-reducing conditions and CO_2 and S concentrations (magnetite, hematite, siderite, sulphides, crystalline and amorphous hydroxides) (b) incorporation of iron cations into the structure of newly formed layer silicates (kaolinite, smectite, secondary micas etc.) (c) adsorption of iron oxides on the surface of kaolinite and covering of surface by iron oxides and (d) formation of insoluble iron containing organic complexes. Organic matter plays a double role in the process of iron circulation. It diminishes the pH value and the redox potential (Eh), accelerating the extraction of iron as soluble ferrous ions. Simple organic acids form soluble complexes with iron acting as an accelerator of iron leaching. Humic and other organic acids of large molecules, form insoluble complexes of iron and stabilizes it.

Extensive research has been carried out on the nature of iron impurities in kaolin, which leads to the conclusion that iron is present as a part of the kaolinite or ancillary mineral (mica or titania) structure ie., "structural iron" or as separate iron minerals such as oxides, hydroxides, oxy-hydroxides, sulphides and carbonates ie., "free iron" (Jepson, 1988). Distinguishing between these two forms of iron is very important from the practical point of view for selecting suitable methods for their removal. Many researchers have shown that iron in kaolin can exist as coatings on the surface of the mineral (Bahranowski et al, 1993; Fysh et al, 1983a, b), or isomorphously substituted for Al in dioctahedral sites (Malden and Meads, 1967). Iron can also occur within the kaolinite structure as occluded ferric oxides (Malengrau et al, 1994) as well as partly dispersed through out kaolinite and partly clustered into segregated isostructural domains within the dicoctahedral sheet of kaolinite (Schroeder et al, 1998). ^{1}H NMR studies by Stone et al (1988) have shown that Fe ordering within kaolinite can be quite variable and that there is no direct correlations between the amount of "Fe" in kaolinite and ordering of "Fe" within the kaolinite structure.

Recently, Schroeder and Shiflet (2000) have carried out the first quantitative measurement of Ti-bearing phases in a pale yellow (cream) east Georgia deposit. Their studies has shown that "Fe" is getting isomorphously substituted into "Ti" in anatase and other Ti-bearing phases and indicating that anatase is formed from the Fe-Ti precursors like ilmenite. Grey and Reid (1975) and Larrett and Spencer (1971) suggested the ferrous

21

to ferric pathway for oxidative weathering of ilmenite, which involves a progressive removal of ferrous Fe by leaching, leaving behind rutile as the end product. During the above process pseudorutile was found to be the intermediate product. Gray kaolins generally contain significant amounts of sulfides and organic matter and the coloration is due to the minor amounts of phases such as pyrite, marcasite, ferrous silicates and kerogen. They remain intact in the reduced conditions underneath as long as they are less chemically disturbed (White et al., 1991).This phenomenon is similar to that observed in soils. Many researchers (Dudas et al, 1988; Evangelou and Zhang, 1995; Lumsdon et al, 2001) have studied the geochemistry of acid sulfate soils ie., soils derived from pyrite parent materials (Fanning and Fanning, 1989) are strongly influenced by the iron and sulfur weathering products (Lumsdon etal., 2001) and the common secondary minerals formed from the weathering of pyrite are iron oxides (eg.,goethite and ferrihydrite) and iron sulfates (jarosite).

1.5 Optical properties of kaolin

The optical properties pertinent to white minerals including kaolin are brightness, whiteness, yellowness and **Lab** color values (expressed in ISO units). Brightness represents the % of reflectance of light at a wavelength of 457 nm. Researchers have monitored the changes occurring in the spectrophotometer curve for material (pulp) throughout the bleaching cycle. They found out that the large changes are occurring in the blue-green region whereas only minor changes are observable in the red region (Figure 1.5a). Based on the results, blue area was chosen to take measurements which would best correlated with observable changes in brightness during the bleaching process (Figure 1.5b). It is on this basis that 457 nm was taken as the effective wave length for measuring brightness .It is worthwhile to mention that, brightness measurement takes into consideration only the blue part of the visible spectrum and ignores the yellow and red portions. Hunter whiteness and yellowness indices have the advantage of single number quantities that are based on the entire visible spectrum. The whiteness formula relates better to people's visual assessment than brightness whereas yellowness indices normally do not correlate well with the visual judgment of yellowness. The **Lab** system based on the color opposites gives a better representation of the colors. The term "**L**" is a measure of lightness / darkness and varies from 100 for perfect white to 0 for absolute black. The

22

red / green color is indicated by "**a**". The more positive is its value; greater is the reddishness and negative value indicating greenish ness. Similarly, the yellow / blue shade is represented by "**b**", positive value for yellow and negative for bluishness.

Kaolins are informally classified on the basis of their color ie., either as gray, pink, red or cream based on its coloration due to the presence of minor amounts of various "Fe" phases. Red kaolins are predominantly colored by hematite and cream kaolins are colored by goethite and anatase. Gray kaolins generally contain significant amounts of sulfides and organic matter and the coloration is due to the minor amounts of phases such as pyrite, marcasite, ferrous silicates and kerogen. (White et al., 1991).

The white colour of kaolin is greatly affected by the presence of iron mineral impurities. Color of a mineral can be best explained by the crystal field formalism and is shown by predominantly ionic crystals containing ions with unpaired electrons. These usually originate in elements with partially filled d shells such as V, Cr, Mn, Fe, Co, Ni, and Cu. Of these transition elements, Fe is the most plentiful (about 5% of the earth's crust) and is therefore the dominant color contributor in minerals. Divalent iron makes silicate minerals dark green or black. Trivalent iron participates in charge transfers that are strongest in the ultraviolet, but somewhat effective in the visible range. Thus the blue end of the spectrum is absorbed and the reddish orange color is imparted to the silicate mineral. Brightness and **Lab** color components are influenced by iron minerals and iron bearing anatase. Iron decreases brightness and "**L**" value whereas anatase increases "**b**" to cause yellowness

1.6 Present work

Extensive studies have been reported on important kaolin deposits all over the world over the years by various research groups. The information provided by their studies has helped the value addition of these particular kaolin deposits to a great extent. Since the processes leading to formation of kaolin during chemical weathering changes from one deposit to another, the formation of kaolinite, its properties and the nature and type of ancillary minerals associated with it varies. This implies that, the information available in the literature can not be taken as such to understand a kaolin deposit of different geological origin. So an exclusive in-depth study of each kaolin deposit is needed to understand the clay mineralogy and impurity mineral species.

In the present work, a comprehensive study has been carried out for the first time on kaolin samples. No such data has been reported so far on any of the kaolin deposits in India. Seven major deposits have been selected from the states of Kerala, Orissa, Gujarat, West Bengal and Rajasthan. Physical, chemical, mineralogical, microscopic and spectroscopic studies were conducted to characterize the samples. Speciation of iron and titanium minerals in these kaolins has been carried out by separating them from kaolin by various methods and characterizing by different techniques. Attempt has also been made to study the influence of iron and titanium on the optical properties of kaolin. It has been established that optical properties of kaolin are not directly related to the quantity of the iron present, but dependent on the form (species) in which "Fe" occurs. A variety of instrumental techniques including X-ray diffraction, spectroscopy (UV-Vis., FTIR, EPR, Mossbauer) and microscopy (Optical Microscopy, SEM, TEM - EDS, EPMA) have been used for getting information and arrive at the conclusions.

Pyrite is found to be the major ancillary iron mineral in china clay sample from Koraput district of Orissa which is one among the samples taken for the present study. Beneficiation of this sample by wet route can not be done by conventional methods due to the high acidity of the clay suspension in water. During the investigation, a Laboratory Level method has been developed for removing the Fe mineral impurity from this clay by which considerable value addition could be achieved.

Most of the findings have been presented in national and international conferences and published in cited journals.

24

References

1. Angel B.R. and Hall P.L. (1972) Electrom spin resonance studies of kaolins, Int. Clay Conference, Madrid, 1, 71-86

2. Anand R.R, Gilkes R.J., Armitage T.M and Hillyer J.W. (1985) Feldspar weathering in lateritic saporolite. Clays and Clay Minerals, 33, 31-43

3. Anon (1987) Kaolin, paper underpins current demand. Industrial Minerals Journal, July, 64-87.

4. Bailey, S.W. (1980) Structures of layer silicates. In Crystal structure of clay minerals and their X-ray identification, G.W. Brindley and G.Brown, eds., Mineralogical Society London, Monograph, 44, 78-114

5. Bahranowski J, Serwicka E.M, Stoch L. and Strycharski P. (1993) On the possibility of removal of non-structural iron kaolinite-group minerals, Clays and Clay Minerals, 28, 379-391

6. Banfield, J.R. and Eggleton, R.A. (1988) Transmission electron microscopic study of biotite weathering. Clays and Clay Minerals, 36, 47-60.

7. Brindley, G.W. and Brown, G. (1980) Crystal structure of clay minerals and their X-ray identification. In: Monograph, Mineralogical Society, London, 495.

8. Banfield, J.F. and Eggleton, R.A. (1990) Analytical transmission electron microscope studies of plagioclase, muscovite and K-feldspar weathering. Clays and Clay Minerals, 38, 77-89.

9. Bennett, H and Reed, R.A. (1971) Chemical methods of silicate analysis. A handbook Academic Press Ind., London, 272 pp.

10. Brindley, G.W., Kao,C.C., Harrison, J.L., Lipsicas, M., and Raythata, R. (1986) Relation between structural and other characteristics of kaolinite and dickite. Clay and Clay Minerals, 34, 239-249

11. Bristow, C.M. (1968) Kaolin deposits of the United Kingdom of Great Briton and Northern Ireland. In Proceedings of symposium I, . Kaolin Deposits of the World: A – Europe, International Geological Congress, Prague, Czechoslovakia, Malkovsky, M. and Vachtl, J. eds., Academia, Prague, 275-288.

12. Bristow, C.M. (1977) A review of the evidence for the origin of the kaolin deposits in South West England. In Proceedings of the 8th International symposium and meeting on Alunite, Madrid-Rome, Galen, E., eds., Madrid, 1-19.

13. Brushwell, W. (1964) What a paint chemist should know about printing inks, American Paint Journal, November, 84-96.

14. Bundy, W.M. (1991) Kaolin in paper filling and coating, Applied Clay Science, 5, 397-420.

15. Bundy, W.M. (1993) The diverse industrial applications of kaolin. Murray, H.H., Bundy, W. and Harvey, C. eds., Special publication No.1, The Clay Mineral Society, 43-74.

16. Chandrasekhar, S., Ramaswamy, S. (2002) Influence of mineral impurities on the optical properties of kaolin and its thermally treated products, Applied Clay Science, 21, 133-142

17. Clarke, O.M. Jr. (1973) Gibbsite in weathered granitic rocks of Albama, Southest, Geology, 14, 203-212.

18. Craw, D., Coombs, D.S. and Kawachi, Y. (1982) Interlayered biotite kaolin and other altered biotites and their relevance to the biotite isograd in estern Otago, New Zealand. Mineralogical Magazine, 45, 79-85.

19. Deer, W.A., Howie, R.A. and Zussman, J.(1976) Rock forming minerals. Volume 3, Longman Group Limited, London, 270 pp.

20. Dolcater D.L, Syers J.K. and Jackson M.L. (1970) Titanium as free oxide and substituted forms in kaolinites and other soil minerals, Clays and Clay Minerals, 18, 71-79

21. Dudas, M.J., Warren, C.J., Spiers, G.A., 1988. Chemistry of arsenic in acid sulphated soils of northern Alberta. Communications in Soil Science and Plant Analysis, 19, 887-895

22. Evangelou, V.P., Zhang, Y.L., 1995. A review: Pyrite oxidation mechanisms and acid mine drainage prevention. Critical Reviews in Environmental Science and Technology, 25(2), 141-199

23. Fanning, D.S., Fanning, M.C.B., 1989. Soil Morphology, Genesis and Classification. Wiley, New York

24. Fysh S.A, Cashion J.D. and Clark P.E. (1983a) Mossbauer effect studies of iron in kaolin I. Structural iron, Clays and Clay Minerals, 31, 285-292

25. Fysh S.A, Cashion J.D. and Clark P.E. (1983b) Mossbauer effect studies of iron in kaolin I. Surface iron, Clays and Clay Minerals, 31, 293-298

26. Gilkes, K.J and Suddhiprakkarn, A. (1979) Biotite in deeply weathered granite. Morphologic, mineralogical and chemical properties. II. The oriented growth of secondary minerals. Clays and Clay Minerals, 27, 349-367.

27. Grey I.E, and Reid A.F. (1975) The structure of pseudorutile and its role in the natural alteration of ilmenite, American Mineral, 60, 898 – 906

28. Hart, R.D., Pierre, T.G., Gilkes, R.J. and Mckinley, A.J. (2002) Iron in soil kaolins from Indonesia and Western Australia. Clay Minerals, 37, 671-685.

29. Hurst, V.J. (1979) Editor. Field Conference on Kaolin and Fuller's Earth. The Clay Minerals Society, Bloomington, Indiana.

30. Hurst, V.J. and Pickering, S. (1989) Cretaceous-Tertiary strata and kaolin deposits in the inner Coastal Plain of Georgia. In : Upper Cretaceous and Cenozoic Geology of the Southeastern Atlantic Coastal Plain, Field Trip Guidebook T172, 28th International Geological Congress, American Geophysical Union, Washington DC, 1-22.

31. Hurst, V.J. and Pickering, S. (1997) Origin and classification of coastal-plain kaolins, southern USA, and the role of ground water and microbial action. Clays and Clay Minerals, 45, 274-285.

32. Jepson W.B. and Rowse J.B. (1975) The composition of kaolinite –an electron microscope microprobe study, Clays and Clay Minerals, 23, 310-317

33. Jeong, G.H. (1998) Vermicular kaolinite epitactic on primary phyllosilicates in the weathering profiles of anorthosite. Clays and Clay Minerals, 46, 509-520.

34. Jepson, W.B., 1988. Structural iron in kaolinites and in associated ancillary minerals, In : Iron in Soils and Clay Minerals (J.W.Stucki, B.A.Goodman and U.Schwertmann, editors). NATO Advanced Science Institutes Series, D.Riedel Publishing Company, Dordrecht, Holland, 467-536

35. Keller, W.D. (1970) Environmental aspects of clay minerals. Journal of Sedimentary Petrology, 40, 788-813.

36. Keller, W.D. (1976 a) Scan electron micrographs of kaolins collected from diverse environments of origin – I, Clays and Clay Minerals, 24, 107-113.

37. Keller, W.D. (1976 b) Scan electron micrographs of kaolins collected from diverse environments of origin – II, Clays and Clay Minerals, 24, 114-117.

38. Keller, W.D. (1976 c) Scan electron micrographs of kaolins collected from diverse environments of origin – III: Influence of parent material on flint clays and flint like clays, Clays and Clay Minerals, 24, 262-264.

39. Keller, W.D. (1977) Scan electron micrographs of kaolins. Clay and Clay Minerals, 25, 347-364.

40. Keller, W.D. (1977) Scan electron micrographs of kaolin collected from diverse environment of origin. – IV. Georgia kaolin and kaolinizing source rocks. Clays and Clay Minerals, 25, 311-345.

41. Keller, W.D. (1978) Classification of kaolins exemplified by their texture in scan electron micrographs. Clays and Clay Minerals, 26, 1-20.

42. Keller, W.D. (1980) Kaolin from the original kauling (Gaoling) mine locality, Krangsi Province, China, Clays and Clay Minerals, 28, 97-104.

43. Keller, W.D. (1985) The nascence of clay minerals. Clays and Clay Minerals, 33, 161-172.

44. Konta, J. (1980) Properties of ceramic raw materials. Ceramic Monographs, Handbook of Ceramics, Verlag Schmid GmbH, Freiburg, 1-22.

45. Larrett M.J.W. and Spencer W.G. (1971) Contributions to Australian Mineralogy, 3, "Pseudorutile" from South Neptune Island, South Australia, Amdel Bulletin, 12, 74-80

46. Lumsdon, D.G., Meeussen, J.C.L., Paterson, E., Garden, L.M., Anderson, P., 2001. Use of solid phase characterization and chemical modeling for assessing the behavior of arsenic in contaminated soils. Applied Geochemistry, 16, 571-581

47. Malden P.J. & Meads R.E. (1967) Substitution by iron in kaolinite, Nature, 215, 844-846

48. Malengrau N., Muller J.P. and Calas G. (1994) Fe-speciation in kaolins: a diffuse reflectance study, Clays and Clay Minerals, 42, 137-147

49. Malengreau, N., Bedidi, A., Muller, J.P. and Herbillions, A.J. (1996) Spectroscopic control of iron oxide dissolution in two ferralitic soils. Euro. Journal of Soil Sciences, 47, 13-20.

50. Maksimovic Z., White, J.L and Logar, M. (1981) Chromium - bearing dickite and chromium – bearing kaolinite from Teslic, Yogoslavia. Clays and Clay Minerals, 229, 213-218

51. Meads R.E and Malden P.J. (1975) Electron spin resonance in natural kaolinites containing Fe+3 and other transition metal ions, Clay Minerals, 10, 313-345

52. Mestdagh, M.M., Vielvoye, L, and Herbillon, A.H. (1980) Iron in kaolinite II. The relationship between kaolinite crystallinity and iron content. Clay Minerals, 15, 1-13

53. Muller, J.P. and Bocquier, G. (1987) Textural and mineralogical relationship between ferruginous nodules and surrounding clayey matrices in a laterite from Cameroon. In Proceedings of International Clay Conference, Denver, 1985, L.G.Shultz, H. Van Olphen and F.A.Mumpton, eds., The Clay Mineral Society, Bloomington, Indiana, 186-196.

54. Murray, H.H. (1963) Industrial applications of kaolin, Clays and Clay Minerals, 10, 291-293.

55. Murray H.H, (1977) "Kaolin – A versatile Pigment", Extender, and Filler," Prepr. Pap. Annu. Meet. Tech. Sect., C.P.P.A, 63rd, A29-34

56. Murray, H.H.., 1986. Clays. Ullmann's Encyclopaedia of Industrial Chemistry, Volume A7, 5th Edition, VCH Publishers, 109-136

57. Murray, H.H. and Keller, W. (1993) Kaolin, Kaolin and Kaolin, In : Kaolin Genesis and Utilization, Murray, H.H.,Bundy, W. and Harvey, C. eds., Special publication No.1, The Clay Mineral Society, 1-24.

58. Muller, J.P. and Calas, G. (1993) Genetic significance of paramagnetic centers in Kaolinite. Pp. 261-289 in : Kaolin Genesis and Utilisation (H.H.Murray, W.Bundy and C.Harvey, editors). Clay Minerals Society, Boulder, Colarado.

59. Muller, J.P., Manceau.A., Calas, G., Allard, T., Ildefone, P. and Hazemann, J.L. (1995) Crystal chemistry of kaolinite and Fe-Mn oxides: Relation with

formation condition of low-temperature systems. American Journal of Science, **295**, 1115-1155.

60. Patterson, S.H. and Murray, H.H. (1975) Clays. In Industrial Minerals and Rocks (Nonmetallics other than Fuels), American Institute of Mining, Metallurgical and Petroleum Engineers, Inc., New York, 519-585.

61. Pevear, D.R. and Nagy, K.L. (1993) Kaolinite growth on mica in sandstones, bentonites and experiments. In Abstract, 10th Int. Clay Conf., 1993, Adelaide, South Australia, 1-141.

62. Plancon, A. and Tchobar, C. (1977a) Determination of structural defects in phyllosilicates by X-ray powder diffraction – I. Principle of calculation of the diffraction phenomenon. Clays and Clay Minerals, 25, 430-435

63. Plancon, A. and Tchobar, C. (1977b) Determination of structural defects in phyllosilicates by X-ray powder diffraction – II. Nature and proportion of defects in natural kaolinites. Clays and Clay Minerals, 25, 436-450

64. Rengasamy P., Sarma V.A.K. and Krishna Murti G.S.R. (1975) Isomorphous substitution of iron for aluminium in some soil kaolinites, Clays and Clay Minerals, 23, 211-214

65. Rengaswamy, P. (1976) Substitution of iron and titanium in kaolinites. Clays and Clay Minerals, 24, 265-266

66. Robertson, I.D.M. and Eggleton, A.A. (1991) Weathering of granite muscovite to kaolinite and halloysite and of plagioclase derived kaolinite to halloysite. Clays and Clay Minerals, 39, 113-126.

67. The Economics of kaolin, 2000, Roskill Information Book

68. Sand, L.B. (1956) On the genesis of residual kaolins. American Minaralogist, 41, 28-40

69. Schroeder, P.A; Le Govlan, J.J. and Roden, M.D. (2002) Weathering of ilmenite from granite and chlorite schist in the Georgia Piedmont, USA. American Mineralogist, 87, 1616-1625.

70. Schroeder P.A., Pruett R.J. and Hurst V.J. (1998) Effects of secondary iron phases on kaolinite 27Al MAS NMR spectra, Clays and Clay Minerals, 46, 429-435

71. Schroeder P.A. and Shiflet J. (2000) Ti-bearing phases in an east Georgia kaolin deposit, Clays and Clay Minerals, 48, 151-158

72. Schroeder, P.A., Pruett, R.J. and Melear, N.D. (2004) Crystal – Chemical changes in an oxidative weathering front in a Georgia kaolin deposit. Clays and Clay Minerals, 52, 211-220.

73. Schwertmann, U. (1985) The effect of pedogenic environments on iron oxide minerals, Advanced Soil Science, 1, 171-200.

74. Sharp, T.G., Olten, M.T. and Buseck, P.R. (1990) Serpentinization of phlogopite phenocrysts from a micaceous kimberlite. Contribution to Mineralogy and Petrology, 104, 530-539.

75. Singh, B. and Gilke, R.J. (1991) Weathering of a chromium muscovite to kaolinite. Clays and Clay Minerals, 39, 571-579.

76. Singh, B. and Gilkes, R.J. (1992) Properties and distribution of iron oxides and their association with minor elements in the soils of south-western Australia. Journal of Soil Science, 43, 77-98.

77. Steigs, F.B. (1959) Effect of extenders on the hiding power of titanium pigments, Official Digest 31, No.408, 52-64.

78. Stoch, L. and Sikora, W. (1976) Transformation of mica in the process of kaolinization of granites and gneisses. Clays and Clay Minerals, 24, 156-162

79. Stoch, L. (1987) Iron in kaolins - mineralogical, crystallo-chemical and technological aspects, Interceram, 6, 21-25.

80. Stone W.E. and Torres-Sanchez R.M.(1988) Nuclear magnetic resonance spectroscopy applied to minerals, Journal of the Chemical Society: Faraday transactions, 84, 117-132

81. Storr, M. (1983) The kaolins of German Democratic Republic. Academie-Verlag, Berlin

82. Stoy, W.S. (1989) Make room for extenders, American Ink Maker, June, 46-50.

83. Tardy, Y., Bocquier, G., Paquet, H and Millot, G. (1973) Formation of clay from granite and its distribution in relation to climate and topography. Geoderma, 10, 271-284.

84. Tchoubar C.A., Plancon A., Ben Brahim J., Clinard C. and Sow C. (1982) Structural characteristics of disordered kaolinites, Bull. Mineral, 105, 477-491

85. Tsuzuki, Y. and Kawabe, I. (1983) Polymorphic transformation of kaolin minerals in aqueous solution. Geochimica et Cosmochimica Acta, 47, 59-66.

86. Weaver, C.E. (1985) Developmentt in sedimentology – Clay, Muds and Shales, Elsevier, Amsterdam, 819 pp.

87. White, N.G, Dixon, J.B., Weaver, R.M. and Kunkle, A.C. (1991) Genesis and morphology of iron sulfides in gray kaolins. Clay and Clay Minerals, 39, 70-76.

88. Wilson, M.J. (1966) The weathering of biotite in some Aberdeenahire soils. Mineralogical Magazine, 35, 1080-1093.

89. Zheng, Z., Lu, D.,Feng, M., Feng, B. and Jin, T. (1982) Kaolin deposit of China. In: Proceedings of International Clay Conference, Development in Sedimentology 35, Van Olphen, H. and Veniale, F., eds., Elsevier, Amsterdam, 719-731.

90. Yvon, J., Garin, P., Delon, J.F., Cases, J.M. (1982 a) Beneficiation of kaolinitic clays from Charentes in natural rubber, Bulletin Mineral, 105 (5), 535-542.

Table 1 Ions found in Phyllosilicate Minerals

Common constituents			Occasional constituents			Cations found in interlayer spaces		
Ion	radius (nm)	r_c/r_o	Ion	radius (nm)	r_c/r_o	Ion	radius (nm)	r_c/r_o
O^{2-}	0.135	-	Ni^{2+}	0.074	0.55	Na+	0.101	0.75
Si^{4+}	0.040	0.30	Ti^{4+}	0.060	0.44	K+	0.134	1.00
Al^{3+}	0.055	0.41	Zn^{2+}	0.057	0.42	Cs+	0.163	1.24
Fe^{2+}	0.080	0.59	Mn^{2+}	0.083	0.61	Ca2+	0.105	0.78
Fe^{3+}	0.067	0.54	Mn^{3+}	0.072	0.53	Ba^{2+}	0.140	1.03
Mg^{2+}	0.078	0.58	Mn^{4+}	0.052	0.39	Sr^{2+}	0.118	0.87
			Li^+	0.076	0.56	H_2O	0.145	..
			Cr^{3+}	0.065	0.48	NH_4^+	0.143	.
			Cu^+	0.095	0.70		..	

Table 2 Approximate cost of commercial kaolins in India

Sl. No	Kaolin Grade	Approx. Indian Market Rate/Ton (Rs)
1	Anhydrous premium coating grade	8,000 – 12,000
2	Anhydrous second coating grade	6,000 - 9,000
3	Anhydrous paper filling grade	5,000 – 8,000
4	Calcined clay (paper coating and paint grade)	23,000 – 20,000
5	Calcined clay (Ceramic grade)	5,000 – 10,000
6	Hydrous filler grade	3,000 – 7,000
7	Raw clay	100 - 350
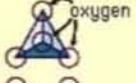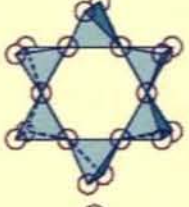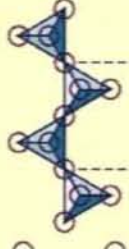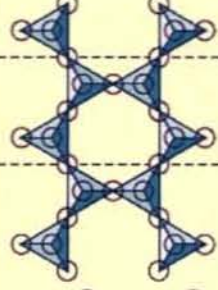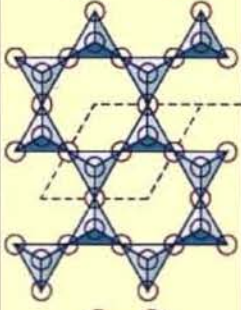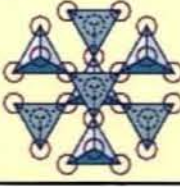
class	arrangement of SiO$_4$ tetrahedrons (central Si^{4+} not shown)	unit composition	mineral example
Nesosilicates	oxygen	$(SiO_4)^{4-}$	Olivine, $(Mg, Fe)_2SiO_4$
Sorosilicates		$(Si_2O_7)^{6-}$	Hemimorphite, $Zn_4Si_2O_7(OH)_2 \cdot H_2O$
Cyclosilicates		$(Si_6O_{18})^{12-}$	Beryl, $Be_3Al_2Si_6O_{18}$
Inosilicates (single chain)		$(Si_2O_6)^{4-}$	Pyroxene e.g., enstatite, $MgSiO_3$
Inosilicates (double chain)		$(Si_4O_{11})^{6-}$	Amphibole e.g., anthophyllite, $Mg_7Si_8O_{22}(OH)_2$
Phyllosilicates		$(Si_2O_5)^{2-}$	Mica e.g., phlogopite, $KMg_3(AlSi_3O_{10})(OH)_2$
Tectosilicates		$(SiO_2)^0$	High cristobalite, SiO_2

Figure 1.1 Two dimensional framework of silica tetrahedrons in Phyllosilicates

34

SERPENTINE - KAOLIN (X - 0)

TALC - PYROPHYLLITE (X - 0)

MICA (X - 1.0) and BRITTLE MICA (X - 2.0)

7.1 - 7.3 A

9.1 - 9.4 A

9.6 - 10.1 A

14.4 - 15.6 A

14.0 - 14.4 A

SMECTITE (X - 0.25 - 0.6) and VERMICULITE (X - 0.6 - 0.9)

CHLORITE (X - variable)

- • Tetrahedral cation
- ● Octahedral cation
- ◑ Interlayer cation
- ○ Exchangable cation

- O Oxygen
- ◑ Hydroxyl group
- ◐ Water molecule
- ● Oxygen + hydroxyl (in projection)

X - layer charge per formula unit
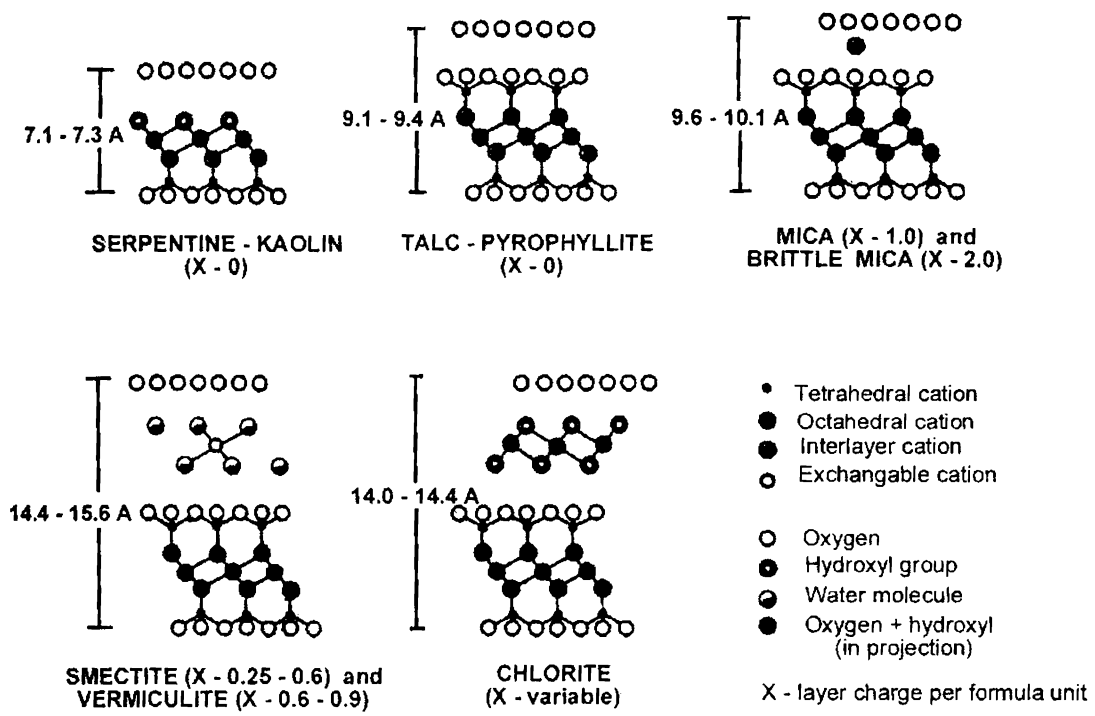
Figure 1.2 Schematic representation of the common clay minerals

35

Orthosilicate anion (a)

Quartz crystal (b)

Octahedral aluminium unit (c)

Gibbsite unit (d)

Three dimensional kaolinite structure as clay micelle (e)

Kaolinite mineral (f)
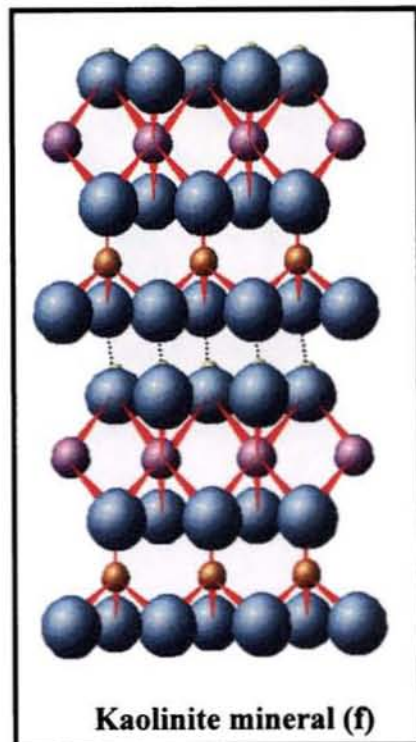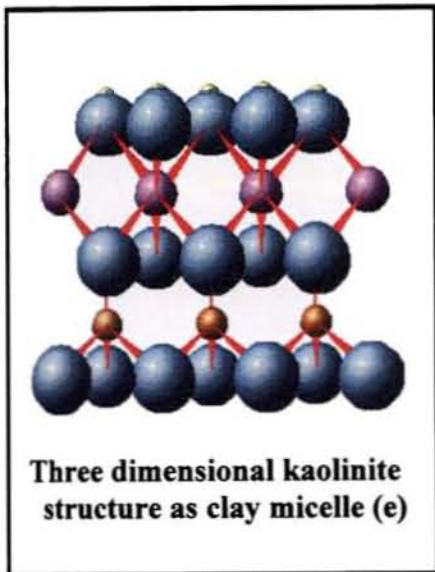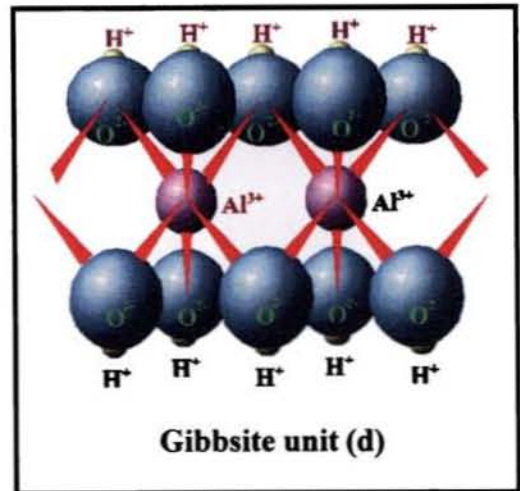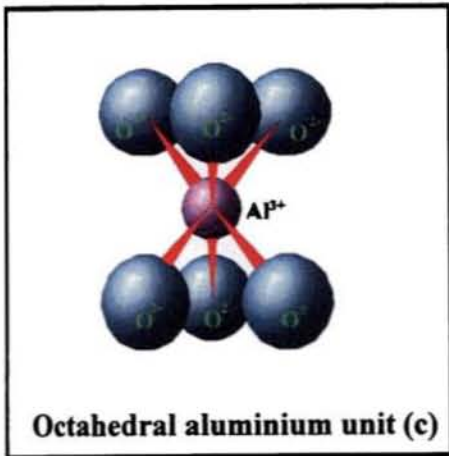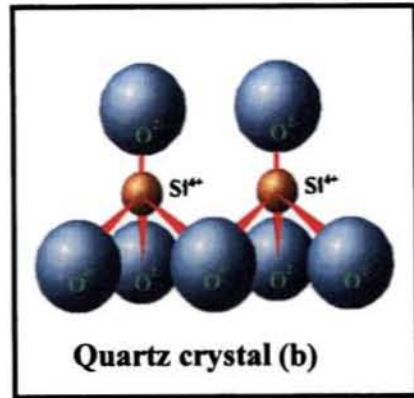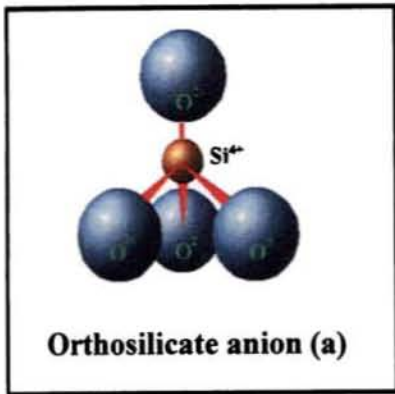
Figure 1.3 Kaolinite and its building blocks

36
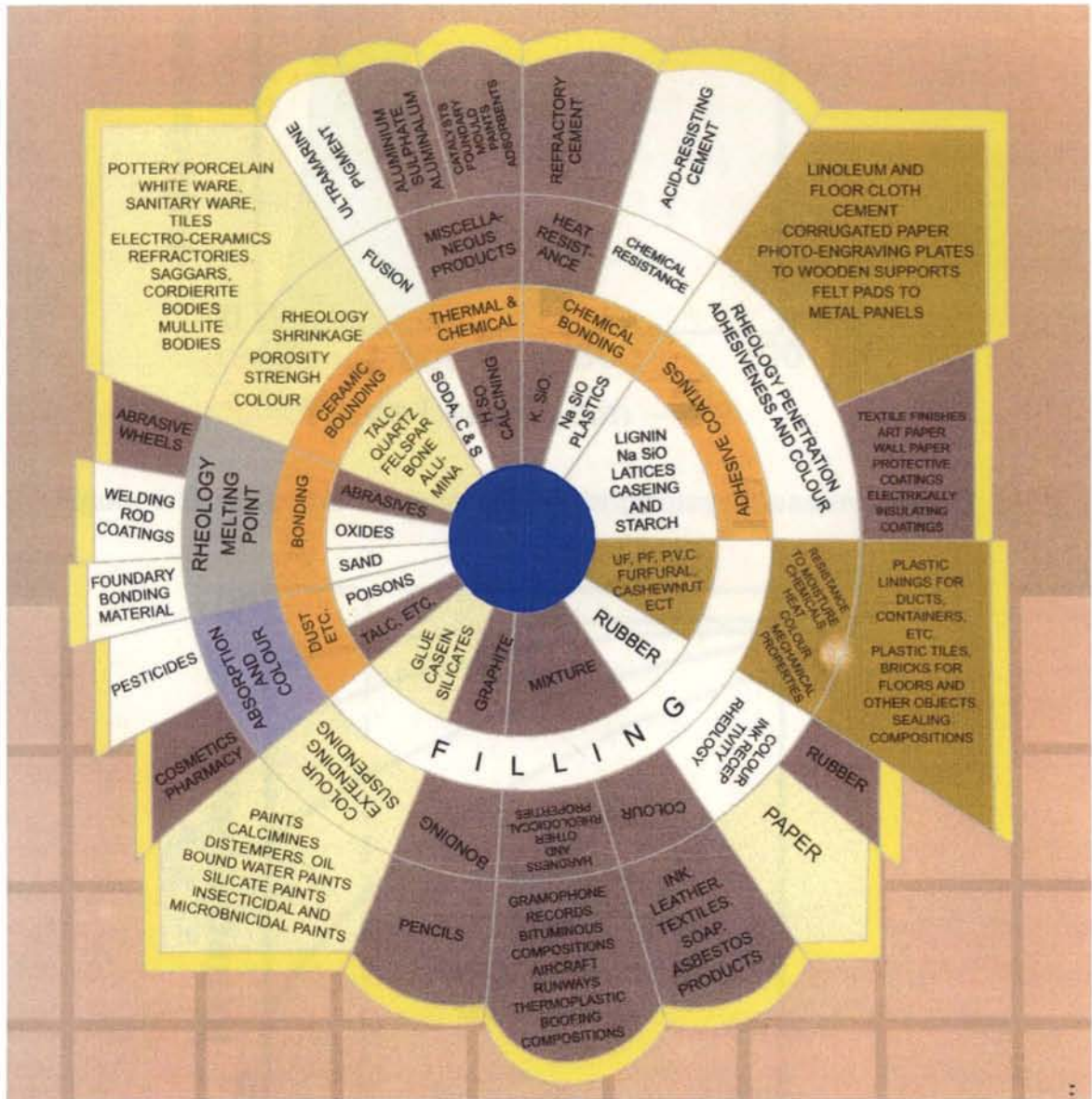
Figure 1.4 Applications of kaolin
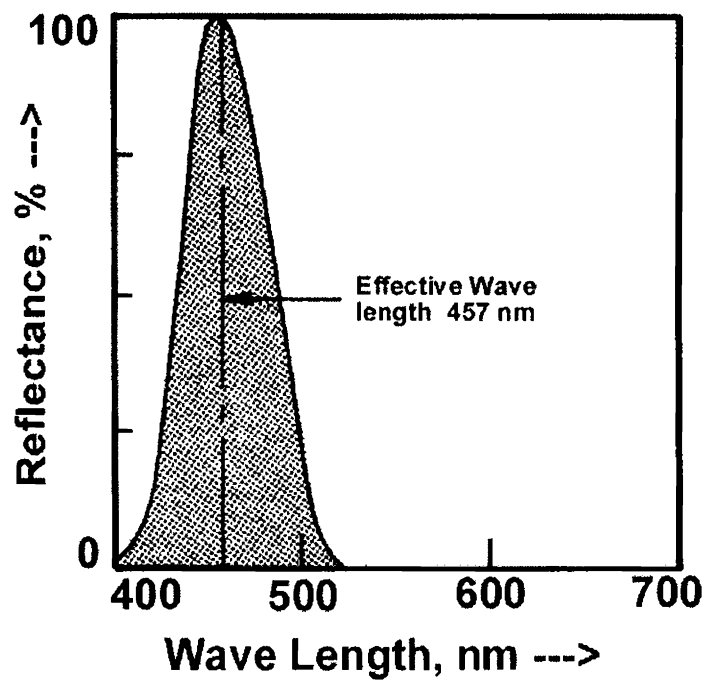
Figure 1.5a Effective wave length for brightness measurement
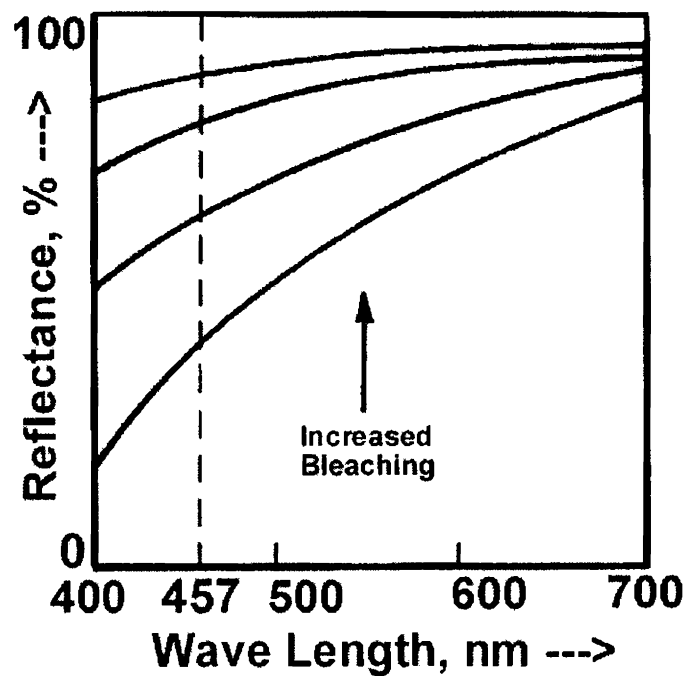
Figure 1.5b Variation in brightness during bleaching process

(Courtesy : M/s. Technidyne Corporation, USA)

38

CHAPTER 2
EXPERIMENTAL PROCEDURES AND INSTRUMENTAL TECHNIQUES

The experimental methods adopted for the characterization of clay samples and ancillary minerals are presented in this chapter. It also deals with the methodologies followed for the size classification of clays, separation of the impurity minerals and the chemical and physical methods to identify the iron and titanium mineral species in kaolin. Principles of the instrumental techniques for X-ray diffraction analysis, particle size distribution analysis, measurement of optical properties, spectroscopic analyses like FTIR, UV-VIS, EPR, Mossbauer and ICP-AES, microscopic studies such as optical microscopy, SEM / TEM-EDS and EPMA are also briefly described here.

In order to prepare a representative sample for the investigation, the run -of -mine (ROM) clay was size reduced to 1-1.5" and thoroughly blended by centre displacement method where the sample heap centre was changed 20 times by 'shoveling' ie., the entire material was shifted by shovel from the original place to another place and again the whole clay was shoveled back to the original place. This blended clay constitutes the bulk feed which was spread with uniform thickness and the required quantities were collected from different spots as representative samples for characterization and size classification. The material was stored in polythene bags.

2.1 Characterization

The ROM clay and the products of size classification are analyzed for their physical, chemical and mineralogical properties. The products obtained after (i) reductive bleaching with hydros (sodium dithionite) and (ii) dithionite-citrate-bicarbonate (DCB) treatment were also analyzed for their chemical assay and optical properties. Spectroscopic and microscopic studies were also conducted on selected samples.

The instrumental / experimental analyses have been carried out as per standard procedures and are categorized as follows:

Chemical   # Major and minor elements – by classical method of chemical Analysis

| | # | Trace elements – by Inductively Coupled Plasma-Atomic Emission Spectroscopy (ICP-AES) |

Physical
- \# Optical properties
- \# Particle size distribution
- \# Relative density
- \# pH
- \# Solubility in water and acid

Mineralogical
- \# X-ray Diffraction Analysis (XRD)
- \# Differential Thermal Analysis (DTA)
- \# Thermo Gravimetric Analysis (TGA)
- \# Rational Analysis

Spectroscopic
- \# Inductively Coupled Plasma-Atomic Emission Spectroscopy (ICP-AES)
- \# Electron Paramagnetic Resonance Spectroscopy (EPR)
- \# Mossbauer Spectroscopy
- \# Fourier Transform Infrared Spectroscopy (FTIR)
- \# UV-Visible Spectroscopy

Microscopic (Morphological)
- \# Optical Microscopy (OM)
- \# Scanning Electron Microscopy (SEM)
- \# High Resolution Transmission Electron Microscopy (with Energy Dispersive X-ray spectroscopy) – (HRTEM-EDS)
- \# Electron Probe Micro Analysis (EPMA)

The details of the instruments by which the characterization has been carried out are as given below:

1. Flame photometer, Systronics, Model 128

2. UV-Visible spectrophotometer Genway, model for colorimetric analysis

UV-Vis. Spectrophotometer, Shimadzu, model UV-2450 for studying the impurity concentrate.

3. Inductively Coupled Plasma-Atomic Emission Spectrometer (ICP-AES)

4. X-ray Diffractometer (Philips analytical) with Ni-filtered Cu K_α radiation (40KV, 20mA)

5. DTA (Seiko Thermal Analyser Model 320) and TGA (Shimadzu Thermal Analyser Model 50 H)

6. Particle size analyzer, Model Sedigraph 5001, Micromeritics, USA

7. Brightnessmeter , Model Color Touch™ Model from Technidyne Corporation, USA.

8. pH meter, Model Systronics

9. FTIR Perkin – Elmer spectrophotometer

10. EPR Varian model E-112 spectrophotometer.

11. Mossbauer spectrometer ([57]Co source in Rh matrix as the Mössbauer source; at IIT, Kanpur and JNV University, Jodhpur)

12. OM Leika model optical microscope, Japan.

13. SEM JEOL JSM 5600 LV

14. HR TEM -EDS (University of Gei , Germany)

15. EPMA Scanning Electron Microscope, JEOL, Model (JXA-8100), Japan at RRL, Bhubaneswar.

2.1.1 Chemical analysis

The oldest and most established determinative method for studying clay minerals is to find out the chemical constituents. Major elemental analysis methods have changed dramatically over the last 50 years. Initially the "Classical Scheme" of analysis, involving decomposition of the sample followed by gravimetric determination, developed by Lundell and Hooffman (1983), Groves (1951) and Hillebrand et al (1953) was adopted as the standard procedure. Subsequent development of colorimetric methods has led to their introduction into more rapid analytical techniques, which needs only small quantities of samples (Shapiro and Brannok, 1953). The recent induction of sophisticated analytical techniques such as flame photometry, atomic emission and absorption, inductively coupled plasma and X-ray fluorescence spectroscopy have greatly reduced analysis time and sample quantity with out affecting the accuracy. With the advent of sophisticated

mineralogical, spectroscopic and microscopic techniques, instrumental techniques are now unquestionably superior to chemical analysis for clay mineral identification. But, for complete characterization, chemical analysis is still essential because the structural formula can be calculated and the distribution of cations in the structure can be defined directly only by this method. A full characterization includes the determination of all the major, minor elements and cation exchange capacity.

The main purpose of chemical analysis is to determine all the elements present in a sample. Unlike many other fields of analysis, where the percentage of a given element present is recorded, the silicate and ceramic analyst report the percentage of oxides. This convention is followed as it represents the truer picture of the constitution of the material. For example, kaolin approximates to a formula $Al_2O_3.2SiO_2.2H_2O$ and if the results are expressed as percentage of SiO_2, Al_2O_3 etc., it will give a more useful picture than merely reporting as Si, Al, O contents. The origin of this convention probably lay in the method of classical analysis wherein most of the constituents were actually weighed as oxides.

A further convention to be noted is that generally the "complete" analysis of kaolin comprises of the determination of SiO_2, Al_2O_3, Fe_2O_3, TiO_2, CaO, MgO, K_2O, Na_2O and Loss on Ignition (LOI). Classical methods of chemical analysis are widely used for the aluminosilicates (Bennett and Reed, 1971). In the present study, the samples were analyzed by standard wet chemical and instrumental methods. The LOI was determined by igniting pre-weighed samples of kaolin at 1025°C for 1h and calculating the percentage of loss in weight. The SiO_2 was estimated gravimetrically, Al_2O_3 by complexometry, Fe_2O_3 and TiO_2 by colorimetry and Na_2O, K_2O and CaO by flame photometry. The elements present in traces such as arsenic, barium, bismuth, cadmium etc were determined by ICP-AES.

2.1.1.1 Loss on ignition

The organic impurities, water molecules associated with clay sample (water of crystallization) and carbonates in the clay mainly contribute to loss on ignition at an elevated temperature. Nearly one gram of finely ground and dried samples (at ~110°C 1h) was weighed accurately and transferred into a tared platinum crucible. It was placed in a muffle furnace and heated slowly at a constant rate of 6°C/min.to 1025°C and soaked for one hour. The sample was then cooled in a desiccator and weighed. Heating and

42

cooling was continued to get a constant weight. The loss in weight gives the ignition loss of the material.

Loss on ignition (%)   = $\dfrac{\text{Loss in weight of the sample} \times 100}{\text{Initial weight of the sample}}$

2.1.1.2 Determination of silica

About 0.5 g of finely agated dried (~110°C 1h) and cooled sample was weighed accurately into a platinum crucible and fused with about 3 g of fusion mixture (equimolar mixture of potassium and sodium carbonates). After cooling, the melt was extracted with 30 ml of 1:1 HCl and 1 ml of 1:1 H_2SO_4. The silicic acid precipitated was dehydrated initially on a water bath and finally baked in an air oven at 110°C for 1 hour. After cooling, 10 ml con. HCl and 40 ml of water was added to it, the contents were warmed and filtered through Whatman No.40 filter paper. The residue was washed first with hot dilute HCl and then with hot water till free from chlorides (checked with dil.$AgNO_3$ solution). The filter paper along with precipitate was transferred to a platinum crucible and heated slowly to 1000°C; cooled and weighed till constant weight (X) is obtained. After moistening the contents of the crucible with water, a few drops of 1:1 H_2SO_4 and 10 ml of HF was added and evaporated to dryness. During this process, the whole SiO_2 is volatilized and removed as SiF_4.

$$SiO_2 + 6HF \longrightarrow H_2\,[SiF_6] + 2H_2O$$
$$H_2\,[SiF_6] \longrightarrow SiF_4 + 2HF$$
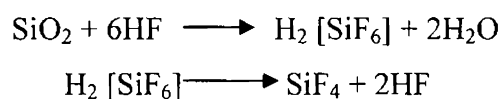
The crucible along with the contents were heated at ~1000°C, cooled and weighed (Y). The difference in weight (X-Y) gives the SiO_2 content.

% Silica content   = $\dfrac{(X - Y) \times 100}{\text{Weight of the sample}}$

2.1.1.3 Estimation of aluminium, iron & titanium

(a) Preparation of stock solution

The first step involved is the preparation of sample solution from which these elements are estimated. About 0.5 g of well agated and dried sample (at ~-110°C 1h) was accurately weighed in a platinum basin, moistened with water and added 10 ml of H_2SO_4 (1:1) and 10 ml of HF (48%). The contents of basin were evaporated on a heated sand bath to fumes of H_2SO_4. The basin was cooled, 10 ml HF was added again and

43

evaporated to copious fumes of SO₃ and ultimately to dryness. The residue was fused with ~3 g of potassium pyrosulphate. After cooling, the melt was treated with 3% H_2SO_4 and heated on a steam bath to obtain a clear solution. The solution was transferred to a 250 ml standard flask and made up to the mark. This is the stock solution for determination of aluminium, iron and titanium.

b) Estimation of Aluminium (by volumetry)

To a 20 ml of stock solution pipetted out into a conical flask, 25 ml EDTA solution (0.02M) was added. A drop of methyl orange solution and 1:1 NH_4OH was added to it until the color changed from red to yellow. 10 ml buffer (pH 5.3) was added and heated to boil for five minutes. After cooling, 5 ml of buffer was added and the solution was titrated against standard zinc acetate solution (0.02M) using xylenol orange as indicator. The end point was indicated by a clear change of colour from yellow to orange. About 1g of NaF was added and it was boiled for 5 minutes. After cooling, 10 ml of buffer was added and was titrated against standard zinc acetate solution to get the second titre value "V" ml.

$$\% \text{ of alumina } (Al_2O_3) = \frac{(V \times a \times 100)}{W} - 0.6378 \text{ Ti}$$

a = equivalents of alumina in g/ml of zinc solution, W = weight of sample and Ti – percent titania in the sample.

When a known excess of EDTA is added to the stock solution, all the aluminium ions form complex with EDTA. The first titre value corresponds to the EDTA remaining after the complexation with aluminium. When NaF is added to this solution and heated to boil, the Al-EDTA complex decomposes to form more stable Al-F and EDTA equivalent to the aluminium content is liberated. This liberated EDTA was titrated against zinc acetate solution and the titre value corresponds to the aluminium present in solution.

c) Estimation of iron and titanium (by colorimetry)

Colorimetric analysis is based on Beer – Lambert Law, which is combination of two theories put forward by Lambert and Beer dealing with the effect of thickness of the absorbing medium and concentration of the colored constituent in the solution on the intensity of the transmitted light. According to this law, when a monochromatic light

44

passes through a transparent medium, the intensity of the transmitted light decreases exponentially as the thickness of the absorbing medium and concentration of the absorbing substance increases arithmetically.

$$\text{ie., } \log I_o/I_t = a \cdot c \cdot l$$

Where I_o - Intensity of the incident light of wavelength λ

I_t - Intensity of the transmitted light

c - Concentration of the medium

l - Thickness of the absorbing medium

a - molar absorption coefficient, if 'c' is expressed in mole L^{-1}

and 'l' in centimeters

Thus the optical density of the solution is directly related to the concentration of the metal ion in solution.

Estimation of iron as Fe_2O_3

Ortho (1:10)phenanthroline ($C_{12}H_8N_2.2H_2O$) forms a red colored complex with ferrous iron $[Fe-(o-phenanthroline)_3]^{2+}$. In this complex, Fe(II) is bonded to the two 'N'-atoms of the ligand to form a chelate, which is stable over a pH range of 2-9. For estimating the iron, Fe (III) in the sample is reduced to Fe (II) using hydroxyl ammonium chloride and complexed with the ligand. Usually, the pH is adjusted between 5 and 6 using tartaric acid to avoid the hydroxide precipitation.

For the estimation of iron, 5 ml of the stock solution (**a**) was transferred to a 100 ml standard flask and 2 drops of para nitrophenol indicator and 10 ml of tartaric acid were added. The solution was neutralized with concentrated ammonia to the yellow color of the indicator and acidified with a few drops of 1:1 HCl. 2 ml of hydroxyl ammonium chloride and 10 ml of 1, 10 phenanthroline were added and diluted to the mark. The optical density of the solution was measured at 510 nm in a cell against the reference blank prepared in the same way without sample. A calibration graph was drawn using a set of values obtained with 0, 2,4,6,8 and 10 ml of standard Fe_2O_3 solutions in the same way as in sample solution and the iron content in the sample was determined from this graph.

$$\% \ Fe_2O_3 \ = \ \frac{\text{iron oxide content (from graph) x made up vol. x 100}}{\text{Sample wt. x vol.of solution taken for measurement}}$$

45

Estimation of titanium as TiO_2

Titanium forms a peroxy complex with hydrogen peroxide. The yellow colored species formed at pH > 2 is believed to be [Ti $(OH)_2(H_2O)$ (H_2O_2)] $^{2+}$ and in order to avoid the hydrolysis of titanium, a dilute sulphuric acid medium is usually used. The maximum optical absorption is observed at 410nm.

For the estimation of titanium, 20 ml of the stock solution was pipetted out into a 100 ml standard flask and 10 ml of 6% hydrogen peroxide was added to it and made up to the mark. A blank was also prepared with out hydrogen peroxide. The absorbance of the colored solution was measured at 410 nm against a blank. Absorbance for a set of standard titania solutions where color was developed in the same way as the sample solution was also measured and a calibration graph was drawn based on the obtained values. The titania content in the sample was obtained from this graph.

$$\% \ TiO_2 \ = \ \frac{\text{titania content (from graph) x made up vol. x 100}}{\text{Sample wt. x vol. of solution taken for measurement}}$$

2.1.1.4 Estimation of sodium, potassium and calcium (Flame photometric method)

The concentration of sodium, potassium and calcium in clay samples were determined by flame photometric technique. The essential features of the instrument are a suitable flame into which the sample solution is aspirated through a nebuliser unit, a collimating lens system to collect light from the flame, a filter designed to transmit only the characteristic emission of a particular element, a photo cell and a digital read out unit. Here the intensity of the radiation of the samples is compared with that of the standard samples measured under the same conditions.

Nearly 0.1 g of finely agated, dried (~110°C 1h) and cooled sample was weighed accurately into a platinum basin, moistened with water and added 1 ml of perchloric acid and 5 ml of HF (48%). The contents of basin were evaporated on a heated sand bath to fumes of H_2SO_4. The basin was cooled, 5 ml HF was added again and evaporated to copious fumes and ultimately to dryness. After cooling, to the melt 5 drops of 1:1 HCl and water was added and heated on a steam bath to obtain a clear solution. The solution was transferred to a 100 ml standard flask and made up to the mark. This is the stock solution for determination of sodium, potassium and calcium The concentrations of K_2O, Na_2O and CaO in the samples were determined by selecting the suitable filter.

46

2.1.1.5 Analysis of trace elements

Determination of elements present in traces is carried out using ICP-AES. When a solution containing various metal ions are introduced into a flame, characteristic colors are produced and when the light from the flame is passed through a spectroscope, several lines are seen, each of which has got a characteristic color. A definite wavelength can be assigned to each radiation, corresponding to its fixed position in the spectrum. Normally an electric arc is used to excite the atoms and the spectra are recorded photographically by means of a spectrograph. Since the characteristic spectra of many elements occur in the ultraviolet region, optical system made from quartz is used for dispersing the radiation.

AES make use the emissions due to line spectra. The line spectra consists of definite lines, characteristic of atoms or atomic ions which have been excited and emit their energy in the form of light of definite wavelengths. According to quantum theory, each atom or ion possess definite energy states in which the various electrons can exist and in the ground state the electrons will have the minimum energy. When application of sufficient energy, one or more electrons can be ejected to the higher energy state further from the nucleus. But these excited electrons tend to return to the ground state by emitting the extra energy as a photon of radiant energy. Since there are definite energy states and only certain changes are possible according to quantum theory, only a limited number of wavelengths are possible in the emission spectrum. The lines in the spectrum from any element always occur in the same positions relative to each other. When sufficient amounts of several elements are present in the source radiation, each will emit its characteristic spectrum and this is the basis of AES.

The intensity of a spectral line depends largely upon the probability of the required energy transition taking place. Also, the number of lines appearing in the spectrum is determined by the energy of the excited atoms, which in turn is depended on the energy of the exciting source. In order to achieve the maximum atomization, plasma can be used as the source for atomization. It produces a cloud of highly ionized gas, composed of ions, electrons and neutral particles. The inductively coupled plasma (ICP) was used for atomization as it produces a greater number of excited emitted atoms, especially in ultraviolet region, than that obtained by the relative low temperatures used

in normal FES. Further, the plasma source has got greater degree of precision, thus making it possible to produce spectra of a large number of elements and this allows carrying out multi element determinations possible over a wide concentration range.

The <45μm fraction samples (2"stub hydrocyclone overflow) of the clays were analyzed for the elements such as arsenic, barium, bismuth, cadmium, cobalt, chromium, copper, magnesium, manganese, nickel, phosphorous, lead, sulphur and zinc.

2.1.1.6 Determination of Ferrous oxide

Ferrous iron forms major part of the iron content of rocks and minerals and its estimation is essential for calculating the structural formulae of the clay minerals. Fe (II) was determined based on the method proposed by Shapiro and Brannok (1952).

As prolonged grinding can result in oxidation of ferrous to ferric iron, a gentle grinding (< 70 mesh size) under alcohol was done (Kolthoff and Sandell(1956). Nearly 0.5 g of agated, dried (110°C for 1h) and cooled sample was weighed accurately into a platinum crucible and to it 10 ml of 1:1 H_2SO_4 and 10 ml of HF (48%) was added .The mixture was boiled over a gas burner and was plunged into a beaker containing 300 ml of 2.5% boric acid solution. The solution was mixed gently and to the above solution, 10 ml of diphenylamine sulphonate indicator was added and titrated immediately with 0.1 N potassium dichromate solutions to a purple end point. A reagent blank was also carried out.

$$1 \text{ ml of } 0.0167M \ K_2Cr_2O_7 = 5.58 \text{ mg Fe(II)}$$

2.1.1.7 Determination of pyrite

Pyrite in clay was estimated as per the analytical procedure given by Schneider and Schneider (1990). The method involved two selective extractions

(a) overnight dissolution of non-pyritic iron (including hematite, Fe_3O_3) in concentrated hydrochloric acid and then diluting the same with distilled water to 2.5 N and boiling it for 1 hour under atmospheric pressure and

(b) dissolution of total pyritic and non-pyritic iron, including hematite, from a separate sample in two steps which involve (i) initial dissolution in concentrated HCl followed by dilution to 2.5 N and boiling for 30 minutes, followed by (ii) the addition of 3 N nitric acid (to dissolve pyrite) and boiling for 30 minutes.

48

The filtrates from the two extractions (a) and (b) were then analyzed for iron. The pyritic iron was determined as the difference in iron content of the two extractions.

(a). Selective extraction of nonpyritic iron

Nearly 1 g of agated, dried (~110°C 1h) and cooled sample was weighed accurately into a 250 ml conical flask, 11 ml of concentrated HCl was added, mixed thoroughly, closed and kept overnight (12 hours). The contents were diluted to 50 ml, an additional 50 ml of 2.5 N HCl was added and boiled for 1 hour in covered condition. Then the contents were cooled, rinsed with 20 ml of HCl (1:10) and filtered through Whatman No.5 filter paper and was washed 5 times with 2 ml of HCl solution (1:10). The transparent or yellow-green colored filtrate was obtained depending on the content of acid soluble compounds. The acid insoluble part, which remained in the filter paper, was discarded and the filtrate was treated with 5 ml Con.H_2SO_4 and 3 ml of HNO_3 and was evaporated to dense SO_3 fumes. After cooling, the residue was diluted with distilled water to 250 ml in the standard flask and the aliquot of the solution was taken for the determination of Fe.

(b) Selective extraction of total (pyritic and nonpyritic) iron

In the case of extraction of total iron, nearly 1 g of agated, dried (~110°C 1h) and cooled sample was weighed accurately into a 250 ml conical flask. The overnight (12 hours) treatment of the sample with 11 ml of concentrated HCl was done as described earlier. The contents were then diluted to 50 ml, an additional 50 ml of 2.5 N HCl was added and boiled for 30 minutes. The sample was then cooled and filtered through Whatman No.5 filter paper after rinsing the flask with 20 ml of 2 N HNO_3. Subsequently, it was washed 5 times with 2 ml 2N HNO_3. The filtrate is treated with 5 ml of conc. H_2SO_4 and evaporated to dense white fumes of SO_3. After cooling, the residue was diluted with distilled water and boiled for a few minutes. The sample solution was then diluted to 250 ml in a standard flask and an aliquot of the solution is taken for the determination of Fe by colorimetric method as described earlier.

% of pyritic Fe = % of Fe from extraction (b) - % of Fe from extraction (a)

From the quantity of pyritic iron, the percentage concentrations of pyrite in the samples were calculated.

49

2.1.1.8 Organic Carbon

The organic carbon content in the clay samples were determined by wet combustion method (Gross, 1971). Nearly 0.5 g of agated dried (~110°C 1h) and cooled sample was accurately weighed into a 500 ml conical flask, 10 ml of $K_2Cr_2O_7$ and 20 ml of H_2SO_4-Ag_2SO_4 solutions were added to it. The flask was gently heated to 150°C for 2 minutes and allowed to cool. The excess $K_2Cr_2O_7$ was estimated by back titration with $FeSO_4$ solution after adding 10 ml of 85% H_3PO_4, 0.2 g of NaF and 30 drops of diphenylamine indicator and diluting it to 200 ml. The end point is a change of color from blue to bright green. A blank analysis was conducted for each series of samples. The percent organic carbon in the sample was calculated as follows,

$$\% \text{ of organic carbon} = \frac{(\text{ml FeSO}_4) \text{ blank} - (\text{ml FeSO}_4) \text{ sample x 0.3}}{\text{Weight of the sample}}$$

2.1.1.9 Sulphur

The method adopted here is usually used for the determination of most of the insoluble sulphides. Here sulphur is oxidized to H_2SO_4 by bromine in carbon tetrachloride solution followed by nitric acid, and is determined as basium sulphate.

$$2FeS_2 + 6HNO_3 + 15Br_2 + 16H_2O = 2Fe(NO_3)_3 + 4H_2SO_4 + 30 HBr$$
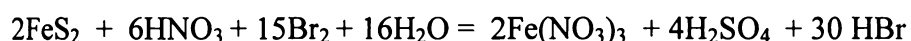
The sample was ground well in an agate mortar and was heated in an air oven at ~110°C for 1 hour. After cooling, a known weight of the samples (~0.5 g) was taken in a dry 400 ml beaker and to it 6 ml of a mixture of 2 volumes of pure liquid bromine and 3 volumes of pure carbon tetra chloride was added . The mixture was kept in the fume cupboard in the closed condition for 20 minutes and with occasional swirling of the contents of the beaker. Then about 10 ml of conc. HNO_3 was added to be beaker and the contents were again kept in the closed condition for another 20 minutes with occasional swirling of the contents. The contents in the beaker were then heated in a hotplate for 1 hour to remove bromine and the remaining liquid was evaporated to dryness in a steam bath. It was then treated with 10 ml HCl and the contents were evaporated to dryness to eliminate most of the HNO_3. Silica present in the sample was then dehydrated by heating the beaker at 90°C for 1 hour in an air oven. The residue obtained was then moistened with 2 ml of conc.HCl and after after 5 minutes, it was diluted with 50 ml of hot water after rinsing the sides of the beaker and cover glass with water. The contents were then digested in steam bath at 100°C for 10 minutes in order to dissolve the soluble salts and after cooling, 0.2 g

of aluminum powder was added to it to reduce the Fe (III). The solution was then gently swirled and after cooling the contents, inner side of the beaker as well as the cover glass was rinsed with water. It was then filtered through a Whatman No 5 paper and the filtrate was collected in a 1 lit beaker. The filter was then thoroughly washed with hot water and the filtrate and the washings were dilute to 600 ml after adding 2 ml of conc.HCl to it. Sulphate was then precipitated in cold by running in from a burette, without stirring, a 5 percent solution of barium chloride at a rate of 5 ml / min (5 ml in excess was added). The content was then gently stirred and was kept undisturbed for overnight (12 hours) for the complete settling of the precipitate. It was then filtered through a Whatman No 5 paper, washed with warm water till free from chloride and ignited to constant weight. The percentage of sulphur was calculated based on the weight of barium sulphate.

2.1.1.10 Cation exchange capacity

A known quantity (~0.5 g) of the well ground, pre-heated (~110 °C 1 h), cooled sample was mixed with 30 ml of ammonium acetate solution was kept was kept overnight (12 hours). To the above mixture, 1 drop of sodium chloride solution was added, mixed well and was centrifuged. The clay is then washed with rectified spirit and was again centrifuged and this is continued till the sample has become free from chloride ions. To the washed sample, 10 ml of distilled water and 0.5 g of .MgO were added and was distilled for 30 minutes. The distillate formed is collected in a stoppered conical flask containing saturated boric acid solution containing a drop of mixed indicator. The colour changes of the solution from pink to green indicates the collection of the distillate. After the distillation is over, 50 ml of the distillate was titrated against standard hydrochloric acid for a colour change of green to pink. One blank titration was also carried out.

$$\text{C.E.C (m. equ. / 100 g of sample)} = \frac{\text{(Blank value – sample value) x Normality of acid x 100}}{\text{Weight of sample}}$$

2.1.2 Physical characterization samples

The physical properties of clay samples such as pH, relative density, solubility (matter soluble in HCl & in water) and grit content were determined as per the procedure given in the Indian Standard Specifications (IS 505, 1995)

2.1.2.1 pH

The hydrogen ion concentration or pH is expressed as the logarithm to the base 10 of the reciprocal of the hydrogen ion concentration. Measurement of pH has significance in understanding the clay surface as well as in the processing steps. Hence, the ROM clay is subjected to this study.

Nearly 25 g of the sample was mixed with 100 ml of freshly prepared distilled water (in the ratio 1:4) and stirred for 5 minutes. The slurry was filtered through Whatman No. 40 filter paper. The first 20 ml of the filtrate was discarded and the pH of the remaining filtrate was measured.

2.1.2.2 Relative Density

About 10g of the clay sample was dried (at $\sim 110^{\circ}C$ 1h) and accurately weighed into a previously dried and weighed specific gravity bottle (W_1). The weight of the bottle and the contents was noted (W_2). The bottle was nearly half filled with water, placed on an evaporating dish and evacuated for air bubbles by using a vacuum pump. The bottle was then filled with boiled water, and the weight was found out (W_3). The weight of the bottle completely filled with water alone was also determined (W_4). From the mass of the sample and its loss in weight in water, relative density of the sample was calculated as given below

$$\text{Relative Density} = \frac{(W_2 - W_1)}{(W_2 - W_1) - (W_3 - W_4)}$$

2.1.2.3 Matter soluble in hydrochloric acid

About 2g of the dried clay was weighed accurately (W_1) and transferred to a round-bottomed flask with 100ml of 0.2 N HCl. A reflux condenser was connected to the flask and the mixture was boiled on a heating mantle for 5 minutes. It was cooled and filtered through a sintered glass crucible (G-4). The residue was washed free from chlorides and the filtrate was taken in a silica basin and evaporated to dryness on a water bath. The mass was cooled and weighed. Heating and cooling was repeated to get constant weights (W_2).

$$\text{Matter soluble in HCl, \% by mass} = 100\ W_2 / W_1$$

2.1.2.4 Matter soluble in water

Nearly 10g of the dry material was weighed accurately into a beaker (W_S). Rectified spirit (5 ml of)was added to wet the sample and mixed thoroughly. Water (250ml) was added, the suspension was boiled for 5 minutes and allowed to cool to room temperature. Sufficient quantity of bromophenol blue indicator was added to give a visible color followed by dil. HCl (0.1 N HCl) until blue color disappears.The contents of the beaker was transferred to a 250 ml volumetric flask, diluted to the mark with water and mixed well by shaking. It was filtered through a filter paper, rejecting the first 50ml of the filtrate. 100ml of the clear filtrate was taken in a porcelain dish and evaporated to dryness on a water bath. The residue was dried at ~110°C, cooled and weighed till constant mass was obtained (W_R).

$$\text{Matter soluble in water, \% by mass} = 250 \times W_R / W_S$$

2.1.2.5 Grit content and recovery (ROM clay)

About 100g of clay was dried, accurately weighed and added to 1 liter of water and allowed to slake overnight. The slurry was agitated mechanically and is passed through a 350 mesh (BS sieve). The material retained in the sieve as well as the material passed through the sieve were separately dried at 100 ± 5°C and weighed. The percentages of particles above and below 45 μm size were calculated, which corresponded to the grit and recovery respectively.

2.1.2.6 Particle size distribution analysis

Usually, particle size distribution analysis is done mainly by sieving techniques, sedimentation techniques, laser diffraction light intensity fluctuation techniques etc. The sedimentation technique is based on Stoke's law, which is the most widely used for clays. According to Stokes law the terminal velocity of a particle falling under the influence of gravity is directly proportional to the density of the particle and the viscosity of the falling medium.

Assuming the particles to be of near spherical shape, Stokes Law is applied to calculate the diameter of particles by correlating the terminal velocity 'V' of particle settling under gravity in a medium of viscosity 'η'. Thus

$$a = \frac{\sqrt{18\eta V}}{(D_P - D_L)g}$$ where $\quad$ a = Stokes' diameter of the particle, D_P =

Density of particle, $\quad D_L$ = Density of liquid and $\quad$ g = Acceleration due to gravity

The clay samples (fraction below 45 μm) were analyzed for its size distribution by sedimentation method. The sample is made into slurry and the particles are dispersed ultrasonically in presence of sodium hexameta phosphate. This slurry is poured into the mixing chamber of the instrument where a magnetic stirrer keeps the particles in suspension. At the appropriate time, the slurry is pumped into the analysis cell, which is placed in the path of X-ray beam, and the particles are allowed to settle under gravity force. The particles in the path of the beam absorb X-rays. The amount of X-ray absorbed at that point in the cell where the beam is located, is determined as percentage of X-ray absorption with the highest particle concentration. Based upon the particle falling rate, this percentage is related to the maximum particle size above that point in the cell. The resulting particle size data are processed by the system computer. The rate of particle fall due to gravity is calculated and X-ray absorption, which is directly related to the concentration of particles, at different heights and time is determined and the results are obtained as graphs and tabular reports. The size distribution as well as the average particle size of the sample was obtained from a graph with cumulative mass % versus particle diameter in micro meters.

2.1.2.7 Optical property measurement

The optical properties pertinent to kaolin are brightness, **Lab** color values, Hunter whiteness (HW) and yellowness (HY) which are measured using a brightness meter

The basis of all color measure is the electromagnetic spectrum (Figure 2.1) and only the region between 400 to 700 nm is visible to human eye. When a ray of light strikes a layer of a material, four possible phenomena occur such as reflection, transmission, scattering and absorption (Figures 2.2a and 2.2b). The phenomenon which influences the whiteness of a material is its light reflecting capacity ie., for a material to appear as white, sufficient amounts of all wavelengths of light has to be scattered back in the direction of the viewer (ie., multiple reflection and refraction inside the material should be minimum). When the light ray strikes the colored matter, the light energy is absorbed and converted to heat. Therefore, the light is not re-emitted from the material

thereby reducing its reflectance. Brightness is the measure of the percentage reflectance of blue light of very specific spectral distribution with reference to a standard material (paper standard) having 100 % light reflecting power and is measured at an effective wave length of 457 nm.

The color values give information on the "shade" of the material in accordance with the visual appearance. The spectrophotometer measures the reflectance of different wavelengths of light, and then it is converted to color scale which matches with the visually observable color. For this purpose, in 1931, Commmission Internationale de l'Eclairage (CIE) introduced the tristimulus functions X (red), Y (green) and Z (blue). This is based on a cone angle of 2 degree viewing and illuminant C, whose spectral power distribution agrees well with that of typical daylight. In 1958 Richard Hunter transformed the CIE color space to more visually uniform and more easily understood L, a, b color space. The concept of color co-ordinates is based on the color opposites (Figure 2.3). Therefore "L" is the measure of lightness and varies from 100 for a perfect white to 0 for absolute black. A positive value for "a" indicates redness, negative "a" greenness, positive "b" yellowness and negative "b" blueness.

The brightness and the color values are measured as per the ISO standards. The clay sample was dried in an air oven at ~110°C for one hour, cooled and pulverized for 10 seconds using an Anglo Pulveriser. Thereafter, this powder was compacted into a disc of 4 cm diameter by applying a uniform load of 55 kg for 30 seconds in a Hand Powder Press Apparatus. Then the pellet was introduced into the brightnessmeter (Color Touch™ Model from Technidyne Corporation, USA) and the optical properties like brightness, Lab color values, HW and HY were measured

2.1.3 Mineralogical Analysis

2.1.3.1. X-ray Diffraction analysis

X-ray powder diffraction (XRD) is the most widely used technique used for the identification and characterization if clay minerals (Brindley and Brown, 1980; Wilson1966).

Clay minerals consist of tiny crystals which are themselves made up of ordered array of atoms arranged in a periodic way. X-ray diffraction can be visualized as a reflection of the incident beam by parallel, closely spaced planes of atom within a crystal.

W.L.Bragg in 1912 gave a geometrical interpretation of the diffraction by a crystal grating. According to him the condition for diffraction is given by the relation,

$$n\lambda = 2d \sin\theta \quad \text{where}$$

n   = order of the reflection

λ = wavelength of X-rays (in Å)

d   = inter planar distance and.

θ = angle of diffraction.

From this, the'd' values pertaining to characteristic reflections of each mineral can be calculated. The identification of the minerals is done by comparing the d-spacings and relative intensities of the sample with the standard reference data (formerly JSPDS file).

Randomly oriented samples were prepared by pressing about 0.5 g of the clay uniformly into the shallow cavity of a glass sample holder using a glass slide. The powder XRD patterns were obtained on a diffractometer on a diffraction range 5-60^0 (2θ).

2.1.3.2 Thermal Analysis

The thermodynamic changes in solids and reaction between the materials are determined by thermo gravimetric analysis (TGA) and differential thermal analysis (DTA). In TGA, the loss in weight of a material is determined as a function of temperature while in DTA, differential temperature due to endothermic and exothermic transition or reaction in a sample is plotted as a function of temperature or time with respect to an inert reference material such as alumina. Thermo chemical methods give information due to decomposition of materials, oxidation, phase transition, vitrification, crystallization etc.

Differential Thermal Analysis

DTA is a technique for studying the thermal behavior of material as they undergo physical and chemical changes during heating. The name is derived from the differential thermocouple arrangement, consisting of two thermocouple wires, where the first one is placed in the sample to be analyzed and the other one in the standard reference material (which does not undergo any thermal transformations over the temperature range being studied). When the temperature of the sample equals that of the reference material, the

56

two thermo couples produce identical voltages and the net output will be zero. But, when there is difference in voltage between the two, it will refer to the difference in temperature between the sample and the reference material at that point of time. The μV outputs from the differential thermocouple pair is then amplified and are recorded. The results are recorded as DTA curves, in which, by convention, $\Delta \mu V$ is plotted on the ordinate with endothermic peaks pointing downward, and exothermic peaks pointing upward from the horizontal base line and the temperature is recorded increasing from left to right on abscissa.

Thermo Gravimetric Analysis

TGA of the sample is done by heating the material at a controlled rate or at a fixed temperature above the ambient. This produces a loss in weight due to the dehydration, desorption, decomposition or oxidation of the material. TGA essentially observes change in weight of the material as a function of temperature (dynamic heating) or time (isothermal heating). In actual practice, it involves the measurement of the mass of a substance as a function of temperature, while the substance is subjected to a controlled heating. In a typical TG curve, the mass of the sample is recorded on the ordinate (decreasing downwards) and temperature is recorded on the abscissa.

In the present study, the DTA experiments were carried out in an air atmosphere at a heating rate of 40°C/minute and using alumina as the reference material.

2.1.3.3 Rational Analysis

Although methods have been suggested from time to time for separating the mineralogical compounds of clays, these have not proved particularly satisfactory. Adequate estimates of the chief components can be made, however, by calculation from the ultimate analysis on the basis of limited assumptions. These so-called proximate analyses or preferably, calculated mineralogical compositions can provide with sufficiently adequate picture for most practical purposes.

The calculated mineralogical composition of clays has followed two main lines ie., "Feldspar" and "Mica" basis. The older method was to consider all basic oxides as occurring as orthoclase feldspar, $K_2O.Al_2O_3.6SiO_2$, so that the oxides Na_2O, CaO and MgO were all regarded as K_2O. The modern trend in calculating the "mineralogical" composition is to use the so-called "mica convention" which deals with the alkalis,

alumina, silica and ignition loss, and to list the remaining elements as oxides unless there is direct evidence of the form in which they occur as, for instance, with TiO_2 which is usually present as anatase. With this calculation the alkalis are calculated separately as "paragonite"(soda mica) and "muscovite"(potash mica), the remaining alumina appears as kaolinite, the remaining silica as "quartz" and any excess LOI as "carbonaceous matter".

The rational analyses of the clay samples including the ROM, beneficiation products and impurity concentrates were calculated based on the "mica convention" from the chemical assay.

2.1.3.4 Crystallinity measurements

The presence of defects in kaolinite structure is often studied using X-ray diffraction (XRD) procedure, as the XRD patterns of different kaolinites vary in peak intensity modulation and peak position. In spite of this, it is very difficult to translate the observed changes in crystal perfection into a coherent and quantitative description of the defect structure. Due to the importance in the estimation of the degree of disorder in kaolinite structure, empirical relations were used.

The most widely used relation. to study the crystal structure of kaolin minerals is the one proposed by Hinckley (1963) and is known as "crystallinity index" or Hinckley index (HI). This index is a ratio of (i) the sum of the heights of the reflections (110) and (1̄11) measured from the inter-peak background and (ii) the height of the (110) peak measured from the general background (Figure 2.4a). The basis of this procedure is that "as crystallinity decreases, the proportion of random shifts between adjacent layers increases by + n b/3 units, resulting in resolution of neighboring peaks and an increase in the inter peak diffraction intensity. At the same time, an increase in the frequency of defects would decrease the absolute intensity of (110) peak. Similarly, DTA can also be used to understand the crystalline nature of the kaolinite. A slope ratio method was introduced by Robertson et al (1954) to detect the differences in the shapes of DTA curves. Slope ratio is defined as the ratio of the angels (α, β) made between a vertical line at the peak maximum and the tangents to the left and right limbs of the peak (Figure 2.4b).

2.1.4 Spectroscopic studies

Molecular spectroscopic techniques, usually used to study the clay minerals, involves the interaction of electromagnetic radiation with materials in order to produce an absorption pattern (ie., a spectrum) from which structural or compositional information can be deduced. Electromagnetic radiation is conventionally divided into a number of distinct regions, each of which covers a range of energies that corresponds to different molecular processes (Figure 2.5). They are,

1. Radio frequency (105– 109 Hz) corresponding to the energy involved in changing the direction of spin of a nucleus (Nuclear Magnetic Resonance, NMR)

2. Microwave (109 to 3x1010 Hz). This range covers the energy involved in changing the direction of electron spin (Electron Paramagnetic Resonance, EPR) and the separations between rotational energy levels of gaseous molecules

3. Infrared (3x1010 to 3x1014 Hz). Separations between vibrational energy states occur in this region and the technique based on infrared absorption is employed in this region.

4. Visible and Ultraviolet (3x1014 to 3x1016 Hz). This region corresponds to the separations between the energy levels of valance electrons.

5. X-rays (3x1016 to 3x1018 Hz). The energies of transitions involving inner-shell electrons occur in this region, and

6. Gamma (γ) rays (3x1018 to 1021 Hz). These correspond to the energies required to change the energy states of nuclear particles (Moss Bauer Spectroscopy)

All of the above energy states are quantized, ie., they occur as discrete values and the energy states of all atoms and molecules are determined by a set of quantum numbers which determine the number and related energies of the states in the various regions of the electromagnetic spectrum.

Molecular spectroscopy involves both absorption and emission spectroscopy. In absorption spectroscopy, the absorption of radiation is monitored as it is swept through a range of frequencies. For example, absorption at a frequency v implies that the specimen contains energy levels separated by hv, where h is the Planck's constant (6.626x10-34). In emission spectroscopy, transitions occur from higher to lower energy states with the

emission of radiation. The sample is excited by a radiation source and the radiation emitted as it returns to thermal equilibrium is detected and analyzed.

2.1.4.1 Electron Paramagnetic Resonance (EPR) spectroscopy

EPR spectroscopy aims at the detection of unpaired electrons and their characterization with respect to their chemical environments. It is a powerful technique for identifying the various types of association of paramagnetic metal ions with clay mineral, ie., on the basal surfaces, within the inter lamellar spaces, or as part of the aluminosilicate structure and can be used to characterize the minor structural or surface components, having unpaired electrons, in clays.

Usually, free electrons (in the absence of crystal or magnetic field) are randomly aligned, but in the presence of an external magnetic field, they can take up 2S+1 (where S is the net spin) different orientations, distinguished by quantum numbers m_s. The relative energies of these two states are proportional to the applied magnetic field B, and is given by

$$E\ m_s = g\mu_B B\ m_s$$

where μ_B - Bohr magneton (9.2731 x 10^{-24} J/T)

g - spectroscopic splitting factor

Electrons in the lower energy state, ms = -1/2, can be excited to the upper state, ms = +1/2 by electromagnetic radiation of appropriate frequency to satisfy the resonance condition, ie.,

$$h\nu = g\mu_B B$$

where v - frequency of the applied radiation (Hz)

h - Planck's constant

At resonance condition, a strong coupling occurs between the electron spin and the radiation. A strong absorption occurs as the electron spin makes the transition between the two states. It implies that the energy at which the resonance occurs is proportional to the applied magnetic field and most of the EPR work is carried out at a frequency of 9 GHz known as X-band.

The actual experimental set up involves measurement of the magnetic fields at which the paramagnetic molecules come into resonance with the applied monochromatic microwave radiation and the different types of paramagnetic species were identified

60

based on the g-value, which varies according to the orientation of orbital containing the unpaired electron relative to the direction of the external magnetic field. For instrumental purposes, an EPR spectrum is usually recorded as the first derivative of the absorption spectrum. The EPR spectral measurements at 9.42 GHz(X-band) of the ROM clays, products of beneficiation and impurity minerals were carried out at room temperature under identical conditions.

2.1.4.2 Mossbauer spectroscopy:

Transitions are observed between the energy levels in an atomic nucleus in the gamma-ray region of the electromagnetic spectrum in Mossbauer spectroscopic analysis. When a gamma ray is emitted from a nucleus in a free state, the nucleus recoils and the energy of recoil is related to mass of the nucleus as follows

$$E_R = mv^2/2$$

When the nucleus is part of a crystalline structure, such as clay mineral, the recoil energy is absorbed by many atoms, to such an extent that a fraction of the emissions is recoil-free. A similar process occurs on absorption and it is the study of the recoil-free absorption of those gamma- rays that are emitted without recoil which forms the basis of Mossbauer spectroscopy.

Nuclear energy levels of the nuclear transitions are precisely defined and their changes with variations in the environment of the nucleus are very small. It is thus necessary to use radiation that has an exceedingly small spread of energies in order to observe the spectral structure from interactions between the nuclei and their surrounding electrons. In Mossbauer spectroscopy, this is achieved by modulating the energy of the gamma rays by simple Doppler motion, where the radiation source is moved relative to the absorbing specimen. Only small velocities are required and ± 1 cm/s covers the range of energies required for ^{57}Fe Mossbauer spectroscopy.

The magnitude of the electric monopole interaction between the nucleus and its surrounding electron is determined by the electron density at the nucleus and the parameter isomer shift (∂), is used to describe the shift in the centre of the spectrum between the sample being investigated and a known standard, usually metallic iron. Isomer shift occurs in aluminosilicate minerals because the radial distributions of the atomic orbitals are such that electrons in 3d orbitals spend part of their time closer to the

nucleus than electrons in core s-orbitals (Figure 2.6). This decreases the attractive coulomb potential between the nucleus and the s-electrons Therefore, any change in the number of d-electrons changes the magnitude of the electron density at the sample leading to a positive isomer shift. Also, the d-electron density on the iron is determined primarily by the oxidation state [Fe (II) has six 3d electrons; where as Fe (III) has five].

The distributions of valance electrons and charges in the surrounding lattice is determined by measuring the magnitude of the quadrupole splitting (ie., splitting of energy levels of a nucleus having a spin, I > ½ by the interaction with an electric field gradient).

A Mossbauer spectrometer consists of a drive unit which moves the source to modulate its energy, a gamma-ray detector, a data storage system along with various amplifiers and a out put devise. The Mossbauer peaks are Lorentzian in shape and the line widths in clay mineral specimens can be broadened due to the in homogeneities in the coordination environment of the iron atoms, leading to the spreading of the spectral peaks over a range of values.

2.1.4.3 Fourier Transformed Infra Red (FTIR) spectroscopy:

The IR spectra originate from the different modes of vibration and rotation of molecules. The IR region of the electromagnetic spectrum is divided into three main sections ie., (a) near IR (overtone region; υ = 12500 to 4000 cm^{-1}), (b) middle IR (vibration – rotation region; υ = 4000 to 400 cm^{-1}) and (c) far IR ; υ = 200 to 10 cm^{-1}). The main region of interest for analytical purposes is the middle IR. At wave numbers below 4000 cm^{-1}, the radiation has got sufficient energy to cause changes in the vibration energy levels of molecules and these are accompanied by changes in the rotational energy levels.

IR spectroscopy has been used as a rapid non-destructive physical method for the structural analysis of clay minerals. The absorption of IR radiation by clay minerals depends critically on atomic mass, and the length, strength and force constants of inter atomic bonds in the structures of these minerals. Also, only those vibrations which undergo a change in dipole moment are IR active. The IR spectrum of a clay mineral can provide fundamental information on mineral identification, crystallinity, size and shape of the mineral particles and on isomorphous substitution.

The clay sample was ground finely to < 2 μm in size using conventional agate mortar and pestle (to minimize the scattering of incident IR radiation and to avoid distortion and broadening of absorption bands). It was then dispersed in KBr in the ratio (1:200) and pressed into discs. The sample is scanned and spectrum is the recorded over a range of 4000 to 300 cm^{-1} and the transmittance (T %) verses wave number (cm^{-1}) plots were taken.

2.1.4.4 UV-Visible spectroscopy:

Solutions of transition metal ions absorb light in the UV or visible regions of the electromagnetic spectrum and can be colored (i.e., absorb visible light) due to the excitation of d electrons within the metal atoms from one electronic state to another.

<u>Electronic transitions</u>

The absorption of UV or visible radiation corresponds to the excitation of outer electrons. There are two types of electronic transition which can be considered;

1. Transitions involving π, σ, and *n* electrons

2. Transitions involving charge-transfer electrons

When an atom or molecule absorbs energy, electrons are promoted from their ground state to an excited state. In a molecule, the atoms can rotate and vibrate with respect to each other. These vibrations and rotations also have discrete energy levels, which can be considered as being packed on top of each electronic level.
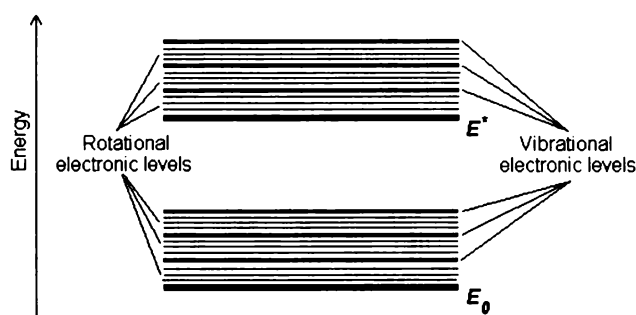
The possible *electronic* transitions of π, σ, and *n* electrons are;

Energy

$n \to \sigma^*$ $\sigma \to \sigma^*$

$n \to \pi^*$ $\pi \to \pi^*$

Antibonding σ^*

Antibonding π^*

Non-bonding n
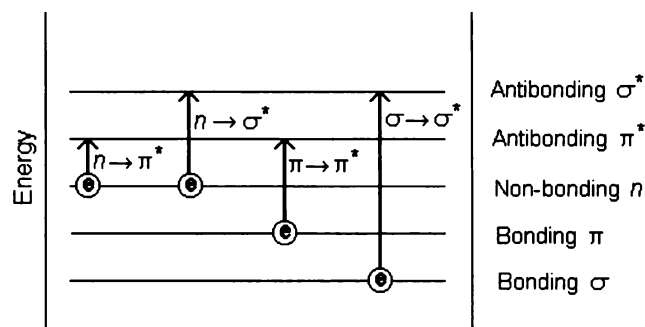
Bonding π

Bonding σ

$\sigma \to \sigma^*$ Transitions

An electron in a bonding σ orbital is excited to the corresponding antibonding orbital. The energy required is large. For example, methane (which has only C-H bonds, and can only undergo $\sigma \to \sigma^*$ transitions) shows an absorbance maximum at 125 nm. Absorption maxima due to $\sigma \to \sigma^*$ transitions are not seen in typical UV-Vis. spectra (200 - 700 nm)

$n \to \sigma^*$ Transitions

Saturated compounds containing atoms with lone pairs (non-bonding electrons) are capable of $n \to \sigma^*$ transitions. These transitions usually need less energy than $\sigma \to \sigma^*$ transitions. They can be initiated by light whose wavelength is in the range 150 - 250 nm. The number of organic functional groups with $n \to \sigma^*$ peaks in the UV region is small.

$n \to \pi^*$ and $\pi \to \pi^*$ Transitions

Most absorption spectroscopy of organic compounds is based on transitions of n or π electrons to the π^* excited state. This is because the absorption peaks for these transitions fall in an experimentally convenient region of the spectrum (200 - 700 nm). These transitions need an unsaturated group in the molecule to provide the π electrons.

Molar absorbtivities from $n \to \pi^*$ transitions are relatively low, and range from 10 to 100 L mol^{-1} cm^{-1}. $\pi \to \pi^*$ transitions normally give molar absorbtivities between 1000 and 10,000 L mol^{-1} cm^{-1}.

The solvent in which the absorbing species is dissolved also has an effect on the spectrum of the species. Peaks resulting from $n \rightarrow \pi^*$ transitions are shifted to shorter wavelengths (*blue shift*) with increasing solvent polarity. This arises from increased solvation of the lone pair, which lowers the energy of the n orbital. Often (but *not always*), the reverse (i.e. *red shift*) is seen for $\pi \rightarrow \pi^*$ transitions. This is caused by attractive polarization forces between the solvent and the absorber, which lower the energy levels of both the excited and unexcited states. This effect is greater for the excited state, and so the energy difference between the excited and unexcited states is slightly reduced resulting in a small red shift. This effect also influences $n \rightarrow \pi^*$ transitions but is overshadowed by the blue shift resulting from solvation of lone pairs.

Charge transfer absorption is exhibited by many inorganic species which are called *charge-transfer complexes*. For a complex to demonstrate charge-transfer behavior one of its components must have electron donating properties and another component must be able to accept electrons. Absorption of radiation then involves the transfer of an electron from the donor to an orbital associated with the acceptor. Molar absorbtivities from charge-transfer absorption are large (greater that 10,000 L mol^{-1} cm-1).

The samples were ground well and a dilute suspension (0.1 mg/10 ml) of the same in distilled water (pH-5.65) was prepared. It was then dispersed well in an ultrasonic bath for 20 minutes and the absorbance was measured using a cell of 5 cm height and 1 cm width. The spectral measurements of the samples were carried out under similar experimental conditions.

2.1.5 Microscopic Studies

Microscopy is defined as any technique used for producing visible images of structures too small to be seen by the human eye, using a microscope or other magnification tool. Microscopy has evolved with the development of microscopes and there are three main branches ie., optical, electron and scanning probe microscopy. Optical and electron microscopy involves the diffraction, reflection, or refraction of radiation incident upon the subject of study, and the subsequent collection of this scattered radiation in order to build up an image. This process may be carried out by wide

field irradiation of the sample (optical microscopy and transmission electron microscopy) or by scanning of a fine beam over the sample (scanning electron microscopy). Scanning probe microscopy involves the interaction of a scanning probe with the surface or object of interest.

2.1.5.1 Optical Microscopy

Optical microscopy involves passing visible light transmitted through or reflected from the sample through a single or multiple lenses to allow a magnified view of the sample. The resulting image can be detected directly by the eye, imaged on a photographic plate or captured digitally. The maximum resolution that can be achieved by this method is approximately 0.2 microns and can be used only for imaging dark or strongly refracting objects. The sample was spread on a glass slide and the individual particles were examined and the micrographs were taken.

2.1.5.2 Electron microscopy

The main feature of electron microscopy is the unusual short wavelength of the electron beams, substituted for light energy and are designed for very high magnification usage. The wavelengths of about 0.005 nm increases the resolving power of the instrument to fractions of a nanometer and makes it possible to clearly see both the nano and macro sized particles. Electrons, which have a much smaller wavelength than visible light, allow a much higher resolution. The main limitation of the electron beam is that it must pass through a vacuum as air molecules would otherwise scatter the beam. Instead of relying on refraction, lenses for electron microscopes are specially designed electromagnets which generate magnetic fields that are approximately parallel to the direction that electrons travel. The electrons are typically detected by a phosphor screen, photographic film or a charged-coupled device (CCD).

Two types of electron microscopes are in use today and they are scanning and transmission.

Scanning Electron Microscopy (SEM)

SEM allows surfaces of objects to be seen in their natural state without staining. The specimen is put into the vacuum chamber and covered with a thin coating of gold to increase electrical conductivity and to avoid blurring of image. The electron beam

then sweeps across the object building an image line by line as in a TV Camera. As electrons strike the object, they knock loose showers of electrons that are captured by a detector to form the image. Magnifications with this microscopy are limited to about 75,000 -100,000 diameters.

Scanning electron microscopic techniques were used for the accurate observation of particle morphology. In the scanning microscope, the electron gun is operated at electron energy of 20KeV with a beam diameter of 20-25 nm. A very dilute suspension of the sample in acetone was dispersed well, to avoid agglomeration, by placing it on a ultrasonic bath for 20 minutes. Then one drop of the dispersed suspension was deposited on a polished stud and the acetone was allowed to evaporate. The surface of the sample was coated with a thin gold film of 10-20 nm thick, by sputtering. This helps to remove the charging effect produced on the sample surface due to high energy beam, by earthing it. The samples were mounted in the chamber and the system is evacuated. The electron beam was scanned on the sample and the maximum magnification possible is 100,000.

A dilute suspension of the sample for SEM analysis was prepared by dispersing it in acetone using ultrasonic bath. A drop of the suspension was put on a polished stud and the dried sample was given gold coating. Then it was examined under the microscope.

Transmission electron microscopy (TEM)

TEM is an imaging technique whereby a beam of electrons (100,000 volt) is transmitted through a specimen and the image formed is magnified and directed to appear either on a fluorescent screen or layer of photographic film or to be detected by a sensor such as a CCD camera. Objects as small as 1 nm can be examined by this method and the total magnification over 20 million times can be achieved. Furthermore, the advent of high resolution transmission electron microscopy (HR-TEM) allows the direct observation of crystal structure and therefore has an advantage over other methods as there is no displacement between the location of a defect and the contrast variation caused in the image. However, it is not always possible to interpret the lattice images directly in terms of sample structure or composition. This is because the image is sensitive to a number of factors (specimen thickness and orientation, objective lens defocus, spherical and chromatic aberration), and although quantitative interpretation of the contrast shown in lattice images is possible, it is inherently complicated and may

67

require extensive simulation of the images. Computer modeling of these images has added a new layer of understanding to the study of crystalline materials.

To stimulate a measurable response from a specimen, an electron or photon beam is aimed down into the sample to be characterized. At rest, an atom within the sample contains ground state ('unexcited') electrons situated in concentric shells around the nucleus. The incident beam, however, excites an electron in an inner shell, prompting its ejection and resulting in the formation of an electron hole within the atom's electronic structure. An electron from an outer, higher-energy shell then fills the hole, and the excess energy of that electron is released in the form of an X-ray. The release of X-rays creates spectral lines that are highly specific to individual elements; thus, the X-ray emission data can be analyzed to characterize the sample in question. Energy dispersive X-ray spectroscopy (EDS or EDX) is an analytical tool predominantly used for chemical characterization. Being a type of spectroscopy, it relies on the investigation of a sample through interactions between light and matter, analyzing X-rays in its particular case. Its characterization capabilities are due in large part to the fundamental principle that each element of the periodic table has a unique electronic structure and, thus, a unique response to electromagnetic waves.

Electron Probe Microanalysis

EPMA is an elemental analysis technique which uses a focused beam of high energy electrons (5 - 30 KeV) to non-destructively ionize a solid specimen surface (including thin films and particles) for inducing emission of characteristic x-rays (0.1 - 15 KeV). The spatial resolution of x-ray microanalysis of thick specimens is limited to a volume with dimensions of approximately 1 micrometer due to electron scattering effects. This volume may be even larger for low energy emission lines that can still be excited by lower energy electrons that have been highly scattered a significant distance from the impinging beam on the specimen surface.

Quantitative matrix (inter element) correction procedures based on first principle physical models provide great flexibility and accuracy in analyzing unknown samples of arbitrary composition. Spatial distribution of elemental constituents can be visualized quantitatively by digital composition maps and displayed in gray scale or false color.

These quantitative procedures have been demonstrated to produce error distributions characterized by a standard deviation of less than 3% relative when the samples are in the ideal form of a metallographically polished bulk solid. Standards utilized in these analyses are in the form of pure elements or simple compounds (e.g., MgO or GaP). This analytical approach provides great versatility in the analysis of multi-element unknowns of virtually any composition, with the significant exception of light elements (atomic numbers less than 8). Detection limits are of the order of 100 ppm with wavelength dispersive spectrometry and 1000 ppm with energy dispersive spectrometry. Typical applications include metallurgical studies, failure analysis, thin film, particulate analysis, mineral analysis, ceramic analysis, and many others.

EPMA basically works by bombarding a micro-volume of a sample with a focused electron beam (typical energy = 5-30 keV) and collecting the X-ray photons thereby induced and emitted by the various elemental species. Because the wavelengths of these X-rays are characteristic of the emitting species, the sample composition can be easily identified by recording WDS spectra (Wavelength Dispersive Spectroscopy). WDS spectrometers are based on the Bragg's law and use various moveable, shaped monocrystals as monochromators.

2.2 Separation

Size Separation of clays

> \# Hydrocyclone

Impurity minerals

> \# Density gradient separation (Panning)
>
> \# Size separation (Hydrocyclone)
>
> \# Chemical method (Alkali treatment)
>
> \# Magnetic separation (Hand magnet)
>
> \# Reductive Bleaching (dithionite method)
>
> \# Dithionite-Citrate-Bicarbonate method

The following equipments were used for the separation studies:

1. Clay Washing Plant (Edward and Jones, UK)

2. Hydrocyclone (Mozley, UK)

2.2.1 Size separation of clay samples

The raw kaolin can be value added by employing suitable beneficiation techniques and the methods of beneficiation depend upon the quantity and nature of impurity minerals associated with it and the end use of the material. The most sophisticated wet process provides not only higher purity but enables production of a broader range of particle sizes and shapes. The general processing methods, adopted for both primary and secondary kaolins, are blunging (forming clay-water suspensions), degritting, particle size classification via hydrocycloning or centrifugation and drying. The size classification produces different grades of kaolin with varying particle size distribution. Increase in the finer fraction can result in improved brightness due to the increase in surface area and hence more light scattering sites. During sizing, coarser (quartz) and / or denser (ilmenite, rutile etc.) impurity minerals get separated The conventional size classification flow sheet is given in Figure 2.7.

The main objective of the size classification experiments is to achieve the optimum possible refinement of the clay ie., removal of the coarse impurity minerals and enrichment of the fines in the clay. In order to achieve the same, in the present study, all the clay samples (except that from Orissa) were blunged and screened though 300 μm screen (coarse desanding) and size classified using a set of hydrocyclones (ie.,for removal of medium sized impurities and enriching the fine clay). The methodology adopted for the size classification of the clays is given below.

Blunging and coarse de-sanding (> 300 μm fraction)

Blunging is the first major processing in clay beneficiation or removal of coarser impurities. During this operation, the aggregated clay-sand particles get loosened thereby achieving liberation of the clay from ancillary mineral impurities. Blunging can be done by providing mechanical energy in the form of shear agitation. De-aggregation of the clay in presence of water was done in a vertical micropilot blunger and the total slurry volume was kept fixed at 40 litres. The solid loading and time for blunging for each clay were fixed based on the grit content and viscosity of the sample.

In the present study, 30 % (w/w) slurry (clay – water suspension) of the ROM clay was prepared and was blunged (de-aggregated) using the high speed blunger (rpm - 1440) in the Clay Washing Plant for 10 minutes. The slurry was then screened though

300 μm screen and the finer fraction (< 300 μm) is taken for the further size classification.

Size separation / classification using Hydrocyclones

(i) Removal of > 45 μm fraction or de-gritting using 2"stub cyclone

Conventionally, medium desanding of the clay is done using hydrocyclone classifier keeping a separation size at about 45 μm. This size has got a lot of significance in china clay processing, since particles below 45 μm are essentially considered as "clay". To achieve separation at 45 μm, 14" diameter standard cyclones are employed in clay processing plants. Since the throughput of 14" cyclone is between 40-175 M^3/hr (40,000 – 1, 75,000 litres/hour) it is impossible to carry out separation experiments with this cyclone in the laboratory or even in pilot plants. Hence, a 2" stub cyclone, which gives a separation size nearer to that of a 14" cyclone but with very low throughput, has been used for de-sanding in this case. Stub cyclone is a short cone cyclone ie., having a large cone angle and a shorter body length.

The clay slurry after wet screening (coarse de-sanding) at 300 μm is homogenized at three levels as follows.

a.   In S.S tank (65 L capacity) using a marine propeller stirrer - by taking batches of about 40 L. This is then transferred to the hydrocyclone test rig for classification studies

b.   In hydrocyclone test rig sump – by pumping and re-circulation and finally

c.   In the sump and hydrocyclone – by pumping after introducing the slurry to the cyclone.

The size classification is carried out at following experimental conditions,

Hydro cyclone – 2" stub; % solids – 24; Inlet feed pressure: 25 psi; Vortex finder / Spigot – 14.3/4.7 mm

The fractions < 45 μm and > 45 μm were taken for further studies and a portion of <45 μm slurry was further size classified for enriching the fines.

(ii) Enrichment of finer fraction (< 2 μm fraction) using 1" hydro cyclone

The <45 μm fraction slurry obtained after 2" stub cycloning was homogenized well as mentioned above and further size classified using 1" hydro cylone (narrow sized cyclone having longer body length) for further enrichment of the fines. The experimental

71

conditions were chosen so as to get a separation cut size of 2 μm. The following are set experimental conditions for the same.

Hydrocyclone – 1 inch; % solids – 15; Inlet feed pressure: 55 psi; Vortex finder / Spigot – 7.0/3.2 mm

The classification of the clay by the 2"stub, and 1"hydro cyclones was carried out at specific experimental conditions so as to achieve maximum efficiency of separation (Table 1). The final product of size classification (FSCP) was the dried sample from the overflow slurry of the 1"hydrocyclone separation

Dewatering and drying

At every stage of size classification, part of the product slurry was dewatered and dried for further characterization. The slurry was kept for a few hours so that maximum solids settled at the bottom. The supernatant portion was decanted; the concentrated slurry was taken in a S.S tray and dried on a water bath to get the dried material.

Koraput clay

The china clay from Orissa was found be acidic in nature due to the presence of pyrite particles. Wet processing of acidic clay is extremely difficult, as it will corrode the metallic parts of the processing equipments. It was observed that most of the pyrite particles in this clay were present in the coarse size range (>45 μm). When the clay was mixed with water for carrying out the wet processing as per the general method, the slurry color changed to yellowish brown and the product clay was found to be yellow in color. The optical properties were found to be inferior to those of the raw clay. Hence, a detailed study was conducted on this clay and a modified process was established for getting a good product. Chapter 7 gives the details of this study.

2.2.2 Impurity minerals

The physical methods for separating the "Fe-rich" minerals are based on the particle size, density and magnetic properties of the impurities. Coarse minerals like quartz, feldspar etc are removed to a great extent during size classification. However, ferruginous, titanoferrous, carbonaceous and micaceous minerals generally exist in finer fractions also which influence the properties of clays for most of its applications. Depending upon the species, techniques for their removal are to be selected. Impurities separated / concentrated by various methods are characterized for their identification and

quantification. They include (1) the underflow solids of hydrocyclone classification, (2) the insoluble portion during the 5M NaOH treatment, (3) the impurity minerals separated by panning and (4) using hand magnet to concentrate only ferro/ferri magnetic materials. The response of clays to the DCB treatment needs special mention since it gives information on the soluble iron minerals in the clays. DCBT is the well-known technique for dissolving and separating the "free" iron in solids and clay minerals. The iron minerals like oxides, hydroxides, oxy hydroxides, carbonates, sulphides etc. dissolve during DCB treatment and can be easily removed and hence termed as "free" iron. Iron present in the structural framework of kaolinite or other minerals like mica, anatase, feldspar etc. is not extractable and hence termed as "structural". Even though the latter type of iron does not generally influence the clay brightness, concentration above a certain limit impart slight coloration to the clay. The iron oxides and oxy hydroxides are often poorly crystalline in nature and present at low concentrations in soils and clays samples (Kampf & Schwertmann, 1982). Hence, the impurity has to be concentrated for characterizing the 'Fe" phases by X-ray diffraction and spectroscopic techniques.

Concentration of impurity minerals by panning

Panning is a combination of water washing and density separation employed to remove kaolinite and quartz and to enrich ancillary minerals. Here the impurity minerals are separated / concentrated based on their density gradient and is well suited method for the concentration of Fe-containing minerals. Concentration of coarser as well as the finer impurity minerals is carried out by this method. A dilute suspension (10% w/w) of the ROM clay was prepared in distilled water and it was stirred well with a low speed mechanical stirrer. Most of the clayey portion was removed by decantation method after washing it with distilled water several times. When it is free from clayey matter, the denser impurity minerals are then separated by panning

ROM clay ⟶ Slurrying ⟶ Stirring (de-aggregation) ⟶ Settling of heavies

Decanting of clayey portion ⟶ water washing ⟶ Wet panning of the
3 times   heavies (to remove quartz)

73
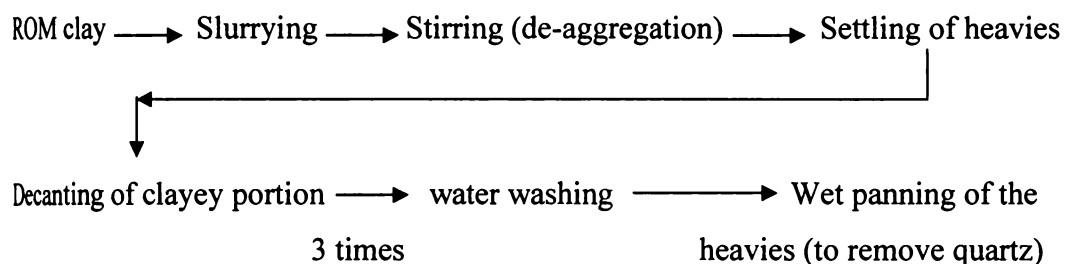
Concentration of impurity minerals using 2" stub hydrocyclone

The impurity minerals having particle size between 300 and 45 μm are separated in the underflow of 2" stub hydrocyclone and quartz is the major impurity removed by this technique. The methodology adopted has been described under 2.7.2.2. The iron minerals of this particle size range also accompany the coarse quartzite minerals.

Concentration of impurity minerals using hand magnet

The samples were washed with acetone and dried in an air oven at 200°C for 12 hours and the magnetically susceptible impurities were separated using a hand magnet.

Concentration of "Fe-oxides" by 5M-NaOH treatment

Identification and quantification of iron oxides in kaolin is very difficult due to their poor crystallinity and low concentration.The Fe-oxides are concentrated by treating the clay with reagents like NaOH and Na_2CO_3. During this treatment, siliceous and aluminous cements, which frequently bind the kaolin particles into aggregates get dissolved and clean up the crystalline compounds, thereby assisting their separation. A high ratio of dissolution reagent to sample weight ensures much better dissolution and avoids saturation of the solution with Si and Al.

The product sample after size classification with 2" stub hydrocyclone (ie., < 45 μm fraction) was subjected to 5M-NaOH treatment. One gm of the sample was mixed with 100 ml of 5M NaOH solution in a 150 ml teflon beaker and the contents were boiled for 60 minutes in a heating mantle. It was then cooled, centrifuged and the supernatant liquid was decanted. The residue was subsequently subjected to a set of washing, centrifuging and decanting ie., once with 25 ml 5M NaOH, twice with 0.5 M HCl (20 minutes contact time) to dissolve the sodalite, twice with 25 ml of 1N $(NH_4)_2CO_3$ to remove NaCl and finally twice with 25 ml dist. water to remove NH_4 and CO_3. The residue was then heated for 12 hours in an air oven at 110°C. The above experiment was repeated many a times (15 times) to get an appreciable quantity (~ 1 g) of Fe-oxides. This method was developed by Norrish and Taylor in 1961 and later modified by B.Singh & Gilkes, 1991 to improve its efficiency.

Reductive bleaching

Bleaching is the processing of whitening a substance through chemical action. It makes color bodies in the substance more soluble and therefore easily removable during

processing. Bleaching can also involve chemical processes that change the ability of the color bodies to absorb light by changing their degree of unsaturation. Sodium dithionite ($Na_2S_2O_4$), commonly known as 'hydros', is the universally used reducing / bleaching agent in china clay processing.

The ferric iron in the clay is reduced to ferrous state by sodium dithionite in acid medium. The latter being more soluble can be removed by filtration and washing. The optical properties like brightness and color values of the clay before and after bleaching are measured and the "bleach response" of the clay is indicated by the change in these properties. There is a disproportionation reaction occurring to the dithionite ion at first

$$S_2O_4{}^{2-} + Fe_2O_3 + 4H^+ \longrightarrow 2HSO^{3-} + 2Fe^{+2} + H_2O$$
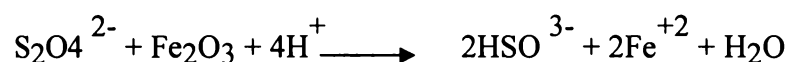
Which is negligibly slow above pH 7.0? The rate of this reaction increases with decreasing pH and the most suitable value is found to be between 2.5 and 3.0.

Nearly 20g of clay (FSCP) was added to 80 ml of double distilled water. The slurry was stirred in a beaker using a magnetic stirrer and its pH was measured. The pH of the slurry was adjusted to 2.5-3.0 by the drop wise addition of dil. H_2SO_4. About 0.06 g (3kg per ton) of sodium dithionite (hydros) and 0.5 ml a 10% solution of of tri sodium phosphate were added to the slurry. After slow stirring, the slurry was kept for about 30 minutes. The clay was then filtered and washed thoroughly till free of iron. The product clay was dried first on a water bath and then in an air oven at ~110°C. The optical properties of the dry products were measured and compared with those of the feed clay for bleaching.

Dithionite-Citrate-Bicarbonate Treatment (DCBT)

DCB treatment is a well established method used to quantify the 'free' and the 'structural' iron content in clays. The beneficiated products ie., the final size classified product (FSCP) of all the clays were subjected to DCBT adopting the method given by Mehra and Jackson (1960) as given below.

$$4OH^- + S_2O_4{}^{2-} \longrightarrow 2SO_3{}^{2-} + 2H_2O + 2e$$
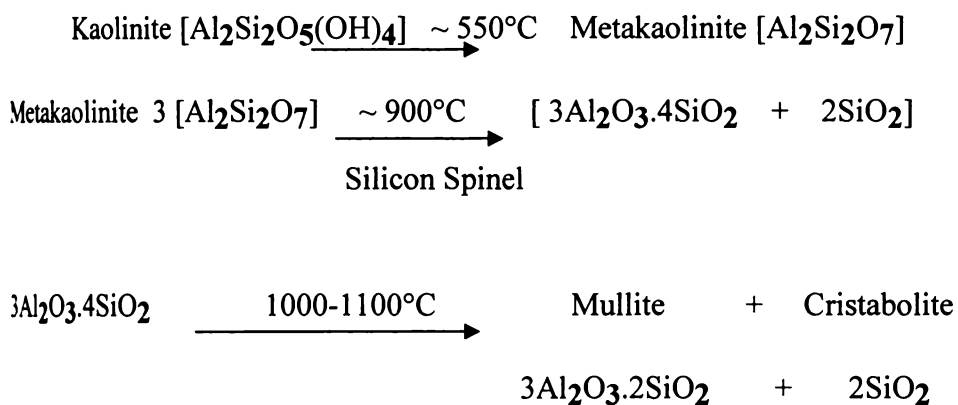
$$2Fe^{+3} + 2e \longrightarrow 2Fe^{+2}$$
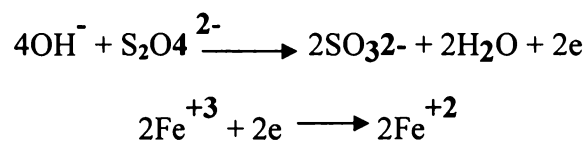
To 25 gm of the clay sample taken in a 250 ml beaker, 100 ml of 0.3 M sodium citrate solution (pH-5.1) and 10 ml of sodium bicarbonate (8.4g/100ml) was added and

75

the contents were mixed manually. It was then immersed in a water bath and heated to ~ 75°C. Then 1 gm of the reducing agent ie., sodium dithionite was added to the reaction mixture, mixed well and the beaker was kept closed for 5 minutes with occasional manual stirring. After 5 minutes, one more gram of the reducing agent was introduced into the reaction medium and the contents were kept closed for another 10 minutes with occasional stirring. The temperature of the reaction mixture was kept at 75-76 °C through out the experiment, which was monitored using a continuous digital temperature recording set-up. After the reaction, the contents were cooled and 10 ml of saturated NaCl solution and 10 ml of acetone were added. It was then filtered, washed with distilled water till free from Fe^{2+} ions [the same was confirmed by checking with acidified (with dil.HCl) potassium thiocyanate solution] and dried. The DCB treatment was carried out three times on the same sample to check the maximum removal of iron.

2.3 Calcination

Calcined clay has got a lot of demand in the clay based industres due to its improved properties, especially due to high brightness value. Heating of the clay at 550 °C produces the meta kaolin and on further heating it gets transformed into silicon spinal at 900 °C and finally to mullite and cristabolite at 1000-1100°C. The changes in kaolinite during thermal treatment are as follows.

Kaolinite $[Al_2Si_2O_5(OH)_4]$ $\xrightarrow{\sim 550°C}$ Metakaolinite $[Al_2Si_2O_7]$

Metakaolinite 3 $[Al_2Si_2O_7]$ $\xrightarrow{\sim 900°C}$ $[3Al_2O_3.4SiO_2 + 2SiO_2]$

Silicon Spinel

$3Al_2O_3.4SiO_2$ $\xrightarrow{1000-1100°C}$ Mullite + Cristabolite

$3Al_2O_3.2SiO_2 + 2SiO_2$

Calcination of the washed samples (fraction <45μm) was carried out and the optical properties of the products were tested for their suitability as pigments. The heating of the clay sample (~ 50 g) was done in a programmable furnace at 1100°C with a heating rate of 6°C / minute. The bed thickness of sample was kept as 1 cm and the temperature was

maintained for one hour. The sample was then cooled; powdered and optical properties were measured.

References

1 Bennett H and Reed R.A. (1971) Chemical methods of silicate analysis. A handbook Academic Press Ind., London, 272 pp.

2 Brindley G.W. and Brown G. (1980) Crystal structure of clay minerals and their X-ray identification. In: Monograph, Mineralogical Society, London, 495

3 Gross M.G. (1971) Carbon Determination, In Procedure in Sedimentary Petrology, Eds. Robert E., Carver. Wiley Interscience, 573-596

4 Groves A.W.(1951)Silicate Analysis, Allen and Unwin, London

5 Hillebrand W.F., Lundell G.E.F., Bright H.A. and Hoffman J.I.(1953) Applied Inorganic Analysis, John Wiley, New York

6 Hinckley D.N.(1963) Variability in "crystallinity" values among the kaolin deposits of the coastal plane of Georgia and South Carolina, Clays and Clay Minerals, 11, 229-235

7 IS 505,1995 Specifications for light kaolin

8 Jeffery et al G.H., Bassett J., Mendham J. and Denney R.C.(1989),Vogel's Text book of Quantitative Chemical Analysis, 741, John Wiley and Sons, USA

9 Lundell G.E.F and Hoffman J.I. (1938) Outlines of Methods of Chemical Analysis, Wiley, New York

10 Robertson R.H.S., Brindley G.W. and MacKenzie R.C. (1954), Mineralogy of kaolin clays from Pugu, Tanganyikka, Americal Mineralogist, 39, 18-139.

11 Shapiro L. and Branock. (1952). Rapid analysis of silicate rocks, US Geological Survey Circular, 165, 17.

12 Schneider J.W., Schneider K., 1990. Indirect method for the determination of pyrite in clays and shale after selective extraction with acid solutions, Ceramic Bulletein, 69, 107-109

13 Wilson M. J. (1966) The weathering of biotite in some Aberdeenahire soils. Mineralogical Magazine, 35, 1080-1093

Table 1 Details of the experimental conditions set for the size classification of kaolin samples at different size ranges

| Sl. No. | Sample | Blunging | | Size Separation | | |
		Percent Solids	Time	Percent Solids	Feed inlet Pressure (Psi)	Vortex Finder/Spigot (mm)
1	Kasargod-1 clay Blunging 2" Stub cycloning 1" cycloning	35	10	 30 12	 25 60	 14.3/4.7 7.0/2.2
2	Kasargod-2 clay Blunging 2" Stub cycloning 1" cycloning	45	10	 20 12	 25 60	 14.3/4.7 7.0/2.2
3	Trivandrum clay Blunging 2" Stub cycloning 1" cycloning	35	10	 19.0 14.8	 25 60	 14.3/4.7 7.0/2.2
4	Kutch clay Blunging 2" Stub cycloning 1" cycloning	35	10	 18.0 14.8	 25 60	 14.3/4.7 7.0/2.2
5	Bankura clay Blunging 2" Stub cycloning 1" cycloning	35	10	 27.0 16.1	 25 60	 14.3/4.7 7.0/2.2
6	Pali clay Blunging 2" Stub cycloning 1" cycloning	35	10	 19.0 14.8	 25 60	 14.3/4.7 7.0/2.2
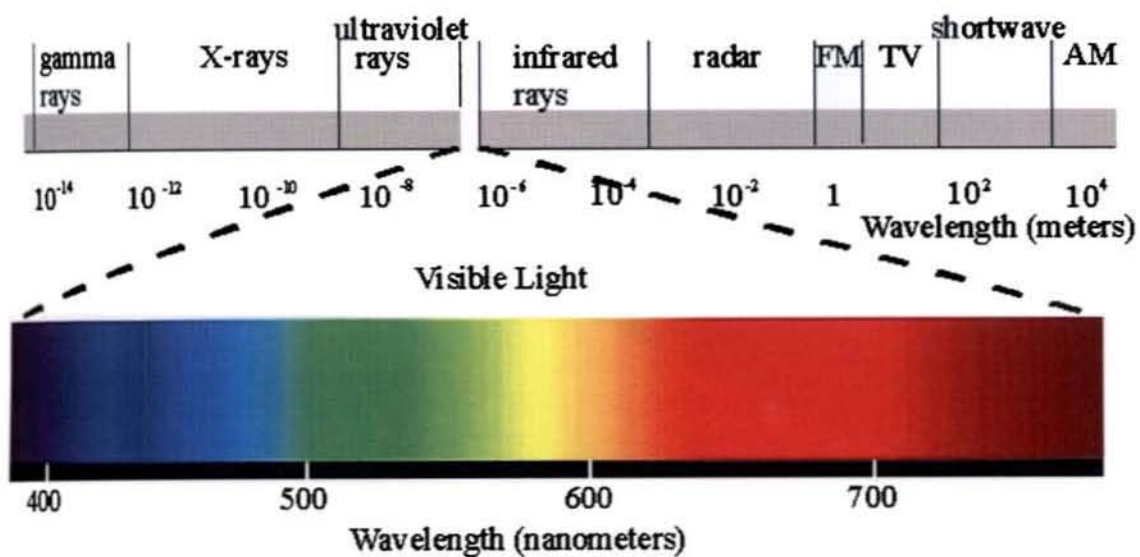
Figure 2.1 Electromagnetic spectrum
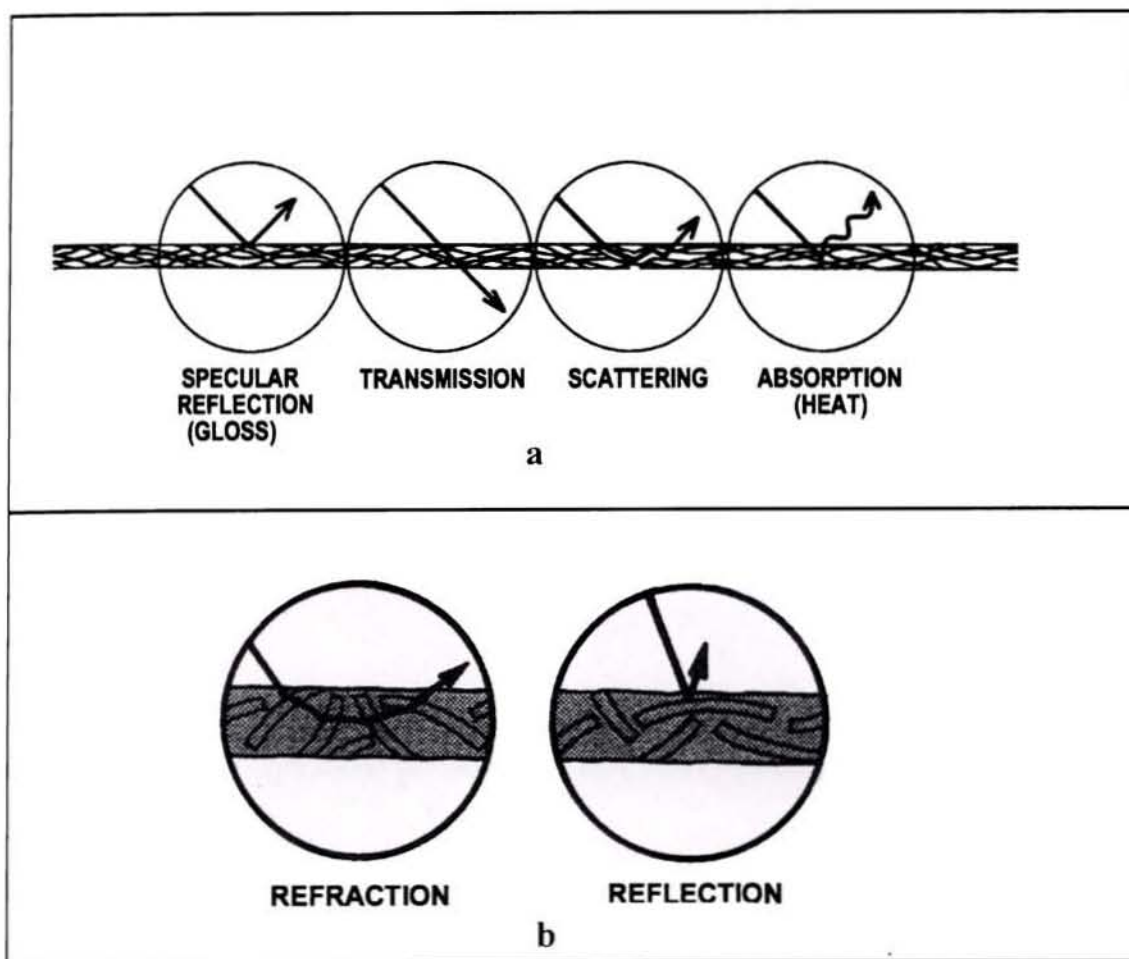
Figure 2.2a and 2.2b Behaviour of light striking the paper
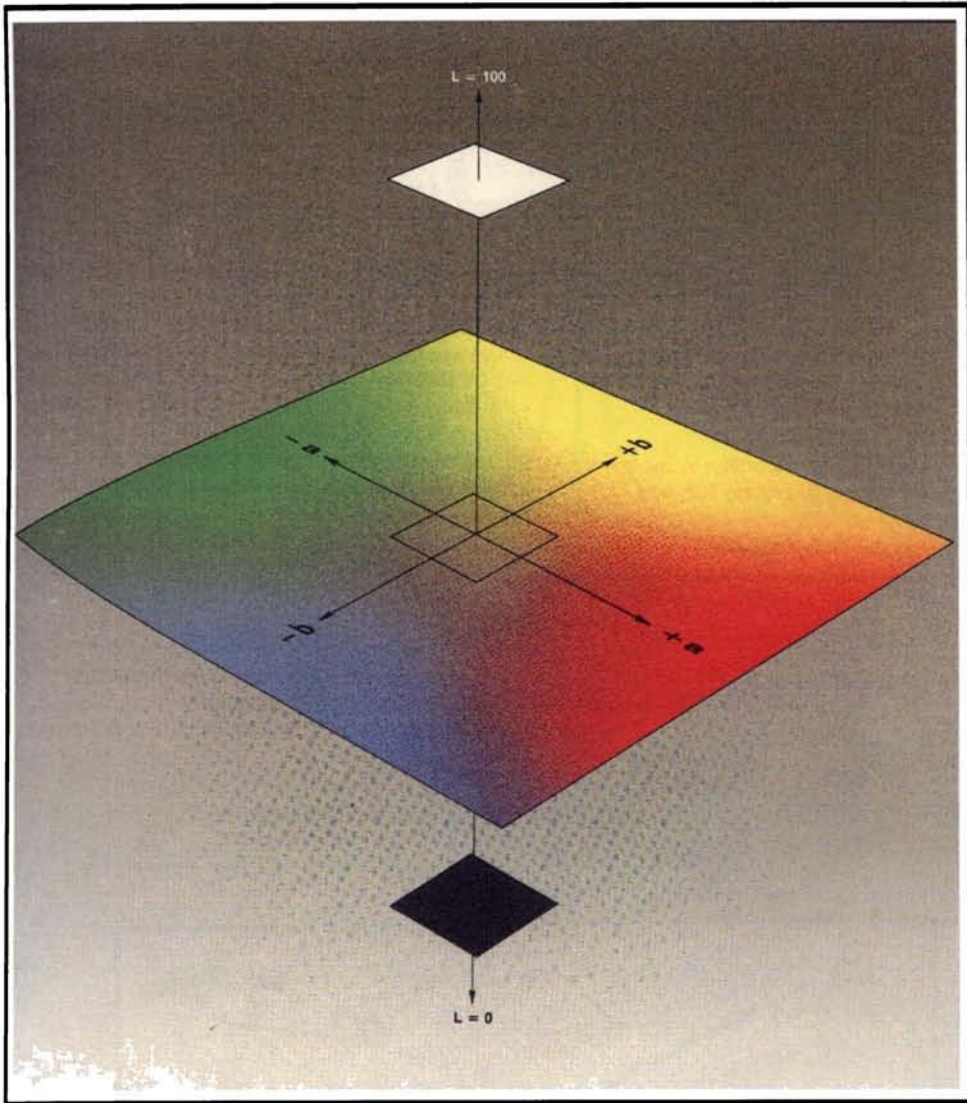
Figure 2.3   L,a,b colour co-ordinates
(Courtesy : M/s. Technidyne Corporation, USA)
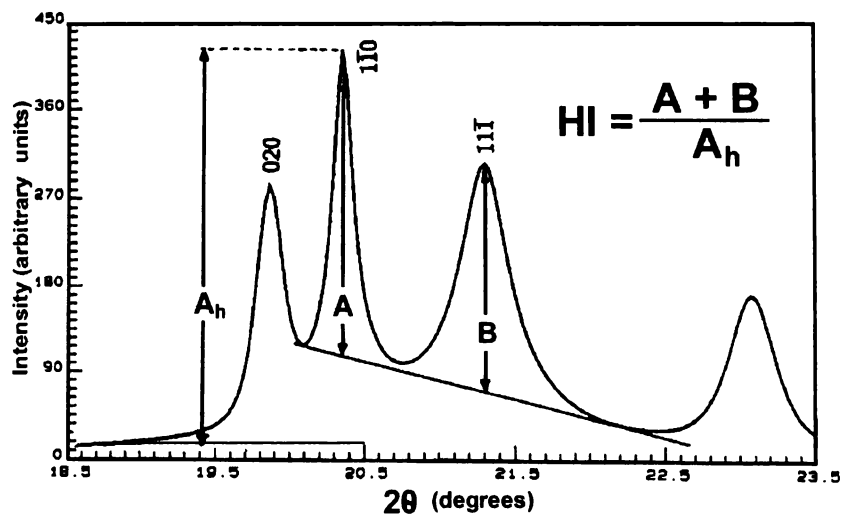
$$HI = \frac{A + B}{A_h}$$

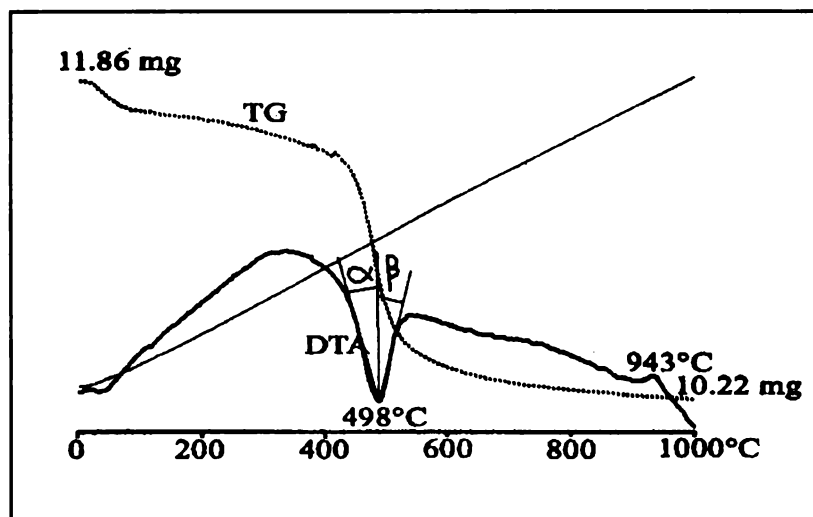**Figure 2.4a Calculation of Hinckley Index**

Figure 2.4b Calculation of Slope ratio from DTA
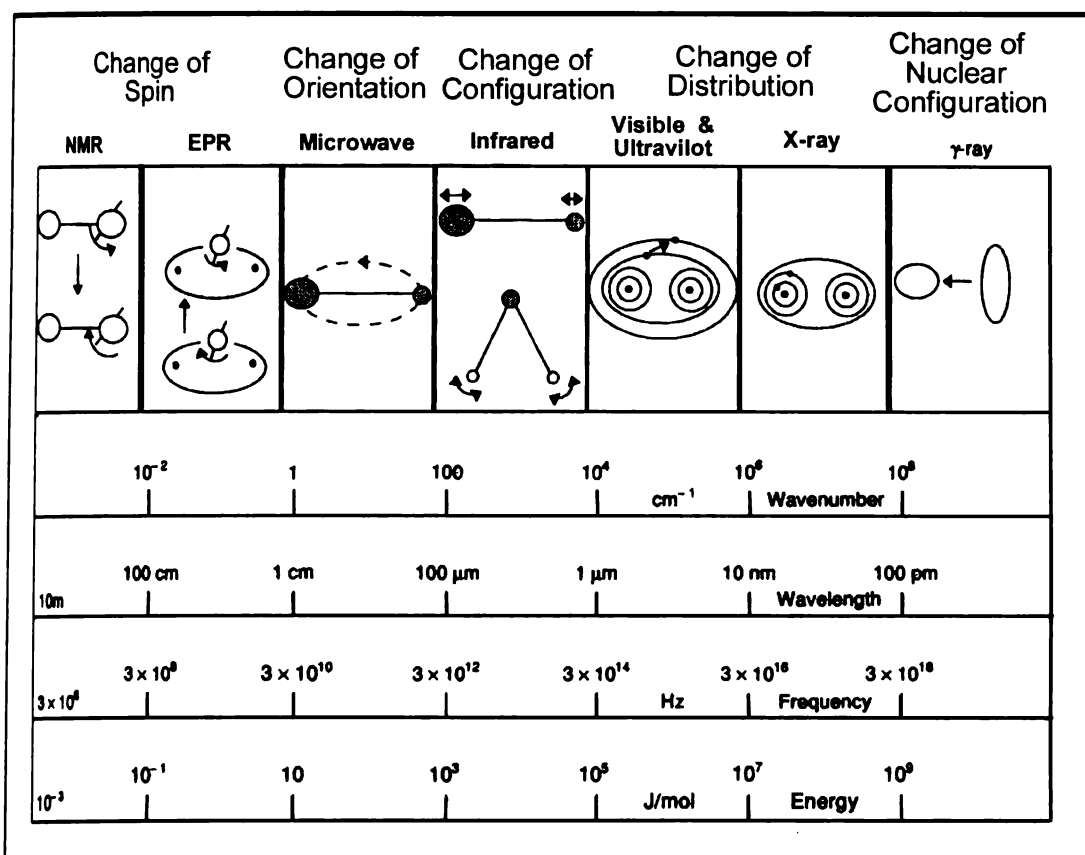
Figure 2.5 The electromagnetic spectrum and corresponding spectroscopic techniques

$$\delta = E_a - E_s$$
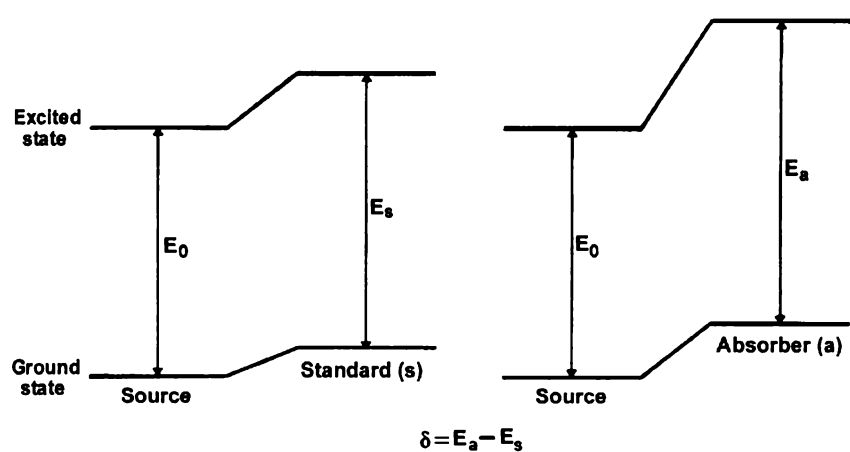
Figure 2.6 Diagrammatic representation of the electronic monopole

ROM Clay

$\downarrow$

Size Reduction (~1 inch size)

$\downarrow$

Mixing (Blending)

$\downarrow$

Blunging/De-aggregation

(Mixing with water + stirring at high rpm)

$\downarrow$

Screening at 300 μm

$\downarrow$

Size Separation with different cyclones (at 45 & 2 μm)

$\downarrow$

Dewatering & drying of the product samples
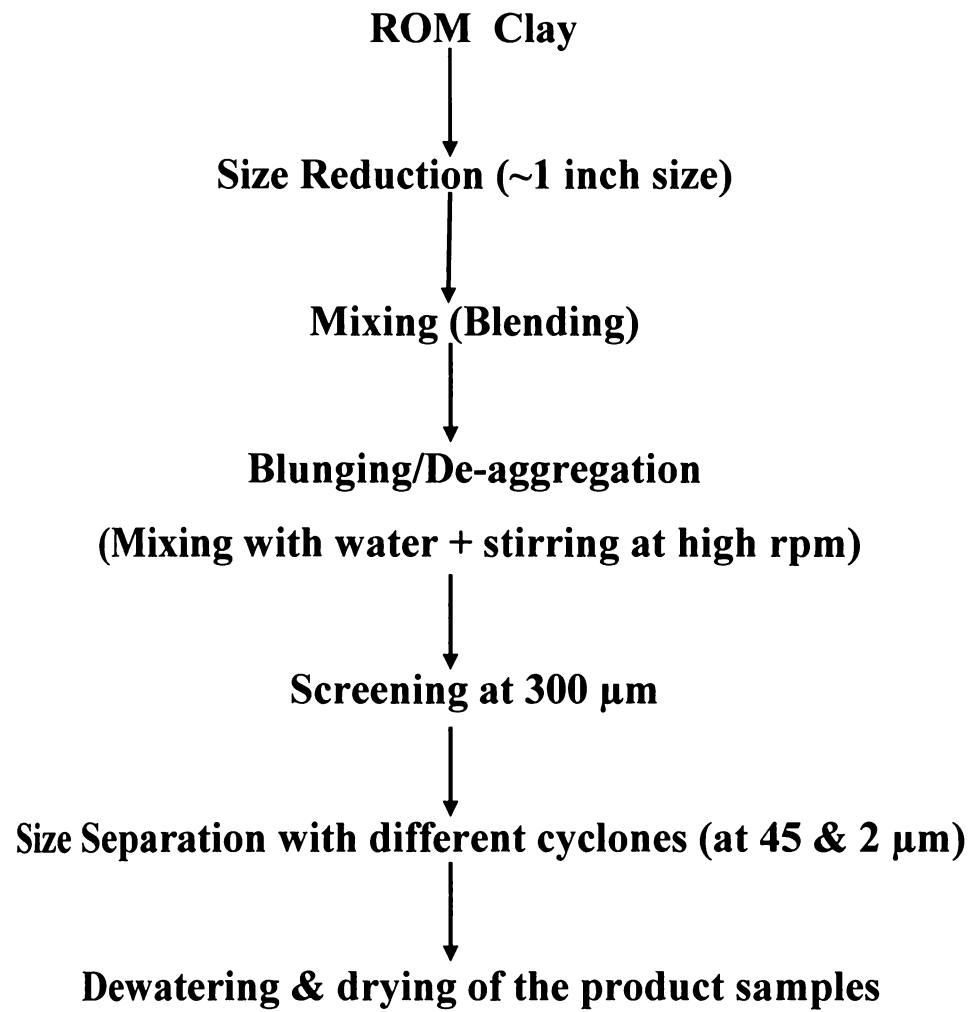
Figure 2.7 Conventional size classification flow sheet for china clay

CHAPTER 3

CHARACTERIZATION AND POSSIBLE VALUE ADDITION
OF THE KAOLINS

Kaolin or china clay is one of the most important "white" minerals and for most of its applications, the clay has to be characterized for its physical, chemical, mineralogical and morphological properties and then value added by suitable processing techniques. Highest value is achieved for paper coating and pigment (in paper and paint) grade products for which superior optical properties and fine particle size are essential. Quartz and parent rock minerals are present in the kaolin mostly in coarse size and the main coloring impurities are ferruginous, titanoferrous, micaceous and carbonaceous minerals. All these impurities are to be removed to achieve specific particle size and good brightness. Kaolin calcined at ~1100°C is used in paper and paints as pigment and as reinforcing material in polymers and plastics.

Identification and quantification of the impurities plays an important role in the selection and sequentialisation of beneficiation processes. Modern techniques for achieving stringent specifications for kaolin are still largely alien to India even though the country has got a vast reserve of this mineral resulting in the underutilization of this non-replenishable resource. The main reason is the difficulty in the speciation of all impurity minerals and lack of technical knowledge on modern beneficiation methods. The modernization will result in better quality processed china clay thereby achieving more value added consumer end products. This will also help in utilizing the marginal / submarginal deposits of the country and reducing or even stopping the imports. Tremendous potential exists for the bulk export of the processed clay to Japan and other Asian countries and also to Europe. Only technological up gradation can make us globally competitive. In this context, a comprehensive study of the major clay deposits of the country is highly relevant.

The present chapter deals with the detailed investigations as given below on kaolin samples from seven major deposits of five states of India.

1. Details and location of the mines

2. Physical, chemical, mineralogical and morphological characterization of the raw clays

3. Beneficiation of the clays by physical and chemical methods such as (a) size classification to enrich the finer fraction and to remove the coarse impurity minerals (b) chemical leaching of the product clay using sodium dithionite for removing the iron impurities and (c) calcination of the < 45 μm fraction samples at 1100°C to test for its application as pigment and in polymers / plastics.

4. Characterization of the beneficiated clays for their relevant properties

5. Comparison of the properties of the beneficiated samples with the International and Indian Standard specifications for various industrial applications.

Details of the samples taken for the present study are given in Table 3.1 and the locations of the mines are marked in the Figure 3.1. Specifications for kaolin for some important industries are also given in this chapter. Comparison of the properties of the samples with the required specifications gives information on the utilitarian aspects of these clays as well as the level of beneficiation to be carried out for each sample.

3.1 Kaolin from Kasargod district of Kerala (Kasargod 1)

3.1.1 Physical properties

The raw clay has a dirty white color, indicating the association of colored impurities. It is easily slaking in nature and has a near-neutral pH (5.63). Specific gravity of the sample is 2.66 which is slightly higher than that of "kaolinite" mineral. The size classified products have lower values almost matching with that of ideal kaolinite (2.6). Small quantities of heavy minerals may be present in the clay and are possibly getting removed during size classification. The matter soluble in acid and water in the raw clay is low and changes marginally in the products of size classification.

The cation exchange capacity of the raw clay is 8.41 meq/100g which falls in the range of values for kaolins (1-15) in general. Cations due to their positive charge are attracted to negatively charged surface of the clay. In kaolinite, the charge is primarily due to the dissociation of the hydroxyl groups and is pH dependent. In strongly acidic clays, the Al-OH polymers adsorbed on the negative exchange sites forms source of pH dependent charges. A higher pH value gives rise to more negative charges which lead to a higher CEC. The cation exchange capacity depends on the amount and type of organic matter and clay apart from its pH dependence (Brady and Weil 1996). The charge on clay minerals is variable and influences the exchangeable ions in solution. A low pH

causes protonation and a positive charge is formed on the surface of the clay minerals (Froth and Ellis, 1996) resulting in low CEC. Generally kaolinites have CEC values in the range 1-10 [Chi Ma & Eggleton, 1999]. Table 3.1.1 gives the general properties of the clay and its beneficiated products.

Particle size distribution analysis of the raw clay shows that the grit content is not high, ~ 10%, but the fines are relatively less (the fraction < 2μm is only 35%). Screening and separation using 2"stub hydrocyclone has resulted in marginal decrease in < 45 μm fraction (from ~ 54.90% to 56.10% along with an increase in the < 2 μm fraction (35.0 % to 43.90%). Further sizing with 1" hydrocyclone is found to enhance the < 2 μm fraction to 62.10 %. The size distributions in the raw and processed samples are given in Table 3.1.1. The variation in the fine fraction during size classification processes is depicted in Figure 3.1.3.

The optical properties of the raw clay are found to be poor. The relatively low lightness (L) and Hunter Whiteness (HW) values indicate the presence of dark/black colored impurities in the sample. At the same time, the color values "a" (redness), "b" (yellowness) and Hunter Yellowness (HY) are found to be high indicating the presence of reddish/yellow impurities in the clay. Size classification increases the brightness of samples only marginally ie., by 3.2 (in SCP1) and 3.48 (in SCP2) units. Though there is a 2.2 unit improvement in the L value of SCP1, only a marginal improvement of the same is observed in the case of SCP2. The reddishness of the material also does not get reduced appreciably during size classification and is evident from the "a" values. But there is slight decrease in the yellowness of SCP1 and SCP2 as indicated by the HY and "b" values. The improvement, even though very small, in the optical properties of the samples may be due to the removal of some of the coarse colored impurities. The marginal reduction in the Fe_2O_3 content of SCP1 and SCP2 also supports the same. Optical properties, % Fe_2O_3 and % TiO_2 values of ROM are given in Table 3.1.1 and those of beneficiated samples in Table 3.1.3. For pigment grade kaolin, brightness should be >80% ISO and beneficiation to achieve this level is one of the challenging tasks in kaolin beneficiation.

The conventional reductive ('hydros') bleaching removes only very small amount of 'Fe' from SCP2. The brightness improvement is also marginal (~ 0.22 units). After the

86

reductive bleaching, only a marginal improvement in the L and HW values and a small reduction in "a"," b" and HY values are observed. This indicates the ineffectiveness of the method to remove the "free" iron to a greater extent. "Structural iron" is the iron substituted in the structure of kaolinite and / or the ancillary minerals like anatase, mica etc. and are not easily leachable. The DCB method (Mehra and Jackson, 1960) removes the free iron oxides with a minimal effect on the crystalline clay and this extractable iron is a fair estimate of pedogenic iron oxides in soils and kaolins (Ole K.Borgaard, 1988). The brightness improvement obtained for the sample SCP2 is almost same for 2nd and 3rd DCB treatments. So the SCP2 sample subjected to two successive treatments is taken as the DCBT product. The brightness is increased by ~8.6 units with a decrease in % Fe_2O_3 from 0.70 to 0.50 indicating that part of the iron in the sample is "free" and leachable. The brightness/whiteness of kaolin is dependent on the overall effect of the "**Lab** " color values. It has been established that the "free iron" is more soluble than the "structural" iron and hence the former is more easily removed by chemical leaching. The "**L**" value of the sample increases on DCB treatment by 2.9 units. The "**a**" value (reddishness) of the sample comes down from 0.91 to 0.32 units indicating the removal of most of the "free" reddish iron oxy hydroxides. Similarly, the "**b**" and HY values are also found to decrease substantially from 3.74 to 1.12 and 5.65 to 1.70 units respectively confirming the decrease in yellowness.

The brightness, L and HW values of SCP1 are found to decrease on calcination. The decrease in "**L**" and HW values indicates the formation of a dark shade on the kaolin during calcination. During the heat treatment, the structure of kaolinite and other minerals breaks down and the iron gets liberated and oxidized to colored oxides, thereby reducing the brightness of the clay. Incidentally, the "**a**" and "**b**" color and HY values of the sample are also found to increase after calcination. Optical properties of the benficiatd products are given in Table 3.1.3.

3.1.2 Chemical assay

The chemical constituents in the raw and beneficiated samples are given in Table 3.1.1. Theoretically, "kaolinite" contains 46.51% SiO_2, 39.54% Al_2O_3 and 13.95% LOI. The silica content in the raw clay is slightly higher and LOI is lower which indicate the presence of "free" silica. Sample SCP1 is found to be more kaolinitic and is evident from

be increased Al_2O_3 content. This shows that 2" stub cycloning has removed the coarse silica particles and enriched alumina in the clay. The LOI value of SCP1 has also increased to almost that of ideal kaolinite, indirectly indicating the removal of silica. But the silica content in the sample SCP2 is slightly higher than that in SCP1 and this may be due to the enrichment of fine silica particles in this particular size region. A marginal increase in the alumina content and LOI supports the same. DCB treatment has produced no change in the chemical assay other than removing part of the iron. This confirms that the aluminium silicate framework of kaolinite mineral is not disturbed by this treatment. It is seen that size classification has produced a marginal decrease in the Fe_2O_3 and TiO_2 content of the samples SCP1 and SCP2 indicating partial removal of denser impurity minerals Figure 3.1.4. The presence of appreciable quantities of Fe_2O_3 (~ 70% of that in ROM) in SCP2 indicates the ultra fine size of the 'Fe' impurities which are retained in the product during size separation. Incidentally, ~ 70% reduction in titania content is observed in SCP2.

Reductive bleaching is found to be ineffective in removing the iron and is evident from the marginal decrease in the Fe_2O_3 content in SCP2 after bleaching. But after DCB treatment, the Fe_2O_3 has come down from 0.70 to 0.50 % and the optical properties are enhanced. The extent of iron removal shows that significant amount of iron in the clay is "free" in nature (ie., as separate iron minerals such as oxides, hydroxides, oxy-hydroxides) and the rest is present in the structure of either kaolinite or ancillary mineral (mica or titania). Also, the sharp decrease in the "a", "b" and HY values, corresponding to the reddish and yellow shade of the material, confirms the removal of the coloring iron impurities such as hematite and goethite. The marked improvement in the optical properties of SCP2 DCB treated product shows that most of the "free" iron is removed and the remaining is in the structure which does not affect the brightness of kaolin. It is also worth mentioning that chemical leaching has not effected any changes in the TiO_2 content. The variation of Fe_2O_3 and TiO_2 content during beneficiation is represented in Figure 3.1.4.

Other impurity minerals of Na, K, and Ca are present only in low concentrations. Their presence in the finer size fractions indicate that they are almost uniformly distributed in all size fractions. Results of the trace elements analysis of the clay is given

in Table 3.1.2. No toxic elements are detected in the clay and the concentration of certain elements such as Mg, Ba, Cr, S, P, Zn and Ni are found to be relatively high. However, the concentrations of all these elements are found to decrease in the products of size classification. DCB treatment is found to remove some of the trace elements like Mg, Zn, Ba, Cr, Mn and Ni appreciably and some of them like As, Bi, Cd, Co, Cu, and Pb) marginally. The properties and distribution of iron oxides and their association with minor elements in soils have been studied [Singh and Gilkes, 1992]. They have observed that most of these elements are concentrated with the iron oxides and their dissolution kinetics in 1M HCl indicate that some may be present in the structure of the iron oxides. A similar dissolution phenomenon is possibly taking place for certain elements during the DCB treatment also.

3.1.3 Mineralogical study

X-ray diffraction and thermal analyses give mineralogy of the clay. In XRD studies, the d values of various peaks are characteristic of various minerals. The major three peaks of kaolinite and the ancillary minerals commonly found in kaolin are represented in Table 3.1.4. The XRD analysis data of the ROM and beneficiation products is given in Table 3.1.1 and the powder patterns are represented in Figure 3.1.1. The major peaks of kaolinite and the ancillary minerals commonly found in kaolin are given in Table   In the raw clay, kaolinite is found to be the major mineral along with quartz, hematite, anatase and rutile as the ancillary mineral impurities. An increase in the intensity of the kaolinite peaks and a decrease in the intensity of quartz peak in the XRD patterns of SCP1, SCP2 and SCP2 DCBT clearly show the enrichment of kaolinite in the sample during the size classification.

Thermal analysis data for kaolinite and ancillary minerals in kaolin is given in Table 3.1.4 which includes the temperatures at which the characteristic endotherms and exotherms are formed (DTA). TGA of the ROM sample shows that the total weight loss on heating is ~12.3%, which is near to that of the kaolinite mineral. The weight loss in the range 450 to 600°C corresponds to the dehydroxylation of kaolinite. The total weight loss on heating increases to ~14.60% in both the SCP1 and SCP2 samples which is near to that of the kaolinite mineral. The DTA patterns of the samples give endotherms and

exotherms which are characteristic of kaolinite mineral. Table 3.1.1 gives the TGA and DTA data of the samples.

Rational analysis data calculated from the chemical assay also indicate the mineralogical picture of the samples. Table 3.1.5 gives the percentages of possible minerals in "Kasargod 1" kaolin as calculated from the chemical assay. The rational analysis data shows that the ROM sample contains kaolinite as the major mineral along with small amounts of quartz, micaceous minerals (both muscovite and paragonite mica), hematite and anatase. In the size classification products, the kaolinite content increases with a simultaneous decrease in other minerals (especially mica) supporting the XRD findings. Figure 3.1.3 shows the variation in kaolinite content during the beneficiation processes.

3.1.4 Morphological characterization

Scanning electron microscopic analysis (SEM) pictures of the ROM and SCP1 samples are presented in Figure 3.1.2, which shows the presence of aggregates of pseudo hexagonal kaolinite particles.

3.2 Kaolin from Kasargod district of Kerala (Kasargod 2)

3.2.1 Physical properties

The ROM clay is soft, easily slaking and its natural pH is 5.21 units (almost neutral). It has a dirty pink color which indicates the presence of colored impurity, probably Fe minerals. Specific gravity values of the sample (2.63) is near to that of kaolinite mineral (2.6) The specific gravities of the size classified product samples are found to be slightly less and they perfectly match with that of ideal kaolinite. The matter soluble in acid and water are also getting reduced marginally during size classification. The cation exchange capacity of the raw clay (9.97 meq/100g) was found to be in the range of values reported for natural kaolins (Table 3.2.1).

The particle size distribution analysis of the raw clay show that the grit content is medium (36.8%) and the fines are relatively less (fraction < 2μm is only 26.83%) in the sample. Screening and separation using 2"stub hydrocyclone has resulted in appreciable increase of < 45 μm fraction (from ~ 36.37% to 54.30%) along with sharp increase in the <2 μm fraction (26.83% to 45.70%). Further sizing using 1" hydrocyclone is found to enhance the <2 μm fraction only upto 59.30 %. The size distribution in the raw and

90

processed samples is given in Table 3.2.1 and the variation in <2μm fraction is depicted in Figure 3.2.3.

The optical properties of the raw clay are found to be poor. The lightness, L (80.12%) and HW (~49%) values are low, indicating the presence of colored impurities. The colour values, "a" (3.33), "b" (5.30) and HY (8.05) are on a higher side confirming the presence of reddish and yellow coloured impurity minerals in the clay. Optical properties, % Fe_2O_3 and % TiO_2 values of ROM and beneficiated samples are given in **Table 3.2.1 & 3.2.3**. For pigment grade kaolin, brightness should be >80% ISO and beneficiation to achieve this level is one of the highest value additions of kaolin. Size classification increases the brightness of samples by 6.1 (SCP1) and 7.0 (SCP2) units. The "L" values of both the samples, SCP1 and SCP2 are found to increase by ~5 units, but there is no significant improvement in the HW values. The increase in the "L" value indicates the removal of materials, which imparts black shade to the clay. It is seen that, the reddishness ("a" value) and yellowness ("b" and HY) of the material has come down marginally during size classification. The improvement in the optical properties of the samples is due to the partial removal of the coloring impurities which are coarser in size. The marginal reduction in the Fe_2O_3 content of the samples SCP1 and SCP2 also supports the same.

The conventional reductive ('hydros') bleaching removes only very small amount of iron. Hence, the brightness improvement of the product sample SCP2 is also marginal, only by ~ 0.52 units. The decrease in iron content, improvement in the L and HW values and reduction in "a"," b" and HY values are found to be very small. It implies that the impurity minerals imparting dark/reddish and yellow shade to the material is unaffected by this reductive bleaching technique and the extent of "free" iron removal is minimal. DCB treatment improves the brightness substantially (~15.7 units) and during this process the Fe2O3 content reduces from 1.01% to 0.61%, indicating that part of the iron in the sample is "free" and leachable. The brightness/whiteness of kaolin is dependent on the overall effect of the "**Lab**" colour values. The "**L**" and HW values of the sample increase after DCB treatment by ~7.0 and ~25 units respectively and it gives an idea about the extent of removal of the dark coloured impurity minerals. After DCB treatment "a" values (reddishness) of the sample has come down appreciably (~3.0 units)

ndicating the removal of most of the "free" reddish iron oxy hydroxides during DCBT. Similarly, there was a marked reduction in the "b" and HY values (~ 2.6 and 4.2 units respectively) in the DCBT product sample which contributes to the substantial decrease in yellowness.

The brightness and HW values of SCP1 sample was found to increase appreciably after calcinations with a small increase in its L value. Correspondingly, there was a marked decrease in the reddishness and yellowness of the sample as indicated by the reduction in the colour ("a", "b" and HY) values (Table 3.2.3).

3.2.2 Chemical assay

The chemical assay of the ROM and various beneficiated samples are given in Table 3.2.1. The ROM clay is siliceous as indicated by the high silica, low alumina and low loss on ignition. Sample SCP1 was found to be more kaolinitic in nature and is evident from the increased Al_2O_3 content. That is, 2" stub cycloning has removed the coarse silica particles and enriched kaolinite content in the clay. The LOI value of SCP1 has also increased to that of ideal kaoilnite, indirectly indicating the removal of silica. But silica content in the sample SCP2 is slightly higher than SCP1 and this may be due to the enrichment of fine silica particles in this particular size region. A marginal decrease in the alumina content and LOI supports the same. It is seen that size classification has produced some decrease in the Fe_2O_3 and TiO_2 content of the sample, indicating the removal (though marginally) of denser impurity minerals (Figure 3.2.4). The presence of appreciable quantities of Fe_2O_3 (~ 88%) and TiO_2 (~72%) in the SCP2 sample indicates the ultra fine size of these impurities which are getting enriched in the product during size separation.

The presence of Fe and Ti and other impurity minerals of Na, K, Ca etc. in the finer size fractions indicate that they are almost uniformly distributed in all size fractions. Results of the trace elements analysis shows that the concentrations of certain elements such as Mg, Ba, Cr, S, P, Zn, Cu, Pb and Ni are relatively high in the raw clay and come down in the beneficiation products (Table 3.2.2).

Reductive bleaching is found to be ineffective in removing the iron and is evident from the marginal decrease in the Fe_2O_3 content of SCP2 R.B sample. But after DCB treatment, the Fe_2O_3 percentage was reduced by 0.54 units with a marked improvement in

92

optical properties of SCP2-DCBT sample. The extent of iron removal shows that ~53% of the total iron in the clay is "free" in nature and the rest is present in the structure of either kaolinite or ancillary mineral (mica or titania). Also, the sharp decrease in the "a", "b" and HY values confirms the removal of the coloring iron impurities such as hematite and goethite. The marked improvement in the optical properties of SCP2 DCB treated sample shows that most of the "structural iron" may be present in the kaolinite structure. It is also worth mentioning that chemical leaching has not effected any changes in the TiO_2 content. The Fe_2O_3 and TiO_2 content and optical properties of the beneficiated samples are given in Table 3.2.3 and Figure 3.2.4 represents the variation in Fe_2O_3 and TiO_2 content.

3.2.3 Mineralogical study

XRD and thermal analysis data of the ROM and beneficiated products is given in Table 3.2.1 and the XRD powder patterns in Fig. 3.2.1. Kaolinite is the major mineral present in the raw clay along with quartz, hematite, anatase and rutile as the ancillary mineral impurities (Table 3.1.4). An increase in the intensity of the kaolinite peak and decrease in the intensity of quartz peak in the case of SCP1, SCP2 and SCP2 DCBT clearly shows the enrichment of kaolinite in the sample during the size classification.

Thermal analyses data of the ROM and beneficiated samples are given in Table 3.2.1. The total weight loss in the raw clay on heating is ~9.46% and this low value can be attributed to low kaolinite and /or high silica content. This value increases, as the ROM clay is beneficiated by size classification confirming the increase in kaolinite content. DTA data indicate that the ROM and the size classification products are similar giving characteristic endotherm and exotherm of kaolinite mineral (Table 3.1.4). DCB treatment does not have any impact on the thermal properties of the sample.

Table 3.2.4 gives the percentages of possible minerals in the raw and processed samples as calculated from the chemical assay. The ROM sample is kaolinitic with minor amounts of quartz, micaceous minerals (both muscovite and paragonite mica), hematite and anatase. During size separation, the kaolinite content increases in the finer fractions with a simultaneous decrease in the impurity minerals. Figure 3.2.3 indicates the increase in kaolinite content during beneficiation. Appreciable quantities of micaceous minerals are getting removed during 2"stub hydrocycloning along with small quantities

of hematite and anatase. However, the data shows that the impurity minerals are retained in all size ranges.

3.2.4 Morphological characterization

Scanning electron microscopic (SEM) pictures of the ROM clay and SCP1 are shown in **Fig. 3.2.2**. Typical "booklet" shaped kaolinite particles are observed in the raw sample. The processed clay appears to have aggregates of pseudo hexagonal platelet shaped particles of approximately 1-2 µm size.

3.3 Kaolin from Trivandrum district of Kerala

3.3.1 Physical characterization:

The ROM clay is soft, pink colored and easily slaking and has a neutral pH (6.89 units). Specific gravity values of the raw and size classified products are almost the same and are near to that of kaolinite mineral (2.6). The matter soluble in water and acid are low and do not change much during processing. The cation exchange capacity of the raw clay (8.43 meq/100g) is found to be in the range of values reported for natural kaolins(Table 3.3.1).

Particle size distribution analysis (Table 3.3.1) of the raw clay shows that the grit content is very low (6.20%), and the fines are quite high (69.29% < 2µm fraction). Screening followed by separation using 2"stub hydrocyclone has resulted in marginal decrease in < 45 µm fraction (from ~ 24.51% to 16.42% along with a sharp increase in the < 2 µm fraction (69.29% to 83.58%). Further sizing using 1" hydrocyclone is found to enhance the < 2 µm fraction to 91.92 % (Figure 3.3.3).

The optical properties of the raw clay appear to be relatively good. But the sample is having a pinkish shade as indicated by the color values. Optical properties and the % Fe_2O_3 and % TiO_2 of the beneficiated samples are given in Tables 3.3.1 and 3.3.3. For pigment grade kaolin, brightness should be >80% ISO and beneficiation to achieve this level is one of the highest value additions of kaolin. Size classification increases the brightness of samples from 77.71 to 78.17 (SCP1) and to 80.86 (SCP2) units. Accordingly, there is a marginal improvement in the "L" as well as HW values of the SCP1 and SCP2 samples.

There is a marginal decrease in the reddishness ("a" value) of the sample SCP1, but at the same time there is an increase in the yellowness values ("b" and HY). In the

ase of the sample SCP2, reddishness and yellowness are found to be less which are indicated by the "a", "b" and HY values. This clearly shows that a portion of the coloring impurities such as hematite and goethite are getting removed during 1" cycloning. The Fe_2O_3 values also show a corresponding decrease.

Only very small quantity of iron is removed by the conventional reductive ('hydros') bleaching and the brightness improvement of the product sample SCP2 is also marginal (80.86 to 81.54). The improvement in the "L" and HW values and reduction in "a", "b" and HY values are also very small. Hence the reductive bleaching is almost ineffective in the removal of "free" iron. However, DCB treatment improves the brightness by from 80.86 to 89.85 with a decrease in % Fe_2O_3 from 0.35 to 0.18 units indicating that most of the iron in the sample is "free" and leachable. The brightness/whiteness of kaolin is dependent on the overall effect of the "**Lab**" color values. The "*L*" and HW values of the sample increase after DCB treatment by 4.0 units and ~13.0 units respectively, indicating the removal of the dark colored minerals in clay. After DCB treatment "*a*" value (reddishness) of the sample has come down from 2.39 to -0.41 indicating the removal of almost all the "free" reddish iron oxy hydroxides. The "-a" value is indicative of the greenish tinge the material has obtained after the removal of all the red colored impurity minerals. Similarly, the "**b**" (yellowness) and HY values are found to decrease substantially from 3.27 to 2.12 and 5.07 to 3.14 units respectively and thereby decreasing the yellow shade of the sample. The decrease in yellowness can be attributed to the removal of goethite during DCB treatment.

The brightness, L and HW values of SCP1 sample are found to increase appreciably after calcination. Similarly, after calcination the reddish tinge of the sample changes to greenish as indicated by the "a" value (1.76 to -0.39). Yellowness of the sample is also getting reduced after calcination and is evident from the decrease in "b" and HY values (Table 3.3.3).

3.3.2 Chemical assay

The chemical assay of the raw and beneficiated samples are given in Table 3.3.1 The ROM clay is found to be highly kaolinitic as indicated by the silica, alumina and LOI values. Sample SCP1 and SCP2 were found to be more kaolinitic than ROM clay and is evident from the increased Al_2O_3 content, ie., size separation has removed the coarse

95

particles and enriched kaolinite content in the clay (Figure 3.3.3). The increase in the LOI values of SCP1 and SCP2 also indicates the marginal removal of the silica and is close to that of ideal kaolinite. DCB treatment has produced no change in the kaolinitic content of the sample.

It is seen that size classification has resulted in a slight decrease in Fe_2O_3 and TiO_2 content of samples SCP1 and SCP2 and which can be attributed to the removal of the coarse coloring impurities (Fig.3.3.4) in the particular finer size ranges. However, these impurities are retained to a great extent in the fine fractions indicating that they are present in the clay in a wide size range.

Reductive bleaching is found to be ineffective in removing the iron as evident from the Fe_2O_3 values in the sample before and after bleaching. But after DCB treatment the Fe_2O_3 % has came down and the optical properties have enhanced. The extent of iron removal shows that ~ 49% of the total iron in the clay is "free" in nature and the rest is present in the structure of either kaolinite or ancillary mineral (mica or titania). Also, the sharp decrease in the "a", "b" and HY values, indicative of reddish and yellow shade of the material, confirms the removal of the coloring iron impurities such as hematite and goethite. In fact, the "-a" value indicates that greenish tinge has replaced the reddishness of the sample. The marked improvement in the optical properties of the DCB treated product shows that most of the "structural iron" may be present in the kaolinite structure. The variation of Fe_2O_3 and TiO_2 content during beneficiation is given in Figure 3.3.4.

Other impurity minerals of Na, K, Ca etc. are present only in low concentrations in the raw clay, but get enriched in the finer size fractions. Results of the trace elements analysis shows that the concentrations of certain elements such as Mg, Cr, Zn, Ni, P and S are relatively high in the raw clay and come down in the beneficiation products (Table 3.3.2).

3.3.3 Mineralogical properties

X-ray diffraction, thermal and rational analyses give an overall picture of the clay mineralogy. The XRD and thermal analysis data of the ROM and processed samples are given in Table 3.3.1 and the XRD powder patterns are represented in Figure 3.3.1. Kaolinite is found to be the major mineral in the raw clay along with quartz, hematite, anatase, rutile, as the ancillary mineral impurities (Table 3.1.4). An increase in the

ntensity of the kaolinite peak and decrease in the intensity of quartz peak in the XRD patterns of SCP1, SCP2 and SCP2 DCBT clearly shows the enrichment of kaolinite in the sample during the size classification.

Thermogravimetric analysis data of the ROM and processed samples are given in Table 3.3.1. The total weight loss on heating increases from raw to fine sized fraction from 12.78% to ~14.2%). This value increases, as the ROM clay is beneficiated by size classification confirming the increase in kaolinite content. The DTA patterns give endotherm and exotherm characteristic of kaolinite mineral (Table 3.1.4). This shows that the both the product samples are highly kaolinitic. DCB treatment does not have any impact on the thermal properties of the sample.

The rational analysis data of the raw and processed samples calculated from the chemical assay gives the percentages of possible minerals in "Trivandrum" kaolin as given in Table 3.3.4. It shows that the ROM sample is highly kaolinitic with small amounts of quartz, micaceous minerals (both muscovite and paragonite mica), hematite and anatase. Size separation enriches the kaolinite content and gives the percentages of possible minerals in SCP1 and SCP2 kaolin as calculated from the chemical assay. An idea about the enrichment of the kaolinite during size separation can be obtained from rational analysis (Figure 3.3.3). From the data it is clear that the kaolinite content in both the processed samples is higher than the ROM clay and SCP2 has got the highest value. The mica, hematite and calcite content in the size classified samples were also on a higher side. The impurity minerals are thus distributed in all size ranges.

3.3.4 Morphological characterization Scanning electron microscopic (SEM) pictures of the ROM and SCP1 samples is presented in Figure 3.3.2, which shows the presence of aggregates of pseudo hexagonal kaolinite particles and bigger quartz particles sticking to the clay.

3.4 Kaolin from Kutch district of Gujarat

3.4.1 Physical characterization:

Physical properties of the raw and processed clay samples are given in Table 3.4.1. The ROM clay is soft and easily slaking and has a neutral pH (6.92 units) and dull white color. Specific gravity values of the sample (2.71) are higher than that of kaolinite mineral (2.6) and this may be due to the presence of heavy minerals. Size classified

97

product samples are found to have slightly less value which matches with that of ideal kaolinite. The matter soluble in water and acid are also getting reduced marginally during size classification. Cation exchange capacity of the raw clay is 9.34 meq/100g which falls in the range of values reported for natural kaolins.

Particle size distribution analysis of the raw clay show that the grit content is very less (3.0%) and the fines are moderately high (58.30% < 2µm fraction) in the sample. Screening and separation using 2"stub hydrocyclone does not make any increase in < 45 µm fraction but it has increased the < 2 µm fraction (58.30% to 70.60%). Further classification using 1" hydrocyclone is found to enhance the <2 µm fraction to 82.30 %. Table 3.4.1 gives the size distribution data of the raw and beneficiated samples and Figure 3.4.3 gives the trend in increase in the fine fraction.

The brightness (70.34) and HW (65.96) values of the raw clay are found to be relatively low. The L value is high (89.18) which may be because the blackish impurities are of low concentration in the clay. However, the clay has a reddish - yellow shade as indicated by the "a" (0.61), "b" (6.01) and HY (10.58) values and this accounts for the dull color of the sample. The optical properties and % Fe_2O_3 and % TiO_2 of the raw clay and beneficiated samples are given in Tables 3.4.1 and 3.4.3. For pigment grade kaolin, brightness should be >80% ISO and beneficiation to achieve this level is one of the challenges in kaolin beneficiation. Size classification increases the brightness marginally i.e., to 72.50 (SCP1) and 73.57 (SCP2) units and there is a simultaneous improvement in the "L" as well as in the HW values. Interestingly, the size separation has not made any impact on the reddishness of the product samples which is evident from their "a" values. The yellowness of SCP1 has remained as such whereas a marginal decrease is observed for SCP2 as indicated by the decrease in HY value. The chemical assay values for Fe_2O_3 and TiO_2 in these samples support this finding.

The conventional reductive ('hydros') bleaching does not improve the optical properties of the product significantly and the reduction in Fe content is also very small. This indicates that only small part of the free iron is getting removed by this method. DCB treatment improves the brightness from 73.57 to 77.81 units with a decrease in % Fe_2O_3 from 0.43 to 0.27 units. Thus only a part of the iron is leachable. Incidentally, the sample is found to contain significant amount of titania which does not change on DCB

98

T477
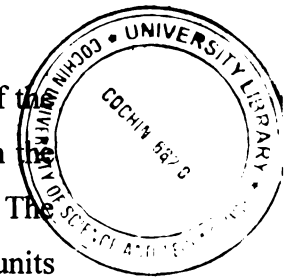
treatment. The brightness / whiteness of kaolin are dependent on the overall effect of the "Lab" color values. It has been established that the "free iron" is more soluble than the "structural" iron and hence the former is more easily removed by chemical leaching. The "L" and HW value of the sample increase after DCB treatment by 1.2 and ~ 7.47 units respectively, indicating that only partial removal of the dark colored minerals is taking place. After DCB treatment, "a" value (reddishness) of the sample has come down from 0.63 to -0.51 units indicating the removal of almost all "free" reddish iron oxy hydroxides. The negative value for "a" is indicative of the greenish tinge achieved by the clay after the removal of red colored impurity minerals. Similarly, the "b" and HY values are found to decrease from 6.09 to 5.16 and 9.67 to 8.03 units respectively. The decrease in yellowness can be attributed to the removal of goethite during DCB treatment. The high yellowness values ("b" and HY) of the DCBT product indicate that considerable amount of colored minerals still remain in the sample.

The brightness, "L" and HW values of SCP1 sample is found to increase marginally after calcination. Both the reddishness as well as yellowness of the sample are decreasing only to a limited extent which is evident from the changes in color values ie., "a" (0.63 to 0.54), "b" (6.09 to 5.78) and HY (9.67 to 9.21) (Table 3.4.3).

3.4.2 Chemical characterization

The chemical assays of the ROM and beneficiated clay samples are given in Table 3.4.1. The ROM clay is found to be highly kaolinitic as indicated by the silica, alumina and LOI values which are close to those of theoretical values for the mineral kaolinite. It is found that size separation is removed the coarse particles, but the kaolinite content has improved only to a limited extent. The silica, alumina and   LOI values of SCP1 and SCP2 confirm the same which is schematically represented in the Figure 3.4.3. DCB treatment has produced no change in the kaolinitic content of the sample. It is seen that size classification has resulted in a marginal decrease in the Fe_2O_3 content of the product samples which can be attributed to coarser particles of the iron containing minerals in the particular finer size ranges. But the TiO_2 content is found to remain as such as in the ROM sample (Figure 3.4.4). The presence of appreciable quantities of Fe_2O_3 (~ 50%) and TiO2 (~ 98%) in the SCP2 sample gives us an idea about

99

the ultra fine size of the 'Fe' and Ti impurities which are mostly retained in the product during size separation.

Reductive bleaching is found to be ineffective in removing the iron and is evident from the marginal decrease in the Fe_2O_3 content of SCP2 R.B sample. Even after DCB treatment the Fe_2O_3 % has come down only by 0.16 units with a marginal improvement in the optical properties. The extent of iron removal shows that ~37% of the total iron in the SCP2 sample is "free" in nature (ie., as oxides, hydroxides, oxy-hydroxides) and the rest is present in the structure of either kaolinite or ancillary mineral (mica or titania). Also, the sharp decrease in the "a" and marginal reduction in "b" and HY values, confirms the removal of iron impurities such as red hematite and yellow goethite. In fact, the negative "a" value indicates that greenish tinge has replaced the reddishness of the sample. The sample is still found to contain appreciable quantities of iron minerals which imparts yellowish-orange tinge to it as shown by the high "b" and HY values. The marginal improvement in the optical properties of SCP2 DCB treated sample shows that it may be possible that most of the "structural iron" is present as part of the titania structure (due to the appreciable titania content in the sample). It is also worth mention that chemical leaching has not effected any changes in the TiO_2 content. The variation of Fe_2O_3 and TiO_2 content during beneficiation is given in Figure 3.4.4.

Impurity minerals of other cations Na, K, Ca etc. are present only in low concentrations and are getting enriched in the finer size fractions. Results of the trace elements analysis shows that the concentrations of certain elements such as Mg, Zn, Ni, Cr, P, S and Ni are relatively high in the raw clay and come down in the beneficiation products. Table 3.4.2 gives the concentrations of trace elements in the ROM and beneficiated samples. DCB treatment is found to decrease the values of Cr, Cu, Ni, Pb and Zn to a great extent.

3.4.3 Mineralogical characterization

The clay mineralogy can be understood by the X-ray diffraction, thermal and rational analyses. The XRD and thermal analysis data of the ROM and processed samples are given in Table 3.4.1 and the XRD powder patterns in Figure 3.4.1. Kaolinite is found to be the major mineral present in the raw clay along with quartz, hematite, anatase and rutile as the ancillary mineral impurities (Table 3.1.4). An increase in the intensity of the

100

kolinite peak and decrease in the intensity of quartz peak in the XRD pattern of SCP1, SCP2 and SCP2 DCBT clearly shows the enrichment of kaolinite in the finer size fractions.

Thermogravimetric analyses of the ROM and processed samples are given in Table 3.4.1. The total weight loss in the raw clay on heating is ~13.20%, which is near to that of the kaolinite mineral (13.95). This value increases, as the ROM clay is beneficiated by size classification confirming the increase in kaolinite content. The DTA curves give characteristic endotherm and exotherm of kaolinite mineral (Table 3.1.4). This shows that the ROM, SCP1 and SCPP2 are highly kaolinitic. DTA data of both the samples indicate that the ROM and the size classification products are similar giving characteristic endotherm and exotherm of kaolinite mineral. DCB treatment does not have any impact on the thermal properties of the sample.

Table 3.4.4 gives the rational analysis data of various samples as calculated from their chemical assay. The rational analysis data shows that the ROM sample is highly kaolinitic with small amount of quartz, micaceous minerals (both muscovite and paragonite mica), hematite and anatase in small quantities. From the data it is clear that the kaolinite content in the ROM and processed samples are more or less the same (Figure 3.4.3). The anatase, hematite and mica content in the size classified samples were also on a higher side. Rational analysis data shows that the impurity minerals are distributed in all size ranges.

3.4.4 Morphological characterization

Scanning electron microscopic (SEM) pictures of the ROM and SCP1 samples are presented in Figure 3.4.2, which shows the presence of aggregates of pseudo hexagonal kaolinite particles and bigger quartz particles sticking to the clay.

3.5 Kaolin from Koraput district of Orissa

The investigation on Koraput clay showed that it is different from the other clay samples under investigation in many properties and conventional size classification procedure can not be adopted for value addition. Hence, only the properties of ROM clay are described here. Beneficiation and characterization of the product samples are dealt separately in Chapter 7.

3.5.1 Physical properties

The ROM clay is soft, easily slaking gray in color with blackish impurities. The pH of the clay is found to be quite low (1.74) and is found to be acidic. High acidity of a clay results in many complications which are described later in Chapter 7. Conventional wet processing of this clay is difficult since the soluble iron gets precipitated on adding more water because of the subsequent increase in pH. Hence, a thorough water wash was given to the clay before size classification.

In the ROM clay the matter soluble in water is on the higher side ie., 4.14% and the reason for the high value can be attributed to mobilization of metals such as Fe^{+3} from the clay by H_2SO_4 . The matter soluble in acid is 9.06% and such high value can be due to the presence of some soluble salts. Specific gravity of the ROM clay is slightly higher than that of pure kaolinite which is possibly due to the presence of heavy mineral impurities. The CEC of the clay is found to have low, 2.1meq /100g clay, which can be attributed to its low pH which causes protonation and formation of a positive charge on the surface of the clay minerals (Froth and Ellis, 1996).Table 3.5.1, gives the general properties of the ROM clay.

Particle size distribution analyses given in Table 3.5.1 show that the grit content is medium (16.80%), and the percentage of fines are moderately high (49.90% < 2µm fraction) in the ROM sample. The brightness (45.87), "L" (67.43) and HW (27.17) values are found to be very poor. The low "L" and HW values show the presence of black/dark colored particles in the clay. The greenish tinge of the sample negative ("a" value) is indicative of the absence of reddish iron compounds in the sample. The "b" (-0.44) and HY (0.94) values show that the overall yellowness of the sample is low. This confirms that low brightness of the sample is due to the presence of the black / dark colored minerals.

3.5.2 Chemical characterization

The percentages of chemical constituents in the ROM clay are given in Table 3.5.1. The clay is kaolinitic as indicated by the silica and alumina content which are close to the theoretical values of kaolinite mineral. However, the LOI value is found to be on a higher side (18.17%) which can be attributed to carbonaceous and / or minerals decomposable with weight loss on heating. The Fe_2O_3 and TiO_2 content in the sample are

found to be relatively high (5.41 and 1.60% respectively). XRD pattern of the clay showed that pyrite is one of the major impurities. Accordingly the chemical analysis is done which confirms that the total "iron content" (as Fe) in the sample is 1.94 % out of which 1.85 % is pyritic iron. The pyrite content in the sample is estimated as 3.97%. The sample is also found to contain 2.07 % of sulphur and 1.2% of carbon. The other impurity minerals of Na, K, Ca etc. are present only in low concentrations. Results of the trace elements analysis of the clay is given in Table 3.5.2. No toxic element was detected in the clay and the concentration of elements such as Co, Ba, Cr, P, Zr and Zn, are found to be quite high. The concentrations of trace elements in this clay are found to be different from that in other clays under study.

3.5.3 Mineralogical characterization

The mineralogical composition of the clay is obtained from its X-ray diffraction, thermal and rational analyses. The XRD and thermal analysis data of the ROM sample is given in Table 3.5.1 and the XRD powder pattern in Figure 3.5.1. Kaolinite is found to be the major mineral along with quartz, pyrite, anatase and rutile as the ancillary mineral impurities (Table 3.1.4).

Thermogravimetric analyses of the ROM sample show that the total weight loss on heating is ~18.27%, which is higher than that of the kaolinite mineral (Table 3.1.4). Again, it can be attributed to the oxidation of carbon and decomposition of pyrite. The DTA curve gives endotherms and exotherms which are characteristic of kaolinite and pyrite minerals.

The rational analysis data in Table 3.5.3 gives the percentages of possible minerals in the ROM sample as calculated from the chemical assay. Kaolinite is the major phase and minerals such as quartz, pyrite, mica (both muscovite and paragonite), hematite, anatase and carbonaceous matter are also found in small quantities.

3.5.4 Morphological characterization

Scanning electron microscopic analysis (SEM) pictures of the ROM clay is presented in Figure 3.5.2, which shows the presence of aggregates of pseudo hexagonal kaolinite particles. Well crystallized pyrite particles of typical octahedral shape are also found.

103

The detailed characterization of the ROM sample shows that, beneficiation of the clay is essential for improving the optical properties as well as the quantity of < 2 micron fraction in the sample. Since the clay is found to be highly acidic, conventional beneficiation techniques may corrode the processing equipments. So a modification in the procedure is essential for the wet processing of the clay. The conventional as well as the modified beneficiation procedures adopted for the size classification of this clay as well as the impact of both on the overall shade / optical properties of the final product are discussed separately in Chapter 7.

3.6 Kaolin from Bankura district of West Bengal

3.6.1 Physical properties

The ROM clay is dull yellow in color indicating the presence of colored minerals. The clay is soft, easily slaking and has neutral pH (7.55 units). Specific gravity values of the sample (2.63) is near to that of kaolinite mineral (2.6) The specific gravity values of the size classified products are found to be slightly less and they perfectly match with that of ideal kaolinite. The matter soluble in acid and water are also getting reduced marginally during size classification. The cation exchange capacity of the raw clay (11.85 meq/100g) was found to be in the range of values reported for natural kaolins. Table 3.6.1 gives the general properties of the clay and the beneficiated products.

The particle size distribution analysis of the raw clay show that the grit content is high (43.09%) and the fines are relatively less in the sample. The fraction < 2μm is only 20.10%. Screening and separation using 2"stub hydrocyclone has resulted in appreciable increase in < 45 μm fraction (from 36.38 to 57.58%) along with sharp increase in the <2 μm fraction (20.10 to 42.42%). Further sizing using 1" hydrocyclone is found to enhance the <2 μm fraction up to 55.76 %. The size distribution in the raw and processed samples is given in Table 3.6.1 and the variation in <2μm fraction is depicted in Figure 3.6.3.

The optical properties of the raw clay are found to be very poor. The brightness (37.69), L (74.29%) and HW (16.01%) values are very low and colored minerals in the clay appear to be in considerable amount. The color values, "b" (16.77) and HY (32.25) are very high, while "a" (0.07) is found to be low. This shows that the impurity is more and yellow in color. Optical properties, % Fe_2O_3 and % TiO_2 values of ROM and beneficiated samples are given in Table 3.6.1 and 3.6.3. The brightness should be >80%

104

ISO for pigment grade kaolin and beneficiation to achieve this level may be very difficult and even impossible for this clay. Size classification increases the brightness of samples to 41.48 (SCP1) and 41.79 (SCP2) units. The "L" value of both SCP1 and SCP2 samples increase by ~ 6 units, while there is a marked improvement in HW values (12 and 15.5 units respectively). The increase in the "L" and HW values indicates the removal of materials, which imparts black shade to the clay. Increase in the "a", "b" and HY values during size classification, confirms the enrichment of reddish and yellow colored impurity minerals. The increase in the Fe_2O_3 content of the products of size classification (SCP1 and SCP2) also supports the same. The marginal improvement in the brightness of the samples is due to the partial removal of the black colored impurity minerals, which are coarser in size.

The conventional reductive ('hydros') bleaching removes only small amount of 'Fe' minerals. Hence, the brightness improvement of the product sample SCP2 is also marginal. The brightness of the sample has improved on hydros bleaching only by ~ 5.0 units with a very small improvement in the L and HW values and marginal decrease in "a," "b" and HY values. The Fe_2O_3 content also does not change much. Thus the impurity minerals imparting dark/reddish and yellow shade to the material is unaffected by this reductive bleaching technique and the extent of "free" iron removal is very low. DCB treatment improves the brightness substantially from 41.79 to 69.67 and during this process the Fe_2O_3 content comes down from 5.66% to 0.94%. This indicates that a good amount of the iron in the sample is "free" and leachable. The brightness/whiteness of kaolin is dependent on the overall effect of the "L a b" color values. The "L" and HW values of the clay increase after DCB treatment by ~5.0 and ~23 units and it gives an idea about the extent of removal of the dark colored impurity minerals. After DCB treatment "a" value (reddishness) of the sample has come down appreciably (from 1.07 to -1.32 units) indicating the removal of most of the "free" reddish iron oxy hydroxides. Similarly, there is a marked reduction in the "b" and HY values (20.99 to 4.03 and 36.98 to 6.68 units respectively) on DCBT which contributes to the substantial decrease in yellowness. Even though the extent of brightness improvement and removal of free by the DCB treatment is very high, the overall brightness of the product is not promising. The sample still contains ~1.0% of iron and the yellowness values ("b" and HY) support

105

x same. Since the sample is found to contain mica, it is possible that the iron remaining iter DCB treatment may be present as part of the mica structure and their by affecting x overall brightness of the sample.

The brightness, "L" and HW values of SCP1 sample is found to decrease appreciably after calcination. Correspondingly, there is a marked increase in the reddishness and yellowness of the sample as indicated by the reduction in the color ("a", "b" and HY) values as given in Table 3.6.3. Since the iron content in the sample is high, it is possible that most of the iron getting liberated during metakaolinisation may not be getting incorporated into the kaolinite structure during calcination. This leads to the formation of reddish iron oxide coating on the clay surface and corresponding appreciable reduction in the optical properties of the calcined clay.

3.6.2 Chemical assay

The chemical assay of the ROM and various beneficiated samples are given in Table 3.6.1. The ROM clay is siliceous as indicated by the high silica, low alumina and low loss on ignition. Samples SCP1 and SCP2 are found to be more kaolinitic which is evident from the increased Al_2O_3 content. That is, 2" stub and 1" cycloning have removed the coarse silica particles and enriched kaolinite content in the clay. Though the LOI value of SCP1 and SCP2 has increased marginally indicating the removal of the silica indirectly, the values are found to be much lower than that of an ideal kaolinite. Even after size classification, the LOI values remain low and silica content is high showing the highly siliceous nature of these products. The Fe_2O_3 and TiO_2 content of the sample are found to increase (Figure 3.6.4) in the fines, indicating the enrichment of finer impurity minerals in these fractions. The presence of appreciable quantities of Fe_2O_3 (5.66 % - due to enrichment) in the SCP2 sample indicates the ultra fine size of these impurities which are getting enriched in the product during size separation.

The presence of Fe and Ti and other impurity minerals of Na, K and Ca etc. in the finer size fractions confirm that they are almost uniformly distributed in all size fractions. Results of the trace elements analysis shows that the concentrations of certain elements such as Mg, Zn,Ba,Cr,Mn,P,S and Ni are relatively high in the raw clay and come down in the beneficiation products(Table 3.6.2).

106

Reductive bleaching was found to be ineffective in removing the iron and is evident from the marginal decrease in the Fe_2O_3 content of SCP2 R.B sample. But after DCB treatment, the Fe_2O_3 percentage was reduced from 5.66 to 0.94 units and is evident from the marked improvement in optical properties of SCP2-DCBT product. The extent of iron removal shows that ~83% of the total iron in the clay is "free" in nature and the rest is present in the structure of either kaolinite or ancillary mineral (mica or titania). Also, the sharp decrease in the "a", "b" and HY values confirms the removal of the coloring iron impurities such as hematite and goethite. Though the extent of brightness improvement and free iron removal of the sample by the DCB treatment is very high, the overall brightness of the sample is not found to be promising. The sample is still found to contain ~1.0% of iron. Since the sample is found to contain mica and less amount of titania, it is possible that the iron remaining after DCB treatment may be present as part of the mica framework and thereby affecting the overall brightness of the sample. The titania content is not affected by the chemical leaching. The weight percentages of Fe_2O_3 and TiO_2 content and optical properties of the beneficiated samples are given in Table 3.6.3 and the variation in Fe_2O_3 and TiO_2 content is schematically represented in Figure 3.6.4.

3.6.3 Mineralogical study

The data from XRD and thermal analysis of the ROM and beneficiated products is given in Table 3.6.1 and the XRD powder patterns in Figure 3.6.1. Quartz is the major mineral present in the raw clay along with kaolinite, mica, anatase and rutile (Table 3.1.4). An increase in the intensity of the kaolinite peak and decrease in the intensity of quartz peak in the case of SCP1 and SCP2 clearly shows the enrichment of kaolinite in the sample during the size classification.

The total weight loss in the raw clay on heating is ~5.02% and this low value can be attributed to high silica content. The weight loss in the range 450 to 600°C corresponds to the dehydroxylation of kaolinite. This value increases, as the ROM clay is beneficiated by size classification confirming the increase in kaolinite content. DTA data indicate that the ROM and the size classification products are similar giving endotherms and exotherms which are characteristic of kaolinite mineral (Table 3.1.4). DCB treatment does not have any impact on the thermal properties of the sample.

107

Rational analysis calculated from the chemical assay gives the percentages of possible minerals in the raw and processed samples and the data is given in Table 3.6.4. The ROM sample is high in silica and low in kaolinite and is found contain minor amounts of muscovite and paragonite mica, hematite and anatase. During size separation, the kaolinite content increases in the finer fractions (Figure 3.6.3) with a simultaneous decrease in the quartz content. But concentrations of all other impurity minerals are found to increase during size classification this shows their enrichment in the finer size fractions. The data shows that the impurity minerals are retained in all size ranges.

3.6.4 Morphological characterization

Scanning electron microscopic (SEM) pictures of the ROM clay and SCP1 are shown in Figure 3.6.2. Typical platelet shaped kaolinite particles are observed in the raw sample. The processed clay appears to have aggregates of pseudo hexagonal platelet shaped particles of approximately 1-2 μm size.

3.7 Kaolin from Pali district of Rajasthan

3.7.1 Physical properties

The ROM clay is soft, easily slaking and has neutral pH (7.00 units). It has a gray color which indicates the presence of colored impurity. Specific gravity value of the sample (2.61) is near to that of kaolinite mineral (2.6) and the values for the size classified product samples are found to be slightly less and are closer to that of ideal kaolinite. The matter soluble in acid and water are low and decrease marginally during size classification. The cation exchange capacity of the raw clay (11.85 meq/100g) was found to be in the range of values reported for natural kaolins. Table 3.7.1 gives the general properties of the clay.

Particle size distribution analysis of the raw clay show that the grit content is negligible (0.4%) and the fines are relatively high (the fraction < 2μm is 72.7%) in the sample. Screening and separation using 2"stub hydrocyclone has resulted in marginal decrease in < 45 μm fraction (from ~ 26.90% to 24.3% along with an increase in the -2 micron fraction (72.7% to 75.7%). However, further sizing using 1" hydrocyclone is found to enhance the <2 μm fraction to 83.3 %.The size distribution in the raw and

processed samples is given in Table 3.7.1 and the variation in $<2\mu m$ fraction is depicted in Figuer 3.7.3.

The optical properties of the raw clay are found to be very good. The lightness (93.01%) and HW (60.02%) values are relatively high, indicating the absence of black/dark colored minerals. At the same time, the color values, **"b"** (4.98) and Hunter Y (7.65) are high with a low value for **"a"** (-0.50). These values indicate the presence of yellow colored impurity minerals in the clay. Optical properties, % Fe_2O_3 and % TiO_2 values of ROM and beneficiated samples are given in Table 3.7.1 and 3.7.3. It is seen that there is not much improvement either in the brightness or "L" and HW values after size classification. In fact, they are getting reduced marginally in SCP1 sample and this can be attributed to the removal of pure white silica sand particles, which usually impart white color to the clay. The reddishness ("a" value) and yellowness ("b" and HY) of the SCP1 and SCP2 samples shows that the yellow colored impurity minerals are not getting removed during size classification. The unchanged Fe_2O_3 content of the samples SCP1 and SCP2 also supports the same. Interestingly, the samples do not have any reddishness and has got a greenish tinge as indicated by the low "a" value.

The conventional reductive ('hydros') bleaching is unable to remove any 'Fe' minerals. No brightness improvement is observed in the product sample SCP2. Similarly, the "L", HW and color values ("a", "b" and HY) remained almost unchanged after reductive bleaching. This shows that the yellow shade to the material is unaffected by this reductive bleaching technique and the extent of "free" iron removal is minimal.

DCB treatment is also found to be ineffective in improving the brightness and during this process the Fe_2O_3 content remained almost unchanged, indicating that the iron in the sample is not "free" and leachable. The brightness/whiteness of kaolin is dependent on the overall effect of the **"Lab"** colour values. The **"L"** and HW values of the sample have not improved and it implies that the dark colored impurity minerals are not getting removed by DCB treatment. After DCB treatment the **"a"** value remains unchanged and the "b" and HY values, which contributes to the yellowness decrease marginally. The product sample is still found to contain ~1.0% of iron and the yellowness can be due to the "Fe" minerals. The fact that clay has high brightness which is not changed by DCB treatment confirms that iron is in the framework of kaolinite or any other ancillary

...neral. Mica is one of the major impurities in this clay and it is possible that the iron remaining after DCB treatment may be present as part of the mica structure.

The brightness, "L" and HW values of SCP1 sample iss found to decrease marginally after calcination. Simultaneously, there is an increase in the reddishness and yellowness of the sample as indicated by the increase in the color ("a", "b" and HY) values (Table 3.7.3). Since the iron content in the sample is on a higher side, it is possible that most of the iron getting liberated during metakaolinisation (from mica structure) may not be getting incorporated into the kaolinite structure during calcination. This leads to the formation of colored iron oxide coating on the clay surface, which in turn may be adversely affecting the optical properties of the calcined product.

3.7.2 Chemical assay

The chemical assay of the ROM and various beneficiated samples are given in Table 3.7.1. The ROM clay is siliceous as indicated by the high silica, low alumina and low loss on ignition. Samples SCP1 and SCP2 are found to be more kaolinitic and is evident from the increased Al_2O_3 content. Thus 2" stub and 1" cycloning have removed the coarse silica particles and enriched kaolinite content in the clay. The increase in the LOI values closer to that of ideal kaolinite in SCP1 and SCP2 also indicates the marginal removal of the silica. DCB treatment has produced no change in the kaolinitic content of the sample.

It is seen that size classification has not made any appreciable change in Fe_2O_3 and TiO_2 content of samples SCP1 and SCP2 (Figure 3.7.4). However, these impurities are retained to a great extent in the finer fractions indicating that they are present in the clay in a wide size range. The presence of appreciable quantities of Fe_2O_3 (~ 95%) in the SCP2 sample gives us an idea about the ultra fine size of the 'Fe' impurities which are getting enriched in the product during size separation.

The presence of Fe and Ti and other impurity minerals of Na, K & Ca etc. in the finer size fractions indicate that they are almost uniformly distributed in all size fractions. Results of the trace elements analysis shows that the concentrations of certain elements such as Mg, Zn, Pb, Ba, Cr, Mn, P,S and Ni are relatively high in the raw clay and come down in the beneficiation products(Table 3.7.2).

110

Reductive bleaching is found to be ineffective in removing the iron and is evident from the unchanged Fe_2O_3 content of SCP2 R.B sample. Even after DCB treatment, the Fe_2O_3 percentage and the optical properties remain more or less unchanged. This shows that almost all the iron in the clay is not "free" in nature and is present in the structure of either kaolinite or ancillary mineral (mica or titania). The "a", "b" and Hun Y values do not show much decrease which confirms the presence of coloring iron impurities in the sample even after DCB treatment. The overall brightness of the ROM and product samples is found to be high in spite of having any improvement on beneficiation. Since the sample is found to contain mica and less amount of titania, it is possible that the iron remaining after DCB treatment may be present as part of the mica structure and their by affecting the overall brightness of the sample. It is also worth mention that chemical leaching has not effected any changes in the TiO_2 content. The Fe_2O_3 and TiO_2 content and optical properties of the beneficiated samples are given in Table 3.7.3 and Figure 3.7.4 represents the variation in Fe_2O_3 and TiO_2 content.

3.7.3 Mineralogical study

XRD and thermal analysis data of the ROM and beneficiated products is given in Table 3.7.1 and the XRD powder patterns in Figure 3.7.1. Kaolinite is the major mineral present in the raw clay along with quartz, mica and anatase (Table 3.1.4). An increase in the intensity of the kaolinite peak and decrease in the intensity of quartz peak in the case of SCP1 and SCP2 clearly shows the enrichment of kaolinite in the sample during the size classification.

Thermal analysis data of the ROM and beneficiated samples are given in Table 3.7.1. The total weight loss in the raw clay on heating is ~13.77% and this relatively low value can be attributed to high silica content. This value increases, as the ROM clay is beneficiated by size classification confirming the increase in kaolinite content. DTA data indicate that the ROM and the size classification products are similar. All of them give endotherms and exotherms of "kaolinite" mineral (Table 3.1.4). DCB treatment does not have any impact on the thermal properties of the sample.

The weight percentages of possible minerals in the raw and processed samples are calculated from the chemical assay and this rational analysis data is given in Table 3.7.4. The ROM clay contains kaolinie as major phase with minor amounts of ancillary

minerals such as quartz, mica, hematite and anatase. During size separation, the kaolinite content increases in the finer fractions (Figure 3.7.3) with a simultaneous decrease in the amount of quartz. But concentration of all other impurity minerals are found to increase during size classification and this shows their enrichment in the finer size fractions. However all size fractions do contain these impurities.

3.7.4 Morphological characterization

Scanning electron microscopic (SEM) pictures of the ROM clay and SCP1 are shown in Fig. 3.7.2. Typical platelet shaped kaolinite particles are observed in the raw sample. The processed clay appears to have aggregates of pseudo hexagonal platelet shaped particles of approximately 1-2 μm size.

3.8 Crystallinity of Kaolins

The presence of defects in kaolinite structure is often studied using X-ray diffraction (XRD) procedure and the Hinckley index (HI) is the most widely used relation for kaolin minerals to study the crystal structure (Hinckley,1963). The HI normally varies between ~0.2 and 1.5 and the larger the value, the greater will be the crystallinity.

Similarly, DTA can also be used to understand the crystalline nature of the kaolinite. Kaolin minerals are characterized by 2 major endothermic peaks and one exothermic peak. The exothermic peak corresponds to the destruction of kaolinite 1:1 structure and the dehydroxylation temperature of most of the kaolinites ranges from 498 to 514°C (Mackenzie, 1970). A well ordered kaolinite has an endothermic peak at ~580°C and any decrease in the dehydroxylation temperature can be attributed to the inferior ordering and crystallinity, plus some effects from the small crystal size (Keller et al, 1966). The slope ratio method was introduced by Robertson et al (1954) to detect the differences in the shapes of DTA curves. This method gives a numeric value to the symmetry of the peak and a value of 0.8 to 1.0 is usually observed for well ordered kaolinite and for disordered one, this value varies from 1.2 to 1.4.

In the present study, above mentioned mineralogical studies were carried out on SCP2 sample (<2μm fraction) and the HI was determined after the deferration of the sample using Dithionite-Citrate-Bicarbonate treatment (Mehra and Jackson, 1969). This was done to avoid the cementing of the particles by iron oxide, as it will inhibit the dispersion of the clay mineral. In addition, Cu radiations are used for the X-ray analysis

112

f the samples and high amount of iron may produce high background radiations, leading in the masking the peaks. The salient features of the study are given in Table 3.8.

Mineralogical data shows that "d" value of all the samples, except that of Bankura us near to that of the characteristic value for kaolinite mineral 7.156. The HI value also found to be less for the Bankura clay while the samples from Kerala are found to have the higher HI value. Koraput and Pali samples are found to have moderate values. Similarly, the slope ratio obtained from the DTA shows the highly ordered nature of the samples from Kerala.

3.9 Possible applications of the beneficiated kaolins

Kaolin finds application in a variety of industries like paper, ceramics, rubber, plastics, cement, ink, catalyst, fiberglass etc. High value addition is achieved when the processed clay becomes suitable as pigment in paper and paint industries (Murray, 1986). For some applications such as cement industry, there is no critical specification for kaolin and the only concern is light color and correct chemical composition. Ceramic industry is a large user of kaolin in white ware, insulators and refractory and the specifications are variable as the individual users may have different requirements with respect to strength, plasticity, fired color, shrinkage and pyrometric cone equivalent (PCE).

For some other uses, kaolin has to meet rigid specifications such as particle size, brightness, color and viscosity. Kaolin has to meet stringent specifications for optical properties (brightness and color) when it is to be used as pigment in paper and paint industries. Particle size distribution of kaolin is of great significance because it affects viscosity, brightness, opacity, gloss, ceramic strength and shrinkage and many other properties. The percentage of < 2 μm fraction constitutes the major portion of paper coating and high glossing paint clays. Brightness is of kaolin determines the potential uses and prices in pigment industry. Viscosity, the flow property of the kaolin used in paper coating is very important and low viscosity kaolins are required for paper coating applications. Fine particle sized kaolin is used in film formation as it greatly enhance the quality of films formed by polymers that are used as binders. This application in film formation includes paper coating, paint and ink. There is no naturally occurring or synthetic pigment which has got better rheology, brightness, opacity in coatings and contributes effectively to film gloss at low cost . The glossy nature arises due to both the

113

in particle size and thin platelet shape of kaolin. Kaolin is used as the usual filler in white papers such as newsprint, printing grades, uncoated book to attain certain desirable properties such as increased opacity, brightness, smoothness and improved ink receptivity and printability. Reinforcing and stiffening properties of kaolin makes it excellent filler in rubber, fiber and plastic industries. Fine kaolin gives good resistance to abrasion and is used extensively in non-black rubber goods. It finds application in plastic industry because kaolin aids in producing a smooth surface finish, reduces cracking and shrinking, obscures the fiber pattern when fiberglass is used as reinforcement, contributes to a high dielectric strength, improves resistance to chemical action and weathering. Fine particle, airfined kaolin (90% < 2 μm) is used as a polishing agent in toothpaste, automobiles and soft metal polishes.

In the present study, beneficiated clays of different grades are produced at various stages and their utilitarian aspect has been explored by comparing their critical properties such as particle size distribution and brightness with the required standard specifications for various end uses. This is done to have an idea about the possible value addition of these clays. The different beneficiated samples taken are the (1) < 45 μm fraction (SCP1) (2) its calcined product at 1100°C (3) <2 μm fraction (SCP2) (4) reductive bleached SCP2 and (5) DCB treated SCP2. The salient features are given in Tables 3.9.12, 3.9.13 and 3.9.14. Though DCB treatment is not a viable option for the beneficiation of kaolin on an industrial scale, here it is carried out to get quantitative information about the removable free iron in the clay. A photograph of the samples before and after DCB treatment is given in Figure 3.9.1. On an industrial scale, their removal is done by employing various sophisticated methods such as high gradient magnetic separation, froth flotation etc. The international / national specifications of the kaolin for various applications are given in Tables 3.9.1 to 3.9.11 (Roskill, The Economics of kaolin 2000; Murray, 1993).

3.9.1 Comparison of properties of the product clays with international specifications

The product of the first level size classification (SCP1) of most of the kaolins under study have got reasonably good optical properties (Kasargod 1, Trivandrum, Kutch and Pali samples) and contain good percentage of particles <2 μm fraction (Trivandrum, Kutch and Pali clays). Table 3.9.12 gives the particle size distribution and brightness of

114

rious products of beneficiation. But critical properties of none of the above samples match with the required specifications for either paper coating or filler grade kaolin. The percentage of finer fraction (<2 μm) in Trivandrum, Kutch, Koraput and Pali clays falls within the range for its use in ceramic industry for the production of white wares (Table 3.9.5). However, the iron content has to be brought down to the required level. This indicates that the samples have to be beneficiated further for it s optimum utilization.

Further size classification has increased the finer size fraction in all clays and is evident from the percentage of < 2 μm fraction in the second beneficiated product (SCP2). The Trivandrum kaolin is found to have maximum fines followed by Pali and Kutch samples and the values of first two samples are comparable with the that of Grade A paper filler grade kaolin of Imerys, UK (Table 3.9.5) and all the samples needs further improvement in optical properties to achieve optimum value addition. Also the critical properties of Trivandrum clay shows that, it is equivalent to the product EG-21 of one of the pioneers of kaolin processing, Thiele Kaolin Company, USA and it can be used as a filler in paper industry (Table 3.9.4). Chemical assay of the samples matches with that of the commercial kaolin products and shows that, except the samples from Bankura and Pali, all others can be used for the different types of coating in paper coating as well as ceramic industries (Table 3.9.9). At the same time, the optical properties of these kaolin samples are to be improved to match with the required specifications of the paper coating industries.

Reductive bleaching has not made any appreciable improvement in the optical properties of clay samples and the properties of the SCP2 RB samples are almost identical to those of SCP2 (Table 3.9.12). Samples can be used in paper coating and paper filling purposes only after further improving their optical properties.

The optical properties of most of the samples have improved appreciably after OB treatment. The extent of brightness improvement shows that they are amenable to alteration and the iron impurities can be removed by employing suitable advanced beneficiation techniques. Out of the seven clays, the sample from Trivandrum district is found to contain maximum fines (<2 μm fraction) and have the maximum brightness value and its superior quality is comparable to that of internationally used high quality coating grade clays (High Brightness No.1) [Tables 3.9.1 and 3.9.2]. Similarly, the

115

properties of samples Kasargod-1, Kasargod-2 and Koraput are found to be matching with the required specifications of commercial grade products of internationally acclaimed companies such as Thiele Kaolin Company (USA) and Imerys (UK) for their end use in paper filling applications. Also, the clay from Pali can be used as Grade C paper filler kaolin (Tables 3.9.4. and 3.9.5). All other samples are found to be promising and can be value added by employing suitable beneficiation techniques.

It is observed that calcination has improved the optical properties of only Trivandrum kaolin. The high brightness of the sample matches well with the international specifications for its possible use in paint industries. Table 3.9.6 shows that it can be used in a variety of paint formulations.

3.9.2 Comparison of properties of the products with IS specifications

Properties of the beneficiated products from six clays, except that from Koraput which is separately dealt in Chapter 7, are compared with the IS specifications for their possible use in paper and ceramic industry. The IS specification s for light kaolin and ceramic grade china clay are represented in Table 3.9.10 and 3.9.11 respectively. The overall properties of the size classification products (SCP1 and SCP2) determined in this study are given in Tables 3.9.13 and 3.9.14.

The SCP1 and SCP2 samples of all the clays are found have the required particle size distribution as per the IS specifications for Grade I (paper) and Grade II (filler) kaolin. But the iron content as well as the brightness values of all these samples, except that of Trivandrum clay, is less compared to the required specifications and further beneficiation of these samples are essential for their value addition. Though the Pali sample has got the required brightness, the iron content is higher for Grade I and II kaolins as per the IS specifications. Other properties of the clays are more or less matching with the specifications and the same can be fine tuned during the subsequent beneficiation of the clay. Reductive bleaching (of SCP2) has not made any significant improvement in optical properties of any of the clay samples and the properties are similar before and after the bleaching. However, the optical properties of all the clays, except that of Kutch and Pali samples, have increased appreciably with simultaneous reduction in Fe_2O_3 values after DCB treatment. This has made the DCB treated product comparable with the Grade I kaolin used in the paper industry. Accordingly, DCBT

116

products of Kasargod-1, Kasargod-2 and Trivandrum clays are found to satisfy the requirements for Grade I kaolin. Kaolins from Kutch, Bankura and Pali can be used as Bar (Grade II) kaolin. It implies that all the six clay samples can be further value added by effecting the iron removal from these samples by sophisticated beneficiation techniques such as high gradient magnetic separation, froth flotation etc. Calcined product from Trivandrum kaolin is found to be of superior quality and can be used in paint and other suitable industries after grinding it to the desired particle size.

In the present work, the plastic and fired properties of the clays have not been studied and the utilitarian aspect of the samples for ceramic industry has been discussed here only on the basis of their chemical assay and particle size distribution. Their possible use in ceramic industry can be truly assessed only after studying their plasticity and firing behaviour.

The SCP1 and SCP2 samples of Trivandrum kaolin are found to have the required particle size distribution and the metal oxide content (Fe, Al and Ti) are as per the specifications. Hence, they can be used in the manufacture of high quality ceramic products (Grade I kaolin). The high (Fe_2O_3 + TiO_2) content makes the Kutch and Pali clays inferior to Trivandrum sample and they can be used only as Grade II kaolin. None of the other SCP1 samples have the required quality to use them in ceramic industry. The enhancement of finer fractions makes the SCP2 samples of Kasargod 1 and 2 suitable for ceramic industry as Grade III kaolin. The very high (Fe_2O_3 + TiO_2) content makes the Bankura clay unsuitable for its use in ceramic industry.

References

Brady N.C., Weil R.R., 1996. The Nature and Properties of Soils, 11th Edition, Upper Saddle River, New Jersey, USA: Prentice Hall.

2 Borggaard O.K., 1988. Phase identification by selective dissolution techniques, In : Iron in Soils and Clay Minerals (J.W.Stucki, B.A.Goodman and Schwertmann Editors). NATO Advanced Science InstitutesSeries, D.Riedel Publishing Company, Dordrecht, Holland, 83-94

3 Chi Ma., Eggleton R.A., 1999. Cation exchange capacity of kaoilnite, Clays & Clay Minerals, 47, No.2, 174-180

4 Foth H. D., Ellis B.G., 1996. Soil Fertility, Lewis Publishers, CRC Press, Inc. New York, p.25-31

5 IS 505, 1999, Specifications for light kaolin

6 IS 2840 : 2002 China clay for ceramic industry

7 Mackenzie R.C. (1970) Simple phyllosilictes, in Differential Thermal Analysis (eds. R.C.Mackenzie), Academic Press, London, 775

8 Mehra, O.P., Jackson M.L., 1960. Fe Oxide removal from soil and clays by a dithionite-citrate system buffered with sodium carbonate. Clays and Clay Minerals, 7, 317-327

9 Murray H.H., 1986. Clays. Ullmann's Encyclopaedia of Industrial Chemistry, 5th Edition, VCH Publishers, 109-136

10 Murray, H.H. and Keller, W. (1993) Kaolin, Kaolin and Kaolin, In : Kaolin Genesis and Utilization, Murray, H.H.,Bundy, W. and Harvey, C. eds., Special publication No.1,The Clay Mineral Society, 1-24.

11 The Economics of kaolin, 2000, Roskill Information Book

12 Searle, A.B., Grimshaw, R.W., 1960. Chemistry and Physics of Clays. Western Printing Services Ltd., Bristol, UK. 944

Table 3.1 Details of kaolin samples under investigation

SLNo.	States & Samples	Mines / Districts	Source
1	**Kerala** Kasargod 1 Kasargod 2	Both from Neeleswar mines, Kasargod	Kerala Clays & Ceramic Products Ltd., Govt. of Kerala, Kannur
	Trivandrum	Thonnakkal mines, Trivandrum	M/s. English Indian Clays Ltd., Veli Trivandrum
2	**Orissa** Koraput	Koraput Taluk, Koraput	M/s Balaji Minerals, Chebrole, AP Mr.Verma, Transworld Services, Vizag
3	**Gujarat** Kutch	Kutch mines	Gujarat Mineral Development Corporation, Ahmedabad
4	**West Bengal** Bankura	Bankura	Dept.Mines & Minerals Govt.of WB, Bankura West Bengal Proj. Ltd., Govt.of WB Kolkatta
5	**Rajasthan** Pali	Jaitaran, Nimaj, Pali	M/s Sikhwal Chemicals, Jaitaran

119

Table 3.1.1 Chemical assay, mineralogy and physical properties of ROM and beneficiated samples of Kasargod 1 kaolin

Particulars	ROM	SCP1	SCP2	SCP2-DCBT
ChemAssay (% wt)				
SiO_2	48.30	45.82	46.76	46.82
Al_2O_3	36.55	37.83	37.46	37.62
Fe_2O_3 (Total iron)	1.02	0.75	0.70	0.50
$TiO2$	0.65	0.49	0.20	0.20
CaO	0.13	0.07	0.06	0.06
Na_2O	0.35	0.24	0.13	0.13
K_2O	0.38	0.20	0.20	0.20
LOI	12.69	14.57	14.48	14.46
FeO	0.14	---	---	---
Physical Properteis				
Particle Size Distribution, wt. %				
>45 μm	10.10	0.00	0.00	0.00
<45 >2μm	54.90	56.10	37.90	37.90
<2μm	35.00	43.90	62.10	62.10
Optical Properties (% ISO)				
Brightness	74.56	77.36	78.04	86.86
L	88.28	90.49	90.98	93.96
a	1.04	0.93	0.91	0.32
b	3.95	3.74	3.58	1.12
HUN W	64.07	64.39	64.65	82.28
HUN Y	6.45	5.87	5.65	1.70
pH	5.63	5.65	5.66	---
Cation exchange capacity ,meq/100 g	8.41	8.37	8.29	---
Water solubles, % w/w	0.437	0.415	0.410	---
Acid soluble, % w/w	0.247	0.157	0.155	---
Specific gravity, g/cc	2.66	2.61	2.60	2.60
Mineralogy				
XRD				
Major phases	K	K	K	K
Minor phases	Q,H,A,R	Q,H,A,R	Q,H,A,R	Q,A,R
DTA				
Endotherm (°C)	538.9	536.6	532.7	532.6
Exotherm (°C)	995.3	995.3	989.9	989.8
TG (wt. loss %)	12.26	14.57	14.60	14.59

Q-Quartz; K-Kaolinite; R-Rutile; A-Anatase; H-Hematite

Table 3.1.2 Trace elements in ROM and beneficiated samples of Kasargod 1 kaolin (µg / g)

Elements	ROM	SCP1	SCP2	SCP2-DCBT
Arsenic	9.80	5.21	3.89	3.13
Barium	89.61	65.09	61.72	20.38
Bismuth	3.43	3.12	2.87	BDL
Cadmium	4.21	3.57	2.94	BDL
Cobalt	2.85	2.28	2.05	1.43
Chromium	99.14	92.09	88.86	81.93
Copper	19.02	13.75	11.55	9.84
Magnesium	383.36	365.42	232.95	134.09
Manganese	52.61	8.57	2.90	BDL
Nickel	34.43	34.29	32.97	28.90
Phosphorous	79.99	59.59	43.95	16.94
Lead	54.33	7.47	1.52	BDL
Sulphur	177.44	93.60	75.38	57.09
Zinc	89.34	63.27	50.53	10.94

BDL - <1 ppm

Table 3.1.3 Optical properties and Fe & Ti content in the beneficiated samples of Kasargod 1 kaolin

Sample	% Fe_2O_3	% TiO_2	B % ISO	L	a	b	HW	HY
SCP1	0.75	0.49	77.36	90.49	0.93	3.74	64.39	5.87
SCP1 calcined	---	---	76.28	88.72	1.09	3.97	63.74	6.17
SCP2	0.70	0.20	78.04	90.98	0.91	3.74	64.65	5.65
SCP2 R.B	0.68	0.20	78.26	91.06	0.88	3.44	65.10	5.41
SCP2 DCBT	0.50	0.21	86.86	93.96	0.32	1.12	82.28	1.70

Table 3.1.4 Characteristic XRD d-values and temperatures of DTA endotherms and exotherms of minerals

Minerals	Three principal XRD peaks d-value (A°)			Main DTA peaks Temp. °C	
				Endotherm	Exotherm
Kaolinite	7.15	3.566	2.331	585 (L)	985 (L)
Quartz	3.35	1.814	4.21	573 (V.S)	--
Anatase	3.51	1.89	1.70	---	---
Rutile	3.24	1.36	1.69	---	---
Pseudo Rutile	3.04	2.47	2.30	---	---
Ilmenite	3.47	1.88	2.90	---	---
Hematite	2.69	2.51	1.69	---	---
Magnetite	2.53	1.48	2.96	620 (S)	---
Goethite	4.15	2.43	2.67	335	---
Calcite	3.03	1.917	1.868	880 (L)	---
Pyrite	1.63	2.42	2.70	---	440 (L)
Zircon	3.29	2.52	1.71	---	---
Muscovite mica	9.98	3.33	2.57	600-900 (B)	---
Paragonite	9.97	4.41	3.10	---	---
Biotite	10.1	3.36	2.65	550 (M) 700-900 (B)	--- ---
Graphite	3.37	2.02	1.16	---	820 (V.L)

B-Broad: L-Large; V.L–Very Large; M-Medium; S-Small; V.S-Very small

Table 3.1.5 Rational analysis data of ROM and beneficiated samples of Kasargod 1 kaolin

Mineral % by wt.	ROM	SCP1	SCP2
Kaolinite	85.39	92.28	91.61
Quartz	5.13	0.99	2.63
Muscovite mica	3.18	1.71	1.69
Paragonite mica	4.28	1.77	1.60
Hematite	1.02	0.75	0.70
Anatase	0.65	0.49	0.20
Calcite	0.23	0.12	0.11

Table 3.2.1 Chemical assay, mineralogy and physical properties of ROM and beneficiated samples of Kasargod 2 kaolin

Particulars	ROM	SCP1	SCP2	SCP2 - DCBT
Chem.Assay (% wt)				
SiO$_2$	51.93	45.26	46.96	46.96
Al$_2$O$_3$	36.90	37.78	36.18	36.18
Fe$_2$O$_3$ (Total iron)	1.15	1.07	1.01	0.61
TiO2	0.57	0.49	0.41	0.34
CaO	0.13	0.06	0.06	0.06
Na$_2$O	0.20	0.10	0.32	0.32
K$_2$O	0.41	0.22	0.20	0.20
LOI	8.39	14.27	14.53	14.53
FeO	0.19	---	---	---
Physical Properteis				
Particle Size Distribution, wt.%				
> 45 µm	36.80	0.00	0.00	0.00
< 45 > 2µm	36.37	54.30	40.70	40.70
< 2µm	26.83	45.70	59.30	59.30
Optical Properties (% ISO)				
Brightness	60.51	66.65	67.56	83.27
L	80.12	85.03	85.66	92.72
a	3.33	3.03	2.60	-0.36
b	5.30	4.93	4.73	2.15
HUN W	49.08	49.33	49.74	74.59
HUN Y	8.05	7.94	7.51	3.31
pH	5.21	5.20	5.20	---
Cation exchange capacity, meq/100 g	9.97	9.76	9.37	---
Water solubles, % w/w	0.29	0.26	0.25	---
Acid soluble, % w/w	1.03	0.81	0.80	---
Specific gravity, g/cc	2.63	2.55	2.55	2.54
Mineralogy				
XRD				
Major phases	K	K	K	K
Minor phases	Q,A,R,H	Q,A,R,H	Q,A,R,H	Q,A,R
DTA				
Endotherm (°C)	527.5	532.1	532.7	532.7
Exotherm (°C)	995.3	993.0	994.7	994.7
TG (wt. loss %)	9.46	12.41	13.13	13.14

Q-Quartz; K-Kaolinite; R-Rutile; A-Anatase; H-Hematite

Table 3.2.2 Trace elements in the ROM and beneficiated samples of Kasargod 2 kaolin (µg / g)

Elements	ROM	SCP1	SCP2	SCP2-DCBT
Arsenic	6.82	4.08	2.12	BDL
Barium	88.91	45.24	43.75	23.42
Bismuth	2.31	2.17	2.05	BDL
Cadmium	3.43	2.98	2.65	BDL
Cobalt	7.34	5.68	2.05	BDL
Chromium	146.08	104.44	100.57	46.87
Copper	65.42	19.30	18.91	10.25
Magnesium	308.08	302.71	93.70	46.98
Manganese	34.53	23.76	18.24	1.65
Nickel	44.05	36.41	32.94	15.87
Phosphorous	110.99	91.16	60.55	35.73
Lead	31.75	27.63	23.04	BDL
Sulphur	241.15	237.16	225.19	187.08
Zinc	91.48	86.62	84.80	38.53

BDL - <1 ppm

Table 3.2.3 Optical properties and Fe & Ti content in the beneficiated samples of Kasargod 2 kaolin

Samples	Fe_2O_3 %	TiO_2 %	B % ISO	L	a	b	HW	HY
SP1	1.07	0.49	66.65	85.03	3.03	4.93	49.33	7.94
SP1 after calcination	---	---	69.07	85.41	1.54	3.25	57.09	5.43
SP2	1.01	0.41	67.56	85.66	2.60	4.73	49.74	7.51
SP2 RB	0.95	0.41	68.12	85.74	2.41	4.47	51.60	7.32
SP2 after DCBT	0.61	0.34	83.27	92.72	-0.36	2.15	74.59	3.31

124

Table 3.2.4 Rational analysis data of ROM and beneficiated samples of Kasargod 2 kaolin

Mineral % by wt.	ROM	SCP1	SCP2
Kaolinite	87.54	92.61	85.95
Quartz	8.46	0.76	4.34
Muscovite mica	3.46	1.88	1.70
Paragonite mica	2,51	1.24	3.97
Hematite	1.06	0.80	1.07
Anatase	0.57	0.49	0.41
Calcite	0.23	0.12	0.11

Table 3.3.1 Chemical assay, mineralogy and physical properties of ROM and beneficiated samples of Trivandrum kaolin

Particulars	ROM	SCP1	SCP2	SCP2-DCBT
Chem.Assay (% wt)				
SiO_2	45.86	46.18	46.35	46.40
Al_2O_3	36.02	36.42	37.88	38.05
Fe_2O_3 (Total iron)	0.75	0.62	0.35	0.18
$TiO2$	0.66	0.53	0.52	0.50
CaO	0.19	0.80	0.19	0.18
Na_2O	0.36	0.12	0.27	0.25
K_2O	0.39	0.04	0.15	0.14
LOI	13.60	14.31	14.10	14.16
FeO	0.09	---	---	---
Physical Properteis				
Particle Size Distribution, wt.%				
>45 μm	6.20	0.00	0.00	0.00
<45 >2μm	24.51	16.42	8.08	8.06
<2μm	69.29	83.58	91.92	91.94
Optical Properties (% ISO)				
Brightness	77.71	78.17	80.86	89.85
L	90.30	90.95	92.20	96.23
a	2.75	2.39	1.76	-0.41
b	3.02	3.60	3.27	2.12
HUN W	65.96	66.01	67.83	80.97
HUN Y	4.78	5.65	5.07	3.14
pH	6.89	6.91	6.90	---
Cation exchange capacity, meq/100 g	8.43	8.43	8.43	---
Water solubles, % w/w	0.79	0.64	0.60	---
Acid soluble, % w/w	1.33	1.17	1.08	---
Specific gravity, g/cc	2.65	2.63	2.61	2.61
Mineralogy				
XRD				
Major phases	K	K	K	K
Minor phases	Q,,A,R,H	Q,A, R,H	Q,A,R,H	Q,A,R
DTA				
Endotherm (°C)	521.9	525.4	525.7	525.8
Exotherm (°C)	999.9	999.9	999.8	999.7
TG (wt. loss %)	12.78	14.24	14.20	14.21

Q-Quartz; K-Kaolinite; R-Rutile; A-Anatase; H-Hematite

Table 3.3.2 Trace elements in the ROM and beneficiated samples of Trivandrum kaolin samples (µg / g)

Elements	ROM	SCP1	SCP2	SCP2-DCBT
Arsenic	BDL	BDL	BDL	BDL
Barium	25.4	20.7	19.8	18.2
Bismuth	1.2	1.1	1.1	BDL
Cadmium	BDL	BDL	BDL	BDL
Cobalt	4.4	3.9	3.1	1.8
Chromium	127.3	102.2	98.4	65.1
Copper	22.8	18.5	16.3	7.9
Magnesium	167.1	143.0	128.3	90.6
Manganese	25.8	20.5	17.4	2.6
Nickel	76.1	64.9	58.1	50.8
Phosphorous	265.8	253.2	184.8	182.0
Lead	22.4	19.7	18.9	10.7
Sulphur	305.0	296.1	295.9	294.3
Zinc	71.4	64.2	47.6	31.1

BDL - <1 ppm

Table 3.3.3 Optical properties and Fe & Ti content in beneficiated samples of Trivandrum kaolin

Samples	Fe_2O_3 %	TiO_2 %	B % ISO	L	a	b	HW	HY
SCP1	0.62	0.43	78.17	90.95	1.76	3.60	64.01	5.65
SCP2	0.35	0.52	80.86	92.20	2.39	3.27	67.83	5.07
SCP1 after calcination	---	---	89.90	96.27	-0.39	2.11	80.96	3.12
SCP2 after reductive bleaching	0.30	0.50	81.54	92.97	2.05	3.12	68.34	4.89
SCP2 after DCBT	0.18	0.50	89.85	96.23	-0.41	2.12	80.97	3.14

127

**Table 3.3.4   Rational analysis data of ROM and
beneficiated samples of Trivandrum kaolin**

Mineral % by wt.	ROM	SCP1	SCP2
Kaolinite	83.39	90.75	91.85
Quartz	3.43	3.28	1.73
Muscovite mica	3.29	0.34	1.27
Paragonite mica	4.43	1.47	3.33
Anatase	0.66	0.53	0.52
Hematite	0.75	0.62	0.35
Calcite	0.34	1.43	0.33

Table 3.4.1 Chemical assay, mineralogy and physical properties of ROM and beneficiated samples of Kutch kaolin

Particulars	ROM	SCP1	SCP2	SCP2-DCBT
Chem.Assay (% wt)				
SiO_2	45.81	45.21	45.39	45.45
Al_2O_3	37.72	37.98	37.96	38.08
Fe_2O_3 (Total iron)	0.86	0.61	0.43	0.27
$TiO2$	1.63	1.53	1.60	1.59
CaO	0.32	0.11	0.06	0.05
Na_2O	0.29	0.33	0.13	0.11
K_2O	0.03	0.01	0.02	0.02
LOI	13.56	14.22	14.31	14.35
FeO	0.10	---	---	---
Physical Properteis				
Particle Size Distribution,wt.%				
> 45 µm	3.00	0.80	0.00	0.00
< 45 > 2µm	28.70	28.60	17.70	17.64
< 2µm	58.30	70.60	82.30	82.36
Optical Properties (% ISO)				
Brightness	70.34	72.50	73.57	77.81
L	89.18	90.12	90.52	91.77
a	0.61	0.61	0.63	-0.51
b	6.01	6.05	6.09	5.16
HUN W	45.14	46.44	49.69	57.16
HUN Y	10.58	10.47	9.67	8.03
pH	5.38	5.31	5.26	---
Cation exchange capacity ,meq/100 g	9.34	9.11	9.04	---
Water solubles, % w/w	0.65	0.48	0.43	---
Acid soluble, % w/w	1.47	1.21	1.15	---
Specific gravity, g/cc	2.7	2.68	2.66	2.66
Mineralogy				
XRD				
Major phases	K	K	K	K
Minor phases	Q, R, A,H	Q,A,R,H	Q,A,R,H	Q,A,R
DTA				
Endotherm (°C)	539.7	524.7	524.9	524.8
Exotherm (°C)	994.4	985.4	985.6	985.7
TG (wt. loss %)	13.20	14.29	14.30	14.31

K-Kaolinite, Q-Quartz, A-Anatase, R-Rutile; H-Hematite

Table 3.4.2 Trace elements in ROM and beneficiated samples of Kutch kaolin (µg / g)

Elements	ROM	SCP1	SCP2	SCP2-DCBT
Arsenic	2.3	BDL	BDL	BDL
Barium	76.3	53.8	47.2	32.1
Bismuth	2.6	2.5	2.0	BDL
Cadmium	1.1	1.0	BDL	BDL
Cobalt	2.3	1.9	1.4	1.1
Chromium	54.4	50.1	46.7	23.7
Copper	10.9	7.9	7.3	1.8
Magnesium	169.3	146.7	133.6	114.6
Manganese	6.7	4.6	4.1	BDL
Nickel	43.2	39.8	37.5	18.3
Phosphorous	258.6	201.6	189.5	178.7
Lead	49.4	35.5	30.8	19.2
Sulphur	593.3	511.2	490.9	476.1
Zinc	54.9	39.4	36.8	14.9
Zirconium	63.0	50.2	48.9	47.1

BDL - <1 ppm

Table 3.4.3 Optical properties and Fe & Ti content in beneficiated samples of Kutch kaolin

Samples	Fe_2O_3 %	TiO_2 %	B % ISO	L	a	b	HW	HY
SCP1	0.61	1.53	72.50	90.12	0.61	6.05	46.44	10.4
SCP2	0.43	1.60	73.57	90.52	0.63	6.09	49.69	9.67
SCP1 after calcination	---	---	74.46	90.99	0.54	5.78	50.13	9.21
SCP2 R.B	0.40	1.60	73.96	90.78	0.57	5.94	49.91	9.58
SCP2 after DCBT	0.27	1.59	77.81	91.77	-0.51	5.16	57.16	8.03

Table 3.4.4 Rational analysis data of ROM and beneficiated samples of Kutch kaolin

Mineral % by wt.	ROM	SCP1	SCP2
Kaolinite	92.75	93.14	94.82
Quartz	1.38	0.47	0.67
Muscovite mica	0.25	0.09	0.17
Paragonite mica	3.58	4.07	1.60
Anatase	1.63	0.61	1.60
Hematite	0.86	1.53	0.43
Calcite	0.57	0.13	0.11

Table 3.5.1 Chemical assay, mineralogy and physical properties of ROM of Koraput kaolin

Particulars	ROM
Chem.Assay (% wt)	
SiO_2	41.81
Al_2O_3	32.01
Fe_2O_3 (Total iron)	5.41
TiO2	1.60
CaO	0.69
Na_2O	0.23
K_2O	0.08
LOI	18.17
Sulphur	2.07
Organic Carbon	1.2
FeO	2.40
Pyrite	3.90
Physical Properteis	
Particle Size Distribution,wt.%	
> 45 μm	16.80
< 45 > 2μm	43.30
< 2μm	49.90
Optical Properties (% ISO)	
Brightness	45.87
L	67.43
a	-0.75
b	-0.44
HUN W	27.17
HUN Y	0.94
pH	1.72
Cation exchange capacity ,meq/100 g	2.1
Water solubles, % w/w	4.14
Acid soluble, % w/w	9.06
Specific gravity, g/cc	2.78
Mineralogy	
XRD	
Major phases	K, Q
Minor phases	P
DTA	
Endotherm (°C)	534.3, 684.9, 73.4
Exotherm (°C)	468.0, 554.8, 983.8
TG (wt. loss %)	18.27

K-Kaolinite; Q-Quartz; P-Pyrite

Table 3.5.2 Trace elements in the ROM of Koraput kaolin

Elements	Concentration µg / g	Elements	Concentration µg / g
Barium	304	Sodium	148
Calcium	569	Nickel	83
Cadmium	<2	Phosphorous	1537
Cobalt	647	Lead	145
Chromium	145	Strontium	212
Copper	36	Vanadium	133
Potassium	134	Zinc	154
Lanthanum	68	Zirconium	403
Magnesium	68		
Manganese	35		

<1 ppm - BDL

Table 3.5. 3 Rational analysis data of ROM of Koraput kaolin

Mineral % by wt.	ROM clay	Mineral % by wt.	ROM clay
Kaolinite	77.54	Hematite	2.84
Quartz	4.10	Anatase	1.60
Muscovite mica	0.68	Calcite	1.78
Paragonite mica	2.84	Carbonaceous matter	4.75
Pyrite	3.87		

Table 3.6.1 Chemical assay, mineralogy and physical properties of ROM and beneficiated samples of Bankura kaolin

Particulars	ROM	SCP1	SCP2	SCP2-DCBT
Chem Assay (% wt)				
SiO_2	72.54	53.85	49.16	49.17
Al_2O_3	16.20	26.70	30.01	32.70
Fe_2O_3 (Total iron)	3.94	5.17	5.66	0.94
$TiO2$	0.44	0.77	0.28	0.28
CaO	0.80	2.31	2.12	2.22
Na_2O	0.28	0.35	0.48	0.59
K_2O	1.25	3.05	2.66	2.85
LOI	4.56	7.77	9.64	10.14
FeO	1.71	---	---	---
Physical Properteis				
Partcle Size Distribution, wt. %	43.09	0.00	0.00	0.00
>45 μm	36.81	57.58	44.24	44.24
<45 >2μm	20.10	42.42	55.76	55.76
<2μm				
Optical Properties (% ISO)				
Brightness	37.69	41.48	41.79	69.67
L	74.29	80.14	81.09	86.16
a	0.07	0.65	1.07	-1.32
b	16.77	20.15	20.99	4.03
HUN W	16.01	28.01	31.50	54.41
HUN Y	32.25	35.92	36.98	6.68
pH	7.55	7.50	7.47	---
Ion exchange capacity ,meq/100 g	11.85	11.54	11.42	---
Water solubles, % w/w	1.28	1.20	1.11	---
Acid soluble, % w/w	2.50	2.48	2.29	---
Specific gravity, g/cc	2.63	2.57	2.54	2.53
Mineralogy				
XRD				
Major phases	Q,K	Q,K	Q,K	Q,K
Minor phases	Mi, R, A, H	Mi, R, A, H	Mi ,R,A, H	Mi,R,A
DTA				
Endotherm (°C)	85.1,532.7,575.8	73.4,525.2	80.2,532.1	80.2,
Exotherm (°C)	975.6	717.0, 963.3	963.3	532.1 963.3 80.2,532.1
Wt. loss %)	5.02	6.22	10.10	10.11

K-Kaolinite, Q-Quartz, Mi-Mica, R-Rutile, A-Anatase; H-Hematite

Table 3.6.2 Trace elements in ROM and beneficiated samples of Bankura kaolin (µg / g)

Elements	ROM	SCP1	SCP2	SCP2-DCBT
Arsenic	18.18	14.14	13.93	5.41
Barium	114.43	43.43	40.62	33.31
Bismuth	2.31	2.19	1.84	BDL
Cadmium	2.24	2.12	2.00	BDL
Cobalt	11.16	10.38	9.00	5.28
Chromium	91.75	70.17	56.46	35.74
Copper	21.62	18.57	27.77	22.86
Magnesium	368.28	294.62	238.71	141.47
Manganese	73.66	55.53	51.32	7.07
Nickel	24.88	22.55	21.50	16.71
Phosphorous	80.79	65.31	54.65	44.56
Lead	39.10	25.20	23.48	5.02
Sulphur	301.03	155.30	72.80	37.34
Zinc	467.61	65.62	62.36	51.72

BDL - <1 ppm

Table 3.6.3 Optical properties and Fe & Ti content in beneficiated samples of Bankura kaolin

Samples	Fe_2O_3 %	TiO_2 %	B % ISO	L	a	b	HW	HY
SCP1	5.17	0.77	41.48	80.14	0.65	20.15	28.01	35.92
SCP1 after calcination	---	---	20.34	59.98	3.32	27.76	20.02	47.11
SCP2	5.66	0.28	41.79	81.09	1.07	20.99	31.50	36.98
SCP2 after reductive leaching	4.86	0.28	46.45	84.67	0.89	20.42	33.04	29.19
SCP2 after DCBT	0.94	0.28	69.67	86.16	-1.32	4.03	54.41	6.68

Table 3.6.4   Rational analysis data of ROM and beneficiated samples of Bankura kaolin

Mineral % by wt.	ROM	SCP1	SCP2
Kaolinite	27.74	38.15	47.31
Quartz	54.22	22.52	14.41
Muscovite mica	10.58	25.80	23.35
Paragonite mica	3.45	4.06	5.89
Anatase	0.44	0.78	0.28
Hematite	3.94	5.17	5.66
Calcite	1.61	4.12.	3.78

Table 7.1 Chemical assay, mineralogy and physical properties of ROM and beneficiated samples of Pali kaolin

Particulars	ROM	SCP1	SCP2	SCP2-DCBT
Chem.Assay (% wt)				
SiO_2	52.52	48.55	46.17	46.17
Al_2O_3	33.04	34.18	35.66	35.66
Fe_2O_3 (Total iron)	1.10	1.13	1.04	1.00
$TiO2$	0.52	0.62	0.55	0.49
CaO	0.34	0.45	0.51	0.51
Na_2O	0.33	0.33	0.37	0.37
K_2O	0.56	0.70	0.62	0.62
LOI	11.79	13.23	14.30	14.30
FeO	0.53	---	---	---
Physical Properteis				
Particle Size Distribution,wt.%	0.4	0.0	0.0	0.0
>45 μm	26.90	24.30	16.70	16.70
<45 >2μm	72.7	75.7	83.3	83.3
<2μm				
Optical Properties (% ISO)				
Brightness	80.16	79.97	81.17	81.27
L	93.01	92.65	93.63	93.71
a	-0.50	-0.44	-0.41	-0.43
b	4.98	4.50	4.20	3.56
HUN W	60.02	61.86	66.59	66.77
HUN Y	7.65	7.72	6.95	5.49
pH	7.00	6.95	6.89	---
Cation exchange capacity ,meq/100 g	9.02	8.73	8.68	---
Water solubles, % w/w	0.53	0.49	0.44	---
Acid soluble, % w/w	1.04	0.92	086	---
Specific gravity, g/cc	2.61	2.58	2.55	2.54
Mineralogy				
XRD				
Major phases	K	K	K	K
Minor phases	Q, Mi, A	Q, Mi, A	Q, Mi, A	Q, Mi, A
DTA				
Endotherm (°C)	75.5,547.1	75.5,547.1	73.2,547.1	73.2,547.1
Exotherm (°C)	975.6	978.0	975.5	975.5
TG (wt. loss %)	13.77	13.93	14.05	14.05

K-Kaolinite; Q-Quartz; M-Mica; A-Anatase

Table 3.7.2 Trace elements in the ROM and beneficiated samples of Pali kaolin

(μg / g)

Elements	ROM	SCP1	SCP2	SCP2-DCBT
Arsenic	9.80	8.67	7.56	1.48
Barium	157.00	84.85	49.61	22.69
Bismuth	4.56	3.97	3.62	BDL
Cadmium	2.53	2.25	2.10	BDL
Cobalt	14.31	13.52	8.53	5.60
Chromium	90.35	67.94	56.20	36.24
Copper	22.84	18.99	16.36	11.05
Magnesium	1766.56	780.24	93.70	72.47
Manganese	37.10	17.06	14.24	1.92
Nickel	34.49	33.09	27.94	14.75
Phosphorous	131.12	71.14	60.55	35.96
Lead	44.89	22.23	13.04	BDL
Sulphur	183.07	179.77	154.19	132.12
Zinc	87.20	32.64	26.80	2.60

BDL - <1 ppm

Table 3.7.3 Optical properties and Fe & Ti content in the beneficiated samples of Pali kaolin

Samples	Fe_2O_3, %	TiO_2, %	B % ISO	L	a	b	HW	HY
SCP1	1.13	0.62	79.97	92.65	-0.44	4.50	61.86	7.72
SCP1 Calcined	---	---	76.36	89.11	-0.24	5.05	61.82	8.11
SCP2	1.04	0.55	81.17	93.63	-0.41	5.06	66.59	6.95
SCP2 R.B	1.03	0.55	81.18	93.64	-0.41	5.05	66.60	6.74
SCP2 DCBT	1.00	0.49	81.27	93.71	-0.43	3.56	66.77	5.49

138

Table 3.7.4 Rational analysis data of ROM and beneficiated samples of Pali kaolin

Mineral % by wt.	ROM	SCP1	SCP2
Kaolinite	74.98	76.77	80.56
Quartz	13.60	8.29	4.16
Muscovite mica	4.75	5.90	5.24
Paragonite mica	4.03	4.01	4.60
Anatase	1.10	1.13	1.04
Hematite	0.52	0.62	0.55
Calcite	0.61	0.79	0.91

Table 3.8 "d" value, HI and slope ratio of kaolins

Samples	"d" value (XRD)	Hinckley index (HI)-XRD	Slope ratio (DTA)
Kasargod-1 clay	7.16	1.38	0.76
Kasargod-2 clay	7.15	1.40	0.81
Trivandrum clay	7.15	1.42	0.80
Kutch clay	7.16	1.32	0.87
Koraput clay	7.14	1.24	0.92
Bankura clay	7.11	0.64	1.31
Pali clay	7.16	1.17	0.98

Table 3.9.1 Specifications of Thiele Kaolin Company(USA) paper coating grade kaolins (Mid Georgia deposit)

		KaoGloss	*Kaobrite*
Brightness (%)		86.5-87.5	86.5-86.6
Particle size	<2 microns, %	90-93	80-83
Viscosity, Brookfield	70% solids (cps, 20 rpm, 1 spindle)	300 (slurry)	300 (slurry)
Screen residue (% 200 mesh)	Rotary dried (acid)	0.003-0.01	0.003-0.02
+325 mesh	Rotary dried (acid)	0.005-0.15	0.001-0.02
Mositure, %	Rotary dried (acid)	2-4	2-4
pH	Slurry (predispersed)	3.5-4.5	3.5-4.6

Table 3.9.2 International Specifications for some coating grade clays

Grade	Particle size, % of < 2μm fraction	Brightness, % ISO
No.3	73	85 - 86.5
No.2	80-82	85.5 - 87.0
No.1	90-92	87.0 - 88.0
Fine No.1	95	86.0 - 87.5
Delaminated	80	88.0 - 90.0
High Brightness No.2	80	90 - 91
High Brightness No.1	92	90 - 91
High Brightness Fine No.1	95	90 – 91

Table 3.9.3 Typical specifications for types of paper coating grades of kaolin

	Brightness (%)	Particle Size (% <2 microns)	Surface Area (m2/g)	325 mesh Residue (max. %)	Moisture, max. %	pH	Viscosity, Brookfield (20 rpm, cps)
High Brightness Fine No.1	90-92	96-100	22	0.01	1.0	6.0-7.7	350
High Brightness No.1	89.5-91	90-92	13	0.01	1.0	6.0-7.6	350
High Brightness No.2	89.5-90.5	80-84	12	0.01	1.0	6.0-7.5	350
No.1 Fine coating	86.5-88	94-97	22	0.01	1.0	6.0-7.1	350
No.1 Standard Coating	86.5-87.5	90-92	13	0.01	1.0	6.0-7.9	350
Delaminated Coating	87.5-89.0	n/a	14	0.01	1.0	6.0-7.1	350

Source: Industrial Mineral Handbook, Third Edition, 1999

Table 3.9.4 Specifications of Thiele Kaolin Company paper filler grade kaolins

Trade name		Kaofill	EG-21
Brightness (%)		82.5-83.5	80.0-82.06
Particle size	<2 microns, %, min	40	86-92
Particle size	> 10 microns, %	0-8	0-2
Screen residue (% 100 mesh)	Rotary dried (acid)	0.003-0.01	0.05-0.1
% 325 mesh	Rotary dried (acid)	0.010-0.25	0.17-0.3
Mositure, %	Rotary dried (acid)	2-4	0.5-1.5
pH	Slurry (predispersed)	3.5-5.5	3.5-5.0

141

Table 3.9.5 Specifications of Imerys (formerly ECCI), UK Grade C paper filler grade kaolin

Properties	
Brightness (%, ISO)	81.0 ± 0.7
Yellowness	5.7 ± 0.5
Particle size % (< 2 microns)	50.0
Particle size % (> 10 microns)	8.0
Particle size % (> 53 microns)	0.05 (maximum)
pH	5.0 + 0.5

Table 3.9.6 Specifications of calcined kaolin for use in various types of paints

	Oleresnous	Primers	Eggshell finish paint	Interior emulsions
Mediun particle size (microns)	0.6	2.2	1.5	0.8
Brightness (%)	90-92	92.5-93.5	90-92	90-92
pH	4.2-5.2	5.0-6.0	4.2-5.2	5.0-6.0
Moisture, max.%	0.5	0.5	0.5	0.5
325 mesh residue, %	0.01	0.02	0.02	0.02
Oil absorption)g/100g)	40-45	70-75	50-55	70-75
Surface area (M^2/g)	19.0	9.0	9.0	9.0

Table 3.9.7 Properties of extender minerals used in paint formulations

Mineral	Particle shape	Particle size (microns)	Oil absorption (g/100g)	Specific gravity (g/cc)
Hydrous kaolin	Lamellar	0.2-50	30-60	2.58
Calcined kaolin	Amorphous	0.2-50	45-60	2.58
Calcium carbonate	Nodular	0.7-3.0	16-30	2.65
Titanium dioxide	Nodular	0.2	14-18	2.61
Talc	Platey/fibrous	2.5-50	25-50	2.80

Table 3.9.8 Specifications of ceramic grade kaolins produced by selected companies

	Topaz [1]	Wilkcaly WC [2]	6Tile[3]	EPK Kaolin[4]
Chemical analysis (%)				
SiO2	48.00	45.60	45.50	45.73
Al2O3	37.00	38.40	38.10	37.36
Fe2O3	0.29	0.74	0.30	0.79
TiO2	0.05	1.58	1.40	0.37
CaO	0.05	0.05	0.40	0.18
MgO	0.05	0.02	0.50	0.01
K2O	0.18	0.15	---	0.33
Na2O	0.1	0.21	0.04	0.06
Loss on ignition	12.80	13.72	13.80	13.91
Particel size distribution				
	0.05	---	---	---
+53 microns	7.00	---	---	---
+10 microns	65.00	75.00	54-65	---
-2 microns				

1 EICL Tableware
2 Wilkinson Kaolin Associates whiteware grade
3 Dry Branch Kaolin Company ceramic grade
4 The Feldspar Corporation ceramic grade

143

Table 3.9.9 Chemical analysis of selected commercial grades of kaolin

%	Coarse coating (Georgia, USA)	Fine coating (Georgia, USA)	Fine coating (Brazil)	Coarse coating (Cornwall, UK)	Ceramic grade (Germany)
SiO_2	45.20	45.00	46.00	47.20	48.30
Al_2O_3	39.20	38.00	37.00	37.60	36.30
Fe_2O_3	0.58	1.00	1.80	0.68	0.50
TiO_2	0.53	1.60	0.98	0.04	0.30
MgO	0.08	0.09	0.07	0.20	0.10
CaO	0.06	0.06	0.02	0.08	0.10
Na_2O	0.03	0.29	0.08	0.08	1.60
K_2O	0.02	0.13	0.00	1.39	0.10
LOI	13.30	14.00	14.30	12.70	---

Table 3.9.10 Indian Standard Specifications for Light kaolin, IS 505:1995 reaffirmed 1999

Sl.No.	Characteristics	Requirements for Grade1(Paper)	Requirements for Grade 2 (Filler)
1	Coarse particles or grit (residue on 53μm IS sieve), %by mass, max.	0.8	1.0
2	Particles larger than 10μm in dia, % by mass, max.	5.0	15.0
3	Particles smaller than 10μm, % by mass, min.	75	60
4	Relative density 27/27°C	2.5 - 2.9	2.5 – 2.9
5	Loss on drying, % by mass, max. Lump Powder	 10 2	 10 2
6	Loss on ignition, % by mass, max	11.0 – 15.5	11.0 – 15.5
7	Matter soluble in water, % by mass, max.	-	0.5
8	Matter soluble in HCl,% by mass, max.	0.5 – 1.0	0.5 – 1.0
9	CuO. % by mass, max.	-	0.007
10	As_2O_3, ppm, max.	-	10
11	Fe_2O_3, % by mass, max.	0.6	0.75
12	MnO, % by mass, max.	-	0.013
13	pH value of aq.extract	4.5 – 7.5	4.5 – 7.5
14	Color reflectance to blue light of wavelength 5040 Å, %	80 - 85	As agreed between the purchaser & supplier

145

Table 3.9.11 . Indian Standard Specifications for China clays for Ceramic industry, IS 2840 : 2002

Sl No	Characteristics	Requirement		
		Grade 1	Grade 2	Grade 3
1	Grit content / fineness (residue on 45 μm IS sieve), % by mass, Max.	0.5	1.0	2.0
2	Particle size distribution, % by mass:			
	a) Coarser than 25 μm, Max.	5	7	10
	b) Finer than 10 μm, Min.	85	80	75
	c) Finer than 2 μm, Min.	70	65	60
3	Plasticity by hand feel test	Very good	Good	Fair
4	Water of plasticity ,% by mass, Min.	32	30	28
5	Atterberg number, Min	12	10	8
6	Loss on Ignition, % by mass Min.	13.0	12.0	10.0
7	Al_2O_3 % by mass, Min.	37.0	34.0	32.0
8	Fe_2O_3, % by mass, Max.	0.8	1.0	1.5
9	TiO_2, % by mass, Max.	0.7	1.0	1.0
10	Fe_2O_3 & TiO_2 together % by mass, Max.	1.5	2.0	2.5
11	Dry linear shrinkage(at 110^0C) percent Max	6	7	8
12	Green MOR, MPa (on drying at 110^0C), Min.	1.0	0.7	0.6
13	Fired characteristic at 1350^0C	Should be free from black specks/spots and cracks	Should be free from black specks/spots and cracks	Should be free from black specks/spots and cracks
14	Fired colour	White	Cream	Light buff
15	Water absorption (Maturity), % by mass, Max.	15	13	11
16	Apparent porosity, Max.	26	24	21
17	Total linear shrinkage (after firing at 1350^0C), % Max.	16	17	18
18	PCE value in Orton, Min.	34	32	28

Table 3.9.12 Brightness and percent <2 μm fraction in the beneficiated products

Kaolins	SCP1 <2 μm, %	SCP1 B, %	SCP1 calcined	SCP2 <2 μm, %	SCP2 B, %	SCP2 RBP B, %	SCP2 DCBTP B, %
Kasargod 1	43.90	77.36	76.28	62.10	78.04	78.26	86.86
Kasargod 2	45.70	66.65	69.07	59.30	67.56	68.12	83.27
Trivandrum	83.58	78.17	89.90	91.92	80.86	81.54	89.85
Kutch	70.60	72.50	74.46	82.30	73.57	73.96	77.81
Bankura	42.42	41.48	20.34	55.76	41.79	46.45	69.67
Pali	75.7	79.97	76.36	83.30	81.17	81.18	81.27

Table 3.9.13 Properties of SCP1 samples

Sl. No.	Characteristics	Kasargod 1 clay	Kasargod 2 clay	Trivand-rum clay	Kutch clay	Bankura clay	Pali clay
1	Coarse particles or grit (residue on 53 μm IS sieve), %by mass	Nil	Nil	Nil	Nil	Nil	Nil
2	Particles coarser than 25 μm, % by mass	2.5	3.0	3.46	3.76	7.72	0.70
3	Particles larger than 10μm in dia, % by mass	10.7	10.0	3.58	7.70	22.13	5.0
4	Particles smaller than 10μm, % by mass	89	90	96.42	92.30	77.87	95.0
5	Particles finer than 2 μm	43.90	45.70	83.58	70.60	42.42	75.70
6	Relative density 27/27°C	2.6	2.6	2.6	2.7	2.57	2.68
7	Loss on ignition, % by mass	14.57	14.27	14.31	14.22	7.77	13.23
8	Matter soluble in water, % by mass	0.42	0.26	0.64	0.48	1.20	0.49
9	Matter soluble in HCl,% by mass	0.16	0.81	1.17	1.21	2.48	0.92
10	CuO. % by mass	0.0014	0.0019	0.0018	0.008	0.0019	0.0019
11	As_2O_3, ppm	5.21	4.08	<1 ppm	< 1 ppm	14.14	8.67
12	Fe_2O_3, % by mass.	0.75	1.07	0.62	0.61	5.17	1.13
13	MnO, % by mass,	0.0085	0.0023	0.002	0.005	0.0055	0.0017
14	pH value of aq.extract	5.61	5.2	6.9	5.3	7.5	7.0
15	TiO_2, % by mass	0.49	0.49	0.53	1.53	0.77	0.62
16	Fe_2O_3 & TiO_2 together % by mass	1.24	1.56	1.15	2.14	5.94	1.75
17	Al_2O_3 % by mass	37.83	37.78	36.42	37.98	26.70	34.18
18	Color reflectance to blue light of wavelength 5040 Å, %	77.36	66.7	78.2	72.5	41.5	79.97

Table 3.9.14 Properties of SCP2 samples

Sl. No.	Characteristics	Kasargod 1 clay	Kasargod 2 clay	Trivand-rum clay	Kutch clay	Bankura clay	Pali clay
1	Coarse particles or grit (residue on 53μm IS sieve), %by mass	Nil	Nil	Nil	Nil	Nil	Nil
2	Particles coarser than 25 μm,	Nil	Nil	Nil	1.70		
3	Particles larger than 10μm in dia, % by mass	10.7	10.0	100.0	98.20	22.13	5.0
4	Particles smaller than 10μm, % by mass	89	90			77.87	95.0
5	Particles finer than 2 μm,	62.10	59.30	91.92	82.30	55.76	83.3
6	Relative density 27/27°C	2.6	2.6	2.6	2.7	2.5	2.6
7	Loss on ignition, % by mass	14.48	14.53	14.10	14.31	9.64	14.30
8	Matter soluble in water, % by mass	0.41	0.25	0.60	0.43	1.11	0.44
9	Matter soluble in HCl,% by mass	0.86	0.80	1.08	1.15	2.29	0.86
10	CuO. % by mass	0.0011	0.0018	0.0016	0.0007	0.0028	0.0016
11	As_2O_3, ppm	3.89	2.12	<1 ppm	< 1 ppm	13.93	7.56
12	Fe_2O_3, % by mass	0.70	1.01	0.35	0.43	5.66	1.04
13	TiO_2, % by mass	0.20	0.41	0.52	1.60	0.28	0.55
14	Al_2O_3, % by mass	37.46	36.18	37.88	37.96	30.01	35.66
15	Fe_2O_3 & TiO_2 together % by mass	0.90	1.42	0.87	2.03	5.94	1.59
16	MnO, % by mass	0.0003	0.0018	0.0017	0.0004	0.0051	0.0014
17	pH value of aq.extract	5.63	5.2	6.9	5.3	7.5	7.0
18	Color reflectance to blue light of wavelength 5040 Å, %	78.04	67.6	80.9	73.6	41.8	81.2

Figure 3.1 Mine Location Map
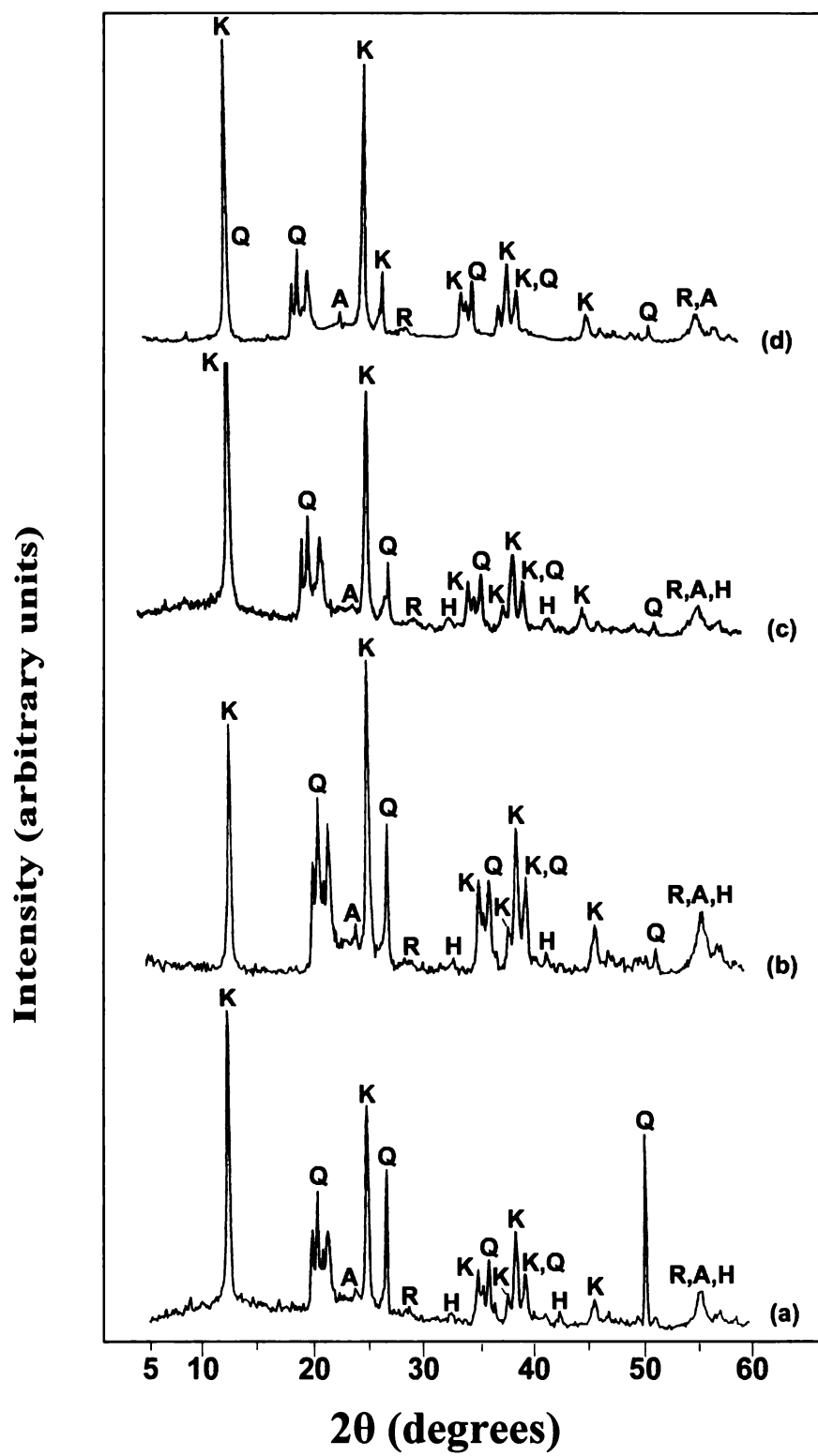
Figure 3.1.1 XRD pattern (a) ROM (b) SCP1 (c) SCP2 and (d) SCP2-DCBT of Kasargod 1 kaolin
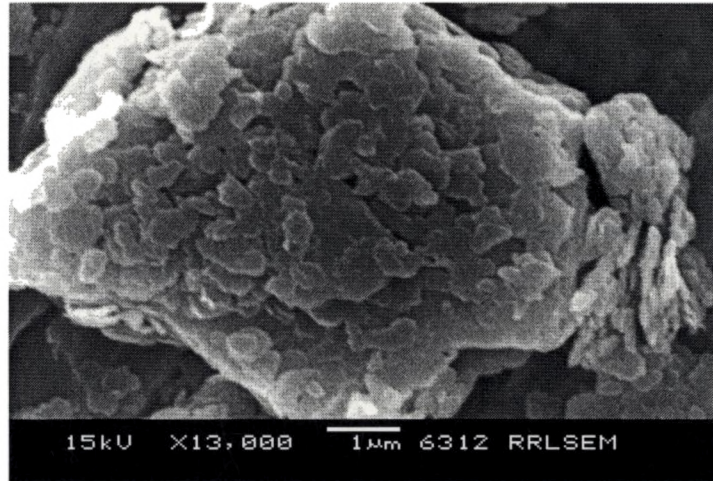
ROM sample
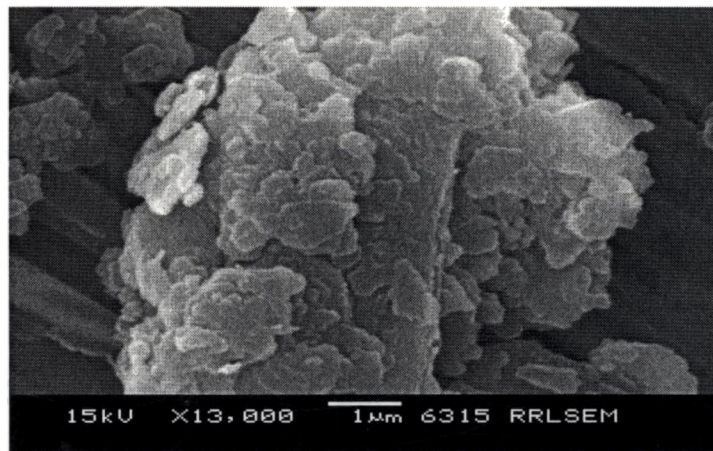
SCP1 sample

Figure 3.1.2 SEM pictures of Kasargod 1 kaolin

152
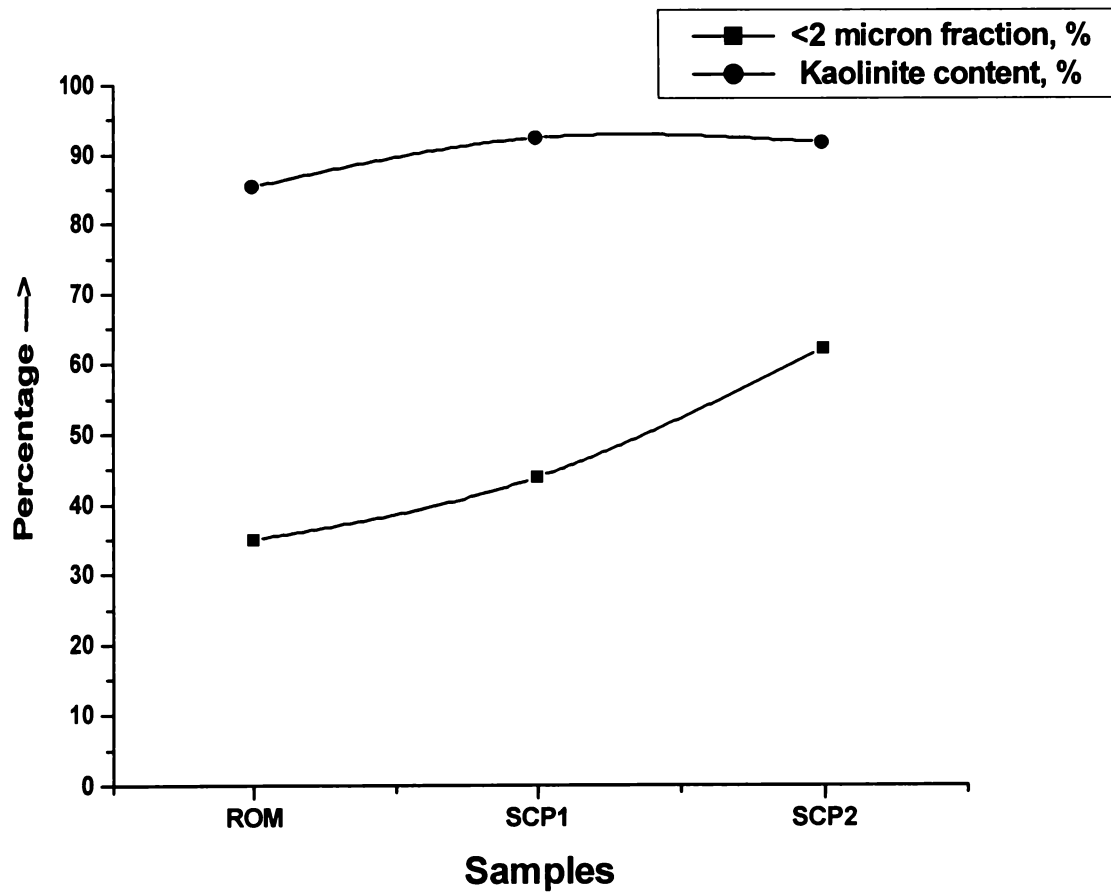
Figure 3.1.3 Variation of <2 μm fraction and kaolinite content during size separation
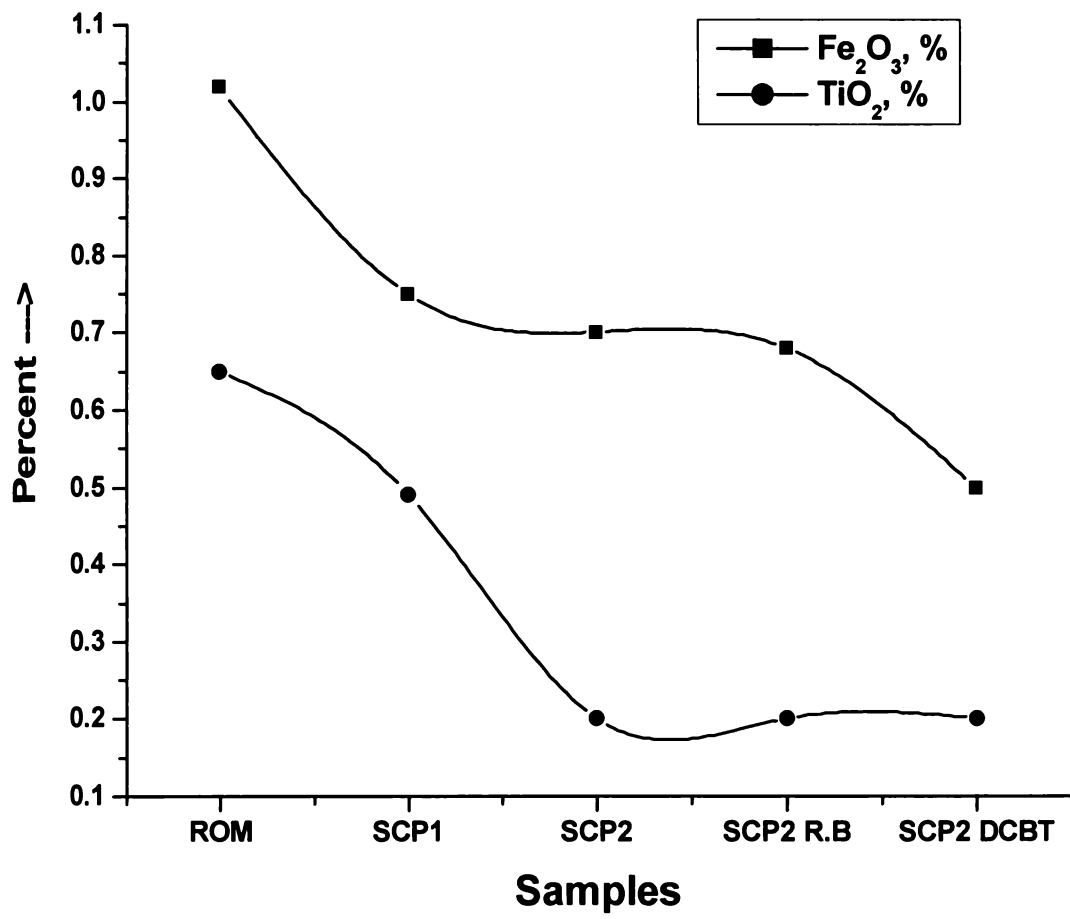
Figure 3.1.4   Variation of Fe_2O_3 & TiO_2 content during
different beneficiation processes
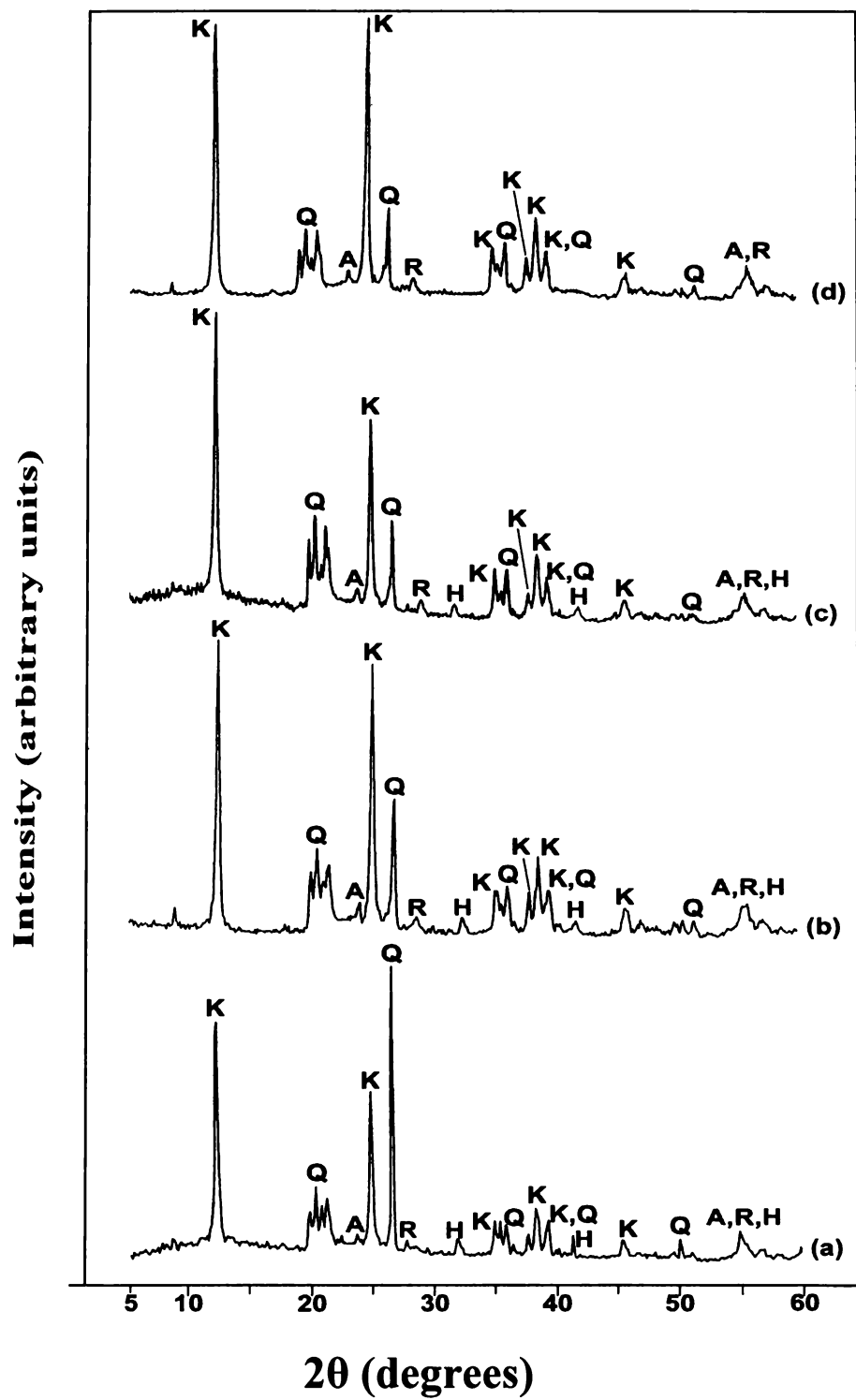
Figure 3.2.1 XRD pattern (a) ROM (b) SCP1 (c) SCP2 and (d) SCP2-DCBT of Kasargod 2 kaolin

155
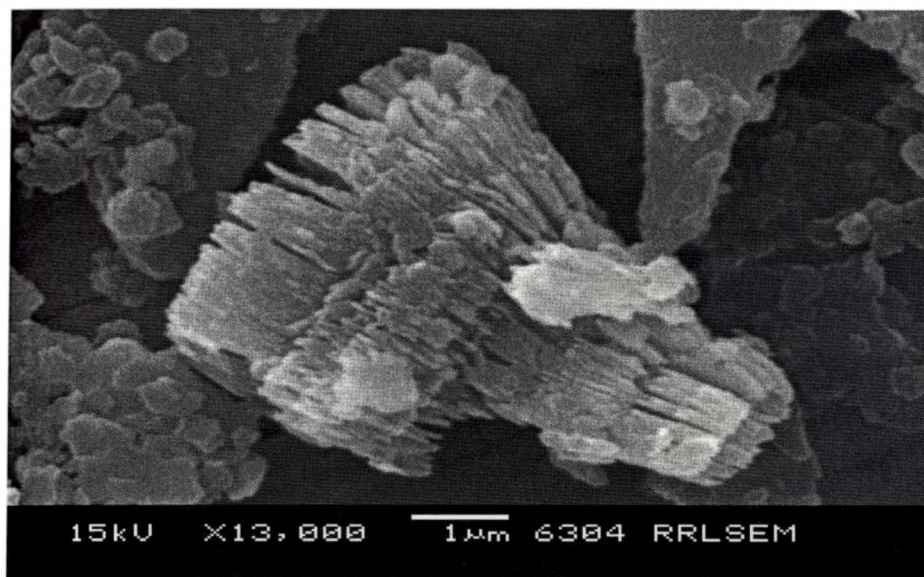
ROM sample
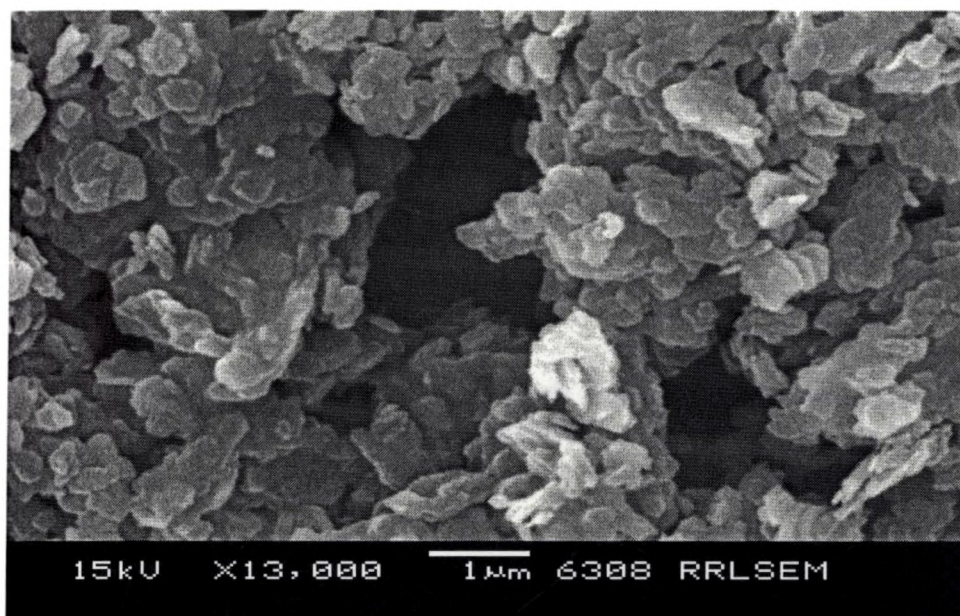
SCP1 sample

Figure 3.2.2 SEM pictures of Kasargod 2 kaolin

156
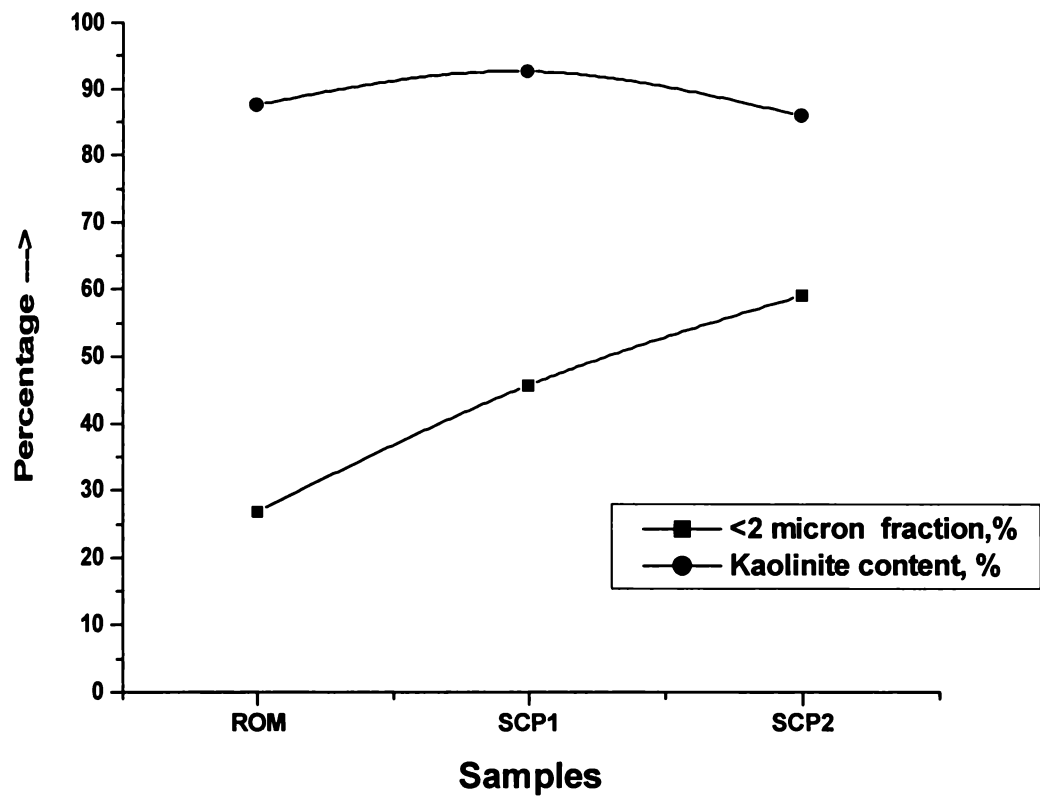
Figure 3.2.3   Variation of < 2 μm fraction & kaolinite content during size separation
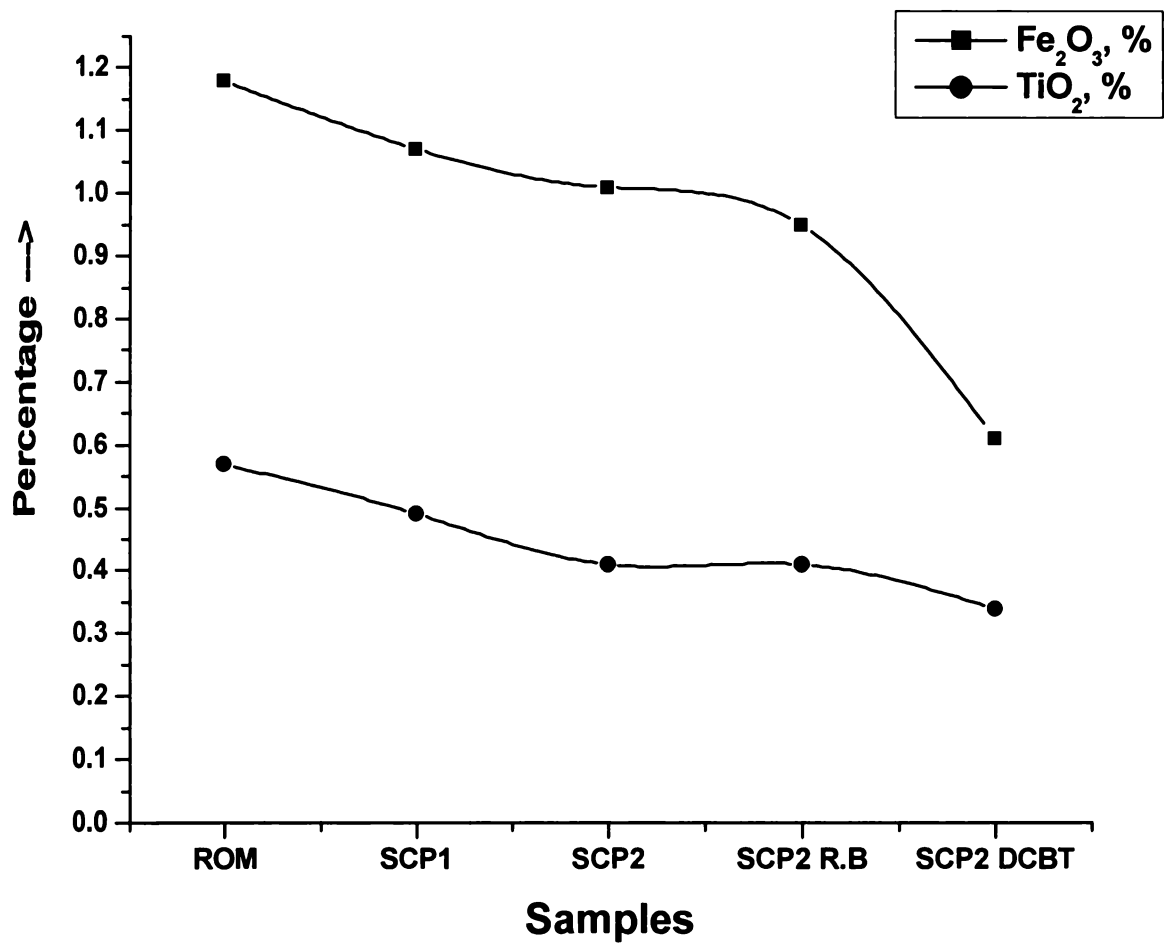
**Figure 3.2.4   Variation of Fe₂O₃ & TiO₂ content during
different beneficiation processes**
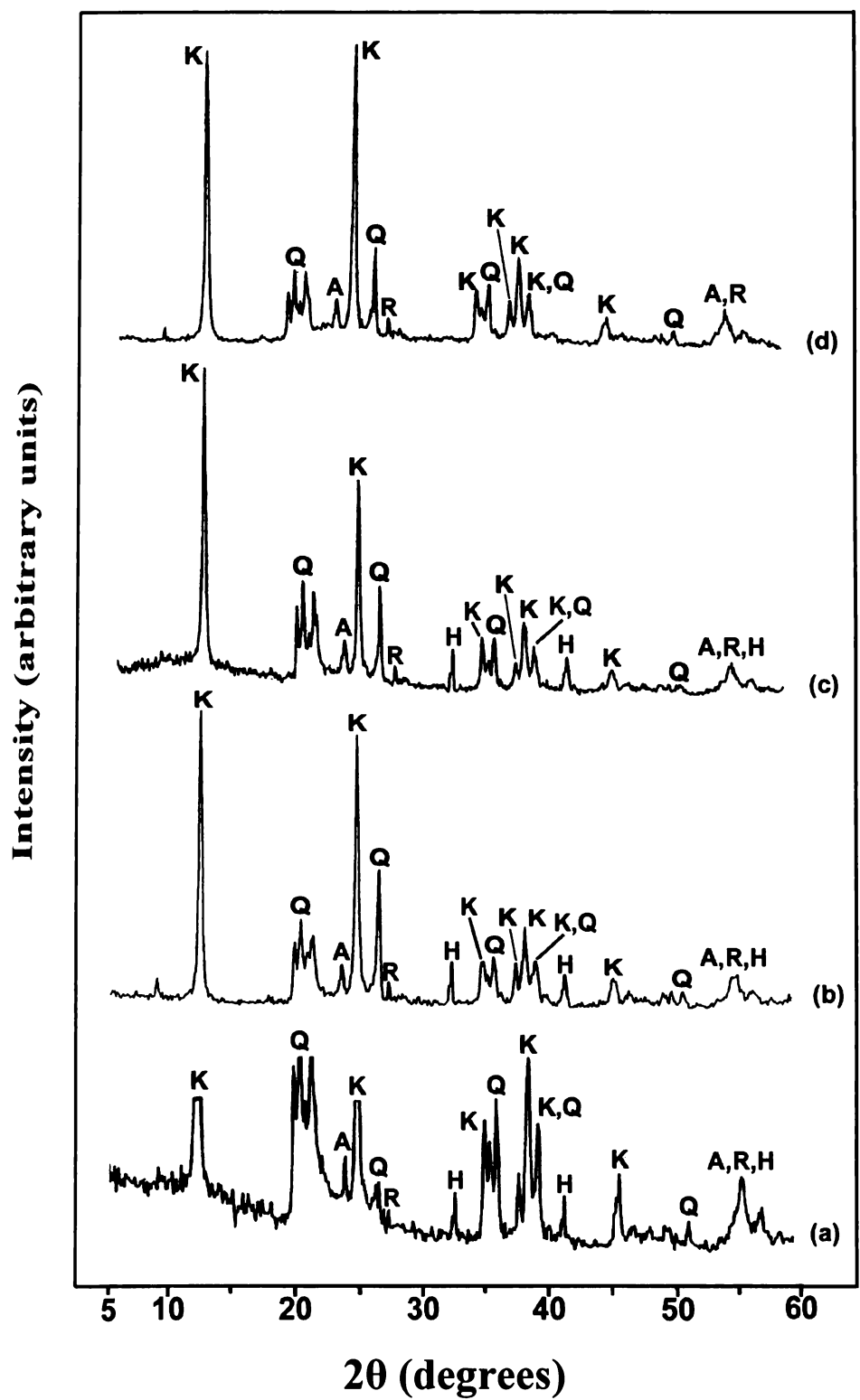
Figure 3.3.1 XRD pattern (a) ROM (b) SCP1 (c) SCP2 and (d) SCP2-DCBT of Trivandrum kaolin

159
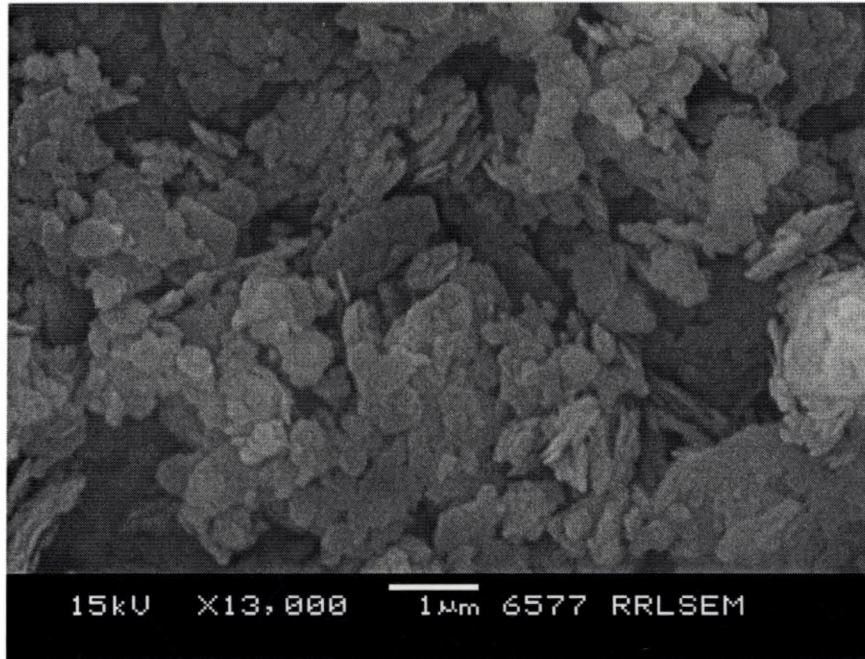
ROM sample
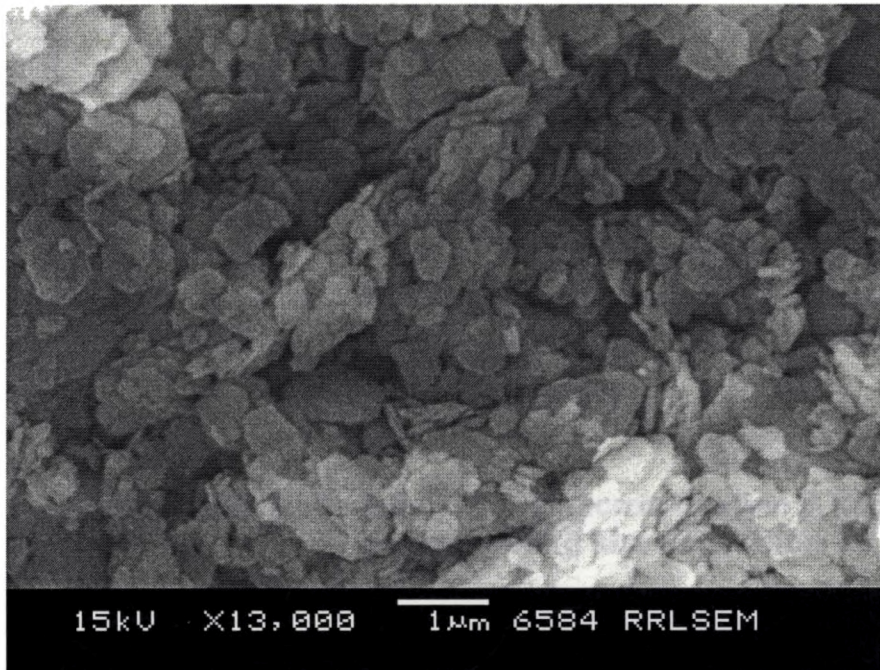
SCP1 sample

Figure 3.3.2 SEM pictures of Trivandrum kaolin

160
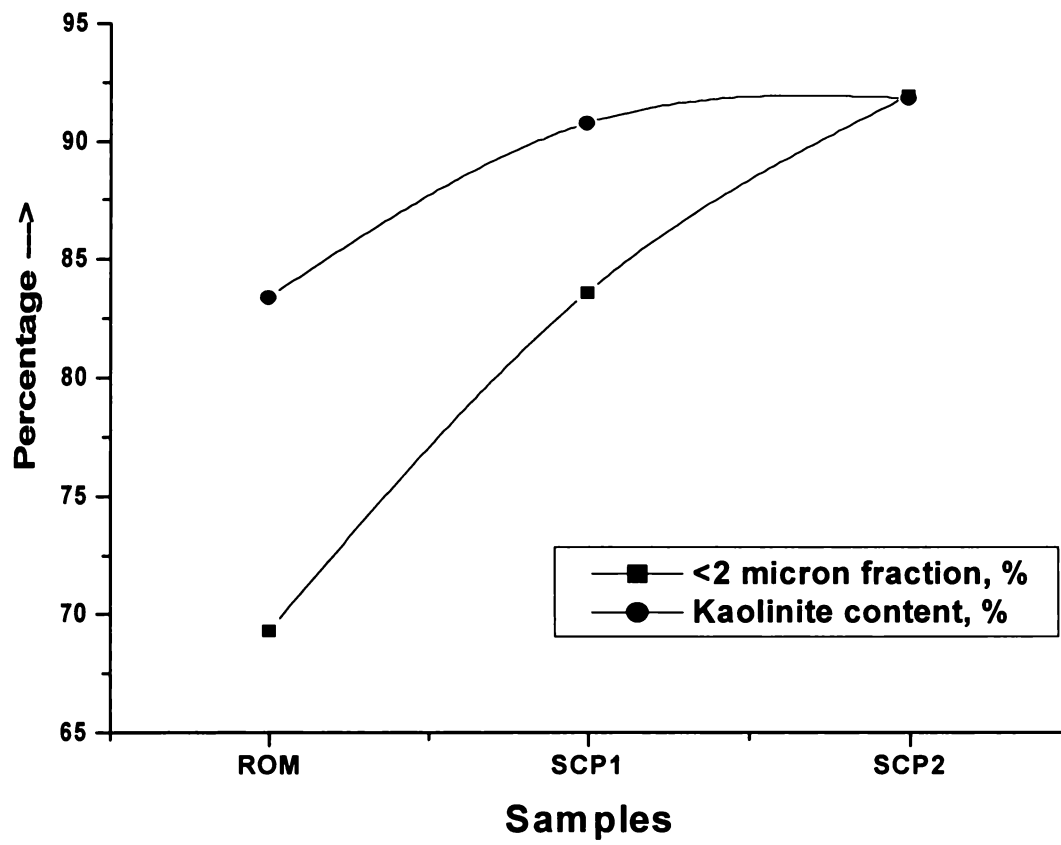
Figure 3.3.3   Variation of < 2 micron fraction & kaolinite content during size separation
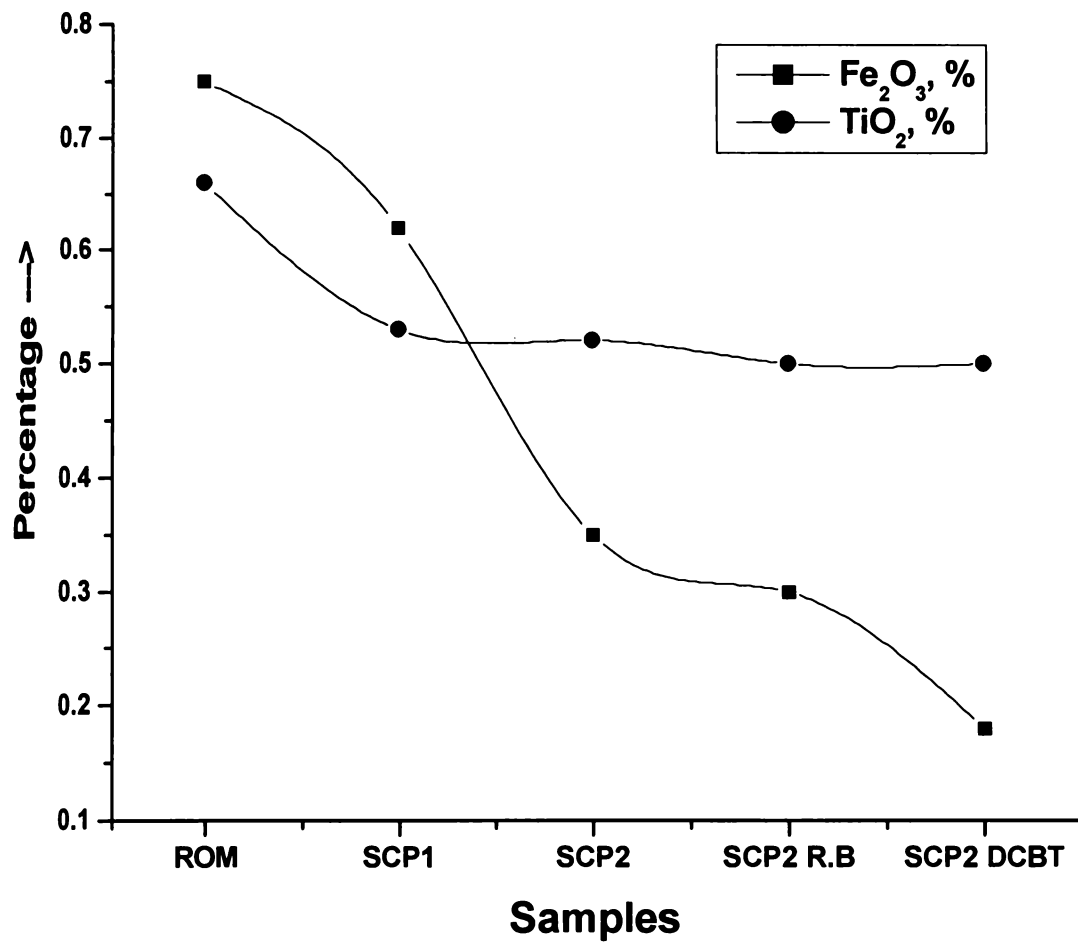
Figure 3.3.4 Variation of Fe₂O₃ & TiO₂ content during different beneficiation processes
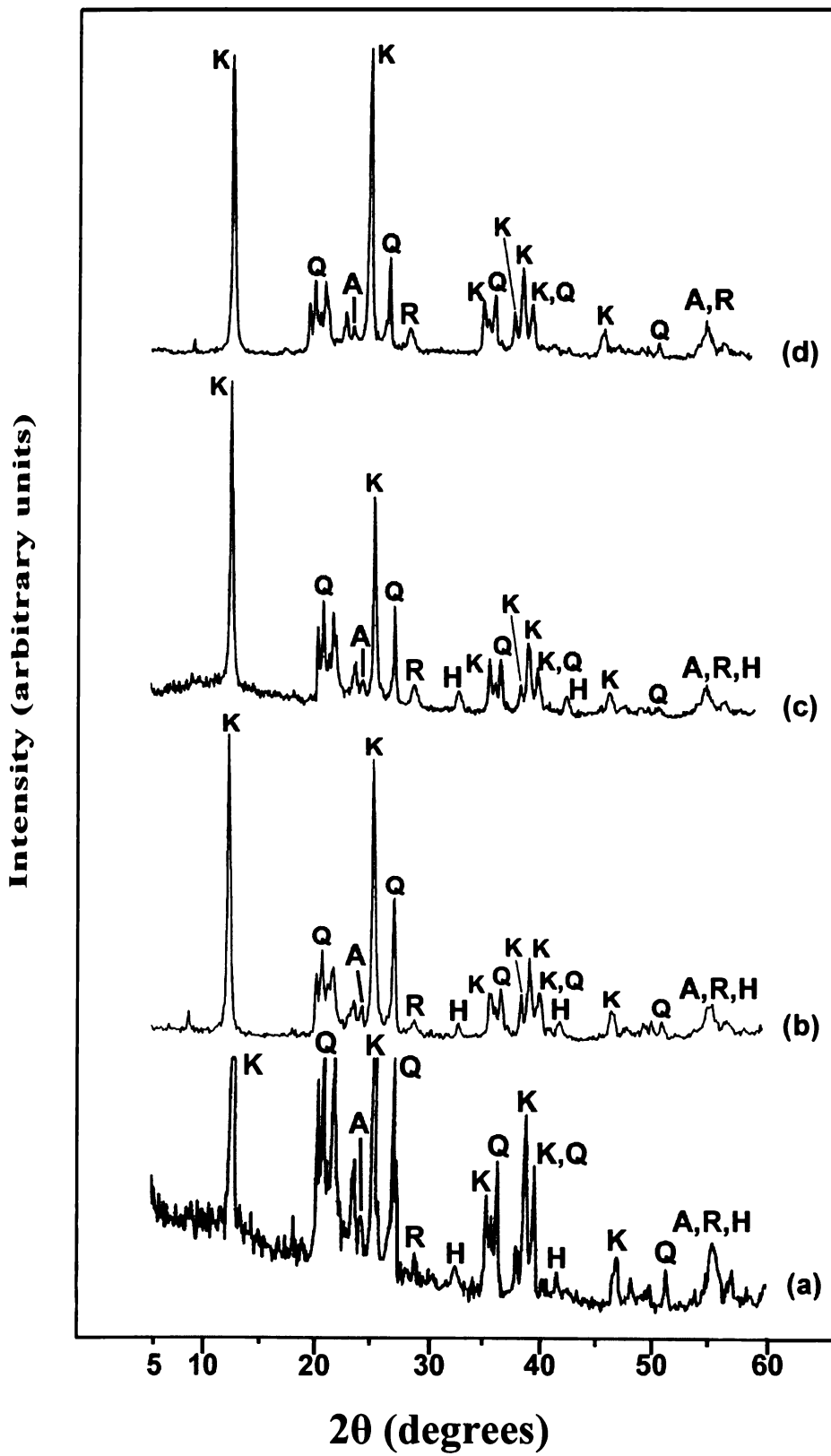
Figure 3.4.1 XRD pattern (a) ROM (b) SCP1 (c) SCP2 and (d) SCP2-DCBT of Kutch kaolin
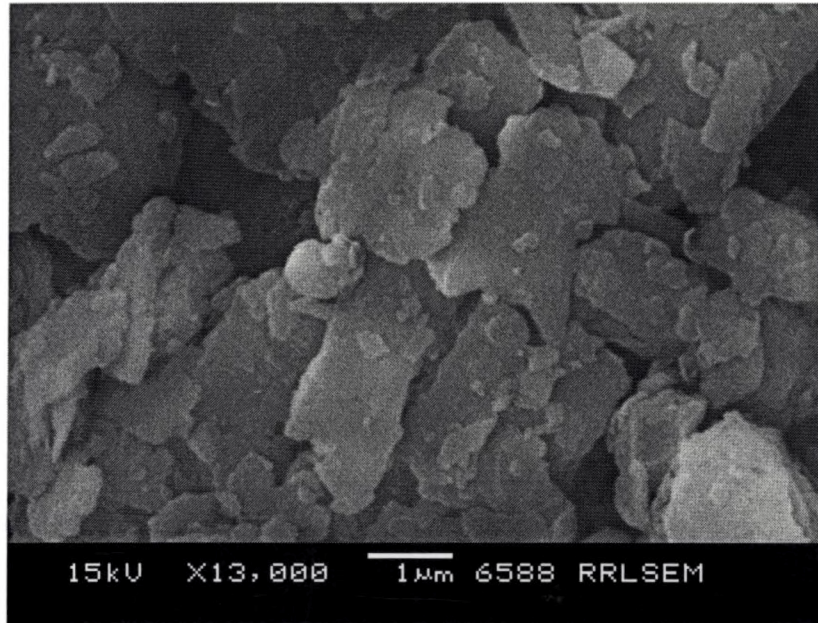
ROM Sample
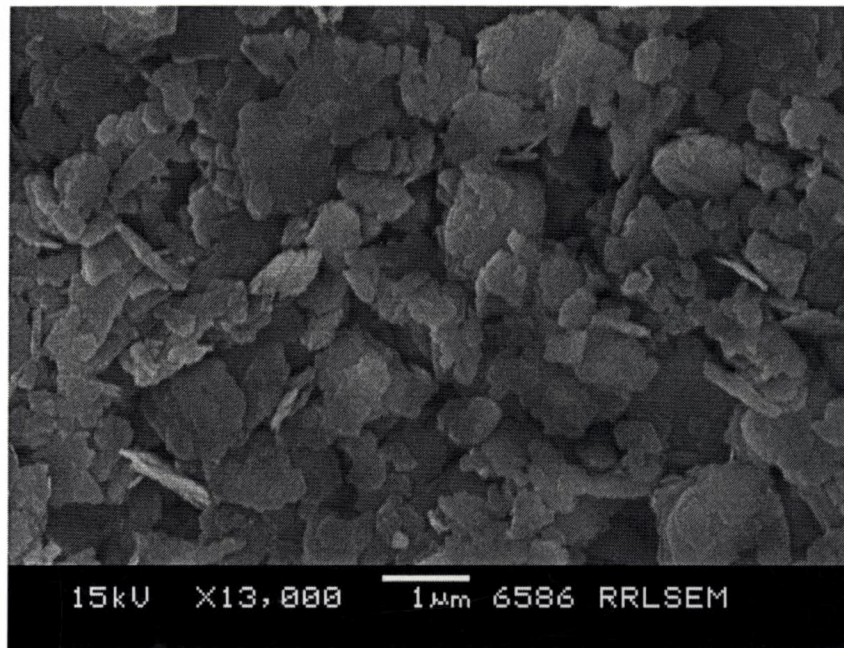
SCP1 Sample

Figure 3.4.2 SEM pictures of Kutch kaolin
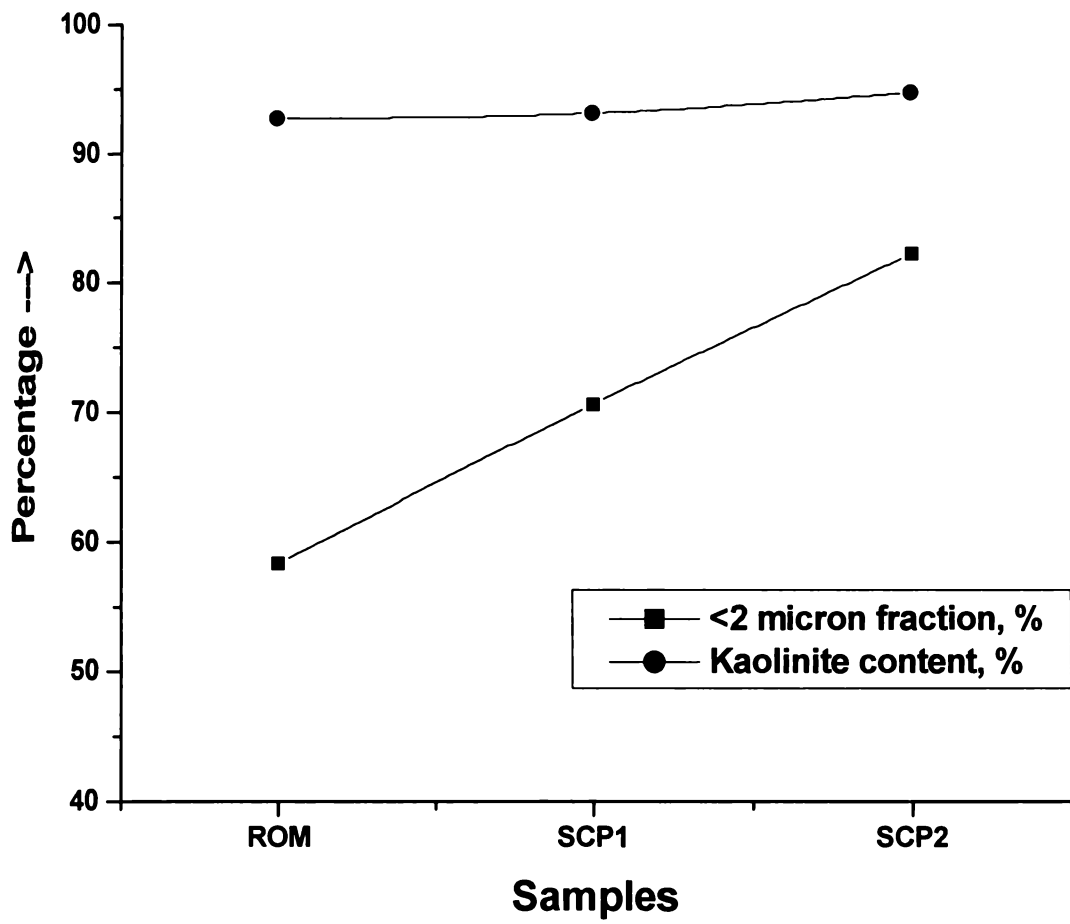
Figure 3.4.3 Variation of <2 micron fraction & kaolinite content
during size separation in Kutch kaolin
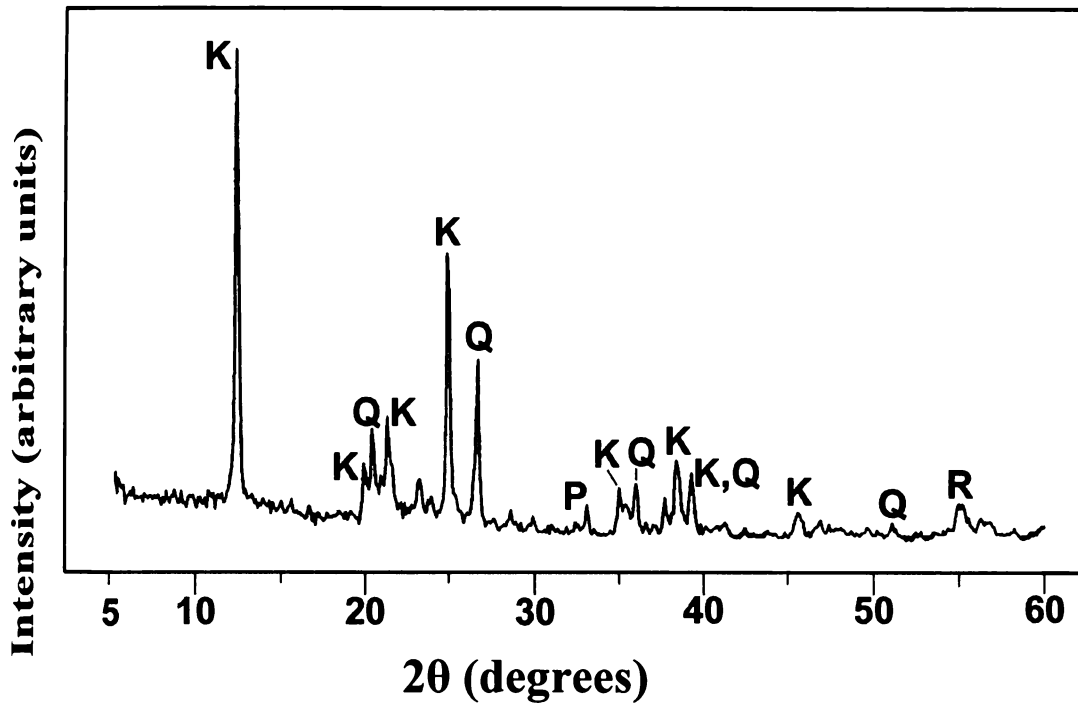
Figure 3.5.1 XRD pattern of ROM of Koraput kaolin
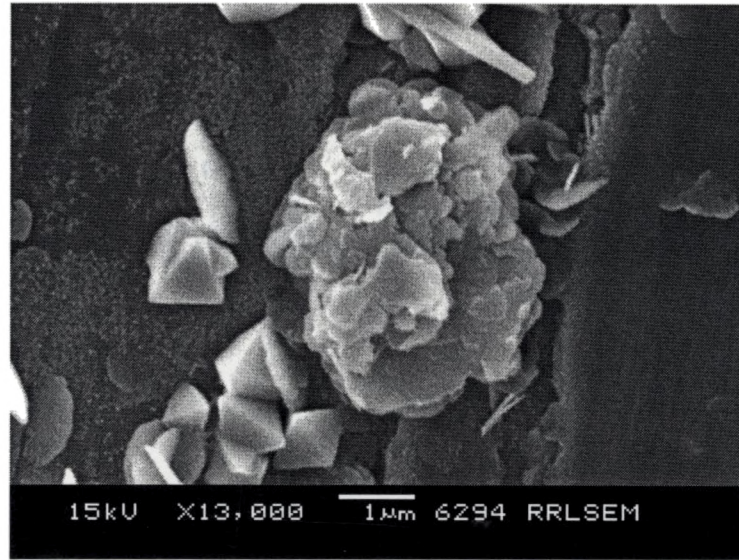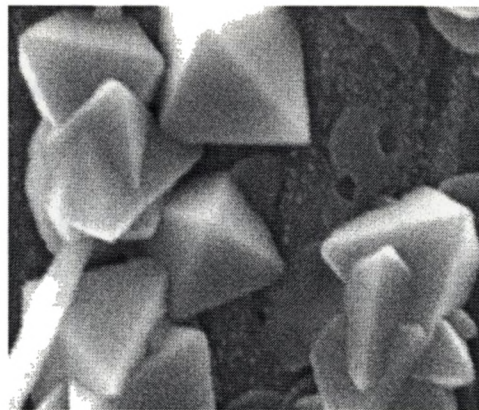
ROM sample

Pyrite crystals

Figure 3.5.2 SEM picture of Koraput kaolin

168
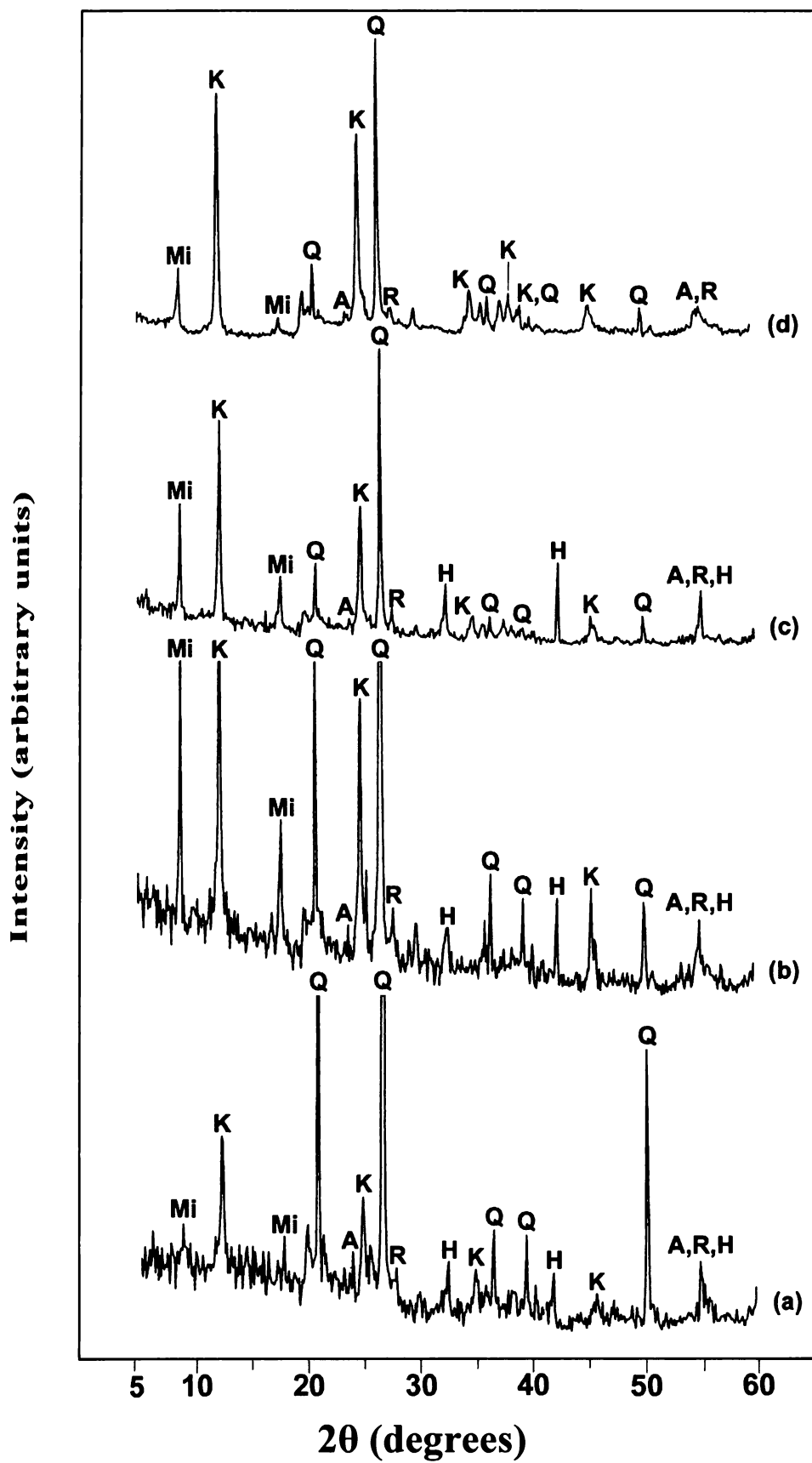
Figure 3.6.1 XRD pattern (a) ROM (b) SCP1 (c) SCP2 and (d) SCP2-DCBT of Bankura kaolin
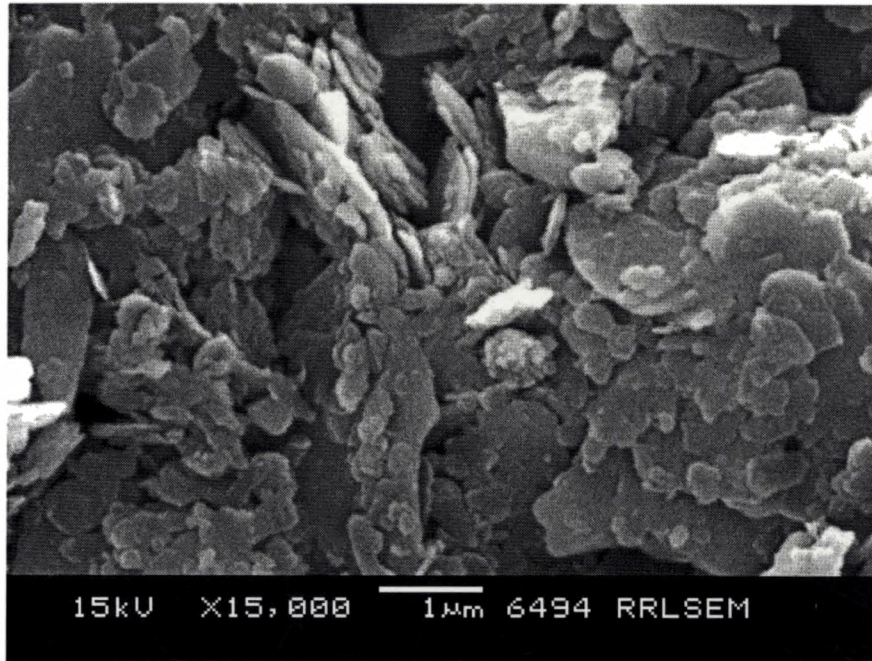
ROM Sample
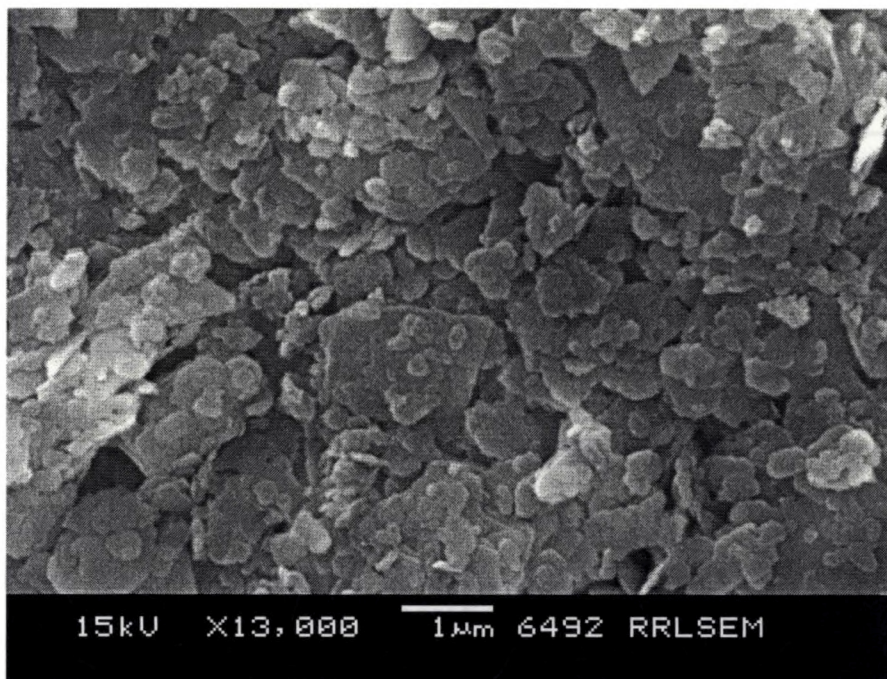
SCP1 sample

Figure 3.6.2 SEM pictures of Bankura kaolin

170
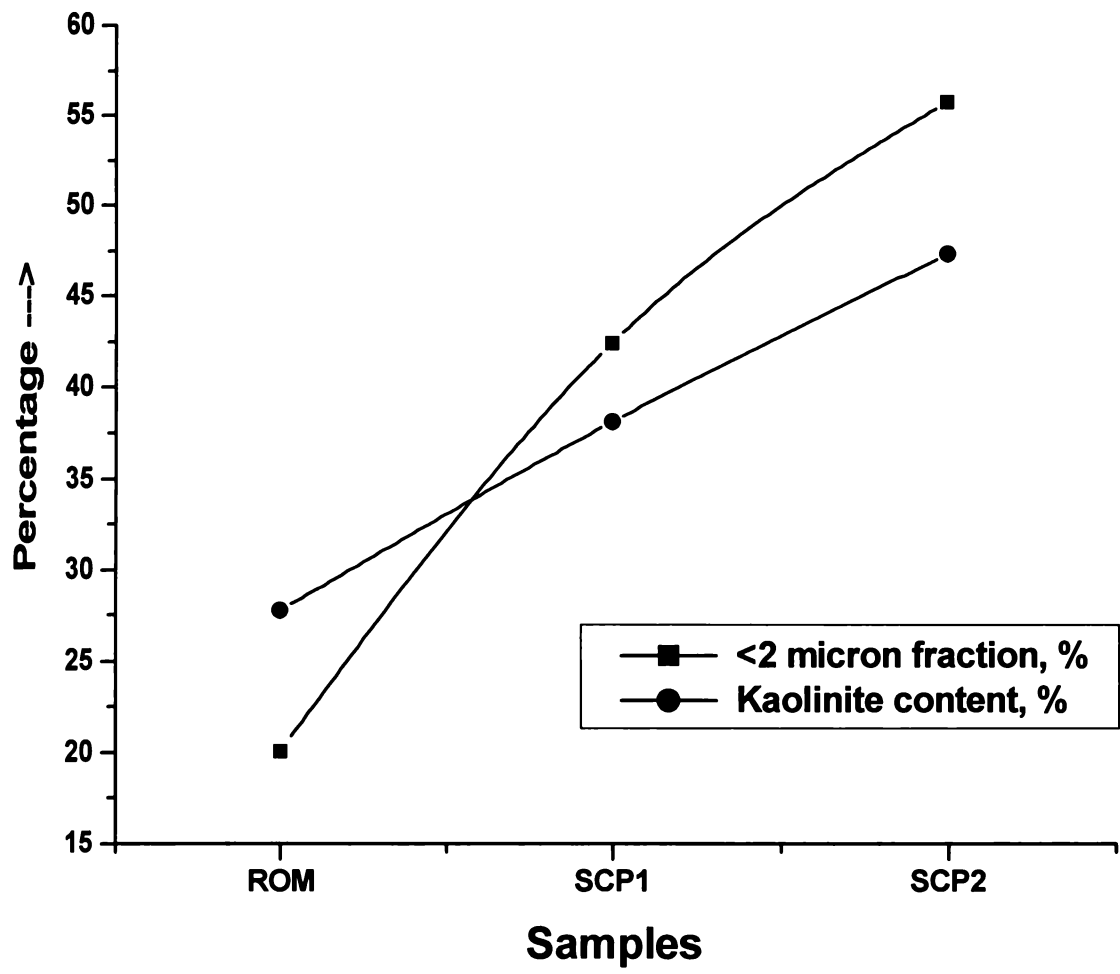
Figure 3.6.3 Variation of <2 micron fraction & kaolinite content
during size separation in Bankura kaolin
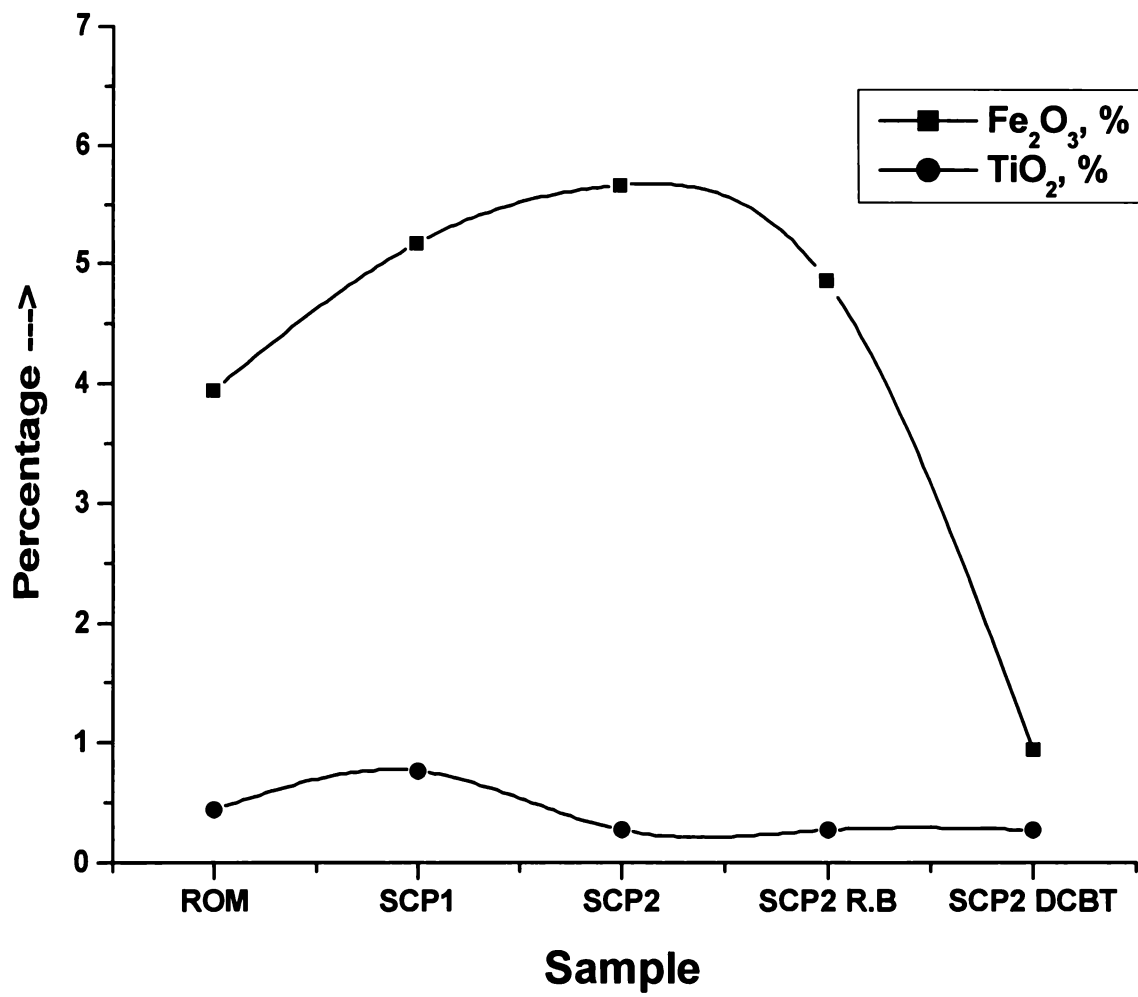
Figure 3.6.4 Variation of Fe_2O_3 & TiO_2 content during different beneficiation processes in Bankura kaolin
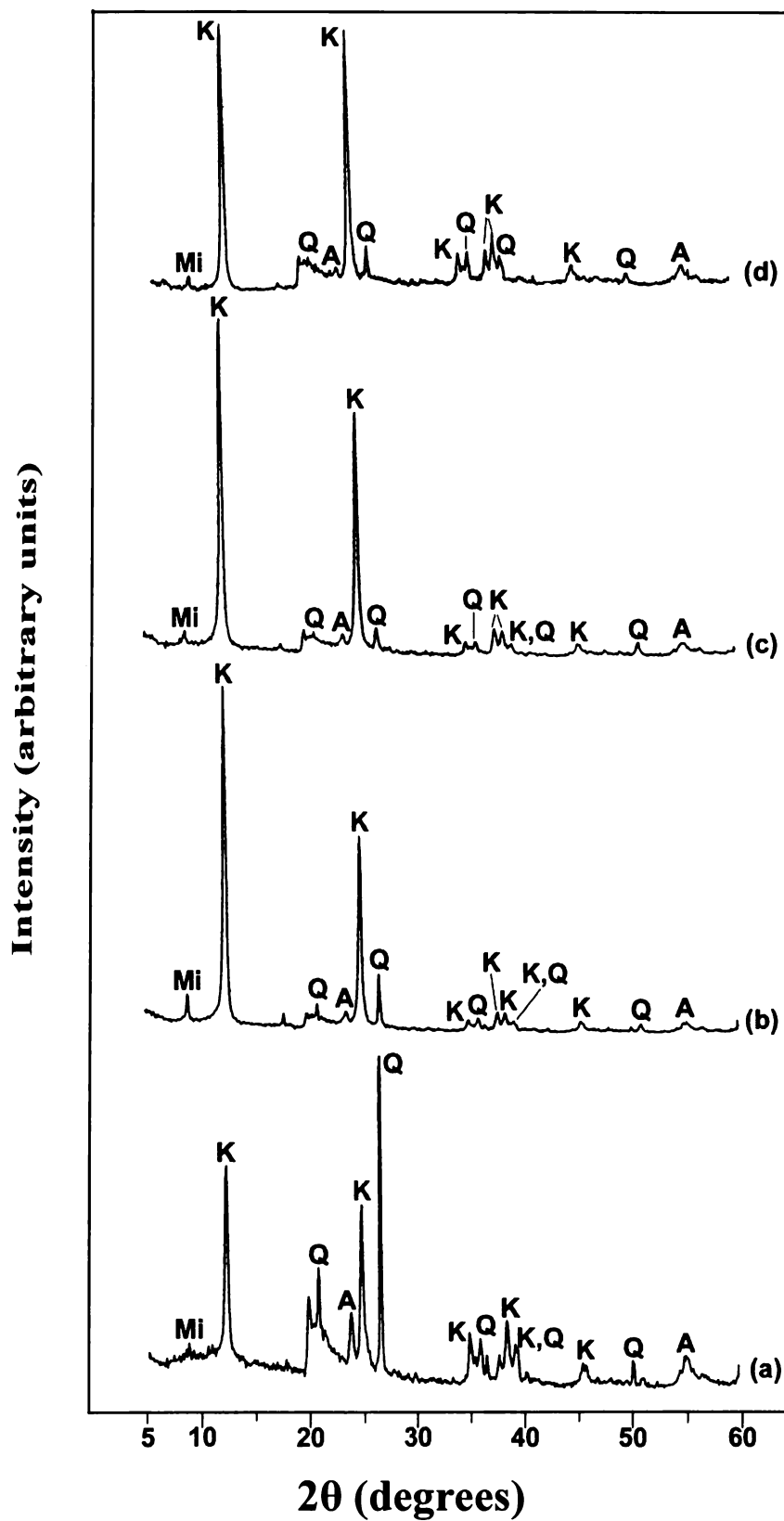
Figure 3.7.1 XRD pattern (a) ROM (b) SCP1 (c) SCP2 and (d) SCP2-DCBT of Pali kaolin

173
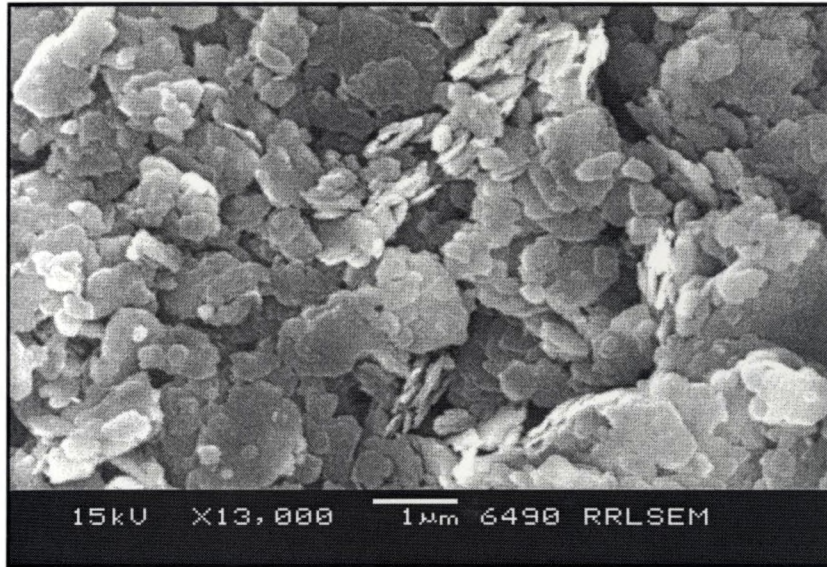
ROM sample
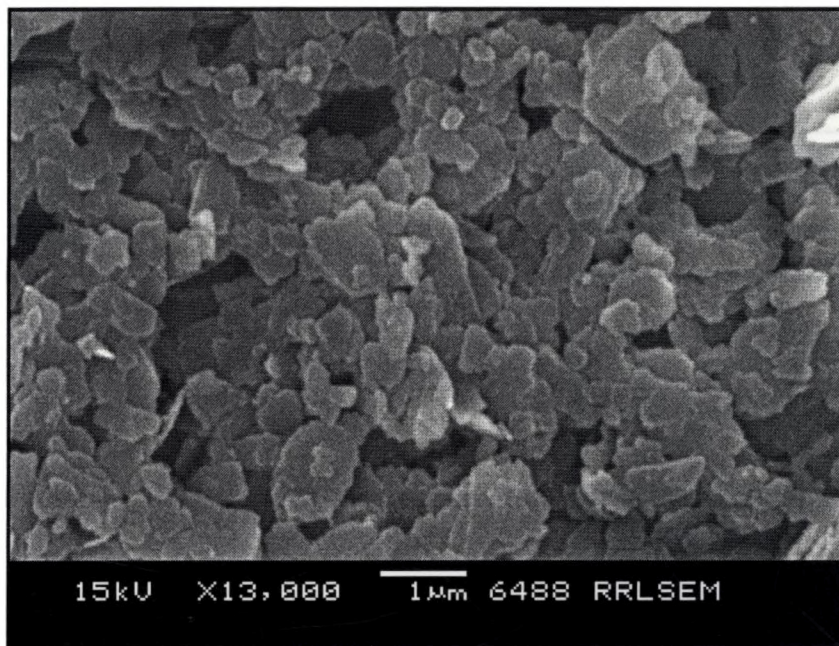
SCP1 sample

Figure 3.7.2 SEM pictures of Pali kaolin
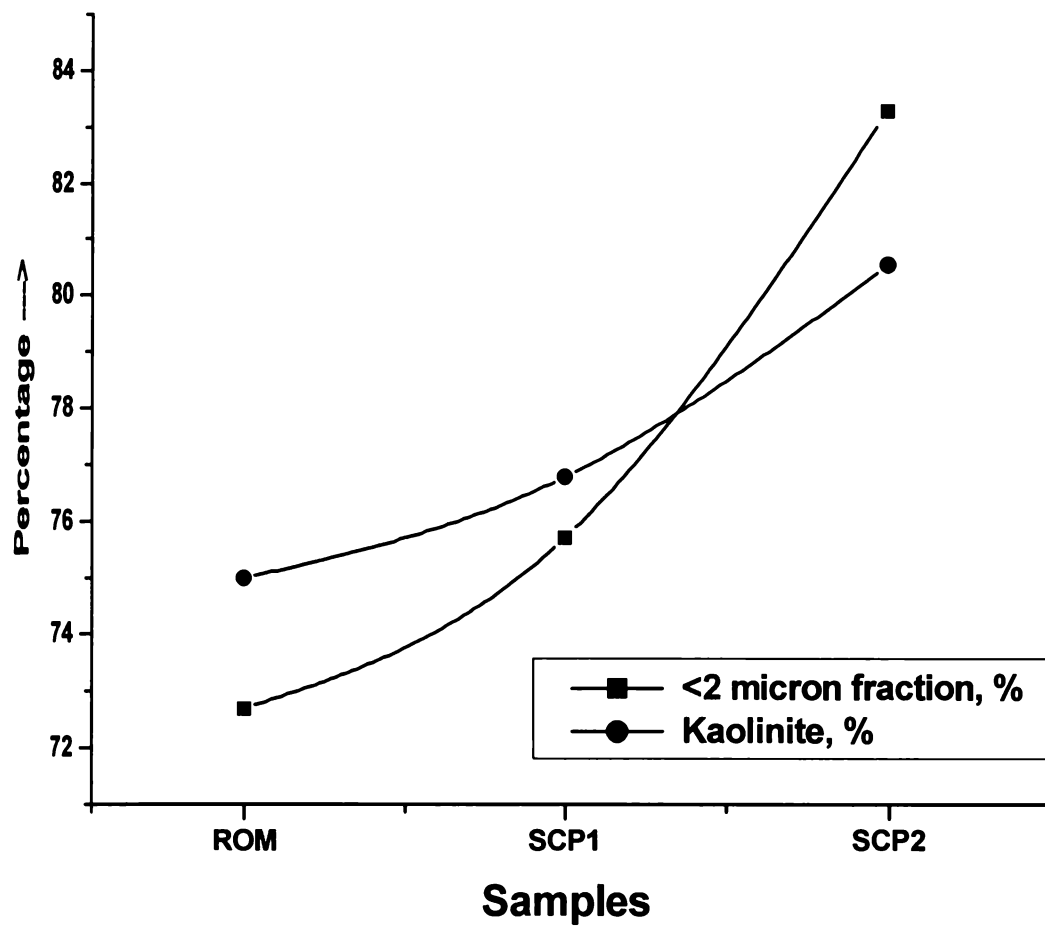
Figure 3.7.3 Variation of <2 micron fraction & Kaolinite content during size separation in Pali kaolin
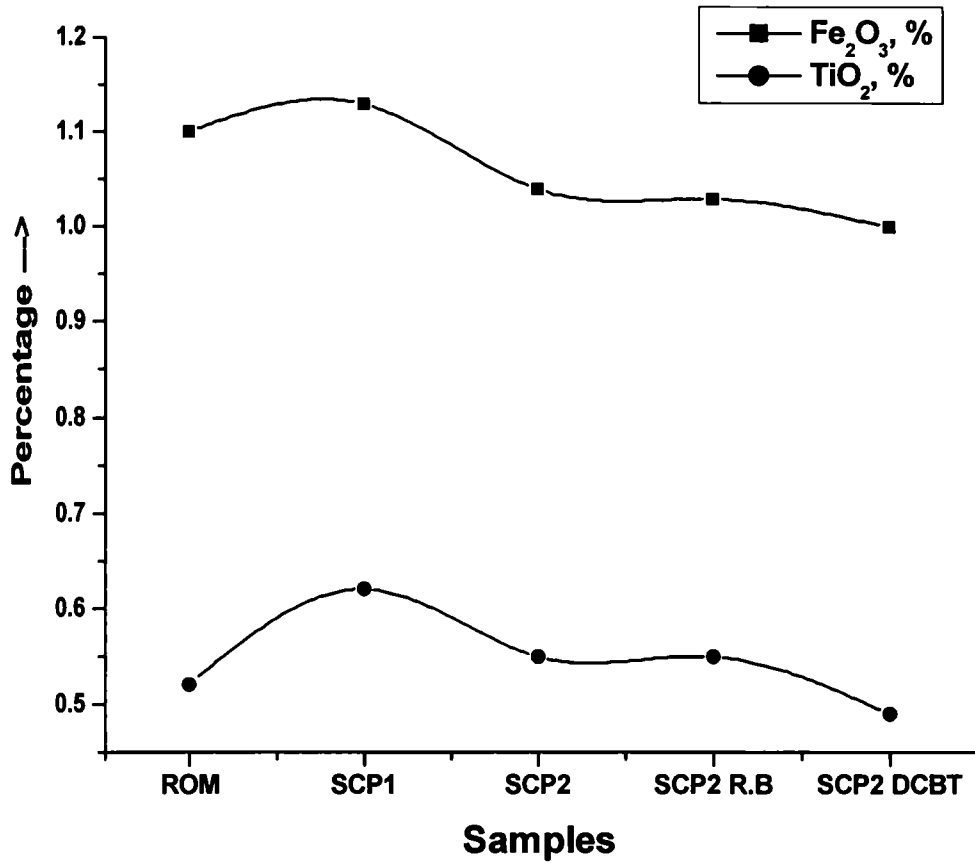
Figure 3.7.4   Variation of Fe_2O_3 & TiO_2 content during different beneficiation processes in Pali kaolin
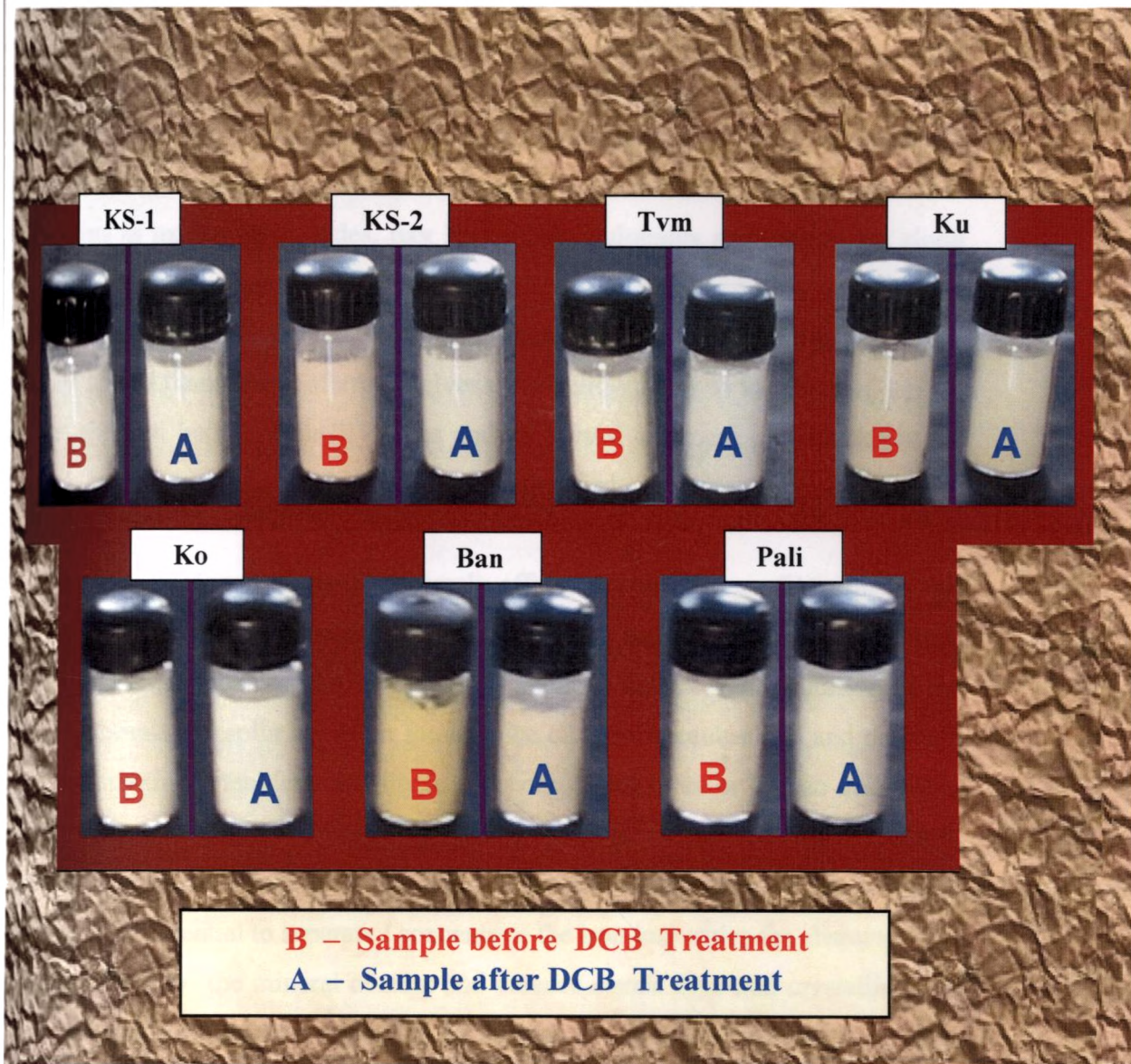
Ks-1 : Kasargod 1; Ks-2 : Kasargod 2; Tvm : Trivandrum; Ku : Kutch;
Ko : Koraput; Ban : Bannkura

Figure 3.9.1   Photograph of samples before and after DCB treatment

CHAPTER 4

IMPURITY MINERALS - CRYSTALLO CHEMICAL STUDY

The common ancillary / impurity minerals occurring with kaolin include parent
als like feldspar and mica, quartz, ferruginous, titanoferrous and carbonaceous
erials etc. Ferruginous and titanoferrous minerals are the common coloring impurities
of iron exists as oxides, hydroxides, oxy hydroxides, sulphides and carbonates along
th iron stained quartz / anatase and mica. Goethite (α-FeOOH) is yellow to brown in
our and hematite (α-Fe$_2$O$_3$) is red. Pyrite and ilmenite are black and give gray color to
aolin. Iron stained titania (titanoferrous) gives dirty yellow color to kaolin. Iron occurs
silicates either in Fe(II) or Fe(III) states and its crystal chemical characteristics are
examined by its valance and ionic size, modified by crystal field (ligand)
considerations.

The presence of iron minerals adversely affects the properties of kaolin. In this
text, the identification and quantification of the impurity mineral phases has relevance
selecting and sequentialising the beneficiation methods for the value addition of the
olin. Iron minerals in kaolin are often found to be of low concentrations and different
rticle size. Sometimes, their crystallinity is also poor giving more or less an amorphous
ure. Generally, the quantity of these "Fe" phases is too low to be detected / estimated
instrumental techniques such as X-ray diffraction and various spectroscopic methods.
nce, it becomes essential to separate / concentrate the iron impurities for characterizing
e same especially for the mineral content and valence states. Free and crystalline iron
des are frequently separated from kaolin by various physical (particle size separation,
nsity gradient separation and magnetic separation) and chemical (selective dissolution
chniques) methods for identification and quantification.

In the present study, impurity mineral phases of iron have been separated /
ncentrated from the seven kaolin samples by various physical and chemical methods
scribed in the experimental part (Chapter 2). Following are the various impurity
ncentrates separated from the kaolin, (1) the underflow solids of hydrocyclone
assification (IM1, >45 μm), (2) the impurity minerals separated by panning (IM2 , <1

m) (3) the insoluble portion after the 5M NaOH treatment of the <45 μm fraction M). The ferro/ferri magnetic materials in the kaolin have been separated using a hand magnet (IM4) and analyzed by XRD to get more information on the iron minerals present in the kaolin. The XRD and DTA results have been compared with the characteristic data of kaolinite and other minerals commonly found in kaolin represented in Table 3.1.4 of Chapter 3. The deviation in the thermal analysis values of kaolinite is attributed to the presence of impurities in the samples.

The sample IM1 is essentially the impurities/particles of large size which contain quartz, parent rocks and other minerals. IM2 contains particles of high specific gravity or "heavy" minerals (including those of Fe and Ti) and their particle size varies from fine to ultrafine. The IM2 samples separated from different kaolins are represented in figure 4.1. The differences in shades/colours are clearly visible. The iron species/minerals in the impurity concentrates separated from the kaolin by different methods are identified by chemical, mineralogical (XRD, DTA, TGA and rational analysis), spectroscopic (EPR, Mossbauer, IR and UV-Visible) and microscopic (TEM-EDS, EPMA and Optical) techniques. This chapter deals with the chemical and mineralogical characterization of these impurity-concentrates while Chapter 5 describes the spectroscopic and microscopic studies.

4.1 Impurities from Kasargode 1 kaolin

The impurity concentrates IM1, IM2 and IM3 have been characterized for their chemical and mineralogical properties and the salient results are given in Tables 4.1 The XRD patterns of these samples along with that of IM4 are presented in Figure 4.2.

Kaolinite mineral has a chemical assay with 46.51% SiO_2, 39.54% Al_2O_3 and 13.95% LOI. The high silica, low alumina and low LOI values in the hydrocylone underflow (IM1) sample confirm the presence of free silica and low amount of kaolinite. The X-ray diffraction analysis shows that quartz and kaolin are the major minerals present in the sample while mica, rutile, anatase and hematite are present in minor quantities. The characteristic "d" values of kaolinite and the common ancillary minerals are given in Table 3.1.4 of Chapter 3. The relative intensity of the quartz peak is found to be on a higher side indicating the presence of free silica and the same is supported by the rational analysis data and the low weight loss indicated by TGA. Considerable amounts

179

ifFe_2O_3 (4.08%) and TiO_2 (3.63%) are present in the sample which indicates the ...ration of these minerals along with quartz in this particular size range. The ...rmation from the XRD analysis and weight percentage of the mineral content ...ined from the rational analysis data also supports the same. Presence of appreciable ...ntities of micaceous impurities is also observed from the analysis data of the sample. ...DTA pattern of IM1 consists of an endotherm at ~532° C and an exotherm at ~997°C ...ich are near to the values for kaolinite. The former corresponds to the dehydroxylation ...kaolinite and the latter to the phase change to primary mullite. The deviation from the ...ues of kaolinite mineral can be attributed to the presence of impurities. The endotherm ...575°C represents the phase change from ß-quartz to α form. Table 3.1.4 in Chapter 3 ...o includes the temperatures at which the exothermic and endothermic reactions taking ...ce in kaolinite and other minerals.

The chemical assay of the impurities separated by panning (IM2) shows the ...sence of appreciable quantities of silica and heavy minerals of Fe and Ti. As expected, ...kaolinite content is less and quartz is high which is also supported by the low LOI ...m chemical assay and TGA. XRD patterns show that quartz, magnetite and rutile are ...major minerals present in the sample along with hematite, goethite, anatase, ilmenite, ...udo rutile and kaolinite in minor quantity. Though the chemical assay shows high iron ...ntent, XRD peaks corresponding to any iron mineral is absent. The iron contaminants ...y be amorphous to X-rays. However, Ti containing mineral is identified as rutile. The ...TA pattern of the IM2 does not show any prominent exotherm of kaolinite even though ...RD indicates its presence. The small endotherm at 523°C is possibly indicating the ...hydroxylation of the small amount of kaolinite. Since the sample is a mixture of many ...nerals, the reactions during heat treatment are complex.

The alkali treated sample (IM3) is found to be free from kaolinite and at the ...me time enriched with the "Fe" and "Ti" mineral phases and this was evident from the ...emical assay of the sample. The relatively high LOI of the sample in comparison to the ...her impurity mineral concentrates can be due to the presence of relatively high ...antities of iron oxides and oxy-hydroxides. XRD analysis data shows the presence of ...artz and rutile as major minerals along with hematite, ilmenite, anatase, goethite and ...udo rutile as minor phases.

It is evident from the X-ray diffraction analysis that magnetite, pseudo rutile and ᵣₐₜite are the major phases present in the fraction separated by hand magnet (IM4) ᵢₙg with minor quantities rutile, goethite, ilmenite and anatase. The presence of quartz : ₜₕₑ magnetic fraction is possibly due to the iron stains which are common in naturally ᵣᵣ₁ng quartz mineral.

₄₂ Impurities from Kasargode 2 kaolin

The chemical and mineralogical properties of the IM1, IM2 and IM3 samples ₑᵣᵢᵥₑd from the Kasargod 2 kaolin are presented in Tables 4.2. The X-ray diffraction ₚₐₜₜₑms of these samples along with that of the IM4 represented in Figure 4.3.

The chemical composition of the cyclone underflow solids (IM1) gives higher ₛᵢₗᵢₑₐ and lower alumina compared to those of the ideal kaolinite. Appreciable quantity of ₜᵣₑ silica appears to be present in this sample. The LOI value is also lower than 13.95% ₖₐₒlinite) confirming this finding. The XRD pattern shows that quartz and kaolinite are ₜ major minerals present while rutile and anatase are also indicated in minor quantities. ₜₕₑ relative intensity of the quartz peak is found to be very high again confirming the ₚᵣₑₛence of free silica. The rational analysis data and the low weight loss on heating from ₜGA also support the same. The percentages of Fe_2O_3 (4.46%) and TiO_2 (3.40%) in the ₛₐₘple indicates the concentration of Fe and Ti impurity minerals separated along with ₑᵤₐrtz in this particular size range. The information from the XRD analysis and weight ₚₑrcentage of the mineral content obtained from the rational analysis data also supports ₜₑ same. The DTA pattern also shows the presence of endothermic and exothermic ₚₑₐks characteristic to that of kaolinite. Endotherm at ~575°C corresponds to the large ₐₘount of quartz in the sample.

Considerable amounts of silica and heavy minerals are present in the impurities ₛₑₚarated by panning (IM2) as evident from the chemical assay. As expected in the ₚₐₙning technique, the alumina content is very low and silica is high. Thus kaolinite ₘᵢₙeral is almost negligible. The low values of loss on heating from chemical assay and ₜGA also support this finding. Absence of characteristic DTA pattern of kaolinite in this ₛₐₘple also confirms this finding. XRD analysis shows that quartz is the major mineral ₐₗₒng with other minerals such as goethite hematite, anatase, rutile, pseudo rutile, ᵢₗmenite and magnetite in minor quantities. The endotherm at ~72°C can be due to the

181

.s of adsorbed water. However, the exotherms do not correspond to any mineral commonly found with kaolin (Table 3.1.4 in Chapter 3) and the mixture of many minerals may be making it complicated.

The alkali treated sample (IM3) is found to be free from kaolinite and at the same time enriched with the "Fe" and "Ti" mineral phases as evident from the chemical assay of the sample. The relatively high LOI of the sample in comparison to the other purity mineral concentrates can be due to the presence of high quantities of iron oxides and oxy-hydroxides. XRD analysis data shows the presence of quartz and rutile as major minerals along with anatase, goethite hematite and ilmenite, as minor phases.

The X-ray diffraction analysis of the magnetic fraction (IM4) separated by hand magnet indicates that quartz (iron stained), hematite, magnetite, rutile and goethite are the major phases present in the sample along with minor quantities pseudo rutile, ilmenite and anatase.

G Impurities from Trivandum kaolin

Results of the chemical and mineralogical analysis of the samples IM1, IM2 and IM3 are given in Tables 4.3. Their XRD patterns along with that of IM4 are represented in Figure 4.4.

The IM1 sample contains higher silica and low alumina compared to the values of typical kaolinite. The loss on ignition is also low which confirms the limited kaolinite content in the sample. The X-ray diffraction analysis shows that quartz and kaolinite are the major minerals while rutile and anatase are present in minor quantities. The relative intensity of the quartz peak is found to be high, which indicates the presence of free silica. The low loss on heating from TGA also confirms that kaolinite content is low. Rational analysis data gives approximate figures for silica, kaolinite and other mineral percentages. The high percentages of Fe_2O_3 (17.69%) and TiO_2 (8.16%) in the sample indicates the extent of separation of Fe and Ti impurity minerals along with quartz in this particular size range. The information from the XRD analysis and weight percentage of the mineral content obtained from the rational analysis data also supports the same. Rational analysis data indicates presence of micaceous impurities in the sample, but XRD analysis does not give corresponding peak. This may be because the concentration is too

s for detection by XRD. The DTA pattern exhibits endotherm at ~528°C and exotherm t 994°C which are near to the values for kaolinite mineral. (Table 3.1.4 in Chapter 3)

The IM2 sample contains appreciable quantities of quartz and heavy minerals of Fe and Ti as evident from the chemical assay. The values of alumina and LOI are low which correspond to low kaolinite content. Panning as expected, concentrates the coarse (quartz) and heavy (Fe and Ti) minerals. XRD analysis shows that quartz, rutile and anatase are the major minerals present in the sample along with minor quantities of other minerals such as kaolinite, hematite, goethite, zircon and pseudo rutile. The DTA pattern is not give any inference on the type of mineral present in the sample.

The alkali treated sample (IM3) is found to be free from kaolinite and at the same time enriched with the "Fe" and "Ti" mineral phases as evident from the higher percentages of Fe$_2$O$_3$ and TiO$_2$ and low alumina in the chemical assay. Silica content is also quite low. XRD analysis data shows the presence of anatase and rutile as major minerals along with hematite, goethite and magnetite as minor phases. Though the analytical iron content is found to be high, the X-ray diffraction pattern does not give any peaks of any iron containing mineral. The reason may be again the amorphous nature of iron contaminants. However, TiO$_2$ containing mineral has been identified as such.

The magnetic faction (IM4) contains magnetite, rutile, goethite, anatase and hematite as major phases present along with minor quantities of iron stained quartz and pseudo rutile as identified by the X-ray diffraction analysis.

4.4 Impurities from Kutch kaolin

The chemical and mineralogical characterization of the samples IM1,IM2 and IM3 has been conducted and the results are given in Tables 4.4. The X-ray diffraction of these impurities along with that of the IM4 sample are presented in Figure 4.5.

The chemical assay of the IM1 sample shows that the ratio of silica and alumina high and the LOI is low compared to the values of kaolinite mineral. This confirms that appreciable quantity of free silica is present in the sample. The X-ray diffraction analysis shows that quartz and kaolinite are the major minerals present in the sample while rutile and anatase are present in minor quantities. The high percentages of Fe$_2$O$_3$ (4.90%) and TiO$_2$ (10.60%) in the sample indicates that the corresponding impurity minerals along

183

quartz are getting concentrated in this particular size range during the hydrocyloning. The XRD results and weight percentages of the minerals obtained from rational analysis data also supports the same. The DTA pattern shows endotherm and exotherm near to the values for kaolinite mineral. The decrease in former and increase in the latter temperatures can be attributed to the presence of impurities present in the sample.

The chemical assay of the IM2 sample shows the presence of appreciable quantities of heavy minerals (of Fe and Ti) and moderate amount of quartz in the sample. As expected in the panning operation, the kaolinite content has reduced considerably as confirmed by the low alumina and LOI values. The high percentages of Fe_2O_3 (20.12%) and TiO_2 (36.11%) in the sample indicates the enrichment of "Fe" and "Ti" impurity minerals in the sample during hydrocycloning. XRD analysis shows that quartz, zircon, rutile and anatase are the major minerals present in the sample along with other minerals such as kaolinite and hematite in minor quantities. Thermogravimetric analysis gives a total weight loss of 8.8 which almost matches with the LOI determined in chemical assay. DTA patterns do not show endotherm and exotherm values characteristic any mineral.

The silica and alumina content in the IM3 sample is low indicating the removal of kaolinite from the clay by the alkali treatment. The Fe_2O_3 and TiO_2 content has increased considerably and the chemical analysis results are given in the table. XRD analysis data shows the presence of rutile and anatase as the major minerals along with hematite as minor phase even though the iron content is quite high. Here again, it is possible that the iron minerals are mostly in the amorphous form whereas TiO_2 is in crystalline forms. The weight loss obtained from TGA is very low and near to the LOI in chemical assay by which the low kaolinite content in the sample is indicated. The DTA peaks do not match with those of kaolinite and the impurities may be undergoing complex reactions during heating.

The X-ray diffraction analysis of the magnetic fraction separated by hand magnet (IM4) confirms the presence of hematite, pseudo rutile, rutile, ilmenite and goethite as the major phases and minor quantities of iron stained quartz and anatase.

Impurities from Koraput kaolin

The Koraput kaolin is quite different from the other samples since it contains appreciable quantity of iron as pyrite. The impurity minerals IM1, IM2 and IM3 have been characterized for their chemical assay and mineralogical properties and the salient results are given in Tables 4.5.1. The pyrite content in these impurity mineral concentrates has been estimated and the values are given Table 4.5.5. The XRD powder patterns of these samples along with that of IM4 (the magnetic fraction separated using a hand magnet) are represented in Fig 4.6.

The IM1 sample contains silica and alumina with a high ratio. Appreciable amount of iron and sulphur is also present. The LOI is slightly high compared to that of kaolinite mineral indicating the presence of volatiles other than the water of crystallinity. From the XRD analysis, quartz, pyrite and kaolinite are found to be the major minerals with rutile and anatase in minor quantities. Presence of carbon / graphite has also been indicated. The iron and sulphur content confirms the presence of pyrite. The carbon and pyrite may be contributing to the higher LOI. The high percentage of Fe_2O_3 (11.90%) and the pyritic content in the sample indicates the extent of concentration of Fe impurity minerals along with quartz in this particular size range during hydrocycloning. The thermal analysis also supports these findings. During TG analysis, the sample loses weight at two steps, which correspond to the oxidation of pyrite to hematite and dehydroxylation of kaolinite. The low concentration of kaolinite in the sample is confirmed by the DTA pattern where the characteristic exotherm at ~998°C and endotherm at ~550°C are insignificant. Prominent exotherms are observed at 440-560°C which corresponds to the decomposition / oxidation of pyrite.

The chemical assay of the IM2 sample shows the presence of appreciable quantities of quartz and heavy minerals (of Fe and Ti). As expected in the panning operation, the kaolinite content in the sample is almost negligible as evident from the very low alumina value and quartz content is high. XRD analysis shows that pyrite and goethite are the major minerals present in the sample along with other minerals such as quartz, rutile, anatase, ilmenite, kaolinite and graphite in minor quantities. Considerable quantity of pyrite is found to be present and is evident from the chemical assay, thermal analysis and XRD findings. The weight loss on heating is high in the chemical assay and

185

TA results. The DTA pattern shows that the characteristic exotherm at ~998°C and xotherm at ~550°C are insignificant which confirms the very low concentration of xlinite in the sample. Prominent exotherms are observed at 440-560°C which responds to the decomposition / oxidation of pyrite. The high percentages of Fe_2O_3 (98%) and TiO_2 (11.77%) indicates that Fe and Ti impurity minerals are getting concentrated to a great extent during panning.

The sample IM3 separated by alkali treatment of the clay is found to be free from kaolinite and at the same time enriched with the "Fe" mineral phases, particularly pyrite and this is evident from the chemical assay of the sample. The high LOI value also indicates the presence appreciable quantities of pyrite in the sample. The titania content is low since part of it may be getting leached into the alkali on heating. XRD analysis data shows the presence of pyrite, quartz and goethite as major minerals along with anatase and rutile as minor phases. It is interesting to note that chemical treatment with 5M KOH solution removes the kaolinite completely but does not decompose the pyrite.

The XRD analysis of the magnetic fraction IM4 separated by hand magnet confirms the presence of magnetite, rutile, goethite, hematite, anatase and ilmenite as the major phases along with minor quantities of iron stained quartz and pseudo rutile.

4.6 Impurities from Bankura kaolin

The characterization studies of Bankura kaolin indicate that the nature of impurities is different from those from other kaolins under investigation. The impurity minerals separated from the kaolin IM1, IM2 and IM3 have been analyzed for their chemical and mineralogical properties and the results are given in Tables 4.6. The XRD patterns of these samples along with that of the magnetic fraction (IM4).are exhibited in Figure 4.7.

Chemical analysis of the sample IM1 shows that the silica percentage is high and the alumina content and LOI are very low in comparison to that of kaolinite mineral. The low kaolinitic content and large amount of free silica are thereby indicated. The X-ray diffraction analysis shows that quartz and kaolin are the major minerals present in the sample while mica is present in significant quantities. Presence of hematite was also detected in the sample. The relative intensity of the quartz peak is found to be very high. The rational analysis data also support these findings. The weight loss in TGA is small,

186

exotherm at ~980 is broad and the endotherm is lowered to 518°C. All these observations again point to the low kaolinite content. The endotherm at ~573°C corresponds to the quartz and /or mica. The percentages of Fe_2O_3 (2.91%) and TiO_2 (.49%) in the sample indicates the concentration of Fe and Ti impurity minerals along with appreciable quantities of quartz in this particular size range. The information from the XRD analysis and weight percentage of the mineral content obtained from the rational analysis data also supports the same. Rational analysis data clearly shows the presence of micaceous impurities in the sample.

The chemical assay of the IM2 sample shows the presence of appreciable quantities of quartz and heavy minerals in the sample. As expected, the kaolinite content in the sample was minimal and Fe_2O_3, TiO_2 and quartz content was high and is evident from the low LOI and TGA values. The sample is found to contain micaceous phases also. The XRD analysis shows that quartz and mica are the major minerals present in the sample along with other minerals such as kaolinite, rutile, anatase, goethite and hematite in minor quantities. The endotherm at ~575°C again corresponds to quartz and or mica.

The alkali treated sample (IM3) is found to be free from kaolinite and at the same time enriched with the Fe and Ti mineral phases which are evident from the chemical assay of the sample. The titania content in the sample is also less. The relatively high LOI of the sample in comparison to the other impurity mineral concentrates can be due to the presence of relatively high quantities of iron hydroxides and oxy-hydroxides. XRD analysis data shows the presence of quartz and rutile as major minerals along with hematite, anatase and goethite as minor phases.

It is evident from the X-ray diffraction analysis that, iron stained quartz, goethite, hematite and pseudo rutile are the major phases present in the magnetic fraction (IM4) along with minor quantities of hematite, anatase, ilmenite and rutile.

4.7 Impurities from Pali kaolin

The chemical and mineralogical properties of the impurity samples IM1, IM2 and IM3 are presented in Tables 4.7. The XRD patterns of these samples along with that of IM4 are represented in Figure 4.8.

The chemical assay clearly shows that the sample IM1 contains larger amount of silica and smaller alumina in comparison to the composition of kaolinite mineral. This

187

gh ratio of silica alumina indicates free silica and low kaolinite content. The percentages of Fe_2O_3 (1.53%) and TiO_2 (0.82%) in the sample indicates that only small amount of Fe" and Ti impurity minerals along with appreciable quantities of quartz are concentrated by hydroycloning in this particular size range. The X-ray diffraction analysis shows that quartz and kaolinite are the major minerals present in the sample while mica, calcite and rutile are present in minor quantities. The peak corresponding to quartz is quite intense indicating the presence of large amount of free silica in the sample. This inference is supported by the rational analysis data and the low weight loss in TGA. Rational analysis data shows the presence of appreciable quantities micaceous impurities in the sample. The endotherms at ~535 and ~575°C correspond to the dehydroxylation of kaolinite and phase change in quartz respectively. Loss of adsorbed water is possibly contributing to the endotherm at ~68°C. Micaceous impurities may be causing the small endotherm at ~750°C. Presence of kaolinite is confirmed by the characteristic exotherm at ~976°C.

The chemical composition of the IM2 sample shows the presence of appreciable quantities of silica, Fe_2O_3 and CaO. The LOI is also relatively high. XRD analysis of this sample shows that quartz is the major mineral content along with calcite, kaolinite, goethite, anatase, rutile and mica in minor quantities. The endotherm at ~579°C and ~830°C in the DTA corresponds to quartz and calcite respectively. The rational analysis data also supports these findings from XRD and thermal analysis. It also indicates small amount of micaceous phases. The high Ca content and LOI are due to the calcite present in the sample.

The alkali treated sample (IM3) contains only very small amount of alumina indicating the removal of most of the kaolinite during alkali treatment. However, free quartz is retained and Fe and Ti minerals are concentrated. The chemical assay is given in the Table 4.7. XRD analysis data shows the presence of quartz as the major mineral along with goethite, rutile and anatase as minor phases. Again the high amount of iron content adds to the fact that considerable amount of the iron is present as amorphous compounds.

It is evident from the X-ray diffraction analysis that, iron stained quartz, magnetite, pseudo rutile and hematite are the major phases present in the magnetic fraction (IM4) along with minor quantities of rutile, goethite, ilmenite and anatase.

188

Chemical assay and mineralogy of impurity minerals from Kasargod 1 kaolin

Properties	IM1	IM2	IM3
Chem.Assay			
(% wt)			
SiO_2	73.18	28.41	20.34
Al_2O_3	12.34	6.21	2.49
Fe_2O_3	4.08	36.08	52.29
$TiO2$	3.63	26.47	14.89
CaO	0.22	0.24	BDL
Na_2O	0.30	0.09	BDL
K_2O	0.37	0.17	BDL
LOI	3.92	2.34	10.48
Mineralogy			
XRD			
Major phases	Q, K	Q,M R, K	Q, R
Minor phases	Mi, R, A	H, P.R, G, A, I, K	H, A, I, G P.R
DTA			
Endotherm (°C)	532.5, 575.8	523.1	---
Exotherm (°C)	997.1	322.1	---
TG (wt. loss %)	3.54	2.26	---
Rational Analysis			
(Mineral % weight)			
Kaolinite	24.47	10.64	
Quartz	58.64	21.09	
Muscovite mica	3.10	1.14	
Paragonite mica	3.72	1.11	
Hematite	4.08	36.08	
Anatase	3.63	26.47	
Calcite	0.40	0.43	

Q-Quartz; K-Kaolinite; R-Rutile; A-Anatase; H-Hematite; I-Ilmenite; G-Goethite
Mi-Mica, P.R-Psuedo Rutile

189

LC Chemical assay and mineralogy of impurity minerals from Kasargod 2 kaolin

~perties	IM1	IM2	IM3
Jem.Assay			
% wt)			
SiO_2	80.78	35.52	17.02
Al_2O_3	7.12	5.89	3.67
Fe_2O_3	4.46	36.69	55.15
$TiO2$	3.40	14.21	13.48
CaO	0.32	0.41	BDL
Na_2O	0.34	0.18	BDL
K_2O	0.21	0.29	BDL
LOI	2.52	2.01	10.21
ineralogy			
XRD			
Major phases	Q, K	Q, G	Q, R
Minor phases	A, R	H, I, R, A, P.R, M	A, G, H, I
TA			
Endotherm (°C)	527.9, 575.8	72.2	---
Exotherm (°C)	180.9, 889.5, 997.1	341.2, 877.1	---
G (wt. loss %)	1.67	1.87	---
ional Analysis			
Mineral % weight)			
Kaolinite	12.13	9.83	
Quartz	72.31	28.58	
Muscovite mica	1.74	2.45	
Paragonite mica	4.15	2.20	
Hematite	0.67	36.69	
Anatase	0.34	20.21	
Calcite	0.29	0.73	

BDL < 0.01 %

Q-Quartz; K-Kaolinite; R-Rutile; A-Anatase; H-Hematite; I-Ilmenite; G-Goethite
P.R – Psuedo Rutile; M-Magnetite

JChemical assay and mineralogy of impurity minerals from Trivandrum kaolin

Properties	IM1	IM2	IM3
Chem.Assay (% wt)			
SiO_2	49.52	25.90	5.64
Al_2O_3	19.66	5.23	2.76
Fe_2O_3	17.69	28.18	62.51
$TiO2$	6.16	35.82	23.14
CaO	0.46	0.62	BDL
Na_2O	0.11	0.32	BDL
K_2O	0.39	0.18	BDL
LOI	3.12	2.96	5.21
Mineralogy XRD			
Major phases	K, Q	Q, R, A	A, R
Minor phases	A, R	K, H, G, Z, P.R	H, G, M, P.R
DTA			
Endotherm (°C)	527.8	196.4	---
Exotherm (°C)	994.0	867.8	---
TG (wt. loss %)	3.12	2.15	---
Rational Analysis (Mineral % weight)			
Kaolinite	44.16	8.36	
Quartz	26.37	19.74	
Muscovite mica	3.30	1.53	
Paragonite mica	1.36	3.95	
Anatase	6.16	35.82	
Hematite	17.69	28.18	
Calcite	0.81	1.10	

BDL < 0.01 %

Q-Quartz; K-Kaolinite; R-Rutile; A-Anatase; H-Hematite; Z-Zircon; G-Goethite; P.R –Pseudo Rutile; M-Magnatite

Table 4.4 Chemical assay and mineralogy of impurity minerals from Kutch kaolin

Properties	IM1	IM2	IM3
Chem.Assay			
(% wt)			
SiO_2	47.20	24.22	8.17
Al_2O_3	21.83	14.18	3.18
Fe_2O_3	4.90	20.12	40.92
$TiO2$	10.60	36.11	36.23
CaO	0.08	0.05	BDL
Na_2O	0.30	0.24	BDL
K_2O	0.11	0.01	BDL
LOI	8.57	2.10	7.47
Zircon	---	3.53	---
Mineralogy			
XRD			
Major phases	K, Q	Q, Z, R	R, A
Minor phases	A, R	K, H	H
DTA			
Endotherm (°C)	528.6	197.9	
Exotherm (°C)	994.7	869.4	
TG (wt. loss %)	8.76	2.28	
Rational Analysis			
(Mineral % weight)			
Kaolinite	51.45	16.06	
Quartz	21.48	15.77	
Muscovite mica	0.93	0.08	
Paragonite mica	3.70	2.96	
Anatase	10.60	38.11	
Hematite	4.90	24.12	
Calcite	0.14	0.09	
Zircon	---	2.60	

BDL < 0.01 %

Q-Quartz; K-Kaolinite; R-Rutile; A-Anatase; H-Hematite; Z-Zircon

Chemical assay and mineralogy of impurity minerals from Koraput kaolin

Properties	IM1	IM2	IM3
Chem.Assay			
(% wt)			
SiO_2	49.76	16.50	15.43
Al_2O_3	20.67	3.62	ND
Fe_2O_3	11.90	47.98	65.71
$TiO2$	1.24	11.77	2.12
CaO	0.92	0.51	BDL
Na_2O	0.44	0.22	BDL
K_2O	0.37	0.19	BDL
LOI	14.60	19.10	16.87
Sulphur	4.50	18.20	27.60
Mineralogy			
XRD			
Major phases	Q, P, K	P, G	Q, P
		Q, R, A, I, K,	
Minor phases	R, A, Gr	Gr	A, R, H
DTA			
Endotherm (°C)	534.4, 563.8	606.9, 80.3	---
Exotherm (°C)	441.1, 542.3, 561.5	444.1, 628.5	---
TG (wt. loss %)	13.31	19.50	---
Rational Analysis (Mineral % weight)			
	43.77	4.98	
Kaolinite	25.41	12.24	
Quartz	3.12	1.60	
Muscovite mica	5.47	2.71	
Paragonite mica	8.41	34.00	
Pyrite	4.69	17.98	
Hematite	1.24	11.77	
Anatase	1.64	0.91	
Calcite			

BDL < 0.01 %

K-Kaolinite; Q – Quartz; R – Rutile; P – Pyrite; G-Goethite; A –Anatase; Gr-Graphite I-Ilmenite; H-Hematite

193

Pyrite content in the impurity minerals from Koraput kaolin

Properties	IM1	IM2	IM3
*Total Iron, % (by estimation)	4.24	16.55	24.40
*Non-Pyritic Iron, % (by estimation)	0.35	0.64	0.96
*Pyritic Iron,% (by calculation)	3.89	15.91	23.43
#Sulphur, %	4.50	18.19	27.61

% of pyrite from
    Pyritic Iron
    Sulphur
	8.36
	8.42
		34.17
		34.05
			50.34
			51.67

* Schneider & Schneider, Ceramic Bulletin, 1990
\# Quantitative chemical analysis, Vogel (Fifth ed.)

4.6 Chemical assay and mineralogy of impurity minerals from Bankura kaolin

Properties	IM1	IM2	IM3
Chem.Assay			
(% wt)			
SiO$_2$	86.52	25.84	9.16
Al$_2$O$_3$	4.92	6.21	0.34
Fe$_2$O$_3$	2.91	52.03	78.23
TiO2	1.49	10.98	5.21
CaO	0.42	2.10	BDL
Na$_2$O	0.12	0.44	BDL
K$_2$O	0.28	1.48	BDL
LOI	1.51	1.55	7.05
Mineralogy			
XRD			
Major phases	Q, K	Q, Mi	Q, R
Minor phases	Mi, H	K, R, A, G, H, M, P.R	H, A, G
DTA			
Endotherm (°C)	518.3, 573.4	575.8	---
Exotherm (°C)	~980 (broad)	Nil	---
TG (wt. loss %)	1.20	1.33	---
Rational Analysis			
(Mineral % wt)			
Kaolinite	8.67	3.23	
Quartz	80.72	18.52	
Muscovite mica	2.35	6.00	
Paragonite mica	1.48	5.42	
Anatase	1.49	10.98	
Hematite	2.91	52.03	
Calcite	0.74	3.75	

BDL < 0.01%

Q-Quartz; K-Kaolinite; M-Mica; R-Rutile; A-Anatase; H-Hematite; I-Ilmenite; G-Goethite; M-Magnetite; P.R-Psuedo rutile

Table 4.7 Chemical assay and mineralogy of impurity minerals from Pali kaolin

Properties	IM1	IM2	IM3
ChemAssay (% wt)			
SiO_2	68.97	26.40	18.48
Al_2O_3	17.99	6.20	1.27
Fe_2O_3	1.53	29.05	61.31
TiO2	0.82	1.00	8.71
CaO	0.59	17.97	BDL
Na_2O	0.44	0.87	BDL
K_2O	0.29	0.62	BDL
LOI	7.96	18.01	10.12
Mineralogy			
XRD			
Major phases	Q,K	Q,C	Q,R
Minor phases	Mi, R, C	G,A, R,K,C	R, G, A, H
DTA			
Endotherm (°C)	68.3, 535.1 575	293.3, 578.8,	--- ---
Exotherm (°C)	779.3, 975.6	820.0 482.5	--- ---
TG (wt. loss %)	8.61	19.32	---
Rational Analysis (Mineral % wt)			
Kaolinite	37.75	0.80	
Quartz	47.78	19.30	
Muscovite mica	2.41	5.25	
Paragonite mica	5.40	10.73	
Anatase	1.53	1.00	
Hematite	0.82	29.05	
Calcite	1.06	32.07	

BDL < 0.01%

Q-Quartz; K-Kaolinite; Mi-Mica; R-Rutile; A-Anatase; H-Hematite; G-Goethite; C-Calcite
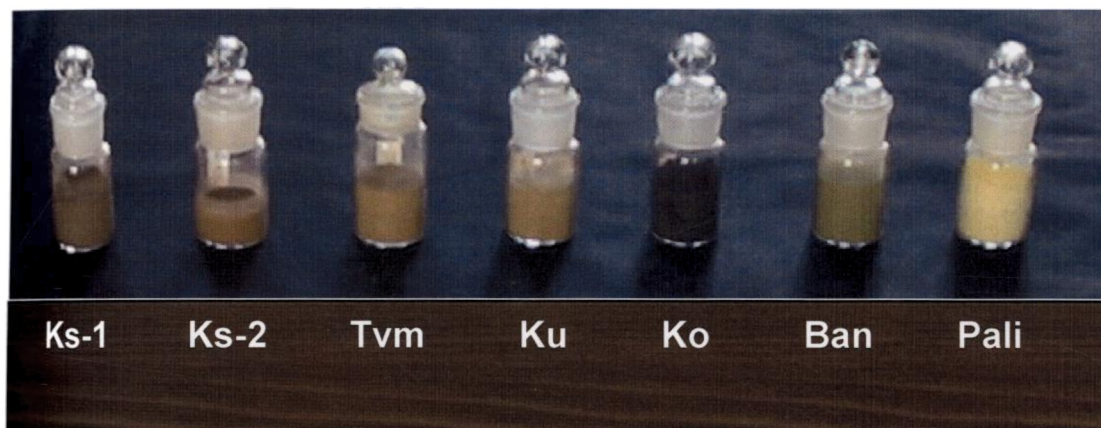
Figure 4.1 Impurity concentrate (IM2) separated from the kaolin samples

Ks-1 **Kasargod 1**
Ks-2 **Kasargod 2**
Tvm **Trivandrum**
Ku **Kutch**
Ko **Koraput**
Ban **Bankura**

197
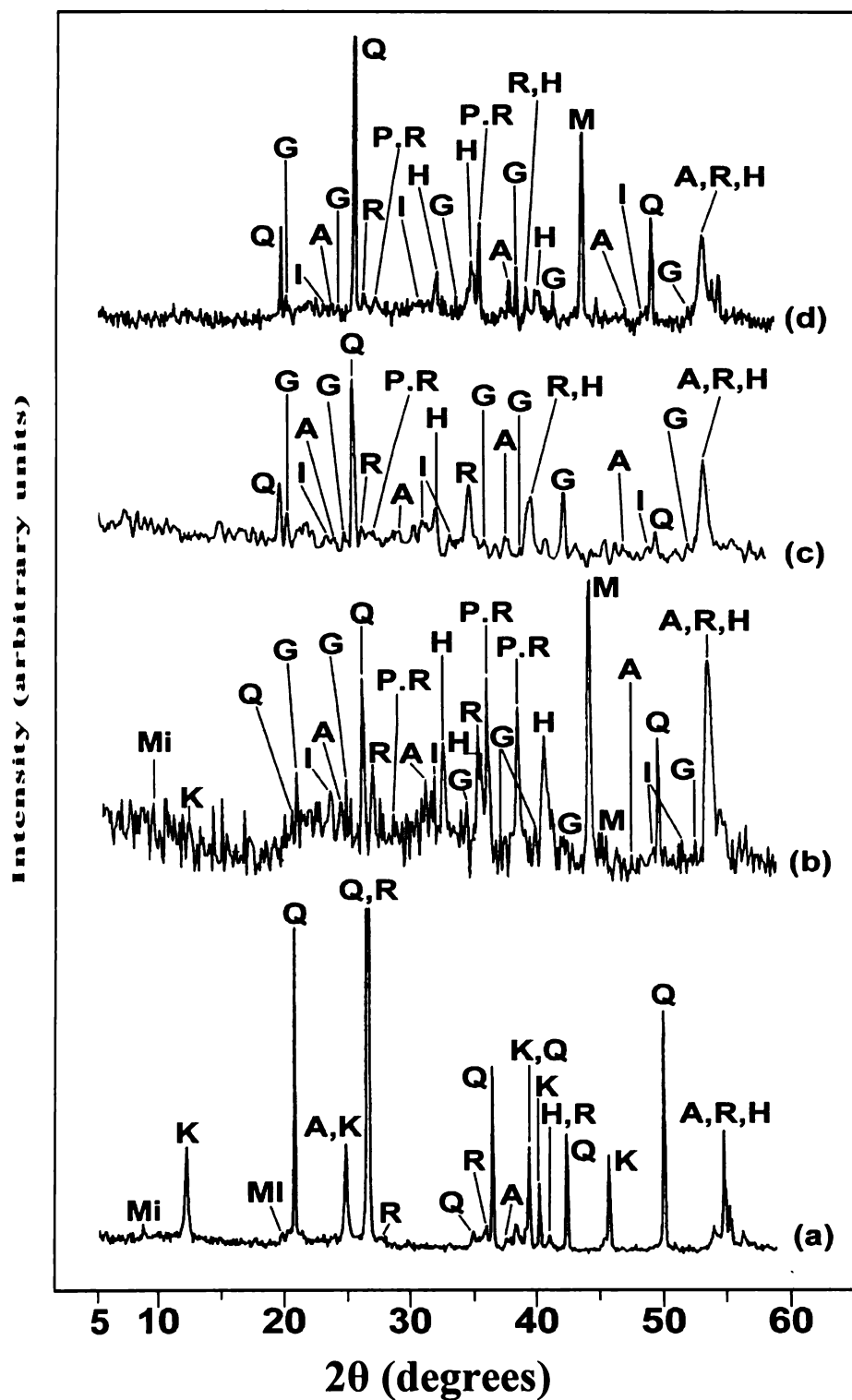
Figure 4.2 XRD patterns of (a) IM1 (b) IM2 (c) IM3 and (d) IM4 of
Kasargod 1 kaolin
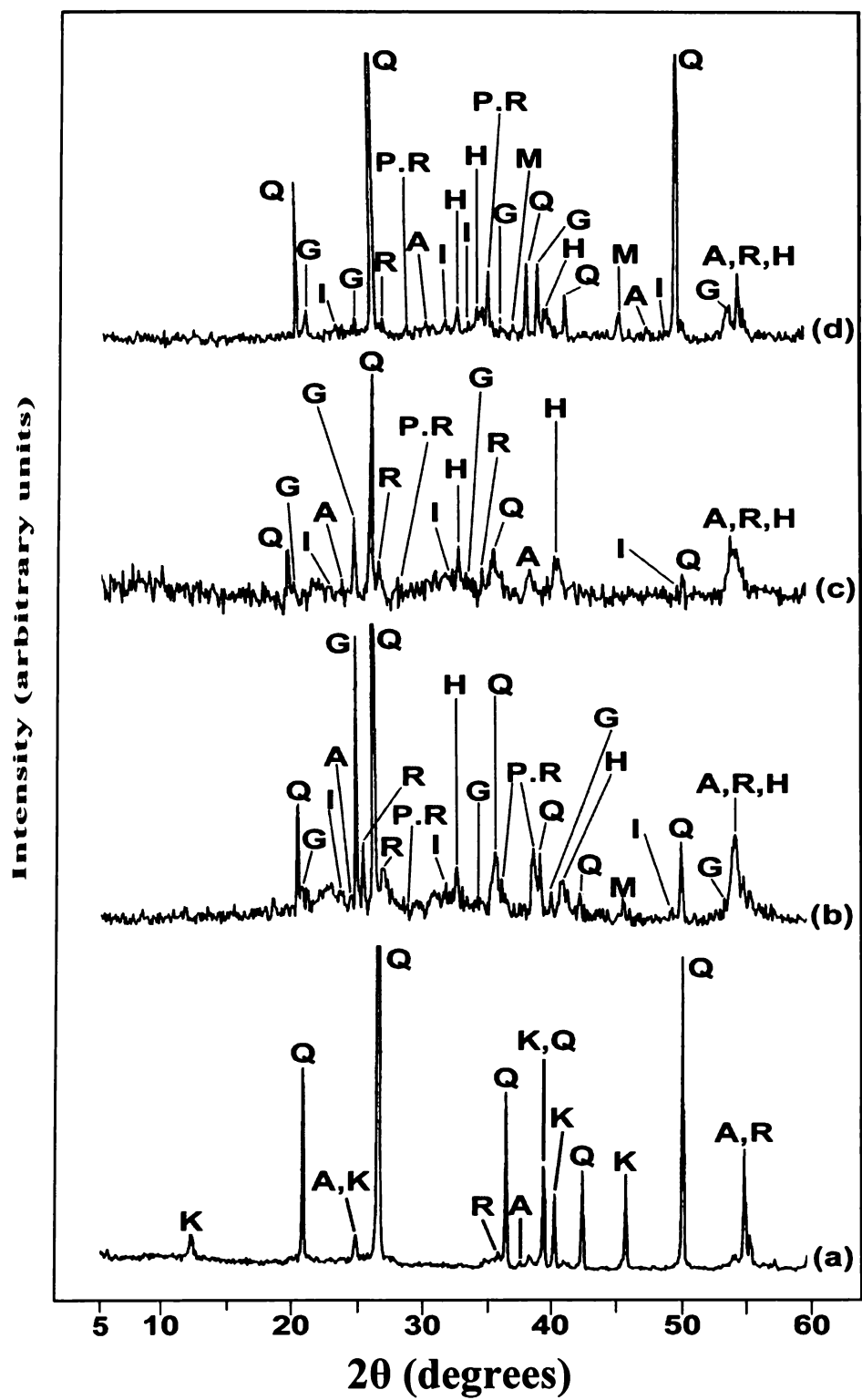
Figure 4.3 XRD patterns of (a) IM1 (b) IM2 (c) IM3 and (d) IM4 of
Kasargod 2 kaolin
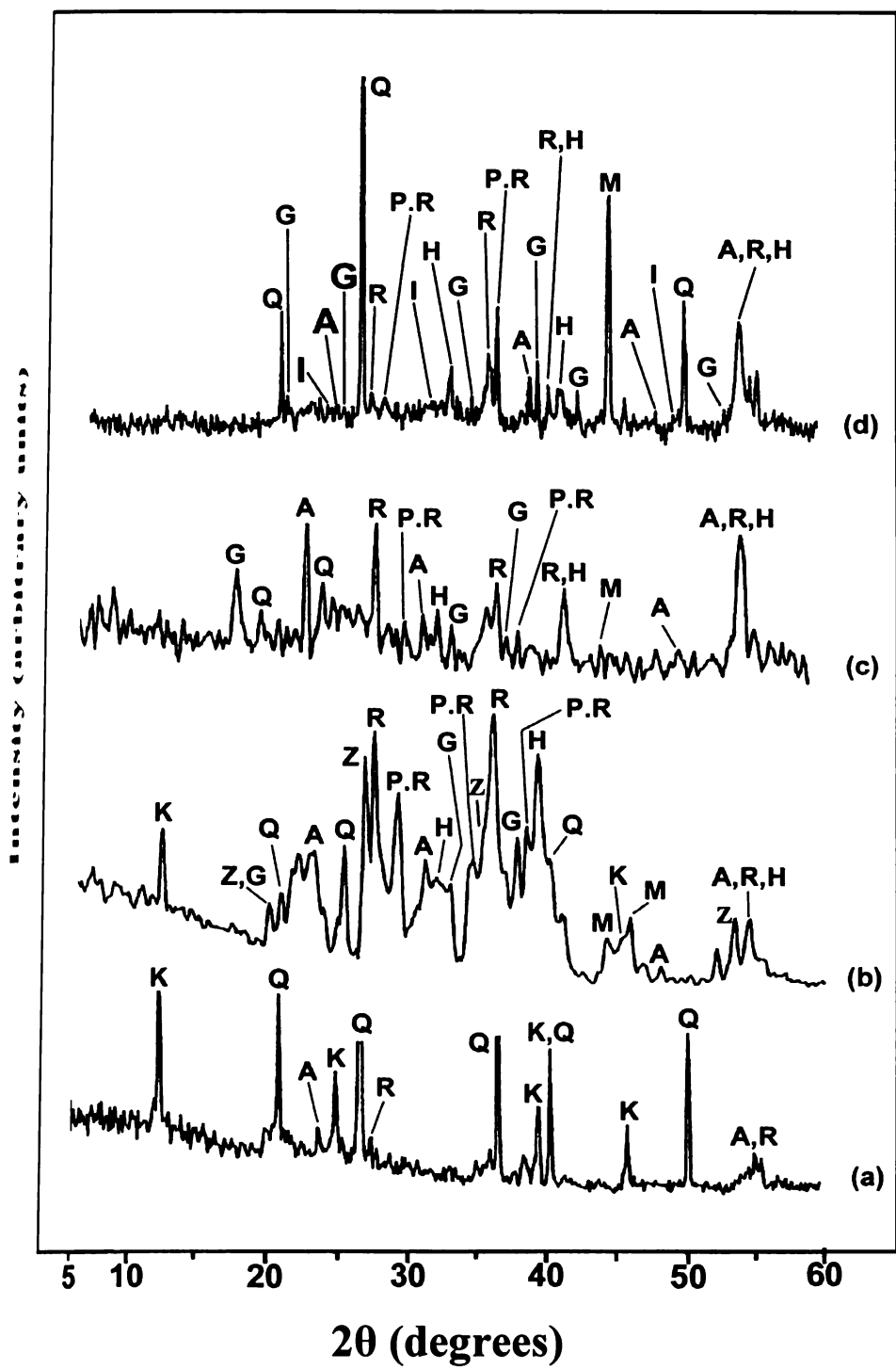
Figure 4.4 XRD patterns of (a) IM1 (b) IM2 (c) IM3 and (d) IM4 of
Trivandrum kaolin
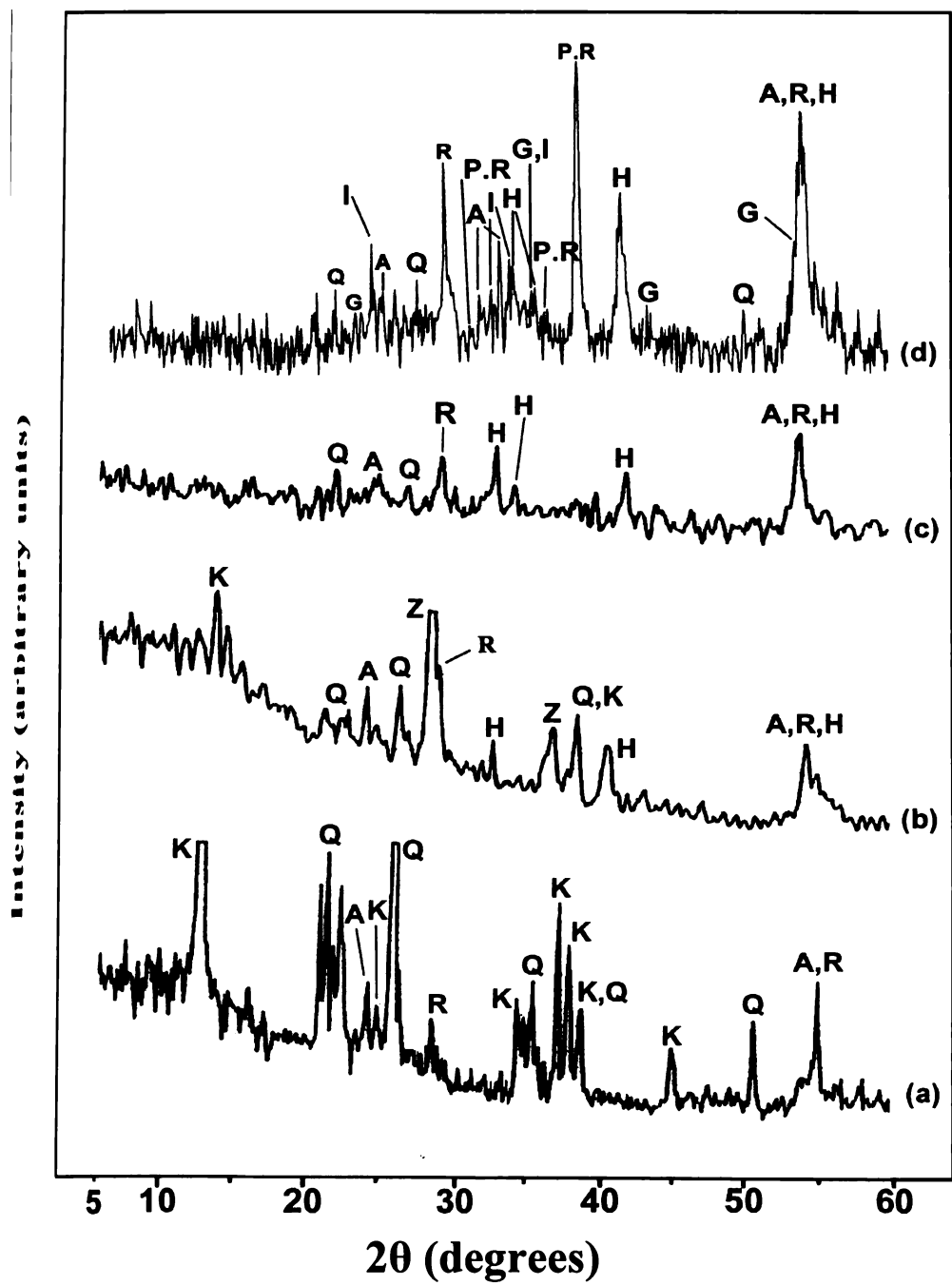
Figure 4.5 XRD patterns of (a) IM1 (b) IM2 (c) IM3 and (d) IM4 of Kutch kaolin
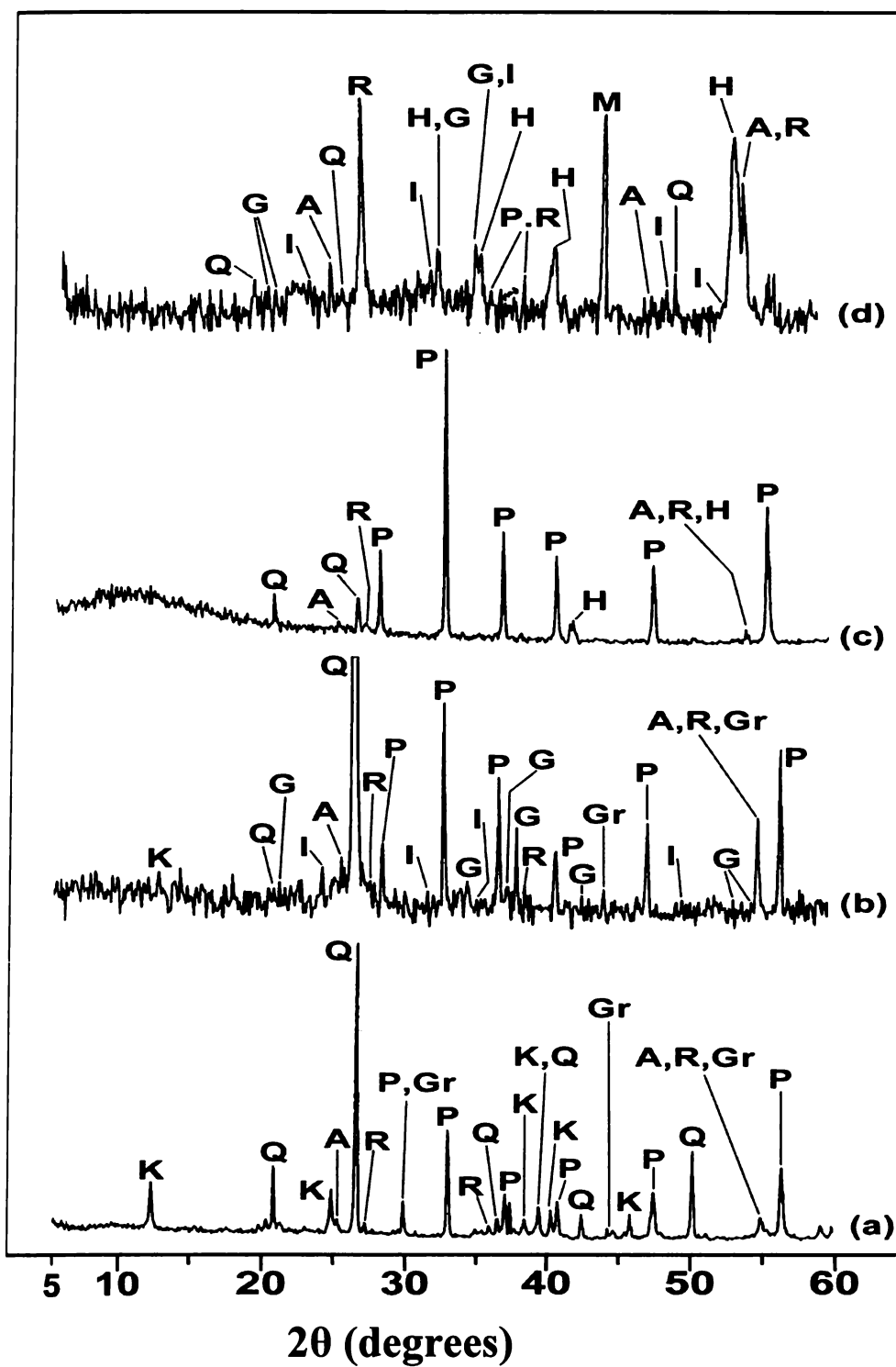
Figure 4.6 XRD patterns of (a) IM1 (b) IM2 (c) IM3 and (d) IM4 of Koraput kaolin
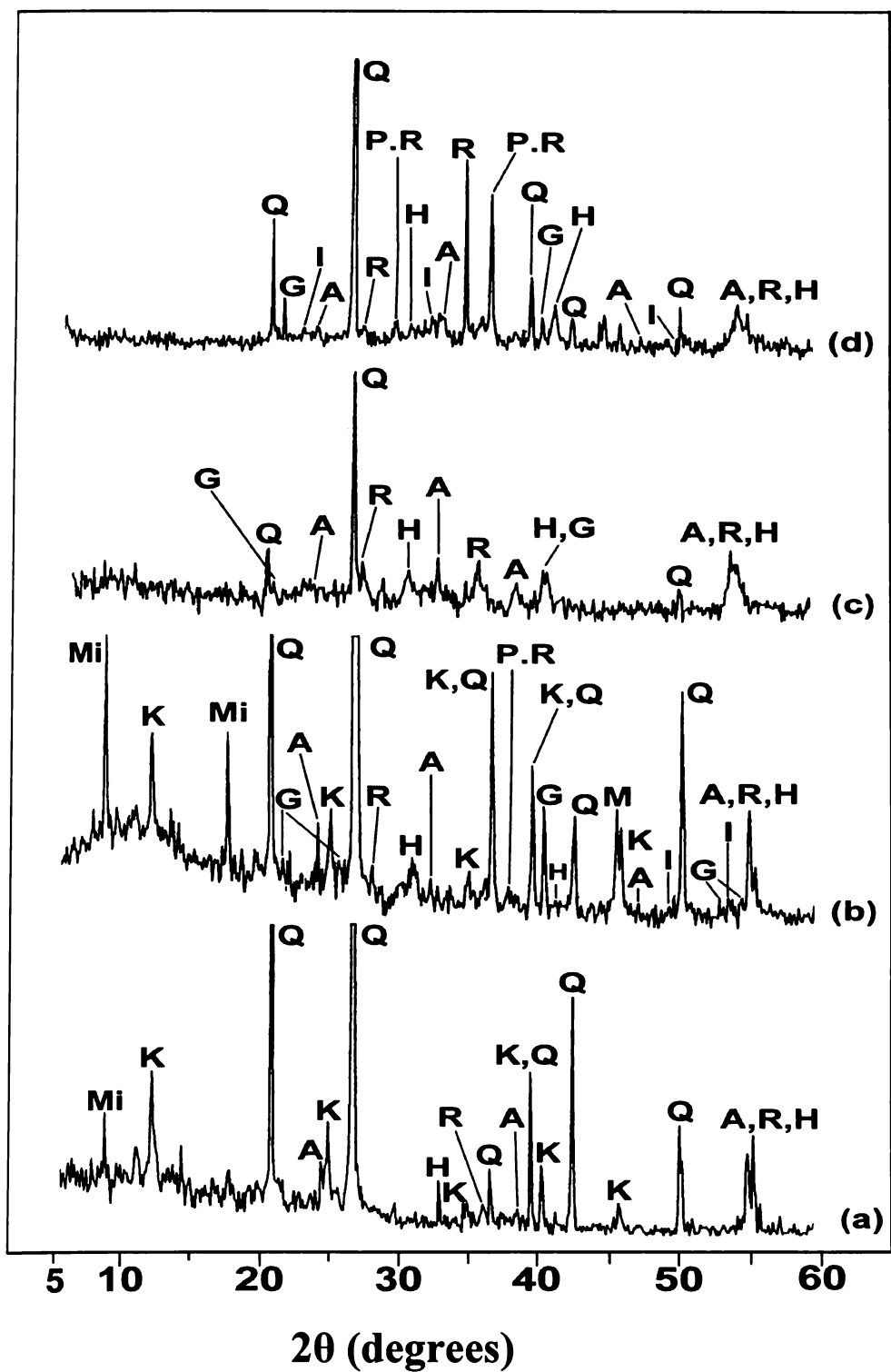
Figure 4.7 XRD patterns of (a) IM1 (b) IM2 (c) IM3 and (d) IM4 of Bankura kaolin
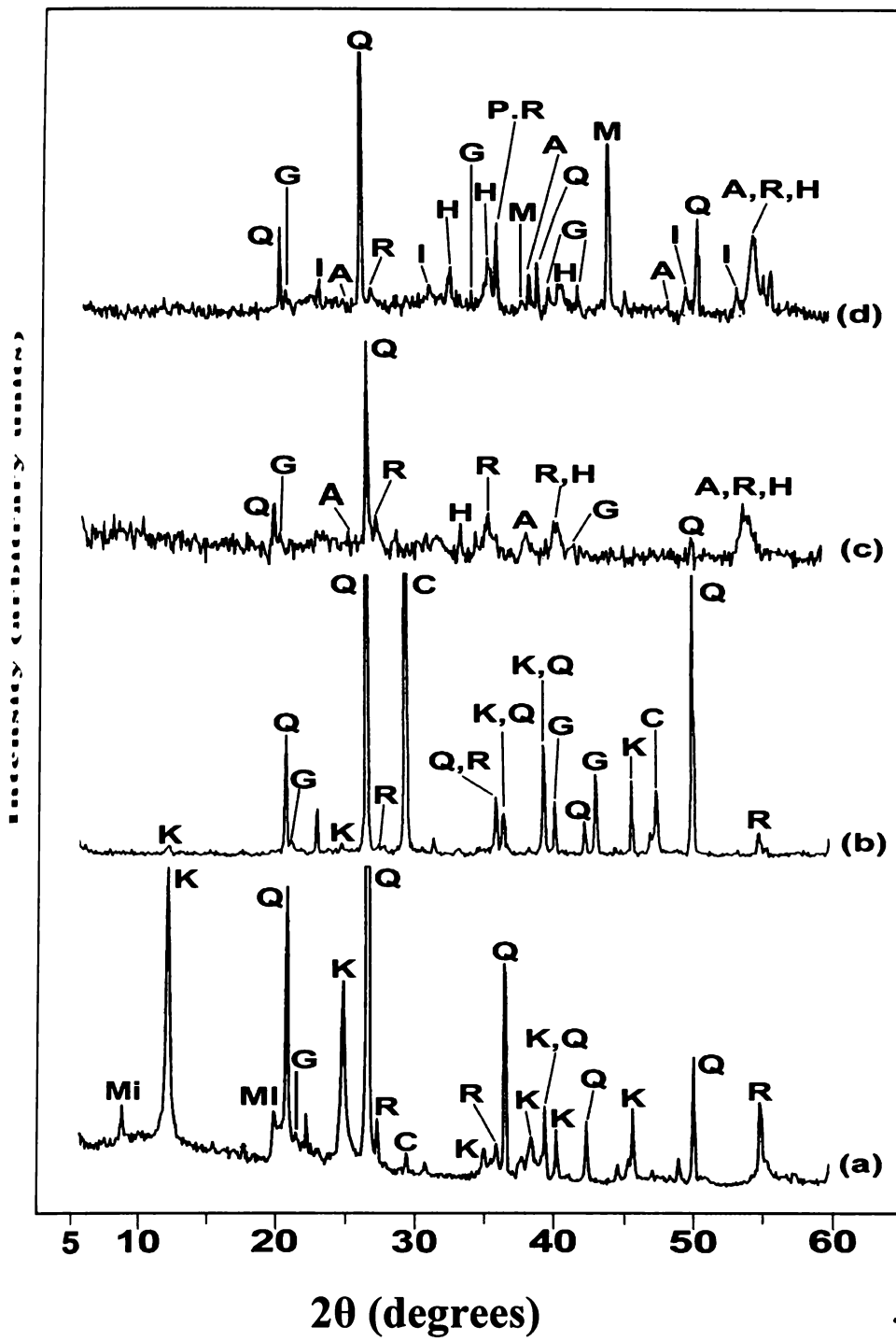
Figure 4.8 XRD patterns of (a) IM1 (b) IM2 (c) IM3 and (d) IM4 of
Pali kaolin

CHAPTER -5

SPETROSCOPIC AND MICROSCOPIC STUDIES

The ancillary impurities especially those of iron strongly influence the physico chemical properties of kaolin during its processing for example specific surface of the kaolinite phase and the rheological properties. The qualities of the finished products related to the different industries (paper coating, paints, ceramic, rubber etc.) are also affected. Extensive studies have been carried out on the relation between the total iron, its size, the structural order and the surface reactivity of kaolin (Cases et al, 1982, 1986). The advent of sophisticated spectroscopic analytical techniques has made easy to understand the state of iron and its effect on the properties of kaolin (Brindley, 1986). The difficulties associated with the low concentration of Fe in kaolin, the complexity of the natural material matrix from which kaolins are obtained and the effect of pre-concentration or extraction methods often requires the use of multiple analytical techniques to investigate the materials. In addition to XRD analysis, the traditional tool for mineral identification, spectroscopic (IR, EPR and Mossbauer) and microscopic (optical, SEM, TEM and EPMA) techniques have been used to define the iron impurities in kaolin.

The crystallo-chemical characteristics and the assembly of kaolinites with the associated iron oxyhydroxides are closely linked to the geological conditions in which the kaolins are formed. Certain mineral impurities such as iron and titanium oxyhydroxides can not be detected and / or analyzed by XRD since they are present in minute quantity and sometimes in amorphous form. The spectroscopic tools are, on the other hand, adapted to their analysis and can bring additional information, ie., they allow to identify and to localize certain impurities, within the minerals or the form of separated neophases (Bonin et al., 1982)

Electron Paramagnetic Resonance (EPR) spectroscopy is concerned with the detection of unpaired electrons and characterization of their chemical environments. It is not a technique that can be used for clay mineral identification, but can be used for characterizing the minor structural or surface components (paramagnetic species) that contain unpaired electrons and which may be of importance in understanding the specific properties of the minerals. It is a powerful technique for identifying the various types of

205

sociation of paramagnetic metal ions with clay minerals, on the basal surfaces, within the interlamellar spaces, or as part of the aluminosilicate structures. Such information will be of vital importance in understanding clay chemistry and EPR has been used extensively over the past two decades for the same.

Over the years extensive EPR studies have been carried out on both natural kaolinites (Angel and Hall, 1973; Meads and Malden, 1975; Herbillon et al, 1976; Clozagh et al, 1980; Brindley et al, 1986; Muller et al, 1990) and synthetic specimens (Angel et al, 1974; Jones et al, 1974; Angel et al, 1977; Cuttler, 1980, 1981) and the main spectral characteristics are now well understood. The EPR spectra of two typical kaolins of sedimentary origin are given in Figure 1 (Meads and Malden, 1975; Hall, 1980). These spectra are a result of the superimposition of different signals described in the literature (a) in the magnetic field , between 1200 and 2000 Gauss (G), a complex signal due to ferric iron in the impurities with in the lattice kaolinites (b) in the elevated magnetic field three overlapped signals centered to about 3300 Gauss, due to the iron oxyhydroxides associated with the kaolinites and the electronic defects within the lattice of the kaolinite (Meads and Malden, 1975; Hall, 1980; Muller and Calas, 1991). It is evident from Figure 5.1 that the intensities of the signals are related to the concentration of the corresponding paramagnetic species and varies from one sample to the other in a significant manner.

The paramagnetic ferric iron can situate in two distinct sites within the kaolinite given in Figure 5.1, which can be referred to as Fe(I) and Fe(II) (Balan et al, 1999). The isotropic signal of Fe(I), centered around 1585G overlaps with the anisotropic signal of Fe(II) having a maxima at 1340G and a minima at 1890G. Even though both of these two sites contain ferric iron substitute for aluminium in the octahedral layer of the kaolinite, they will have different symmetry and will affect the structural order / crystalline nature of the kaolinite differently. The replacement of aluminium ion from the lattice of kaolinite by Fe(II) will not make any noticeable deformation of the crystal lattice indicating that Fe(II) is associated with the crystalline domain with a high crystalline nature. On the contrary, the replacement of lattice aluminium of kaolin by Fe(I), probably at the periphery of the crystalline domains, is accompanied by the site deformations of substitution (rhombic distortion), which disturbs the regular stacking up

206

layers in the kaolinite lattice (Brindley et al, 1986) showing that the Fe(I) is associated with the weak crystalline nature domains. Based on their studies on soil kaolinites, Allard al.(1994) has shown that an appreciable increase of the area of the signal Fe(II) does produce a significant modification in the crystalline nature of the kaolinite, but at the same time a modest change in the area of the signal of iron Fe(I) makes an appreciable increase in the crystalline nature of kaolin.

The isotropic signal centered around regions 2000G and 3300G are due to the presence of iron oxyhydroxides (hematite and/or gothite) in nanometric particles (<10 nm) and / or of ferric gels. There exists a relationship between the area of this signal to concentration of the super-paramagnetic phases and the concentration of Fe(I) in the structure of kaolinites and is evident from the EPR specta of the samples subjected to iron removal by various methods. The intensity of this signal will be high, if, concentrations of Fe(I) is high. This relation can be linked with the existence of very close structural relations between the iron oxyhydroxides and the kaolin (Bonin et al, 1982). Typical EPR spectra different kaolin samples are given in Figure 5.2.

Mossbauer spectroscopy is a very important technique which can be used for the identification and characterization of less crystalline iron oxide and oxy-hydroxide minerals present in kaolin samples. It is powerful technique, which gives the information about the oxidation state and the coordination environments of the iron in mineral phases. The oxidation states can be determined from the magnitude of the inner shifts and the typical values for Fe^{+2} and Fe^{+3} bound to oxygen in different coordination environments are given in Figure 5.3.

Hematite (alpha-Fe_2O_3), Maghemite (gama-Fe_2O_3), Magnetite(Fe_3O_4), Goethite(α-FeOOH), Lepidocrocite(γ-FeOOH), Akaganeite(β-FeOOH) Ferrihydrite ($Fe_5HO_8.4H_2O$), feroxyhite(∂-FeOOH) are the oxide and oxyhydroxide species of iron generally associated with kaolin in nature. All these minerals will order magnetically and only magnetite and maghemite are strongly ferromagnetic due to their spinel type structures. others are either antiferromagnetic or very weakly ferromagnetic, although the arrangement of spins in the poorly crystalline mineral, ferrihydrite has been described as ferrimagnetic (Coey and Readman, 1973). The Mossbauer spectra of iron oxides have reviewed by many researchers (Bowen and Weed, 1984; Murad and Johnston, 1987; and

207

and, 1988). Recently, Pollard et al (1992) has suggested that the use of large applied magnetic fields in low temperature Mossbauer spectra is the most effective approach to distinguish the various oxyhydroxide species, since it reduces particle size effects. Since it is a costly procedure, it is used only when the differentiation can not be made with measurements at higher temperature Mossabauer spectroscopic studies on iron in various kaolin deposits are reported (Fysh et al, 1983; Komusinski et al, 1981; Weaver et al, 1967; Malden and Meads; 1967, Jefferson et al, 1975; Murad and Wagner, 1991; Olowe et al 1990; Cuttler, 1980, Rossiter & Hodgson, 1965; Hart et al, 2002; Sei et al, 2004). The isomer shift (∂) and quadrupole splitting (ΔE) values of various iron species are sorted by these researchers. In 1983, Fysh et al. has reported that it possible to identify structural and surface iron in kaolin using Mossbauer spectroscopy.

Infrared absorption spectroscopy is a rapid, economical method universally used structural analysis. Absorption of infrared radiation by clay minerals is influenced by atomic mass, degree of crystalline order and the size and shape of the mineral particles (Marev, 1974; Farmer and Russell, 1966, Rendon and Serna, 1981, Serna et al, 1982). The infrared spectrum of a clay mineral is sensitive to the chemical composition, isomorphous substitution and crystallinity and provides fundamental information for the mineral identification and surface properties of the minerals. The IR band assignments in the kaolin (Farmer and Russell, 1964, Ledoux and White, 1964, Rouxhet et al, 1977) as well as for the various iron phases (Rendon and Serna, 1981; Yariv et al, 1979; Russell and Fraser, 1994) are available in the literature. The IR band due to the Fe^{+3} substitutions in Al^{+3} in kaolinite structure has been reported by Mendelovici et al in 1979.

Similarly, it is possible to identify the mineral phases in the impurity concentrates using *UV-Vis spectroscopy* based on the band assignments given for various iron minerals reported in the literature (Sherman et al, 1985 Karickhoff et al, 1973; Lehmann 1970 and Manning P. G., 1967).

Under microscopic studies, SEM pictures give the morphology and size of the particles. TEM gives information on nanoparticles and with EDS facility it provides the chemical assay (in atomic percentage) of individual particles and this information can be used for the identification of various mineral phases. The "iron staining", ie., the impurity Fe phases which are present as coatings (approximately 100 A° units) bound

the kaolin surface or incorporated in gel coatings on the surface of the kaolin particles easily identified and quantified by various researchers (Ferris and Jepson, 1975). ing et al (1975) and Jefferson et al (1975) have used TEM for understanding the red matite) and yellow (gothite) coating on kaolin while, Weaver (1976) has used the unique for studying the titanoferrous impurity (Ti,Fe)O_2 present in Georgia kaolin. M-EDS have also been used to understand the incorporation of Fe in anatase and anatie structure (Jepson and Rowse, 1975).

Electron Probe Micro Analysis (EPMA) and Optical Microscopic analysis are used to understand the various mineral phases present in kaolin.

In the present study, the spectroscopic and microscopic methods have been used in identifying the species of iron in kaolin samples and to see how the information given by each technique complement each other and supplement the findings. The ROM and products of beneficiation have been subjected to EPR spectral studies whereas the panned mineral impurities (IM2) are analyzed by Mossbauer and UV-Vis spectroscopy. IR spectra of ROM and impurity separated by hydrocyclone (IM1) and IM2 have been run. The ROM and size classified products (SCP1) are examined by SEM whereas IM and IM1 have been studied by EPMA. The ROM, SCP1 and IM1 samples of Kutch and Koraput kaolins have been subjected to HRTEM

EPR spectral studies

EPR spectroscopy is used to characterize Fe^{+3} ions that contain unpaired electrons (Komusinski et al., 1981; Balan et al, 2000). EPR spectra distinguishes two forms of Fe^{+3} isolated Fe^{+3} ions isomorphously substituted for Al^{+3} within the kaolinite structure "dilute" structural Fe^{+3}) and (ii) poorly understood domains in which Fe^{+3} ions reside in close proximity to one another. Fe^{+3} occurring in these domains are referred to as "concentrated / clustered" Fe^{+3}. Dilute structural Fe exhibits a paramagnetic signal at low magnetic field.

The characteristic EPR resonance lines of kaolinite are found in low magnetic (F1) and high magnetic (F2) fields with "g" values near 4.0 and 2.0 respectively. The resonances at F1 are attributable to structural Fe^{+3} and those at F2 may result from crystal imperfections, holes, free radicals etc. Fe^{+3} ions occupy two different sites denoted as $Fe_{(I)}$ and $Fe_{(II)}$ in the F1 region. Though both sites are due to Fe^{+3} substituting for Al^{+3} in

lattice, their symmetry is different. The degree of structural order of the kaolinite and relative populations of $Fe_{(I)}$ and $Fe_{(II)}$ sites are interrelated. Replacement of Al^{+3} by of $Fe_{(I)}$ probably at the periphery of the crystalline domains is accompanied by cubic distortion (deformation of the site of substitution), disturbing the regularity of kaolinite lattice (Balan et al, 2000). Replacement of Al^{+3} with Fe^{+3} at $Fe_{(II)}$ makes no gible deformation in the crystal lattice showing that it is associated with high crystalline nature. Thus $Fe_{(I)}$ substitution is associated with poorly crystalline nature and even a small increase will result in appreciable decreases in crystallinity. In other words the signal corresponds to the changes of the site symmetry owing to the random distribution of vacant octahedral site in successive layers and $Fe_{(II)}$ corresponds to the ions within low defect kaolin (Allard et al, 1994). Therefore an increase in the number of these sites and decrease in the number of $Fe_{(II)}$ sites leads to an increase in structural order. The wide resonance at g =2.0 (obscuring region II) is due to the contaminants of Fe_2O_3 and ore minerals. Fe removal by sodium dithionite solution completely eliminates or weakens this resonance. Thus EPR spectral method can be used to assess effectiveness of bleaching of kaolin.

Dehydroxylation of produces strong anisotropy of the crystal field in the position occupied by Fe^{+3} and the positions B of higher symmetry turn into A-type ones. This causes the rise of a small peak at g = 4.28 in region I and a very broad one at g = 2.0. The density of the resonance in region I decrease when the sample is heated nearly 1000°C due to the formation of spinel phase. Dehydroxylation causes the rise of a broad peak at g =2.0 caused by cluster of iron ions, because it supports the rearrangement of the iron and in consequence domains with a higher concentration of Fe+3 ions arise inside the metakaolinite structure or as a separate oxygen phase.

In the present work, the ROM clay as well as the beneficiated product samples ie., SCP1,SCP2 and SCP2-DCBT have been studied by EPR spectroscopy. The studies have been conducted on their heated (400°C & 1100°C) products also. The effect of heating on the intensities of the resonance bands gives an idea about the structural changes occurred in the clay during heating. Almost in all the ROM samples, the heating at 400°C has caused an increase in intensity of the broad band at g =2.0 and this is very much marked in Bankura and Koraput samples. This may be due to the cluster of iron ions, because it

site is found to decrease from ROM to the SCP2-DCBT product samples with a simultaneous increase in the number of $Fe_{(II)}$ lines and their intensity. This clearly indicates that the Fe^{+3} substituting for Al^{+3} in $Fe_{(I)}$ is less compared to that in $Fe_{(II)}$ site and the beneficiation of the sample has actually led an increase in structural order of the kaolinite

5.1.2 Kasargod -2 kaolin

The EPR spectra of the ROM and products of beneficiation and their heated products are given in.Figure 5.1.2a, Figure 5.1.2b and Figure 5.1.2c. The samples at RT show EPR lines at F1 and F2 regions. The ROM sample produces broad line at g ~ 4.86, 4.31 and 3.26 in the F1 region and g ~ 2.44 and 2.02 in F2 region. Sharper lines are observed in the F1 region (at g ~ 4.93, 4.31 and 3.77) for the SCP1 sample with a broad line at g ~ 2.69 in F2 region along with the g ~2.0 line. The SCP2 sample has also shown similar features, but the line at g ~2.85 more intense indicting the presence of free iron impurities. In the case of the SCP2DCBT product sample, the intensity of line at g ~2.56 is decreased considerably, thus confirming the removal of free iron contaminants by DCBT. The reduction in iron content and the sharp improvement in brightness of the sample support the findings. The other lines in the F1 region of the spectra are found to be sharper. Both the lines at $Fe_{(I)}$ and $Fe_{(II)}$ sites in F1 region are due to Fe^{+3} substituting for Al^{+3} in the kaolinite lattice but they have different symmetry. It is reported that and increase in the number of $Fe_{(I)}$ sites and decrease in the number of $Fe_{(II)}$ sites lead to an increase in structural disorder. Intensity of the line at $Fe_{(I)}$ site is found to decrease from ROM to the SCP2-DCBT product samples with a simultaneous increase in the number of $Fe_{(II)}$ lines and their intensity. This clearly indicates that the Fe^{+3} substituting for Al^{+3} in $Fe_{(I)}$ is less compared to that in $Fe_{(II)}$ site and the beneficiation of the sample has actually led an increase in structural order of the kaolinite.

5.1.3 Trivandrum kaolin

Figure 5.1.3a, Figure 5.1.3b and Figure 5.1.3c give the EPR spectra of the ROM, products of size classification and their heated products. All the samples in the RT show EPR lines at F1 and F2 regions. The ROM sample produces broad line at g ~ 4.66 and 3.9 in the F1 region and g ~ 2.81 and 2.02 in F2 region. The lines observed in the F1 region (at g ~4.61 and 4.17) are found to be sharper for SCP1 with a broad line at g ~

212

...in F2 region along with the g ~2.0 line. The SCP2 has also shown similar features, with the line at g ~2.85 more intense indicting the presence of free iron impurities. In the case of the SCP2DCBT product sample, the intensity of line at g ~2.80 has decreased considerably, thus confirming the removal of free iron contaminants by DCBT. The reduction in iron content and the sharp improvement in brightness of the sample support the findings. The other lines in the F1 region of the spectra are found to be sharper. Both the lines at $Fe_{(I)}$ & $Fe_{(II)}$ sites in F1 region are due to Fe+3 substituting for Al+3 in the kaolinite lattice but they have different symmetry. It is reported that and increase in the number of $Fe_{(I)}$ sites and decrease in the number of $Fe_{(II)}$ sites lead to an increase in structural disorder. Intensity of the line at $Fe_{(I)}$ site is found to decrease from ROM to the SCP2-DCBT product samples with a simultaneous increase in the intensity of $Fe_{(II)}$ line. This clearly indicates that the Fe^{+3} substituting for Al^{+3} in $Fe_{(I)}$ is less compared to that in $Fe_{(II)}$ site and the beneficiation of the sample has actually led an increase in structural order of the kaolinite.

5.1.4 Kutch kaolin

The EPR spectra of ROM clay, the beneficiated products and their heated products are given in Figure 5.1.4a, Figure 5.1.4b and Figure 5.1.4c. All the samples in the RT show EPR lines at F1 and F2 regions. The ROM sample produces broad line at g ~4.88, 4.33 and 3.74 in the F1 region and g ~ 2.79 and 2.01 in F2 region. Sharper lines are observed in the F1 region (at g ~ 4.91, 4.38 and 3.74) for the SCP1 sample with a weak line at g ~ 2.64 in F2 region along with the g~ 2.01 lines. The SCP2 sample has also shown similar features and the line at g ~2.64 was not much intense indicting the minimal presence of free iron impurities. In the case of the SCP2DCBT product sample, the intensity of line at g ~2.64 has not decreased much, thus showing that most of the iron in the sample is in the "structural" form and DCB treatment was ineffective. The minimal reduction in iron content and the minimal improvement in brightness of the sample support the findings. The other lines in the F1 region of the spectra are found to be sharper. Both the lines at $Fe_{(I)}$ and $Fe_{(II)}$ sites in F1 region are due to Fe^{+3} substituting for Al^{+3} in the kaolinite lattice but they have different symmetry. It is reported that and increase in the number of $Fe_{(I)}$ sites and decrease in the number of $Fe_{(II)}$ sites lead to an increase in structural disorder. Intensity of the line at $Fe_{(I)}$ site is found to decrease from

213

OM to the SCP2-DCBT product samples with a simultaneous increase in the intensity if Fe$_{(II)}$ line. This clearly indicates that the Fe^{+3} substituting for Al^{+3} in Fe$_{(I)}$ is less compared to that in Fe$_{(II)}$ site and the beneficiation of the sample has actually led an increase in structural order of the kaolinite.

iii) Koraput kaolin

The EPR spectra of the ROM, beneficiated products and their heated products are given in Figure 5.1.15a, Figure 5.1.5b and Figure 5.1.5c. EPR lines at F1 and F2 regions are exhibited by all samples but the lines are found to be weak. The ROM sample induces broad line at g ~ 4.83, 4.23 and 3.65 in the F1 region and g ~ 2.35 and 2.02 in F2 region. Sharper lines are observed in the F1 region (at g ~ 4.90 and 4.31) for the SCP1 sample with a broad line at g ~ 2.24 in F2 region along with the g ~ 2.02 lines. The SCP2 sample has also shown similar features, but the line at g ~2.54 more intense indicting the presence of free iron impurities. In the case of the SCP2DCBT product sample, the intensity of line at g ~2.56 has decreased considerably, thus confirming the removal of free iron contaminants by DCBT. The reduction in iron content and the sharp improvement in brightness of the sample support the findings. Chemical assay and XRD analysis shows that the EPR silent pyrite (Ferrous sulphide) is the major iron impurity in the clay. The other lines in the F1 region of the spectra are found to be sharper. Both the lines at Fe$_{(I)}$ & Fe$_{(II)}$ sites in F1 region are due to Fe^{+3} substituting for Al^{+3} in the kaolinite lattice but they have different symmetry. It is reported that and increase in the number of Fe$_{(I)}$ sites and decrease in the number of Fe$_{(II)}$ sites lead to an increase in structural disorder. Intensity of the line at Fe$_{(I)}$ site is found to decrease from ROM to the SCP2-DCBT product samples with a simultaneous increase in the intensity of Fe$_{(II)}$ line. This clearly indicates that the Fe^{+3} substituting for Al^{+3} in Fe$_{(I)}$ is less compared to that in Fe$_{(II)}$ site and the beneficiation of the sample has actually led an increase in structural order of the kaolinite.

iv) Bankura kaolin

The ROM clay, beneficiated products and their heated products are studied by EPR spectroscopy and the spectra are given in Figure 5.1.6a, Figure 5.1.6b and Figure 5.1.6c. Strong EPR lines at F1 and F2 regions are shown by all samples. The ROM clay induces broad line at g ~ 4.83, 4.40 and 3.78 in the F1 region and g~ 2.51 and 2.01 in F2

214

Sharper lines are observed in the F1 region (at g ~4.70 and 4.36) for the SCP1 sample with a more intense broad line at g ~ 2.81 in F2 region along with the g~ 2.0 line. The SCP2 sample has also shown similar features, but the line at g~2.70 more intense indicting the presence of free iron impurities. In the case of the SCP2DCBT product sample, the intensity of line at g ~2.68 has decreased considerably, thus confirming the removal of free iron contaminants by DCBT. The reduction in iron content and the sharp improvement in brightness of the sample support the findings. The other lines in the F1 region of the spectra are found to be sharper. Both the lines at $Fe_{(I)}$ & $Fe_{(II)}$ sites in F1 region are due to Fe^{+3} substituting for Al^{+3} in the kaolinite lattice but they have different symmetry. It is reported that and increase in the number of $Fe_{(I)}$ sites and decrease in the number of $Fe_{(II)}$ sites lead to an increase in structural disorder. The line at $Fe_{(I)}$ site is found to be prominent (due to the more Fe^{+3} substitution for Al^{+3}) in all the samples indicating the structural disorder in kaolinite

5.1.7 Pali kaolin

The EPR spectra of the ROM, products of beneficiation and their heated products are given in Figure 5.1.7a, Figure 5.1.7b and Figure 5.1.7c. All these samples in the RT show strong EPR lines at F1 and F2 regions. The ROM sample produces sharp line at g ~ 4.34 and 3.70 in the F1 region and g~ 2.61 and 2.0 in F2 region. The well defined lines at F1 region shows that most of the iron is in the kaolinite structure and intensities these lines do not show any significant difference among those for the ROM and other beneficiated samples. In the case of SCP1 sample, lines are observed in the F1 region (at g~4.85 and 4.33) with a broad line at g ~ 2.63 in F2 region along with the g ~ 2.0 lines. The SCP2 sample has also shown similar features, and the line at g~2.64 was not much intense, thus indicting the absence of free iron impurities. In the case of the SCP2DCBT product sample, there was only minimal decrease in the intensity of line at g~2.64, showing that most of the iron in the sample was in "structural" form. This is supported by the fact that neither the iron content not the brightness of the sample changed during reclassification and DCB treatment. The other lines in the F1 region of the spectra are found to be sharper. Both the lines at $Fe_{(I)}$ & $Fe_{(II)}$ sites in F1 region are due to Fe^{+3} substituting for Al^{+3} in the kaolinite lattice but they have different symmetry. It is reported that and increase in the number of $Fe_{(I)}$ sites and decrease in the number of $Fe_{(II)}$

is lead to an increase in structural disorder. The line at $Fe_{(I)}$ site is found to be prominent (due to the more Fe^{+3} substitution for Al^{+3}) in all the samples indicating the structural disorder in kaolinite.

5.2 Mossbauer spectroscopic studies

Mossbauer spectroscopy is a very important technique which can be used for the identification and characterization of less crystalline iron oxide and oxy-hydroxide minerals present in kaolin samples. It is powerful technique, which gives the information about the oxidation state and the coordination environments of the iron in mineral phases. The Mossbauer spectral studies of the impurity minerals concentrated by mining (IM2 samples) of all the 7 kaolins have been carried out at room temperature and the salient features are given in the Table 5.2.1 and the spectra are depicted in Figures 5.2.1 to 5.2.7

5.2.1 Kasargod 1 kaolin IM2

The IM2 sample from this kaolin shows isomer shifts of 0.36 and 0.38 mm/sec and quadrupole splitting of 0.64 and -0.08 mm/sec. respectively. The more intense doublet, having the higher quadrupole splitting is due to the Fe(III) in the kaolin lattice (Fysh et al;1983). The sextuplet with a hyperfine splitting of 497 kOe and isomer shift and quadrupole splitting of +0.38 mm.sec. and -0.08 mm/sec. respectively is attributed to hematite. The hyperfine field of hematite at 300Kis 517 kOe and its quadrupole splitting is -0.21 mm/sec. The possible reason for the observation of a decreased hyperfine field in hematite may be due to its small particle size and it have been observed to persist even at 4.2 K (Fysh and Clark, 1982 b). The reason for the decrease in kOe value may be due to the reduced hyperfine field experienced by the nuclei near the surface of the particles and small fluctuations in the magnetization of the particles about the easy direction.

5.2.2 Kasargod 2 kaolin IM2

Isomer shifts of 0.36 and 0.38 mm/sec and quadrupole splitting of 0.62 and -0.10 mm/sec. are exhibited by the IM2 of this kaolin. Fe(III) in the kaolin lattice contributes to the more intense doublet, having the higher quadrupole splitting (Fysh et al;1983). The sextuplet with a hyperfine splitting of 497 kOe and isomer shift and quadrupole splitting of +0.38 mm.sec. and -0.08 mm/sec. respectively is attributed to hematite. The hyperfine

216

ﬁd of hematite at 300K is 517 kOe and its quadrupole splitting is -0.21 mm/sec. The possible reason for the observation of a decreased hyperfine field for hematite may be due to its small particle size and it have been observed to persist even at 4.2 K (Fysh and ﬁt, 1982 b). The reason for the decrease in kOe value may be due to the reduced hyperfine field experienced by the nuclei near the surface of the particles and small fluctuations in the magnetization of the particles about the easy direction.

3.3 Trivandrum kaolin IM2

The spectra of the IM2 sample consist of only one doublet with an isomer shift of 0.3 mm/sec and quadrupole splitting of 0.62 mm/sec. These features are characteristic of Fe(III) located in the distorted octahedral environment of the oxygen anions(Sei et al, 1984).

3.4 Kutch kaolin IM2

A similar spectra consisting of only one doublet with an isomer shift of 0.33 mm/sec and quadrupole splitting of 0.60 mm/sec is exhibited by the IM2 of this kaolin. These features are characteristic of Fe(III) located in the distorted octahedral environment of the oxygen anions.

3.5 Koraput clay IM2

The clay is found to show isomer shifts of 0.35 & 0.88 mm/sec and quadrupole splitting of 0.64 and 1.32 mm/sec. respectively. The one having the lower isomer shift and quadrupole splitting is due to the Fe(III) in the kaolin lattice (Fysh et al;1983). The doublet with larger isomer shift and quadrupole splitting values is due to Fe(II) in pyrite (Typical Pyrite - isomer shift larger than 0.37 mm/s and quadrupole splitting value 1.2 mm/s; Imbert et al., 1963). The sample is found to contain appreciable quantities of pyrite.

3.6 Bankura kaolin IM2

The clay is found to show isomer shifts of 0.28 & 1.23 mm/sec and quadrupole splitting of 0.62 and 3.21 mm/sec. respectively. The one having the lower isomer shift and quadrupole splitting is due to the Fe(III) in the kaolin lattice (Fysh et al;1983). The doublet with larger isomer shift and quadrupole splitting values is due to Fe(II) in illite mica) (Typical Mica - isomer shift larger than 0.37 mm/s and quadrupole splitting

...2.7 mm/s; Heller-Kallai & Rozenson, 1981) and the appreciable quantities of mica in the sample supports the same.

7 Pali kaolin IM2

The clay is found to show isomer shifts of 0.54, 0.42 & 1.55 mm/sec and quadrupole splitting of 1.40, -0.06 and 2.62 mm/sec. respectively. The Mossbauer parameters of isomer shift ∂ = 0.54 mm/sec. and quadrupole splitting, ΔE = 1.40 mm/sec. are quite unusual for iron in kaolinite. The compilation of ^{57}Fe isomer shifts in a large number of iron oxides (Menil, 1985) showed that the isomer shift value of ∂ = 0.54 mm/sec. lie well out side the typical domains of Fe(II) and Fe(III) but is lying exactly between them. Therefore this doublet can be attributed to an intermediate valance state of +2.5 resulting from a rapid electron exchange between Fe(II) and Fe(III) sites (Sei et al, 2004).

The sextuplet with a hyperfine splitting of 305 kOe and isomer shift and quadrupole splitting of +0.42 mm/sec. and -0.086 mm/sec. respectively are characteristic of poorly crystallized goethite, the Fe(III) oxy hydroxide commonly associated with kaolins (Rossiter & Hodgson, 1965; Murad, 1982).

The doublet with larger isomer shift (∂ = 1.55 mm/sec.) and quadrupole splitting values (ΔE = 2.62 mm/sec) is due to Fe(II) in illite (mica) (Heller-Kallai & Rozenson, 1981) and the presence of appreciable quantities of mica in the sample supports the above.

3 IR Spectral Studies

The IR technique is so versatile that it can be used in clay mineralogy for identifying the constituent minerals based on the characteristic absorption features as well as to understand the structural ordering in the kaolin samples. Kaolin minerals display four sharp stretching bands between 3600 and 3700 cm-1. The strong band of 3700cm-1 arises from the surface hydroxyls and produces an in-phase vibration that is quasi-perpendicular to the 1:1 layers. Two other bands at 3670 and 3652 cm-1 arise from stretching vibrations that are sub-parallel to the 1:1 layers. The lowest frequency 3620 cm-1 band has been assigned to the fourth inner OH group (Giese, 1988). This doublet is characteristic of kaolin sub-group. The presence of 3676 and 3650 cm-1 bands along with the above bands suggests an increase in ordering of kaolinite (Russell and Fraser, 1995).

218

spectral features can change due to the reorientation of OH groups in response to stresses. The gradual reduction in size of the 3676 cm-1 band and broadening of 3650 cm-1 band (disappearance of the doublet and formation of a singlet) are typical disordered kaolinites. In addition to above bands, kaolinite shows features at 938 & cm-1 (due to vibrations of the inner and inner surface –OH groups, respectively). A well crystallized kaolinite can be distinguished in the spectral region between 750 800 cm-1. In the highly crystalline kaolinite, the two weak bands found here at 795 758 cm-1 are of about equal intensity whereas in the case of disordered kaolinite the intensity of this band has an intermediate value. Another potentially useful means assessing the crystallinity of kaolinites is based on the ratio of the 3700 and 915 cm-1 hydroxyl band absorbencies following the method of Neal and Worrall (1977). The magnitude of the absorbancy ratio of the bands and the crystallinity of the kaolinites are closely related.

Quartz is the common constituent in most clay materials and iron hydroxides and hydroxides are the iron minerals commonly found in kaolin. Hematite, an anhydrous oxide, occurs in two morphological forms, namely, a platy (kidney ore) and a more form (specularite). Their spectra are generally similar, but show considerable differences in detail due to the differences in crystal size and particularly in shape. Due to this the characteristic bands of 532, 450 and 317 in kidney ore shift to higher frequencies at 562, 480 and 352 cm-1 in specularite. Again the weaker bands at 643 and cm-1 in kidney ore shift to lower frequencies and merge with the stronger bands in specularite, where the 378cm-1 band will be getting resolved (Rendon and Derna, 1981; et al., 1982). The specularite form is the more common in clay minerals. Characteristic bands of minerals are given in Table 5.3.1.

Interpreting the IR spectra of clay minerals requires a positive identification of as characteristic absorption bands of individual minerals possible and will obviously depend on the complexity of the mineral suite present and the degree of overlap of the component spectra. The –OH stretching region is the most important region of the spectrum and since other minerals present may or may not be having hydroxyl groups in structure, a full spectrum is required for the best possible interpretation. High and

w concentrations of sample must also be used, so that full weight can be given to weak
d strong mineral bands.

In the present study the IR spectral studies of the ROM clay and the
purity concentrates, ie., IM1 and IM2 samples of all the 7 china clay samples were
ried out and the details of the various mineral phases identified are given in Table
5.2

5.3.1 Kasargod 1 kaolin

The ROM clay as well as the impurity concentrate samples ie., IM1 and IM2 were
died by IR spectroscopy and the IR spectra's are given in Figure.5.3.1a. Also, the
spectra of all the samples in the 1200 - 350 cm⁻¹ region and that of the ROM clay in
3700 - 3600 cm⁻¹ region are depicted in Figure.5.3.1c and Figure.5.3.1b respectively. The
spectra of the ROM clay shows the sharp OH doublet of kaolin mineral at 3693, 3618
cm⁻¹, with supporting bands at about 800 and 700 cm-1. In addition to that, characteristic
bands of quartz along with   iron minerals, goethite, and hematite were also observed in
the spectrum. The features of the hematite bands shows that the mineral is in the
specularite form (Hs) ie., having particles with   fairly equant shape (common
morphology).The kaolinite is found to be ordered in nature and is evident from the
presence of doublets at 3664   & 3652 cm-1 in the –OH stretching region in addition to
the normal 3620 & 3700 cm-1 bands. Also, the intensities of the two weak bands found
at 792 and 754 cm-1 are of almost equal intensities, indicating that the kaolinite is highly
ordered in nature. The ratio (0.61) of the 3700 and 915 cm-1 hydroxyl band absorbencies
also supports the above.

As expected, in the IR spectra of both the impurity concentrates, the bands due to
kaolinite mineral are very weak and the features associated with the iron minerals are
found to be very prominent. IR spectra show the presence of goethite, hematite (Hs)
along with quartz and kaolinite in samples IM1 & IM2. Sample IM2 is found to contain
lepidocrocite also.

5.3.2 Kasargod 2 kaolin

The ROM clay as well as the impurity concentrate samples ie., IM1 and IM2 were
died by IR spectroscopy and the IR spectra's are given in Figure 5.3.2a. Also, the
spectra of all the samples in the 1200 - 350 cm⁻¹ region and that of the ROM clay in 3700

$400 \, cm^{-1}$ region are depicted in Figure.5.3.2c and Figure.5.3.2b respectively.The IR spectrum of the ROM clay shows the sharp OH doublet of kaolin mineral at 3693, 3618 cm-1, with supporting bands at about 800 and 700 cm-1. In addition to that, characteristic bands of quartz along with iron minerals, goethite, and hematite were also observed in spectrum. The features of the hematite bands show that the mineral is in the specularite form (Hs). The kaolinite is found to be ordered in nature and is evident from the presence of doublets at 3664 & 3654 cm-1 in the –OH stretching region in addition to the normal 3620 & 3700 cm-1 bands. Also, the intensities of the two weak bands band at 793 and 754 cm-1 are of almost equal intensities, indicating that the kaolinite is highly ordered in nature. The ratio (0.79) of the 3700 and 915 cm-1 hydroxyl band absorbencies also supports the above.

As expected, in the IR spectra of both the impurity concentrates, the bands due to kaolinite mineral are very weak and the features associated with the iron minerals are found to be very prominent. IR spectra show the presence of goethite, maghemite, hematite along with quartz and kaolinite in samples IM1 & IM2. Lepidocrocite was also found to be present in sample IM1. While both the forms (specularite and kidney ore) of hematite particles are present in IM2 sample, only 'specularite'' form was detected in IM1.

Trivandrum kaolin

The ROM clay as well as the impurity concentrate samples ie., IM1 and IM2 were studied by IR spectroscopy and the IR spectra's are given in Figure 5.3.3a. Also, the spectra of all the samples in the 1200 - 350 cm^{-1} region and that of the ROM clay in 3700 $400 \, cm^{-1}$ region are depicted in Figure.5.3.3c and Figure.5.3.3b respectively. The IR spectra of the ROM clay shows the sharp OH doublet of kaolin mineral at 3692, 3618 cm-1, with supporting bands at about 800 and 700 cm-1. In addition to that, characteristic bands of quartz along with iron minerals, goethite, and hematite were also observed in spectrum. The features of the hematite bands show that the mineral is in the specularite form (Hs). The kaolinite is found to be ordered in nature and is evident from the presence of doublets at 3664 & 3647 cm-1 in the –OH stretching region in addition to the normal 3620 & 3700 cm-1 bands. Also, the intensities of the two weak bands band at 798 and 748 cm-1 are of almost equal intensities, indicating that the kaolinite is

221

ordered in nature. The ratio (0.74) of the 3700 and 915 cm-1 hydroxyl band absorbencies also supports the above.

As expected, in the IR spectra of both the impurity concentrates, the bands due to kaolinite mineral are very weak and the features associated with the iron minerals are found to be very prominent. IR spectra show the presence of goethite, maghemite, lepidocrocite along with quartz and kaolinite in samples IM1 & IM2. Hematite (Hs) was also found to be present in sample IM1.

Kutch kaolin

The ROM clay as well as the impurity concentrate samples ie., IM1 and IM2 were studied by IR spectroscopy and the IR spectra's are given in Figure 5.3.4a. Also, the spectra of all the samples in the 1200 - 350 cm^{-1} region and that of the ROM clay in 3700 - 400 cm^{-1} region are depicted in Figure.5.3.4c and Figure.5.3.4b respectively. The IR spectra of the ROM clay shows the sharp OH doublet of kaolin mineral at 3692, 3618 cm-1, with supporting bands at about 800 and 700 cm-1. In addition to that, characteristic bands of quartz along with iron minerals, goethite, hematite, lepidocrocite, maghemite are also observed in the spectrum. The features of the hematite bands shows that the mineral is in the specularite form (Hs). The kaolinite is found to be ordered in nature as is evident from the presence of doublets at 3666 & 3653 cm-1 in the –OH stretching region in addition to the normal 3618 & 3692 cm-1 bands. Also, the intensities of the weak bands found at 785 and 754 cm-1 are of almost equal intensities, indicating that the kaolinite is highly ordered in nature. The ratio (0.80) of the 3700 and 915 cm-1 hydroxyl band absorbencies also supports the above.

As expected, in the IR spectra of both the impurity concentrates, the bands due to kaolinite mineral are very weak and the features associated with the iron minerals are found to be very prominent. IR spectra show the presence of goethite, hematite, lepidocrocite, maghemite, along with quartz and kaolinite in samples IM1 & IM2. Specularite and kidney ore forms of hematite particles are present in both the samples.

Koraput kaolin

The ROM clay as well as the impurity concentrate samples ie., IM1 and IM2 were studied by IR spectroscopy and the IR spectra's are given in Figure 5.3.5a. Also, the spectra of all the samples in the 1200 - 350 cm^{-1} region and that of the ROM clay in 3700

3700 cm^{-1} region are depicted in Figure.5.3.5c and Figure.5.3.5b respectively. The IR spectra of the ROM clay shows the sharp OH doublet of kaolin mineral at 3692, 3618 cm-1, with supporting bands at about 800 and 700 cm-1. In addition to that, characteristic bands of quartz along with iron minerals, goethite, hematite, lepidocrocite, maghemite are also observed in the spectrum. The features of the hematite bands show that the mineral is in the specularite form (Hs). The kaolinite is found to be ordered in nature and evident from the presence of doublets at 3664 & 3653 cm-1 in the –OH stretching region in addition to the normal 3618 & 3692 cm-1 bands. Also, the intensities of the two weak bands found at 792 and 754 cm-1 are of almost equal intensities, indicating that the kaolinite is highly ordered in nature. The ratio (0.94) of the 3700 and 915 cm-1 hydroxyl band absorbencies also supports the above.

As expected, in the IR spectra of both the impurity concentrates, the bands due to kaolinite mineral are very weak and the features associated with the iron minerals are found to be very prominent. IR spectra show the presence of goethite, hematite (Hs), maghemite, along with quartz and kaolinite in samples IM1 & IM2. Lepidocrocite was also present in IM2 sample.

5.3.6 Bankura kaolin

The ROM clay as well as the impurity concentrate samples ie., IM1 and IM2 were studied by IR spectroscopy and the IR spectra's are given in Figure 5.3.6a. Also, the spectra of all the samples in the 1200 - 350 cm^{-1} region and that of the ROM clay in 3700 – 3000 cm^{-1} region are depicted in Figure.5.3.6c and Figure.5.3.6b respectively. The IR spectra of the ROM clay shows the sharp OH doublet of kaolin mineral at 3695, 3620 cm-1, with supporting bands at about 800 and 700 cm-1. In addition to that, characteristic bands of quartz along with iron minerals, goethite, hematite (Hs), and maghemite were also observed in the spectrum. The features of the hematite bands show that the mineral is in the specularite form (Hs). The kaolinite is found to be disordered in nature and is evident from the presence of a singlet at 3653 cm-1 in the –OH stretching region in addition to the normal 3620 & 3695 cm-1 bands. Also, the intensities of the two weak bands at 798 and 752 cm-1 are not comparable and in fact the former band is in the form of a very weak inflexion, indicating that the kaolinite is highly disordered in nature.

223

As expected, in the IR spectra of both the impurity concentrates, the bands due to xinite mineral are very weak and the features associated with the iron minerals are nd to be very prominent. IR spectra show the presence of goethite, hematite (Hs), yhemite, along with quartz and kaolinite in samples IM1 & IM2. Also, kidney ore m hematite and lepidocrocite was found to be present in samples IM2 and Im1 spectively.

7 Pali kaolin

The ROM clay as well as the impurity concentrate samples ie., IM1 and IM2 were nied by IR spectroscopy and the IR spectra's are given in Figure 5.3.7a. Also, the xtra of all the samples in the 1200 - 350 cm^{-1} region and that of the ROM clay in 3700 300 cm^{-1} region are depicted in Figure.5.3.7c and Figure.5.3.7b respectively. The IR xtra of the ROM clay shows the sharp OH doublet of kaolin mineral at 3693, 3620 z. with supporting bands at about 900, 800 and 700 cm^{-1}. In addition to that, aracteristic bands of quartz and calcite along with iron minerals, goethite, hematite, didocrocite, maghemite were also observed in the spectrum. The features of the matite bands show that the mineral is in the specularite form (Hs). The kaolinite is nd to be ordered in nature and is evident from the presence of doublets at 3664 & 43 cm-1 in the –OH stretching region in addition to the normal 3618 & 3692 cm-1 nds. Also, the intensities of the two weak bands found at 792 and 754 cm-1 are of most equal intensities, indicating that the kaolinite is highly ordered in nature. The ratio Il) of the 3700 and 915 cm-1 hydroxyl band absorbencies also supports the above.

As expected, in the IR spectra of both the impurity concentrates, the bands due to xinite mineral are very weak and the features associated with the iron minerals are nd to be very prominent. IR spectra show the presence of goethite, hematite (Hs), didocrocite, maghemite along with quartz, calcite and kaolinite in samples IM1 & IM2.

4 UV-Visible Spectral studies

The electronic spectra of iron oxides (eg. hematite) and oxy-hydroxides (eg. pethite) are relevant to several current problems in geochemistry. Though these minerals r the most common minerals on earth's surface, their electronic spectra are poorly aterstood. Three types of electronic transitions occur in optical spectra of Fe(III) merals. First, there are the Fe+3 ligand field transitions; second, there are ligand to

224

ral charge transitions; and, third, there are transitions which result from the simultaneous excitation of magnetically coupled Fe+3 cations which occupy adjacent sites i.e., (i) Ligand Field Transition (L.F.T) - in the region 290-310 nm & 360-380 nm & this can be attributed to hematite (ii) Ligand to Metal Charge Transitions (L.M.C.T) in the region below 270 nm, due to Fe+3 oxides and inorganic materials with Fe-O bonds as hematite and (iii) condensed Fe^{+3} in the region 485 - 550 nm and this also is assigned to hematite.

In the present study the UV-Vis. Spectra of the IM2 samples were taken and the band assignments for the mineral phases were done exactly the same way as reported in the literature (Sherman et al, 1985 Karickhoff,.et al, 1973; Lehmann, G, 1970 and Canning, P. G. 1967). The band assignments given for all the 7 samples are given in table 5.4.1 and the UV-vis. Spectra's of the samples are depicted in Figures 5.4.1 to 5.4.7.

All the samples are found to show characteristic L.M.C.T and L.F.T bands, indicating the presence of iron oxides (hematite / maghemite) and oxy hydroxides (goethite / Lepidocrocite) in all the samples. The Trivandrum clay is found contain one additional band at 485 – 550 nm range and this is due to the simultaneous excitation of magnetically coupled Fe^{+3} cations which occupy adjacent sites (hematite / maghemite).

5.5. Electron Probe Micro Analysis

Electron Probe Micro Analysis of the ROM and IM1 samples of the seven kaolins are carried out. A semi quantitative analysis of the samples was obtained by the standardless technique. Figures 5.5.1a to 5.5.7b give the electron micrographs of the samples along with the distribution pattern of the elements. Table 5.5.1 and 5.5.2 give the mineral distribution in each sample which has been interpreted based on the concentration levels of pixels corresponding to different elements.

5.5.1 Kasargod 1 kaolin

Figure 5.5.1a shows the electron micrograph of the ROM sample along with the weight percentages of the constituents. However, here the loss on ignition in the kaolinite is not considered. Kaolinite is found to be the major mineral with small amounts of illite, montmorillonite, ilmenite and rutile as the probable impurities. Figure 5.5.1b gives the electron micrograph of the IM1 sample (>45μm fraction). The alumina content in the

ple is less with a subsequent increase in the silica and other elements. The mineral composition of IM1 is almost the same as that of ROM clay, but for the increase in concentration of ilmenite and rutile.

5.5.2 Kasargod 2 kaolin

Figure 5.5.2a represents the electron micrograph of the ROM clay sample along with the weight percentages of the constituents. Kaolinite is found to be the major mineral with small amounts of illite, montmorillonite, ilmenite and rutile as the probable impurities The potassium and alumina content are found to be relatively high. EPMA analysis of IM1 shows the presence of ilmenite and montmorillonite, in addition to kaolinite. Figure 5.5.2b gives the electron micrograph of IM1 sample. The alumina content in the sample is low with a subsequent increase in silica and other impurities like Si, K, Ti, Ca and sulphur.

5.5.3 Trivandrum kaolin

Kaolinite is found to be the major mineral in the ROM clay with small amounts of montmorillonite, hematite, rutile, and ilmenite as the probable impurities. The IM1 sample is found to contain kaolinite as major mineral and it is seen that the impurity minerals (ilmenite and rutile) are present in higher concentration. Figures 5.5.3a and 5.5.3b show the EPMA of the ROM and IM1 samples respectively.

5.5.4 Kutch kaolin

The electron micrographs of ROM and IM1 samples with elemental analysis are given in the Figures 5.5.4a and 5.5.4b respectively. Kaolinite is found to be the major mineral in the ROM clay with small amounts of montmorillonite and ilmenite and rutile as the probable impurities. Kaolinite is the major mineral in IM1. The sample contains less alumina and the increase in the concentration of other constituents such as silica, Fe, etc. indicates the increase in concentration of the illite, rutile and ilmenite.

5.5.5 Koraput kaolin

EPMA figures of the ROM and the IM1 along with the weight percentages of the constituents are given in Fig 5.5.5a and 5.5.5b respectively. Kaolinite is found to be the major mineral in the ROM clay with small amounts of illite, montmorillonite, rutile, pyrite and hematite as the probable impurities. The major impurity in the ROM sample appears to be Fe and sulphur. Kaolinite is the major mineral in IM1 and the impurity

minerals like pyrite and hematite are getting concentrated in the sample. XRD analysis confirms the presence of pyrite in the samples. Illite, Ilmenite, rutile and gypsum are also present in the sample.

5.5.6 Bankura kaolin

The ROM and the IM1 samples give electron micrographs with elemental analysis in the Figures 5.5.6a and 5.5.6b respectively. Kaolinite is found to be the major mineral in the ROM clay with small amounts of illite, montmorillonite, ilmenite and goethite as the probable impurities. Kaolinite is the major mineral in IM1. The sample contains less alumina and the increase in the concentration of other constituents such as silica, Fe, K etc. indicates the increase in concentration of the illite and iron impurities, ilmenite and goethite.

5.5.7 Pali kaolin

Kaolinite is found to be the major mineral in the ROM clay with small amounts of illite, montmorillonite, ilmenite and dolomite as the probable impurities. The ROM clay contain good amount of calcium, indicating the presence of dolomite which is frequently found in the Rajasthan area. The IM1 sample is found to contain kaolinite as major mineral and it is seen that the impurity minerals are present in higher concentration. The mica content in the sample is high. Figures 5.5.7a and 5.5.7b show the EPMA of the ROM and IM1 samples respectively.

5.6 Scanning Electron Microscopy (SEM) Analysis

5.6.1 Kasargod 1 kaolin

Figures 5.6.1.a & b represent the SEM pictures of ROM and SCP1 samples. The SEM picture shows presence of aggregates of pseudo hexagonal kaolinite particles and bigger quartz particles in the ROM clay. As seen in the Figure 5.6.1b, submicron sized kaolinite particles are observed in the SCP1 sample and is free from quartz grains. The mineral content calculated from the chemical assay also supports the same.

5.6.2 Kasargod 2 kaolin

The SEM pictures of ROM and SCP1 samples are depicted in Figures 5.6.2 a & b. Typical booklet type stacking of the pseudo hexagonal kaolinite particles along with aggregates of kaolinite particles alone or sticking to the quartz crystal are clearly seen in

ROM sample. The SEM picture of SCP1 sample shows layers of pseudo hexagonal ьs of very small size (<1 micron).

) Trivandrum kaolin

As seen in the SEM Figure 5.6.3a,   most of the particles in the ROM clay was d to be very fine (<3 micron) in nature. The picture shows the presence of platlets xteristic of kaolinite and the quartz particles are found to be minimum. As seen in Figure 5.6.3b, kaolinite particles of <1 micron size was observed in the SCP1 sample the quartz content was found to be minimal. The mineral content calculated from the nical assay also supports the same.

(Kutch kaolin

The SEM pictures of ROM and SCP1 samples are depicted in Figure 5.6.4a & b. do hexagonal kaolinite particles along with aggregates of kaolinite particles are ly seen in the ROM sample. The SEM picture of SCP1 sample shows layers of do hexagonal plates of very small size (<1 micron). The presence of quarz particles th the samples was minimal.

) Koraput kaolin

Scanning electron microscopic analysis (SEM) pictures of the ROM clay is ated in Figure 5.6.5a and it shows the presence of aggregates of pseudo hexagonal nite particles along with well crystallized pyrite particles of typical octahedral shape. SEM picture of SCP1 shows only the pseudo hexagonal kalonite platelets of icron size as depicted in Figure 5.6.5b.

) Bankura kaolin

The SEM pictures of ROM and SCP1 samples are depicted in Figure 5.6.6a & b. SEM picture of the sample shows lot of aggregates of quartz crystal along with to hexagonal kaolinite particles. The quartz particle in the sample was found to be and the minarological data of the sample supports the same.   The SEM picture of (sample shows layers of pseudo hexagonal kaolinite plates of very small size (<1 яn) alone or sticking to the quartz crystal. The presence of quarz particles is found to inimal.

228

As seen in the SEM Figure 5.6.7a, most of the particles in the ROM clay was and to be very fine (<2 micron) in nature. The picture shows the presence of pseudo ugonal kaolinite particles and fine quartz particles sticking to the kaolnite. As seen in Figure 5.6.7b, kaolinite particles of <1 micron size was observed in the SCP1 sample. ser number of quartz particles are observed in the sample and the mineral content isolated from the chemical assay supports the same.

Electron microscopic analysis by HRSTEM

High resolution transmission electron microscopic analysis of the selected apks of Kutch and Koraput kaolins were carried. The impurity minerals present in set samples are found to be typical in nature and the microanalysis of these samples are done get a atomic level chemical composition of these impurity minerals.

Kutch kaolin

Figure 5.7.1a represents the TEM picture and micro analysis data of ROM clay. knlinite particles are mostly observed as pseudo hexagonal sharp edged particles with al composition (Al/Si ratio ~1.0) as confirmed by the EDS analysis of particles A, B, D, E and L. These particles also possess a little K and Fe contents. Particles G,H,I and J are found to contain appreciable concentration of "Ti" along with small quantity of "Fe" and this confirms the presence of the titanoferrous minerals (<50nm) in the sample. Presence of "Fe" rich particle (F) associated with a little "Ti" was also observed in the sample.

Figure 5.7.1b gives the TEM picture of the SCP1 sample. Sharp edged pseudo hexagonal platelets with lower deformation are present. The kaolinite predominantly possesses a high Al content and the Al/Si ratio comes close to 0.95:1 which is nearer to that of the ideal kaolinite 1:1 and is evident from the particles A, B, D, H and I. Particles E and F are rich in "Ti" content and found to contain "Fe" in low concentrations, their confirming the presence of the titanoferrous minerals (<50nm) in the sample. The Ti/Fe ratio in the particle C was found to be ~ 1:0.6 and it is possible that it may corresponds to ilmenite. The highest value obtained for "Ti" & "Fe" during analysis are 41 and 24.3 atomic percentage. The K, Na and Ca contents in the kaolinite particles

229

very low. Small amounts of "P" and chlorine are clearly observed in almost all the particles.

The TEM picture of the IM1 is shown in Figure 5.7.1c. The picture shows near all kaolinite platelets (B,C,F) with very fine kaolinite sticked Ti(Fe) particles (A, E,G & I) of dimension <50nm. This shows the very fine nature of the titanoferrous minerals present in the sample. The highest values obtained for "Ti" & "Fe" during analysis are 57.4 and 4.0 atomic percentage. Presence of P, Na, K and Cl are indicated in EDS analysis of all the particles. Small amounts of phosphate minerals appear to be associated with this clay which is also confirmed by the trace analysis values (Table 2).

2 Koraput kaolin

Figure 5.7.2a represents the TEM picture and micro analysis data of ROM clay. Kaolinite particles are mostly observed as pseudo hexagonal sharp edged particles with al composition (Al/Si ratio ~1.0) as confirmed by the EDS analysis of particles A, B, and L. These particles also possess a little K, Fe, S contents. A strong S – Fe concentration is available in the analysis of particle M.

Figure 5.7.2b gives the TEM picture of the SCP1 sample. Sharp edged pseudo hexagonal platelets with lower deformation are present. The kaolinite predominantly possesses a high Al content and the Al/Si ratio comes close to 0.9:1 which is nearer to that of the ideal kaolinite 1:1. The highest value obtained during analysis of sulphur is 4%. In spite of the small Fe content (0.115) the % of sulphur obtained during the analysis is 0.85%. Most of the particles clearly shows sulphur content and the highest that obtained was in particle B ie., 3.89 and 3.88m % S and Fe respectively (Fe:S 1:1). Although S and Fe values do not exactly tally each other, it can be seen that high S & Fe content are available in the sample. Particle E is not clearly bordered and the very fine particles contain a clear content of K. The composition shows a reduced or degraded it. The K content in the kaolinite is very low. Small amounts of Na and chlorine are only observed.

The TEM picture of the IM1 is shown in Figure 5.7.2c. The picture shows near all kaolinite platelets (B,C,E,F) with very fine kaolinite sticked pyrite particle (D) of dimension <50nm. The high iron and sulphur contents in particles A & G indicate that

230

ʾare rich in pyrite content. Particle A is rich in iron and is found to contain more Fe
ʿthat required for the pyrite formation. This indicates the presence of iron minerals
ʿthan pyrite in the sample. The chemical assay of the sample also supports the
ʾnce of non-pyritic iron in the sample. Presence of Na & Cl is indicated in the EDS
ʾysis of particle A and G respectively.

lOptical **Microscopy**

The color is formed due to the selective absorption of light by matter and
ʾtion elements are the major causes of color in minerals. They impart colouration to
ʾmineral by various crystal fields and chare transfer transitions. Luster of a mineral
ʾnds on the way in which light is reflected from the surface of the mineral. Minerals
ʾng metallic bonding and high degree of covalent bonding is found to show metallic
ʾr (An introduction to rock forming minerals,
ʾ Deer et al.)

The optical micrographs of IM1 and IM2 of kasargod 1 kaolin are given in Figure
ʾ Grains of black and yellow/orange color, which are almost similar sizes are seen
ʾth samples. Reddish coloured coating, most probably of iron is observed on a bigger
ʾn in IM2.

The IM1 and IM2 of Kasrgod 2 kaolin are found to contain a lot of yellow and
ʾn coloured particles along with black grains. Red coloured stains, most probably of
ʾ is seen on one grain in IM2. The coloured minerals are found to be coarser in nature
ʾre uniformly distributed. Yellowish orange coloured coating on some particle are
ʾseen in IM1. The Optical micrograph are given in Figure 5.8.2.

The optical micrographs of IM1 and IM2 of Trivandrum kaolin are given in
ʾre 5.8.3. Both the samples are found to contain opaque black grains, which are
ʾibly of ilmenite. The yellowish and reddish brown coloured grains in these samples
ʾcorrespond to the iron oxide minerals. The grains are found to be fine in nature (<45
ʾize).

Opaque black coloured ilmenite grains (I) along with zircon(Z) are observed in
ʾptical micarograph of both IM1 and IM2 samples of Kutch clay (Figure 5.8.4) In
ʾsample metallic luster appears on the grain. Brown coloured coating, probably that

231

iron mineral is also seen on some black particles. Grains having different sizes are reserved in micrographs.

Greenish tinged Pyrite grains (>45 µm size) are observed in the optical micrographs of IM1 of Koraput kaolin (Figure 5.8.5). Some of the pyrite grains shows a metallic lustre also. The pyrite grain in IM2 is found to be greenish black in colour and coarser (> 100 µm) in size.

The optical micrographs of IM1 and IM2 of Bankura show the presence of black and yellow/red coloured minerals of very fine particle size (Figure 5.8.6).

The coloured impurities in IM1 and IM2 samples appears to be very fine and coating of the agglomerated yellow grains are also seen in the optical micrograph of Pali clay (Figure 5.8.7).

References

Allard T., Muller J.P., Dran J.C. and Menager M.T. (1994) Radiation induced paramagnetic defects in natural Kaolinites : Alpha dosimetry with ion beam irradiation. Physics and Chemistry of Minerals, 21, 85-96.

Angel B.R. and Hall P.L. (1972) Electrom spin resonance studies of kaolins, Int. Clay Conference, Madrid, 1, 71-86

Angel B.R. and Hall P.S. (1973) Electron spin resonance studies of kaolins, Proc.Int. Clay Conf. Madrid, 47-60.

Angel B.R., Jones J.P.E. and Hall P.L. (1974) Studeis of doped synthetic kaolinite. I, Clay Minerals, 10, 247-256.

Angel B.R., Cuttler A.H., Richards K.S. and Vincent W.E.J. (1977) Synthetic kaolinites doped with Fe+2 and Fe+3 ions, Clays and Clay Minerals, 25, 381-383.

Balan A., Allard, T., Biozot, B., Morin, G. and Muller J.P. (1999) Structural Fe^{+3} in natural kaolinites: New insights from electron paramagnetic resonance spectra fitting at X and Q – band frequencies. *Clays and Clay Minerals*, 47, 605-616

Balan A., Allard T., Biozot, B., Morin G. and Muller J.P. (2000) Quantitative measurement of paramagnetic Fe^{+3} in kaolinite. *Clays and Clay Minerals*, 48, 439

Bonnin D., Muller S. and Calas G. (1982) Iron in kaolins. A study by EPR spectrometry,Mossbauer, EXAFS, Mineral Bulletin, 105, 467-475

Bowen L.H. and Weed S.B. (1984) Mossbauer spectroscopy of soils and sediment, in Chemiccal Mossbauer Spectroscopy (ed. R.H.Herber), Plenum, New York, 217-242

Brindley G.W., Kao C.C., Harrison J.L., Lipsicas M., and Raythata R. (1986) Relation between structural and other characteristics of kaolinite and dickite. Clay and Clay Minerals, 34, 239-249

Cases J.M., Lietard O., Yvon J. and Delon J.F (1982) Etude des properties crystallographiques,morphologiques et superficielles de kaolinites desordonnees, Bull. Soc. Fr. Min. Crist., 105, 439-457

Cases J.M.l, Cunin P.,Grillet Y., Poinsingnon C. and Yvon J. (1986) Methods of analyzing morphology of kaolinite : relations between crystallographic and morphological properties. Clay Minerals, 21, 55-68

Coey J.M.D. and Readman P.W. (1973) Chacaracterisation and magnetic properties of natural ferric gel, Earth and Planetary Science Letters, 21,45-51

Cuttler A.H. (1980) The behaviour of a synthetic ^{57}Fe-doped kaolinite: Mossbauer and EPR studies. Clay Minerals, 15, 429-444

Cuttler A.H. (1981) Further studies of a ferrous iron doped synthetic kaolin: dosimetry of X-ray induced defects, Clay Mineral, 16

Delineau T., J.Yvon (1999) Evidence of structural Fe(II) ions in Font-Bouillant kaolinites : a Mossbauer study. Clays and Clay Minerals, 34, 515-518

Farmer V.C. and Russell J.D. (1964) The infrared spectra of layered silicates, Spectrochemica Acta, 20, 1149-1173

Farmer V.C. and Russell J.D. (1966) Effects of particles size and the structure on the vibrational frequencies of layer silicates, Spectrochemica Acta, 22, 389-398.

233

Farris A.P. and Jepson W.B. (1975) The exchange capacities of kaolinite and the preparation of homoionic clays, Journal of Colloid Interfaces Science, 51, 245-259.

Fysh S.A., and Clark P.E.(1982b) Aluminous Hematite – a Mossbauer study, Phys. Chem. Minerlals, 8, 257-267

Fysh S.A., Cashion J.D. and Clark P.E.(1983) Mossbauer effect studies on iron in kaolin.I, Structural iron, Clays and Clay Minerals, 31, 285-292.

Giese R.F.(1988) Kaolin minerals: Structure and stabilities, in Hydrous Phyllosilicates (Ed. S.W.Bailey), Reviews in mineralogy, 19, 29-66, Mineralogical S Society of America, Washington, DC

Hall P.L (1980) The application of electron spin resonsnce to studies of clay minerls, lsomorphous substitution and external surface properties, Clay Minerals, 15, 321-335

Hart R.D., St Pierre T.G., Gilkes R.J., Mckinley A.J., Siradz S. and Singh B. (2002), Iron in soil kaolins from Indonesia and Western Australia, Clay Minerals, 37, 671-685

Heller-Kallai L. and and Rozenson I. (1981) The use of Mossbauer spectroscopy of iron in clay mineralogy. Phys. Chem. Min., 7, 223-238

Herbillon J.A, Mestdagh M.M., Vielvote L. And Derouane E.G. (1976) Iron in kaolinite with special reference to kaolinite from tropical soil, Clay Minerals, 11, 201-220

Hogg C.S., Malden P.J and Meads R.E (1975). Identification of iron-containing impurities in natural kaolinites using Mossbauer effect, Mineral. Mag., 40, 89-96

Jefferson D.A., Tricker M.J. and Winterbottom A.P (1975) Electron -microscopic and Mossbauer spectroscopic studies of iron-stained kaolinite minerals. Clays and Clay Minerals, 23, 355-360.

Jepson W.B. and and Rowse J.B. (1975) The composition of kaolinite – an electron microprobe study, Clays and Clay Minerals, 23, 310-317.

Jones J.P.E., Angel B.R. and Hall P.L (1974) Studies of doped synthetic kaolinites II, Clay Minerals, 10, 257-270

Karickhoff S.W. and Bailey G.W.(1973) Optical absorption spectra of clay minerals, Clays and Clay Minerals, 21, 59-70

Komusinski J., Stoch L. and Dubiel S.M.(1981) Application of election paramagnetic resonance and Mossbauer spectroscopy in the investigation of kaolin group minerals, Clays and Clay Minerals, 29, 23-30.

Lazarev A.N.(1974) The dynamics of crystal lattices, in The Infrared Spectra of Minerals (ed. V.C.Farmer), Mineralogical Society, London, 69-86

Ledoux R.L. and White J.L.(1964) Infrared of selective deuteration of kaoliniteand halloysite at room temperature, Science, 145, 47-49.

Lehmann G.(1970) Ligand Field and charge transfer spectra in Fe(II) O complexes. Zeitsschrift fur Physikalische Chemie Neue Folge, 72, 279-297

Malden P.J. and Meads R.E. (1967) Substitution by iron in kaolinite. Nature, 215, 844-846

Manning P.G. (1967) The optical absorption spectra of some andradites and the identification of the 6A1 + 4A1. 4E transition in octahedraally bonded Fe+3,

Canadian Journal of Earth Sciences, 4, 1039 – 1047

Mendelovici E.,Yariv S. and Villalba R.(1979) Iron bearing kaolinite in Venezuelan laterites. 1, Infrared spectroscopy and chemical dissolution evidence, Clay Minerals, 14,323-331

Meads R.E. and Malden P.J.(1975) Electron spin resonance in natural kaolinites containing Fe+3 and other transition metal ions, Clay Minerals, 10,313-345

Mestagh et al, 1980

Menil (1985) Systamatic trends of the 57Fe Mossbauer isomer shifts in (FeOn) and (Fe Fn) polyhedra. Evidence of a new coorelation between the isomer shifts and the inductive effect of the competeting bond T-X ($\rightarrow$ Fe) [where X is O or F and T any element with a formal positive charge], Journal of Physics and Chemistry of Solids, Vol. 46, issue 7, 1985, 763-789

Mitra S. (1989) Fundamentals of optical, spectroscopic and x-ray mineralogy,1-18, Wiley Eastern Limited, New Delhi

Muller J-P., Ildefonse Ph. And Calas G. (1990) Paramagnetic defect centers in hydrothermal kaolinite froman altered tuff in the Nopal uranium deposit, Chihuahua, Mexico, Clays and Clay Minerals, 38, 600-608

Murad E.(1982) The characterization of goethite by Mossbauer spectroscopy. American Mineral, 67, 1007-1011

Murad E.and Johnston J.H. (1987) Iron oxides and oxyhydroxides, in Mossbauer Spectroscopy Applied to Onorganic Chemisty, Vol. 2 (ed. G.J. Long, Plenum, New York, 507-582

Murad E. (1988) Properties and behaviour of iron oxides as determined by Mossbauer Spectroscopy, in Iron in Soils and Clay Minerals (eds) J.W. Stucki, B.A.Goodman and U Schwertmann). D.Reidel, Dordrecht, 309-350

Murad E. and Wagner U. (1991) Mossbauer spectra of kaolinite, halloysite and the firing products of kaolinite: new results and a reappraisal of published work. Neues Jahrb. Min. Abh., 162, 281-309

Neal M. and Worrall W.E.(1977) Mineralogy of fire clays: part 1. The crystallinity of kaolinite in fireclays, Transactions of British Ceramic Society, 76, 57-61

Olowe A. A., Refait Ph. And Genin J.-M.R. (1990) Super paramagnetic behaviour of goethite prepared in sulphated medium. Hyperfine Interactions, 57, 2037-2041

Pollard R.J., Cardile C.M., Lewis D..G and Brown L.J. (1992) Characterization of FeOOH polymorphs and ferrihydrite using low-temperature applied field Mossbauer spectroscopy, Clay Minerlas, 27, 57-71.

Rendon J.L. and Serna C.J.(1981) IR spectra of powder Hematite; effects of particle size and shape, Clay Minerals,16, 375-382

Rossiter M.J. and Hodgson A.E.M.(1965) A Mossbauer study of ferric oxyhydroxide. Journal of Inorganic Nuclear Chemistry, 27, 63-71

Rouxhet P.G., Samudacheata N., Jacobs H., and Anton O. (1977) Attribution of the – OH stretching bands of kaolinite, Clay Minerals, 12, 171-180.

Russell J.D. and Fraser A.A.(1994) Infrared methods, in Clay Mineralogy, 11-67 (Ed. M.J.Wilson), Chapman and Hall, London

Russell J.D and Fraser A.A (1995) Infrared methods, 18-67 in : Clay mineralogy (Ed. M.J.Wilson), Chapman and Hall, London

Sei J., Abba Toure A., Olivier-Fourcade J., Quiquampoix H., Staunton S., Jumas

235

.C. and Womes M. (2004) Hyperfine Interactions, 155, 51-64.

·ema C.J, Rendon J.L and Iglesis J.E (1982) Infrared surface modes in corundum ype microcrystalline oxides, Spectrochem Acta, 38A, 797-802

·Sherman D.M. (1985) Electronic spectra of Fe+3 oxides and oxides hydroxides in the near IR to near UV, American Mineralogist, Volume 70, 1262-1269.

: Weaver C.E., Wampler J.M. and Pecuil T.E (1967) Mossbauer analysis of iron minerals, Science, 156, 504-510

: Weaver C.E. (1976) The nature of TiO2 in in kaolinite,Clays and Clay Minerals,24, 215-218

· Wauchope R.D. and Haque R.(1971) ESR in clay minerals, Nature Phy. Sci., 233, 41

Yariv S.H. and Mendelovici E. (1979) The effect of degree of crystallinity on the infrared spectrum of hematite. Applied Spectroscopy, 33, 410-411

Table 5.2.1 Mossbauer Spectral data of IM2 samples

S.No	Impurities separated from	Isomer shift (∂) (mm/s)	Quadrupole splitting (ΔE) (mm/s)	Hyperfine Field (kOe)	Assignment
1	Kasargod 1 clay	0.36 0.38	0.64 -0.08	497	Structural Fe(III) Hematite
2	Kasargod 2 clay	0.36 0.38	0.62 -0.10	498	Structural Fe(III) Hematite
3	Trivandrum clay	0.33	0.62	0	Fe(III) – O6
4	Kutch clay	0.33	0.60	0	Fe(III) – O6
5	Koraput clay	0.35 0.88	0.64 1.32	0 0	Structural Fe(III) Fe(II) in pyrite
6	Bankura clay	0.28 1.23	0.62 3.21	0 0	Structural Fe(III) Structural Fe(II) - in mica
7	Pali clay	0.54 0.42 1.55	1.40 -0.06 2.62	305	Fe (i.v)* Fe(III) Structural Fe(II) - in mica

(i.v)* - Fe(+2.5)

237

Table 5.3.1 Characteristic bands of minerals

S.No	Mineral	Characteristic bands cm⁻¹
1	Kaolinite	3697, 3669, 3652, 3620, 1108, 1036, 1014, 938, 916, 795, 758, 701, 540, 474, 433, 348
2	Quartz	1085, 800, 781, 697, 516, 462, 399, 374
3	Hematite (kidney stone)	643, 532, 450, 400, 317
4	Hematite (specularite)	562, 480, 378, 352,
5	Maghemite	724, 692, 636, 584, 562, 476, 445, 423, 397, 370, 330
6	Goethite	3153, 893, 794, 633, 495, 455, 409, 377, 296
7	Lepidocrocite	3175, 1154, 1128,1022, 742, 543, 474, 360, 270
8	Calcite	1798, 1452, 1428, 878,714,358,323,228

Table 5.3.2 Mineralogical data of the samples obtained from IR spectral studies

S.No	Samples	ROM	IM1	IM2
1	Kasargod-1 clay	K, Q, G, H	K, Q, G, H	K, Q, G, H, L
2	Kasargod-2 clay	K, Q, G, H	K, Q, G, L, M, H	K, Q, G, M, H
3	Trivandrum clay	K, Q, G, H	K, Q, G, M, L, H	K, Q, G, L, H, M
4	Kutch clay	K, Q, G, L, M, H	K, Q, G, L, M, H	K, Q, G, L, M, H
5	Koraput	K, Q, G, M, L, H	K, Q, G, L, M, H	K, Q, G, M, H
6	Bankura	K, Q, G, M, H	K, Q, G, L,M, H	K, Q, G, H, M
7	Pali	K, Q, G, L, H, M, C	K, Q, G, L, H, M, C	K, Q, G, L, H, M, C

K-Kaolinite; Q-Quartz; G-Goethite; L-Lepidocrocite; H-Hematie; M-Maghemite
C-Calcite

T.5.4.1 UV-Vis. Spectral data of IM2 samples

S.No	Impurity separated from	Bands	Assignment
1	Kasargod 1 clay	Broad – below 270 nm 290-310 nm, 360-380 nm	L.M.C.T L.F.T
2	Kasargod 2 clay	Sharp – below 270 nm 290-310 nm, 360-380 nm	L.M.C.T L.F.T
3	Trivandrum clay	Broad – below 270 nm 290-310 nm, 360-380 nm 485-550 nm	L.M.C.T L.F.T $Fe^{+3} - Fe^{+3}$ pair
4	Kutch clay	Broad – below 270 nm 290-310 nm, 360-380 nm	L.M.C.T L.F.T
5	Koraput clay	Sharp – below 270 nm 290-310 nm, 430 nm	L.M.C.T L.F.T
6	Bankura clay	Broad – below 270 nm 290-310 nm, 430 nm	L.M.C.T L.F.T
7	Pali clay	Broad – below 270 nm 290-310 nm, 430 nm	L.M.C.T L.F.T

L.M.C.T : Ligand to metal Charge Transitions
L.F.T　 : Ligand Field Transition

239

Table 5.5.1 Relative distribution pattern of mineral phases in ROM clay samples

Samples	Major Mineral	Minor	Traces	Occasional
Isargod 1 dry	Kaolinite	Illite Montmorillonite	Ilmenite Rutile	
Isargod 2 dry	Kaolinite	Illite Montmorillonite	Rutile	
Irvandrum dry	Kaolinte	Montmorillonite Hematite	Ilmenite Rutile	
Latch clay	Kaolinite	Montmorillonite	Ilmenite Rutile	
Input dry	Kaolinite	Montmorillonite	Rutile Illite Pyrite	Hematite
Inkura dry	Kaolinite	Goethite Illite	Ilmenite Montmorillonite	
Ni clay	Kaolinite	Illite Montmorillonite	Ilmenite	Dolomite

Note: Interpretation is based on concentration level of pixels corresponding to different elements

Table Relative distribution pattern of mineral phases in IM1 samples

IM1 samples from kaolins	Mineral phase			
	Major	**Minor**	**Trace**	**Occasional**
Isargod 1	Kaolinite	Ilmenite Rutile Illite	Montmorillonite	
Isargod 2	Kaolinite	Ilmenite	Montmorillonite	
Irvandrum dry	Kaolinte	Ilmenite Rutile		
Latch clay	Kaolinite	Illite Ilmenite Rutile	Ilmenite Rutile	
Input clay	Kaolinite	Pyrite Hematite	Ilmenite Rutile Illite	Gypsum
Iakura clay	Kaolinite	Ilmenite Illite Goethite	Montmorillonite	
hi clay	Kaolinite	Montmorillonite	Illite	

Note: Interpretation is based on concentration level of pixels corresponding to different elements.

241
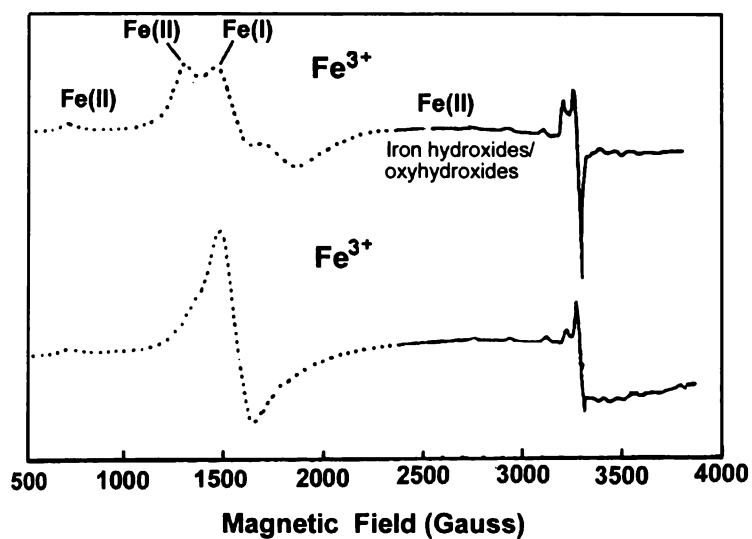
Figure 5.1 EPR spectra of two typical kaolins of sedimentary origin
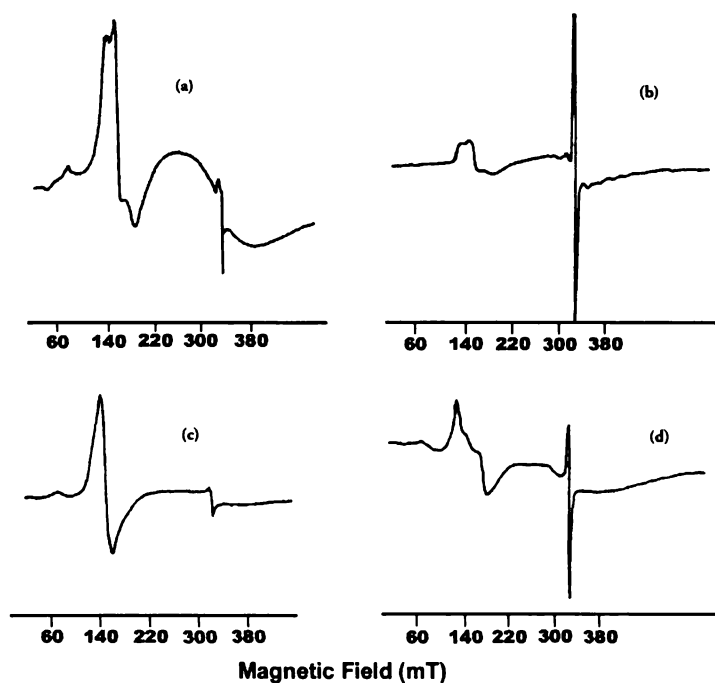
Figure 5.2 EPR spectra of four natural kaolin samples from (a) Mount Crawford, Australia [Fe2O3 %-1.38] (b) Georgia, USA [Fe2O3 %- 0.34] (c) Pugu Tanzania [Fe2O3 %-1.43] and (d) La Frontina, Mexico [Fe2O3 %- 0.62]

242
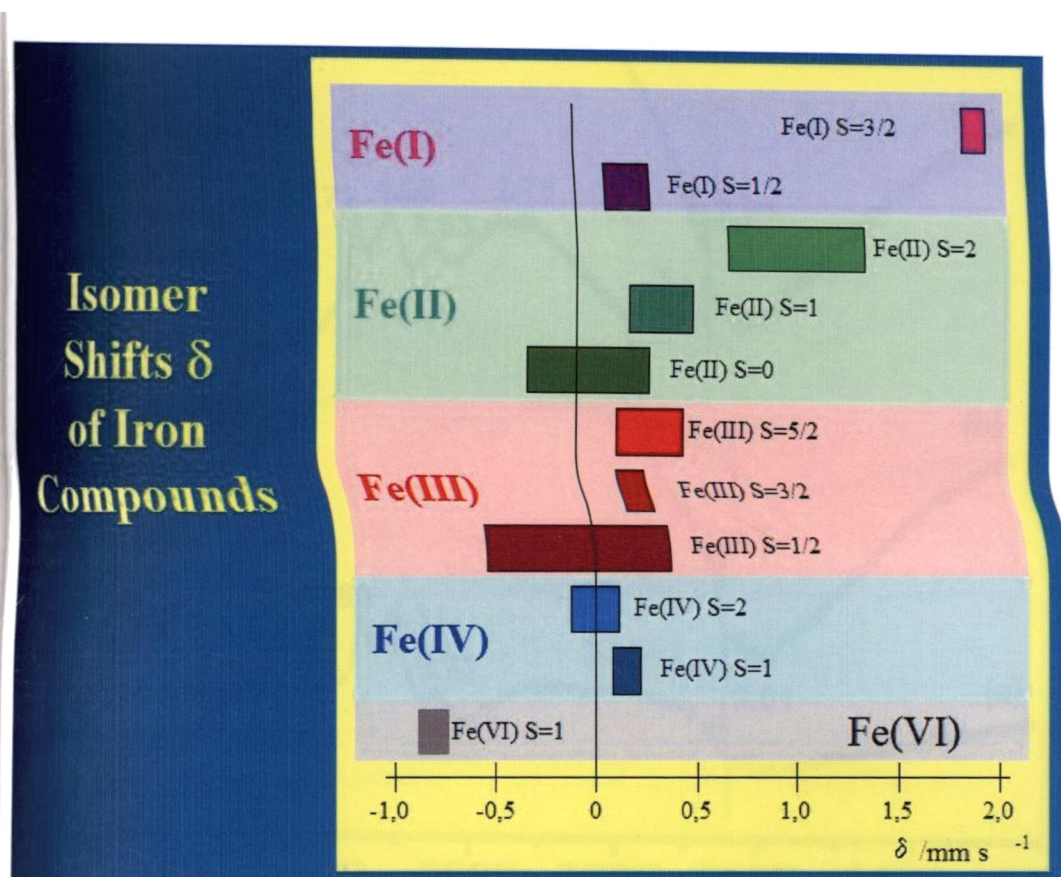
Figure 5.3 Standard isomer shifts of iron compounds
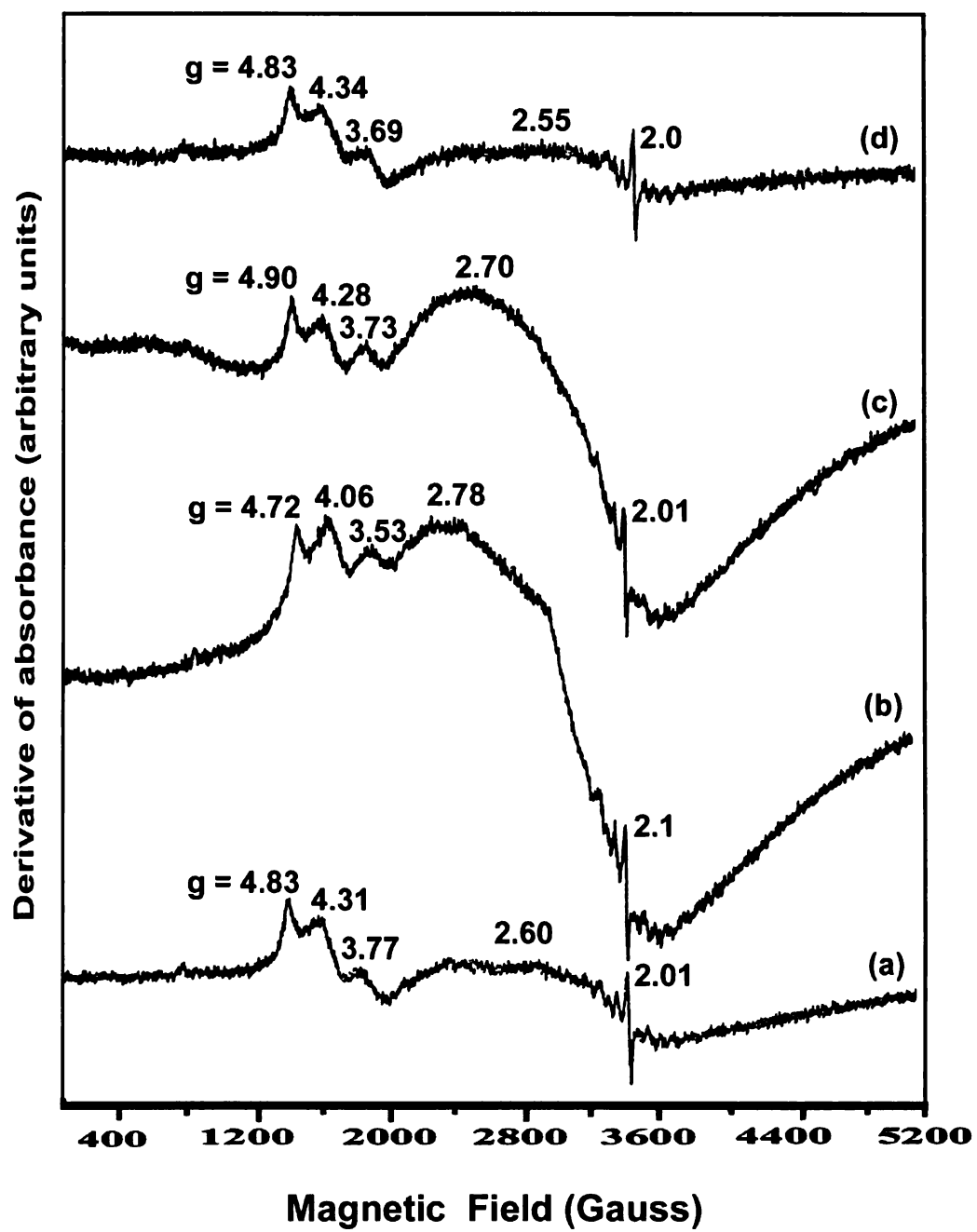
Figure 5.1.1a   EPR spectra of (a) ROM (b) SCP1 (c) SCP2 and
(d) SCP2-DCBT of Kasargod 1 kaolin
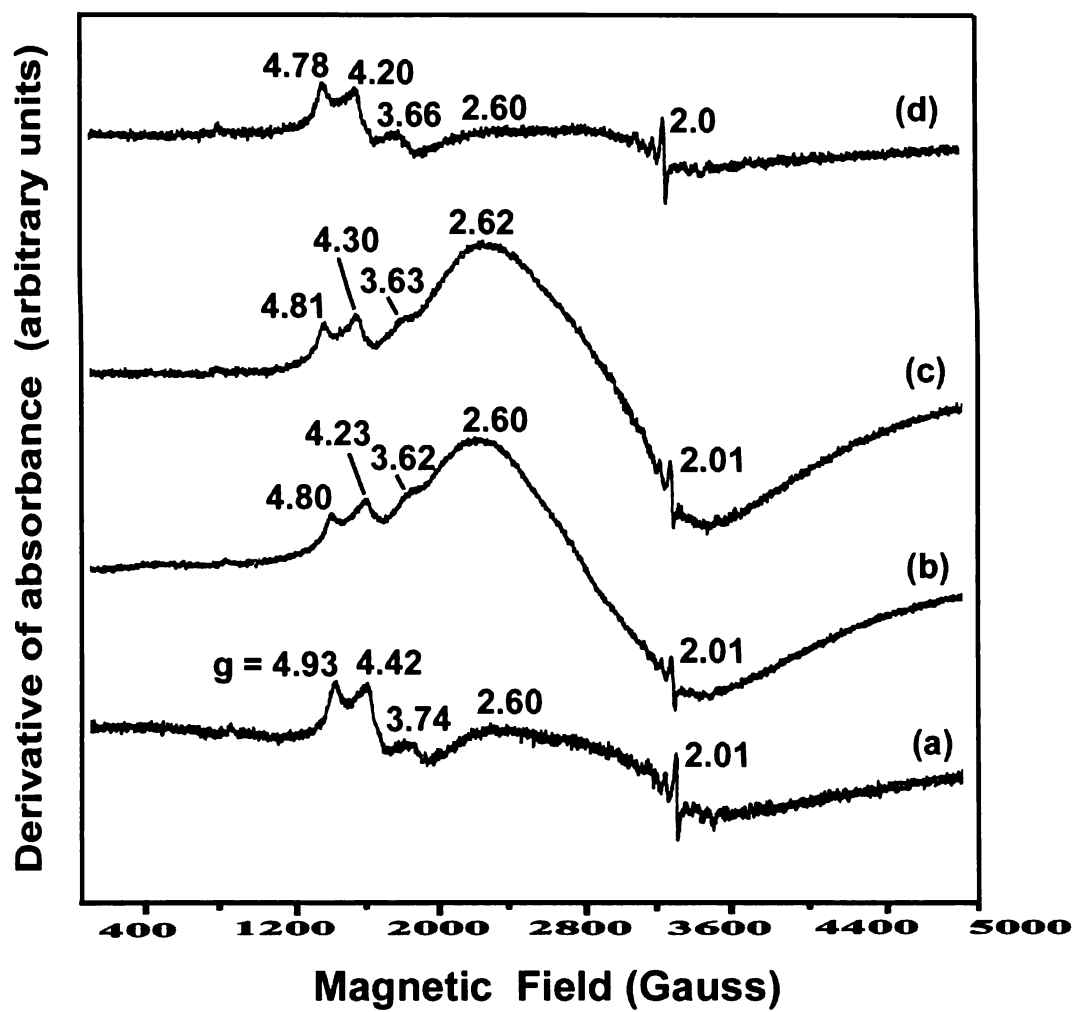
Figure 5.1.1b   EPR spectra of (a) ROM (b) SCP1 (c) SCP2 and

(d) SCP2-DCBT of Kasargod 1 kaolin heated at 400°C
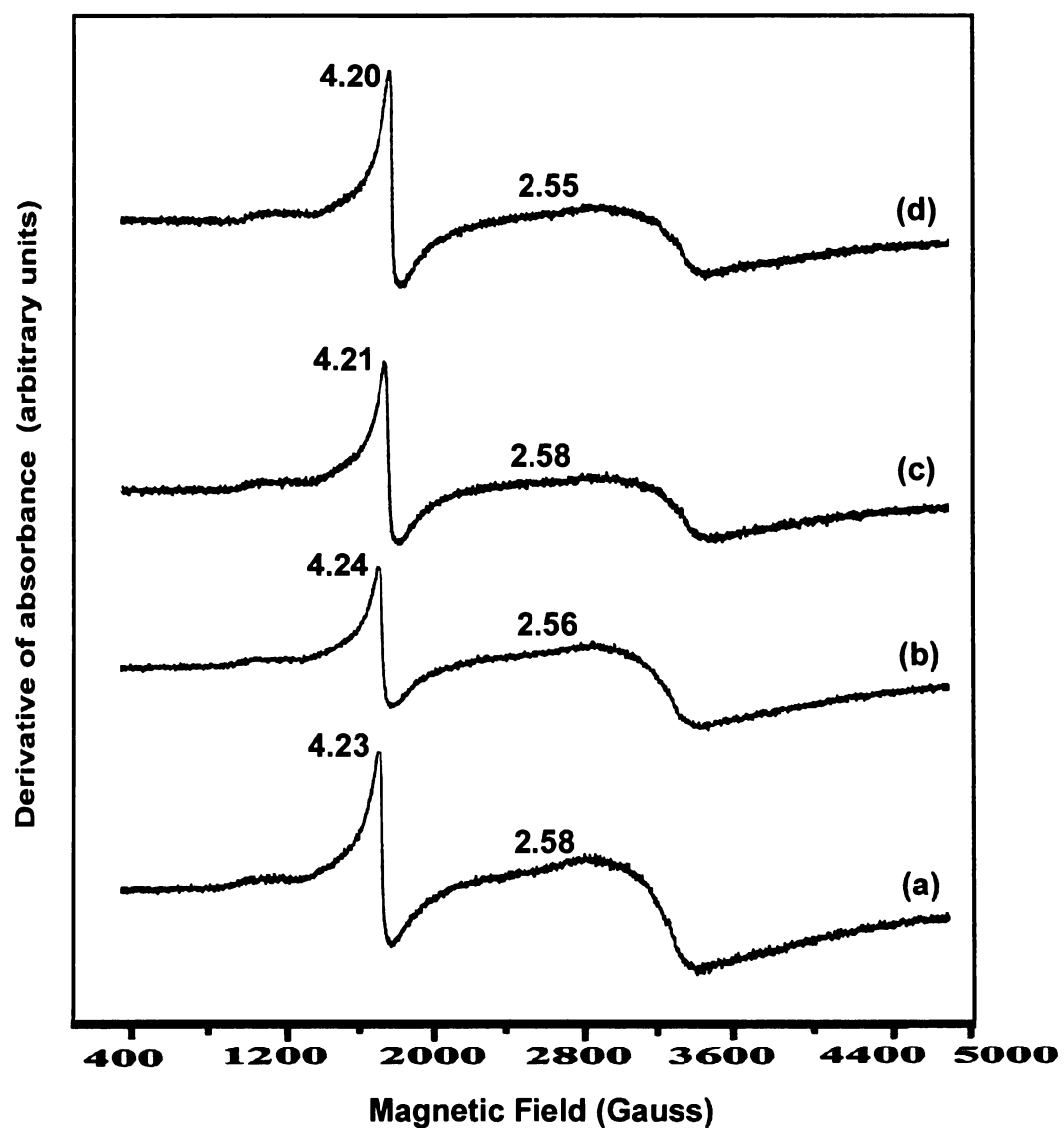
Figure 5.1.1c EPR spectra of (a) ROM (b) SCP1 (c) SCP2 and
(d) SCP2-DCBT of Kasargod 1 kaolin heated
at 1100°C
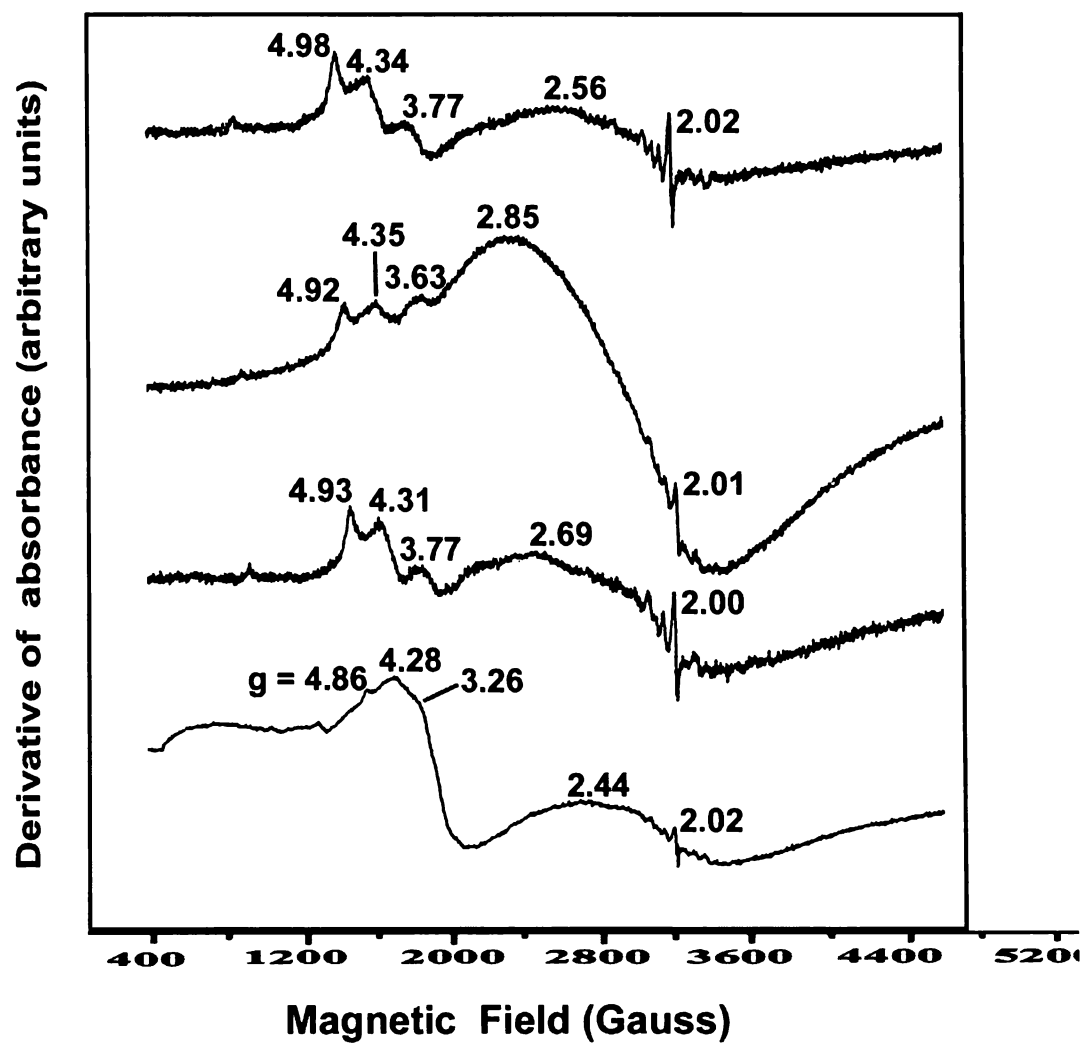
Figure 5.1.2a   EPR spectra of (a) ROM (b) SCP1 (c) SCP2 and
(d) SCP2-DCBT of Kasargod 2 kaolin
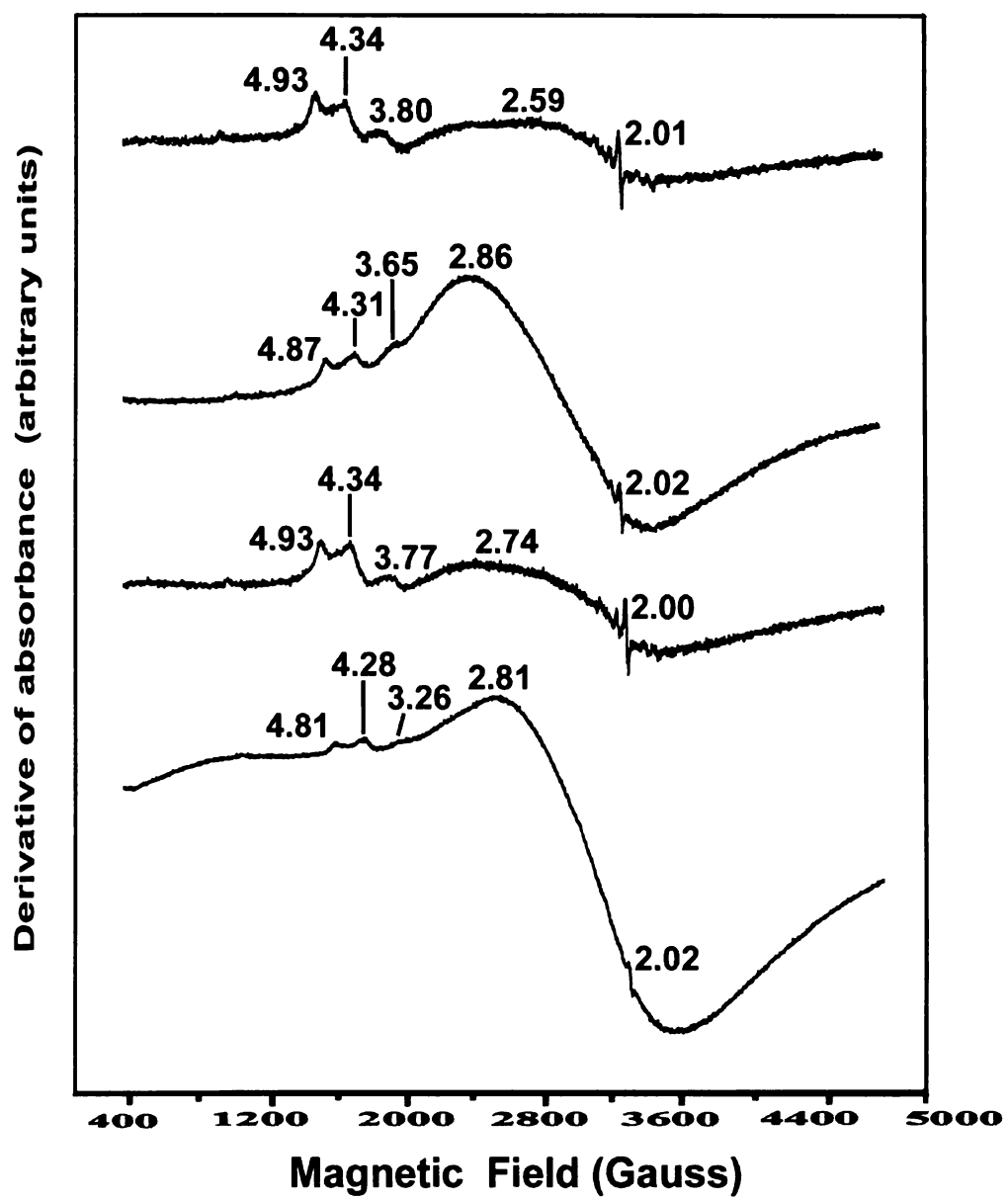
Figure 5.1.2b EPR spectra of (a) ROM (b) SCP1 (c) SCP2 and (d) SCP2-DCBT of Kasargod 2 kaolin heated at 400°C
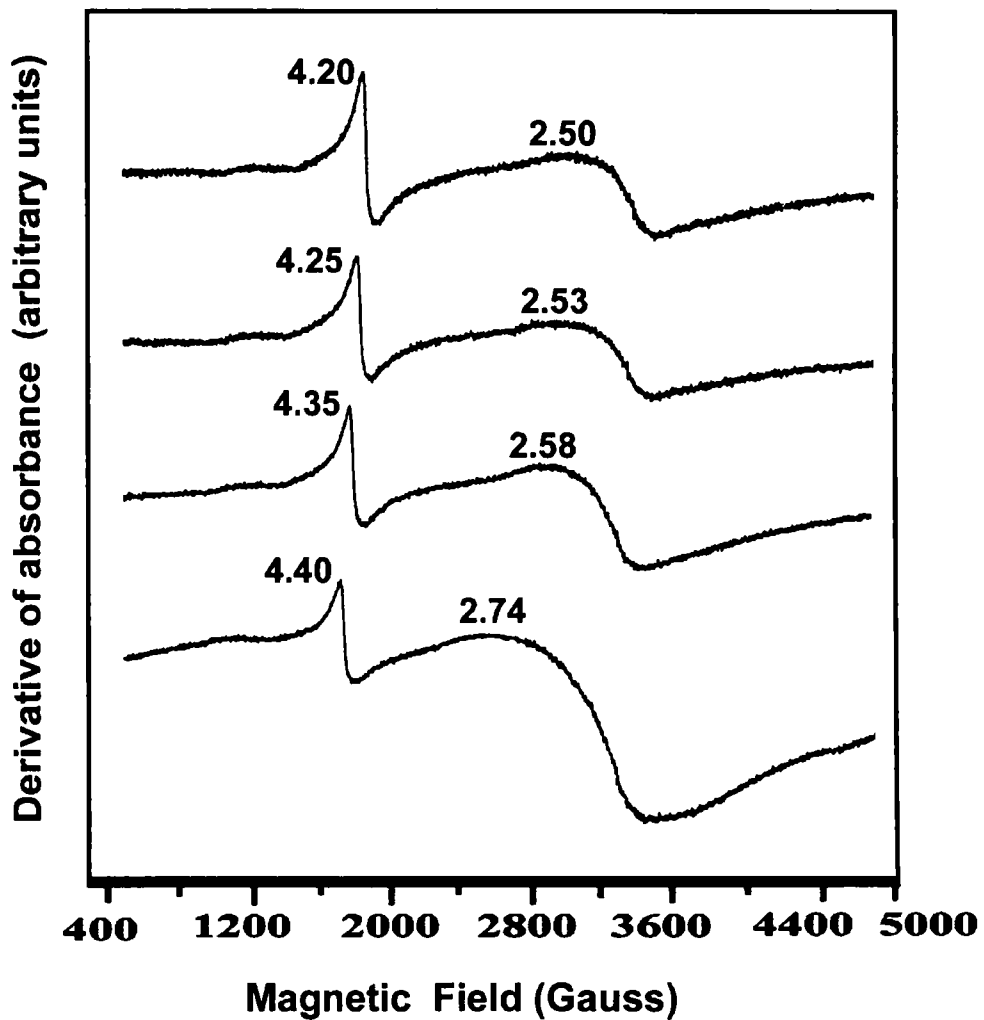
**Figure 5.1.2c EPR spectra of (a) ROM (b) SCP1 (c) SCP2 and
(d) SCP2-DCBT of Kasargod 2 kaolin heated at 1100°C**
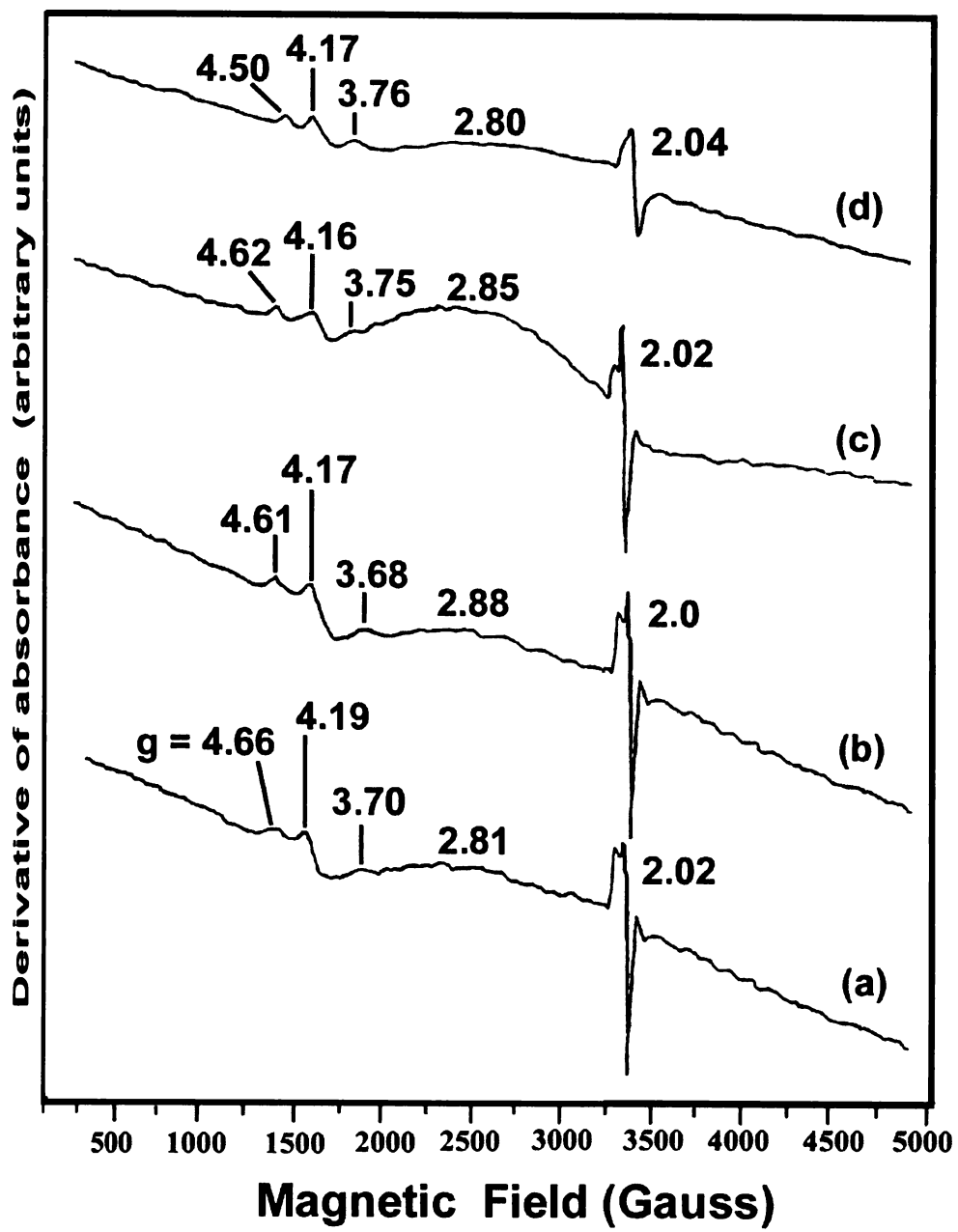
Figure 5.1.3a EPR spectra of (a) ROM (b) SCP1 (c) SCP2 (d) SCP2-DCBT of Trivandrum kaolin

250
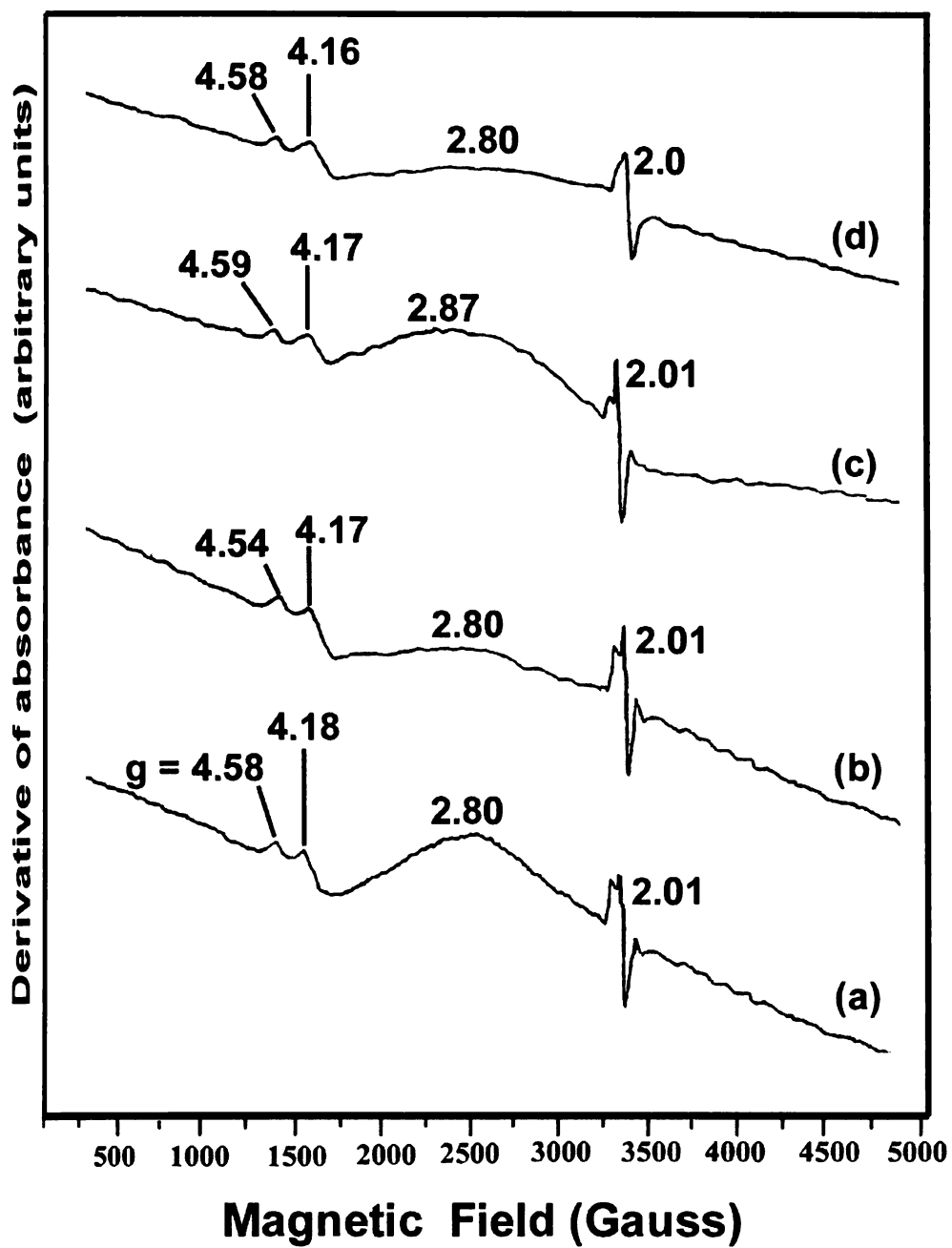
Figure 5.1.3b EPR spectra of (a) ROM (b) SCP1 (c) SCP2 and
(d) SCP2-DCBT of Trivandrum kaolin heated at 400°C
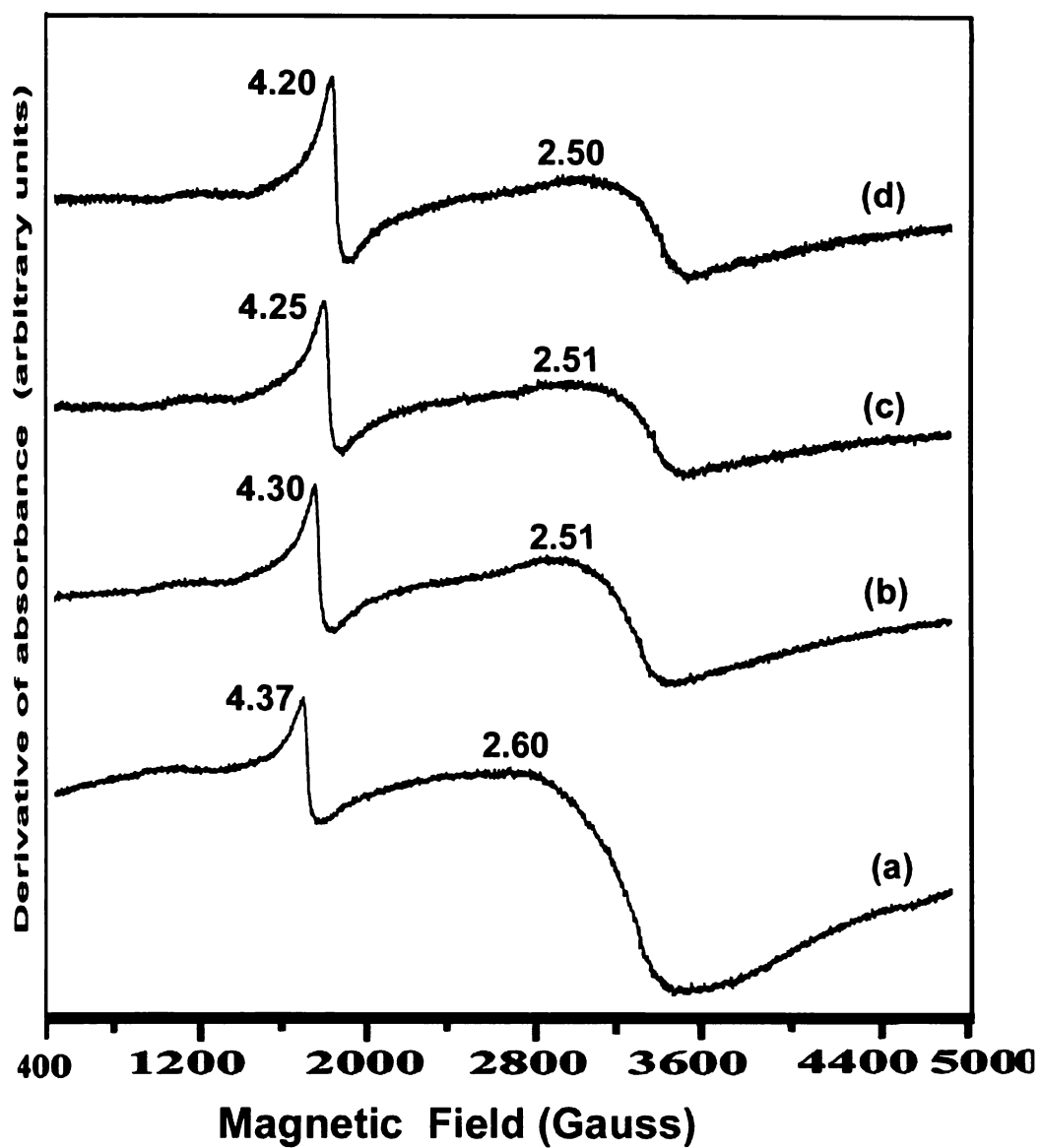
Figure 5.1.3c   EPR spectra of (a) ROM (b) SCP1 (c) SCP2 and
(d) CP2- CBT Trivandrum kaolin heated at 1100°C
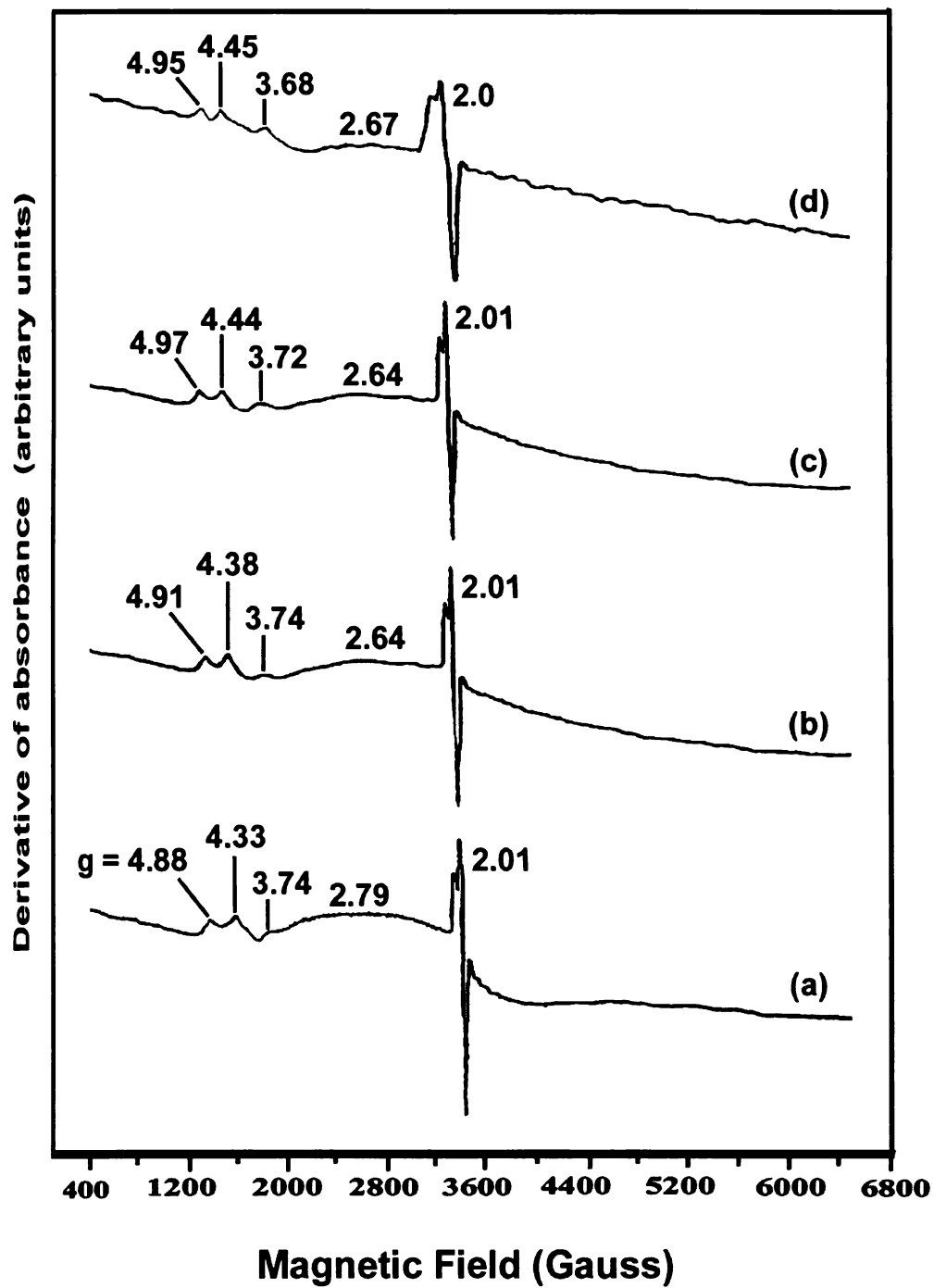
**Figure 5.1.4a   EPR spectra of (a) ROM (b) SCP1 (c) SCP2
and   (d) SCP2-DCBT Kutch kaolin**

253
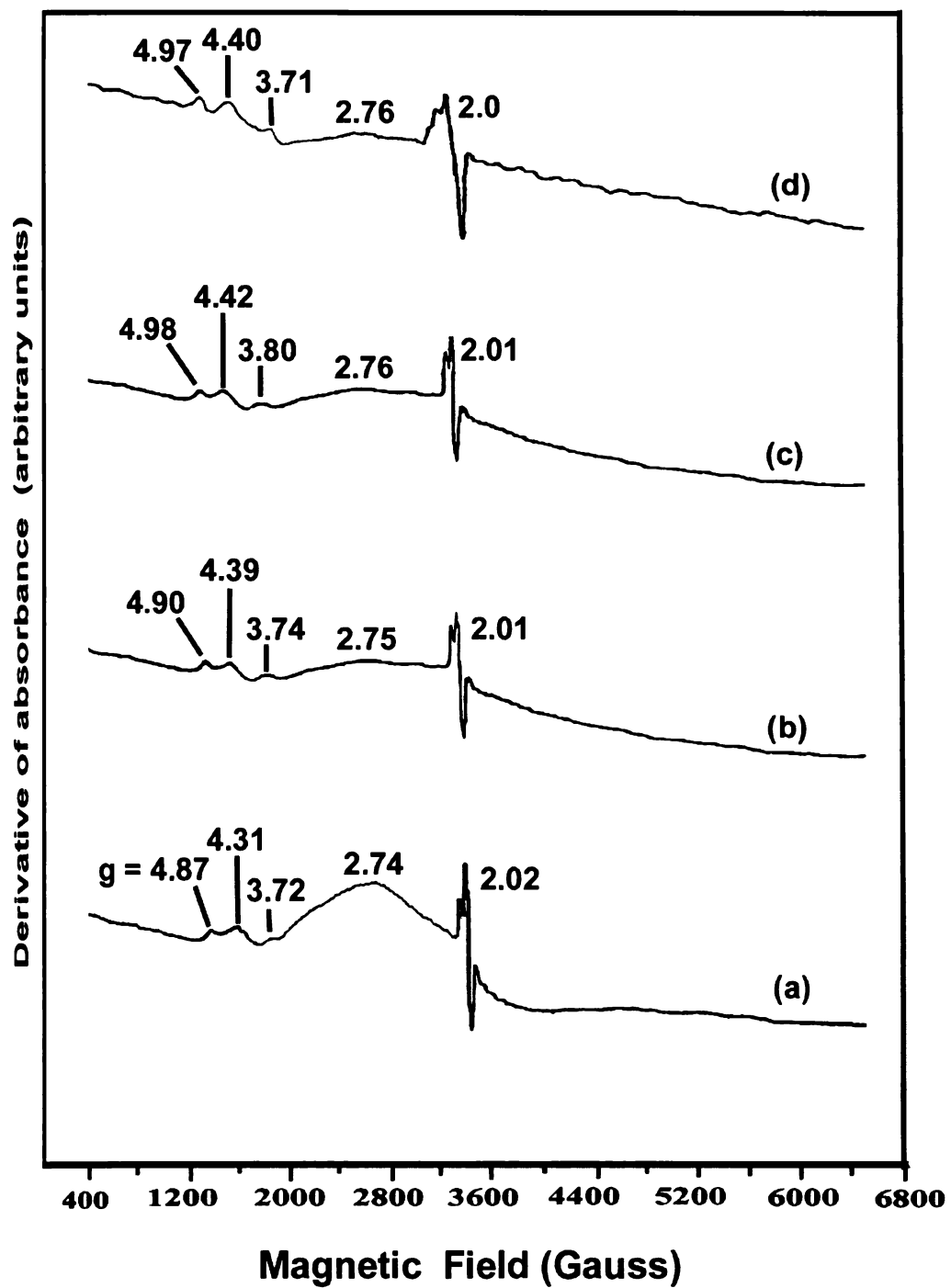
Figure 5.1.4b EPR spectra of (a) ROM (b) SCP1 (c) SCP2 and
(d) SCP2-DCBT Kutch kaolin heated at 400°C

254
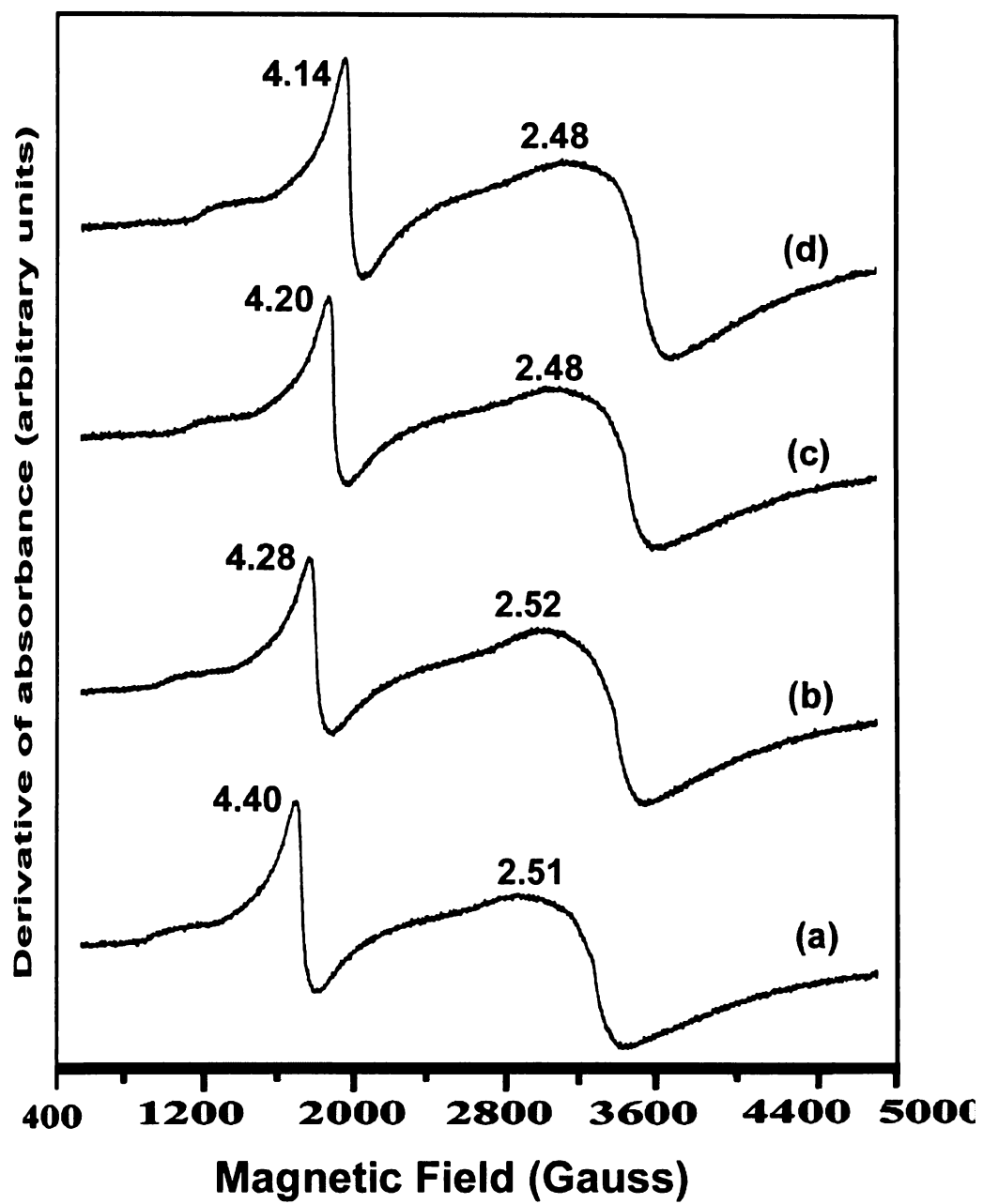
Figure 5.1.4c EPR spectra of (a) ROM (b) SCP1 (c) SCP2 and
(d) SCP2-DCBT Kutch kaolin heated at 1100°C

255
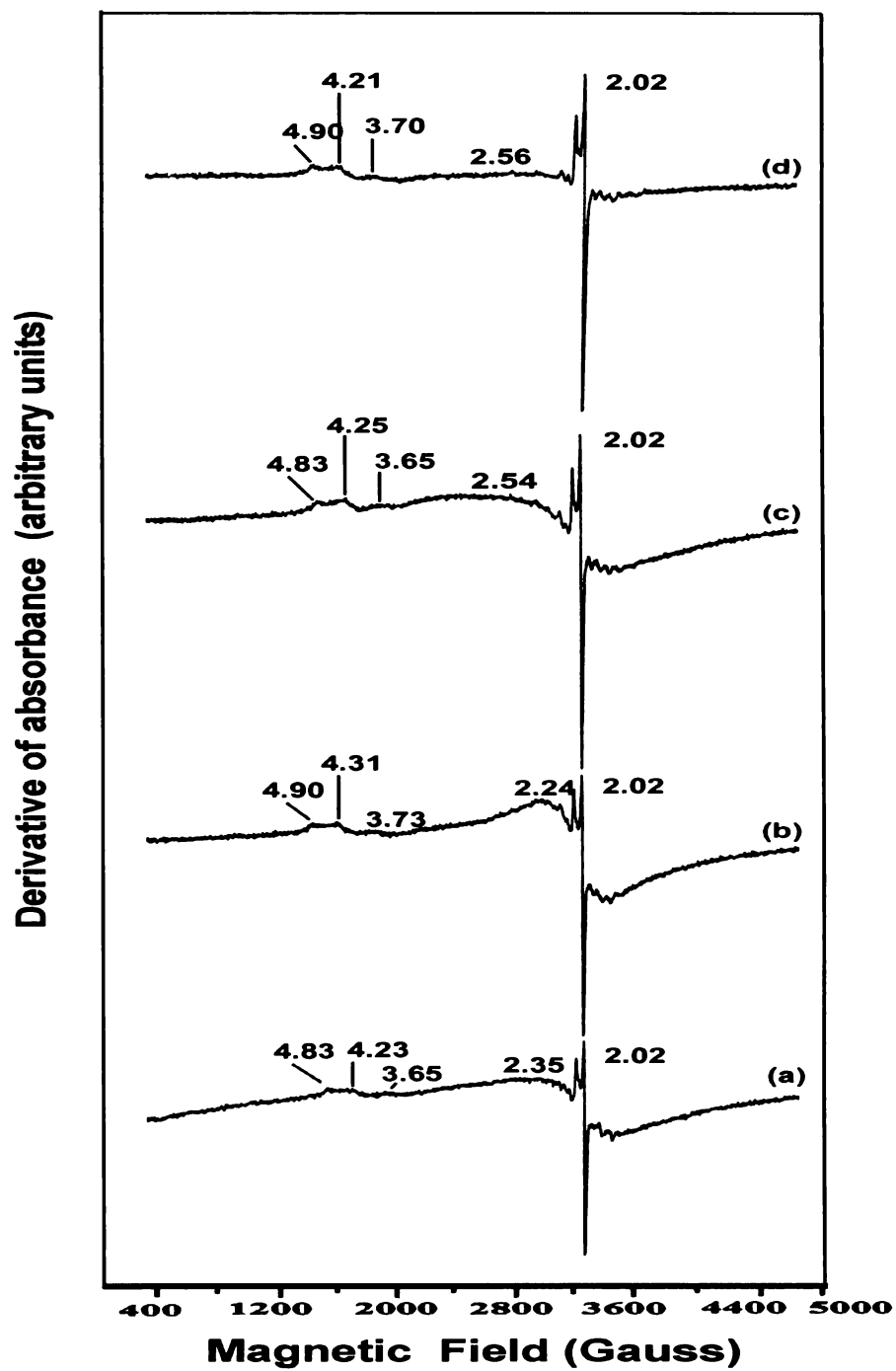
Figure 5.1.5a EPR spectra of (a) ROM (b) SCP1 (c) SCP2 and
(d) SCP2-DCBT Koraput kaolin
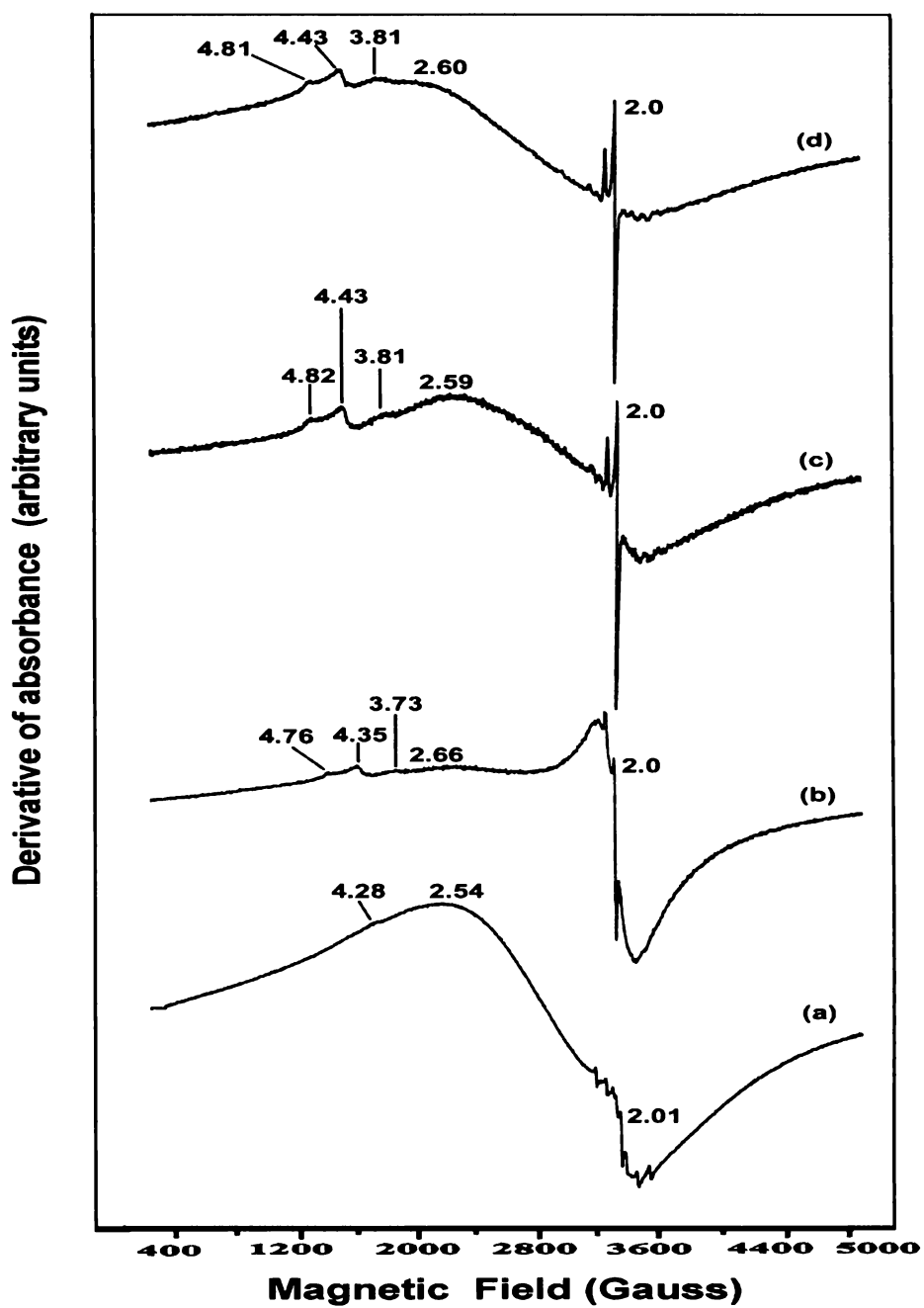
**Figure 5.1.5b EPR spectra of (a) ROM (b) SCP1 (c) SCP2
and (d) SCP2-DCBT Koraput kaolin heated at 400°C**
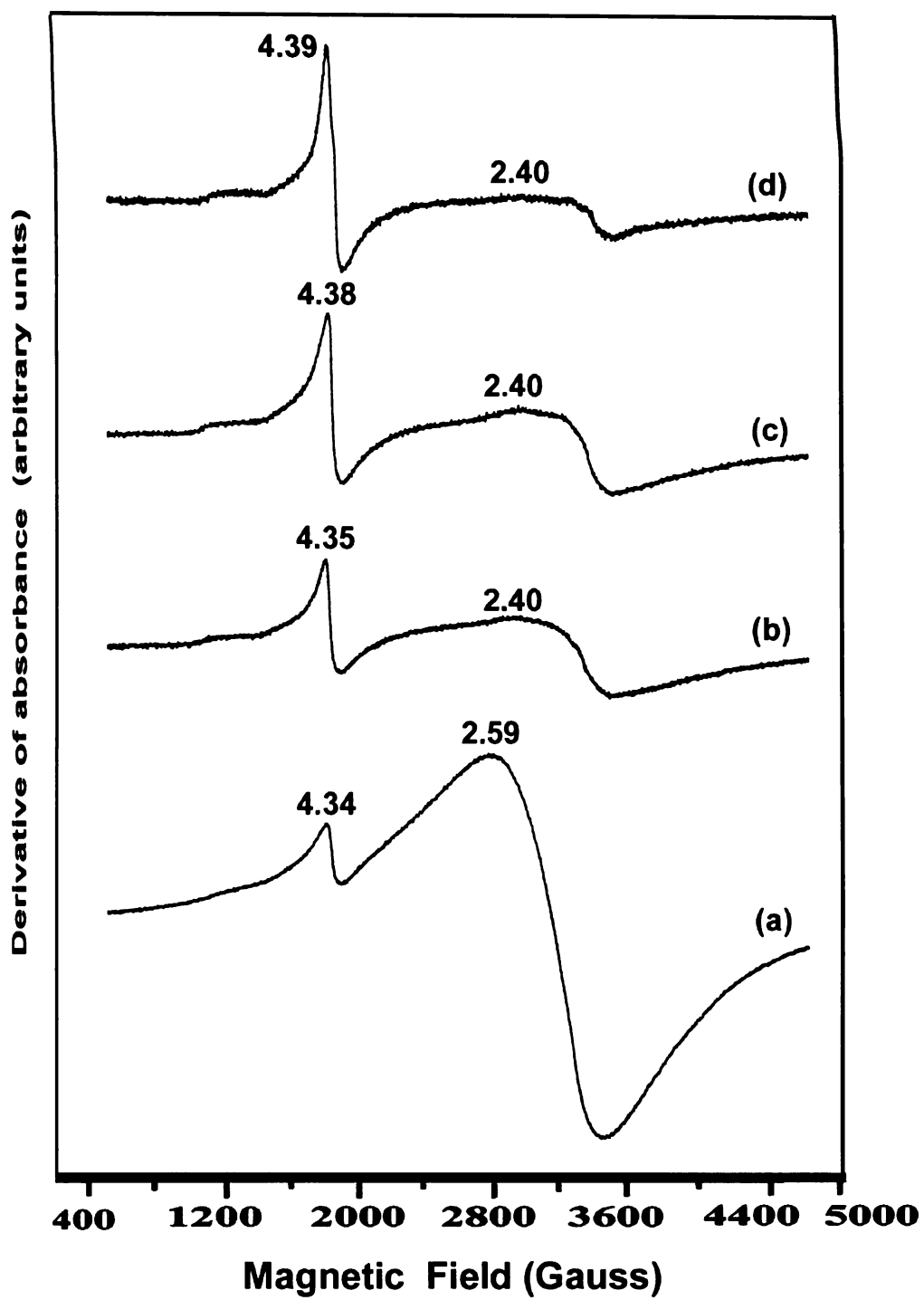
Figure 5.1.5c   EPR spectra of (a) ROM (b) SCP1 (c) SCP2 and
(d) SCP2-DCBT Koraput kaolin heated at 1100°C
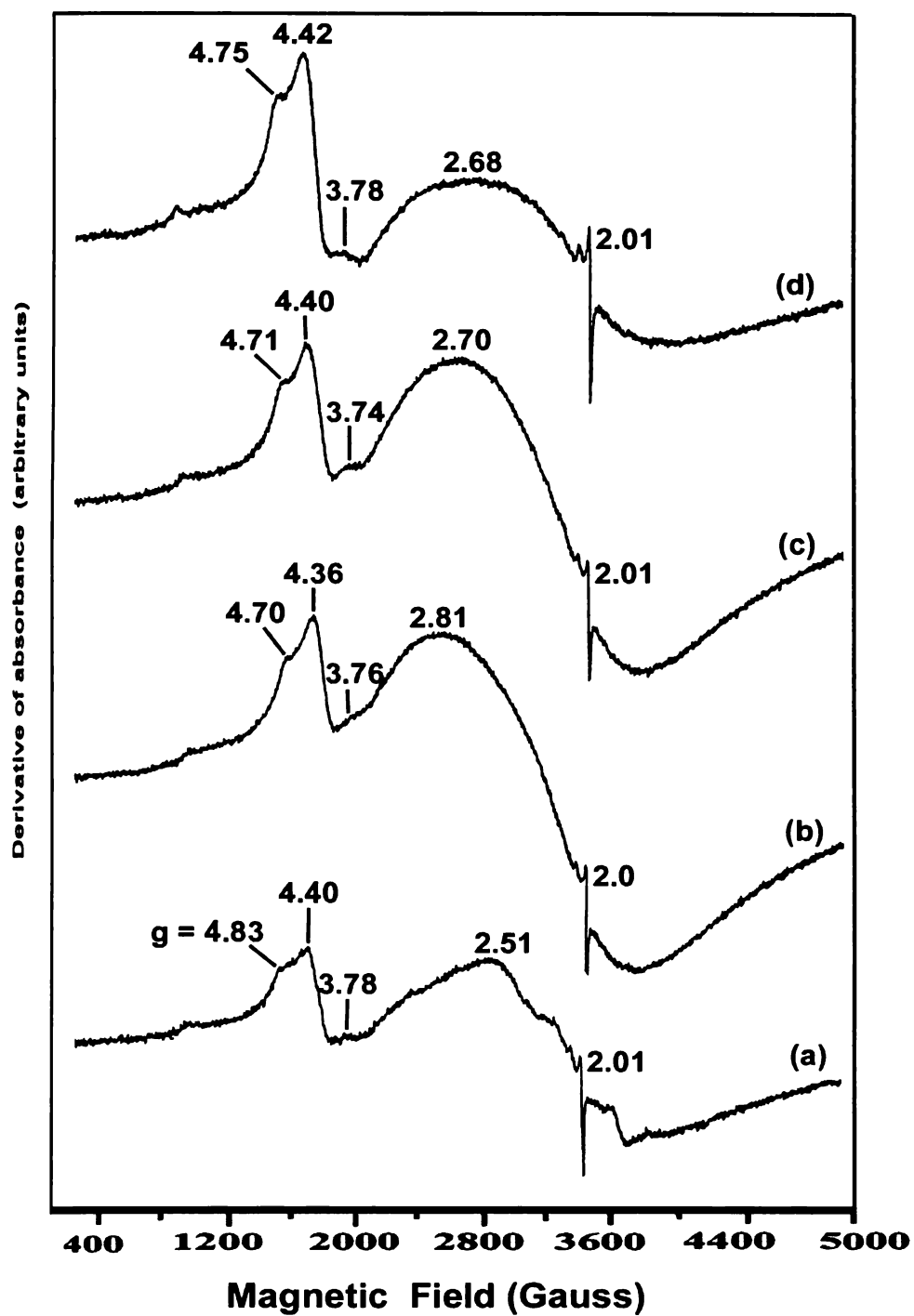
Figure 5.1.6a   EPR spectra of (a) ROM (b) SCP1 (c) SCP2 and
(d) SCP2-DCBT Bankura kaolin

259
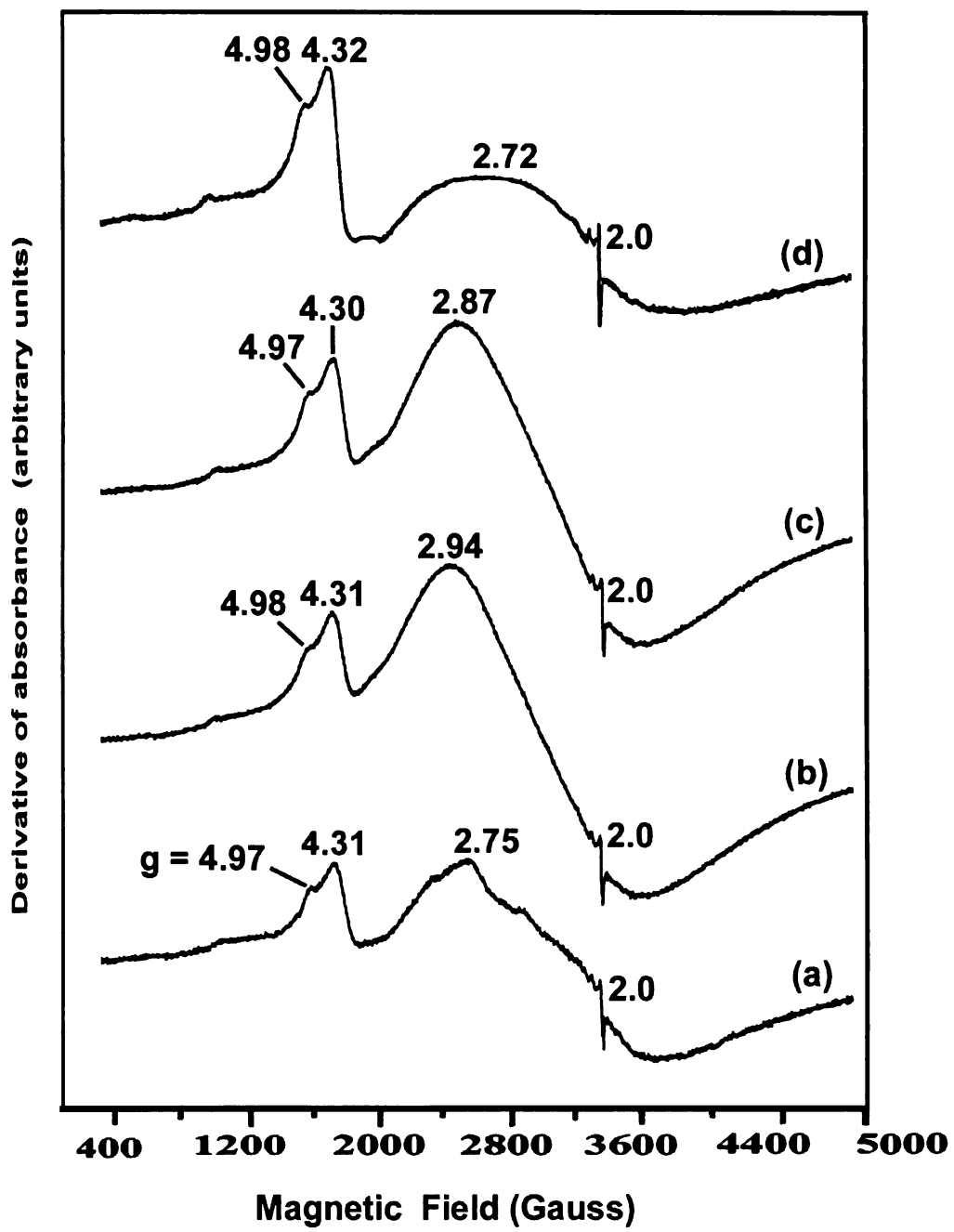
Figure 5.1.6b EPR spectra of (a) ROM (b) SCP1 (c) SCP2 and
(d) SCP2-DCBT Bankura kaolin heated at 400°C
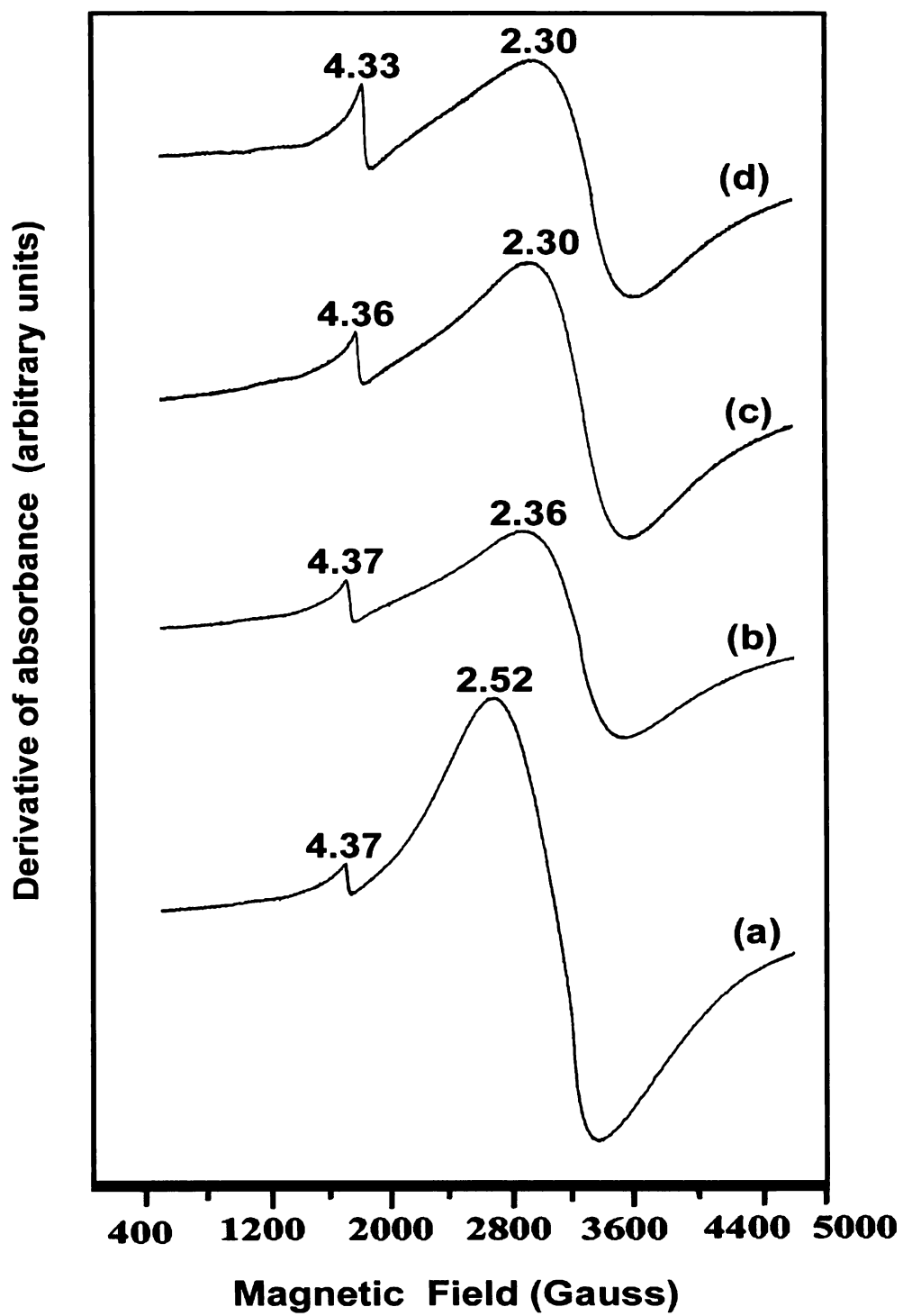
**Figure 5.1.6c EPR spectra of (a) ROM (b) SCP1 (c) SCP2 and
(d) SCP2-DCBT Bankura kaolin heated at 1100°C**
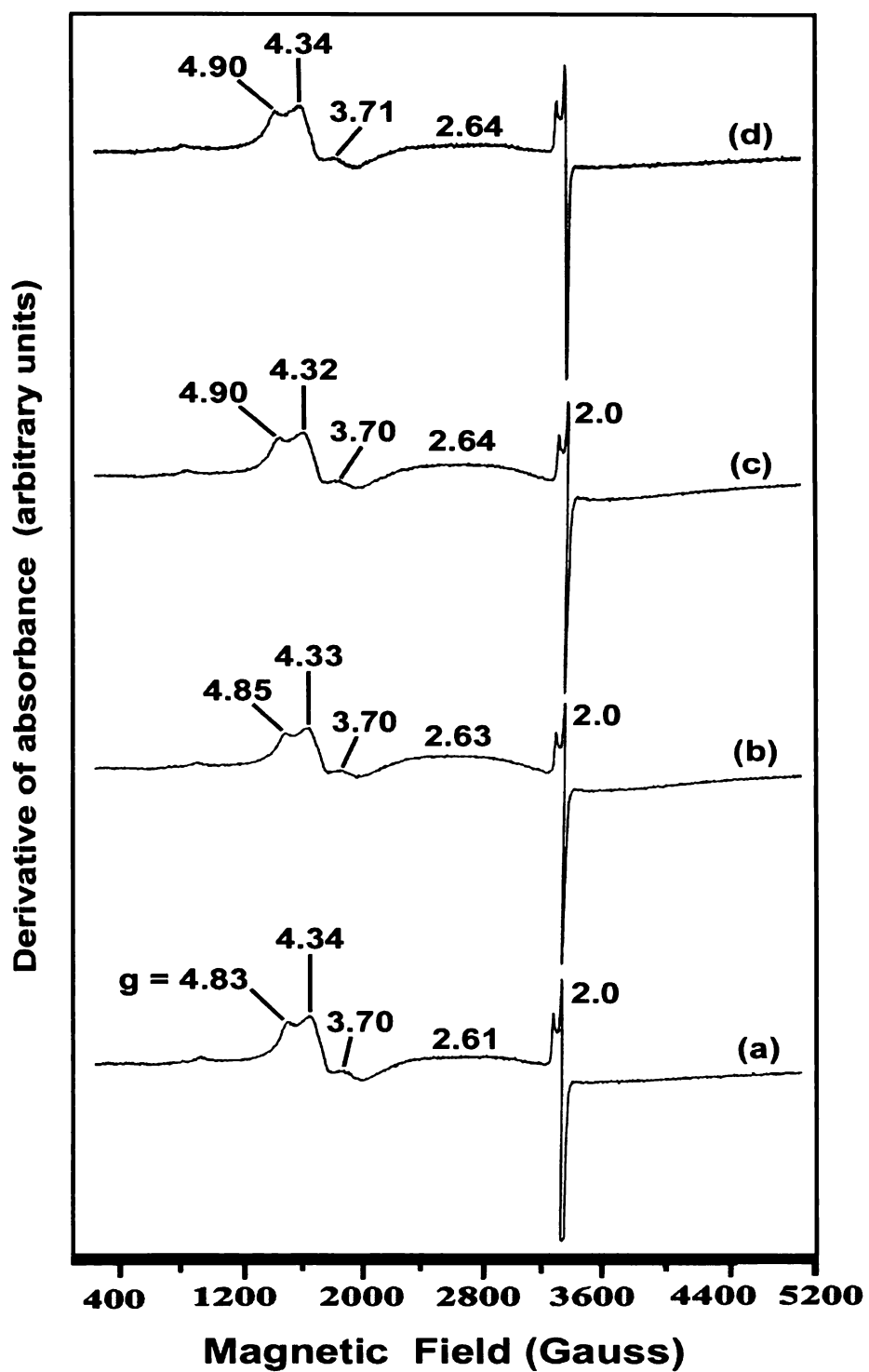
Figure 5.1.7a   EPR spectra of (a) ROM (b) SCP1 (c) SCP2
and (d) SCP2-DCBT Pali kaolin

262
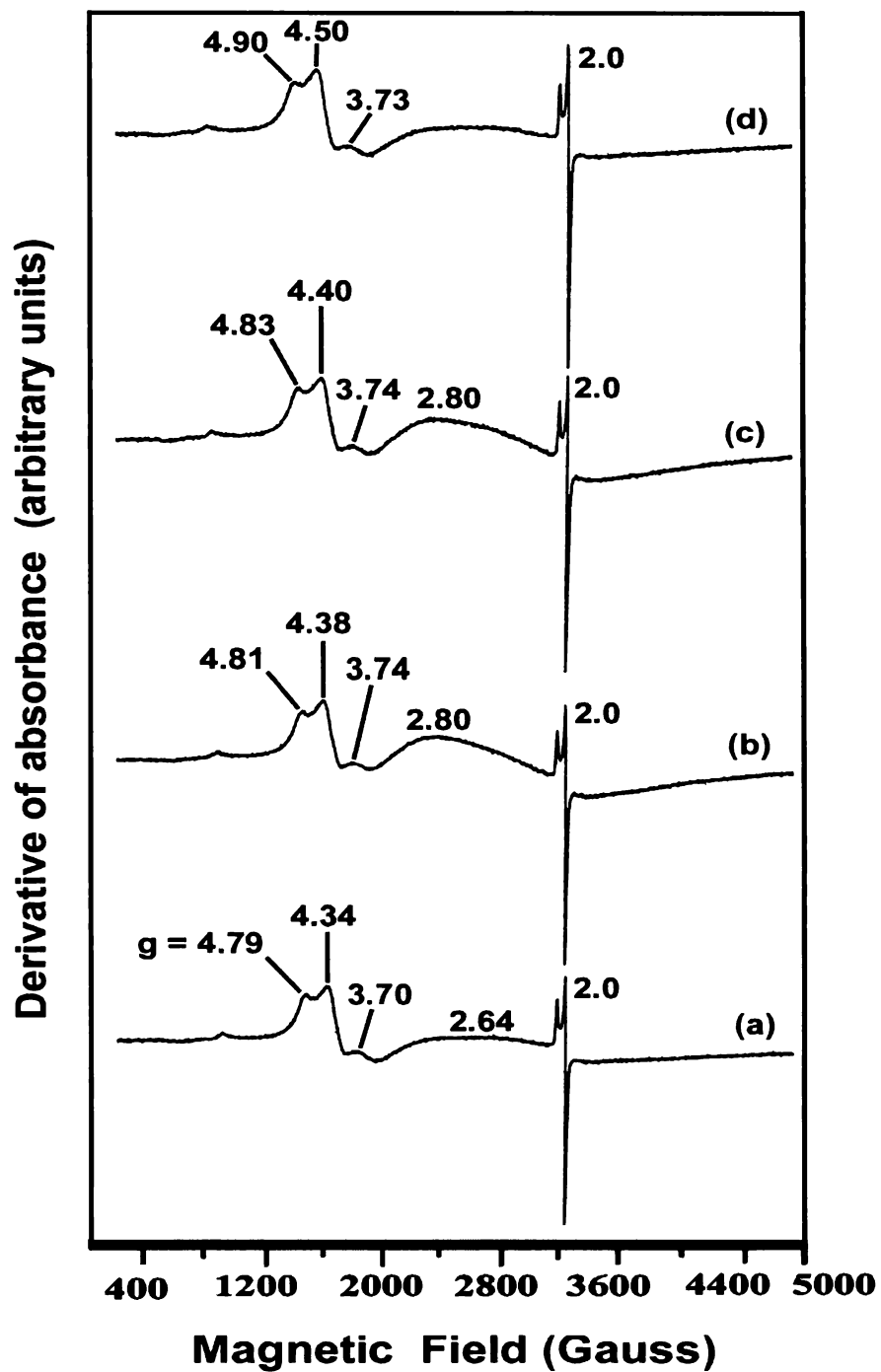
Figure 5.1.7b EPR spectra of (a) ROM (b) SCP1 (c) SCP2 and (d) SCP2-DCBT Pali kaolin heated at 400°C
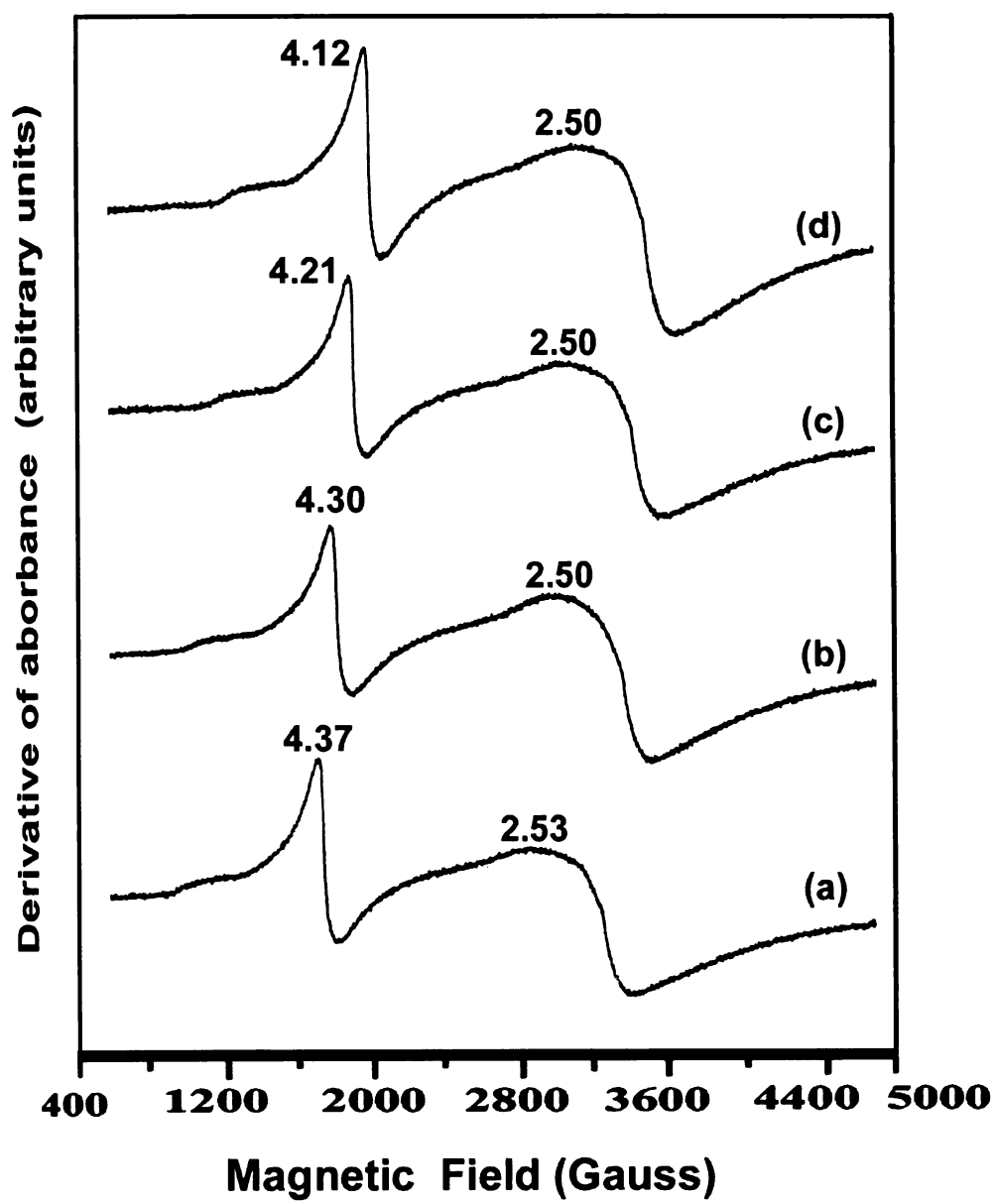
Figure 5.1.7c EPR spectra of (a) ROM (b) SCP1 (c) SCP2 and
(d) SCP2-DCBT Pali kaolin heated at 1100°C
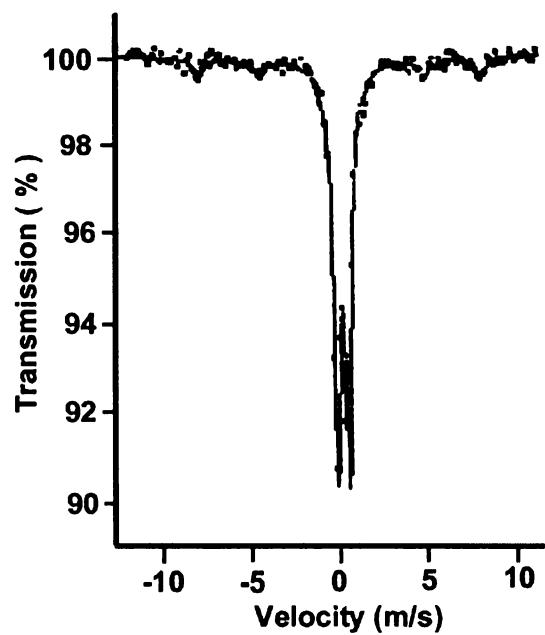
Figure 5.2.1 Mossbauer spectra of IM2 - Kasargod 1 kaolin
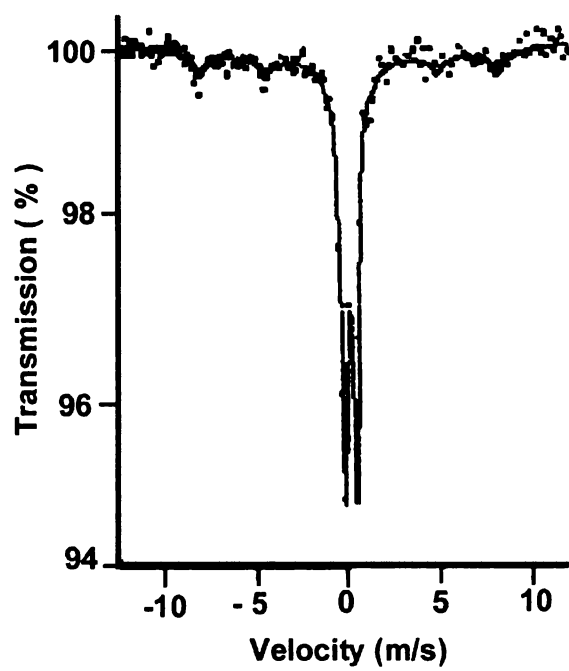
Figure 5.2.2 Mossbauer spectra of IM2 - Kasargod 2 kaolin
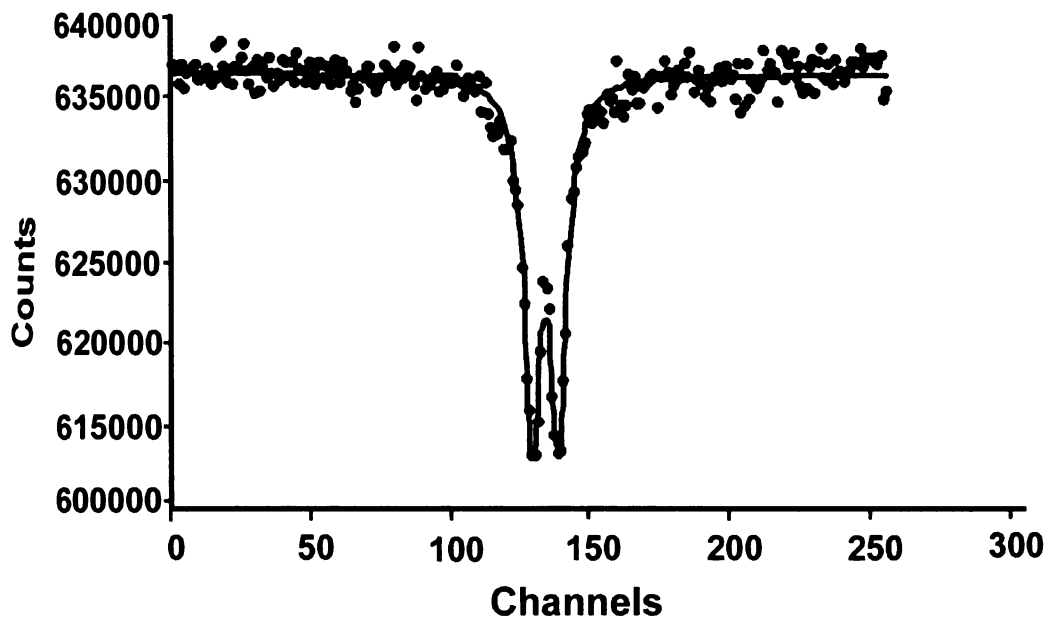
Figure 5.2.3 Mossbauer spectra of IM2 -Trivandrum kaolin
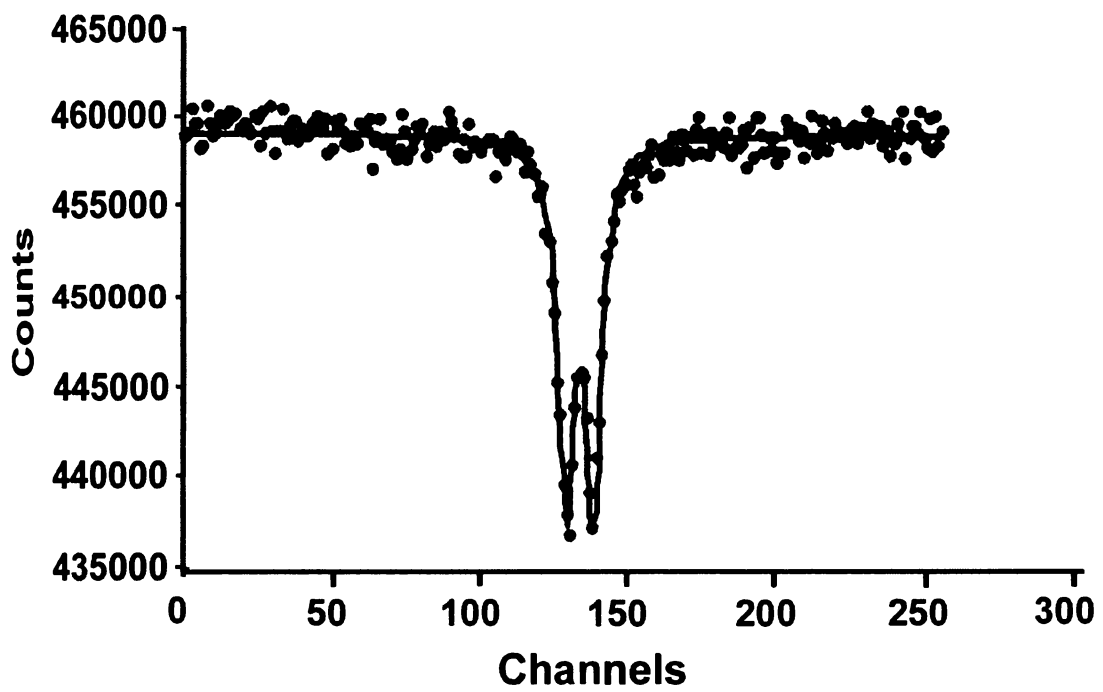

Figure 5.2.4 Mossbauer spectra of IM2 - Kutch kaolin
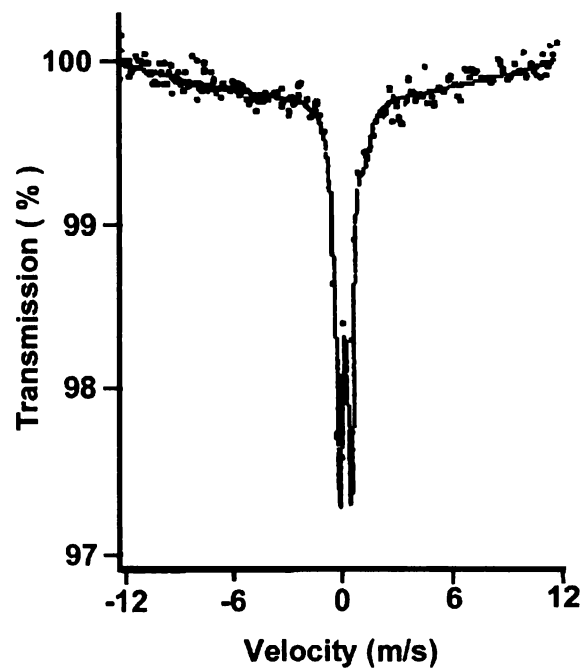
**Figure 5.2.5 Mossbauer spectra of IM2 - Koraput kaolin**
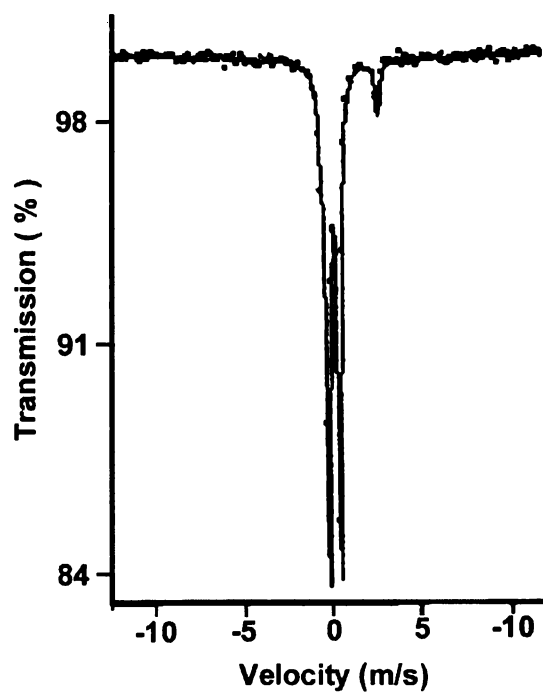
Figure 5.2.6 Mossbauer spectra of IM2 - Bankura kaolin
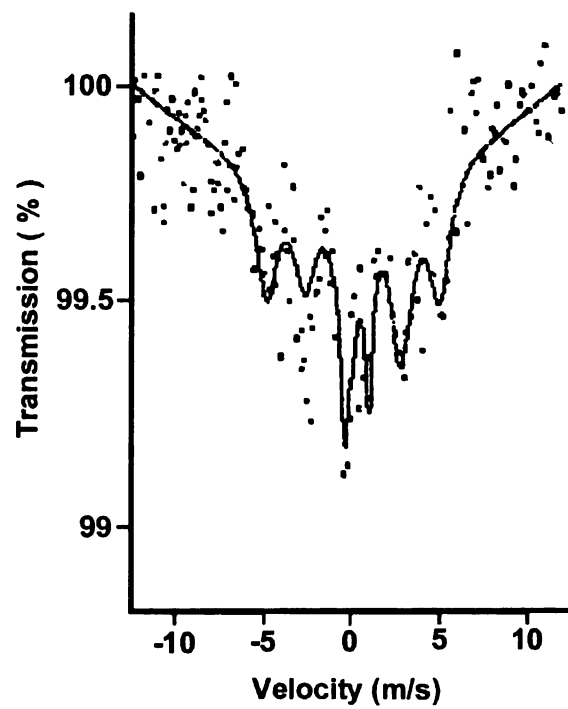
Figure 5.2.7 Mossbauer spectra of IM2 - Pali kaolin
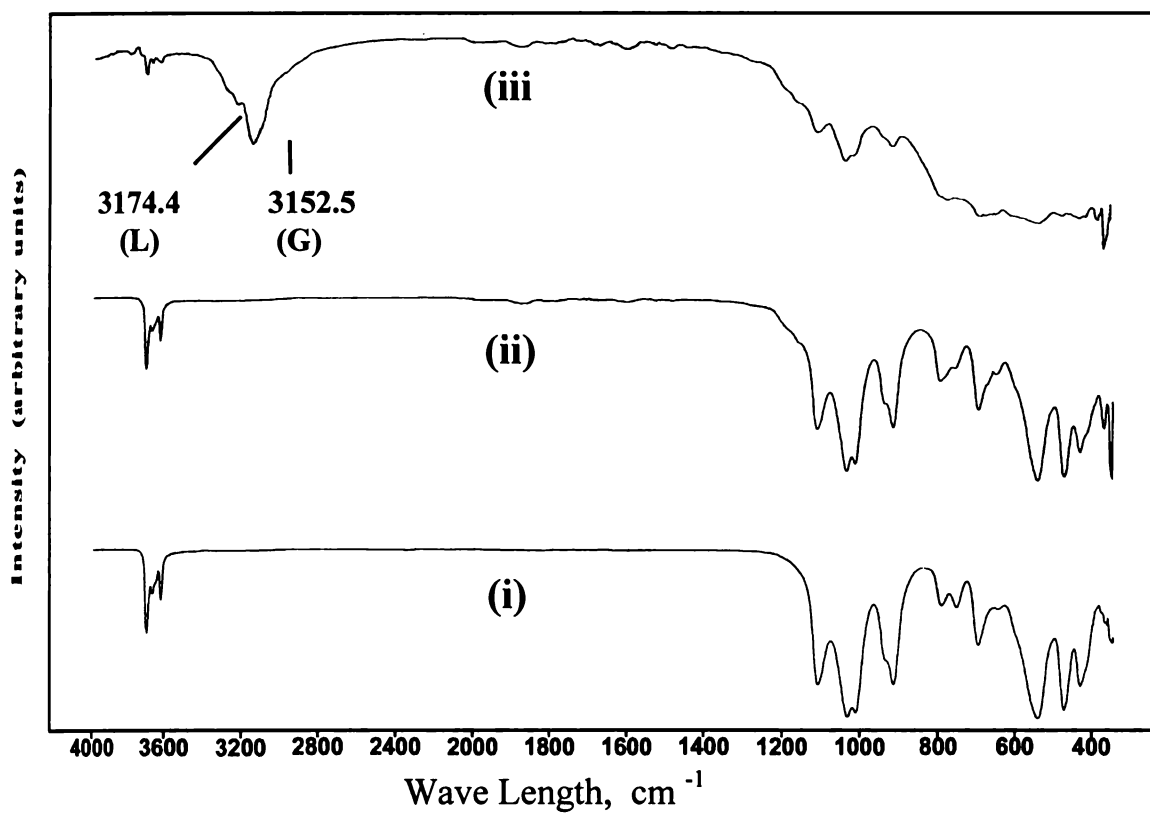
**Figure 5.3.1a IR spectra of (i) ROM (ii) IM1 and (iii) IM2 samples
of Kasargod 1 kaolin**
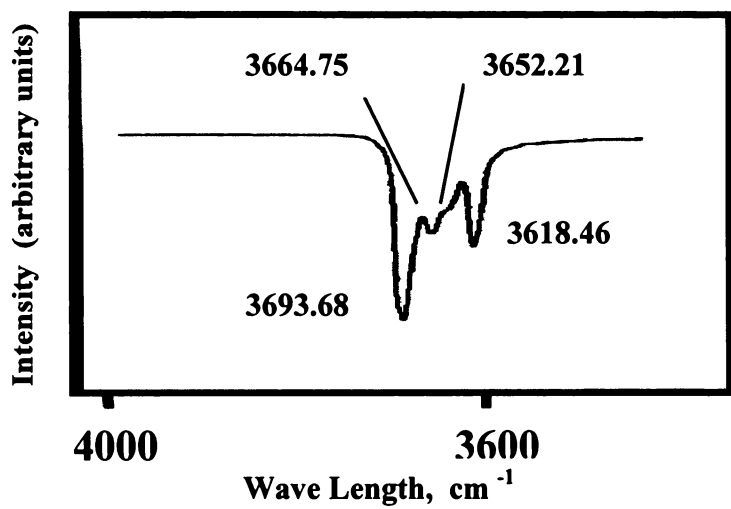
Figure 5.3.1b IR spectrum of   ROM (3700 – 3600 cm^{-1})
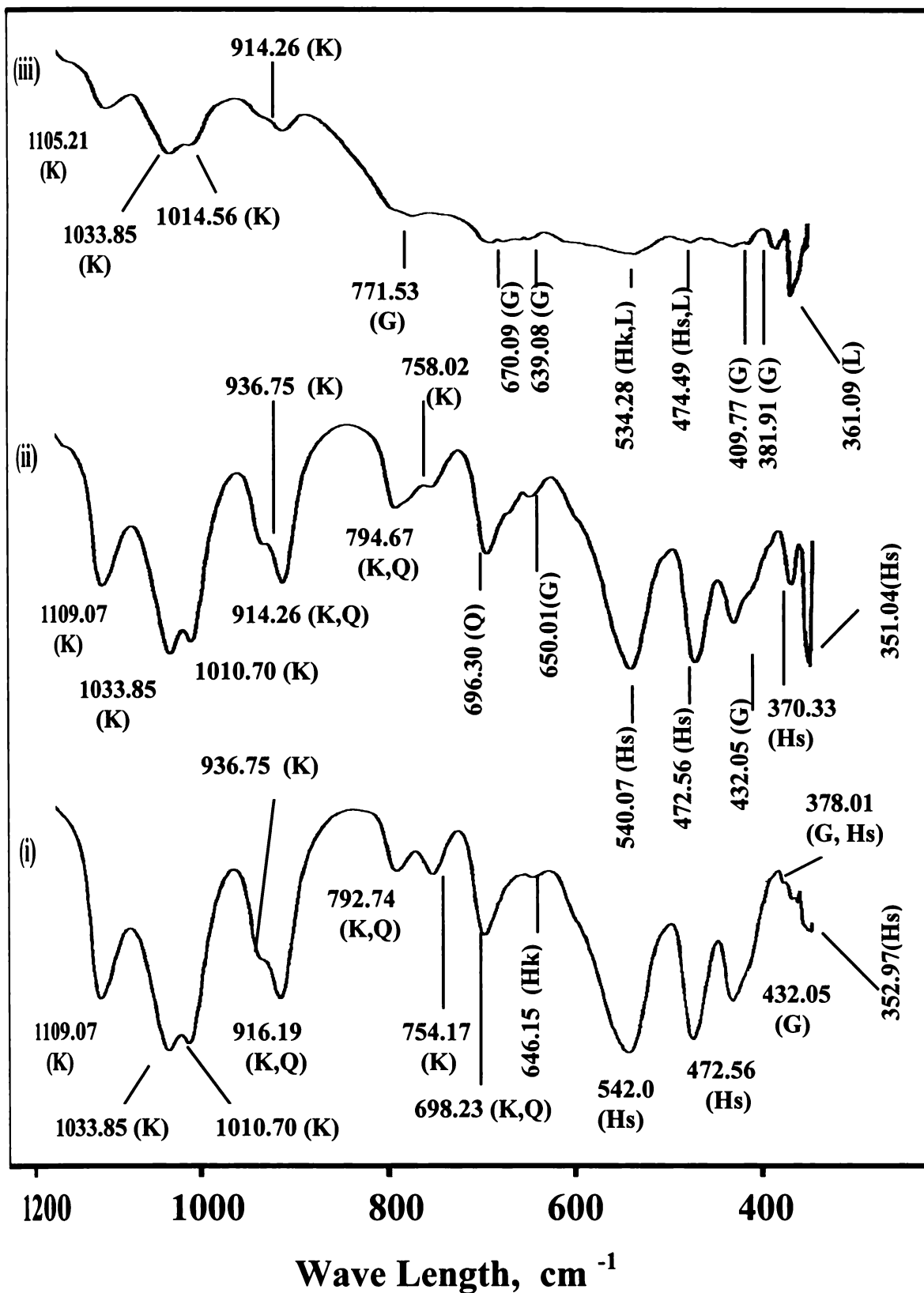
Figure 5.3.1c IR spectra of (a) ROM (b) IM1 (c) and (c) IM2 samples (1200 - 350 cm⁻¹)
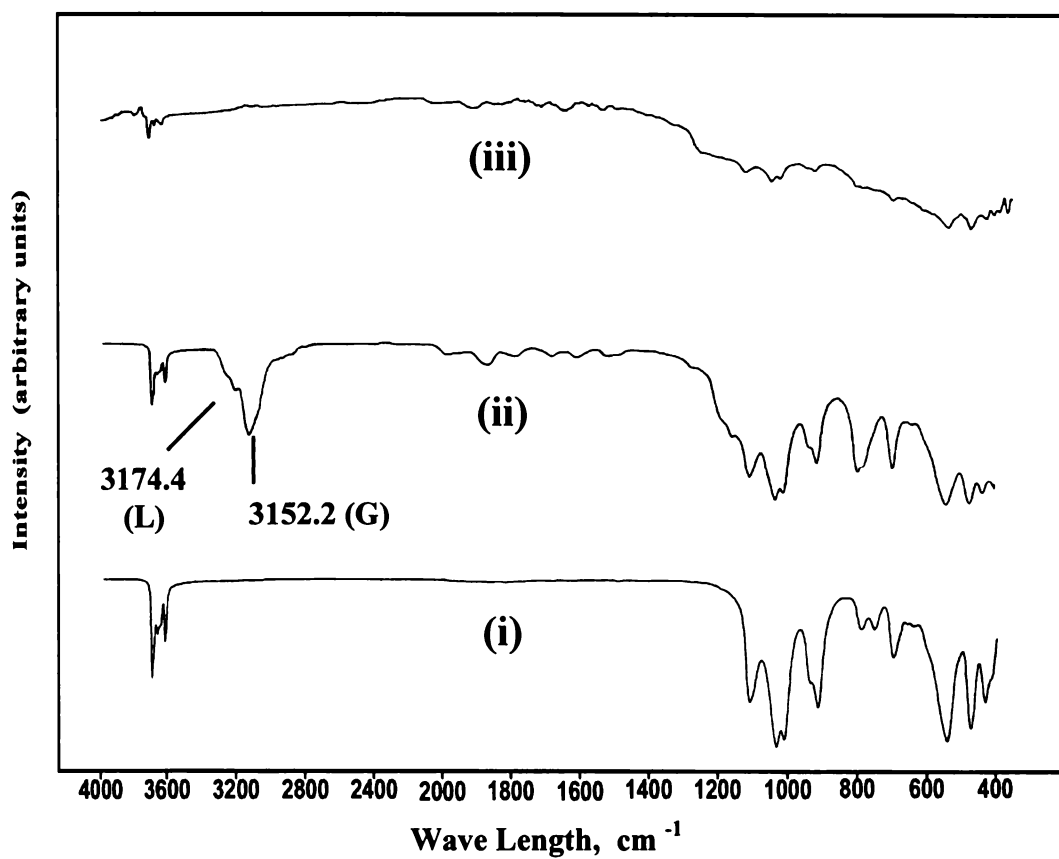
Figure 5.3.2a IR spectra of (i) ROM (ii) IM1 and (iii) IM2 samples of Kasargod 2 kaolin
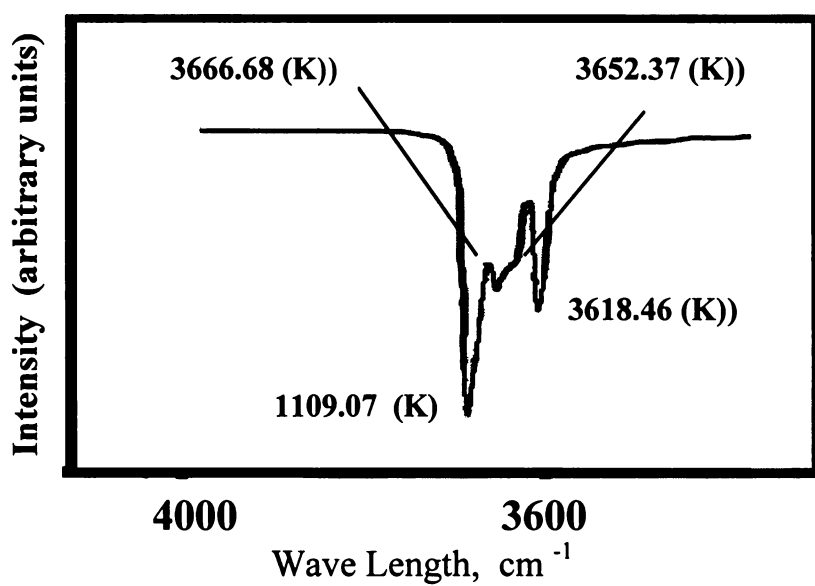
Figure 5.3.2b IR spectrum of ROM (3700 – 3600 cm⁻¹.
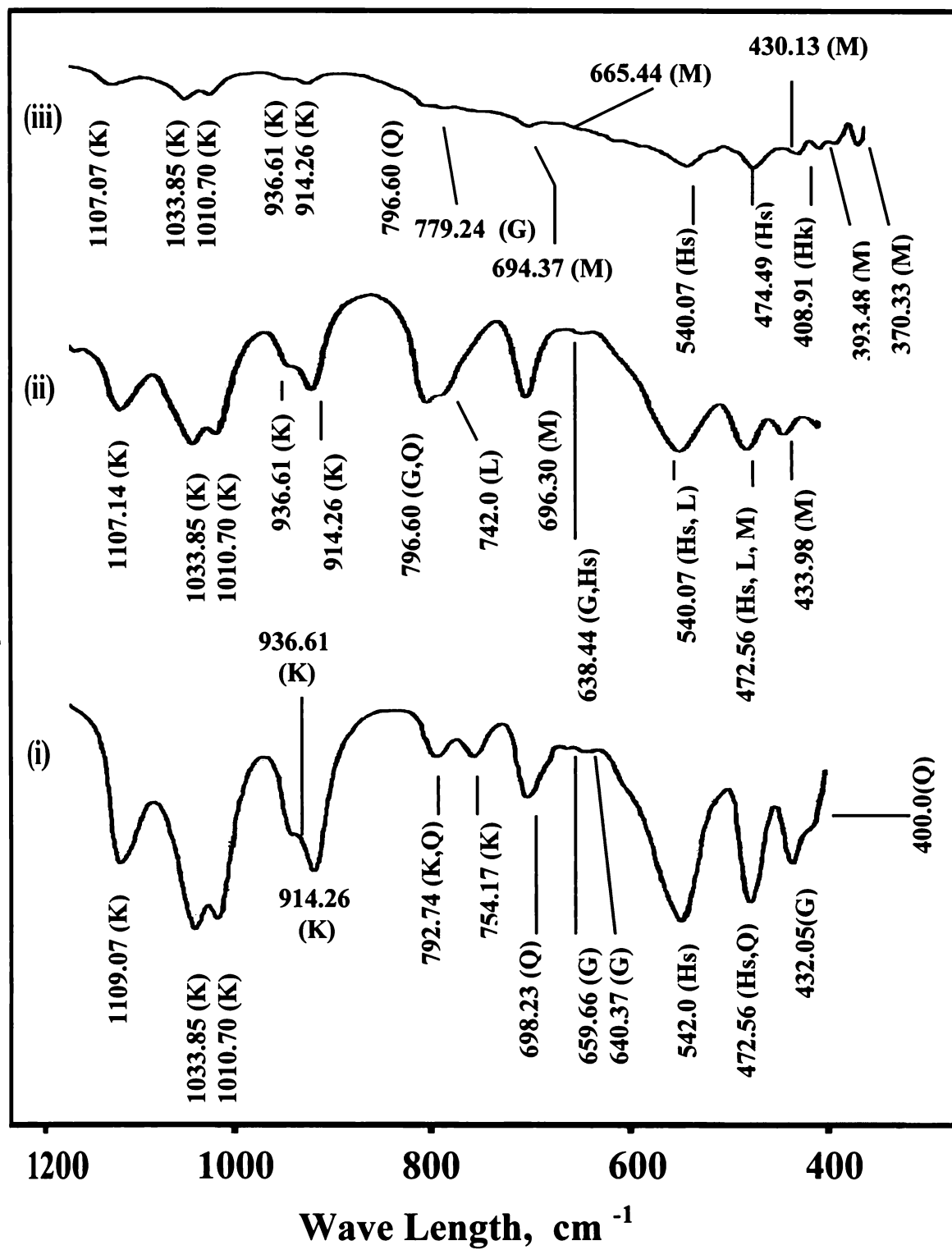
Figure 5.3.2c IR spectra of (a) ROM (b) IM1 (c) and (c) IM2 samples (1200 - 350 cm⁻¹)
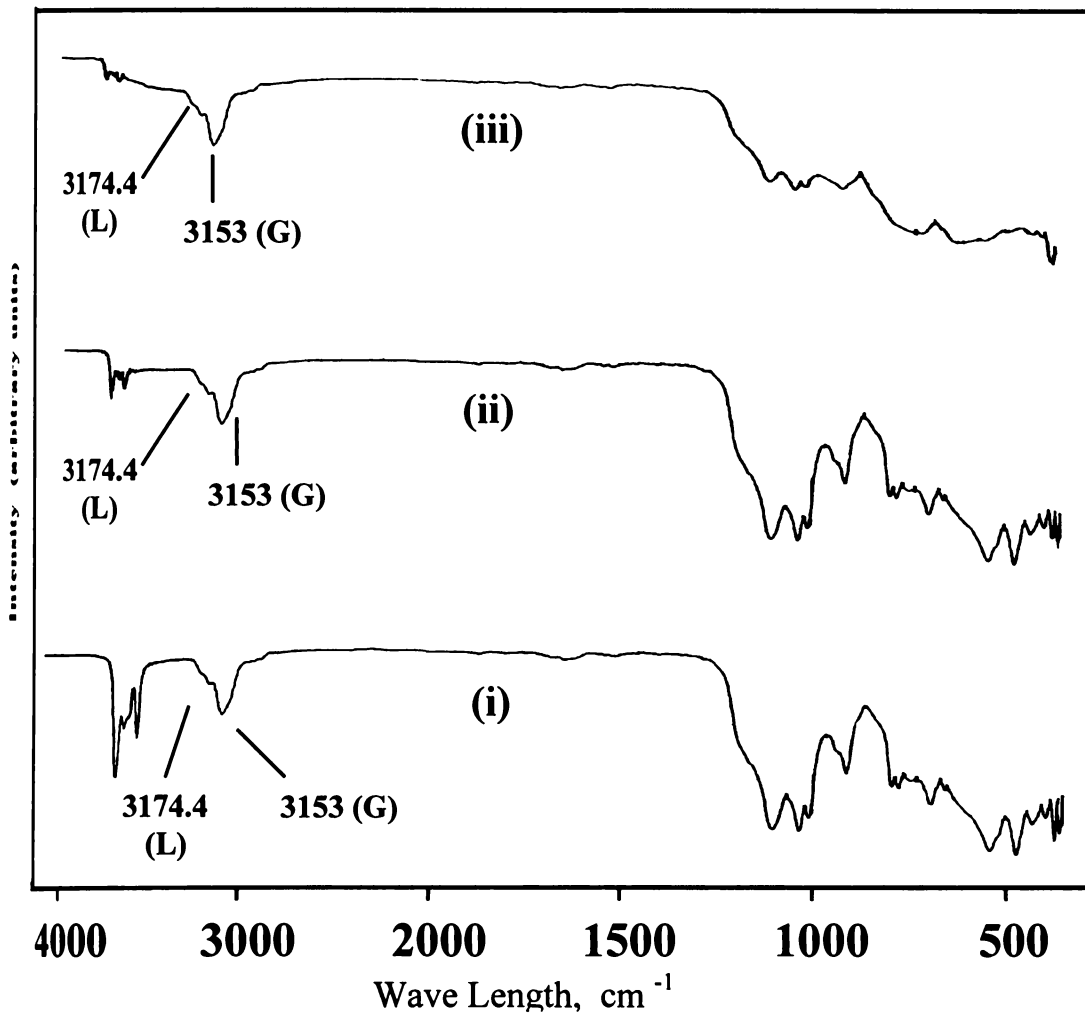
Figure 5.3.3a IR spectra of (i) ROM (ii) IM1 and (iii) IM2 samples of Trivandrum kaolin
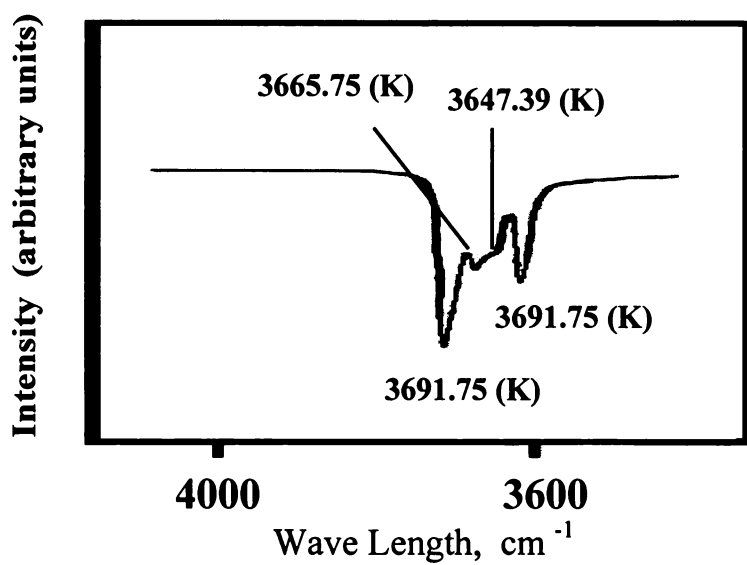
Figure 5.3.3b IR spectrum of   ROM (3700 – 3600 cm⁻¹
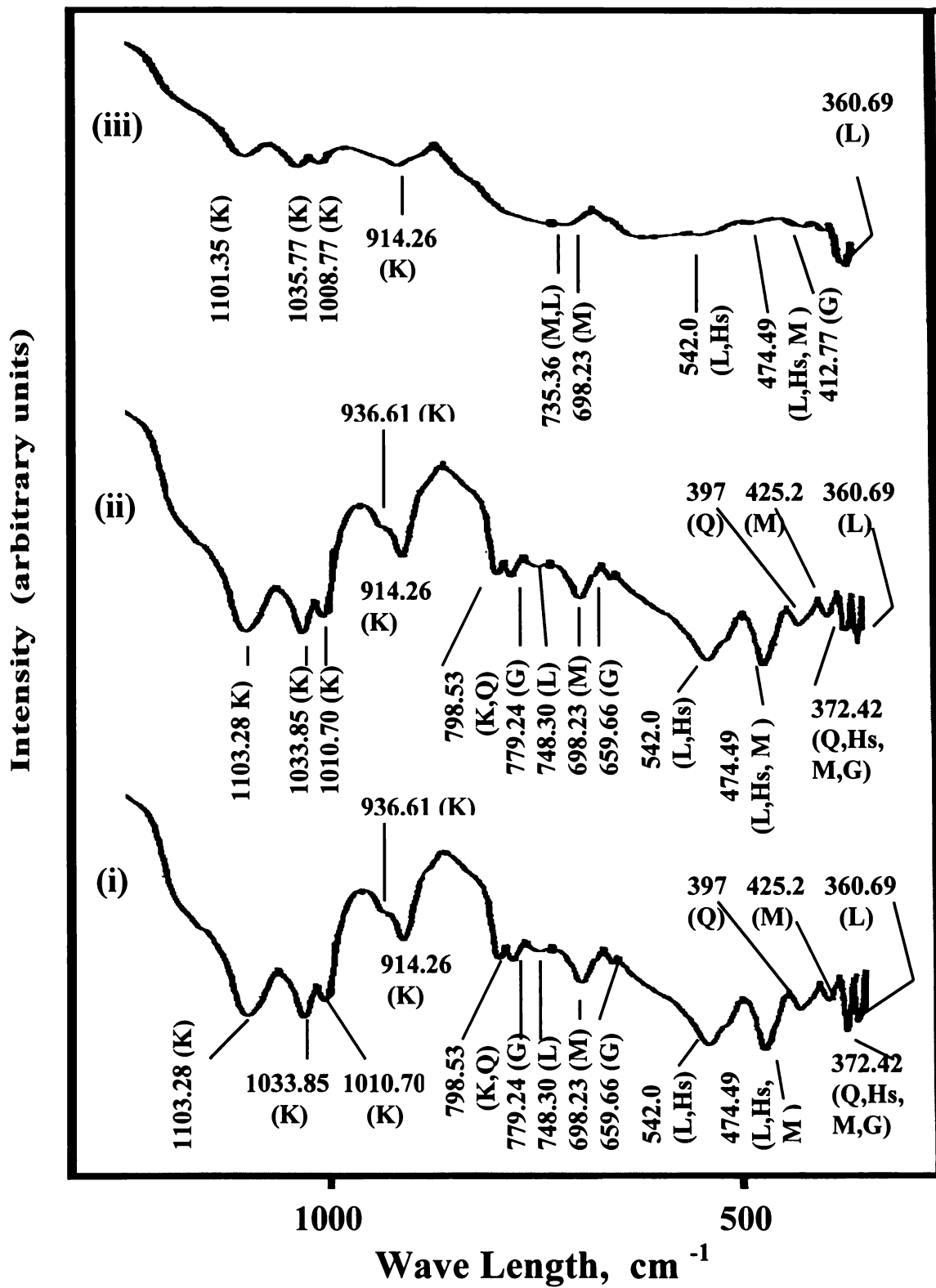
Figure 5.3.3c IR spectra of (a) ROM (b) IM1 (c) and (c) IM2 samples (1200 - 350 cm^{-1})
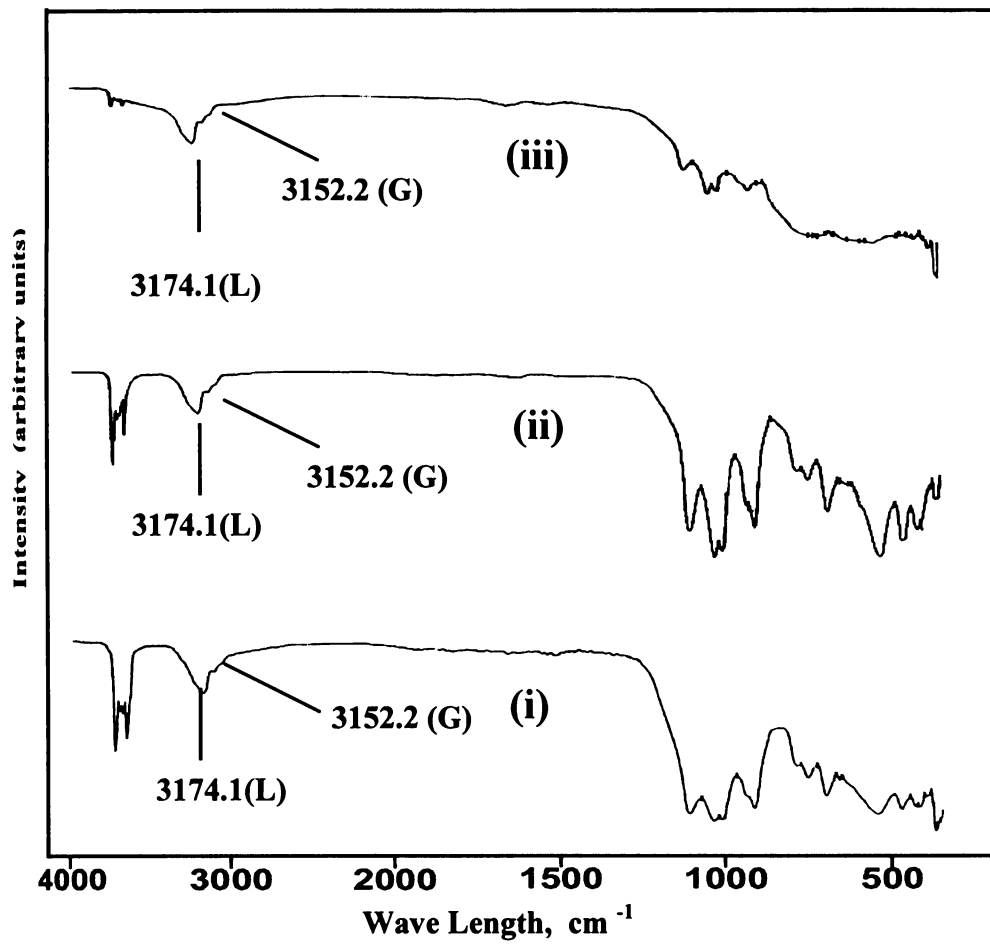
Figure 5.3.4a IR spectra of (i) ROM (ii) IM1 and (iii) IM2 samples of Kutch kaolin
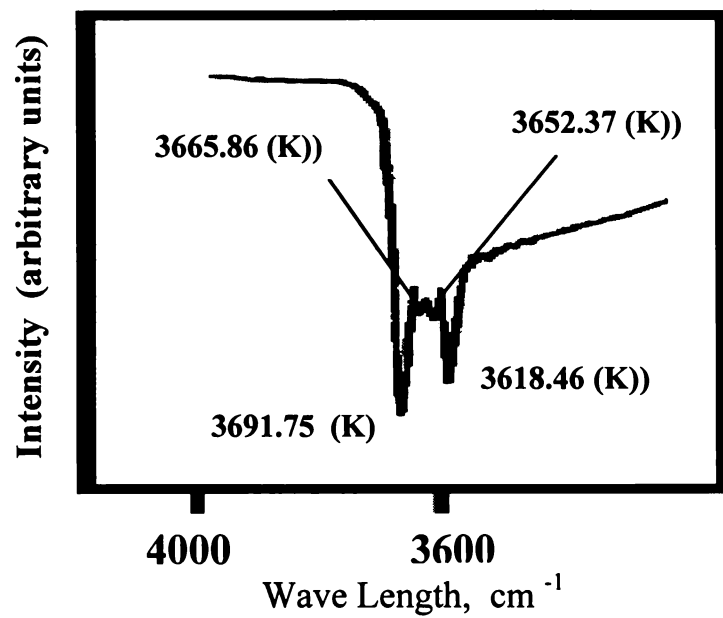
Figure 5.3.4b IR spectrum of ROM (3700 – 3600 cm⁻¹
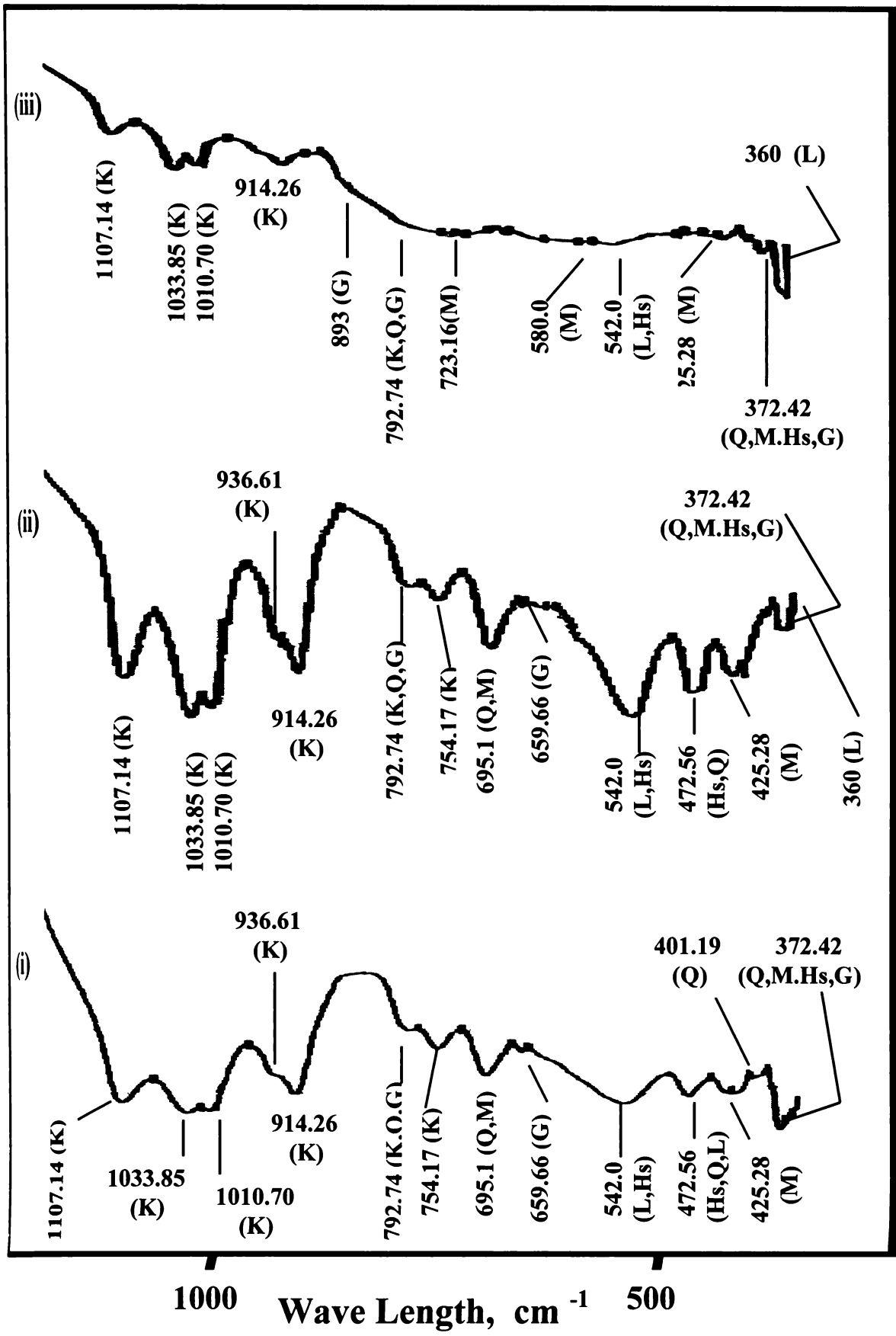
Figure 5.3.4c IR spectra of (a) ROM (b) IM1 and (c) IM2 samples
of Kutch kaolin
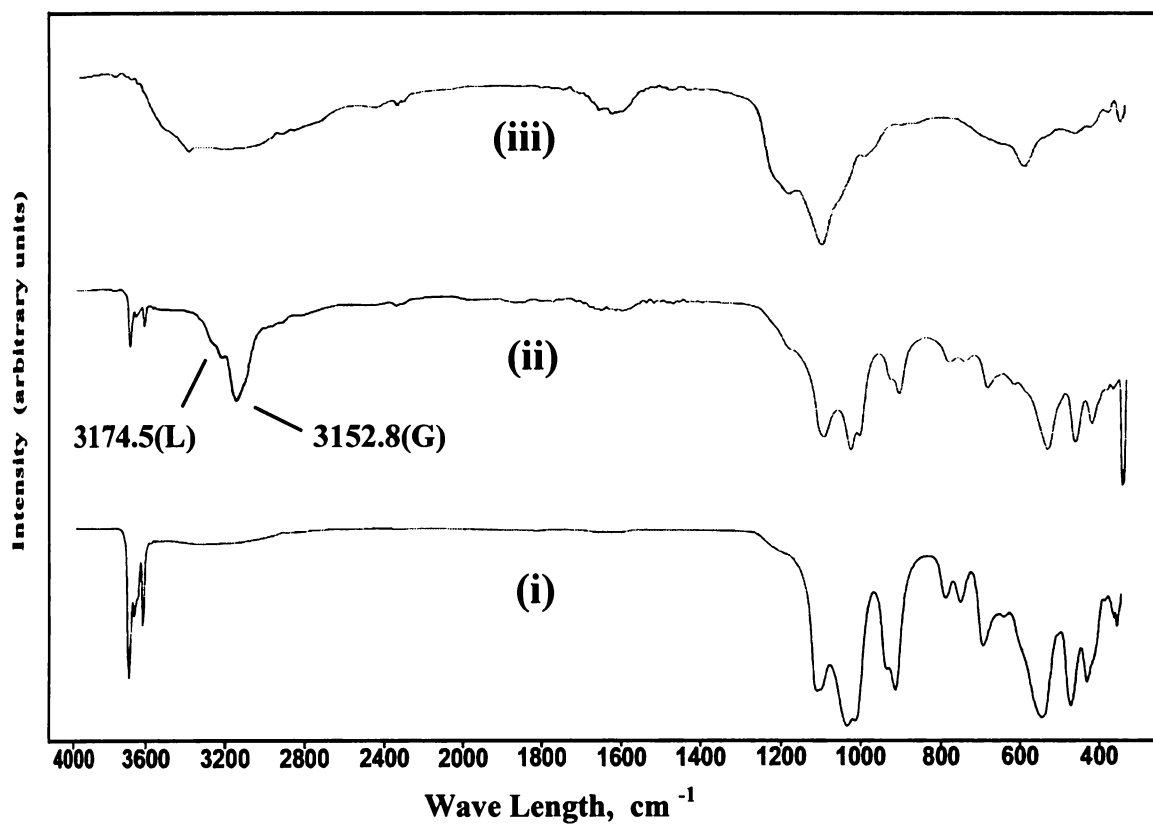
**Figure 5.3.5a IR spectra of (i) ROM (ii) IM1 and (iii) IM2 samples
of Koraput kaolin**
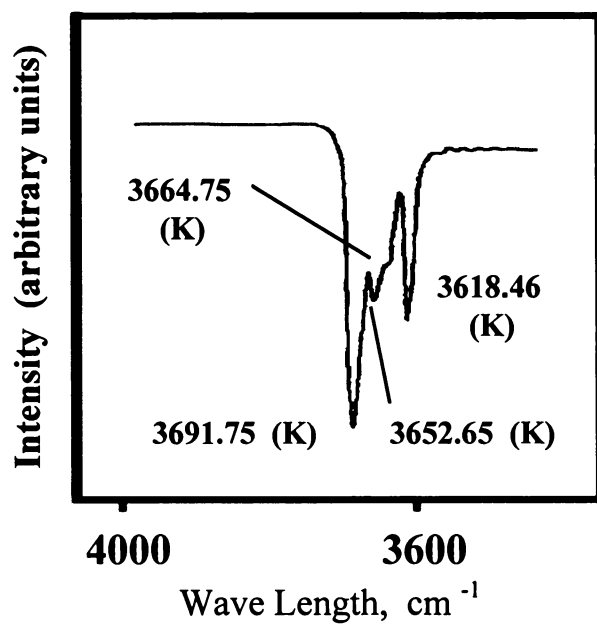
Figure 5.3.5b IR spectrum of   ROM (3700 – 3600 cm⁻
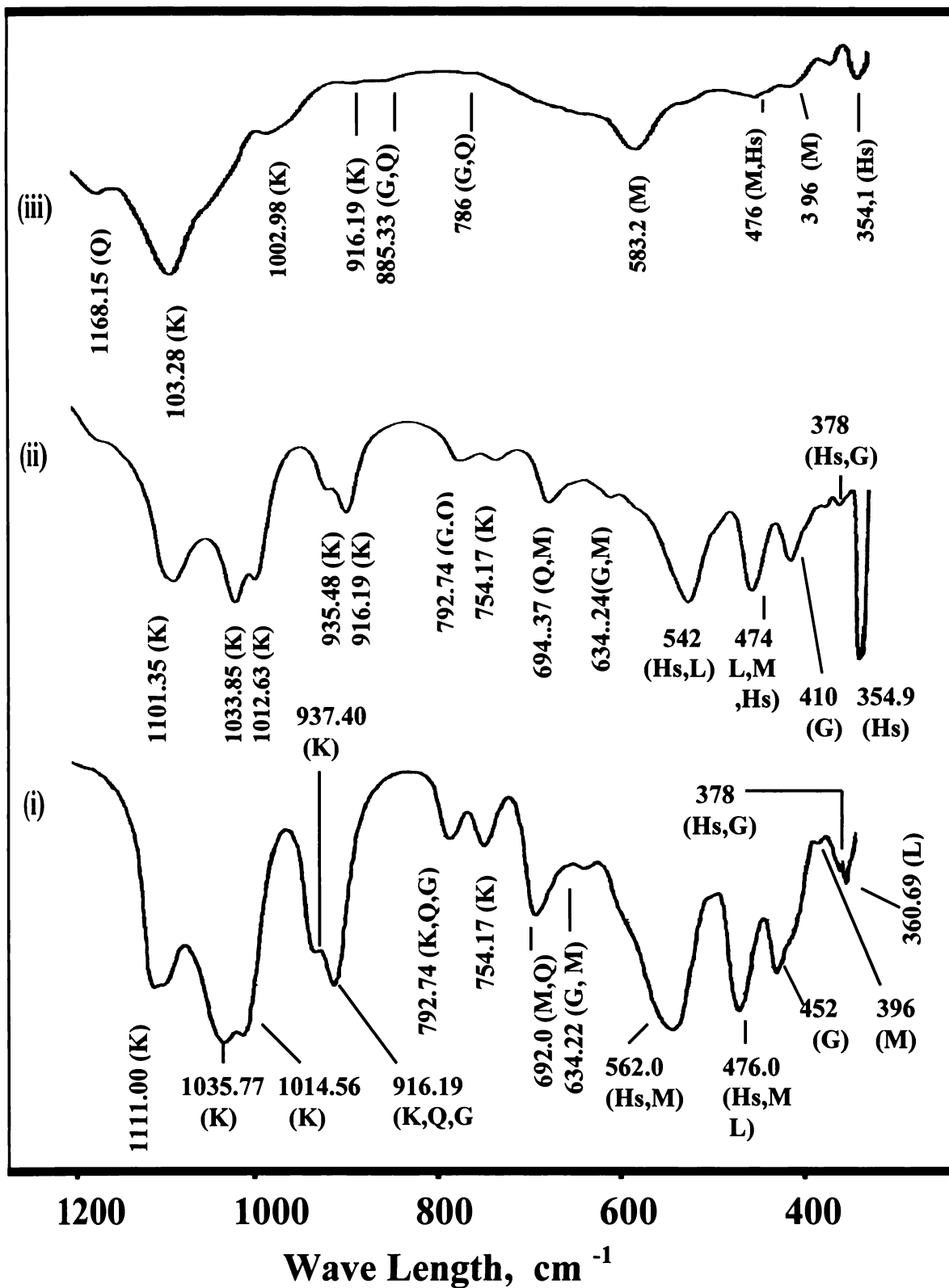
Figure 5.3.5c IR spectra of (a) ROM (b) IM1 (c) and (c) IM2 samples
(1200 - 350 cm^{-1})

278

3175 (L)

3153 (G)
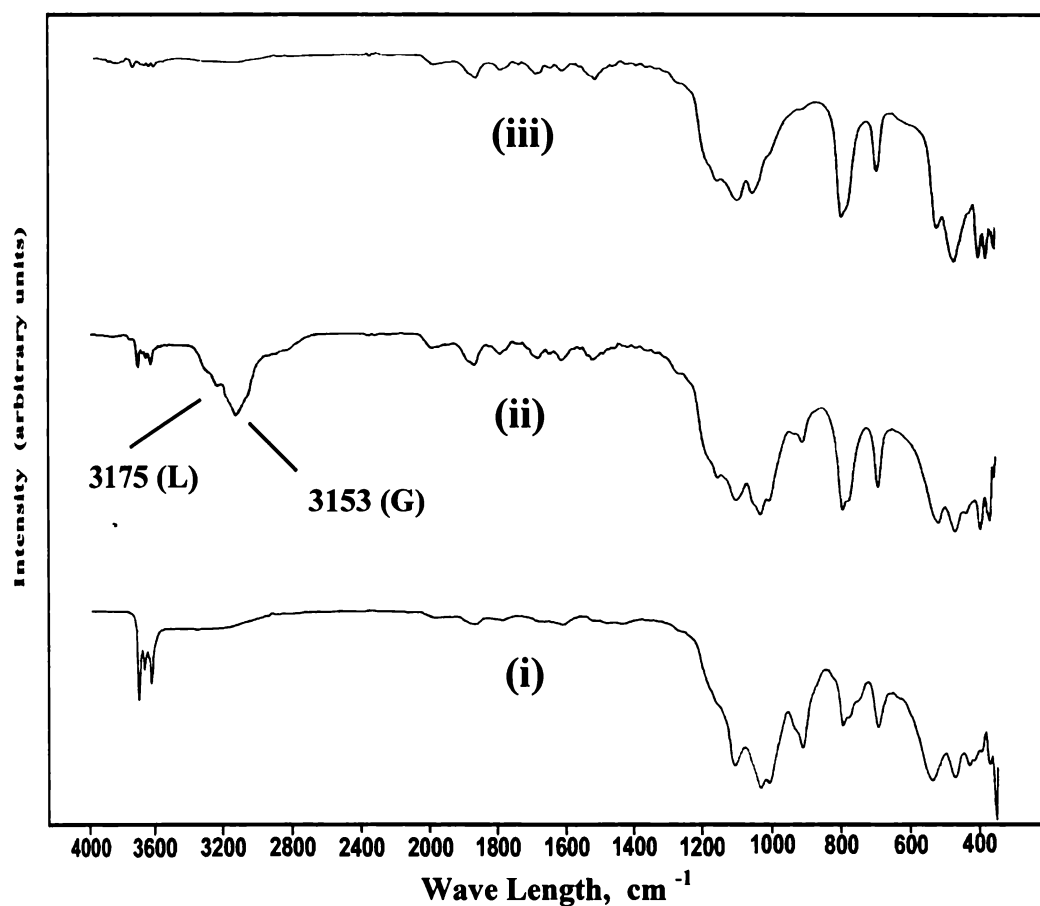
**Figure 5.3.6a IR spectra of (i) ROM (ii) IM1 and (iii) IM2 samples
of Bankura kaolin**

3653 (K)

3695.61 (K)   3620.39(K)

4000   3600

Wave Length, cm $^{-1}$
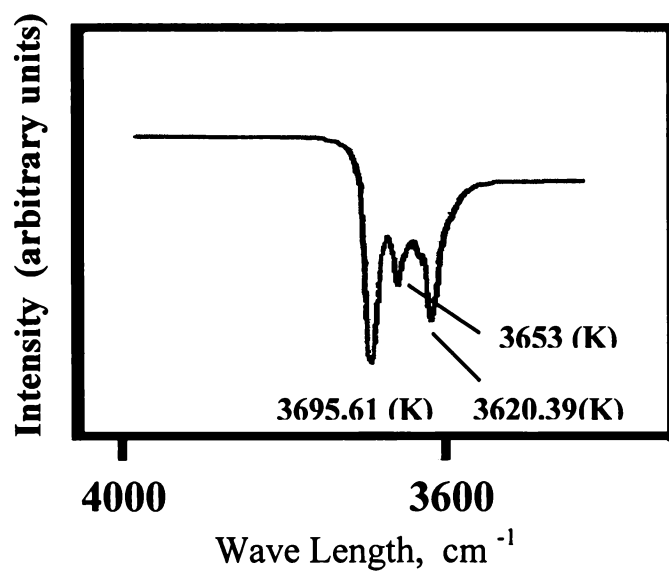
Figure 5.3.6b IR spectrum of   ROM (3700 – 3600 cm
-1.

(ii)

1154.23 (L)
1097.50 (K)
1055.06 (K)
918.12 (K)
796.60 (Q)
792.81(G)
694.31 (M)
532 (Hs)
477.56 (Hs,M)
446.0 (G)
399.56 (M)
372.33 (Q,M,Hs)

(ii)

937.40 (K)
1154.23 (L)
1105.21 (K)
1035.77 (K)
1010.70 (K)
914.26 (K)
798.53 (Q)
792.81(G)
694.31 (M)
548 (L,Hs)
477.56 (Hs,M,L)
445.0 (G)
399.56 (M)
372.33 (QM,Hs)
352 (Hs)

(i)

937.0 (K)
1109.07 (K)
1033.85 (K)
1010.70 (K)
914.26 (K,Q)
798.53 (K,Q)
791.26 (G,Q)
724.10 (M)
694.30 (M,Q)
542 (Hs)
477 (Hs,M)
446.0 (G)
399.56 (Q)
372.42 (Q,Hs,M,G)
352 (Hs)

Wave Length, cm $^{-1}$

1200   1000   800   600   400
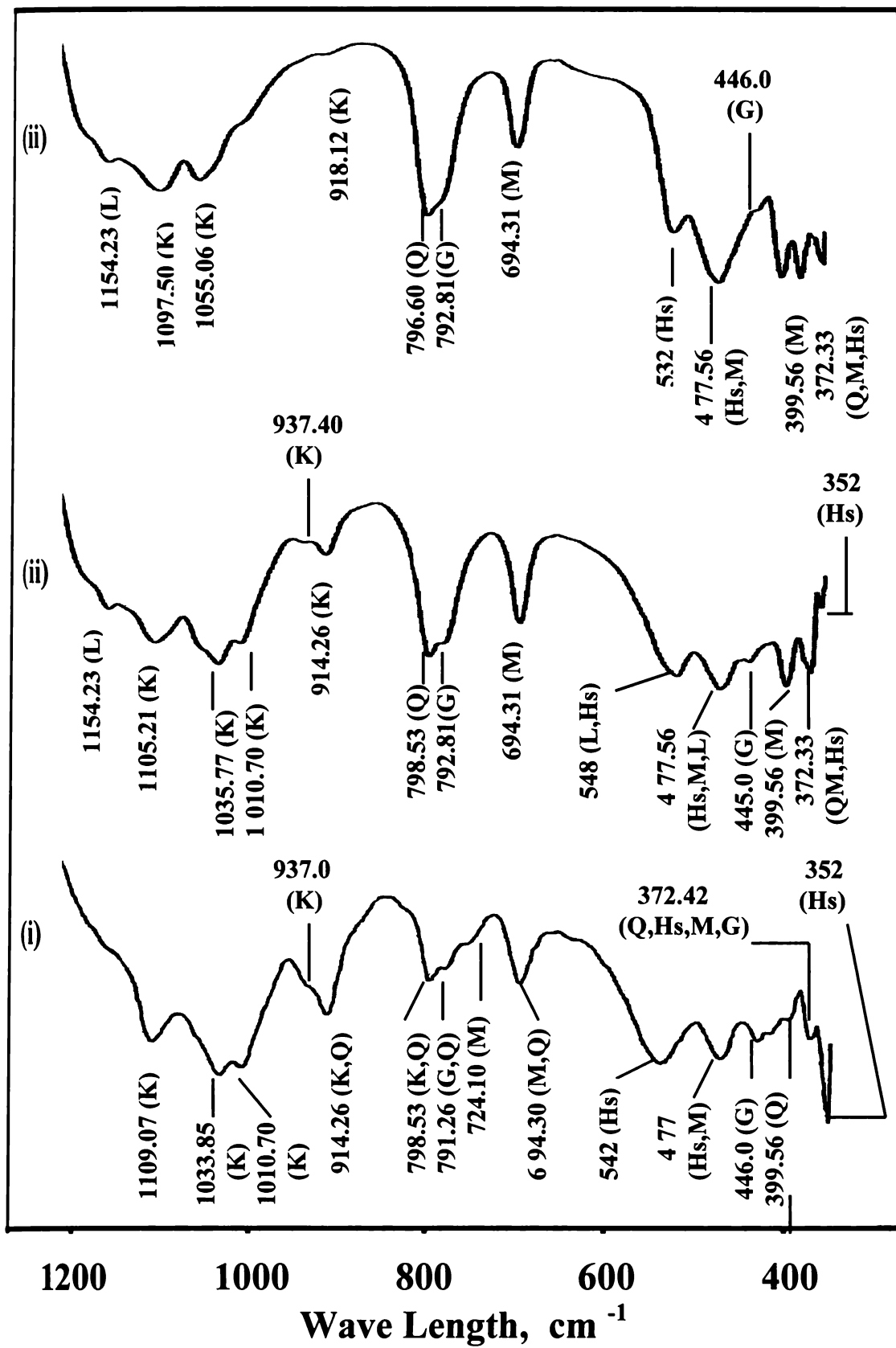
Figure 5.3.6c IR spectra of (a) ROM (b) IM1 (c) and (c) IM2 samples (1200 - 350 cm^{-1})

280
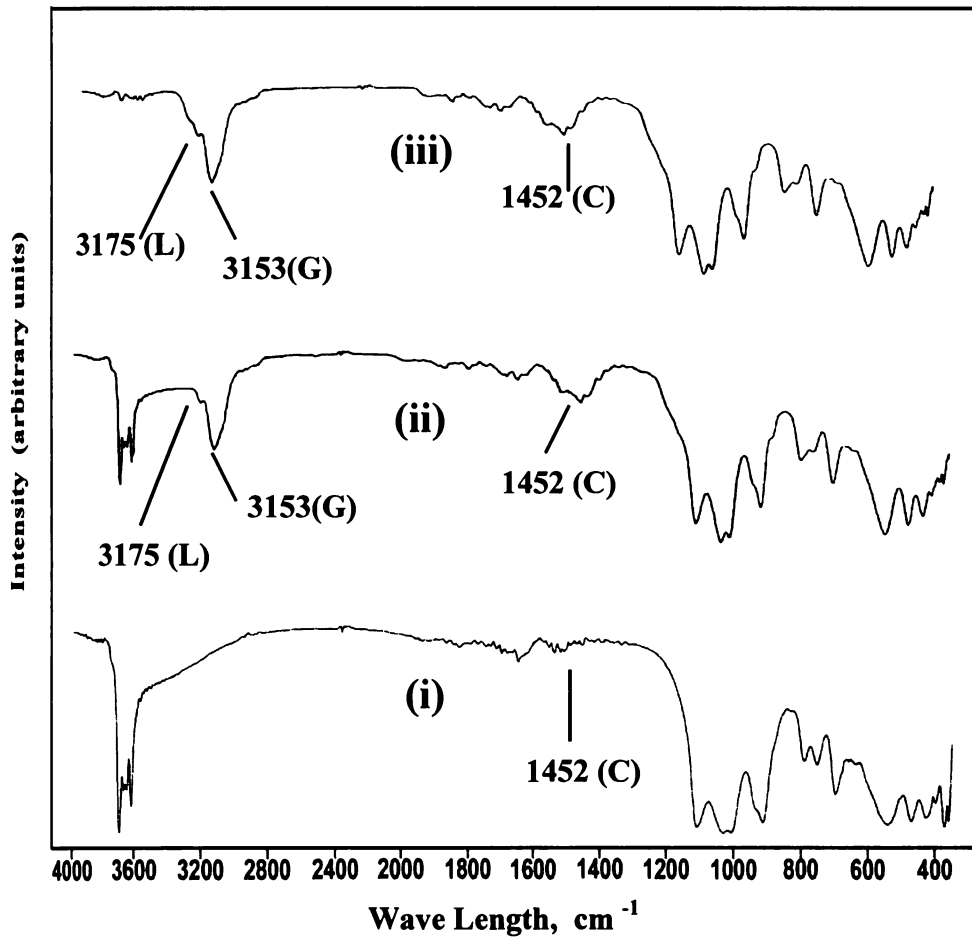
Figure 5.3.7a IR spectra of (i) ROM (ii) IM1 and (iii) IM2 samples of Pali kaolin
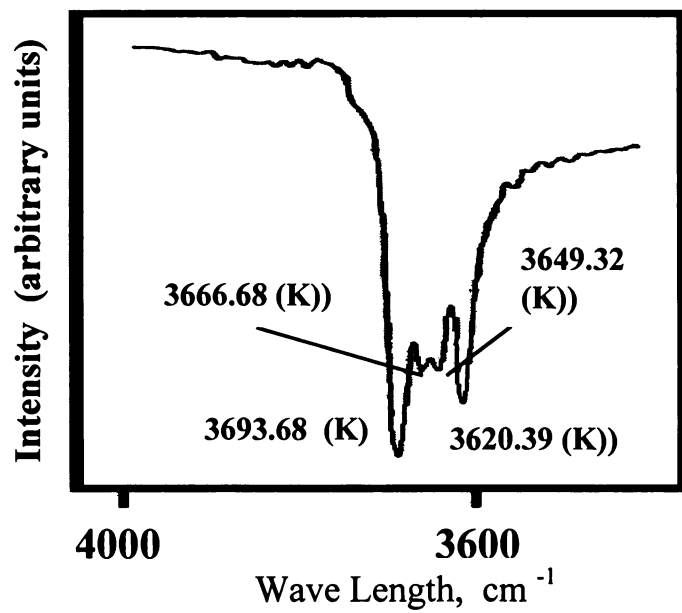
Figure 5.3.7b IR spectrum of   ROM (3700 – 3600 cm⁻¹

281
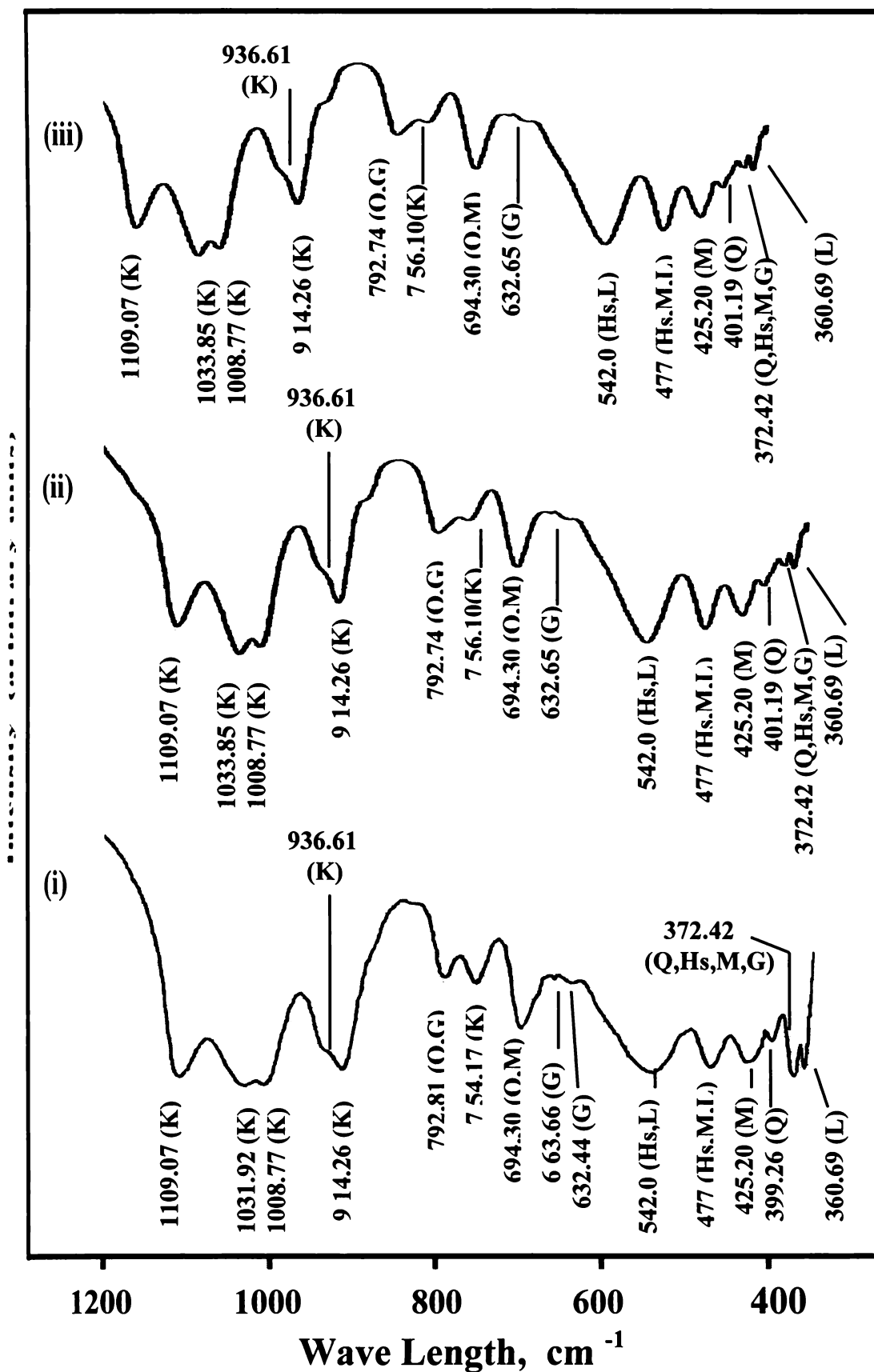
Figure 5.3.7c IR spectra of (a) ROM (b) IM1 (c) and (c) IM2 samples
(1200 - 350 cm⁻¹)
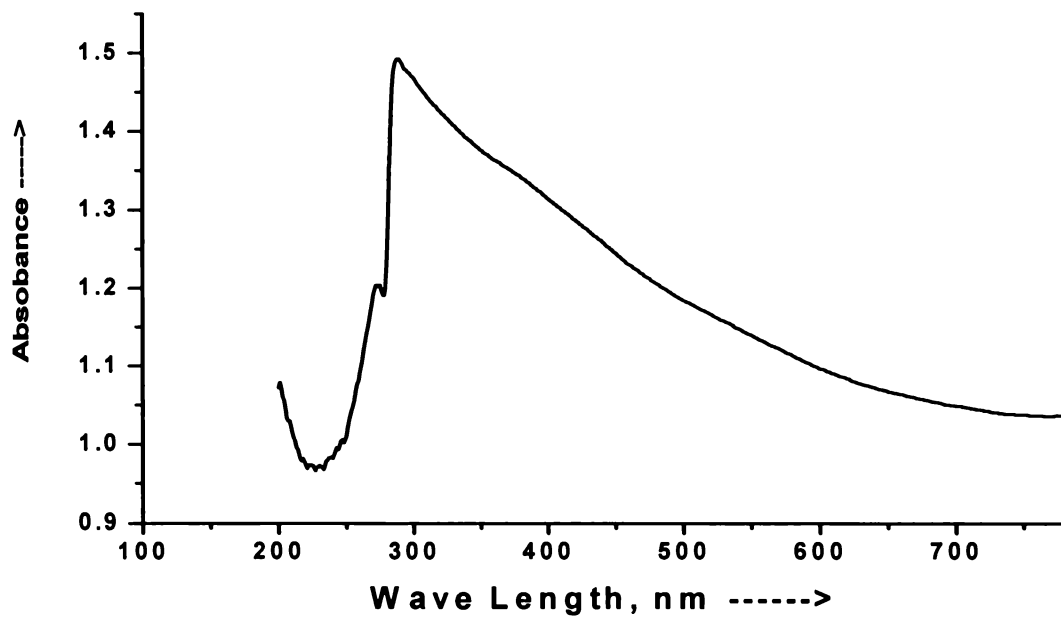
Figure 5.4.1 UV-Visible Spectra of IM2 - Kasargod 1 kaolin
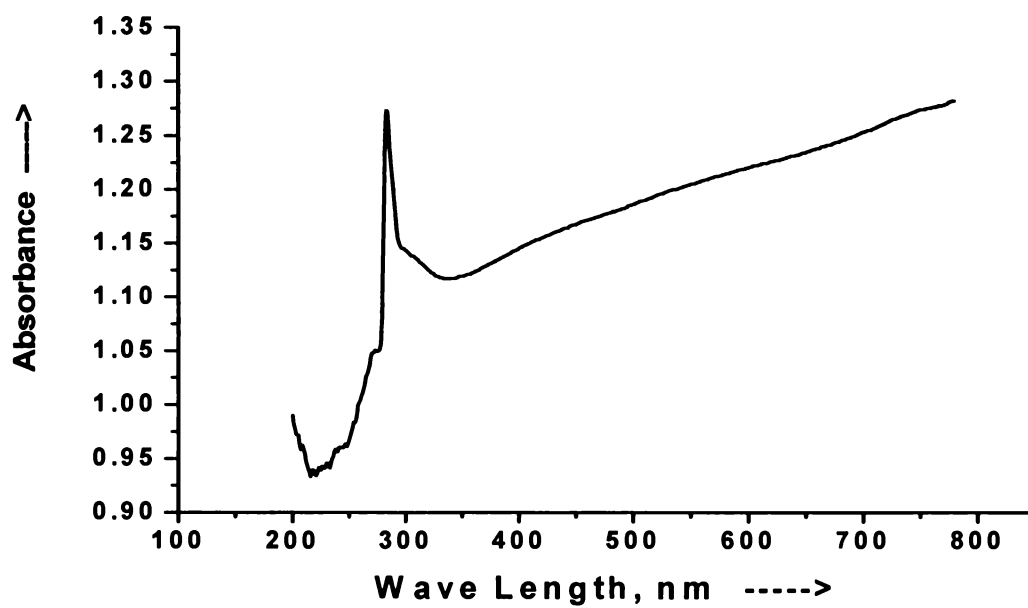
Figure 5.4.2 UV-Visible spectra of IM2 - Kasargod 2 kaolin

283
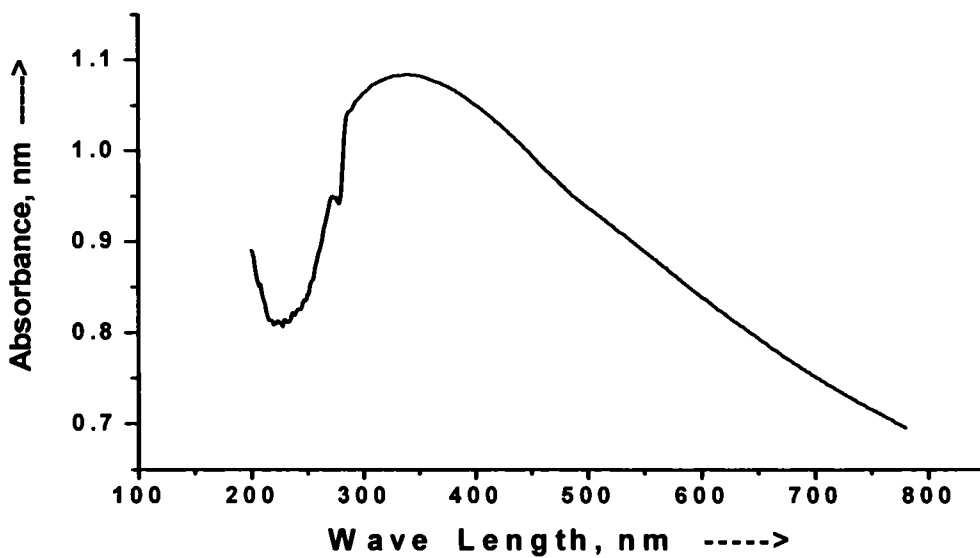
Figure 5.4.3 UV-Visible spectra of IM2 - Trivandrum kaolin
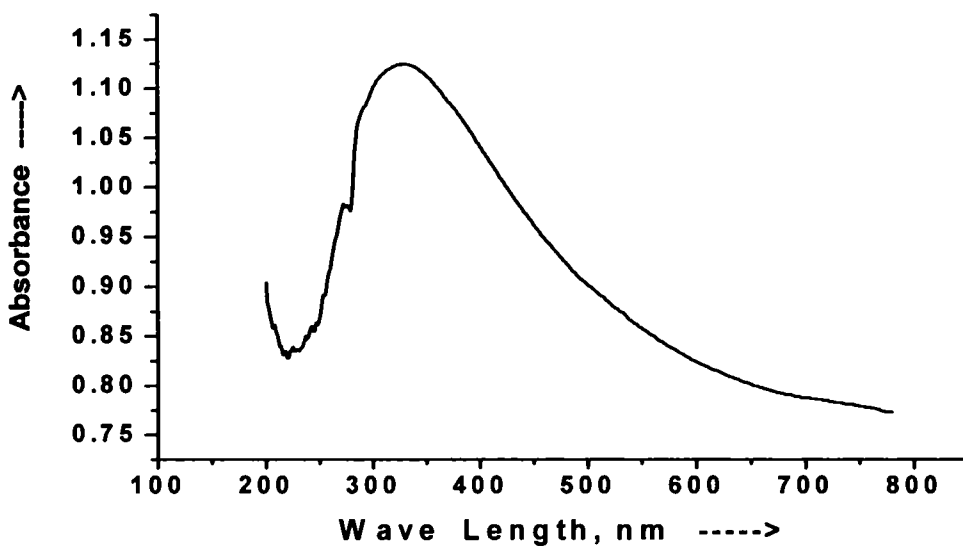
Figure 5.4.4 UV-Visible spectra of IM2 - Kutch kaolin
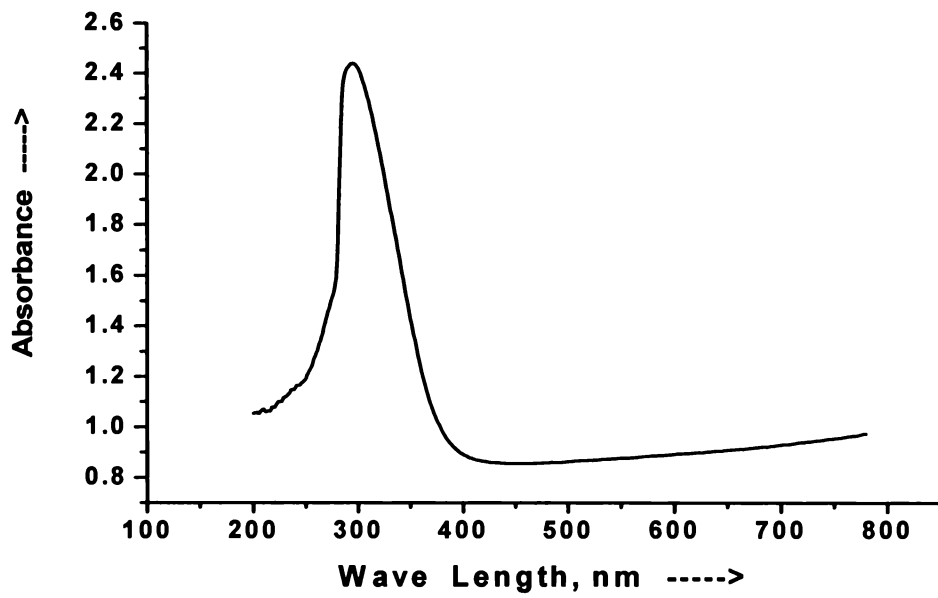
Figure 5.4.5 UV-Visible spectra of IM2 - Koraput   kaolin
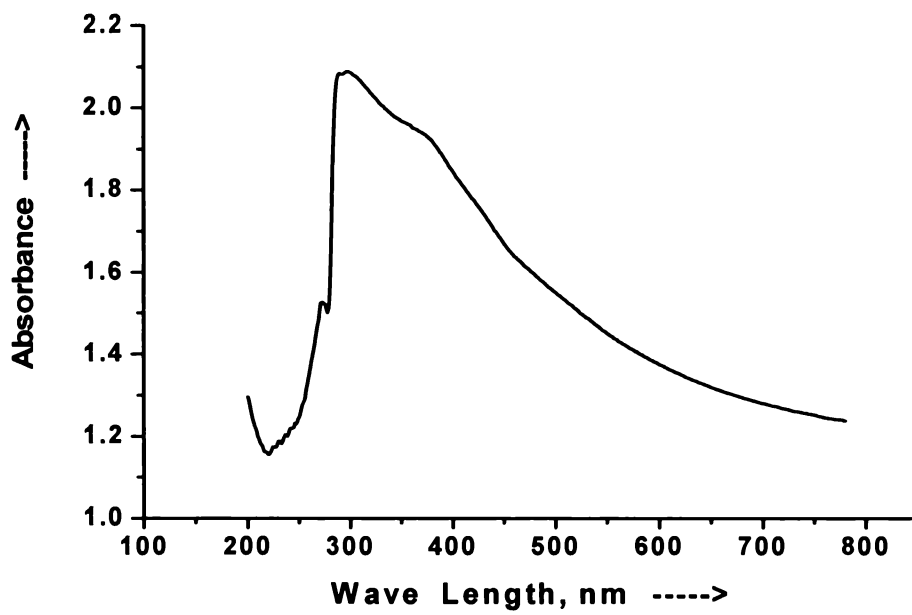
Figure 5.4.6 UV-Visible spectra of IM2 - Bankura kaolin
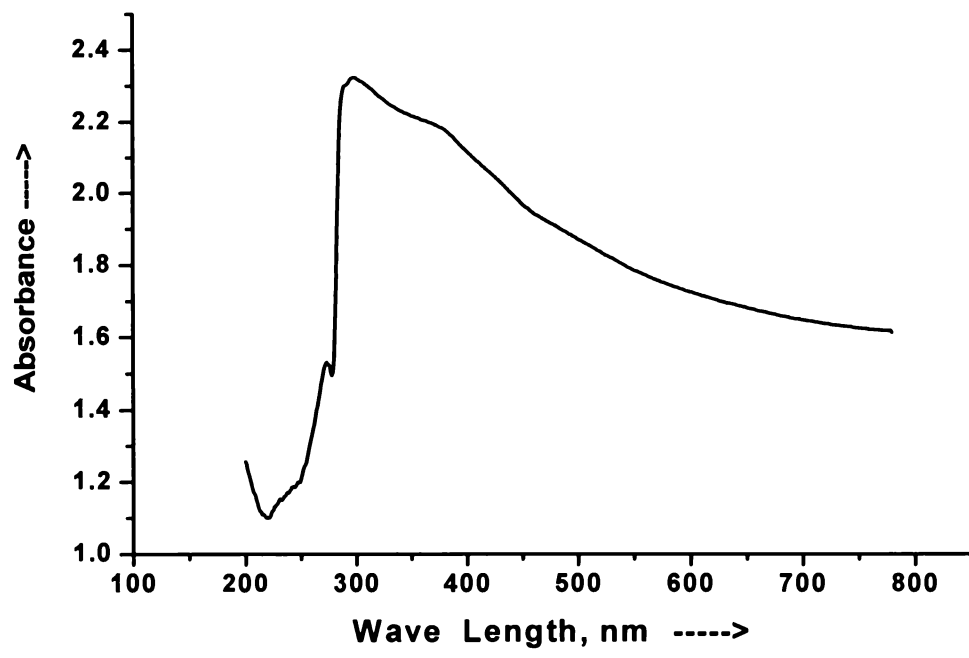
Figure 5.4.7 UV-Visible spectra of IM2 - Pali kaolin
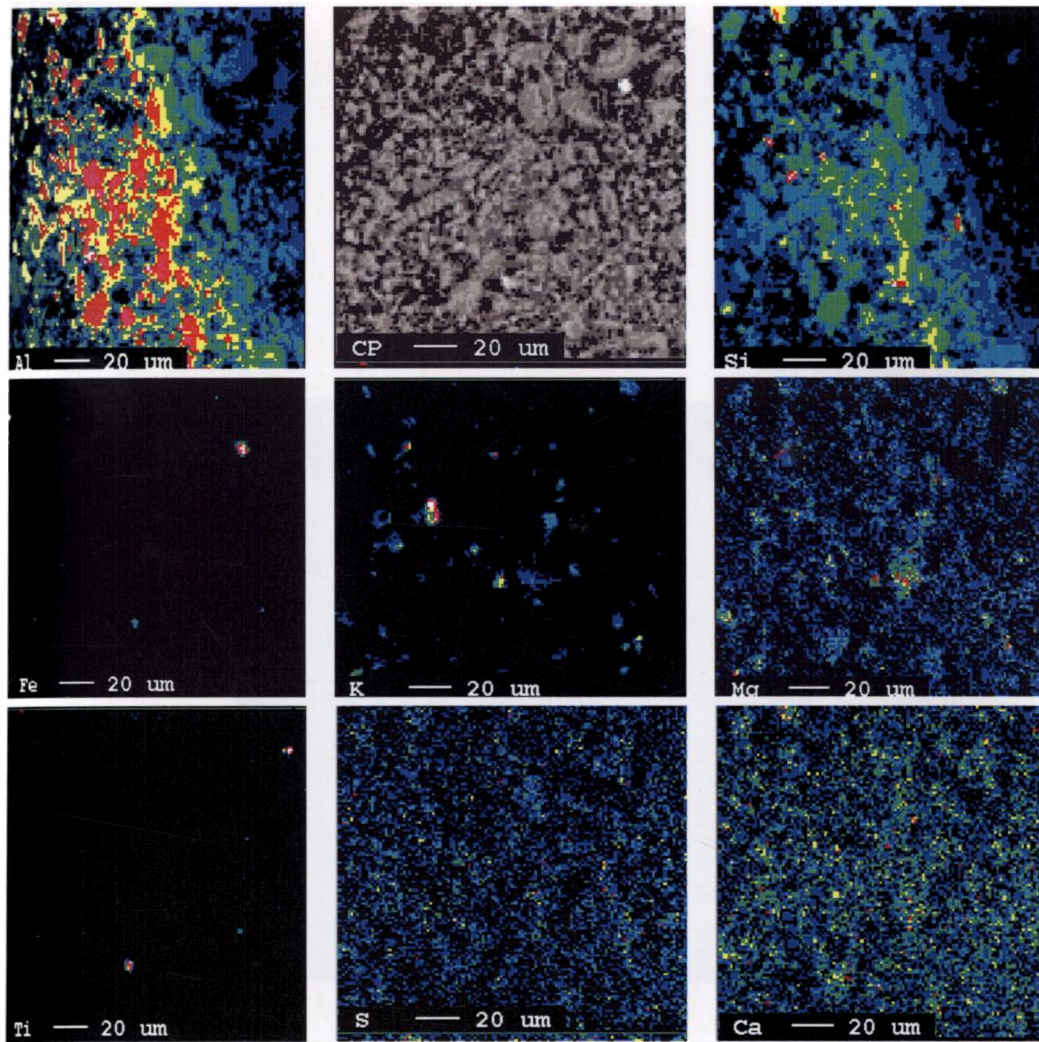
Elements→ in wt%	Al₂O₃	SiO₂	K₂O	FeO	TiO₂	MgO	CaO	SO₃
	42.80	50.71	2.27	1.59	0.53	0.51	0.63	0.92

Figure 5.5.1a Electron micrograph of ROM Kasargod 1 kaolin
(CP - Back scattered image)

287
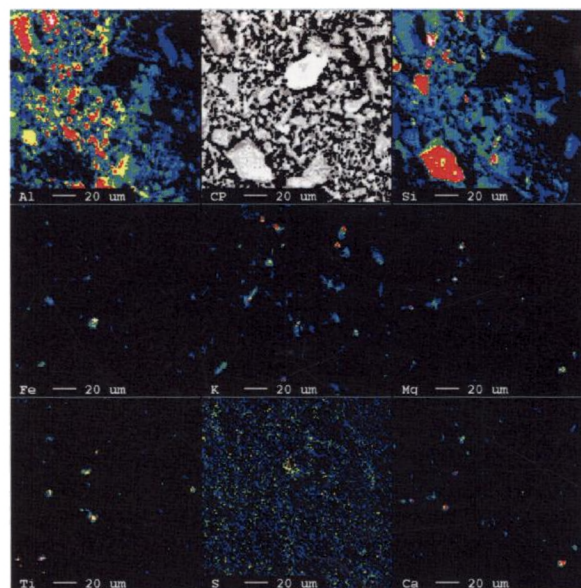
Elements→ In wt%	Al₂O₃	SiO₂	K₂O	FeO	TiO₂	MgO	CaO	SO₃
	34.83	55.12	1.61	2.75	2.26	0.84	1.62	0.98

. **Figure 5.5.1b Electron micrograph of IM1 - Kasargod 1 kaolin**
(CP - Back scattered image)

288
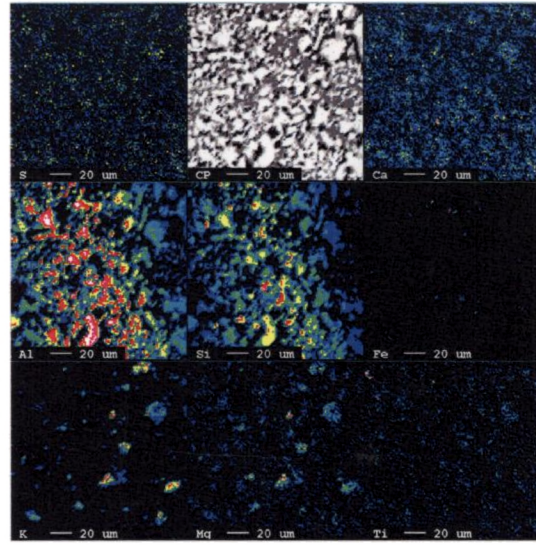
Elements, in wt. % →	Al$_2$O$_3$	SiO$_2$	K$_2$O	FeO	TiO$_2$	MgO	CaO	SO$_3$
	55.63	38.38	3.57	0.87	0.42	0.17	0.43	0.51

Figure 5.5.2a Electron micrograph of ROM Kasargod 2 kaolin
(CP - Back scattered image)
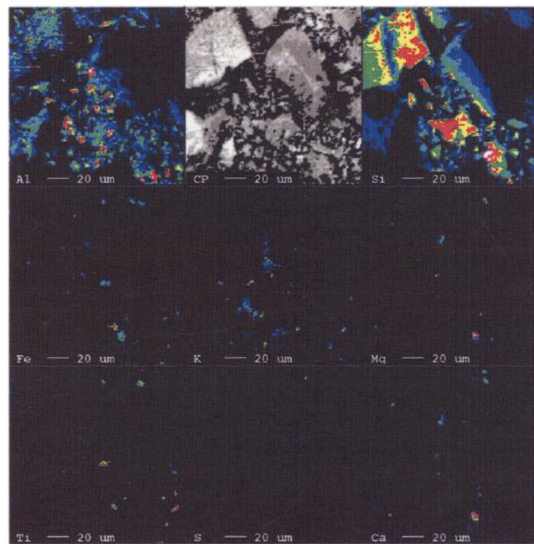
Elements→ In wt%	Al$_2$O$_3$	SiO$_2$	K$_2$O	FeO	TiO$_2$	MgO	CaO	SO$_3$
	20.68	66.21	2.14	5.12	2.50	0.64	1.27	1.44

Figure 5.5.2b Electron micrograph of IM1 - Kasargod 2 kaolin

289
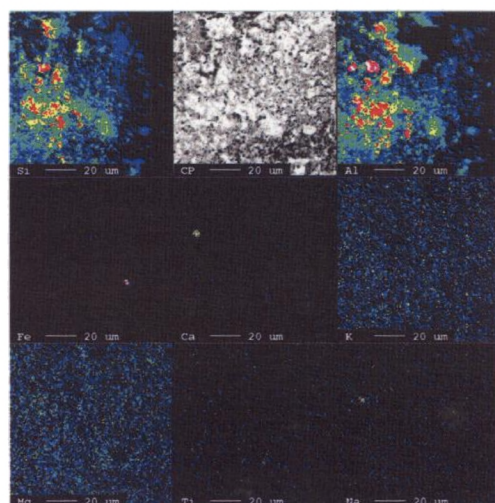
Elements→ In wt%	Al₂O₃	SiO₂	K₂O	FeO	TiO₂	MgO	CaO	Na₂O
	42.533	53.005	0.619	0.973	0.611	0.910	0.791	0.558

Figure 5.5.3a Electron micrograph of ROM Trivandrum kaolin
(CP - Back scattered image)
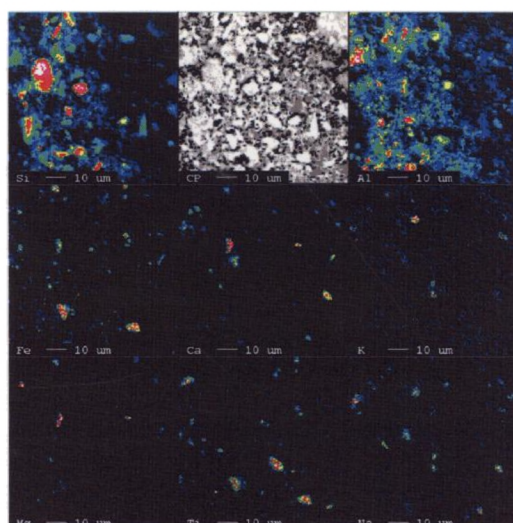
Elements In wt%	Al₂O₃	SiO₂	K₂O	FeO	TiO₂	MgO	CaO	Na₂O
	22.919	62.267	1.378	4.515	4.693	0.849	2.618	0.761

Figure 5.5.3b Electron micrograph of IM1 - Trivandrum kaolin
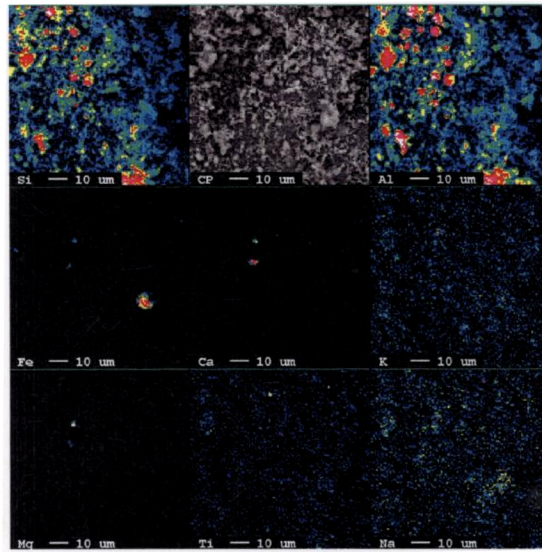
Elements→ in wt%	Al₂O₃	SiO₂	K₂O	FeO	TiO₂	MgO	CaO	Na₂O
	41.061	52.436	1.569	1.221	1.005	0.452	1.153	1.103

Figure 5.5.4a Electron micrograph of ROM Kutch kaolin
(CP - Back scattered image)
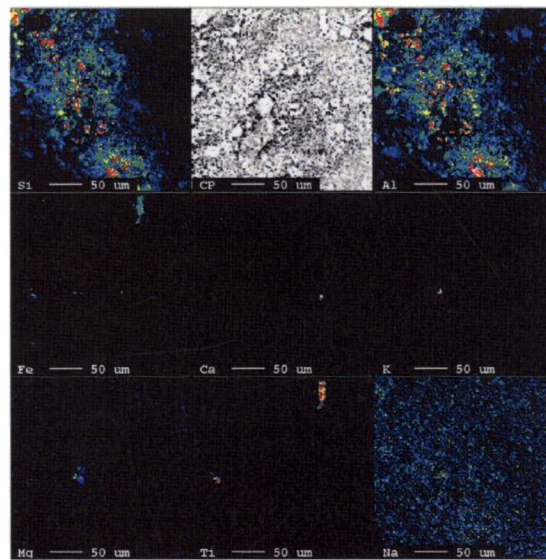
Elements→ In wt%	Al₂O₃	SiO₂	K₂O	FeO	TiO₂	MgO	CaO	Na₂O
	43.679	43.505	1.551	3.531	4.121	0.809	1.721	1.083

Figure 5.5.4b Electron micrograph of IM1 - Kutch kaolin
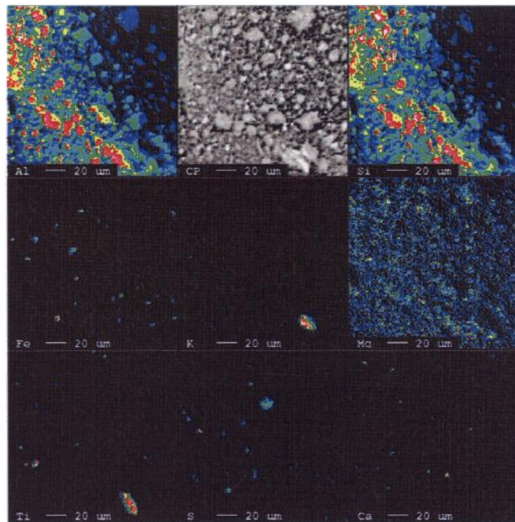
Elements→ In wt%	Al₂O₃	SiO₂	K₂O	FeO	TiO₂	MgO	CaO	SO₃
	43.55	48.03	0.42	2.14	1.77	0.22	0.67	3.21

Figure 5.5.5a Electron micrograph of ROM Koraput kaolin
(CP - Back scattered image)
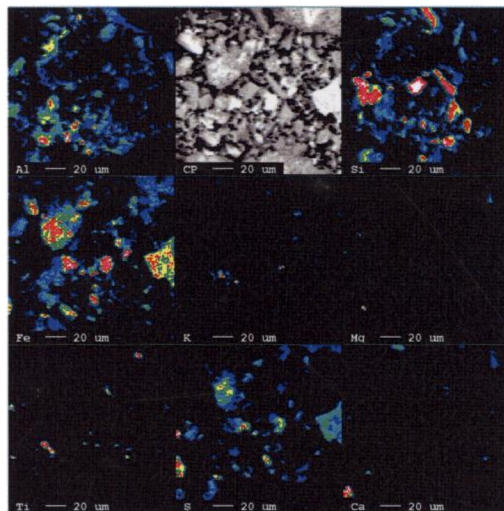
Elements→ In wt%	Al₂O₃	SiO₂	K₂O	FeO	TiO₂	MgO	CaO	SO₃
	12.70	31.60	1.63	14.65	2.84	0.86	1.27	35.03

Figure 5.5.5b Electron micrograph of IM1 - Koraput kaolin

Elements→ In wt%	Al₂O₃	SiO₂	K₂O	FeO	TiO₂	MgO	CaO	SO₃
	22.65	61.75	6.74	4.11	1.46	1.03	1.10	1.17

**Figure 5.5.6a Electron micrograph of ROM Bankura kaolin**
(CP - Back scattered image)

Elements→ In wt%	Al₂O₃	SiO₂	K₂O	FeO	TiO₂	MgO	CaO	SO₃
	14.97	64.76	5.23	8.90	2.37	1.17	1.40	1.22

Figure 5.5.6b Electron micrograph of IM1 - Bankura kaolin

Elements→ In wt%	Al_2O_3	SiO_2	K_2O	FeO	TiO_2	MgO	CaO	SO_3
	22.65	61.75	6.74	4.11	1.46	1.03	1.10	1.17

Figure 5.5.6a Electron micrograph of ROM Bankura kaolin
(CP - Back scattered image)

Elements→ In wt%	Al_2O_3	SiO_2	K_2O	FeO	TiO_2	MgO	CaO	SO_3
	14.97	64.76	5.23	8.90	2.37	1.17	1.40	1.22

Figure 5.5.6b Electron micrograph of IM1 - Bankura kaolin

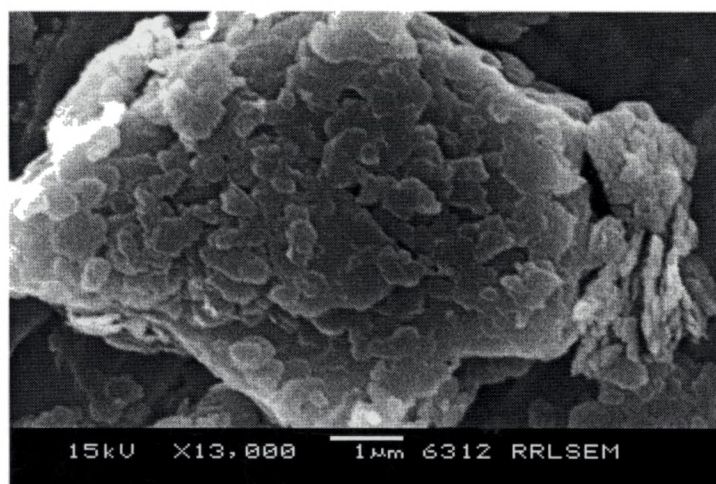| Elements→ In wt%	Al₂O₃	SiO₂	K₂O	FeO	TiO₂	MgO	CaO	SO₃
	39.41	53.20	1.63	1.99	1.48	0.60	1.09	0.60

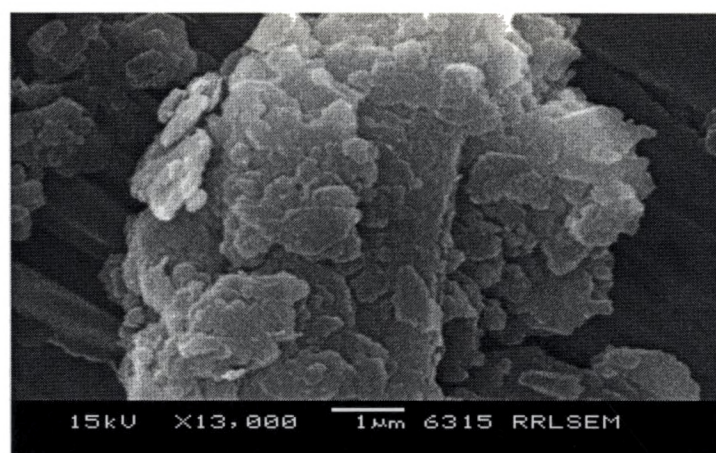**Figure 5.5.7a Electron micrograph of ROM Pali kaolin**
(CP - Back scattered image)
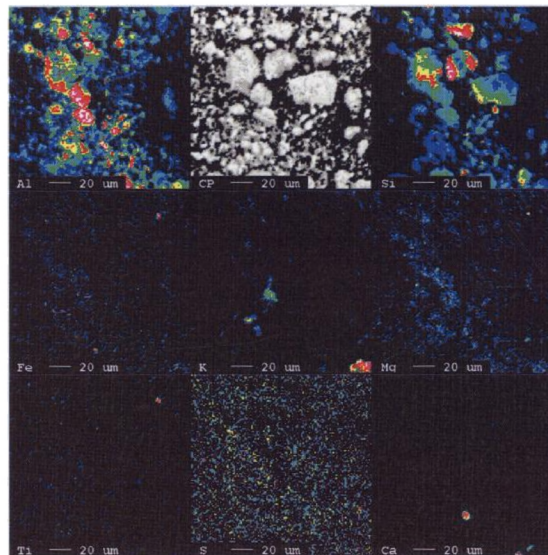
Elements→ In wt%	Al₂O₃	SiO₂	K₂O	FeO	TiO₂	MgO	CaO	SO₃
	35.38	50.62	2.35	2.57	2.09	0.92	4.75	1.33

Figure 5.5.7b Electron micrograph of IM1 - Pali kaolin

(a) ROM sample

(b) SCP1 sample
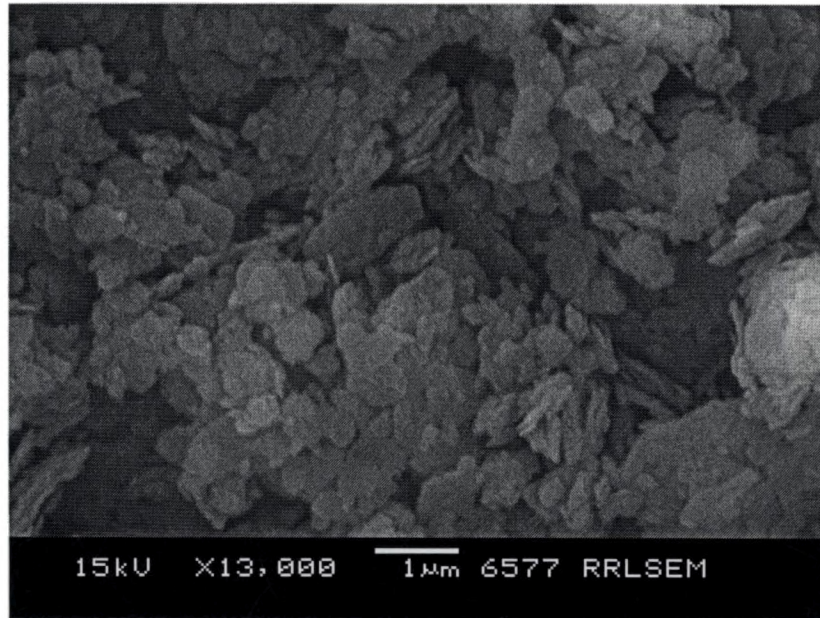
Figures 5.6.1 SEM pictures of Kasargod 1 kaolin
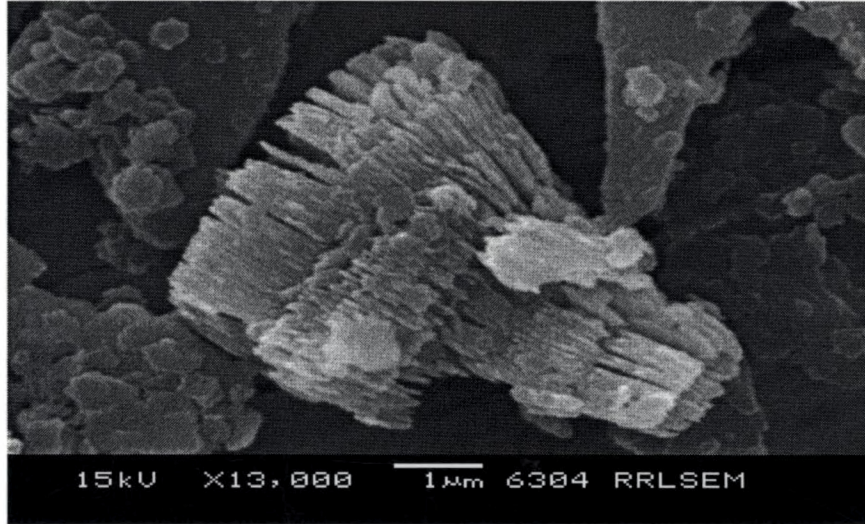
(a) ROM sample
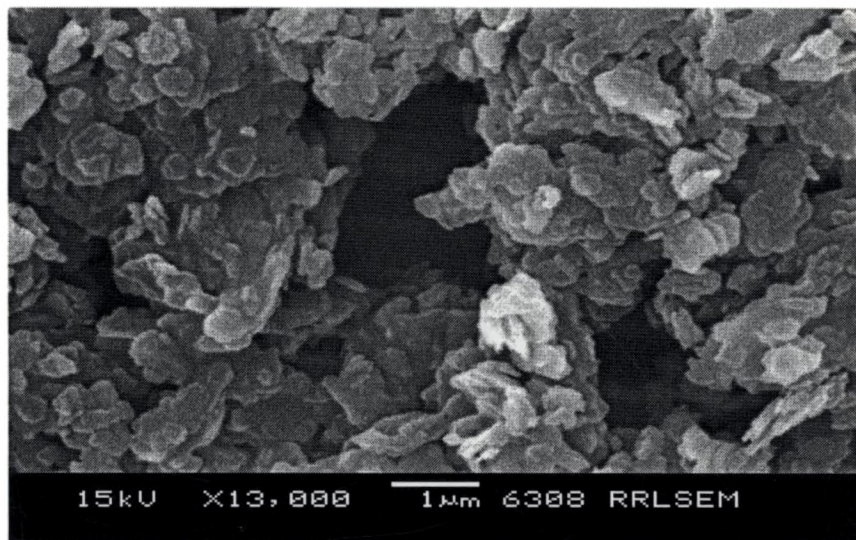
(b) SCP1 sample
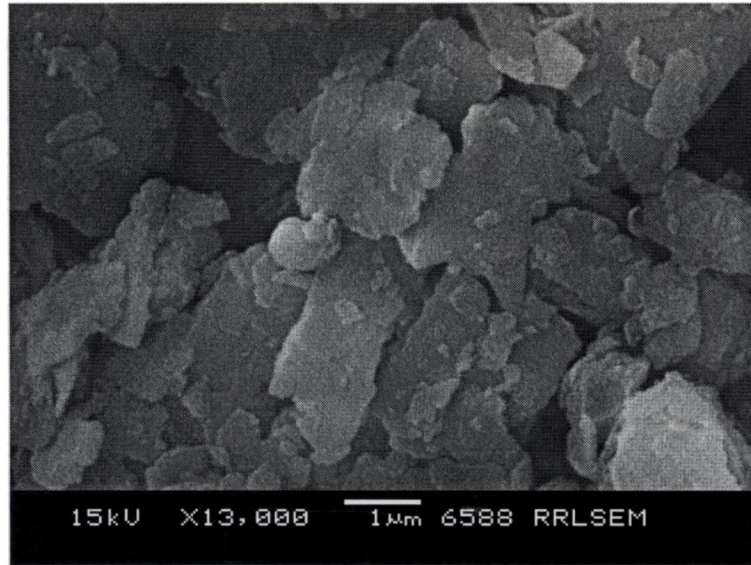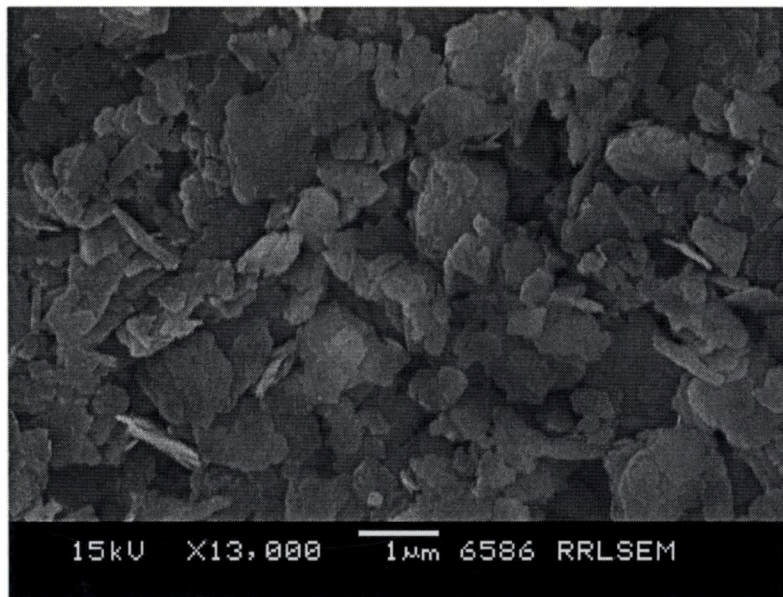
Figures 5.6.2 SEM pictures of Kasargod 2 kaolin

15kU   X13,000   1μm 6577 RRLSEM

(a) ROM sample

15kU   X13,000   1μm 6584 RRLSEM

(b) SCP1 sample
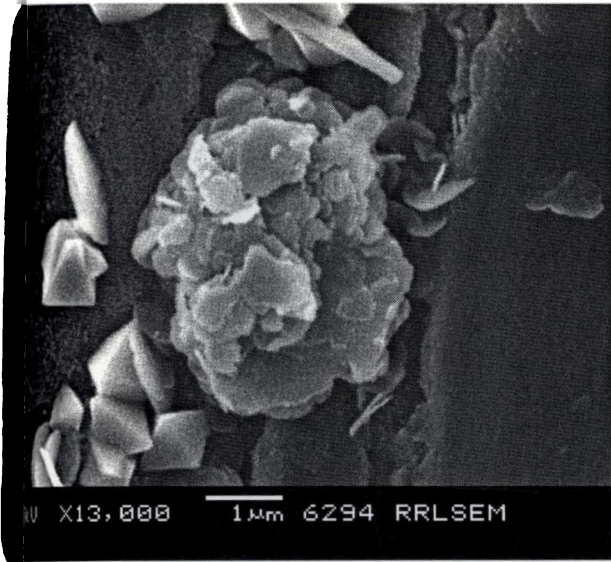
Figures 5.6.3 SEM pictures of Trivandrum kaolin

297

(a) ROM Sample
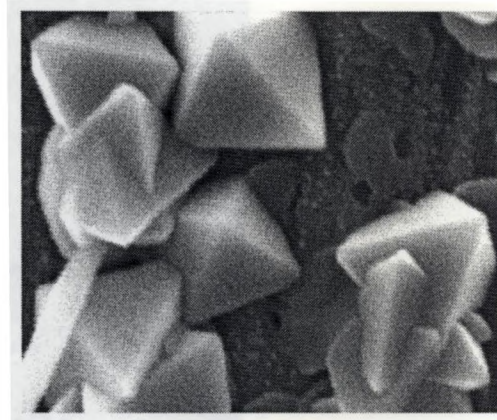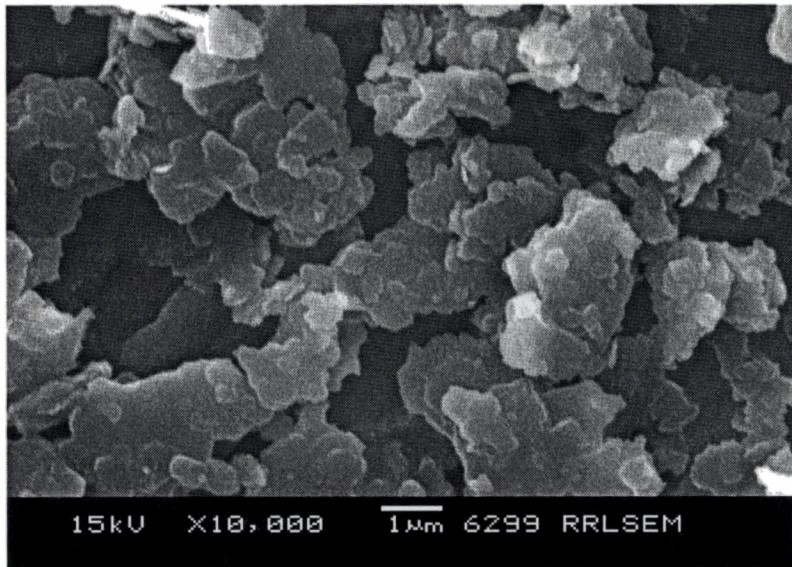

(b) SCP1 Sample

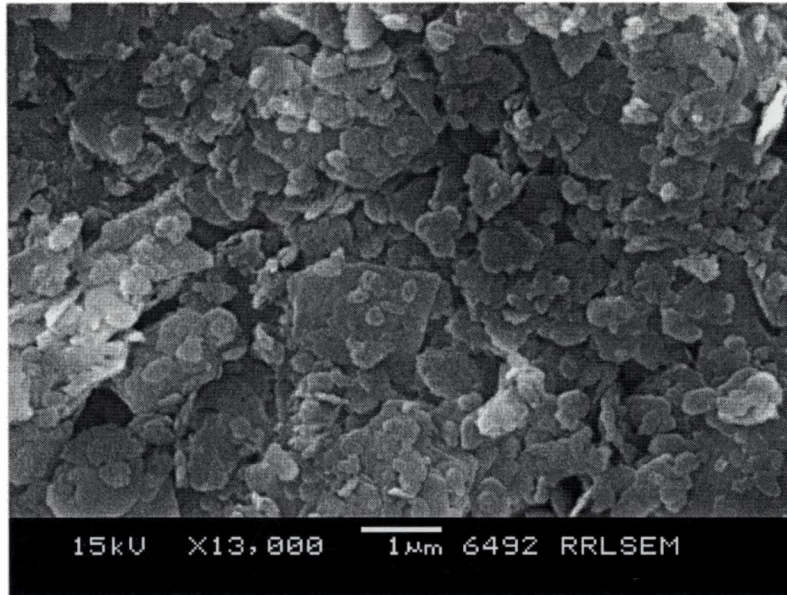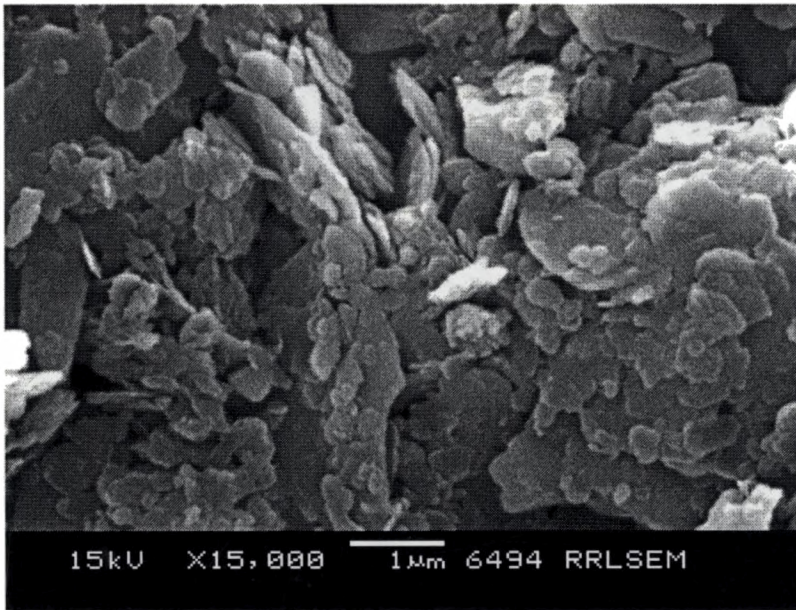**Figures 5.6.4 SEM pictures of Kutch kaolin**

(a) ROM sample

Pyrite particles

(b) SCP1 sample

Figures 5.6.5 SEM pictures of Koraput kaolin

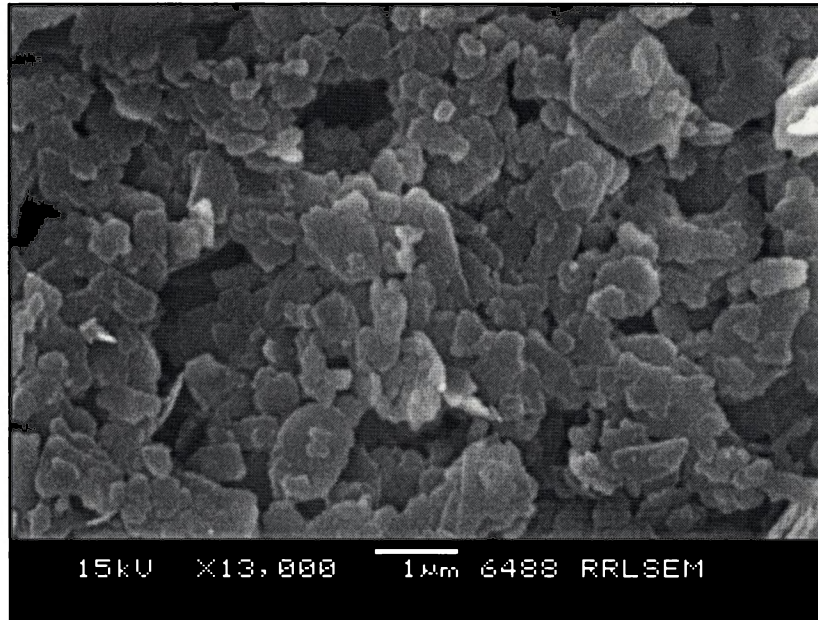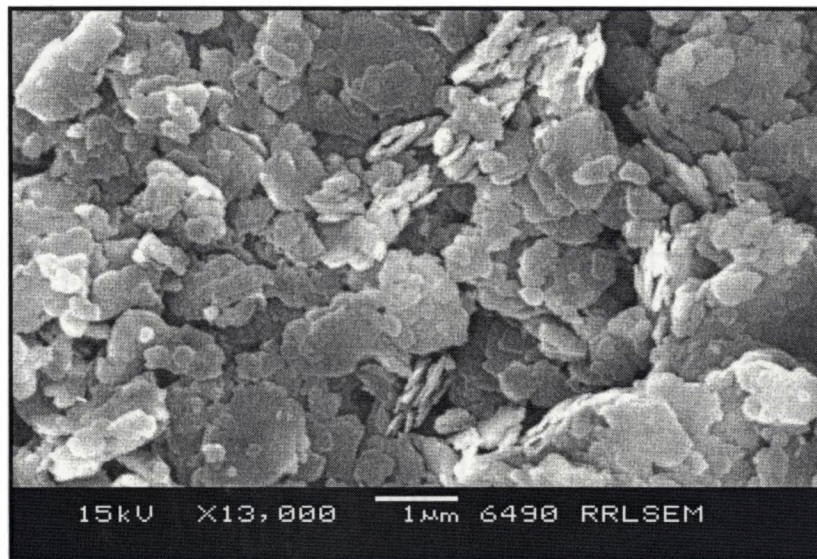(a) ROM Sample

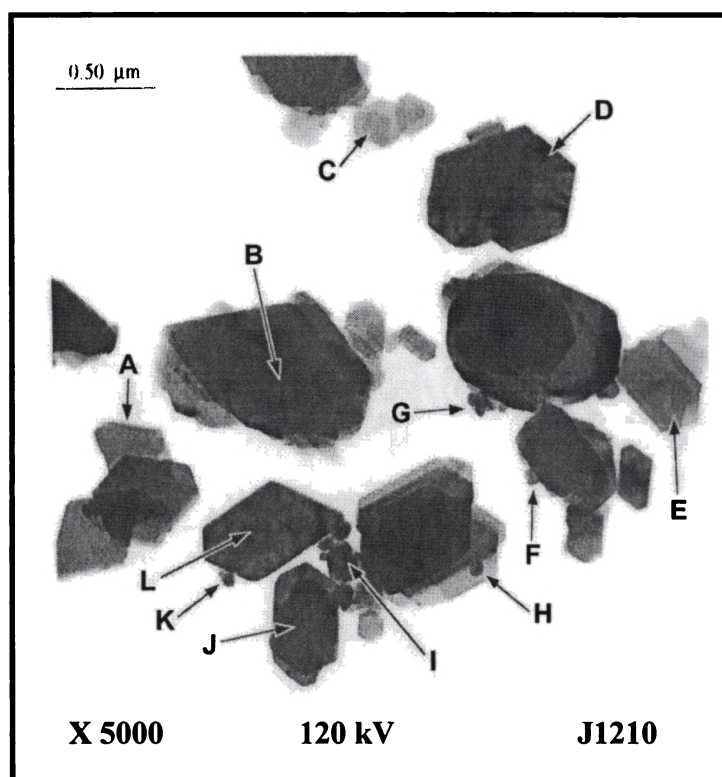(b) SCP1 sample

Figures 5.6.6 SEM pictures of Bankura kaolin

300

15kU X13,000 1μm 6488 RRLSEM

(a) ROM sample

15kV X13,000 1μm 6490 RRLSEM

(b) SCP1 sample

Figures 5.6.7 SEM pictures of Pali kaolin

301

	A	B	C	D	E	F	G	H	I	J	K	L
	K	K	K	K	K	Fe	Ti	Ti	Ti	K	Ti	K
O	54.3	52.8	43.9	55.5	56.5	39.1	34.9	39.3	25.1	58.8	39.2	51.4
Si	22.5	23.4	22.6	22.1	21.4	8.9	0.8	9.2	0.5	23.7	1.0	22.6
Al	22.4	23.1	22.1	21.7	21.6	8.2	0.6	7.5	0.4	16.8	1.7	22.6
Ti	0.0	0.1	0.0	0.1	0.0	3.2	57.3	42.4	71.7	0.1	52.4	2.4
Fe	0.3	0.2	0.4	0.3	0.1	37.7	2.2	1.4	0.8	0.1	2.0	0.3
Mg	0.0	0.0	0.1	0.0	0.0	0.0	0.6	0.0	0.6	0.0	0.5	0.0
Ca	0.0	0.0	0.0	0.0	0.0	1.3	0.4	0.0	0.0	0.1	0.0	0.0
K	0.2	0.1	0.3	0.1	0.2	0.0	0.8	0.1	0.2	0.2	0.5	0.2
Na	0.0	0.0	0.5	0.0	0.0	0.9	1.7	0.0	0.5	0.0	1.7	0.2
S	0.0	0.0	0.0	0.0	0.0	0.0	0.0	0.0	0.1	0.0	0.0	0.1
Cl	0.2	0.3	0.2	0.2	0.2	0.8	0.6	0.2	0.0	0.2	0.8	0.2
P	0.0	0.0	0.0	0.0	0.0	0.0	0.5	0.0	0.1	0.0	0.3	0.0

Figure 5.7.1a   HR TEM-EDS picture of ROM Kutch kaolin

302
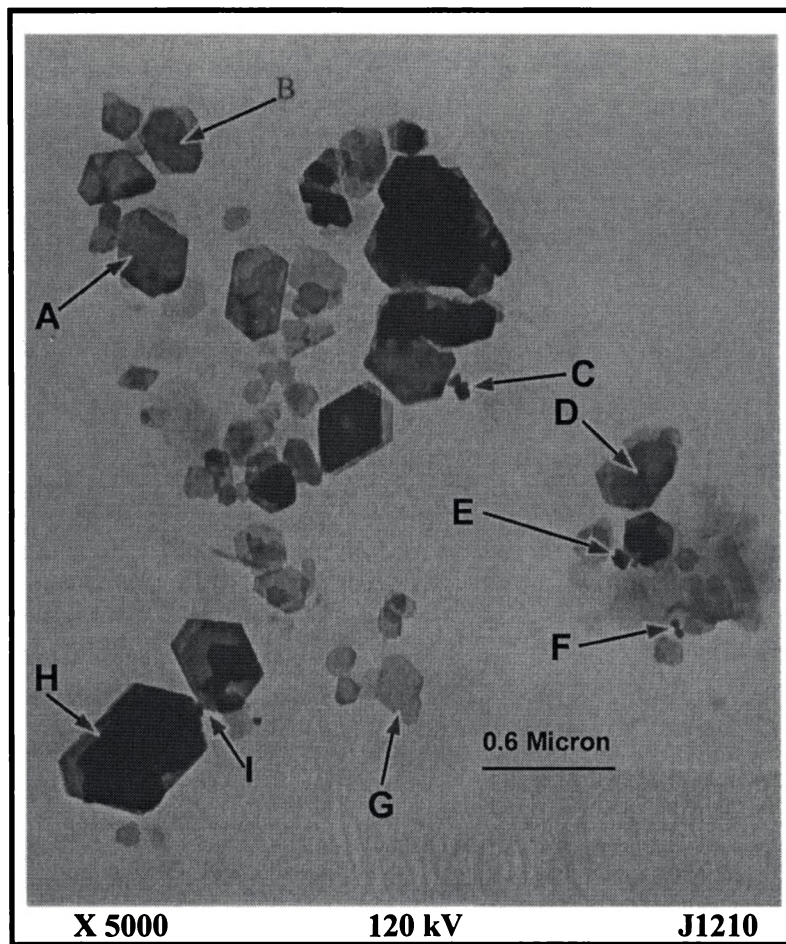
	A	B	C	D	E	F	G	H	I
	K	K	Ti	K	Ti	Ti	K	K	K
O	51.8	52.2	32.4	52.2	29.5	38.3	54.5	52.5	50.9
Si	23.9	23.5	1.0	22.9	0.9	5.4	20.9	23.1	23.9
Al	23.6	23.3	0.3	22.9	0.8	3.9	22.1	23.4	24.1
Ti	0.0	0.0	40.4	0.1	65.3	49.9	0.0	0.0	0.1
Fe	0.4	0.1	24.3	1.2	2.2	1.0	0.5	0.4	0.3
Mg	0.0	0.0	0.0	0.0	0.0	0.0	0.0	0.0	0.0
Ca	0.0	0.1	0.0	0.0	0.0	0.2	0.0	0.1	0.1
K	0.1	0.2	0.0	0.3	0.0	0.0	0.0	0.1	0.3
Na	0.0	0.2	0.4	0.1	0.0	0.5	0.1	0.1	0.0
S	0.1	0.0	0.4	0.0	0.4	0.2	0.0	0.0	0.0
Cl	0.2	0.1	0.4	0.1	0.0	0.7	0.2	0.1	0.1
P	0.1	0.4	0.5	0.2	1.0	0.0	0.7	0.2	0.3

Figure 5.7.1b HR TEM-EDS picture of SCP1 of Kutch kaolin

303
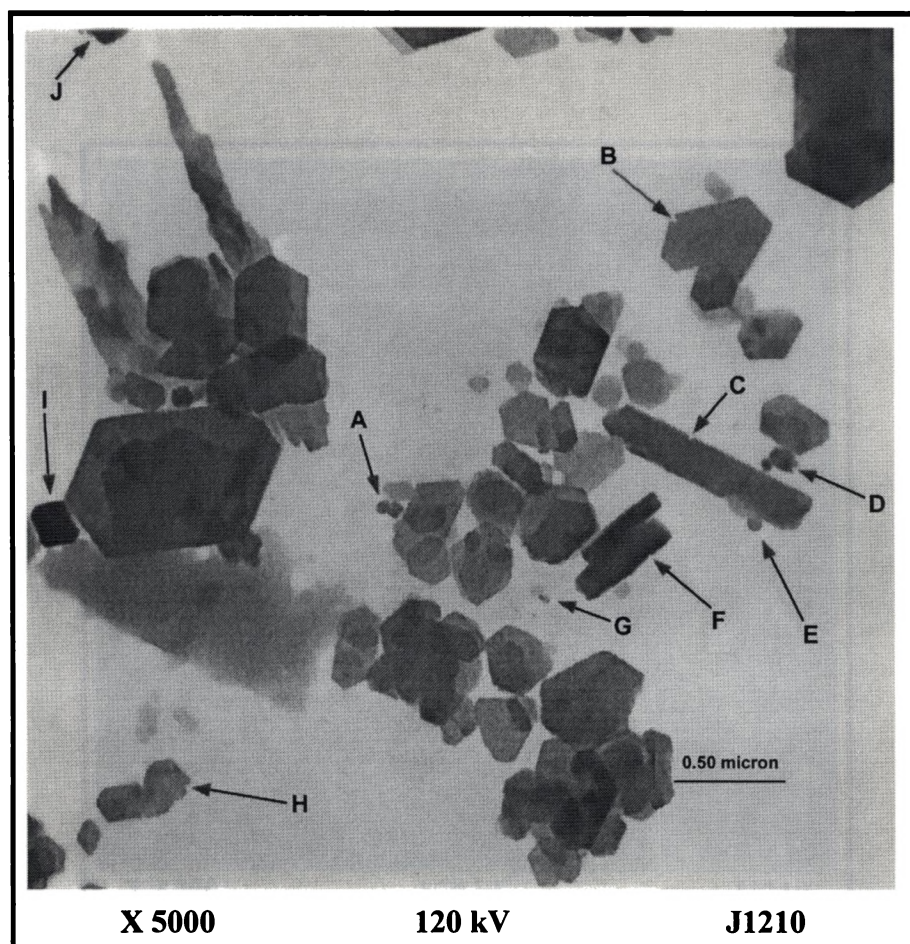
	A	B	C	D	E	F	G	H	I	J
	Ti	K	K	Ti	Ti	K	Ti	K	Ti	Ti
O	41.8	50.9	50.8	36.7	34.5	49.9	37.8	50.9	40.1	50.9
Si	7.5	24.9	24.9	1.0	1.7	25.9	9.3	24.9	0.6	1.8
Al	5.7	23.5	23.0	1.0	0.9	23.4	1.2	21.5	1.2	2.0
Ti	39.0	0.0	0.0	57.4	55.5	0.0	22.6	0.0	53.2	55.6
Fe	2.1	0.0	0.1	1.7	4.0	0.1	5.9	0.4	1.9	1.6
Mg	0.2	0.1	0.0	0.0	0.0	0.0	1.2	0.4	0.6	0.1
Ca	0.2	0.0	0.2	0.4	0.0	0.0	0.7	0.0	0.1	0.0
K	1.1	0.1	0.4	0.2	0.1	0.1	4.3	0.2	0.0	0.0
Na	1.4	0.0	0.3	1.0	1.9	0.2	7.5	0.2	0.7	0.5
S	0.3	0.0	0.0	0.0	0.6	0.1	1.3	0.8	0.2	0.0
Cl	0.8	0.2	0.5	0.3	0.9	0.0	2.8	0.4	0.1	0.0
P	0.7	0.2	0.0	0.2	0.0	0.0	1.1	0.6	0.5	0.4

Figure 5.7.1c   HR TEM-EDS picture of IM1 of Kutch kaolin

304
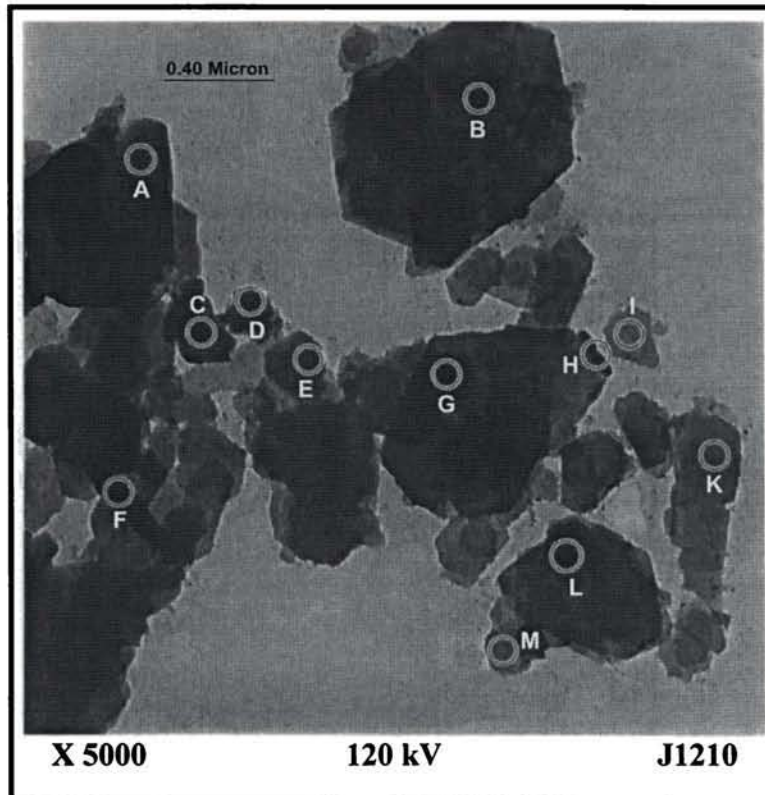
	A	B	C	D	E	F	G	H	I	K	L	M
O	65.91	65.29	64.22	65.70	66.65	66.15	64.36	64.77	68.70	66.36	64.57	61.78
Si	16.61	17.57	16.70	18.80	17.58	15.27	17.85	18.15	18.58	18.29	17.48	13.50
Al	16.70	17.26	15.51	15.44	15.77	15.40	17.39	16.78	16.52	14.33	17.07	13.07
Fe	0.11	0.12	2.69	0.22	0.51	0.48	0.11	0.11	0.44	0.28	0.20	4.72
S	0.01	0.04	0.25	0.02	0.17	1.21	0.03	0.00	0.09	0.04	0.07	3.38
Ti	0.06	0.06	0.00	0.00	0.00	0.00	0.00	0.08	0.00	0.02	0.00	0.04
Na	0.39	0.00	0.27	0.00	0.00	0.70	0.17	0.08	0.00	0.39	0.24	2.24
K	0.07	0.06	0.20	0.07	0.08	0.39	0.03	0.23	0.27	0.05	0.19	0.43
Mg	0.08	0.02	0.00	0.04	0.00	0.00	0.00	0.00	0.00	0.07	0.01	0.00
Ca	0.04	0.00	0.01	0.08	0.03	0.62	0.04	0.00	0.02	0.10	0.04	0.10
Cl	0.03	0.19	0.26	0.15	0.33	0.21	0.17	0.28	0.22	0.25	0.10	0.58
P	0.00	0.00	0.10	0.29	0.00	0.00	0.15	0.01	0.00	0.09	0.18	0.01

Figure 5.7.2a   HR TEM-EDS picture of ROM Koraput kaolin

305
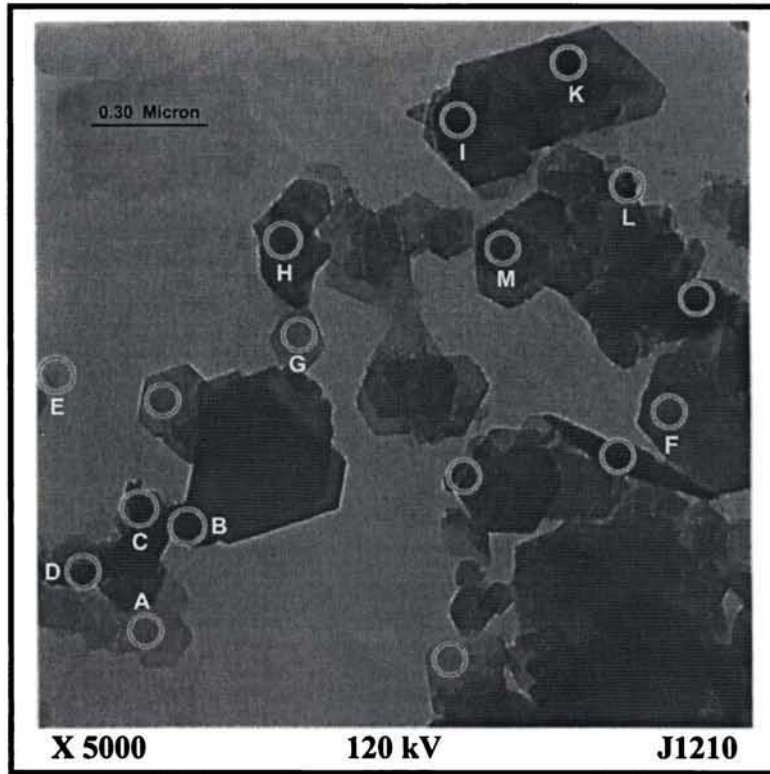
	A	B	C	D	E	F	G	H	I	K	L	M
O	63.45	62.92	64.13	64.92	78.42	67.40	65.69	64.86	64.57	65.79	64.88	65.32
Si	18.08	13.90	16.65	16.19	11.97	16.64	15.92	18.04	17.67	17.46	15.15	17.41
Al	16.19	13.30	16.34	15.63	5.36	15.26	14.94	16.12	16.40	16.16	12.67	16.20
Fe	0.59	3.88	1.08	1.01	0.31	0.52	0.37	0.25	0.32	0.20	2.66	0.36
S	0.52	3.89	0.80	0.73	0.00	0.62	1.01	0.40	0.29	0.17	1.84	0.17
Ti	0.00	0.02	0.00	0.00	0.00	0.00	0.00	0.02	0.00	0.00	0.00	0.04
Na	0.63	1.79	0.59	0.99	1.16	0.00	1.22	0.25	0.36	0.25	1.58	0.31
K	0.22	0.21	0.24	0.33	2.56	0.20	0.44	0.07	0.11	0.09	0.42	0.18
Mg	0.13	0.00	0.00	0.00	0.00	0.11	0.13	0.00	0.01	0.00	0.00	0.00
Ca	0.00	0.05	0.00	0.007	0.40	0.00	0.00	0.00	0.00	0.00	0.03	0.00
Cl	0.00	0.32	0.16	0.19	0.84	0.23	0.15	0.18	0.11	0.01	0.35	0.04
P	0.23	0.09	0.17	0.00	0.00	0.15	0.16	0.00	0.19	0.00	0.55	0.00

Figure 5.7.2b HR TEM-EDS picture of SCP1 of Koraput kaolin

306
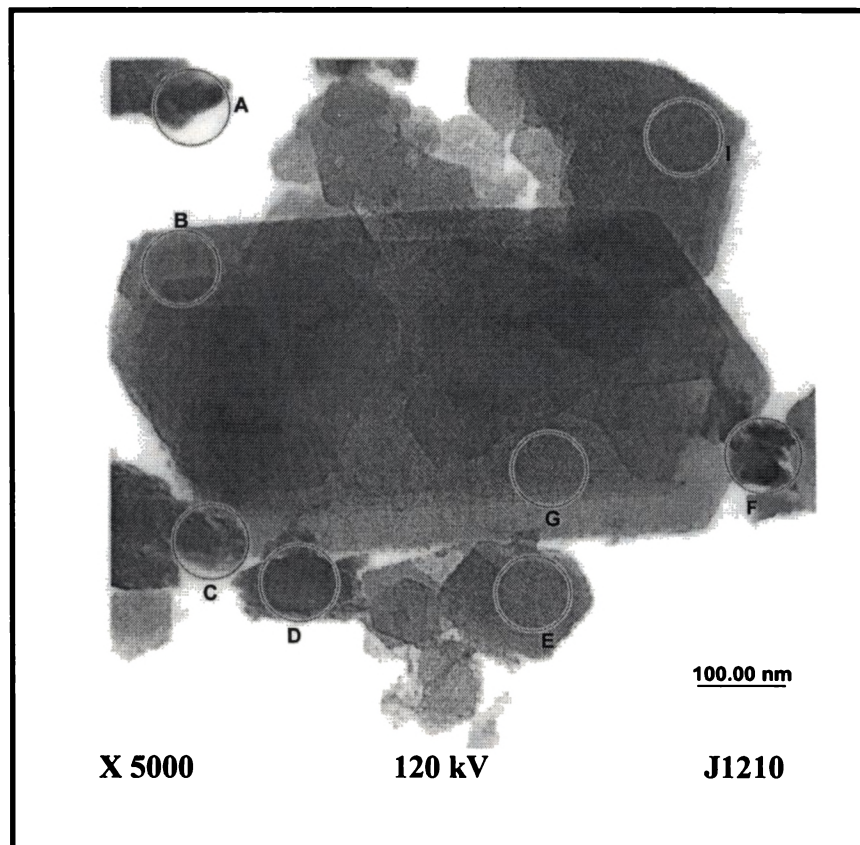
Element	A	B	C	D	E	F	G
O	64.96	65.78	63.70	54.73	63.85	64.70	27.02
Si	1.78	18.16	19.05	16.78	18.53	18.11	3.59
Al	2.53	16.46	16.64	15.19	17.21	17.45	4.80
Fe	15.90	0.31	0.54	4.67	0.33	0.29	21.34
S	9.53	0.00	0.00	7.37	0.05	0.03	40.57
Ti	0.01	0.03	0.00	0.00	0.02	0.00	0.43
Na	4.46	0.00	0.06	0.26	0.00	0.00	0.82
K	0.64	0.05	0.13	0.26	0.24	0.15	0.91
Mg	0.10	0.00	0.00	0.10	0.00	0.00	0.00
Ca	0.07	0.00	0.00	0.05	0.07	0.00	0.00
Cl	0.11	0.03	0.14	0.32	0.00	0.21	1.39
P	0.22	0.00	0.00	0.27	0.16	0.00	0.00

Figure 5.7.2c   HR TEM-EDS picture of IM1 of Koraput kaolin

307
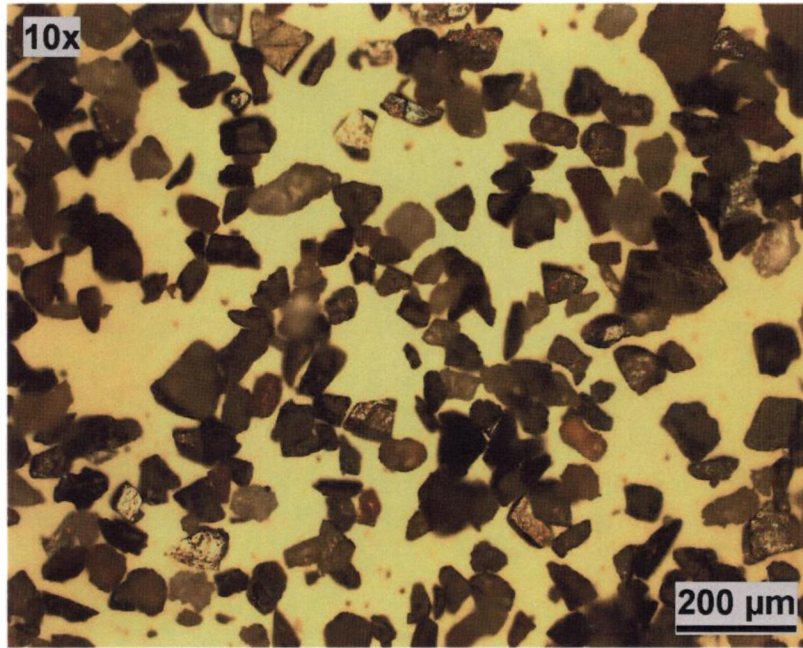
IM1 Sample

IM2 Sample

Figure 5.8.1 Optical micrographs of impurity concentrates from Kasargod 1 kaolin
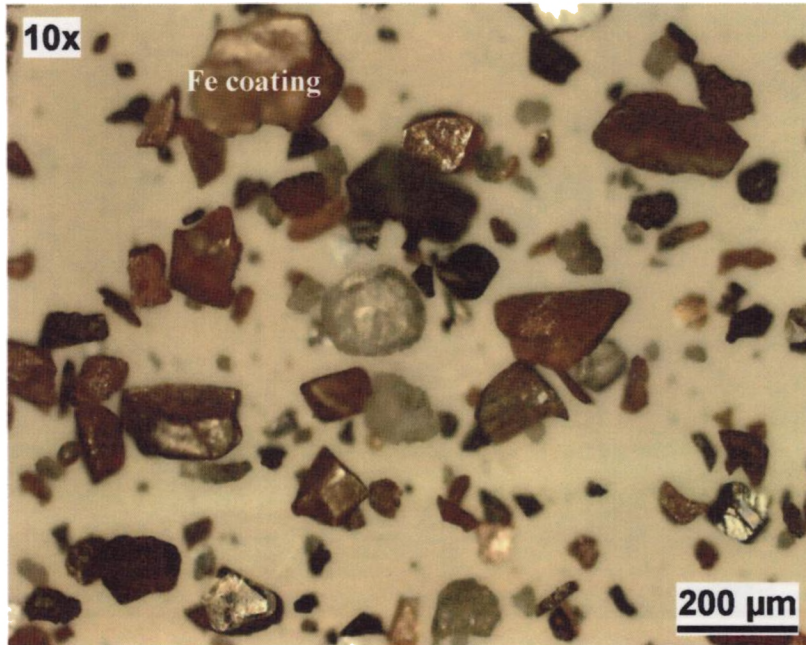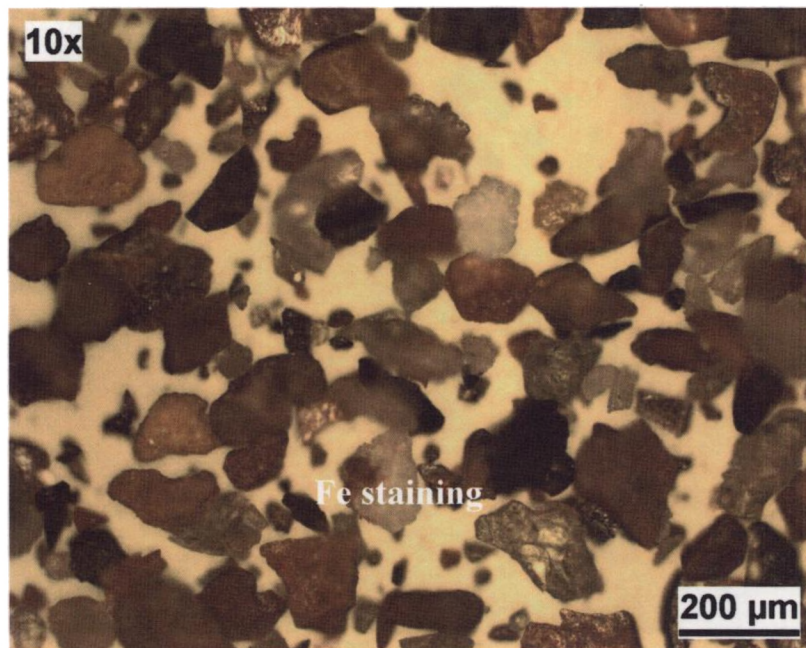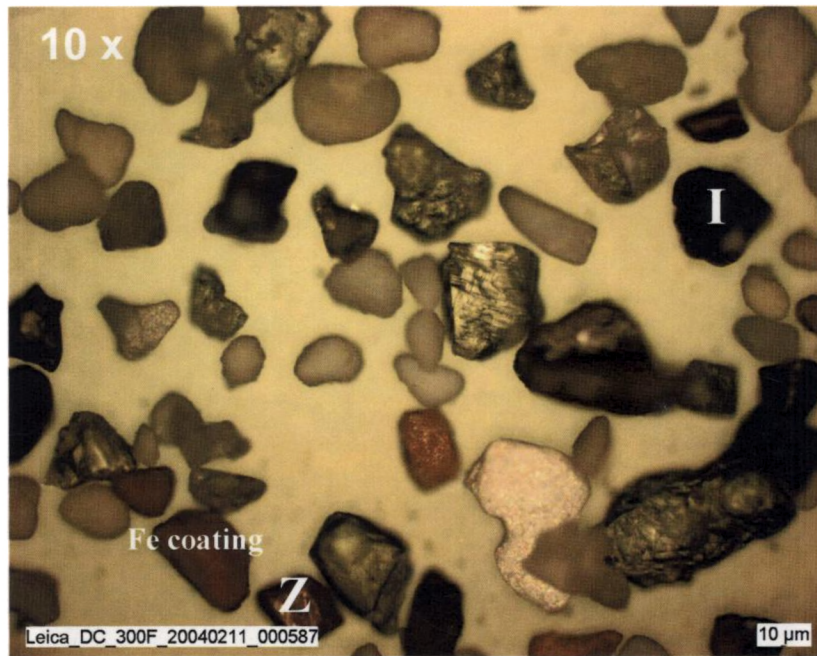
IM1 Sample

IM2 Sample

**Figure 5.8.2 Optical micrographs of impurity concentrates
from Kasargod 2 kaolin**

IM1 Sample

IM2 Sample

Figure 5.8.3 Optical micrographs of impurity concentrates from Trivandrum kaolin

310

IM1 Sample

IM2 Sample

**Figure 5.8.4 Optical micrographs of impurity concentrates
from Kutch kaolin**

311

IM1 Sample

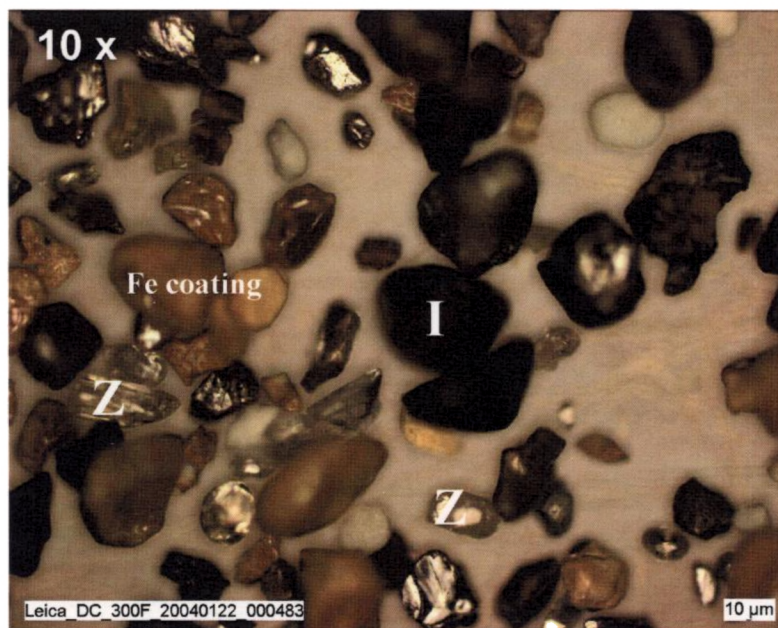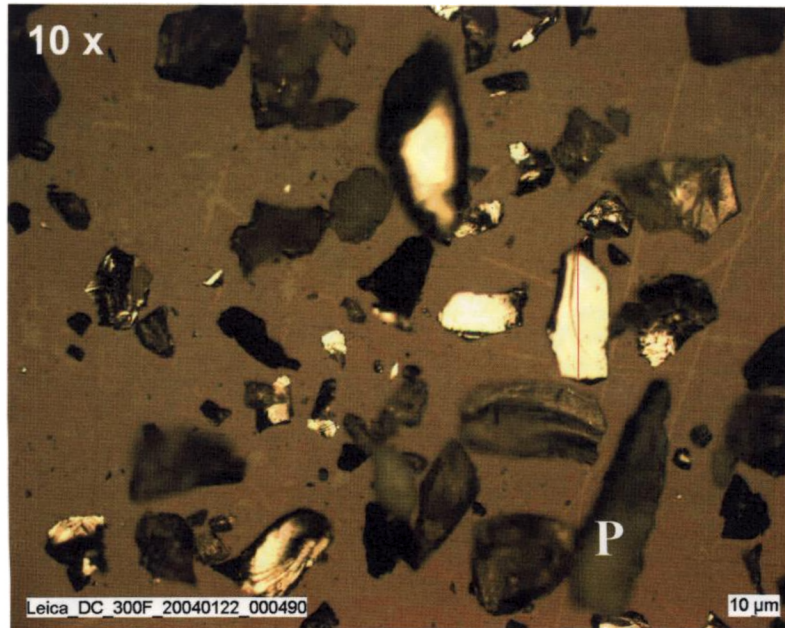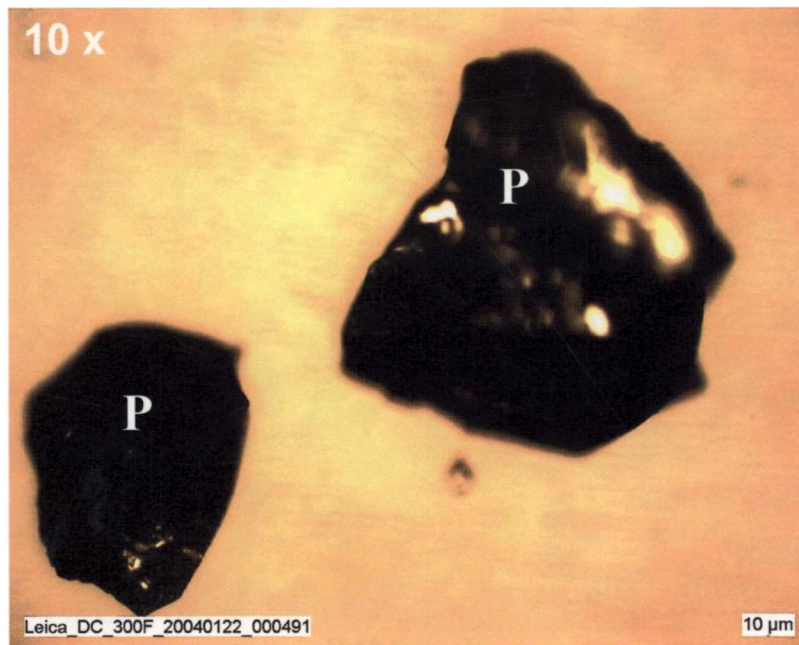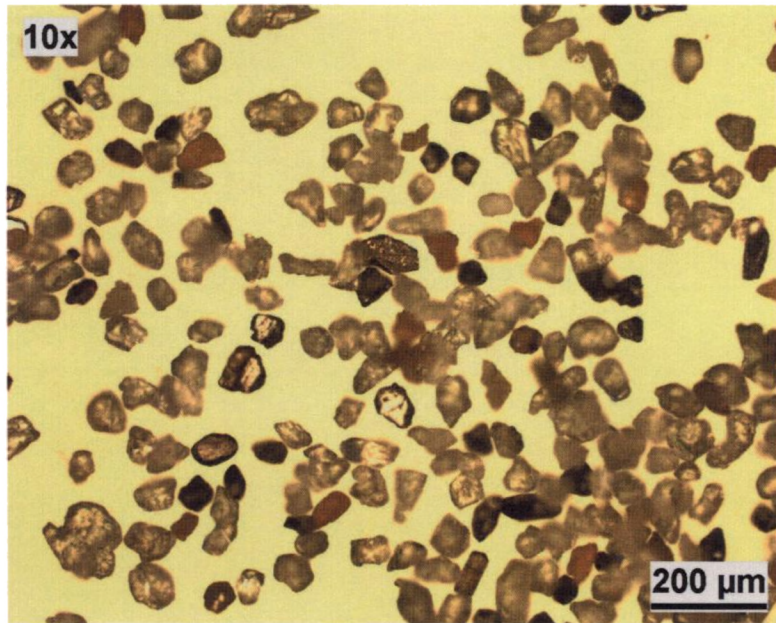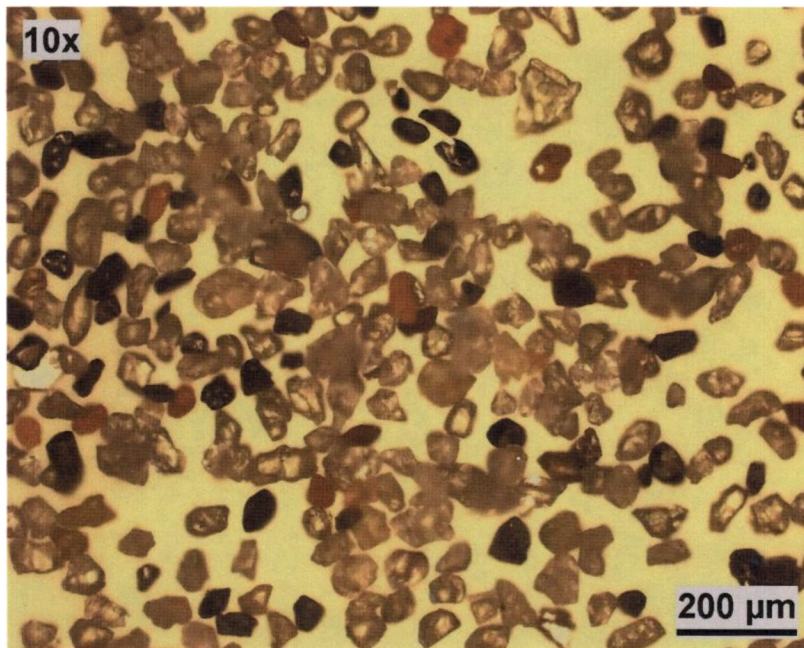**IM2 Sample**

Figure 5.8.5 Optical micrographs of impurity concentrates from Koraput kaolin
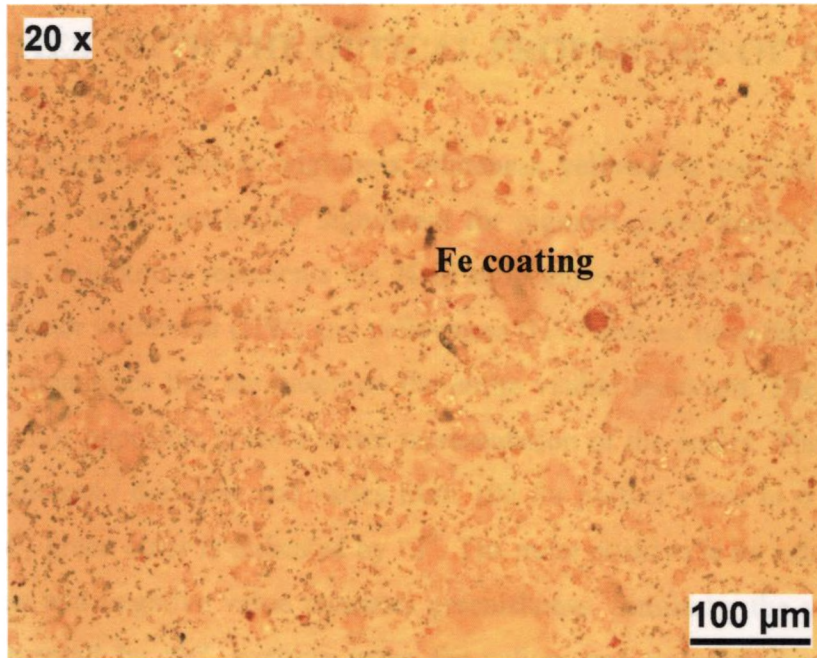
IM1 Sample

IM2 Sample
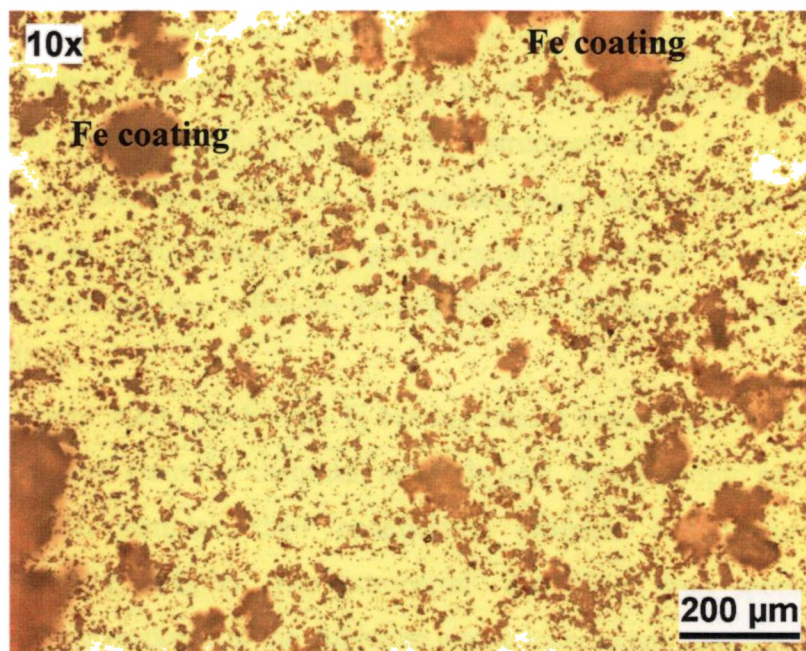
Figure 5.8.6 Optical micrographs of impurity concentrates from Bankura kaolin

313

IM1 Sample

IM2 Sample

**Figure 5.8.7 Optical micrographs of impurity concentrates
from Pali kaolin**

314

CHAPTER 6

POSSIBLE CORRELATION OF IRON AND TITANIUM IMPURITIES WITH THE OPTICAL PROPERTIES OF KAOLIN

Optical properties such as brightness, whiteness, yellowness and Lab color values (expressed in ISO units) are highly significant for pigment grade kaolin in paper and paint industries. Brightness represents the % of reflectance of light at a wavelength of 457 nm and Hunter whiteness (HW) and yellowness (HY) indices have the advantage of single number quantities that are based on the entire visible spectrum. The Lab system based on the color opposites gives a better representation of the colors. The term L is a measure of lightness / darkness and varies from 100 for perfect white to 0 for absolute black. The red / green color is indicated by "a". The more positive is its value; greater is the reddishness and negative value indicates greenishness. Similarly, the yellow / blue shade is represented by "b", positive value for yellow and negative for blueishness. Brightness and Lab color components are influenced by iron minerals and iron bearing anatase. Iron decreases brightness and L values whereas anatase increases "b" to cause yellowness. Extensive research has been carried out on the nature of iron impurities in kaolin, which leads to the conclusion that iron is present as a part of the kaolinite or ancillary mineral (mica or titania) structure ie., "structural iron" or as separate iron minerals such as oxides, hydroxides, oxy-hydroxides, sulphides and carbonates ie., "free iron" (Jepson, 1988). Identification and quantification of various Fe and Ti phases in kaolin and understanding their effect on the brightness of kaolin is an indispensable part in its value addition.

In the present study, the Fe and Ti bearing phases have been identified based on the inferences deduced from the chemical, mineralogical, spectroscopic and microscopic data of the kaolin samples, their beneficiated products and impurity minerals concentrated from the samples. The "structural" and 'free' iron species has been distinguished by their response to the dithionite citrate bicarbonate treatment. The former does not get leached out whereas the latter dissolves and gets easily separated. The "structural" iron can be either in kaolinite or in ancillary minerals such as mica and anatase. A small amount of iron in kaolinite structure does not affect the brightness

because the Fe atoms are too far apart to allow any electronic transition. However, the same amount of Fe if present in the small quantities of ancillary minerals undergoes electronic transitions due to their nearness and imparts color and affects the kaolin brightness. When free iron is present, chemical leaching is very effective and beneficiation becomes relatively easy. Advanced techniques like SC HGMS, selective flocculation, ultra flotation etc are found to partially remove the ancillary minerals even with structural iron.

The results of investigation as described in Chapter 3 and 4 give the properties of the ROM and beneficiated samples and the probable mineral phases of iron and titanium in the kaolin. Table 6.1 gives the minerals identified in the kaolin and / or impurity concentrates separated from the kaolin and the possible iron species. The chemical assay (Fe_2O_3 and TiO_2) and brightness values of the ROM and products of beneficiation are given in Table 6.2. Analysis of the results indicates that the total or analytical iron in a sample is not directly related to its optical properties. The distribution of iron as "structural" or "free' shows variations from sample to sample. Iron compounds such as oxides, hydroxides, sulphides etc indicating the "free" iron are colored and reduce the kaolin brightness. In addition, the ancillary minerals having iron in their structure are also colored. The ROM samples of Kasargod 1, Kasargod 2 and Pali kaolins have almost same iron content, but their brightness values are quite different. The Kasargod 2 kaolin appears to contain more iron in the "free" form and in the ancillary minerals and less iron in the kaolinite structure. Under these conditions, the brightness is low. The Kasargod 1 sample, on the other hand, has more iron in kaolinite structure than in the ancillary minerals and the "free" iron compounds are also less. This may be contributing to a higher brightness (than that of the former sample). In the Pali kaolin, most of the total iron is in the kaolinite structure and hence has the highest brightness among the three samples. The Koraput kaolin contains more iron than that in Bankura sample, but the brightness of the former is higher. Most of the iron in Koraput sample is in the pyrite form whereas mica is the major impurity in Bankura kaolin. Even though the total iron content is less, the quantity of iron containing mica is high which gives a dark shade to the kaolin. Similarly, Kutch kaolin is inferior in brightness to the Kasargod 1 and Pali

316

samples in spite of the lower iron content. This is again due to the same reason that most of the iron is in the structure of anatase which is the major impurity in the clay.

A similar pattern is shown by the products of size classification (SCP1 and SCP2) also. A schematic representation of the total iron content vs brightness in SCP 2 samples is given in Figure 6.1. The overall results confirm that there is no direct relation between the iron content and brightness of kaolin.

It has been established that the "free iron" is more soluble than the "structural" iron and hence the former is more easily removed by chemical leaching. DCB treatment of the SCP2 samples has been carried out to quantify the "free" leachable iron. The iron remaining after DCBT may be either in the structure of kaolinite or any ancillary mineral. The percentage removal of iron and the corresponding brightness improvement during DCBT are given in Table 6.2. The Kasargod 1, Kasargod 2, Trivandrum, Koraput and Bankura samples show a marked improvement in brightness indicating that most of the iron in these samples exists in "free" form ie., essentially in the form of iron oxides / hydroxides. Iron speciation data also supports the same (Table 6.1). Though Pali clay has got the highest brightness, no improvement has been observed after DCBT. The deferration process has improved the brightness of Trivandrum clay to ~ 90.0 (% ISO) and a marked improvement in the overall shade of Kasargod 1, Kasargod 2 and Koraput clays has been observed. The improvement in brightness indicates the extent of removal of the dark colored impurity minerals.

The Kasargod 1 and Kasargod 2 samples after DCBT treatment has improved their brightness appreciably (by ~9 and 16 units respectively) followed by a corresponding reduction in the analytical iron content (~29.0 and 43.0% respectively). Figure 6.3a gives the variation in brightness, L and HW values in the ROM and products of beneficiation of Kasargod 1sample and Fig 6.3b represent the changes in the "a", "b" and HY values. Figures 6.4a and 6.4b represent the corresponding patterns for Kasargod 2 sample and its products. The reduction in reddishness ("a") and yellowness ("b" & "HY") indicates the removal of iron hydroxides and oxy hydroxides and the negative "a" value shows the complete removal of reddish colored material from Kasargod 2 sample. The removal of dark colored impurities has resulted in an appreciable increase (~25 units

in Kasargod 2) in HW value. The high brightness of the DCBT products of these clays shows that the "structural iron" may be present in the kaolinite framework

The changes in the brightness, L and HW values of Trivandrum kaolin and its beneficiation products are depicted in Figure 6.5a and those in "a", "b" and HY values in Figure 6.5b.The sharp decrease in the "a", "b" and HY values, indicative of reddish and yellow shade of the material, confirms the removal of the coloring iron impurities such as hematite and goethite. Appreciable reduction in iron content (~49%) in the sample also supports the same. In fact, the negative "a" value indicates that greenish tinge has replaced the reddishness of the sample. The marked improvement in the optical properties of the DCB treated product shows that most of the "structural iron" may be present in the kaolinite framework and are far apart so that it is not affecting the kaolin brightness.

Though the percentage iron removal (~37%) in Kutch clay during DCBT was not bad, the brightness improvement was found to be very minimal (~ 4.0 units only). Thus only a part of the iron is leachable. Incidentally, the sample is found to contain significant amount of titania which does not change on DCB treatment. The brightness / whiteness of kaolin are dependent on the overall effect of the "L a b" color values. The changes in the brightness, L and HW values of the Kutch kaolin and its products of beneficiation are depicted in Figures 6.6a and the "a", "b" and HY values in Figure 6.6b. The "L" and HW value of the sample increase after DCB treatment by 1.2 and ~ 7.47 units respectively, indicating that only partial removal of the dark colored minerals is taking place. After DCB treatment, "a" value (reddishness) of the sample has come down from 0.63 to -0.51 units indicating the removal of almost all "free" reddish iron oxy hydroxides. The negative value for "a" is indicative of the greenish tinge achieved by the clay after the removal of red colored impurity minerals. Similarly, the "b" and HY values are found to decrease from 6.09 to 5.16 and 9.67 to 8.03 units respectively. The decrease in yellowness can be attributed to the removal of goethite during DCB treatment. The high yellowness values ("b" and HY) of the DCBT product indicate that considerable amount of colored minerals still remain in the sample.

The sharp improvement in brightness in Koraput kaolin after DCBT is due to the removal of "free" iron (pyrite) from the sample. The percentage iron removal is found to

318

be as high as 60% and this has led to ~13 unit improvement in brightness value. The changes in brightness, L and HW values of the ROM and beneficiated products are depicted in Figure 6.7a. The corresponding "a", "b" and HY values are represented in Figure 6.7b. The HW has increased by 34 units which can be attributed to the removal of yellow colored iron oxy hydroxides during DCBT. The marked reduction in "b" (~7.0 to 1.5) and "HY (11 to 2.4) values and absence of dark/red shade imparting materials indicated by the negative "a" value account for the high brightness and HW values.

DCB treatment improves the brightness Bankura clay substantially from 41.79 to 69.67 (~ 28 units) and during this process the Fe_2O_3 content comes down from 5.66% to 0.94%. This indicates that a good amount of the iron in the sample is "free" and leachable. The changes in the brightness, L and HW values of the ROM and beneficiated products are depicted in Figures 6.8.a and the "a", "b" and HY values in Figure 6.8b. The brightness/whiteness of kaolin is dependent on the overall effect of the "L a b" color values. The "L" and HW values of the clay increase after DCB treatment by ~5.0 and ~23 units and it gives an idea about the extent of removal of the dark colored impurity minerals. After DCB treatment "a" value (reddishness) of the sample has come down appreciably (from 1.07 to -1.32 units) indicating the removal of most of the "free" reddish iron oxy hydroxides. Similarly, there is a marked reduction in the "b" and HY values (20.99 to 4.03 and 36.98 to 6.68 units respectively) on DCBT which contributes to the substantial decrease in yellowness. Even though the extent of brightness improvement and removal of free by the DCB treatment is very high, the overall brightness of the product is not promising. The sample still contains ~1.0% of iron and the yellowness values ("b" and HY) support the same. Since the clay is found to contain mica, it is possible that the iron remaining after DCB treatment may be present as part of the mica structure which affect the overall brightness of the sample. The iron speciation data of the sample confirms the same (Table 6.1).

The response of Pali clay to DCB treatment is found to be very poor and is evident from the negligible improvement in brightness (0.07 units) with very small decrease in iron content (3.8%). The changes in the brightness, L and HW values are depicted in Figures 6.9a and the "a", "b" and HY values in Figure 6.9b. The "L" and HW values of the sample have not improved and it implies that the dark colored impurity

319

minerals are not getting removed by DCB treatment. Similarly, the "a", "b" and Hun Y values do not show much decrease which confirms the presence of coloring iron impurities in the sample even after DCB treatment. The product sample is still found to contain ~1.0% of Fe_2O_3 and the yellowness can be due to the "Fe" minerals. This indicates that almost all the iron in the sample in the "structural form". Since the clay contains more mica than titania, it is possible that most of the iron remaining after DCB treatment may be present as part of the mica structure (not much in kaolinite) which affects the overall brightness of the sample. The data from Mossbauer studies confirms the presence of Fe (II) in mica.

The influence of ancillary minerals, containing "structural" iron, on the optical properties of kaolin is interesting. For example, "iron stained titania", as described by Jepson is a deleterious coloring mineral in some of the important deposits in the world such as Georgia kaolin. It is well known that pure TiO_2 does not absorb light in the visible region and is considered to be the best white pigment. However, it strongly absorbs in the UV region due to the metal oxygen charge transfer process in the reaction.

$$O \times O \longrightarrow Ti(IV) \text{ transition}$$

When iron is present in the structure of TiO2, a Fe (II) $\longrightarrow$ Ti (IV) transition is possible. It has been reported that when Fe and Ti are present together in a glass, a charge transfer or electron hopping process takes place between Fe and Ti ions via an intermediate oxygen ion (Hogg and Noble, 1979).

$$Fe^{+2} - O - Ti^{+4} = Fe^{+3} - O - Ti^{+3}$$
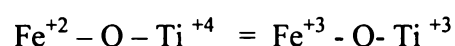
This charge transfer process has an absorption centered at 350 nm in the near-UV region tailing into the visible at the blue end of the spectrum. Intensities of charge transfer bands are reported to be 100-1000 times stronger (in terms of extinctions coefficient) than other transitions like d-d type. Thus, the amount of iron may be small but it has a major effect on the shade of kaolin, which is called 'titania effect' (Weaver, 1976). This confirms that it is the iron containing titanium (titanoferrous) mineral which is adversely affecting the optical properties of Kutch sample. A similar charge transfer may be taking place between iron and any other transition metal ion present in the ancillary mineral like mica which enables absorption resulting in the coloration of the mineral.

Hence it can be concluded that the optical properties of kaolin are not directly related to the quantity of the iron present, but dependent on the form (species) in which "Fe" occurs.

References

1. Hogg C.S., Noble F.R. (1979). A Kubelka - Munk analysis of the influence of iron and titanium oxides on the optical properties of hard porcelain, Science of Ceramics, Volume 10, Berchtesesgaden, Germany, 703-710

2. Weaver C.E. (1976), The nature of TiO_2 in kaolinite, Clays and Clay Minerals, 24, 215-218

321

Table 6.1 Iron and titanium minerals and probable iron species in the kaolins

Samples	Mineral phases identified	Species of Fe – as "Structural" in	Species of Fe – as "Free" in
Kasargod 1 kaolin	H, G, A, R, Mi, L, I, P.R	K, Mi, I, P.R, A, R	H, G, L,
Kasargod 2 kaolin	H, G, R, A, M, I, Mi, Ma, P.R, Fe-stained quartz	K, I, P.R, Mi, A, R	H, G, Ma
Trivandrum kaolin	H, G, R, A, M, Ma, P.R, Fe-stained quartz	K, Mi, A, R	H, G, M, Ma,
Kutch kaolin	H, M, R, A, P.R, Ma, Fe-stained quartz	K, A, P.R, R	H, M, Ma,
Koraput	P, H, G, M, R, A, I, L, Ma, P.R, Fe-stained quartz	K, P.R, I, A, R	P, H, G, M, L
Bankura	H, G, R, A,,Mi, L, Ma	Mi, K	H, G, L, Ma
Pali	G, H, R, A, Mi, L, Ma	Mi, K	G, H, L, Ma

H-Hematite; **G**-Goethite; **K** - Kaolinite; **L**-Lepidocrocite; **M**-Magnetite; **Ma**-Maghamite; I-Ilmenite; **R**-Rutile; **A**-Anatase; **P.R**-Pseudo Rutile; **Mi**-Mica

Table 6.2 Fe$_2$O$_3$ and TiO$_2$ content and brightness of ROM and beneficiated samples

Properties	Kasargod 1 clay	Kasargod 2 clay	Trivandrum clay	Kutch clay	Koraput clay	Bankura clay	Pali clay
ROM							
Fe$_2$O$_3$, %	1.02	1.15	0.66	0.86	5.41	3.94	1.10
TiO$_2$, %	0.65	0.57	0.19	1.63	1.60	0.44	0.52
Brightness,%	74.56	60.51	77.71	70.34	45.87	37.69	80.16
SCP1							
Fe$_2$O$_3$, %	0.75	1.07	0.62	0.61	2.05	5.17	1.13
TiO$_2$, %	0.49	0.49	0.53	1.53	0.80	0.77	0.62
Brightness,%	77.36	66.65	78.17	72.50	68.13	41.48	79.97
SCP2							
Fe$_2$O$_3$, %	0.70	1.07	0.35	0.43	1.16	5.66	1.04
TiO$_2$, %	0.20	0.41	0.52	1.60	0.66	0.28	0.55
Brightness,%	78.04	67.56	80.72	74.08	70.45	41.48	81.17
SCP2-R.B							
Fe$_2$O$_3$, %	0.68	0.95	0.30	0.40	0.93	4.86	1.03
TiO$_2$, %	0.20	0.41	0.50	1.60	0.66	0.28	0.55
Brightness,%	78.26	68.12	81.54	73.96	73.32	46.45	81.18
SCP2- DCBT							
Fe$_2$O$_3$, %	0.50	0.61	0.18	0.27	0.50	0.94	1.00
TiO$_2$, %	0.20	0.34	0.50	1.59	0.66	0.28	0.49
Brightness,%	86.86	83.27	89.85	77.81	83.41	69.67	81.10
Percent iron removal	28.6	43.0	48.6	37.2	56.9	83.4	3.8
Brightness improvement, units	8.82	15.51	9.13	3.73	12.96	28.19	0.07
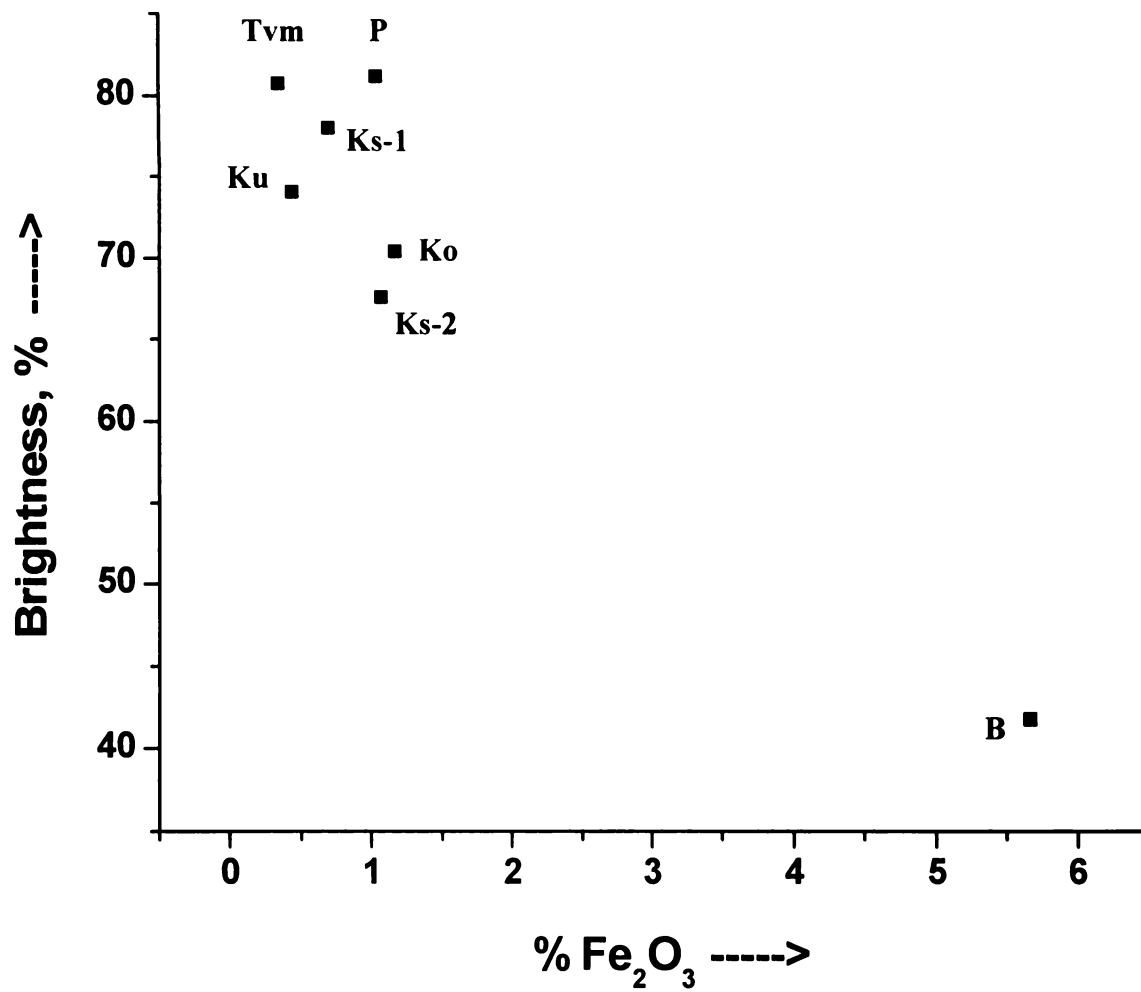
Ks-1 - Kasargod 1 kaolin ; Ks-2 - Kasargod 2 kaolin; Tvm - Trivandrum kaolin;
Ku -   Kutch kaolin; Ko – Koraput kaolin; B- Bankura kaolin; P – Pali kaolin

Figure 6.1 Iron content and brightness of the samples(SCP2) before DCBT
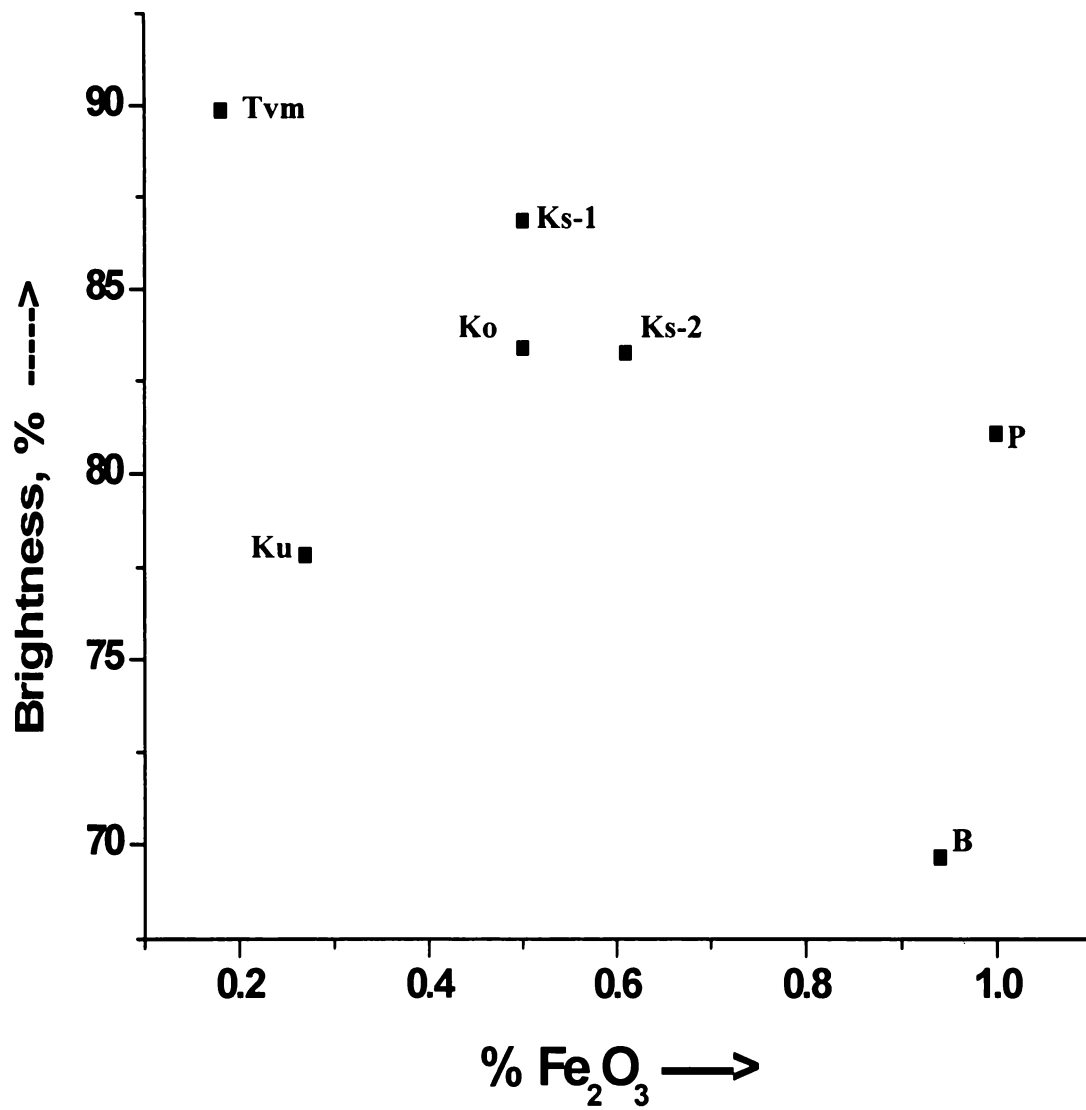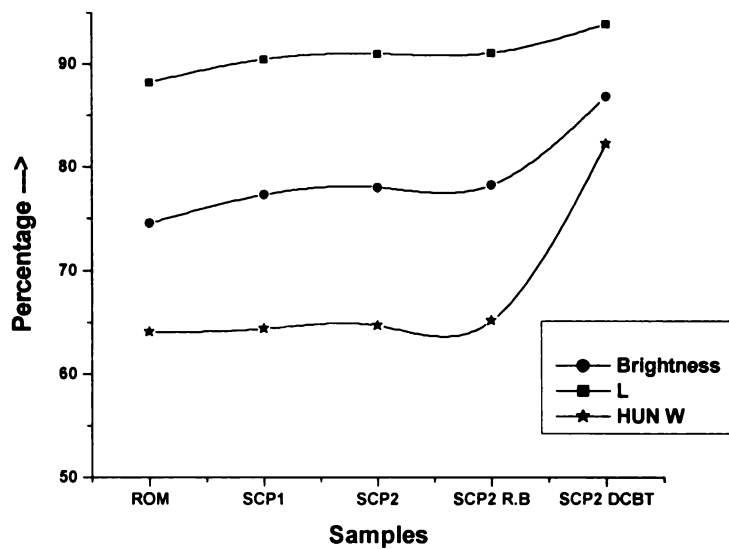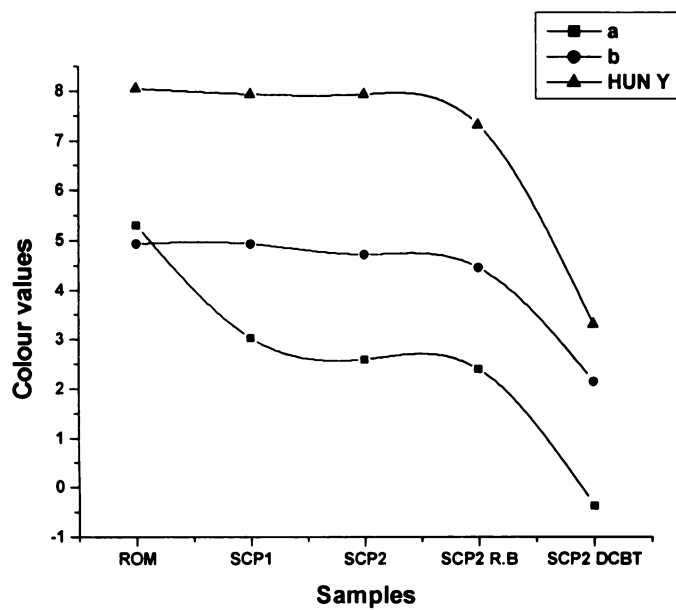
Ks-1 - Kasargod 1 kaolin ;   Ks-2 - Kasargod 2 kaolin; Tvm - Trivandrum kaolin;

Ku -   Kutch kaolin; Ko – Koraput kaolin; B- Bankura kaolin; P – Pali kaolin

Figure 6.2 Iron content and brightness of the samples(SCP2) after DCBT

Fig. 6.3a Variation of brightness, L and HW values during beneficiation of Kasargod 1 clay

Fig. 6.3b Variation of a, b and HY values during beneficiation of Kasargod 1 clay
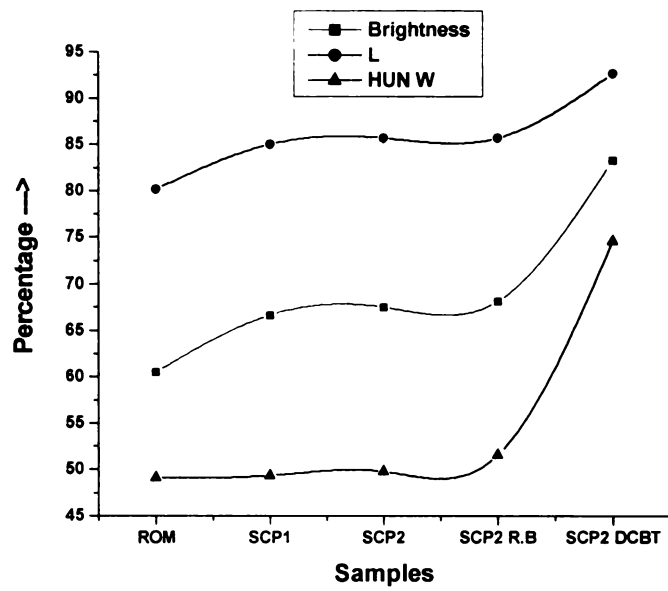
Fig. 6.4a Variation of brightness, L and HW values during beneficiation of Kasargod 2 clay
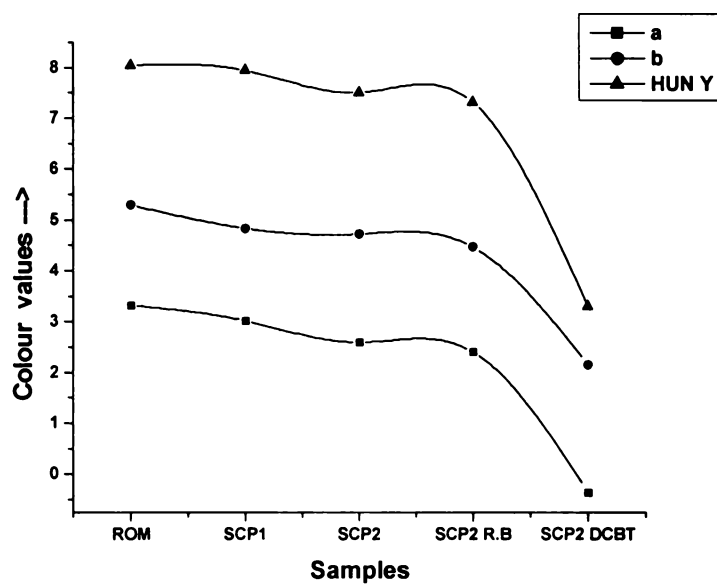

Fig. 6.4b Variation of a, b and HY values during beneficiation of Kasargod 2 clay

327

**Fig. 6.5a Variation of brightness, L and HW values during
beneficiation of Trivandrum clay**

**Fig. 6.5b Variation in a, b and HY values during beneficiation
of   Trivandrum clay**

Fig. 6.6a Variation of brightness, L and HW values during beneficiation of Kutch clay

Fig. 6.6b Variation in a, b and HY values during beneficiation of Kutch clay

329

Fig. 6.7a Variation of brightness, L and HW values during beneficiation of Koraput clay

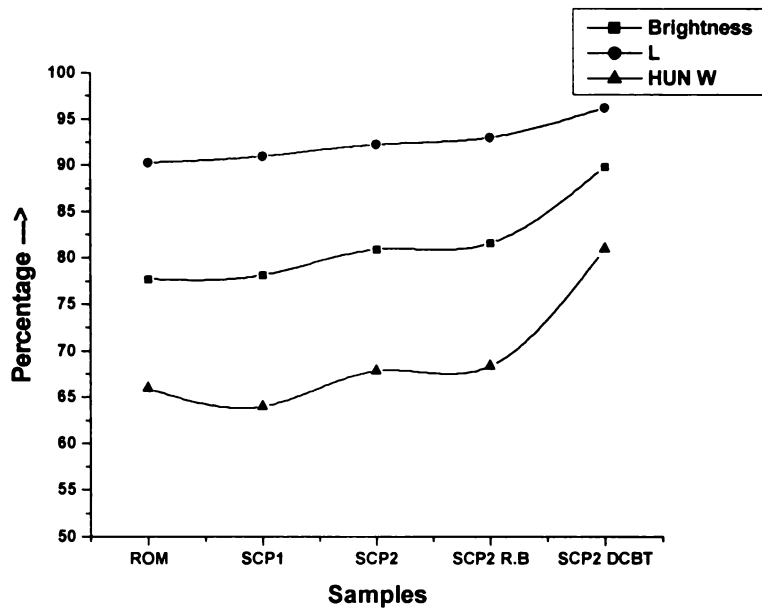**Fig. 6.7b Variation in a, b and HY values during beneficiation of Koraput clay**

330

Fig. 6.8a Variation of brightness, L and HW values during beneficiation of Bankura clay

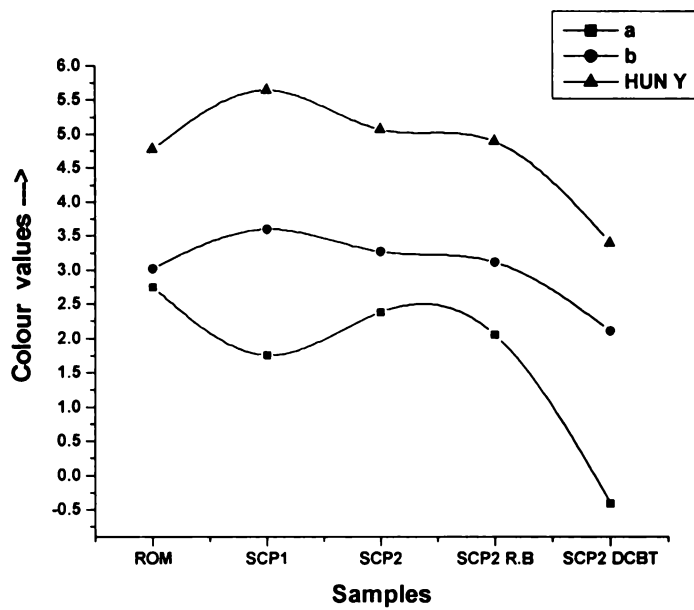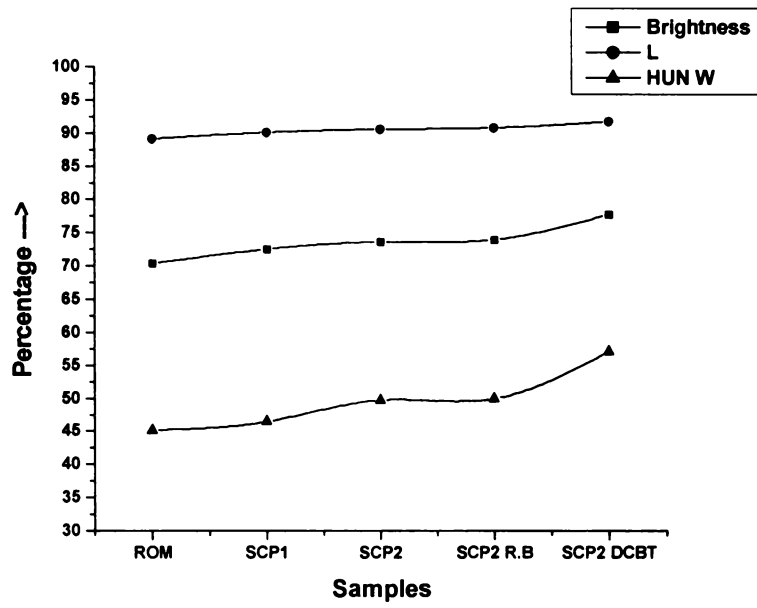**Fig. 6.8b Variation in a, b and HY values during beneficiation of Bankura clay**

331
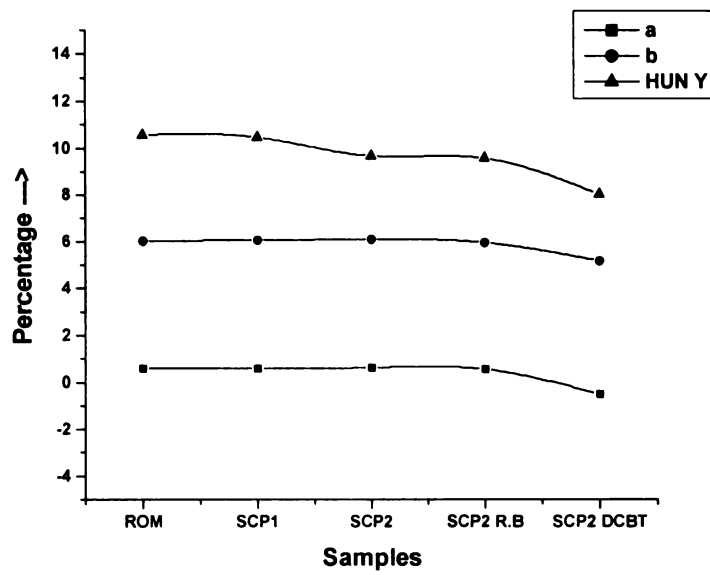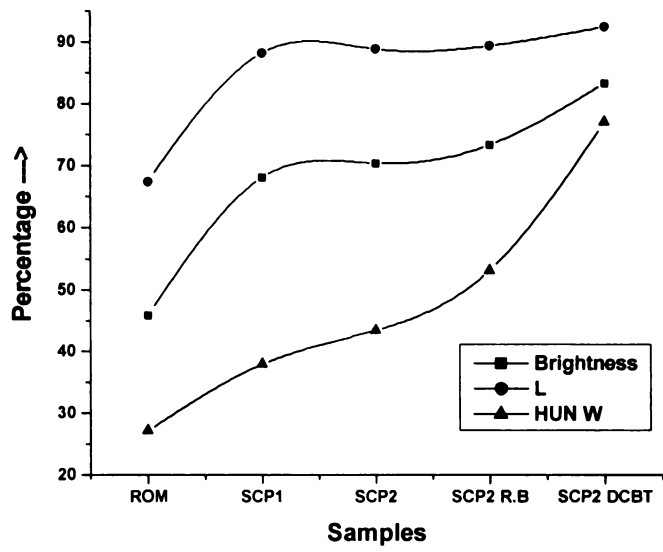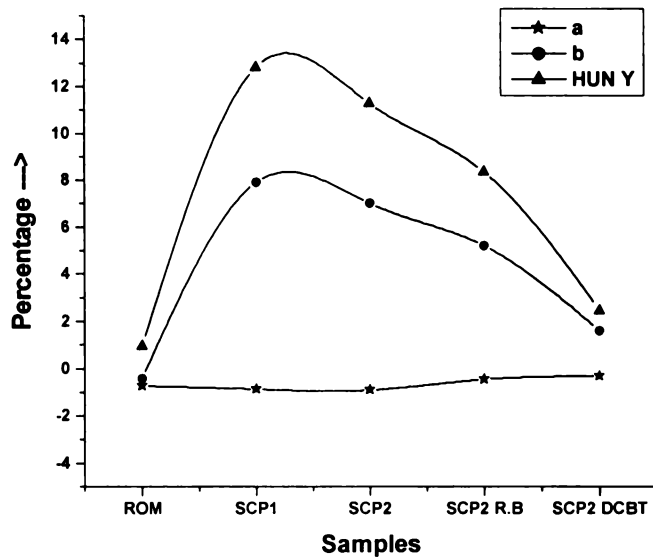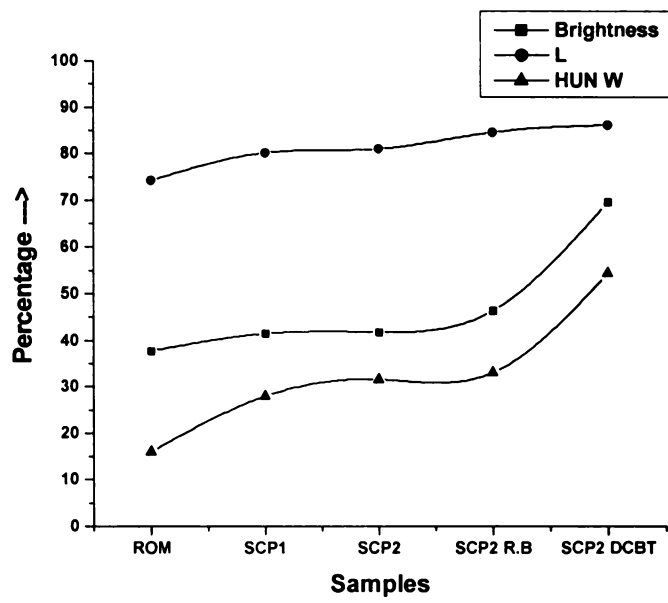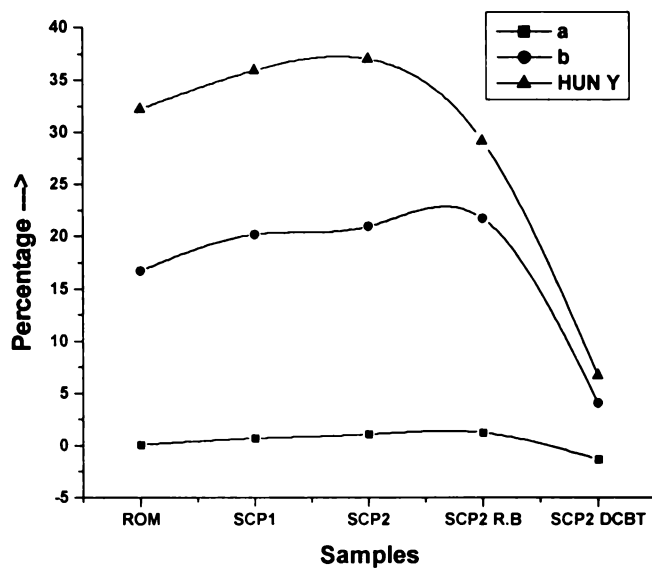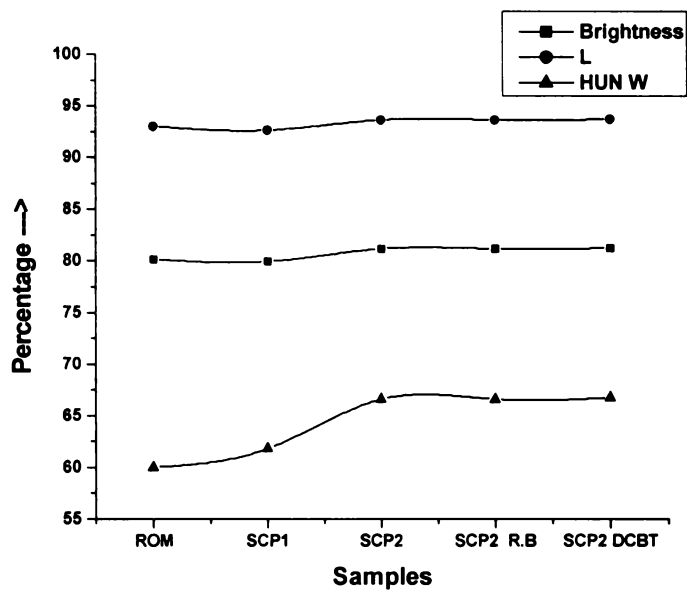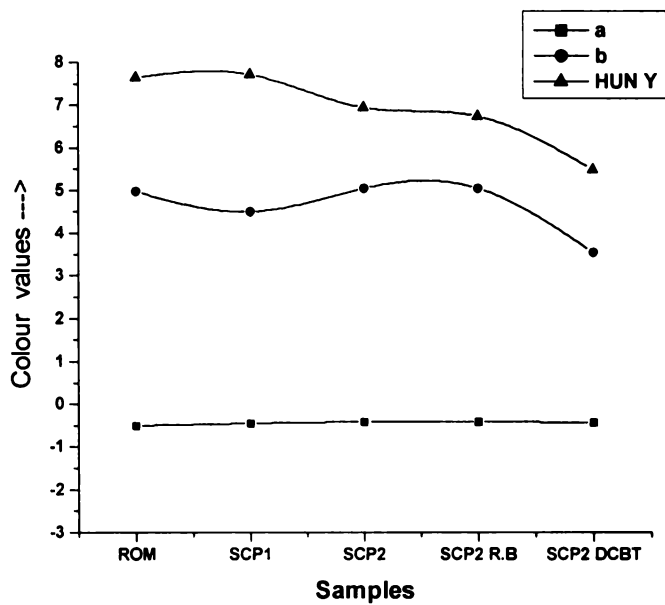
Fig. 6.9a Variation of brightness, L and HW values during beneficiation of Pali clay

Fig. 6.9b Variation in a, b and HY values during beneficiation of Pali clay

CHAPTER - 7
BENEFICIATION OF THE ACIDIC KAOLIN
FROM KORAPUT

The kaolin from Koraput district of Orissa has been found to be highly acidic due to the presence of pyrite and is different from all other samples under the present investigation. Addition of water to the clay makes pH of the slurry in the range 1-2 which corrodes the processing machinery. Hence, the conventional method may not be adopted for the size classification and other beneficiation studies. The detailed properties of the ROM kaolin have been described in Chapter 3. The beneficiation and characterization of the products has been dealt in this chapter and the possible industrial use has been discussed.

The main objective of the size classification experiments is to achieve the optimum possible refinement of the clay ie., removal of the coarse impurities and enrichment of the fines in the clay. Conventional size classification procedure involves

(i) slurry preparation - mixing of clay with water to make a clay-water suspension,

(ii) blunging - high speed stirring of the water suspension to achieve maximum de-aggregation,

(iii) screening of the blunged slurry through 300 μm screen and

(iv) further size classification using a series of small diameter hydrocyclones for removal of medium sized impurities and enriching the fine clay and to separate the desired size fractions.

7.1 Size classification using conventional method

Initially, the conventional size classification methodology has been adopted for the size separation of Koraput clay as done in the case of other clay samples (Figure 7.1). But when the clay is mixed with water and diluted to 25 % solids w/w, the clay suspension is found to acquire a pale yellow color. This phenomenon is due to the dissolution of iron in the acidic medium followed by the formation of colloidal hydroxides because of the subsequent increase in pH. As the highly acidic slurry has detrimental effect on the processing equipments, further downstream processing of the clay is found difficult. When the pH of the slurry is modified to ~ 5.0 by adding dilute

alkali (NaOH solution), the slurry color is changed to dark yellow. The processing of the slurry is then continued by adopting the conventional size classification method by high shear blunging followed by screening (300μm) and size separation using 2"stub (separation size 45 μm) and 1" cyclone (separation size 2μm). At every stage of size classification, part of the product slurry is dewatered, dried and characterized for relevant properties. Interestingly, the dried final size classified product (SCP2) is found to be yellowish-orange in color. This has led to deterioration in optical properties.

The experimental conditions are given below

(i) Blunging :

Feed slurry - % solids 25.0; blunging time – 10minutes; total slurry volume – 70 lit.

ii) 2"Stub hydrocycloning :

Feed slurry - % solids 20.0; Inlet feed pressure – 25 psi; Vortex finder /spigot – 14.3 / 4.7 mm; Total slurry volume – 65 lit.

(iii) 1" hydroycloning :

Feed slurry - % solids16.0; Inlet feed pressure – 60 psi; Vortex finder / spigot – 7.0 / 2.2 mm; total slurry volume – 30 lit.

Subsequently, studies at laboratory level have been carried out to understand the reason for yellowing of the Koraput clay during wet processing and to find a solution to overcome the same.

7.2 Laboratory studies

A detailed study was conducted in the laboratory devise a method for removing the yellow coloration developing in the clay slurry (Figure 7.2.1). The yellow color of the supernatant liquid of the clay-water (slurry) suspension and its chemical analysis indicate that the color is due to the water soluble iron. In order to remove this species, a series of water washing and subsequent decantation of the supernatant liquid after each washing was carried at particular clay – water ratio. The contact time as well as the number of washes required for the maximum removal of the water soluble iron was optimized by estimating the iron content of the supernatant liquid after each test.

The following procedure was adopted for the study. ROM clay of approximately <500 μm in size was taken and a slurry with 25% solids (w/w) was prepared in distilled water (pH-6.76). The slurry (100ml) was taken in a 250 ml glass beaker and mixed well

334

with a glass rod. The optimum contact time required for maximum dissolution of iron in water was determined by withdrawing the supernatant solution at regular intervals and analyzing for iron. The supernatant liquid was filtered through Whatman No.40 filter paper and the iron in the filtrate was determined by colorimetric method using 1,10-phenanthoroline. Tests were conducted both at broad and narrow range time intervals and the details of the same as well as the iron content in the filtrate are given in Table 7.2.1 and Figure 7.2.2

The results of the optimization studies with the broad range time interval of contact time shows that the supernatant liquid taken after 15 minutes is found to contain 0.30% of iron (as Fe_2O_3, %) and the same increases to 0.41% after 30 minutes. No appreciable change was noticed in the iron values in the supernatants collected after 45 and 60 minutes. The results of narrow range time intervals also shows that the maximum extraction of water soluble iron was achieved after 30 minutes of contact time.

The extent of removal of the water soluble iron, indicated by the iron concentration in the supernatant liquid, clearly shows that three washings are sufficient for achieving the maximum removal. The maximum iron concentration obtained in the soluble form is ~0.50 % and this constitutes about 9.3 % of the total iron present in the ROM clay. The results are given in Table 7.2.8 and Figure 7.2.3. Even though the concentration of the water soluble iron is only 9.3%, if not removed, it adversely affects the optical properties of the product clay to a great extent. The reason is that the pH will automatically rise during further dilution of the slurry and will lead to the precipitation of hydrated "Fe" species / hydroxides.

The supernatant liquid containing the water soluble iron is found to have yellow color and this can be due to the presence of hydrated species of iron along with other colored metal sulphates which are leached out from the clay at this pH. The colored complexes of organic compounds in the clay are also contributing to this coloration. It is seen that, during pH modification (to pH~5 unit), these hydrated compounds are precipitated to ultrafine brownish/orange particles. These particles get coated all over the clay surface and make them brownish yellow in color.

The laboratory studies have further shown that, after removing the water soluble iron, pH modification either by further dilution or by adding alkali does not impart any

coloration to the slurry. Based on this inference, the size classification of the clay was carried out by incorporating the necessary changes in the conventional beneficiation procedure.

7.3 Size classification by modified method

Based on the laboratory level studies, experiments were conducted to evolve a micro-pilot level method for the beneficiation of this kaolin. The water soluble iron was removed by a combination of operations such as thorough mixing of the clay with water by low speed stirring, allowing the clay portion to settle and removing the colored solution by decantation. Even though the optimum contact time required at the laboratory level was 30 minutes, this duration was not sufficient during scale-up. The whole process was repeated three times for the maximum removal of the color imparting species. After removing all the soluble iron, the pH was raised to the desired level ~ 5 units and further down stream processing of the clay was carried out. It is worth mentioning that, now the pH modification has not led to any yellowing of the slurry, which indirectly indicates the complete removal of the limonite like materials for the clay. Also, the chemical analysis has shown that ~ 65% of the pyrite particles are in coarser size ranges (> 45 µm in size). That means, if we adopt the conventional high shear blunging procedure used for the de-aggregation of the particles, it will ultimately led to the breaking down of the coarse pyrite particles to finer sizes and their spreading to the finer portions of the clay. It is therefore advisable to remove the pyrite particles in the coarser range itself and in order to achieve this, the aggressive high shear blunging was replaced with low speed stirring in the modified method. The down stream processing of the blunged slurry was then screened through 300 µm sieve and then size classified using 2"stub (separation size 45 µm) and 1" cyclones (separation size 2 µm). The final product (SCP2) obtained after processing by the modified size separation method is found to be white in color with improved optical properties (Figure 7.3.1). The flow sheets of the conventional and modified methods of size separation are given in Figure 7.1 and Figure 7.3.2 respectively.

The actual experimental conditions are given below.

(i) Water washing and screening

The clay slurry (25% solids equivalent to 15 Kg.of dry clay) was taken in the Stainless Steel tank of 65 L capacity and was mixed slowly using a marine propeller

stirrer for 3 minutes. The slurry was then allowed to settle for 3 hours, the supernatant liquid was siphoned off and the percent solids of the slurry was maintained at 25% by adding the required quantity of water. This process was repeated three times. After this water washing, pH of the slurry became slightly high (~ 1.93). It was further raised to 4.85 by adding 20% NaOH solution (dosage 15 kg/ton). The slurry was then passed through a 300 micron screen to collect the undersize (<300 μm fraction) for subsequent processing using hydrocyclones.

(ii) 2" stub hydrocycloning

The experimental conditions for 2" stub cyclone classification are given below.

Feed percent solids - 20.0; Feed inlet pressure - 25 psi;

Vortex finder – 14.3 mm; Spigot – 4.7 mm

(iii) 1" hydrocycloning

The overflow slurry of 2" stub cyclone separation was diluted to 16% and the 1" cycloning was done at the following fixed experimental conditions

Feed inlet pressure - 60 psi; Vortex finder – 7.0 mm; Spigot – 2.2 mm

At every stage of size classification, part of the product slurry was dewatered and dried for further characterization. The slurry was kept for a few hours so that maximum solids settled at the bottom. The supernatant portion was decanted; the concentrated slurry was taken in a S.S tray and dried on a water bath to get the dried material

7.4 Characterization of the product samples

The size classified samples produced by the modified beneficiation method were characterized for their physical, chemical, mineralogical and morphological properties. The detailed property evaluation of the ROM clay has been discussed in Chapter 3.

7.4.1 Physical properties

As discussed in Chapter 3, the ROM clay is soft and easily slaking in nature and is gray in color with blackish impurities. Table 7.4.1 gives the properties of the ROM clay along with those of the beneficiated products. The low pH and high specific gravity of the ROM clay are due to the presence of pyrite. Most of the pyrite particles are removed during size classification and the size classified products have lower values almost matching with that of ideal kaolinite. In the ROM clay the matter soluble in water

337

and acid are on the higher side which changes appreciably in the products of size classification.

The particle size distribution analyses (Table 7.4.1) show that the grit content is moderate (16.80%), and the fines are moderately high (49.90% < 2μm fraction) in the ROM sample. Screening and separation using 2"stub hydrocyclone has resulted in marginal decrease in < 45 μm fraction (from ~ 43.30% to 38.90% along with an increase in the -2 μm fraction (49.30 % to 61.90%). Further sizing with 1" hydrocyclone is found to enhance the <2 μm fraction to 73.90 %.

The brightness, lightness (L) and Hunter whiteness (HW) values of ROM sample are found to be very poor. The low "L"and HW values are due to the presence of black/dark coloured particles in the clay. The greenish tinge of the sample ("-a" value) is indicative of the absence of reddish colored minerals in the sample. The "b" value and Hunter Yellowness (HY), shows that the overall yellowness of the sample is low. This indicates that low brightness of the sample is due to the presence of black / dark colored minerals. Size classification increases the brightness of samples appreciably ie., by 22.3 (SCP1) and 24.6 (SCP2) units. Similarly, there is a sharp increase in the lightness "L" value (~21 units) and moderate increase in the HW (~11 and 16 units for SCP1 and SCP2 respectively) of the beneficiated samples which is due to the removal of the colored impurities. The "greenishnes" of the material increases marginally during size classification and is evident from the "a" values. But there is appreciable increase in the yellowness of the sample SCP1 and SCP2 as indicated by the HY and "b" values. The sharp improvement in the optical properties of the samples may be due to the removal of some of the coarse dark colored impurities such as pyrite. The appreciable reduction in the Fe_2O_3 content of SCP1 and SCP2 also supports the same. Optical properties, % Fe_2O_3 and % TiO_2 values of ROM are given in Table 7.4.1 and those of beneficiated samples in 7.4.4. For pigment grade kaolin, brightness should be >80% ISO and beneficiation to achieve this level is one of the highest value additions of kaolin.

The conventional reductive ('hydros') bleaching removes only small amount of 'Fe' minerals. Hence, the brightness improvement of the product sample SCP2 is also marginal. The brightness of the sample has improved on hydros bleaching only by ~ 3.0 units with small reduction in the Fe_2O_3 content and only a marginal improvement in the L

and HW values and reduction in "a"," b" and HY values. It implies that the impurity minerals imparting dark/reddish and yellow shade to the material is unaffected by this reductive bleaching technique and the extent of "free" iron removal is low. DCB treatment improves the brightness substantially (~13.0 units) and during this process the Fe2O3 content reduces from 1.16% to 0.50%, indicating that part of the iron in the sample is "free" and leachable. The brightness/whiteness of kaolin is dependent on the overall effect of the Lab color values. The "L" value and HW of the sample increase after DCB treatment by ~3.5 and ~34 units and it gives an idea about the extent of removal of the dark colored impurity minerals. After DCB treatment "a" value (greenishness) of the sample has come down marginally (~0.6 units). Similarly, there is a marked reduction in the "b" and HY values (~ 5.5 and 8.8 units respectively). The sample is still found to contain ~0.50% of Fe_2O_3 and the yellowness values ("b" and HY) support the same. Since the brightness of the sample is promising, it is possible that the iron remaining after DCB treatment may be present as part of the kaolinite framework structure.

The brightness, "L" and HW values of SCP1 sample was found to decrease after calcination. Correspondingly, there is increase in the reddishness and yellowness of the sample as indicated by the increase in the colour ("a", "b" and HY) values (Table 7.4.4). Since the iron content in the sample was on a higher side, it is possible that most of the iron getting liberated during metakaolinisation may not be getting incorporated into the kaolinite structure during calcination. Since almost 85% of the iron in the sample corresponds to pyrite (Table 7.4.2) and other forms of iron are small, the blakish-gray shade of the calcined material is possibly due to the presence of oxidation products of pyrite.

7.4.2 Chemical assay

The percentages of chemical constituents in the samples are given in Table 7.4.1. The silica alumina values in the ROM clay are found to be near to those of kaolinite mineral, but the LOI value is on a higher side (18.17%) The higher LOI value is possibly due to the presence of carbon and oxidization of pyrite. Samples SCP1 and SCP2 are found to be more kaolinitic in nature and is evident from the increased Al_2O_3 content. That is, 2" stub and 1" cycloning have removed the coarse silica particles and enriched kaolinite content in the clay (Figure 7.4.3). Though the LOI values of SCP1 and SCP2

have decreased marginally, the values are still higher than that of kaolinite mineral. This shows that some amount of carbon and / or pyrite is still present in these samples.

The Fe_2O_3 and TiO_2 content in the sample are 5.41 and 1.60% respectively. The total "iron content" (as Fe) in the sample was found to be 1.94 % and out of this 1.85 % was found to be pyritic iron. The pyrite content in the sample was found to be 3.97%. The sample is also found to contain 2.07 % of sulphur and 1.2% of carbon. After size classification, there is a reduction in the Fe_2O_3 and TiO_2 content in the sample and a corresponding decrease is observed in the pyrite content. It is seen that ~72% of the iron remaining in SCP2 sample is pyritic in nature (Table 7.4.2).The presence of moderate quantities of Fe_2O_3 (~ 22%) and TiO_2 (41%) in the SCP2 sample indicates the ultra fine size of these impurities which are getting enriched in the product during size separation. The organic carbons as well as sulphur contents are also found to decrease during size classification. The other impurity minerals of Na, K, Ca etc. are present only in low concentrations. The presence of Fe and Ti and other impurity minerals of Na, K and Ca etc. in the finer size fractions indicate that they are almost uniformly distributed in all size fractions. Results of the trace elements analysis shows that the concentrations of certain elements such as Zn,Pb,Ba,Ca,Co,Cr,Mn,Sr,V,Z,P,S and Ni are relatively high in the raw clay and come down in the beneficiation products (Table 7.4.3).

Reductive bleaching is ineffective in removing the iron and is evident from the marginal decrease in the Fe_2O_3 content of SCP2 R.B sample. But after DCB treatment, the Fe_2O_3 percentage is reduced by ~13.0 units and the optical properties are improved to a great extent. The iron removal shows that ~57% of the total iron in the clay is "free" in nature and the rest is present in the structure of either kaolinite or ancillary mineral (mica or titania). Also, the sharp decrease in the "a", "b" and HY values confirms the removal of the coloring iron impurities such as pyrite, hematite and goethite. The sample is still found to contain ~0.50% of iron. Since the sample has got good optical properties, it is possible that the iron remaining after DCB treatment may be present as part of the kaolinite structure and their by not appreciable affecting the overall brightness of the sample. It is also worth mention that chemical leaching has not effected any changes in the TiO_2 content. The Fe_2O_3 and TiO_2 content and optical properties of the beneficiated

340

samples are given in Table 7.4.1 and Figure 7.4.4 represents the variation in Fe_2O_3 and TiO_2 content.

7.4.3 Mineralogical study

X-ray diffraction and thermal analyses give mineralogy of the clay. The XRD analysis data of the ROM and beneficiation products is given in Table 7.4.1 and the powder patterns are represented in Figure 7.4.1. In the raw clay, kaolinite is the major mineral along with quartz, pyrite, hematite, anatase and rutile as the ancillary mineral impurities. An increase in the intensity of the kaolinite peaks and a decrease in the intensity of quartz peak in the XRD patterns of SCP1, SCP2 and SCP2 DCBT clearly show the enrichment of kaolinite in the sample during the size classification.

Thermogravimetric analyses of the ROM sample (Table 7.4.1) shows that the total weight loss on heating is ~18.27%, which is higher than that of the kaolinite mineral. Again, it can be attributed to the oxidation of the pyrite. The weight loss in the range 450 to 600°C corresponds to the dehydroxylation of kaolinite. This value decreases, as the ROM clay is beneficiated by size classification confirming the increase in kaolinite content and removal of pyrite mineral. The DTA patterns of the samples have given characteristic endotherm and exotherm of kaolinite and pyrite minerals(Table 7.4.1).

Table 7.4.5 gives the percentages of possible minerals in "Koraput" kaolin as calculated from the chemical assay. The rational analysis data shows that the ROM sample is kaolinitic in nature. It is also found to contain quartz, pyrite, micaceous minerals (both muscovite and paragonite mica), hematite, anatase and carbonaceous matter in small quantities. In the size classification products, the kaolinite content increases with a simultaneous decrease in other minerals (especially pyrite) supporting the XRD findings.

7.4.4 Morphological characterization

Scanning electron microscopic analysis (SEM) pictures of the ROM clay and SCP1 are presented in Figure 7.4.2, which shows the presence of aggregates of pseudo hexagonal kaolinite particles along with well crystallized pyrite particles of typical octahedral shape. The SCP1 sample shows only the pseudo hexagonal kaolinite particles.

341

7.5 Possible industrial utilization of the beneficiated products

In the present study, beneficiated clays of different grades are produced and their utilitarian aspect was explored by comparing their critical properties such as particle size distribution and brightness with the required standard specifications for various end uses. This is done to have a idea about the possible value addition of these clays. The different beneficiated samples taken are the < 45 micron fraction (SCP1), its calcined product at 1100°C, <2 micron fraction (SCP2) and its reductive bleached and DCB treated products and their salient features are given in Tables 7.4.1, 7.4.4 and 7.5.1. Though DCB treatment is not a viable option for the beneficiation of kaolin on an industrial scale, here it is carried out to get an quantitative information about the removable free iron in the clay. On an industrial scale, their removel is done by employing various sophisticated methods such as High gradient magnetic separation. The international / national specifications of the kaolin for various applications are given in chapter 3 (Tables 3.9.1 to 3.9.11).

The properties of the beneficiated samples were compared with the international specifications for various applications and Table 7.4.4 shows that, the optical properties of SCP1 and SCP2 samples are not very good and they contain appreciable quantities of <2 μm fraction particles. It is seen that these values does not match with the required specifications for either paper coating or filler grade kaolins. Though the percentage of finer fraction (<2 μm) in the clays falls within the range for its use in ceramic industry for the production of whitewares the higher iron content makes it unsuitable for the same (Table 3.9.8) and can be used in the whiteware industry only after removing iron to the required level. This indicates that the sample has to be beneficiated further for it s optimum utilization. The reductive bleached product (third beneficiated product) is also found not suitable for any of the above mentioned applications due to its poor optical properties and high iron content. DCB treatment is found to remove appreciable quantities of iron from the sample and is evident from the improved optical properties of the fourth beneficiated product (Table 7.4.4). Though the optical properties and chemical assay of the DCBT product matches well with that of the commercial grade coating kaolins (Table 3.9.3 and 3.9.9), the low value of <2 micron fraction makes it unsuitable for paper coating application. Properties of the clay matches with the specifications of

342

commercial paper filler grade kaolin of Imerys (UK) [Table 3.9.5] and ceramic grade kaolins for whitewares (Table 3.9.8). Further value addition of the clay is possible by enriching the finer fractions in the clay and improving its optical properties. This can be achieved by fine tuning the size classification step as well as by ensuring maximum removal of the iron from the clay by using sophisticated techniques such as high gradient magnetic separation. Calcined clay (fifth beneficiated product) is found to be inferior in quality and is evident from the low brightness value (Table 7.4.4).

The beneficiated samples are also compared with the IS specifications for their possible use in paper and ceramic industry. The properties of the samples are given in Table. 7.5.1. The SCP1 and SCP2 (beneficiated products 1 & 2) samples did not have the desired particle size distribution as per the IS specifications for Grade I (paper). The iron content as well as the brightness values of the samples, are also not matching with the required specifications and it is clear that further beneficiation of these samples are essential to improve its quality to Grade I level. But both these samples are found to fulfill the criteria for Grade II (filler) kaolin and they can be used as filler clay. Though the reductive bleaching has not produced any appreciable reduction in iron values of the sample, DCB treated sample is found to have improved optical properties. Though the high brightness value of the DCBT product makes it suitable for paper coating (Grade I), it can be used for such applications only after improving the finer fraction (<2 micron) content.

The SCP1 & SCP2 samples did not possess the required particle size distribution and the metal oxide content (Fe,Al & Ti) and they can not be used in making of high quality ceramic products (Grade I kaolin). The SCP1 sample can be used only as Grade III kaolin due to the high (Fe_2O_3 + TiO_2) content. The enhancement of finer fractions as well as the reduction in iron content makes the SCP2 sample suitable for its use in ceramic industry as Grade II kaolin.

The inputs from the study shows that further value addition of the clay for high end applications is possible by improving its size distribution pattern and optical properties by employing suitable beneficiation methods.

Table 7.2.1 Iron content in the washings at different contact timings

Sl. No.	Contact Time (minutes)	Water soluble iron as Fe_2O_3, %
	Broad range	
1	15	0.22
2	30	0.30
3	45	0.41
4	60	0.42
	Narrow range	
1	20	0.2642
2	25	0.3106
3	30	0.4133
4	35	0.4139
5	40	0.4142

Table 7.2.2 Iron content in the washings after various periodic washes

Sl. No.	Number of washes	Water soluble iron as Fe_2O_3, %
1	0	0.4133
2	1	0.4371
3	2	0.4729
4	3	0.4960
6	4	0.4972
7	5	0.4998

Contact time – 30 minutes

Raw clay

↓

Mixing with water

↓

Stirring at high rpm for max. de-aggregation

↓

Screening/ size separation using Hydrocyclones

↓

Drying

↓

Final Product
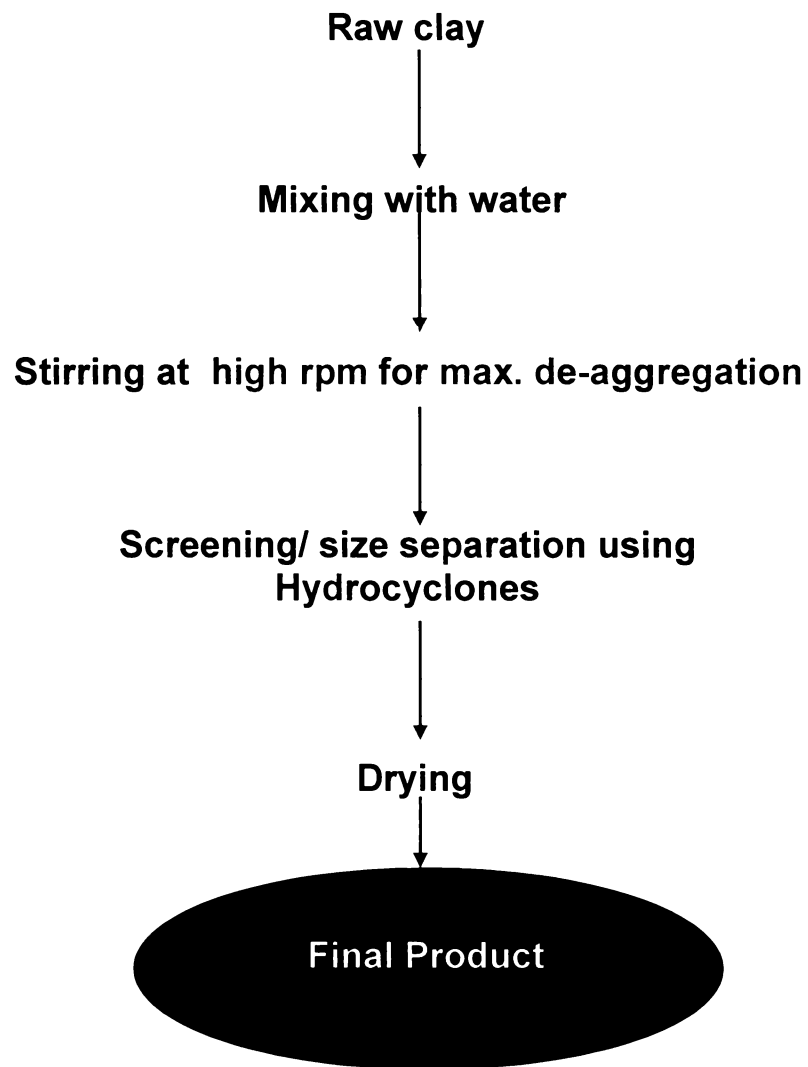
Figure 7.1 Flow sheet for conventional size separation

Figure 7.2.1 Colored supernatant liquid from water washing

346
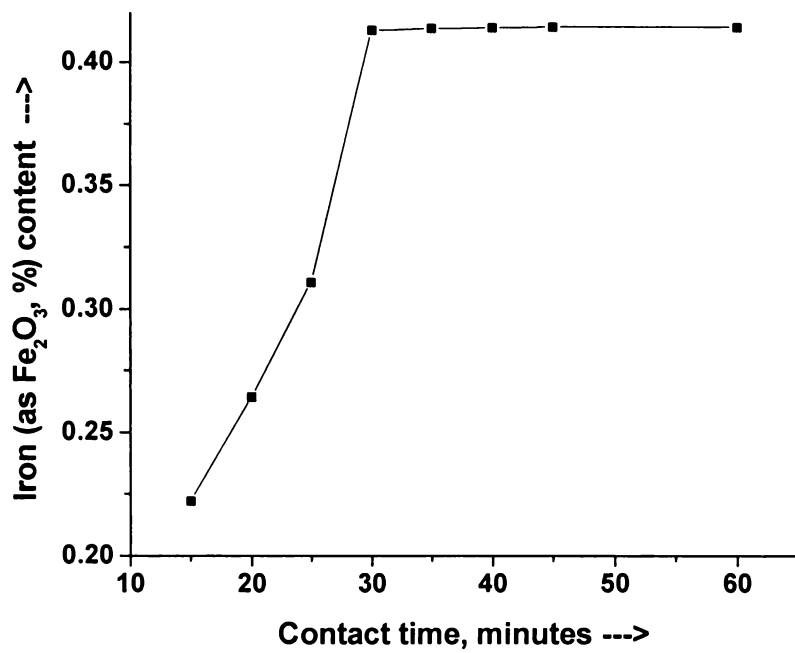
Figure 7.2.2 Variation of Fe₂O₃ content vs contact time
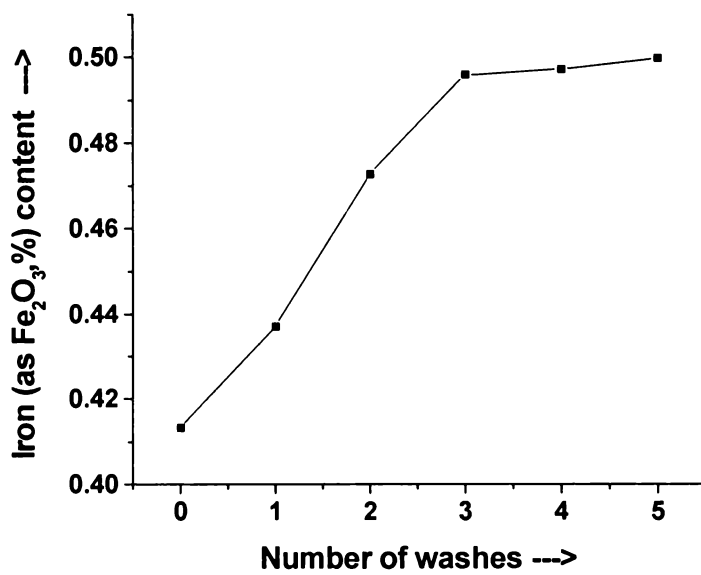
Figure 7.2.3 Variation of Fe₂O₃ content Vs number of washes

347
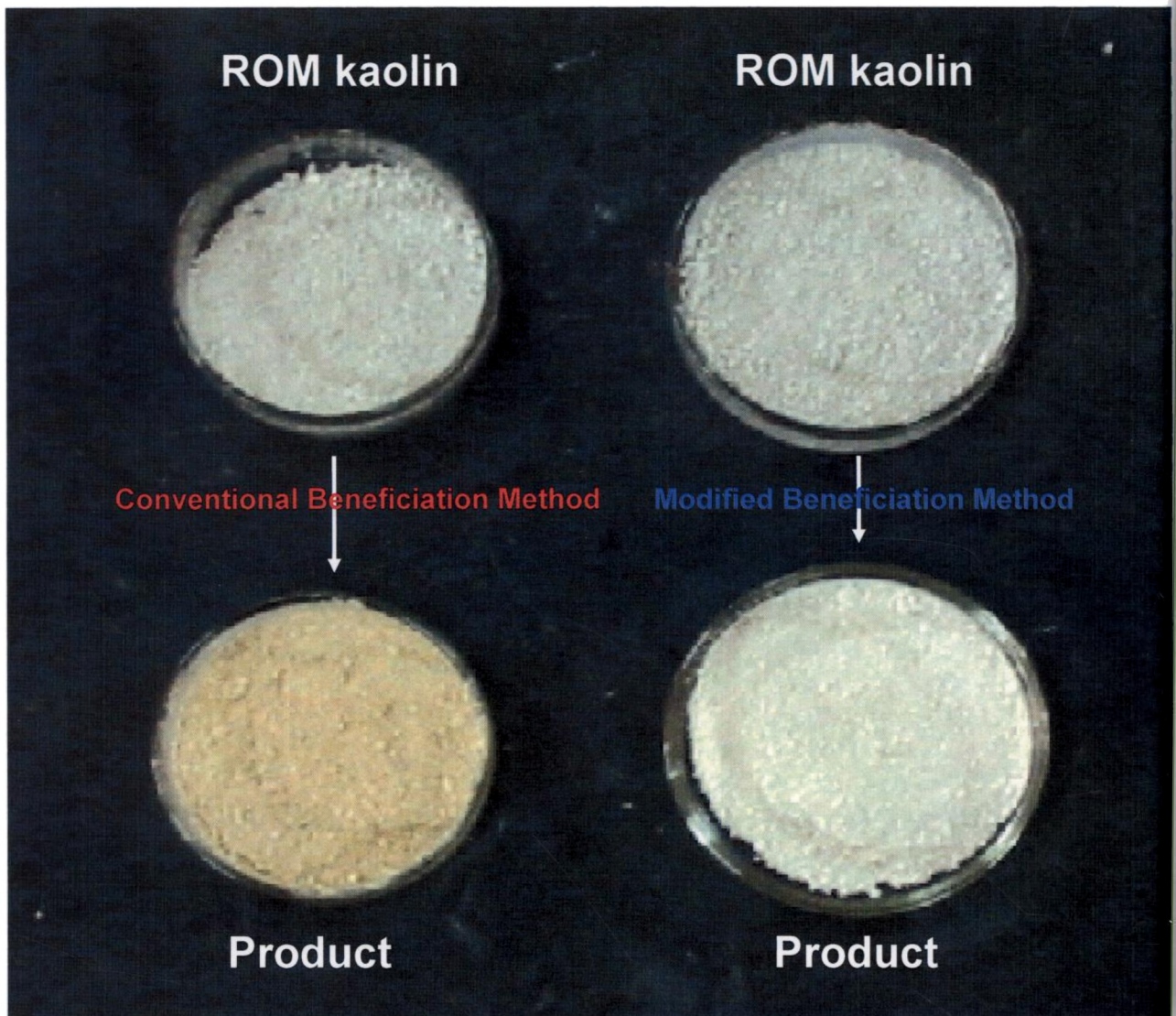
Figure 7.3.1 Colour of the ROM and final size classified product samples (SCP2) - conventional and modified methods

Raw clay

↓

Mixing with water

↓

**Mild Stirring at low rpm for de-aggregation
(to avoid size reduction of coarse pyrite particles)**

↓

Settling of the clay mass

↓

Decantation of the supernatant liquid

↓

(3 water washings) **Water washing with mild mixing
(to remove water soluble Fe impurities)**

↓

pH modification using NaOH solution (to neutral pH)

↓

Screening/ size separation using a set of hydrocyclones

↓

Drying

↓

Final Product

Figure 7.3.2Modified flow sheet for size separation

349

Table 7.4.1 Chemical assay, mineralogy and physical properties of ROM and beneficiated samples of Koraput kaolin

Particulars	ROM	SCP1	SCP2	SCP2-DCBT
Chem.Assay (% wt)				
SiO_2	41.81	42.47	42.52	44.08
Al_2O_3	32.01	37.71	38.41	38.91
Fe_2O_3	5.41	2.05	1.16	0.50
$TiO2$	1.60	0.80	0.66	0.66
CaO	0.69	0.58	0.69	0.69
Na_2O	0.23	0.20	0.23	0.23
K_2O	0.08	0.08	0.02	0.02
LOI	18.17	17.12	15.98	14.71
Sulphur	2.07	0.69	0.33	0.08
Total Carbon	1.2	0.50	0.41	0.38
FeO	2.40	---	---	---
Physical Properteis				
Particle Size Distribution,wt.%				
> 45 μm	16.80	Nil	Nil	Nil
< 45 > 2μm	43.30	38.90	26.10	26.10
< 2μm	49.90	61.10	73.90	73.90
Optical Properties (% ISO)				
Brightness	45.87	68.13	70.45	83.41
L	67.43	88.21	88.92	92.41
a	-0.75	-0.86	-0.89	-0.31
b	-0.44	7.91	7.02	1.58
HUN W	27.17	37.95	43.41	77.06
HUN Y	0.94	12.81	11.27	2.44
pH	1.72	----	-----	-----
Cation exchange capacity ,meq/100 g	2.1	----	----	----
Water solubles, % w/w	4.14	1.94	0.52	---
Acid soluble, % w/w	9.06	7.94	1.07	---
Specific gravity, g/cc	2.78	2.61	2.60	2.59
Mineralogy				
XRD				
Major phases	K, Q	K	K	K
Minor phases	P,A,R,H	Q,A,R,H	Q,A,R,H	Q,A,R
DTA				
Endotherm (°C)	534.3, 684.9, 73.4	534.4, 671.3	563.8, 671.6	---
Exotherm (°C)	468.0, 554.8, 983.8	438.5, 981.6	695.5, 749.1, 992.2	---
TG (wt. loss %)	18.27	16.49	16.20	---

Q-Quartz; K-Kaolinite; P-Pyrite; A-Anatase; R-Rutile; H-Hematite

Table 7.4.2   Pyrite content in ROM, beneficiated samples and IM1 of Koraput kaolin

Properties	ROM	SCP1	SCP2	IM1
Total Iron, % (by estimation)	1.94	0.75	0.43	4.24
Non-Pyritic Iron, % (by estimation)	0.09	0.13	0.12	0.35
Pyritic Iron,% (by calculation)	1.85	0.63	0.31	3.89
Sulphur, %	2.07	0.69	0.33	4.50
% of pyrite from Pyritic Iron Sulphur	3.97 3.87	1.35 1.29	0.67 0.62	8.36 8.42

Table 7.4.3 Trace elements in the ROM and beneficiated samples of Koraput kaolin

(µg / g)

Elements	ROM	SCP1	SCP2	SCP2 – DCBT
Barium	304	1094	1274	ND
Calcium	569	414	358	ND
Cadmium	<2	<1	<2	<1
Cobalt	647	28	41	5
Chromium	145	126	130	15
Copper	36	28	20	<1
Potassium	134	66	115	ND
Lanthanum	68	60	55	10
Magnesium	68	45	67	ND
Manganese	35	7	18	<1
Sodium	148	47	72	ND
Nickel	83	69	57	8
Phosphorous	1537	1250	1089	ND
Lead	145	137	121	17
Strontium	212	178	143	ND
Vanadium	133	99	142	7
Zinc	154	149	145	6
Zirconium	403	301	274	18

<1 ppm - BDL

352

Table 7.4.4 Optical properties and Fe & Ti content in the beneficiated Koraput kaolin

Samples	Fe_2O_3, %	TiO_2, %	B	L	a	b	HW	HY
SCP1	2.05	0.80	68.13	88.21	-0.86	7.91	37.95	12.81
SCP1 Calcined	---	---	65.58	83.46	2.65	8.45	33.23	12.92
SCP2	1.16	0.66	70.45	88.92	-0.89	7.02	43.41	11.27
SCP2 R.B	0.93	0.66	73.32	89.31	-0.47	6.22	46.10	10.36
SCP2 DCBT	0.50	0.66	83.41	92.41	-0.31	1.58	77.06	2.44

Table 7.4.5 Rational analysis data of ROM and beneficiated samples of Koraput kaolin

Mineral % by wt.	ROM clay	SCP1	SCP2
Kaolinite	77.54	88.99	87.09
Quartz	4.10	----	---
Muscovite mica	0.68	0.69	0.17
Paragonite mica	2.84	2.48	2.84
Pyrite	3.87	1.29	0.62
Hematite	2.84	1.19	0.74
Anatase	1.60	0.80	0.66
Calcite	1.78	1.04	1.23
Carbonaceous matter	4.75	1.70	3.33
Free alumina	----	1.32	3.32

353

**Table 7.5.1 Properties of beneficiated products (SCP1 & SCP2)
of Koraput kaolin**

| Sl.No.	Characteristics	SCP1	SCP2
1	Coarse particles or grit (residue on 53μm IS sieve), %by mass	Nil	Nil
2	Particles coarser than 25 μm,	8.20	Nil
3	Particles larger than 10μm in dia, % by mass	13.90	8.51
4	Particles smaller than 10μm, % by mass	86.10	91.49
5	Particles finer than 2 μm,	61.10	73.90
6	Relative density 27/27°C	2.6	2.6
7	Loss on ignition, % by mass	17.12	15.98
8	Matter soluble in water, % by mass	1.94	0.52
9	Matter soluble in HCl,% by mass	7.94	1.07
10	CuO. % by mass	0.0028	0.0020
11	As_2O_3, ppm	Not detcted	Not detected
12	Fe_2O_3, % by mass	2.05	1.16
13	TiO_2, % by mass	0.80	0.66
14	Al_2O_3, % by mass	37.71	38.41
15	Fe_2O_3 & TiO_2 together % by mass	2.85	1.82
16	MnO, % by mass	0.0007	0.0018
17	pH value of aq.extract	6.54	6.52
18	Color reflectance to blue light of wavelength 5040 Å, %	68.13	70.45
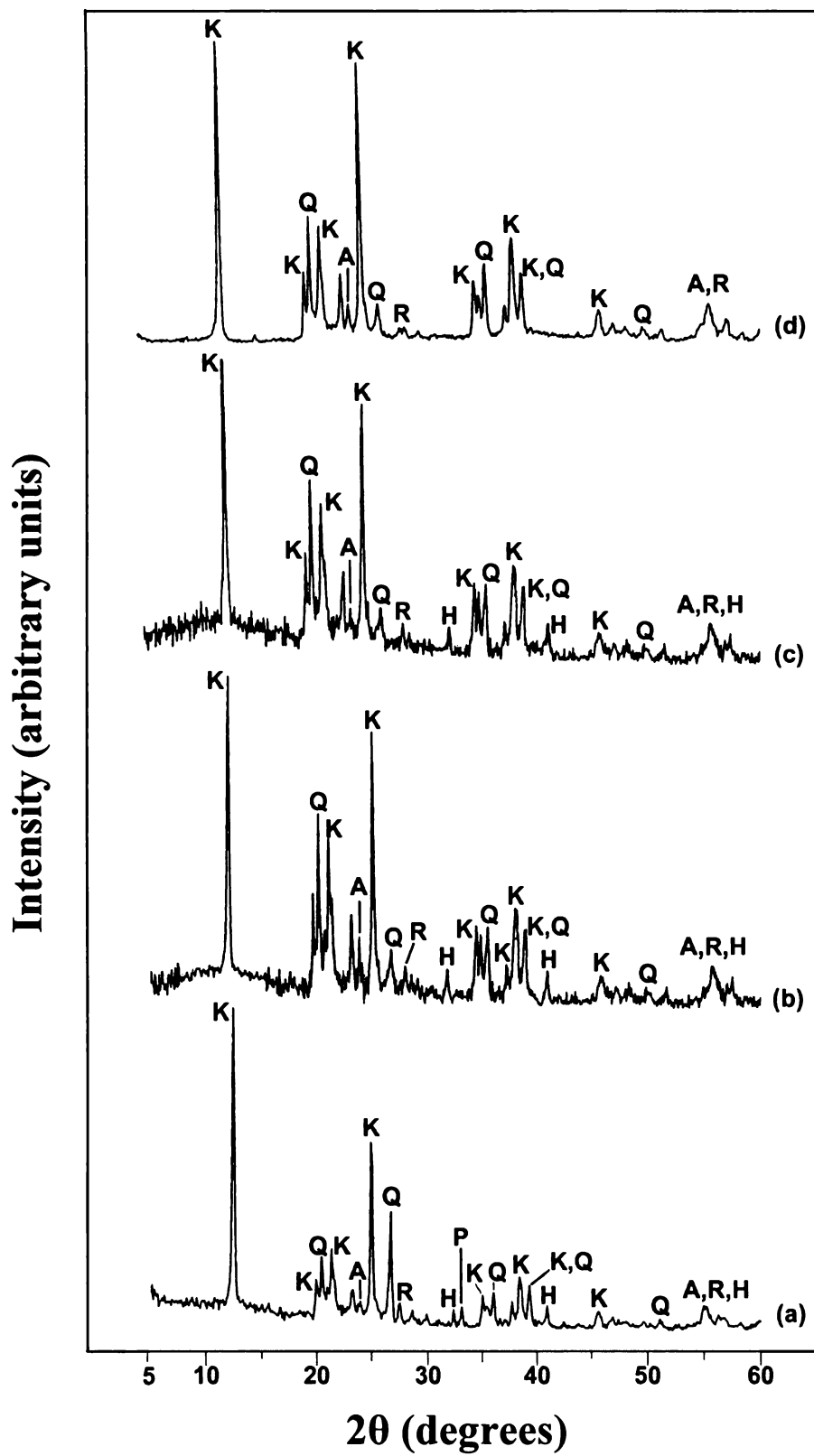
Figure 7.4.1 XRD patterns of (a) ROM (b) SCP1 (c) SCP2 and (d) SCP2-DCBT of Koraput kaolin
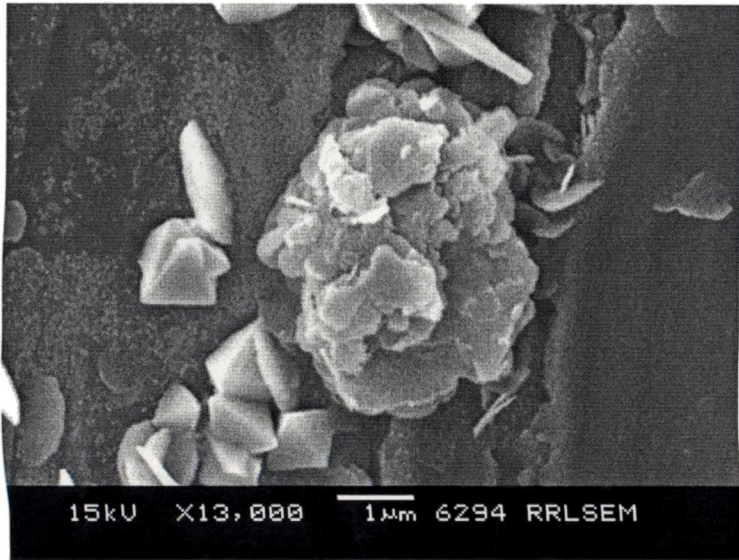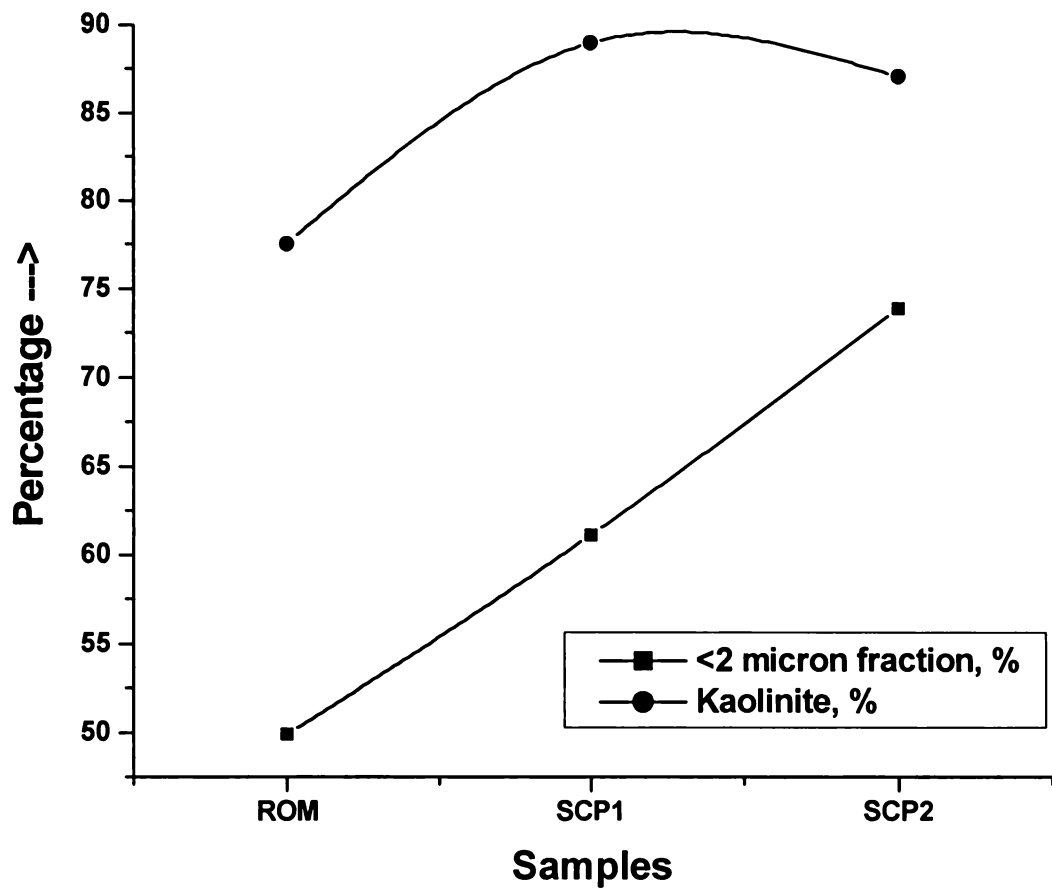
ROM sample
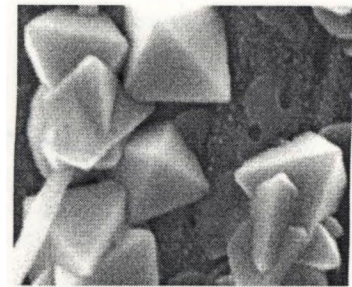
Pyrite particles
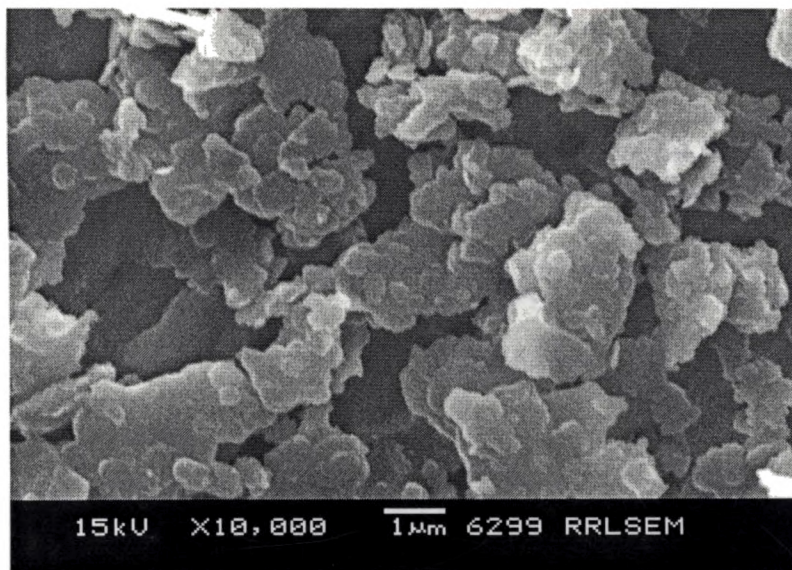
SCP1 sample

Figure 7.4.2 SEM picture of Koraput kaolin

Figure 7.4.3   Variation of <2 micron fraction & kaolinite content during size separation in Koraput kaolin
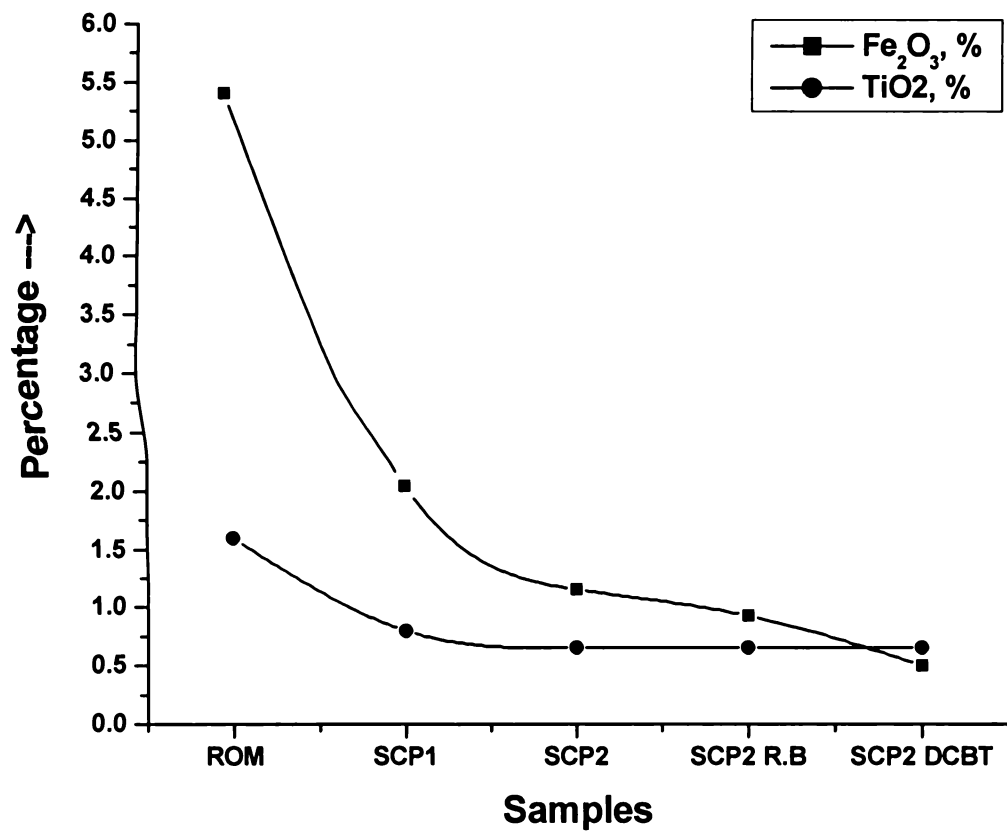
Figure 7.4.4 Variation of Fe_2O_3 & TiO_2 content during various beneficiation processes in Koraput kaolin

CONCLUSIONS

Detailed investigation has been conducted on kaolins from major deposits of the country, Kasargod and Trivandrum (Kerala), Koraput (Orissa), Bankura (West Bengal), Kutch (Gujarat) and Pali (Rajasthan). Valuable information has been obtained on the basic characteristics of the deposits and possibility of beneficiation to give value added products. The identification and quantification of the iron and titanium minerals associated with kaolin has enabled to understand their influence on the kaolin brightness.

All the ROM clay samples are found to be highly kaolinitic except that from Bankura which is more siliceous. Quartz is the major impurity and minor amounts of colored minerals of iron and titania are also present. Kasargod and Trivandrum clays are relatively superior to the others. Mica is dominant in Bankura and Pali samples whereas iron stained titania is the coloring impurity in Kutch clay. Due to the presence of pyrite, Koraput clay is highly acidic. The particle size distribution and optical properties of these clays show wide variation. The brightness values of Koraput and Bankura samples are very poor while that of Trivandrum and Pali kaolins are quite high. All other samples have got moderate brightness. The crystallinity studies by XRD, DTA, FTIR and EPR techniques indicated the disordered nature of the Bankura clay.

Size classification of the samples has resulted in an increase of finer size fractions (<2μm) in the product (SCP1) and removal of coarser particles which include quartz and small quantities of other minerals. Simultaneously, the kaolinite content increases and there is a marginal improvement in brightness also. The Bankura clay is found to be still siliceous. The highest percentage of < 2 μm fraction is in Trivandrum clay (~84%) and the same in Pali, Kutch and Koraput kaolins are promising. The maximum improvement in brightness on the SCP1 is observed in Koraput clay due to the removal of appreciable quantities of pyrite. But the overall brightness of the sample is found to be low. A moderate increase is observed in the brightness of SCP1 from Kasargod 2 and Trivandrum kaolins, but Pali clay does not show any improvement. An enrichment of iron minerals is occurring in the SCP1of Bankura clay which gives a low brightness. The SCP2 samples also show a similar trend and the percentage of <2μm fraction has improved appreciably in all clay samples and the maximum is observed in Trivandrum clay (~92%), followed by Pali and Kutch samples. The SCP2 of Pali is having the highest

359

brightness (~81.2%), followed by Trivandrum and Kasargod 1 clay. Brightness values of all other clays are found to be on a lower side. The reductive bleaching has not made any appreciable improvement in the overall shade of the samples.

The conventional method of size classification could not be adopted for the Koraput clay due to the high acidity. During the slurry preparation, some of the impurities including part of the pyritic iron are dissolved initially and then get precipitated on dilution giving yellowish brown color to the product clay. Hence, a modified method has been suggested for avoiding this problem and getting product clay of acceptable brightness.

DCB treatment is used to leach out the "free" iron and gives a quantitative measure of the same. The "structural" iron does not respond to this treatment and hence the two types can be differentiated. Improvement in the optical properties has been achieved by most of the samples and the highest is for Trivandrum clay. The improvements in Kutch and Pali clays are minimal as most of the iron in these samples is incorporated in the structure of anatase and mica respectively. The Bankura kaolin contains considerable amount of mica and the low brightness of is due to iron containing mica. Calcination has not given any improvement in brightness of the SCP2 samples, except in the case of Trivandrum kaolin.

Comparison of the critical properties ie., particle size distribution and brightness of the beneficiation products with international specifications shows that none of the SCP1 samples fulfill the requirement for either paper coating or filler grade kaolins and further beneficiation is required for their optimum utilization. Properties of SCP2 of Trivandrum and Pali kaolins show that they can be used as Grade C paper filler. SCP2 of Trivandrum clay is even comparable with the commercially available filler grade kaolin used in paper industry. All other samples need further improvement in optical properties for their optimum utilization. The DCB treated sample from Trivandrum is found to have the maximum brightness and fine particle content (<2μm fraction) and is comparable to the international high quality coating grade clays. Kasargod 1, Kasargod 2 and Koraput samples are comparable to the international commercial grade paper filler clays. Koraput kaoin can also be used for the manufacture of white wares (ceramic grade). The

properties of calcined product from Trivandrum match well with the international specifications for paint formulations.

The properties of the product clays have been compared with the IS specifications. Optical properties of SCP1 and SCP2 of all samples except Trivandrum clay need further improvement for their possible use as Grade I (paper) and Grade II (filler) kaolin. The Trivandrum clay can also be used in the manufacture of high quality ceramic products (Grade I kaolin). Kasargod 1, Kasargod 2 can be used as filler (Grade II) kaolin only after removing some of the iron impurities. While SCP2 of Kutch, Koraput and Pali kaolins can be used as Grade II kaolin, Kasargod 1 and 2 and Koraput clays can be used as Grade III kaolin in ceramic industry.

Characterization of the impurities concentrated by different methods has enabled to have a closer look on the nature of iron and titanium minerals. The hydrocyclone underflow (IM1) represents the coarser particles whereas the panned impurities (IM2) have higher density. NaOH treatment of the clay removes the kaolinite and the IM3 is much more concentrated in impurities. The minerals separated by magnet (IM4) are essentially ferruginous. A combination of the characteristics of these four concentrates gives an overall picture of the total impurities present in the clay.

Compared to the other kaolins, the enhancement in optical properties of Kutch and Pali samples after DCBT is not promising. Though there has been a marked improvement in brightness of Bankura sample, the overall shade of the product is not acceptable. Bankura and Pali samples contain mica and appreciable quantities TiO_2 is found in Kutch clay. These ancillary minerals contain "structural" iron and reduce the brightness of the clay. It is difficult to remove these impurities by DCBT and hence the optical properties do not improve.

The EPR spectral studies have been used to understand the extent of iron removal. The spectral data, based on the decrease in intensity of the line at g ~2.6 shows that the iron removal in these samples are minimal. The spectral analysis of the ROM, products of size classification and DCB treatment confirms that most of the iron is ferric and "structural" in Pali clay. Koraput sample contains mostly iron in ferrous state. Most of the iron is "free" in Trivandrum clay whereas Kasargod 1, Kasargod 2 and Bankura samples contain both "structural" and "free" iron where the DCB treatment removes the "free"

iron. The Kutch sample contains only very small part of iron as "free" and the remaining exists in the "structure" of anatase (as titanoferrous). Mossbauer spectra confirm the presence of ferrous iron in Bankura and Koraput samples. The presence of oxides and hydroxides of iron in most of the samples is again indicated by the IR and UV-Visible spectral studies. The HR TEM- EDS clearly shows the presence of ultrafine titanoferrous and pyritic particles in the Kutch and Koraput kaolins respectively.

It has been confirmed that the clays contain different types of impurities in varying concentration and conventional methods of beneficiation alone can not give optimum value addition. DCB treatment is not commercially viable, but it gives very crucial information on the nature of impurities. Hence, advanced techniques of beneficiation such as super conducting high gradient magnetic separation (SC HGMS), froth flotation, selective flocculation have to be adopted in combination with the conventional screening, size classification and reductive bleaching to get maximum and / or optimum value addition of these kaolins.

An attempt has been made to study whether any correlation can be made between the quantities of iron and titanium minerals in the clay with the optical properties. Analysis of the results clearly indicates that the total or "analytical" iron in a sample is not directly related to its optical properties. The type of iron in the ancillary mineral as "structural" or "free" plays significant role in determining the color of the kaolin. The oxides, hydroxides, carbonates, sulphides etc where iron is in the "free" form are colored and have direct influence on the kaolin brightness. A small amount of iron in the structure of kaolinite does not affect the brightness because the iron atoms are too far apart to allow any electronic transition. However, the same amount of iron if present in the structure of ancillary mineral undergoes transitions due to the nearness of the iron atoms. A charge transfer or electron hopping is also possible between iron and any other transition element in the sample. This phenomenon is observed in the titanoferrous impurity in the Kutch clay. Clay is a naturally occurring mineral and the distribution of "analytical" iron among the two species, "structural" and "free", changes from sample to sample resulting in brightness variations. Hence, a direct correlation between the "analytical" iron and brightness is not possible.

362

Publications

International Journals

1. Influence of mineral impurities on the properties of kaolin and its thermally Treated products, Applied Clay Science, Vol.21, 133-142, Elsevier, S.Chandrasekhar & **S. Ramaswamy** (2002).

2. Iron minerals and their influence on the optical properties of two Indian Kaolins, Applied Clay Science, Vol.33, 269-277, S. Chandrasekhar & **S. Ramaswamy** (2006).

3. Investigation on a gray kaolin from south east India, Applied Clay Science, Vol. 37, 32-46, S. Chandrasekhar & **S. Ramaswamy** (2007).

4. Mossbauer Spectroscopic study of china clay samples collected from different Indian States; R. P. Tripathi, H. C.Verma, S. Chandrasekhar, **S. Ramaswamy** Hyperfine Interactions, 2007 (Communicated).

(Applied Clay Science: <u>Impact Factor – 1.652</u>)

National Journals & Seminar Proceedings

1. Chemical leaching of Kaolins and their thermally treated products, Transactions of Indian Ceramic Society, Vol. 61(2), 87-92, S. Chandrasekhar & **S. Ramaswamy** (2002).

2. Investigations on Selected Indian Kaolins for their possible value addition, Proceedings of the International Seminar on Mineral Processing Technology, MPT-Chennai, Allied Publishers, 119-127, S. Chandrasekhar & **S. Ramaswamy** (2006).

3. Removal of Iron mineral impurities from Kaolin – An EPR spectral study, Proceedings of the International Seminar on Mineral Processing Technology, MPT-07, Allied Publishers, Mumbai, 94-99, S.Chandrasekhar & **S. Ramaswamy** (2007).

4. Mossbauer Spectroscopic study of china clay samples collected from different Indian States; R. P. Tripathi, H. C.Verma, S. Chandrasekhar, **S. Ramaswamy**, International Conference on the Application of Mossbauer Effect (ICAME 2007), held in IIT, Kanpur in October 2007.

5. Crystallochemical and spectroscopic investigations on Indian kaolins Part I. Kaolins from Kerala and West Bengal, **S. Ramaswamy** and S. Chandrasekhar, International Workshop on Porous Ceramics (POROCER-2008) and 71st Annual Session of the Indian Ceramic Society, 8-11th January 2008 (Accepted).

6. Crystallochemical and spectroscopic investigations on Indian kaolins Part II. Kaolins from Kerala and Rajasthan, **S. Ramaswamy** and S. Chandrasekhar, International Workshop on Porous Ceramics (POROCER-2008) and 71st Annual Session of the Indian Ceramic Society, 8-11th January 2008 (Accepted).